REPORT DOCUMENTATION PAGE

1. Recipient's Reference	2. Originator's Reference	3. Further Reference	4. Security Classification of Document
	AGARD-LS-195	ISBN 92-835-0749-5	UNCLASSIFIED/ UNLIMITED

5. Originator Advisory Group for Aerospace Research and Development
North Atlantic Treaty Organization
7 rue Ancelle, 92200 Neuilly sur Seine, France

6. Title TURBOMACHINERY DESIGN USING CFD

7. Presented on 24th–25th May 1994 in Ohio, United States, 6th–7th June 1994 in Ankara, Turkey, and 9th–10th June 1994 in Munich, Germany.

8. Author(s)/Editor(s)	9. Date
Various	May 1994
10. Author(s)/Editor's Address	**11. Pages**
Various	252

12. Distribution Statement There are no restrictions on the distribution of this document. Information about the availability of this and other AGARD unclassified publications is given on the back cover.

13. Keywords/Descriptors

Computational fluid dynamics
Design
Gas turbines
Jet flow
Turbulent flow
Unsteady flow
Aircraft engines

14. Abstract

Computational Fluid Dynamics (CFD) has become a major design tool for designers of turbomachinery. The progress in this area is fast, and the use of 3-D methods is becoming increasingly applicable to the design process. This Lecture Series will improve the knowledge in the NATO nations on how to utilize the modern tools of CFD to increase the efficiency, reduce the fuel consumption, and increase the affordability of aircraft engines. Its aim is a unique forum in which the designers from leading gas turbine manufacturers and CFD code developers will present their points of view on the role of CFD in design.

The Lecture Series will cover the recent advances in the use of CFD for turbomachinery design. The role of CFD in the final design phase and the use of computational techniques in the preliminary design phases will be emphasized. Topics to be covered will include:

- Computational methods for preliminary design and geometry definitions;
- Methods for computing through-flows, blade-to-blade flows and geometry generation;
- Optimization strategies;
- Designing in three dimensions;
- Code validation, mesh influence on solution accuracy;
- Turbulence and transition modelling;
- Comparison of time averaged flow solvers and 3-D unsteady CFD codes;
- Industrial use of CFD and the points of view of the designers.

This Lecture Series, sponsored by the Propulsion and Energetics Panel of AGARD, has been implemented by the Consultant and Exchange Programme.

AGARD-LS-195

AGARD
ADVISORY GROUP FOR AEROSPACE RESEARCH & DEVELOPMENT
7 RUE ANCELLE 92200 NEUILLY SUR SEINE FRANCE

AGARD LECTURE SERIES 195

Turbomachinery Design Using CFD

(La Conception des Turbomachines par l'Aérodynamique Numérique)

The material in this publication was assembled to support a Lecture Series under the sponsorship of the Propulsion and Energetics Panel of AGARD and the Consultant and Exchange Programme of AGARD, presented on 24th–25th May 1994 in Ohio, United States, 6th–7th June 1994 in Ankara, Turkey, and 9th–10th June 1994 in Munich, Germany.

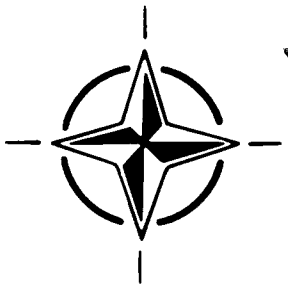

NORTH ATLANTIC TREATY ORGANIZATION

Published May 1994

Distribution and Availability on Back Cover

AGARD

ADVISORY GROUP FOR AEROSPACE RESEARCH & DEVELOPMENT

7 RUE ANCELLE 92200 NEUILLY SUR SEINE FRANCE

AGARD LECTURE SERIES 195

Turbomachinery Design Using CFD

(La Conception des Turbomachines par l'Aérodynamique Numérique)

The material in this publication was assembled to support a Lecture Series under the sponsorship of the Propulsion and Energetics Panel of AGARD and the Consultant and Exchange Programme of AGARD, presented on 24th–25th May 1994 in Ohio, United States, 6th–7th June 1994 in Ankara, Turkey, and 9th–10th June 1994 in Munich, Germany.

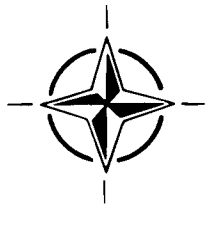

North Atlantic Treaty Organization
Organisation du Traité de l'Atlantique Nord

The Mission of AGARD

According to its Charter, the mission of AGARD is to bring together the leading personalities of the NATO nations in the fields of science and technology relating to aerospace for the following purposes:

- Recommending effective ways for the member nations to use their research and development capabilities for the common benefit of the NATO community;
- Providing scientific and technical advice and assistance to the Military Committee in the field of aerospace research and development (with particular regard to its military application);
- Continuously stimulating advances in the aerospace sciences relevant to strengthening the common defence posture;
- Improving the co-operation among member nations in aerospace research and development;
- Exchange of scientific and technical information;
- Providing assistance to member nations for the purpose of increasing their scientific and technical potential;
- Rendering scientific and technical assistance, as requested, to other NATO bodies and to member nations in connection with research and development problems in the aerospace field.

The highest authority within AGARD is the National Delegates Board consisting of officially appointed senior representatives from each member nation. The mission of AGARD is carried out through the Panels which are composed of experts appointed by the National Delegates, the Consultant and Exchange Programme and the Aerospace Applications Studies Programme. The results of AGARD work are reported to the member nations and the NATO Authorities through the AGARD series of publications of which this is one.

Participation in AGARD activities is by invitation only and is normally limited to citizens of the NATO nations.

Published May 1994

ISBN 92-835-0749-5

Printed by Specialised Printing Services Limited
40 Chigwell Lane, Loughton, Essex IG10 3TZ

Abstract

Computational Fluid Dynamics (CFD) has become a major design tool for designers of turbomachinery. The progress in this area is fast, and the use of 3-D methods is becoming increasingly applicable to the design process. This Lecture Series will improve the knowledge in the NATO nations on how to utilize the modern tools of CFD to increase the efficiency, reduce the fuel consumption, and increase the affordability of aircraft engines. Its aim is a unique forum in which the designers from leading gas turbine manufacturers and CFD code developers will present their points of view on the role of CFD in design.

The Lecture Series will cover the recent advances in the use of CFD for turbomachinery design. The role of CFD in the final design phase and the use of computational techniques in the preliminary design phases will be emphasized. Topics to be covered will include:

- Computational methods for preliminary design and geometry definitions;
- Methods for computing through-flows, blade-to-blade flows and geometry generation;
- Optimization strategies;
- Designing in three dimensions;
- Code validation, mesh influence on solution accuracy;
- Turbulence and transition modelling;
- Comparison of time averaged flow solvers and 3-D unsteady CFD codes;
- Industrial use of CFD and the points of view of the designers.

This Lecture Series, sponsored by the Propulsion and Energetics Panel of AGARD, has been implemented by the Consultant and Exchange Programme.

Abrégé

L'aérodynamique numérique est devenu l'outil de conception de choix des concepteurs des turbomachines. L'évolution est rapide dans ce domaine, où les méthodes tridimensionnelles sont de plus en plus appliquées au processus de conception. Ce cycle de conférences fera évoluer les connaissances dans les pays membres de l'OTAN en ce qui concerne l'utilisation des outils modernes de l'aérodynamique numérique CFD pour améliorer le rendement, pour réduire la consommation de carburant et pour rendre plus abordable le coût des moteurs d'avion. Il constitue un forum unique, où les concepteurs des principaux fabricants de turbines à gaz et les créateurs de codes CFD présenteront leurs points de vue sur le rôle du CFD dans l'étude des moteurs.

Le cycle de conférences couvrira les derniers progrès réalisés dans l'application du CFD à la conception des turbomachines. L'accent sera mis sur le rôle du CFD dans la phase terminale de l'étude ainsi que l'emploi de techniques de calcul lors des phases préliminaires. Les sujets suivants seront traités:

- les méthodes de calcul pour l'étude de l'avant-projet sommaire et la définition de la géometrie;
- les méthodes de calcul des écoulements internes, des écoulements inter-aube et l'élaboration de la géometrie;
- les stratégies d'optimisation;
- la conception tridimensionnelle;
- la validation des codes et l'influence des maillages sur la précision des résultats;
- les tourbillons et la modélisation de la transition;
- la comparaison des résolveurs d'écoulement à moyenne temporelle et les codes CFD instationnaires tridimensionnels;
- l'utilisation du CFD à l'échelle industrielle et le point de vue des concepteurs.

Ce cycle de conférences est présenté dans le cadre du programme des consultants et des échanges, sous l'égide du Panel de Propulsion et d'Enérgetique de l'AGARD.

List of Authors/Speakers

Lecture Series Director: Dr Ahmet S. Üçer
Department of Mechanical Engineering
METU (ODTÜ)
Makina Müh. Bölümü
06531 Ankara
Turkey

AUTHORS/SPEAKERS

Prof. Klaus Broichhausen
MTU München
Postfach 50 06 40
Dachauer Strasse 665
D-8000 München 50
Germany

Dr Michael Casey
Fluid Dynamics Laboratory
Sulzer Innotec
CH-8401 Winterthur
Switzerland

Prof. John D. Denton
University of Cambridge
Department of Engineering
Whittle Laboratory
Cambridge CB3 0DY
United Kingdom

Prof. Dr Ir Ch. Hirsch
Vrije Universiteit Brussel
Dienst Stromingsmecchanica
Plainlaan 2
1050 Brussel
Belgium

Dr Ian K. Jennions
Manager
Computational Turbomachinery Aerodynamics
GE Aircraft Engines
One Newmann Way MD X409
Cincinnati OH 45215-6301
United States

Dr Om P. Sharma
Turbine Group
Commercial Engineering
United Technologies
Pratt & Whitney
400 Main Street M/S 163-01
East Hartford,
Connecticut 06108
United States

Mr Christophe Vuillez
SNECMA
Centre de Villaroche
77550 - Moissy Cramayel
France

Mr Bertrand Petot
SNECMA
Centre de Villaroche
77550 - Moissy Cramayel
France

Contents

INTRODUCTION AND OVERVIEW

by

Dr Ahmet S. Üçer
Department of Mechanical Engineering
Middle East Technical University
(ODTÜ)
Makina Müh. Bölümü
06531 Ankara
Turkey

WHY CFD IN DESIGN?

The trend in the aircraft gas turbine engines is towards energy efficient, compact, lightweight systems. In terms of propulsion parameters the goal is to increase the thermal efficiency, the specific power and specific weight. Higher thermal efficiency means lower specific fuel consumption and it is a direct function of the overall cycle pressure ratio and thermodynamic efficiencies of individual components. The specific power primarily depends on the maximum cycle temperature. Lightweight and high strength materials and reduced number of turbomachinery stages are the primary elements for obtaining higher specific weight. The key technology area for achieving aerodynamic efficiency and increased stage pressure ratio that lead to fewer stages is the use of Computational Fluid Dynamics (CFD) methods in the aerodynamic design process.

Design methods that use CFD techniques produce competitive advantages by increasing the speed of the design cycle, reducing the testing time and therefore the necessary investment. Design of a turbomachine was highly empirical and it required extensive development testing. As computers and their associated design software became tools of design offices, development time reduces appreciably. CFD improves the design techniques when used in making computational experiments to understand the flow physics. The application of computational techniques to the design started in the offices of the aero-engine designers because of the strict requirements of the engines designed to fly. Later computational techniques and CFD codes disseminated into the land based turbomachinery industries.

CFD codes solve the fluid flow equations at many different levels of approximation. By computing the flow field they are capable of simulating and analyzing the flow as accurate as the approximations permit. The application of analysis codes in the design process is done by using the code iteratively for optimizing the component geometry to achieve the desired level of performance. The effectiveness of the process depends on the background and experience of the designer.

Due to the recent cuts in defense budgets throughout the world, there is a danger that enough experience can not be accumulated by the present day designers. Therefore experienced designers will not be available when needed in the future. The experienced designer of the present day will no longer be available in the next decade. There might be two ways of avoiding this unfavorable situation. The first way is to develop "inverse design" techniques. The second, which is complementary to the first is to use artificial intelligence techniques. The two dimensional inverse design methods compute the blade profile necessary to obtain the prescribed flow behavior in the blade to blade plane whereas the 3-D inverse method computes the prescribed blade geometry to produce a prescribed swirl schedule.

AGARD (1989) conference proceedings on "Computational Methods for Aerodynamic Design and Optimization" have several papers on inverse design techniques used in the turbomachinery blade design. Cedar and Stow reported a finite element method for inverse design purposes in 1985. In the recent years 3D inverse design methods emerge (Borges, 1990 and Dang, 1992).

Artificial intelligence tools are incorporated both in the preliminary and detailed aerodynamic design phases. Tong and Gregory (1990) used artificial intelligence in the preliminary design. Shelton et al (1993) attempted to use artificial intelligence tools in the final aerodynamic design.

Presented at an AGARD Lecture Series on 'Turbomachinery Design Using CFD', May to June 1994.

A BRIEF REVIEW

The rapid progress in the computer hardware technology in the last decade or two made computational techniques an indispensable asset in the design of turbomachines. The first application of computers to the design process was the programming of mean-line analysis and simple radial equilibrium methods. The one dimensional nature of the mean-line analysis needs estimation of turning and loss by using various correlation's. Isentropic and non-isentropic radial equilibrium computation procedures were devised in the 60's and early 70's. The early computer codes for the analysis of blade to blade flow used either streamline curvature method, stream function method, or methods using the potential function. Computer codes for defining the geometry of the turbomachine evolved at the same time. These programs were later used in obtaining input data to the computer controlled milling machines.

Streamline curvature method (Novak, 1967), was commonly used in the early years of flow analysis on the blade to blade and hub to shroud surfaces of Wu (1952). The streamline curvature method become instrumental in the development of through-flow codes. Smith (1966) developed the performance prediction capability using through-flow analysis code. Later finite difference solutions of through-flow model were reported by Marsh (1968), Davis and Millar (1975), Smith (1974) and Bosman et al (1977). Finite element method appeared promising in the middle 70's. Works of Hirsch and Warzee (1974, 1979), Adler and Krimerman (1974) are worth mentioning. Above references are some of the first examples of computational fluid dynamics used in the prediction of flow in turbomachines. Axisymmetric through- flow solutions were used extensively in the prediction of radial distribution of flow properties in multi-stage environment. These codes are capable of predicting the overall performance of the turbomachine both at design and off design conditions. Real flow effects are introduced by the use of design and off-design correlation's for loss, deviation and blockage. In the later years spanwise mixing is also introduced to the passage averaged through-flow formulation (Adkins & Smith, 1982., Gallimore, 1986., Ucer & Shreeve, 1992). It is worthwhile to note that due to the complexity of the flow and challenging aspects of solution techniques a large number of researchers were involved in these code development efforts.

Solution of Euler equations on the blade to blade surface of revolution or through linear cascades was attempted because of the limitations of stream function and potential function formulation to solve rotational flows with shocks. Potential function formulation is unable to capture shocks due to the non-conservative form of the discretized principle equation. Stream function formulation is on the other hand restricted to two dimensional flows. Solution of Euler equations was initially performed in two dimensions through cascade of blades (McDonald, 1971; Denton, 1974). Later, with the increase of computing power three-dimensional flow in the blade passages was computed (Thompkins, 1981., Denton, 1982., Arts, 1984). Quasi-three-dimensional representation of the flow as proposed by Wu (1952) was also used in the design and analysis purposes. Consecutive solution of the S1 and S2 axisymmetric surfaces and the transfer of necessary information between the S1 and S2 surfaces was attempted by various researchers in different sophistication's (Jennions & Stow, 1984., Ucer et al, 1983). A comprehensive list of through-flow literature is given by Serovy in the AGARD report AR-175 (1981).

It is very well known that the flow in radial and mixed flow machines are highly three dimensional. In the case of axial flow machines' three-dimensional flow has to be considered if the blade rows are highly loaded. Low aspect ratio highly loaded compressor stages and highly loaded turbine stages are common practice as the efforts of increasing the specific weight of the aircraft engines become the prime objective. Transonic stages become rather common in the present day designs. Historically three dimensional inviscid solvers were developed using finite volume methods in the late 70's, after having mature through-flow methods. A lot of progress has been made with inviscid analysis until the mid 80,s. At the same time it was realized that viscous effects become very significant, especially those associated with shock boundary layer interaction. Many phenomena of key interest as tip clearance flows can only be analyzed by the use of viscous modeling and solution. Tip clearance flow has a major effect on the performance and stability of the compressor. The strong coupling between the boundary layer and core flow and strong probability of boundary layer separation have let to two main approaches to the flow prediction problem. The first is the viscous-inviscid interaction method (Calvert, 1983., Singh, 1982) . A review of schemes used for inviscid-viscous interaction is given by Meauze (1985). The other approach is to solve the Reynolds averaged Navier-Stokes equations with appropriate turbulence models for 2D and 3D flows (Moore, 1985., Dawes, 1987., Hah, 1986., Chima, 1987). A good review of the state of the art of viscous flow solutions for internal flows can be found in AGARD CP-510 (1992). The most commonly used turbulence models are Baldwin and Lomax or κ–ϵ models. Until direct numerical simulation of Navier-Stokes equations for high Reynolds numbers will be available, we shall rely on the turbulence models and hope to have better ones for internal flows of turbomachinery.

Unsteady compressible flow solutions started to emerge in the late 1970's (Hodson,1984., Rai, 1987., Giles, 1990, Gerolymos, 1993). AGARD Conference proceedings (1990) is a collection of work on the unsteady flow in Turbomachinery. The unsteady codes are

meant to simulate the four principle sources of unsteadiness in a stage of turbomachinery. These are wake rotor interaction, potential interaction, vortex shedding and flutter. It was found that the blade wake interaction might be solved by inviscid codes.

A large number of different discretization techniques have been used for the solution of Euler and Navier-Stokes equations. These were the finite difference, finite element and finite volume methods. Space discretization techniques of many types have been developed and used. Time marching methods using both implicit and explicit schemes were practiced. Hirsch (1988) is a valuable reference in which all the available methods are explained. A Proper and accurate specification of the boundary conditions is one of the major factors that effect the success of the code when comparisons are made with the experimental data. AGARD Advisory Report (1990) offers a collection of test cases that can be used for code validation purposes.

Space discretization is based on the so called mesh generation techniques. The mesh generation codes for the complicated geometry's of turbomachine environment became one of the major areas in which research and code development were concentrated. This was because all solvers need a discretized domain on which they are to be solved. Grid generation predefines the quality of the solution with respect to the geometry, the physics and numerical accuracy and stability. Concerning the structure of meshes there are structured and unstructured grids. The most important requirements to the grid arrangement are accurate representation of geometric boundaries, clustering of grids in the regions of strong gradients, smooth distribution of the grid points without singularities and possible orthogonality. These requirements are difficult to satisfy. The structural grid generators were found to be very time consuming in obtaining acceptable grids in and around complicated geometry's. Multiblock techniques were developed in order to reduce the generation time and enhance interactive generation capability. The unstructured grid generation in and around the complicated geometry's is less time consuming. However visual grid quality assessment is difficult even with very sophisticated post processors. Grid adaption enables optimization of the grid during solution. Grid enrichment techniques that refine the grid, considering the physics of the flow, are well suited for unstructured meshes. More information on the grid generation techniques is given in references Thomson et al (1985) and Weitherill (1989).

We should also mention the need of powerful post processors for analyzing the enormous amount of data that is generated by CFD codes. The analysis of the information obtained from a solution takes an appreciable time and effort. Commercially available post processors reached to enough maturity and power that they can be used safely for design and analysis purposes.

The CFD literature might be divided into several categories. Most of the literature is on the solution techniques and algorithms. A large amount of literature is concerned with the efficiency, robustness, and the reliability of the solvers. An important number in this category covers validation studies. More recently, computational experiments using Navier-Stokes codes started to emerge. Such solutions are used to simulate complicated flow phenomena in order to understand the physics that might help to produce better designs.

The main aim of developing, demonstrating and validating the CFD codes is to produce tools for the designer of gas turbines. If the tools are not reliable and user friendly, it would be rather difficult to expect the designer to use the tools that are offered. The reliability of the tools is very important so that the designer can use the tool with confidence and complement the CFD results with his or hers experience. Therefore, in the last few years organized validation studies for CFD codes have started. Some of these studies are restricted to internal flows only. In this regard, it is worth mentioning the efforts of ASME International Gas Turbine Institute (CFD Code Assessment in Turbomachinery) and AGARD Propulsion and Energetics Panel WG 26 (CFD Validation for Propulsion System Components).

PURPOSE AND CONTENT

The codes that might be used in the design process are many. However, it is not clear how often these codes are used actually in the design process. This lecture series is intended to bring the code developers and the CFD specialists of the leading gas turbine manufacturers together. The aim is to discuss how useful the state of the art CFD, in the design environment of companies. The points of view of the users and developers in using CFD as a design tool will be deliberated.

This lecture series will start with the presentation of preliminary design methods. Although preliminary design does not use CFD techniques it was decided that these methods should be addressed in a lecture series on the design of turbomachinery. Several aspects of computational methods for the preliminary design process are discussed for axial and radial compressors. Examples of modern turbomachinery geometry definition methods involving Bezier surfaces and B-splines are described.

The second lecture will be on an aerodynamic design system that consists of many parts like through

flow, secondary flow, geometry generators, blade-to-blade and full 3D analysis.

The next lecture will cover the direct use of three dimensional calculations for turbomachinery design. It will be demonstrated that with a flexible geometry package that directly generates a 3D data set, changes in blade geometry can be made in a short time. Modern 3D calculations will be introduced which can solve the complete stage, adequate for design purposes in the order of one hour on a workstation.

Forth lecture will review the present state of the art of CFD methodology with emphasis on quality and accuracy of numerical approximations related to viscous flow computations. The basic problems of turbulence and transition modeling will be discussed. Integrated interactive mesh generation and graphical post processing systems will be illustrated by specific examples.

The fifth lecture will be on the impact of recent research activities, in unsteady flows in turbines and on flow simulation methods used in the turbine design process. An overall discussion will be presented to distinguish flow parameters that can be modeled with existing steady CFD codes, from those that require unsteady CFD codes. This lecture will also mark the beginning of deliberations of the company specialists on the use of CFD in aerodynamic design of turbomachinery.

Next four lectures will be on the experiences of R&R, SULZER, GE, SNECMA and MTU in the use of CFD in their design processes. These presentations will address the important issues, particular to the company, on the use of CFD. The papers will also address the codes used in the companies. The critical assessments of usefulness of the codes will also be given.

REFERENCES

Adkins, G.G. and Smith, L.H., 1982, "Spanwise Mixing in Axial Flow Turbomachines", ASME Journal of Engineering for Power, Vol. 104, pp-97-110.

Adler, D., and Krimerman, Y., 1974, "A Numerical Calculation of the Meridional Flow Field in turbomachines Using Finite Element method", Israel Journal of Technology Vol 12, p 286-274.

AGARD Adv. Rep., 1990,"Test Cases for Computation of Internal Flows in Aero Engine Components", Ed. Fottner, L., AR-275.

AGARD Con. Pro.,1989,"Computational Methods for Aerodynamic Design (Inverse) and Optimization", CP-463.

AGARD Con. Pro.,1990, "Unsteady Aerodynamic Phenomena in Turbomachines", CP-468

AGARD Con. Pro.,1992,"CFD Techniques for Propulsion Applications", CP-510

AGARD Report, 1981,"Through Flow Calculations in Axial Turbomachines", AR-175.

Arts,T.,1984, "Calculation of the Three Dimensional Steady, Inviscid Flow in a Transonic axial Turbine Stage", ASME paper 84-GT-79.

Borges, J.E., 1990,"A Three-Dimensional Inverse Method in Turbomachinery, Parts 1 and 2", Journal of Turbomachinery, Vol.112, No.3 pp 346-361

Bosman, C., and El-Shraawi, M.A.I.,1977, "Quasi-Three-Dimensional Numerical Solution of Flow in Turbomachines", Trans ASME J. of Fluids Engineering., Vol. 99, p 132-140.

Calvert, W.J., 1983, "Application of an Inviscid-Viscous Interaction Method to Transonic Compressor Cascades", NGTE Report R83001.

Cedar, R.D., and Stow, P., 1985, "A Compatible Mixed Design and Analysis Finite Element Method for the Design of Turbomachinery Blades", Int J. for Num. Meth. in Fluids, Vol 5, p 331-345

Chaima, R.V.,1987, "Explicit Multigrid Algorithm for Quasi-Three-Dimensional Viscous Flows in Turbomachinery", J. Propulsion and Power, Vol.3, No.5, p 397-405.

Dang, T.Q.,1992,"A Fully Three-Dimensional Inverse Method for Turbomachinery Blading in Transonic Flows", ASME Paper 92-GT-209.

Davis, W.R. and Millar, D.A.J., "A Comparison of the Matrix and Streamline Curvature Methods of Axial Turbomachinery Analysis, from a Users point of View", ASME Trans. J. of Eng. and Power, Vol 97, p 549-560.

Dawes, W.N.,1987,"A Numerical Analysis of Three Dimensional Viscous Flow in Transonic Compressor Rotor and Comparison with Experiment", ASME Journal of Turbomachinery, Vol.109, p 83-90.

Denton, J.D., 1974, "A Time Marching Method for Two and Three Dimensional Blade to Blade Flow", Aero. Res. Co., R.&M., 3775.

Denton, J.D., 1982,"An Improved Time Marching Method for Turbomachinery Calculations", ASME Paper 82-GT-239.

Gallimore, S.J., 1986, "Spanwise Mixing in Axial Flow Compressors.: Part 2 Througflow Calculations Including Mixing", ASME Journal of Turbomachinery, Vol. 108, pp- 10-16.

Gerolymos, G.A.,1993, "Advances in the Numerical Integration of the Three Dimensional Euler Equations in Vibrating Cascades", ASME J. of Turbomachinery, Vol 115, No 4, p 781.

Giles, M.B.,1990,"Stator/Rotor Interaction in a Transonic Turbine", AIAA Journal of Prop. and Power., Vol 6, No 5.

Hah, C.,1986, "A numerical Modeling of Endwall and Tip Clearance Flow in an Isolated Compressor Rotor", ASME J. Eng. for Power., Vol.108 p15-21.

Hirsch, Ch., 1989 &1990, "Numerical Computation of Internal and External Flows" Vol 1 and 2, John Wiley and Sons.

Hirsch, Ch., and Warzee, G., 1974, "A Finite Element Method for Flow Calculations in Turbomachines", Vrije Univ.Brussel, Dienst Stromingsmechanica, VUB-STR-5.

Hirsch, Ch., and Warzee, G.,1979, "An Integrated Quasi-3D Finite Element Calculation Program for Tubomachinery Flows", ASME Trans., J. of Eng. for Power, Vol. 101, p 141-148.

Hodson, H.P.,1984, An Inviscid Blade to Blade Prediction of Wake-Generated Unsteady Flow", ASME paper 84-GT-43

Jennions, I.K. and Stow,P.,1984, "A Quasi-Three-Dimensional Turbomachinery Blade Design System", Part1-Through Flow Analysis, ASME paper 84-GT-26, Part2-Computerized System, ASME paper 84-GT-27.

Marsh, H.,1968, "A Digital Computer Program for the Through-Flow Fluid Mechanics in an Arbitrary Turbomachine Using Matrix Method", ARC Rep. and Memo. 3509.

McDonald, P. 1971, "The Computation of Transonic Flow Through Two Dimensional Gas Turbine cascades", ASME Paper 71-GT-89.

Meauze, G.,1985, "Viscous-Inviscid Flow iterraction Methods & Shock Boundary Layer Interaction", Thermodynamics and Fluid Mechanics of Turbomachinery, Ed. by A.S.Ucer, P.Stow, C.Hirsch. Martinus Nijhoff Pub.

Novak, R.A.,1967,"Streamline Curvature Computing Procedures for Fluid Flow Problems", ASME,J.of Eng. for Power, p 478-490.

Rai, M.M.,1987,"Unsteady Three-Dimensional Navier-Stokes Simulations for Turbine Stator Interaction" AIAA Paper 87-2058.

Shelton, M.L., Gregory, B.A., Lamson, S.H., Moses, H.L., Doughty, R.L., and Kiss, T., 1993, "Optimization of a Transonic Turbine Aoirfoil Using Artificial Intellegence, CFD and Cascade Testing", ASME Paper 93-GT-161.

Singh, U.K., 1982,"A Comnputation and Comparison With Measurements of Transonic Flow in an Axial Compressor Stage With Shock and Boundary Layer Interaction", ASME J. of Eng. for Pow., Vol 104,

Smith, D.J.L.,1974," Computer Solution of Wu's Equations for Compresible Flow through Turbomachines" NASA SP-304, Part 1.

Smith, L.H.,1966, "The Radial Equilibrium Equation of Turbomachinery", ASME J.of Eng . for Power, Vol.88, p 1-12.

Thompkins, W.T.,1981, "A Fortran Program for Calculating 3D, inviscid rotational flow with Shock Waves in Axial Flow Compressor Blade Rows", MIT GT and PDL Report No.162.

Thomson, J.F., Warsi, Z., Mastin, C.W.,1985,"Numerical grid generation, Foundations and Applications", Pub. North Holland.

Tong, S.S., and Gregory, B.A., 1990, "Turbine Preliminary Desigh Using Artificial Intelligence and Numerical Optimization Techniques", ASME Paper 90-GT-148.

Ucer, A.S. and Shreeve, R.P.,1992, "A Viscous Axisymmetric Throughflow Prediction Method for Multistage Compressors", ASME Paper 92-GT-293.

Ucer, A.S., Yegen, I. and Durmaz, T.,1983,"A Quasi-Three-Dimensional Finite Element Solution for Steady Compressible FlowThrough Turbomachines", ASME J.Eng.Power, Vol.105,pp 536-542.

Weatherill, N.P.,1989, "Mesh generation in computational Fluid Dynamics" VKI LS1980-4,

Wu, C.H.,1952,"A General theory of Three Dimensional Flow in Subsonic and Supersonic Turbomachines of Axial, Radial, and Mixed Flow Types", Transe/ctions of the ASME p1363-1380.

COMPUTATIONAL METHODS FOR PRELIMINARY DESIGN AND GEOMETRY DEFINITION IN TURBOMACHINERY

M. V. Casey

Fluid Dynamics Laboratory
Sulzer Innotec AG
CH-8401, Winterthur
Switzerland

1. SUMMARY

A review of the turbomachinery preliminary design process is given with particular emphasis on axial and radial compressors. The review covers the selection of machine type, mean-line analysis and correlations, stage-stacking calculations and the use of design charts and optimisation techniques to find optimum values for design parameters. A comparison is made between the most successful correlations for endwall losses in axial compressors to highlight the different approaches that are possible.

The preliminary design process provides an initial definition of the skeletal geometry of the blading and the annulus of the turbomachine. Turbomachinery design systems are then based on design by analysis, whereby the blading is assessed using CFD codes and is iteratively refined. A numerically based parametric blade geometry definition system makes the use of CFD considerably more effective. Examples of modern turbomachinery geometry definition methods involving Bezier surfaces and B-splines are described.

2. INTRODUCTION

A turbomachine is usually designed to achieve optimum performance for the customer, with minimum development time and cost. The enormous range of possible turbomachinery geometry, particularly in multistage machines, makes it impossible to investigate all of the interesting parameter options with CFD computations. It is vital for the engineer to eliminate inadequate designs and to obtain a near optimum configuration during the preliminary design process before proceeding with the final design refinements using CFD, see figure 1.

Preliminary design methods still tend to be based on elementary one-dimensional mean-line (or pitch-line) methods of analysis. These are able to predict the performance of a turbomachine from basic design information to an accuracy of a few percent. They are thus sufficiently accurate to allow the main geometric and aerodynamic parameters to be selected before a refined design is attempted. An additional advantage of one-dimensional methods is that they allow the large body of empirical information and accumulated company experience to be incorporated in the design, via semi-empirical correlations for flow losses, blockage and turning. The high quality of such methods can be seen from the fact that one-dimensional blade loading criteria developed from the classic works of Lieblein (1959), de Haller (1955) and Zweifel (1945) are still used to determine the loading levels in axial machines. The author has come across very few examples where CFD computations during the blading design process have identified a subsequent need to change the number of blades selected by proper use of these classical blade loading criteria.

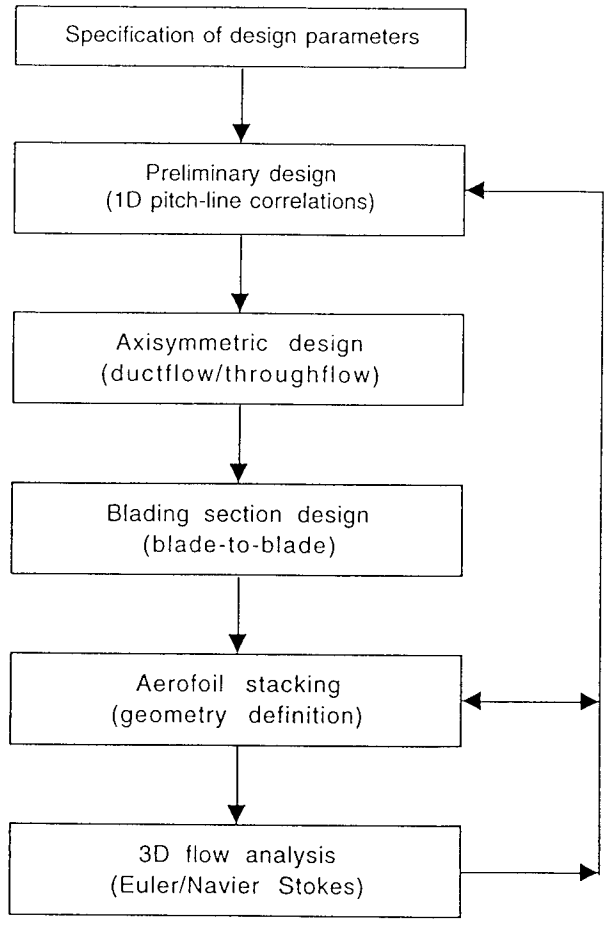

Figure 1: Typical turbomachinery aerodynamic design system

During the preliminary design process all of the fundamental engineering decisions that determine the ultimate performance potential of a machine and the degree of difficulty (in terms of risk, time and cost) of

Presented at an AGARD Lecture Series on 'Turbomachinery Design Using CFD', May to June 1994.

attaining this performance are made. The preliminary design determines both the critical dimensions (for example the annulus geometry and aspect ratio) and the values of the key aerodynamic parameters (such as the mean-line velocity triangles, Mach numbers and loading levels). If the values of any of these parameters selected during the preliminary design process are not consistent with the performance required by the customer, no amount of subsequent CFD computational effort or development testing will enable the performance to be achieved. Thus despite the mundane simplicity of the methods used, the preliminary design process remains crucially important in the aerodynamic design of turbomachinery.

The preliminary design methods used by individual companies tend to be based on correlations of their own experience-base and, as a consequence, new designs often tend to be rather similar to those preceeding them. Because of this, the major differences between the products of different turbomachinery manufacturers probably stem more from the preliminary design methods in use than the CFD methods. In fact, the extensive effort devoted to CFD validation has ensured that the CFD tools in use by different companies provide essentially similar results, and in many cases the same CFD code is in use within many companies, for example, that of Dawes (1988). This is not the case with preliminary design methods, since very few are commercially available, and those in most use are unique to the company using them.

The basic tools for the preliminary design of turbomachinery have not been greatly affected by the rapid change in blading design methods since the introduction of CFD. The techniques currently used for preliminary design are not widely different from those in use for turbomachinery final design two to three decades ago, when many turbomachines were conceived and developed by looking at the flow process in the middle of the annulus only. The main change in preliminary design methods that has occurred in recent years is that the computational techniques and details of the correlations have been refined and improved. In addition, much better graphical techniques are now used to present the results, and, in some cases, numerical optimisation techniques have been developed to aid the search for the optimum design.

With each introduction of more complete CFD modelling of the flowfield as the final design step, many of the the tools currently used in the design process (such as throughflow calculations and Q3D blade-to-blade calculations) can now, to some extent, be classified as preliminary design methods. In radial compressor design, the preliminary design process determines both the skeletal geometry of the blading and the annulus geometry of the machine for subsequent analysis and refinement by throughflow methods or CFD computations. In axial compressors, the one-dimensional preliminary design process is used to estimate the annulus shape, the number of stages, the aspect ratio, the number of blades, the mean-line velocity triangles and the blade loading levels in each stage. A throughflow analysis is then used for the detailed air-angle design. This determines the spanwise variation of the velocity triangles from which a preliminary estimate can be made of the blading geometry for analysis with CFD methods.

The sections that follow review aspects of the preliminary design and geometry definition of both axial and radial compressors. The author has less personal experience of the preliminary design of turbines, so readers are referred to some of the many recent publications on turbine preliminary design methods for more details of this (see, for example, Wilson (1987), Gyarmarthy (1990), Whitfield and Baines (1990), Schobeiri (1992), Schobeiri and Abouelkheir (1992) and many other earlier references given by these authors).

This review first describes some of the successful correlation methods for selecting the machine type and estimating the mean-line performance of axial and radial compressor blade rows. The various methods of stage-stacking, using either blade row performance data or stage characteristics, to compute the performance of multistage machines is then considered. The use of various engineering tools, from design charts to numerical optimisation methods, in conjunction with mean-line prediction methods for the optimisation of designs is discussed. Finally a brief review of modern geometry definition methods for the numerical definition of turbomachinery blade and channel geometry is given.

3. CORRELATIONS FOR AXIAL AND RADIAL COMPRESSORS

3.1 Selection of machine type

The first question to be asked in the selection of a turbomachine is whether an axial or radial machine is appropriate for the duty being considered. For pumps, sufficient experience is available for this question to be answered on the basis of relatively simple correlations using the concept of specific speed without any detailed numerical computations. An example of such a correlation is given in figure 2 from Spengler (1976). The definition of specific speed is based on the duty of the machine as specified by values of the volume flow, V, the head, H, and the rotational speed, n, as

$$n_q = nV^{0.5} / H^{0.75}$$

(Note that specific speed correlations of this type require special care with the units being used: often, as in this case, inconsistent units are used and the result is not truly non-dimensional).

The curves shown in figure 2 demonstrate the optimum values of head rise coefficient, flow coefficient, blade number, outlet width ratio and inlet diameter for a given specific speed. The pump manufacturer would also correlate the inlet and outlet blade angles and the expected value of the efficiency in this way. Deviations of the geometry from the values obtained from such curves are possible, but the peak efficiency is likely to be lower. and the use of CFD in the detailed design of the pump blading would be unlikely to recover this loss in efficiency.

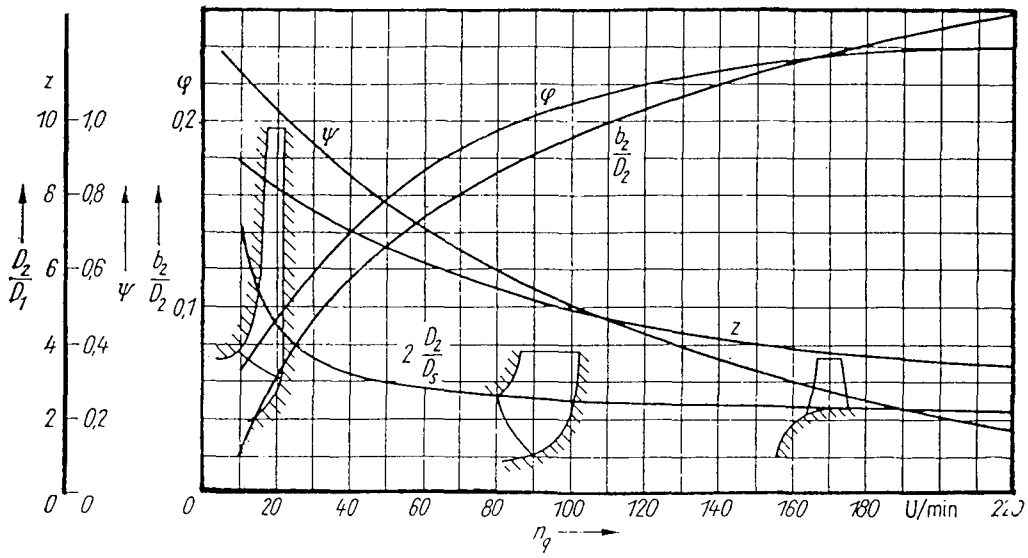

Figure 2: Correlation for the selecton of pump type and global geometry based on specific speed n_q, Spengler (1976).

Key: ϕ = impeller outlet flow coefficient (Cm_2/U_2)
Ψ = impeller work coefficient ($2gH/U_2^2$)
z = impeller blade number
b_2 = impeller outlet width
D_2 = impeller outlet diameter
D_s = impeller eye diameter

For radial compressors, such correlations need to take into account the Mach number and the compressibility of the fluid. Casey and Marty (1986) have published a typical correlation for the efficiency of low Mach number industrial radial compressors based only on the value of the inlet flow coefficient, see figure 3. Rodgers (1980) has published a correlation for high Mach number impellers based on the specific speed using the flow volume derived from the mean density of the gas between the inlet and outlet of the compressor. Such correlations are adequate for radial compressors up to moderate specific speeds but become less useful for high specific speeds where a mixed flow compressor could be used. Balje (1981) has published a correlation for the whole range of compressor applications including mixed flow impellers. The importance of these correlations is that they define the general level of performance that can be expected for particular types of design; high efficiency cannot be expected of a low specific speed design, even if the very best CFD methods are used for its detailed design.

An additional factor to be taken into account is the absolute flow capacity and size of the turbomachine. Correlations based on the value of the exit flow function ($m\sqrt{(T)}/P$) have often been used in aeroengine compressor applications to delineate the change from axial to radial machines, see for example Birdi (1992). For values of the exit flow function lower than 3 (imperial units [$lb/s\sqrt{K}/psi$]) a radial compressor tends to be used, and for values greater than 6 an axial compressor is used. Mixed flow impellers are used for intermediate values and have the advantage that they allow a larger exit flow function to be achieved for a given frontal area than purely radial impellers. Often the experience-base of a particular compressor manufacturer allows a radial compressor to be used when another manufacturer with more experience with axial compressors would use an axial compressor.

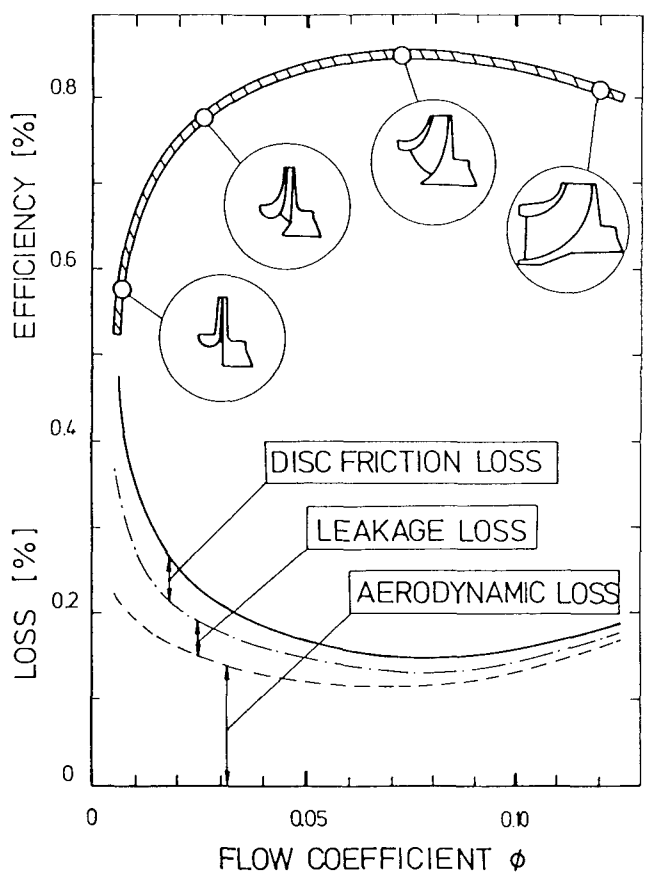

Figure 3: The variation in optimum efficiency, loss and impeller shapes with design flow coefficient for process impellers, Casey and Marty (1986), (ϕ = impeller flow coefficient ($V/U_2D_2^2$).

In practice, correlations of this type are not used that often for the preliminary design process, since in most cases the new design is derived from an existing design. Most customers for turbomachinery are aware of the many difficulties and risks associated with completely new compressor designs and favour derivative designs. This limits the degree of freedom available to the designer. Typically he would examine the following options for derivative designs before carrying out a new design:

(a) Reblading an existing compressor in the same annulus to meet changed requirements,
(b) Changing the blading and the casing annulus line whilst retaining an existing rotor ("cropping" or "growing" the blading),
(c) Scaling an existing compressor to a new size,
(d) Cutting back the trailing edge of an impeller to change its head rise characteristics,
(e) Rematching the diffuser of a radial impeller to change the mass flow - pressure rise characteristics,
(f) Adding a "zero" stage to the front, or additional stages to the rear, of an axial compressor.

In view of the fact that such changes can be requested several times over the lifetime of a particular design, the importance of the preliminary design process, especially with regard to axial length and aspect ratio becomes clear.

Following the selection of machine type, it is necessary to make predictions of the performance for various tentative designs, with a view to selecting those that are most likely to achieve the required performance for more detailed analysis. The preliminary design process thus requires an ability to correctly predict the performance for the various geometrical options. This requires accurate and reliable correlations of the effects of geometrical changes on performance, as outlined below. In view of the fact that one of the major technical problems of compressor design is the achievement of adequate surge margin, these techniques need to be able to examine the off-design performance as well as to predict the design point efficiency.

3.2 Correlations for axial compressors

For the successful prediction of the performance of an axial compressor blade row four different types of aerodynamic problem have to be looked at:

(a) cascade aerodynamics (that is, profile losses and deviation as a function of incidence and Mach number),
(b) casing and hub boundary layers (clearance losses, annulus losses, secondary losses and endwall blockage as a function of stage loading and clearance levels),
(c) the onset of rotating stall, and
(d) the choking of the blade row.

Much research effort has been dedicated to these problems, and fairly universal techniques exist for the correlation of some of the effects of geometrical changes on performance based on semi-empirical physical models of the flow.

Practical compressor preliminary design methods still tend to rely on highly empirical techniques to calculate the magnitude of the endwall losses and the inception of stall from the geometrical parameters (see Cumpsty (1989)). The initial estimates of the profile losses, the deviation angles and the choking of the blade rows are also estimated from empirical correlations, but subsequent analysis with CFD methods is able to provide more precise information. The limitations of CFD methods for the various aspects of performance prediction are reviewed in a companion paper to this, Casey (1994).

3.2.1 *Cascade correlations*

There is widespread agreement on the general form of the best correlations for the cascade performance of an axial compressor section, following the work of Lieblein (1959) and Koch and Smith (1976), although there is often some discrepancy between the detailed form that the correlations take. The profile losses at the minimum loss incidence are generally correlated in terms of the Lieblein diffusion factor with corrections for the effect of thickness/chord ratio, Mach number, axial velocity ratio and Reynolds number. Simple polynomials are used to predict the loss bucket giving the rate of increase of loss with incidence up to and beyond the "stalling" incidence, where the losses are twice their minimum value.

The performance range of a single section of an axial blade row operating in cascade is usefully documented in the form of an "alpha-Mach" diagram showing the operating range of the cascade in terms of inlet flow angle versus inlet Mach number, see for example Cumpsty (1989). An example of such an empirical correlation for a DCA (double circular arc) cascade based on that given by Raw and Weir (1980) is given in figure 4. The lines shown on this diagram are:

(a) The choking limit of the cascade, which for isentropic flow is a unique function of the Mach number, throat area and flow inlet angle. At Mach numbers above the critical Mach number, shock losses modify the ideal choke line in the way shown.
(b) The high loss boundary on the choke side of minimum loss, where the loss coefficient starts to rise above twice its minimum loss value. At higher Mach numbers the losses rise because of the proximity to choke, but at lower Mach numbers they rise because of negative incidence stall.
(c) The locus of minimum loss incidence as a function of the Mach number.
(d) The high loss boundary on the stall side of minimum loss, where the losses rise above twice the minimum loss value because of flow separation losses at positive incidence. The precise location of this line above the critical Mach number depends on the aerofoil type.

No generally valid correlations for these lines have been published, and individual compressor manufacturers have their own data-base and correlations for classical blade profiles (NACA 65, C4 and DCA profiles) to generate such diagrams (see the examples given by Koch and Smith (1976), Raw and Weir (1980), Casey (1987), Miller and Wasdell (1987) and Wright and Miller (1991)). The "alpha-Mach" diagrams can be generated from

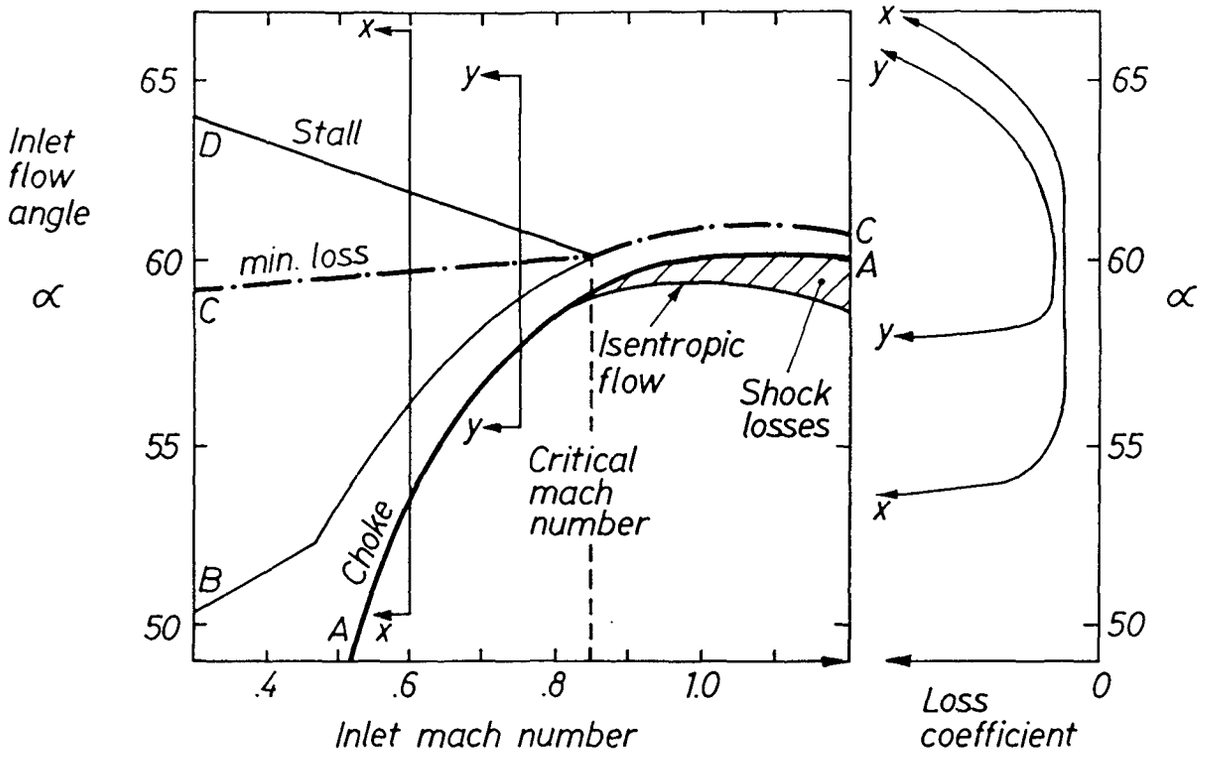

Figure 4: "Alpha-Mach" (inlet flow angle versus inlet mach number) diagram for a compressor cascade section showing limits of operation, based on that given by Raw and Weir (1980)

Key: Line A Choke (with correction for non-isentropic flow)
Line B High loss boundary (choke side of loss bucket)
Line C Minimum loss
Line D High loss boundary (stall side of loss bucket)

relatively few geometrical parameters for the blade row (such as space/chord ratio, thickness/chord ratio, stagger and camber angles) using information based on correlations of low speed cascade data and geometrical correlations to give the throat area.

In addition to the losses, the deviation angle between the blade metal outlet angle and the flow outlet angle needs to be predicted, along with its variation with incidence. Correlation methods based on that of Lieblein (1960) or that of Carter (1950) are in general use for the deviation of classical blade profiles, but most companies have empirical corrections to these to improve the fit to their data-base. Examples of such corrections are given by Cetin et al. (1987) to match measured performance data on transonic compressor stages. The prediction of the variation of deviation with incidence is less straightforward and several different methods have been suggested, varying from a linear increase in deviation with incidence, Lieblein (1969), to the use of generalised curves relating deviation to incidence, Wasdell and Miller (1987). Blade-to-blade codes are generally quite reliable for the prediction of deviation at the minimum loss incidence, but less accurate with respect to the variation with incidence.

Correlation data is, of course, only available for classical profile families on circular arc camber lines, and is not suitable for use with non-standard profiles (such as modern forms of controlled diffusion blading). In order to apply these correlations with profiles of this type it is necessary to define an equivalent blading to the non-standard aerofoil. This can be done (approximately) by choosing a DCA blade with an inlet blade angle that gives the same throat area as the non-standard aerofoil and hence the same choke boundary. The stall and minimum loss lines for the non-standard aerofoil can then be obtained from the DCA correlations relative to the choke line. It would be a great step forward for the compressor designer if a CFD blade-to-blade code were available which could accurately predict these features of cascade aerodynamics and generate such profile loss buckets, the "alpha-Mach" diagrams and flow deviation for all blading types. The work of Youngren and Drela (1991) appears to provide the closest approach to such a code that has been developed so far.

The cascade correlations are not only used in preliminary design to predict the performance of cascades, but also during the throughflow design to suggest a preliminary blading geometry (stagger, camber and space/chord ratio) for a given set of air angles. This is particulary useful as it provides a basis for the establishment of the blade loading levels at an early stage in the design and gives the designer the opportunity to modify the air-angle design to balance the distribution of loading before the detailed blading design process. It also allows preliminary blading

to be available for mechanical analysis and refinement with blade-to-blade codes.

3.2.2. *Endwall losses and blockage*

There is very little agreement in the turbomachinery literature on the most appropriate form of correlation for the prediction of the endwall losses and blockage, and a number of radically different techniques are used, see the recent reviews by Cumpsty (1989) and Denton (1993). The most reliable correlations appear to be those of Smith (1970), as modified by Koch and Smith (1976) and Casey (1987), that of Hunter and Cumpsty (1982), and that given by Wright and Miller (1991), which is based on work by Freeman (1985).

The correlation of Smith (1970) predicts the endwall blockage and tangential force deficit thickness of the hub and casing boundary layers in a repeating stage, see figures 5 and 6. These boundary layer thicknesses are correlated as functions of the clearance/staggered gap ratio and the nearness to stall (as expressed by the pressure rise as a fraction of the maximum pressure rise of the stage).

In a later form of this correlation, given by Koch and Smith (1970), see figure 7, the boundary layer parameters of the hub and casing were combined to produce a correlation with rather less scatter. Another more subtle change introduced by Koch and Smith was to use a different definition of the nearness to stall as the abscissa scale. The initial Smith correlation took the pressure rise coefficient based on mean blade speed as a measure of the pressure rise, whereas the later correlation uses a pressure

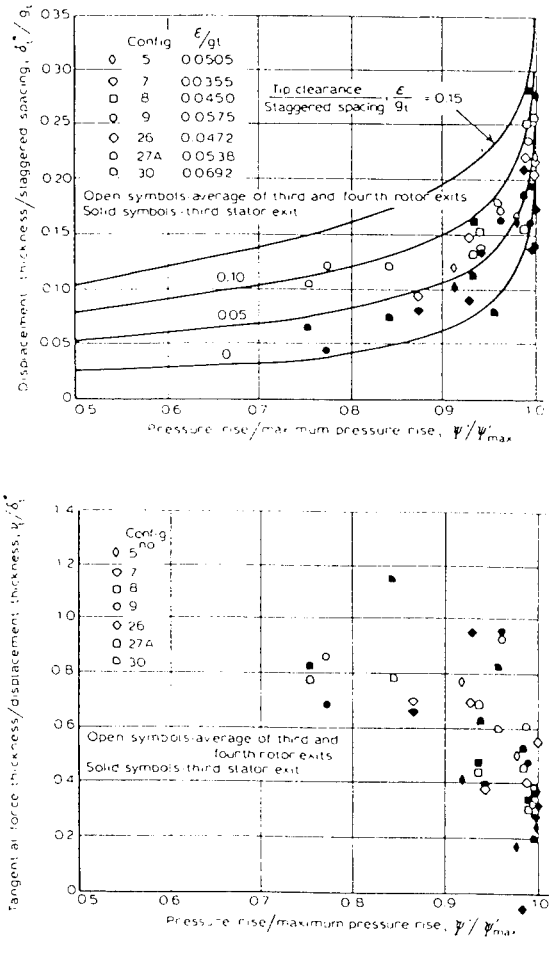

Figure 5: Endwall boundary layer blockage and tangential force deficit thickness correlation for casing boundary layers, Smith (1970)

Key: δ^* = displacement thickness
υ = tangential force thickness
ψ = Pressure rise coefficent ($2\Delta p/\rho U_m^2$)
U_m = mean blade speed
ε = tip clearance
g = blade staggered spacing

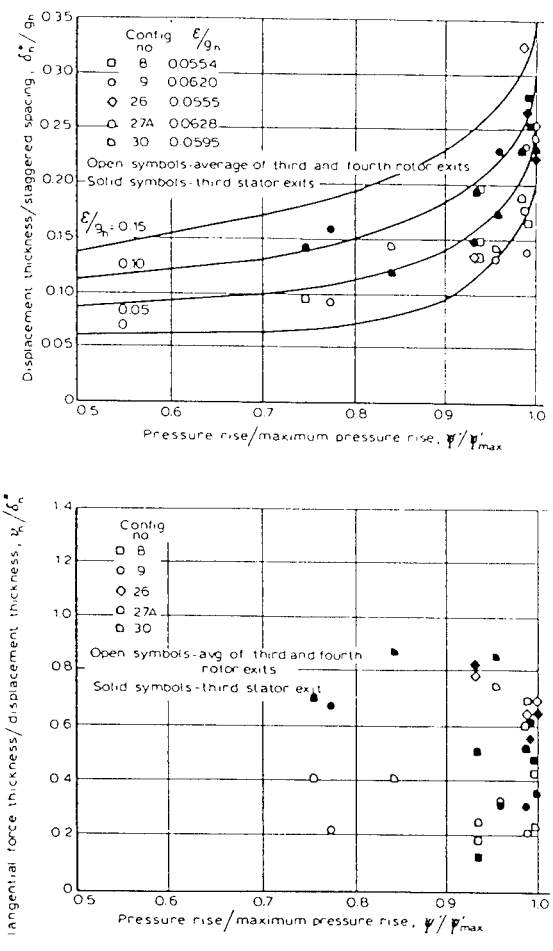

Figure 6: Endwall boundary layer blockage and tangential force deficit thickness correlation for hub boundary layers, Smith (1970)

Key: δ^* = displacement thickness
υ = tangential force thickness
ψ = Pressure rise coefficent ($2\Delta p/\rho U_m^2$)
U_m = mean blade speed
ε = tip clearance
g = blade staggered spacing

rise coefficient based on the inlet velocity to the blade row. This has the effect of spreading out the data close to stall and avoids the trend that the correlated data lies on a vertical line close to stall, as can be seen by comparison of figures 6 and 7. Casey (1987) further modified these correlations to make use of the more recent stall prediction criterion of Koch (1981) for the calculation of the nearness to stall. In the original paper Smith qualifies this correlation as coming "from engineering judgement seasoned by boundary layer data", which is certainly very true for the correlation of the tangential force deficit thickness. The disadvantages of the Smith and Koch correlation are that it does not separate the blockage in the rotors and stators, that it applies only to repeating stages and that a separate correlation for stall is needed before it can be used.

The correlation of Hunter and Cumpsty (1982), see figure 8, also predicts the displacement thickness and the tangential force deficit thickness as a function of the nearness to stall. In this correlation the boundary layer blockage is non-dimensionalised with the tip clearance. This data was taken from measurements on an isolated rotor and it is interesting to note that it agrees well with the Smith data. The correlation is, of course, unsatisfactory for blades with no tip clearance gap (rotor roots and stator casing, for example).

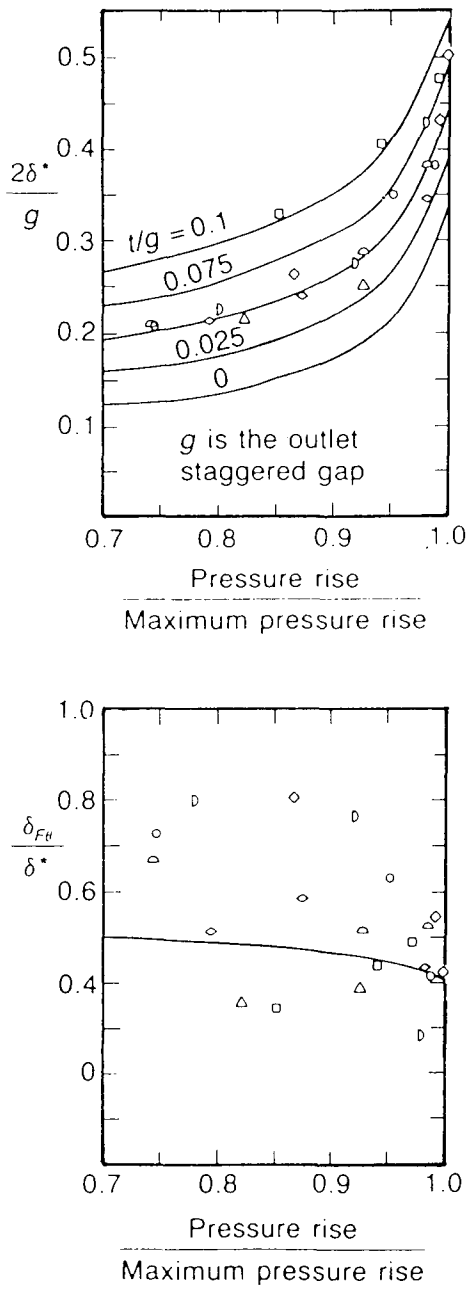

Figure 7: Endwall boundary layer blockage and tangential force deficit thickness correlation for hub and casing boundary layers, Koch and Smith (1976) as given by Cumpsty (1989).

Key: δ^* = displacement thickness
$\delta_{F\theta}$ = tangential force thickness
ψ = Pressure rise coefficent ($2\Delta p/\rho W^2$)
W = mean relative inlet velocity
t = tip clearance
g = blade staggered spacing

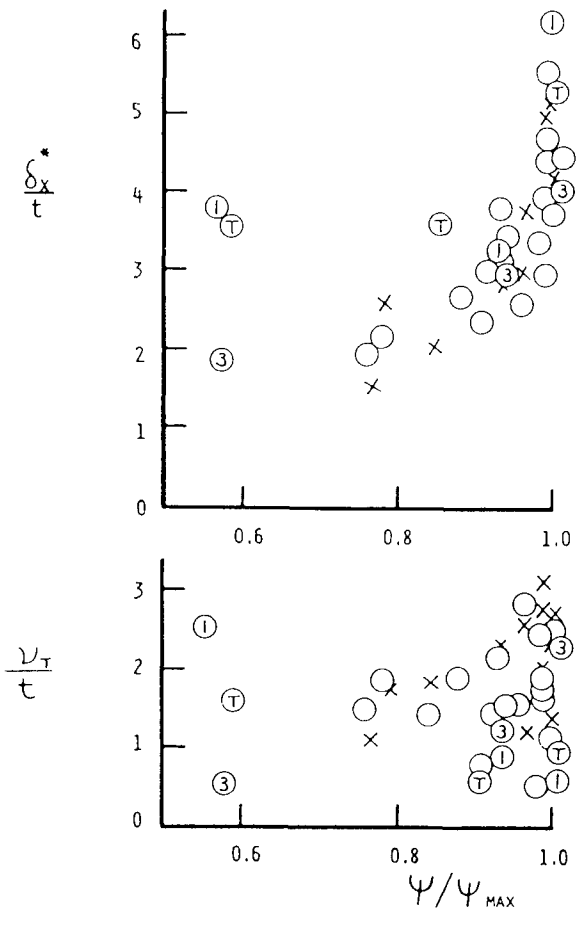

Figure 8: Endwall boundary layer blockage and tangential force deficit thickness correlation for rotor casing boundary layers, Hunter and Cumpsty (1982)

Key: δ^* = displacement thickness
υ = tangential force thickness
ψ = Pressure rise coefficent ($2\Delta p/\rho U_t^2$)
U_t = blade tip speed
t = tip clearance

The effect on stage efficiency due to the endwall blockage and the reduction in tangential blade force in the endwall boundary layer is then calculated by an equation given by Smith (1970) as:

$$\eta = \tilde{\eta}\frac{1-\frac{2\delta^*}{h}}{1-\frac{2v}{h}}$$

where $\tilde{\eta}$ is the stage efficiency without endwall boundary layers δ^* is the displacement thickness,υ is the tangential force thickness and h the annulus height.

The correlation of Freeman (1985), as given by Wright and Miller (1991), see figure 9, predicts directly the loss coefficient due to the endwall boundary layer losses. The endwall loss parameter is correlated as a function of the clearance to chord ratio and the blade loading (as expressed by the mean-line blade diffusion factor). The use of the Lieblein diffusion factor on the mean-line as the measure of endwall loading in this correlation is convenient for calculation purposes, but unlikely to be justified from the physics of the endwall flow. The value of the diffusion factor at which the endwall losses dramatically rise is a function of the clearance/chord ratio and is consistent with the maximum loading criterion also given by Freeman, see figure 11 and section 3.2.3 below.

Wright and Miller calculate the blockage of the endwall boundary layer using a separate annulus wall boundary layer prediction model with numerous empirical coefficents. It should be noted, however, that the equation above can be rederived in a form that allows the boundary layer blockage of the hub and casing boundary layers to be predicted directly from the endwall loss coefficient as follows:

$$\frac{2\delta^*}{h} = \frac{a}{(1-b+ba)}$$

where $a = \omega_r\left(\frac{W_r^2}{2\Delta H}\right) + \omega_s\left(\frac{C_s^2}{2\Delta H}\right)$, and

ΔH is the stage work input, ω_r is the rotor endwall loss coefficient, W_r the rotor inlet relative velocity, ω_s is the stator endwall loss coefficient, C_s the stator inlet velocity. $b = v/\delta^*$ is the ratio of the tangential force thickness to the displacement thickness of the endwall boundary layers, which can be estimated from figure 7, typically b = 0.5.

The contrast between these four different techniques highlights the very serious inadequacy of our current understanding of endwall boundary layer losses and blockage. About the only similarities between the various methods is the trend for an increase in blockage and losses with clearance level and as stall is approached. This increase in blockage and losses with loading towards stall is an important factor in the accurate prediction of stage characteristics which become flatter as stall is approached. The slope of these characteristics has a strong influence on the prediction of surge onset using stability theory (Moore and Greitzer (1986)).

It is interesting to note that although these methods have been derived primarily for use in preliminary design codes, they are usually the most accurate way of calculating endwall losses and blockage over the whole axial compressor design system! The review of endwall flows given by Cumpsty (1989) explains the many inadequacies of endwall boundary layer methods for the prediction of these features of the flow. None of the correlation methods available deals adequately with the problem of shrouded blade rows with a leakage flow over the shroud. A new synthesis of the best features of each of these methods is required, perhaps making use of improved understanding of endwall flows obtained from CFD computations.

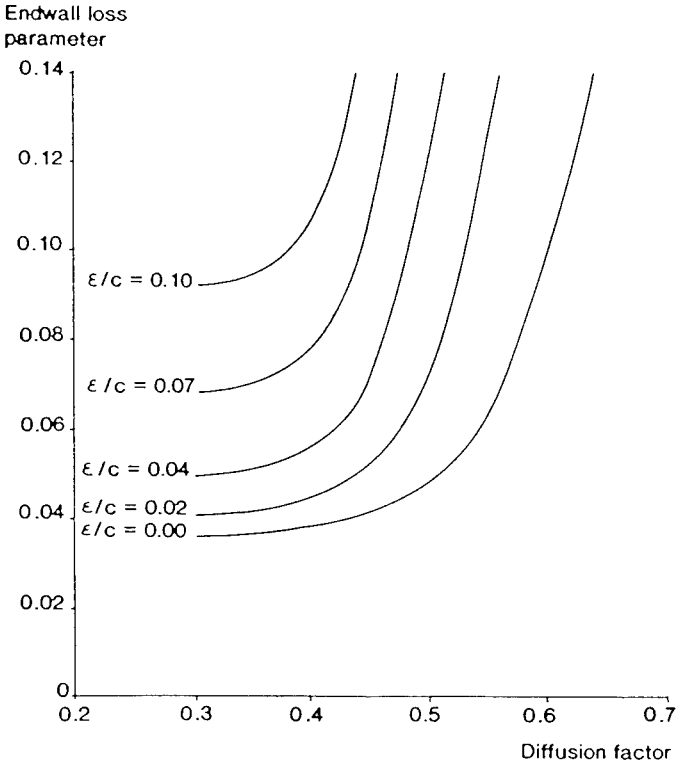

Figure 9: Endwall loss parameter as a function of loading based on work by Freeman (1986), as given by, Miller and Wright (1991)

Key: Endwall loss parameter = $\omega\frac{h}{c}\left(\frac{W_1}{W_2}\right)^2$

ω = endwall loss coefficient
ε = tip clearance
c = blade chord
h = blade span

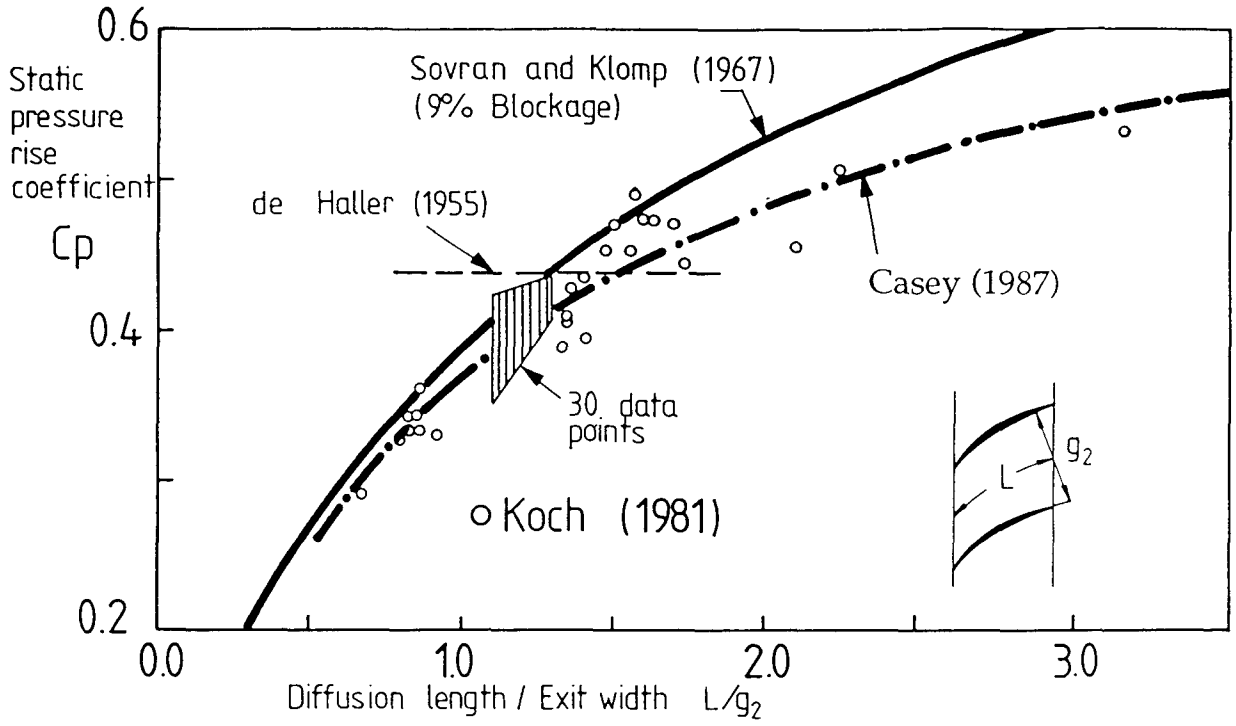

Figure 10: Correlation for the maximum stage pressure rise coefficient from a diffuser analogy, Koch (1981)

3.2.3 *Blade loading, stall and surge*

A reliable prediction method for the onset of stall, and the true functional dependence of stall on blade loading, have remained the most elusive aspects of axial compressor aerodynamics. There are several well-known candidates for the fluid dynamic mechanism of rotating stall inception:

(a) Separation of the blade profile boundary layers due to excessive incidence (as in stall of an isolated aerofoil).

(b) Separation of the blade profile boundary layers due to excessive diffusion along the blade suction surface (see Leiblein (1959)).

(c) Separation of the casing or hub boundary layers (de Haller (1955)).

Recent research has concentrated on the growth and separation of the endwall boundary layers as the central cause of rotating stall (Greitzer et al. (1979), Koch (1981), Schweitzer and Garberoglio (1984)). This is not a new idea. De Haller (1955) recognised that the endwall boundary layers limit the pressure rise acheivable by any cascade of compressor blades and suggested that

$$Cp_{max} = \Delta p / \left((1/2)\rho W^2\right) = 0.44$$

He wrote that "if we try to increase the diffusion above this limit, then the boundary layers on the sidewalls separate and no further pressure increase takes place", (author's translation).

Koch (1981) extended the idea of de Haller by correlating the maximum pressure rise coefficent with a geometrical parameter derived from classical diffuser studies (see Sovran and Klomp (1967)). The geometry parameter used by Koch is the arc length of the cambered airfoil divided by the cascade trailing edge staggered spacing, L/g_2, that is a length-to-outlet-width ratio, see figure 10. This is similar to the conventional type of correlation used for diffuser flows, except that the outlet width rather than the inlet width is used. The justification for using the outlet width instead of the more usual inlet width is that in a compressor cascade it is the exit flow area that remains roughly constant over the range of operation, while the effective flow area at inlet changes with the inlet flow angle. The stage average value of the L/g_2 ratio is calculated by using the bladerow inlet dynamic head of rotor and stator as the weighting factor. Corrections are applied for the effects of tip clearance, Reynolds number and the form of the inlet velocity triangle. Although there is considerable scatter between the actual presure rise achieved in multistage compressors and that predicted by the correlation of Koch, no compressors achieve more pressure rise than that predicted by this correlation. Because of this, Casey (1987) used lower values of the peak pressure rise coefficient for stall prediction in his mean-line method, as shown in figure 10.

Another correlation based on the diffuser analogy has been given by Schweitzer and Garberoglio (1984). The correlation offered by Freeman (1985) is rather simpler, giving the maximum diffusion factor of an axial blade row as a function of the stage tip clearance to chord ratio, see figure 11. Higher diffusion factors and blade loading can be achieved with low clearance levels. In the abscence of better correlations, the designer is advised to check each of these correlations during the preliminary design process to ensure that his design does not exceed the limits given by these authors. It should be noted that even when a good correlation for the stall of an isolated blade row is available, it is still difficult to predict the surge of a multistage machine from the individual stage characteristics (Moore and Greitzer (1986)).

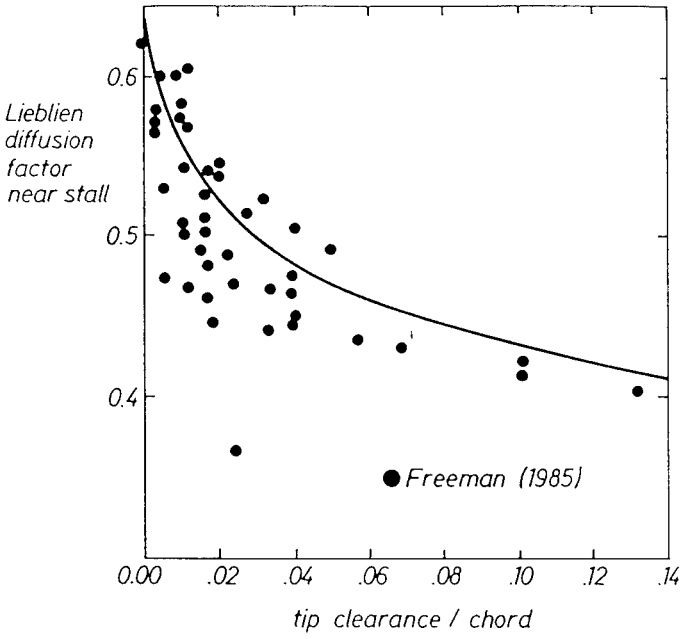

Figure 11: Correlation for maximum diffusion factor as a function of clearance / chord ratio, Freeman (1985).

3.2.4 *Accuracy of correlation techniques*

It is crucially important to realise that correlation techniques are limited in accuracy, especially for stage types not included in the data used to generate the correlations. An example of the accuracy of a such a correlation-based performance prediction method for axial compressor stages has been given by Casey and Hugentobler (1988), see figure 12. The efficiency is predicted to within ±2%, except for stages with poor measured efficiency. It should be noted that the level of agreement is good, but not excellent. Axial turbine mean-line prediction methods tend to be more accurate, see figure 13 from Tong and Gregory (1990).

3.3 Correlations for radial compressors

Unlike the case for axial stages, there are no generally accepted correlation techniques and there is no comprehensive body of literature giving standard forms of correlations for the loss, flow turning and blockage of radial compressor stages. Different authors use radically different approximations and techniques and all of the available methods appear to work well on the types of stage from which the correlations have been derived.

The two main problems in generating universally valid prediction methods for radial stages are our lack of understanding of the loss generating mechanisms (Denton (1993)), and the fact that the flowfield of radial impellers is highly three-dimensional and not easily amenable to physical description by the use of one-dimensional models. The technical literature gives the impression that there are as many different schools of radial compressor preliminary design as there are manufacturers and research institutes working on the subject. The publications of Herbert (1980), Japikse (1985), Van den Braembussche (1985), Cumpsty (1989), Whitfield (1989) and Whitfield and Baines (1990) are probably the best starting points for an examination of the most recent literature.

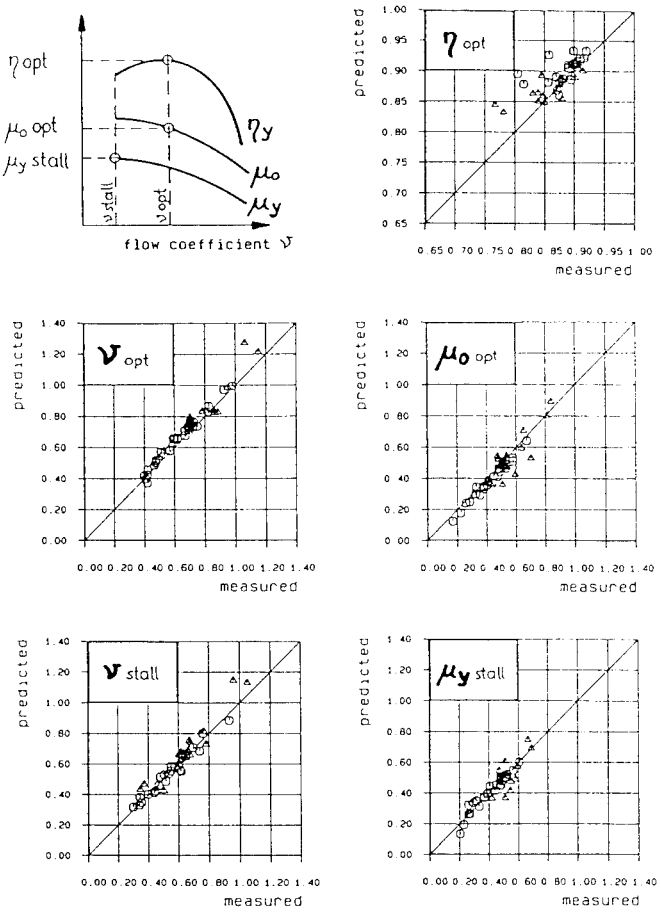

Figure 12: Accuracy of a multiradius method for axial compressor stage characteristic predictions, Casey and Hugentobler (1988).

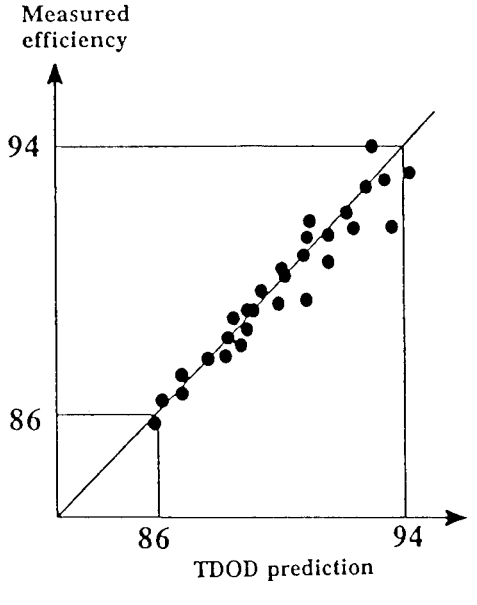

Figure 13: Accuracy of mean-line method for axial turbine efficiency predictions with TDOD (Turbine Design and Off Design code), Tong and Gregory (1990).

Because of the diversity of the methods available, it is not possible to recommend universally valid correlations and a review of the methods available would inevitably be quite patchy. Given the present state of the art, the most consistent and reliable techniques for radial stages are those based purely on a correlation of the measurement data available, using non-dimensional parameters that have been selected on the basis of dynamic and geometric similarity without too much attempt to understand the physics of the flow. To demonstrate this type of method, the outlines of an unpublished procedure developed by the author for the correlation of the performance of industrial compressor stages in this way is described briefly below.

The method is based on a separate analysis of the performance characteristics of the impeller and diffuser. Radial compressor performance tests, in which a measurement of the impeller outlet static pressure has been carried out, can be analysed to generate separate performance characteristics for the impeller and the diffuser and to specify the one-dimensional flowfield at the impeller outlet, see Dalbert et al. (1988). For industrial impellers it is common practice to make use of highly standardised components, such that similar diffuser geometries are used with a range of impellers. In the example presented here, the standard diffuser design uses 24 circular arc vanes of constant thickness and curvature, which may be staggered with variable blade inlet angle. The specification of the vane inlet angle and the diffuser width ratio b_2/D_2, is then sufficient to define the geometry of a wide number of standard diffusers.

This makes it possible to correlate the diffuser off-design performance purely in terms of the vane setting angle, the flow angle at inlet to the diffuser and the inlet Mach number to the diffuser. The impeller off-design characteristics can also be correlated in terms of the variation in the impeller inlet flow coefficient and the inlet Mach number, see figures 14 and 15. Note that these correlations define the shape of the performance characteristic relative to the peak efficiency point, such that separate correlations are needed to define the absolute efficiency and its location in terms of flow coefficient or flow angle. This can be done using correlations based on specific speed for the impeller performance or correlations based on two-dimensional diffuser charts or experience with similar diffusers for the diffuser. The stage performance characteristics for a new diffuser and impeller combination can then be estimated by simple one-dimensional mean-line calculations. In this mean-line procedure a reliable correlation for the slip factor (such as that given by Wiesner (1967)) is also needed to generate the impeller outlet velocity triangle.

Other forms of correlation for radial compressor impeller and diffuser characteristics may be more suitable for high pressure ratio impellers.

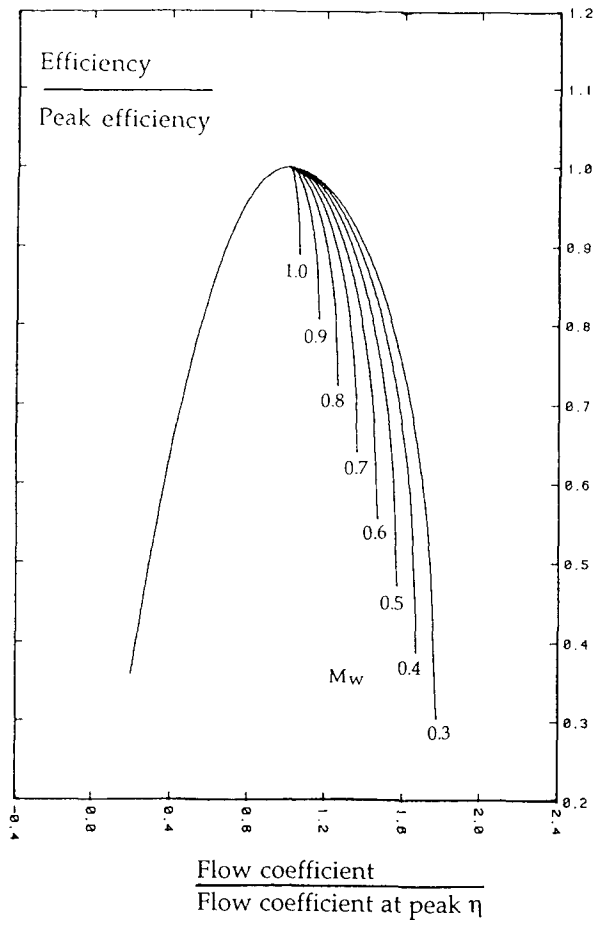

Figure 14: Correlation of measured impeller efficiency data for process radial impellers, (M_W is the inlet relative Mach number at the impeller eye)

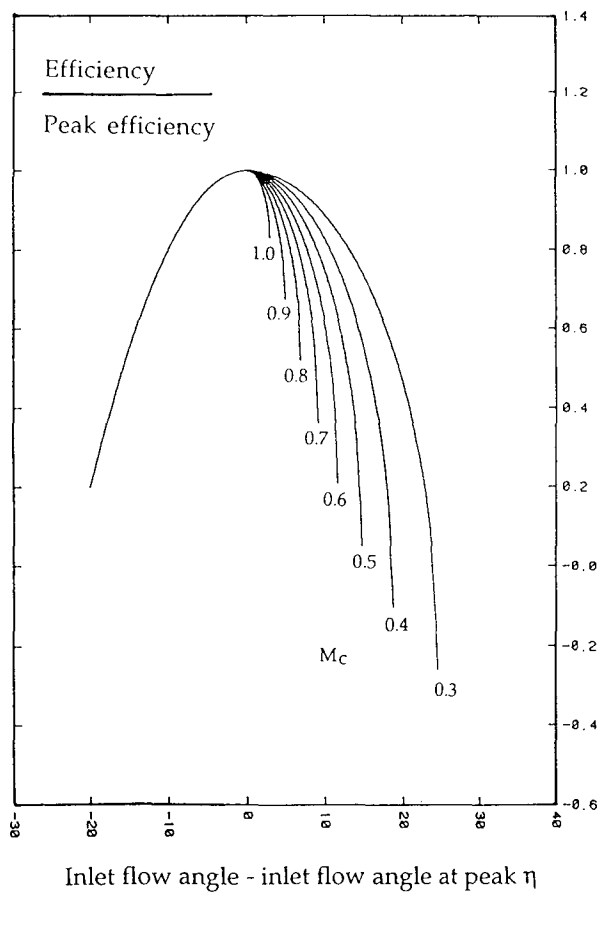

Figure 15: Correlation of measured efficiency data for standardised radial impeller diffusers, (M_C is the diffuser inlet Mach number)

4. STAGE STACKING OF AXIAL AND RADIAL COMPRESSORS

A "stage-stacking" procedure is a method of performance calculation in which the performance of the machine is calculated as the cumulative performance of the individual blade rows or stages. Calculation methods of this type were among the first successful methods available for the calculation of the overall performance of compressors (Robbins and Dugan (1956) and Stone (1958)), and are still under development for the preliminary design and analysis of modern aeroengine compressors (Howell and Calvert (1978) and Wright and Miller (1991)). Their use for design-point calculations of multi-stage compressors has been partly superceeded by more sophisticated methods which use meridional throughflow calculations combined with correlations for blade element performance and endwall losses (Hirsch and Denton (1981)).

For the calculation of the full performance map of compressors at a number of operating conditions simple stage-stacking methods have considerable advantages over throughflow methods:

(a) They are one-dimensional algebraic methods with relatively simple input data.

(b) Being one-dimensional they are very easy to understand, require low computational effort and their results are relatively easy to interpret.

(c) They work well even if individual blade rows are operating at extreme incidence with choke or stall conditions.

(d) They are particularly suitable for identifying problems associated with the mismatch of stage components at off-design operating points and for examining means of overcoming these problems by the use of variable geometry.

Stage-stacking calculations are faster by more than an order of magnitude than meridional throughflow calculations for multistage compressors. Typically the whole performance map of an axial compressor at several speeds or several guide vane settings can be calculated more quickly by stage-stacking than a single operating point using throughflow methods. This makes these types of calculation particularly useful for incorporation into more complicated simulation models for examining the off-design operation (start-up and shut-down) of industrial processes or gas turbines.

The two different ways of carrying out stage stacking calculations, on a stage-by-stage basis and on a row-by-row basis, are described below. The most important aspect of such calculations is a clear thermodynamic accounting procedure for taking into account the losses, blockage and turning, and in some cases the leakage flows, through the machine, Traupel (1977).

4.1 Stage-by-stage stacking calculations

Stage-by-stage stacking calculations are in regular use for industrial compressor performance prediction. Here the calculation proceeds from the inlet to the outlet of the compressor, and the performance of each successive stage determines the inlet conditions (P, T, and V) and the operating point of the next stage (in terms of flow coefficient, ϕ, impeller Mach number, Mu_2, efficiency, η_p, work input coefficient, $\mu_o=\Delta H/U^2$ and pressure rise coefficient $\mu_p=\eta_p\mu_o$). The performance of the machine is then determined by the cumulative performance of the individual stages.

The main requirement for accurate stage-stacking calculations is the availability of reliable one-dimensional characteristics for the individual stages. Industrial axial and radial compressors use standardised types of blading for all machines and suitable stage characteristics can be readily obtained from measurement on similar machines or in dedicated test stands. Stage characteristics can also be derived from theoretical models or correlations; for example, semi-empirical methods of generating suitable stage characteristics for subsonic industrial axial compressors have been given by Casey (1987) and by Casey and Hugentobler (1988). Such calculations can also be used in the design of transonic multistage compressors and fans to examine the effects of different types of stage matching at the design point on the part-speed performance of the machine, Calvert (1994).

Figure 16 provides an illustration of some of the interesting interactions that can occur between the performance of a multistage centrifugal compressor and the characteristics of its stages. In this somewhat idealised example, taken from Casey and Marty (1986), the performance of a five stage compressor using impellers of the same diameter and of the same family has been calculated. The effect of the Mach number on the stage characteristic has, for convenience, been neglected. Figure 16 shows the performance of the machine and the operating points of the individual stages for different inlet volume flows and rotational speeds. Each column of figure 16 represents a certain rotational speed and each row contains the following diagrams:

row A: pressure-volume (π - V) characteristic of the machine

row B: operating points of the individual stages on their efficiency - flow coefficient (η_p - ϕ) characteristic curves

row C: operating points of the stages on their pressure coefficient - flow coefficient (μ_p - ϕ) characteristics.

The diagrams in column 3 show the operating characteristics of the machine at its design speed (n = 100%). At the design point (∇) all of the stages operate at their best efficiency point - the stage efficiency and the pressure coefficient reduce towards the end stages because here the flow coefficients are low and the impellers are narrow. If we reduce the inlet volume flow below the design point then the first stage moves to the left along its characteristic and produces more pressure rise than at design. As a consequence, the second stage receives proportionately less volume than at its design point and lies further to the left on its own stage characteristic. This behaviour continues through all the stages. When the first stage has a certain minimum inlet volume, the last stage lies so far to the left of its characteristic that it reaches its limit of stability and the machine can go into surge ($\bullet$). With an increase in inlet volume, the first stage moves to the right along its characteristic. Each successive stage receives progressively more volume flow than at its design point. At a certain maximum inlet

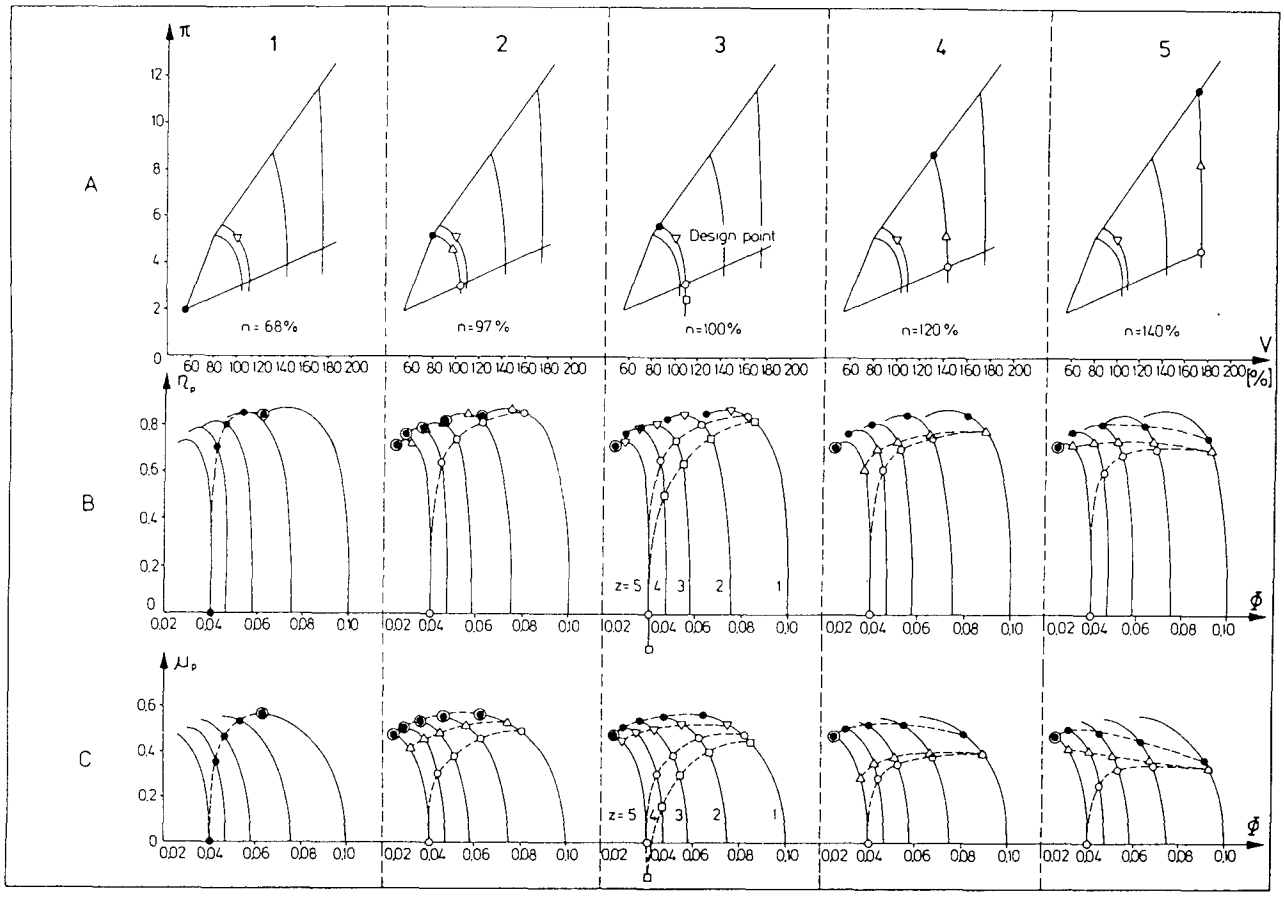

Figure 16: Stage-stacking calculations of a five-stage radial compressor, showing the operating points on the machine characteristic and the working points of the individual stages.

volume flow the last stage produces no pressure rise at all and operates at its choke point (o). Any further increase in inlet volume flow is impossible, although the machine can still operate at lower pressure ratios since the last stage can move into a region of expansion with an efficiency of less than zero (❑). Columns 4 and 5 show the operation of the machine at speeds above its design speed. With a moderate speed increase (n = 120%, column 4) the stages each produce more pressure ratio than at the design speed. A relatively small change in volume flow in the first stage is amplified by succeeding stages. The first stage can now only move a short way along its characteristic whilst the last stage moves all the way fom surge to choke. The machine characteristic becomes steeper than at the design speed. Column 5 shows that the machine characteristic would become even steeper at a speed of 140% of design, and that the first stage barely moves along its characteristic curve. This is only of academic interest, however, as the influence of the Mach number on the characteristic curves of the stages has not been taken into account, and the mechanical limit on the tip-speed is likely to have been exceeded! Stage stacking calculations of high Mach number compressors in which the first stage becomes choked, and therefore experiences no change in inlet flow volume, is best carried out from the last stage forwards.

Columns 1 and 2 show the performance at speeds less than design. Column 2 illustrates that at 97% of design speed all of the stages operate near their stability point when the machine surges. Below this speed the first stage becomes responsible for the surge of the machine, giving rise to the kink in the surge line on the machine characteristic. At much lower speeds a configuration occurs where the first stage operates at its stability point whilst the last stage is in choke (n = 68%, column 1).

This very simplified example highlights some of the important features of the design of multi-stage compressors, in particular the fact that at part-speed the first stages become responsible for the stability of the compressor and the last stages can operate close to choke. It shows clearly that exact stage characteristics for the individual stages are needed in order to avoid an accumulation of errors in the calculation. Some of the complications of real centrifugal machines that have not been included are:-

(a) Each stage is usually of a different type with different characteristic curves,

(b) The effect of the Mach number on the shape of the stage characteristic,which has been neglected here, can be quite large.

(c) The best efficiency point of each stage and the design point of the machine do not necessarily coincide. It may be worthwhile matching the stages at the design point with the front stages closer to choke and the rear stages closer to surge. An example demonstrating the benefits of this for a multi-stage axial compressor has been given by Cumpsty (1989).

(d) To improve the off-design performance some degree of variable geometry may be included (such

as inlet guide vanes, variable diffuser vanes, or variable stagger stator vanes). An example of a stage matching calculation of a constant speed industrial axial compressor with variable stagger stator vanes in all blade rows is given by Goede and Casey (1988).

In practice, stage-stacking methods are usually combined both with interpolation procedures for the characteristics of the individual stages, taking into account the change in the characteristic with Mach number, and with the appropriate real gas equations for the gas properties. This means that sophisticated software becomes essential.

4.2 Row-by-row stacking calculations

Row-by-row stacking calculations are widely used in the preliminary design of axial compressors for gas turbine applications. In methods of this type the blade row performance correlations, described in section 3.2, are combined with the continuity equation, the Euler turbine equation and with the gas equations to stack the performance of the individual blade rows along the mean-line of the compressor. The overall performance characteristics of the machine, as well as those of the individual stages, can be computed with methods of this type. As the rotors and stators are modelled individually it is possible to identify any axial mismatch between the stator and rotor blade rows, as well as between the individual stages.

Methods of this type allow the mismatch of stages at part-speed to be examined, so that the best compromise for the choice of design incidence can be made. Figure 17 shows an example of the type of presentation of results possible with this method. The working point of the mid-section of each rotor at each speed is displayed in the "alpha-Mach" number diagram. The tendency at part-speed for the first stage to move into stall and the last stage to move towards choke can be identified from this. To eliminate some of the difficulties caused by this, the first stage is matched closer to choke and the last stage closer to stall at the design point.

During the preliminary design of an axial compressor methods of this type are used to predict the performance characteristics of the different geometrical options. Typical details that will be examined with these methods are:

(a) The relative advantages of a rising hub-line design compared with a constant hub-line.

(b) The choice of aspect ratio of the stages and the number of stages. For example, for a given length of the compressor, the effect of using more stages of high aspect ratio compared with fewer stages of lower aspect ratio could be examined.

(c) The choice of swirl distribution through the compressor. For example, the use of an inlet guide vane for the first rotor row, leading to low reaction and lower rotor inlet Mach numbers in the front stages, could be compared to a design without an inlet guide vane.

(d) The distribution of the blade loading through the compressor could be examined and the preliminary selection of the number of blades could be made. The number of blades selected would be only tentative at this stage, because of feedback from mechanical design.

(e) The need for variable geometry. For example, how many stages with variable stagger stator vanes are needed to achieve the part-speed surge margin requirements.

In general, the engineer will examine by trial and error those design options which he feels from experience are of most interest until he believes he has got the best solution for the particular application. The success of huge investments in new turbomachinery configurations often depends on the effectiveness of this process. Since there are a large number of possible alterations the examination of the options may take some considerable time. The use of design charts and numerical optimisation techniques make it possible to shorten this process, see below.

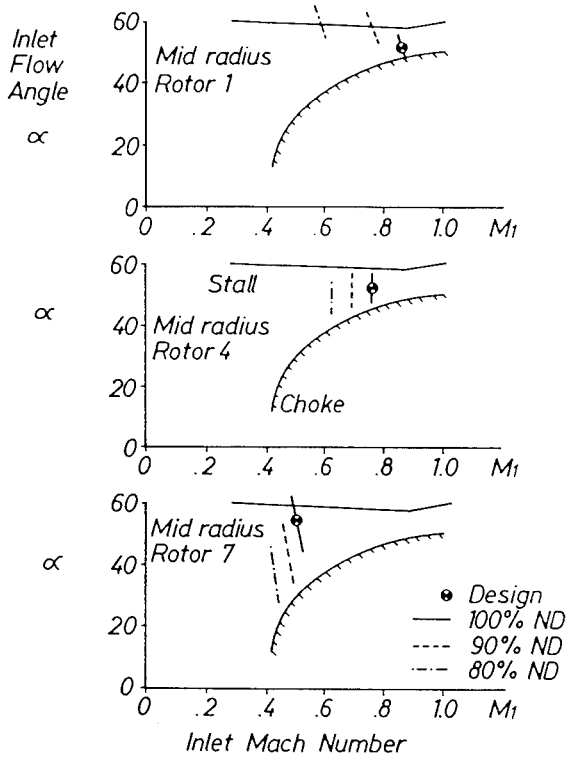

Figure 17: Operating points of the first, fourth and last stages of a 7 stage axial compressor plotted in the rotor "alpha-Mach" number diagrams.

5. OPTIMISATION TECHNIQUES FOR PRELIMINARY DESIGN

5.1 Design charts

The most effective design charts for use in the preliminary design process are those that allow the engineer to rapidly identify designs that are unacceptable or provide guidance on the route towards the optimum design. With the aid of such simple tools the designer can reduce to manageable proportions the number and range of design parameters that must be examined during the preliminary design. Three examples taken from the recent design experience of the author are given below.

5.1.1 *Radial impeller inlet blade angle*

The choice of the best blade angle for the inlet eye of a radial impeller with an axial inducer-type inlet could be considered to be a difficult optimisation problem and its solution by means of trial and error calculations with a 3D CFD method would require considerable computational effort. Fortunately, there is a simple one-dimensional analysis that can be carried out to minimise the relative inlet Mach number of the impeller for a given mass flow. This was first published by Shepherd (1956) but has been subsequently republished in a different form by many authors. A low inlet Mach number is a good thing since it leads to low shock losses, low friction losses and reduces the level of diffusion in the impeller.

Figure 18 plots the mass flow function at the inlet of an impeller with axial flow as a function of the inlet absolute Mach number for a range of relative inlet Mach numbers and flow inlet angles. It can be seen that an inlet flow angle close to 30° gives the largest mass flow function and that the optimum is relatively flat. There is clearly no need for an impeller designer to spend a long time deliberating over the best choice of inlet flow angle.

It is worthwhile noting that a similar analysis for the optimum flow angle at the inlet to a pump can be carried out, based on eliminating cavitation by maximising the static pressure in the suction peak at the impeller leading edge, see Pfleiderer (1957). This leads to optimum inlet angles that are much lower than in compressors, typically around 15°. Clearly it is important for the designer to know what needs to be optimised in the design process.

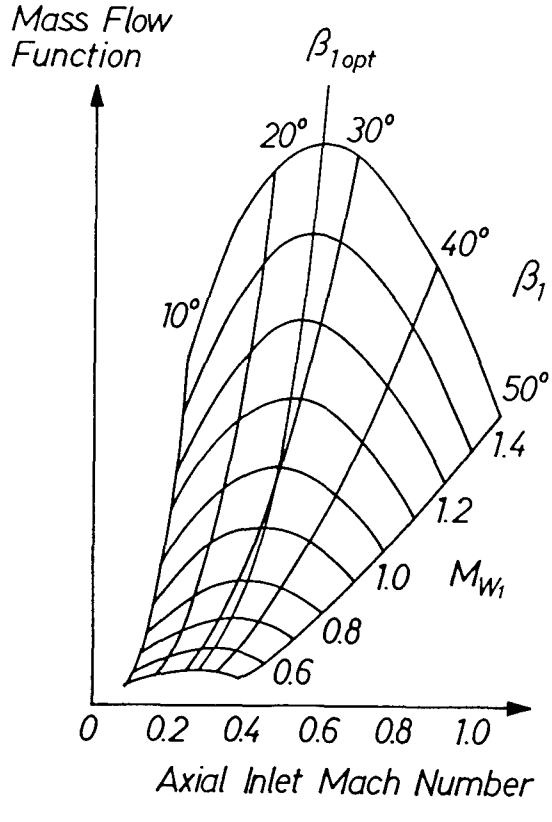

Figure 18: Mass flow function at the inducer inlet of a radial impeller.

5.1.2 *De Haller number in radial impellers*

Figures 19 and 20 show carpet plots of the relationship betwen the velocity components at the inlet and outlet of a radial impeller, for a range of flow angles. The ordinate and abscissa of both plots are logarithmic and to the same scale. In figure 19 the ordinate is the meridional inlet velocity and the abscissa is the inlet relative velocity made non-dimensional with the impeller tip speed. In figure 20 the ordinate and abscissa are the outlet meridional velocity and the outlet relative velocity.

Transparent copies of the two charts placed over each other in different orientations allow the effect of impeller meridional velocity ratio and relative velocity ratio (de Haller number) to be examined. For example, by moving the two charts relative to each other in a vertical plane or in a horizontal plane the relationship of the inlet and outlet velocity triangles of a range of impellers designed for different meridional velocity ratios and de Haller numbers can be examined. The inlet and outlet velocity triangles of an impeller can be marked by points on the charts and by placing these points above each other the meridional velocity ratio and de Haller number may be determined from the relative position of the axes.

These charts were developed by the author during the preliminary design of the low specific speed impellers reported by Casey et al. (1990). They allowed a rapid assessment of the use of high backsweep combined with low outlet meridional velocity for the design of low flow coefficient impellers with wide flow channels and high work coefficients. In such impellers the use of more backsweep can lead to a higher pressure rise !

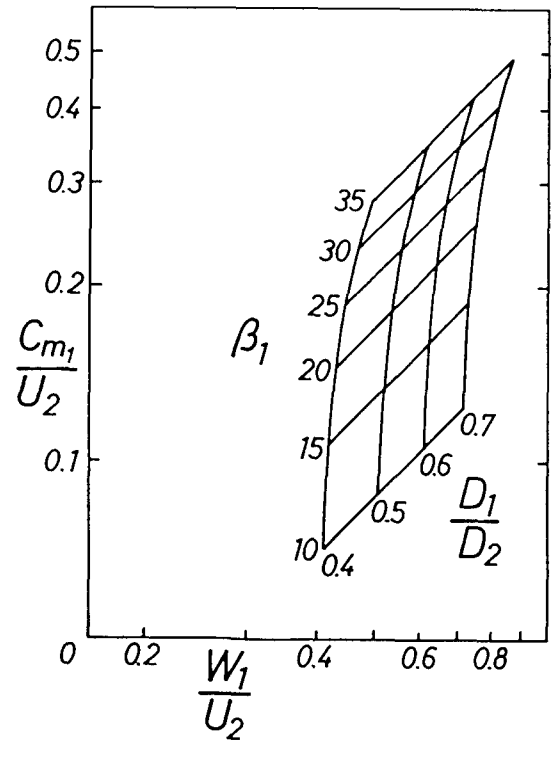

Figure 19: Carpet plot of velocity components in the impeller inlet velocity triangles for different inlet radii and inlet relative flow angles.

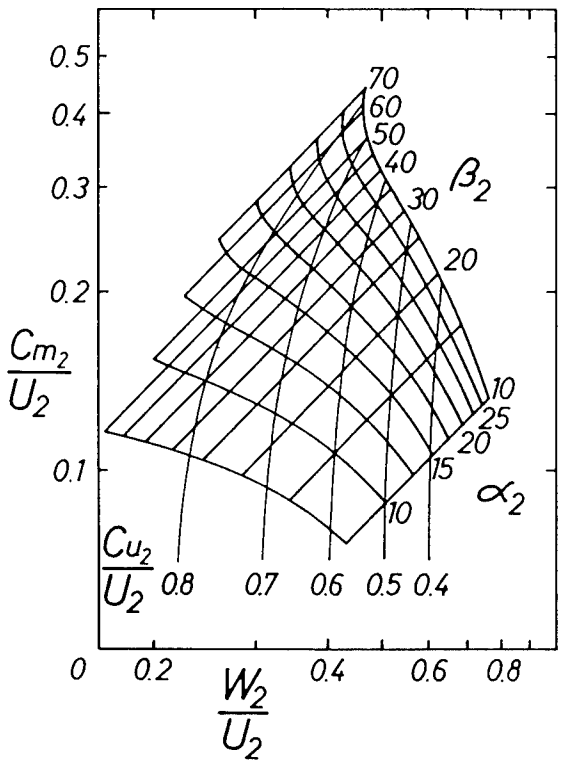

Figure 20: Carpet plot of velocity components in the impeller outlet velocity triangles for a range of relative and absolute flow angles.

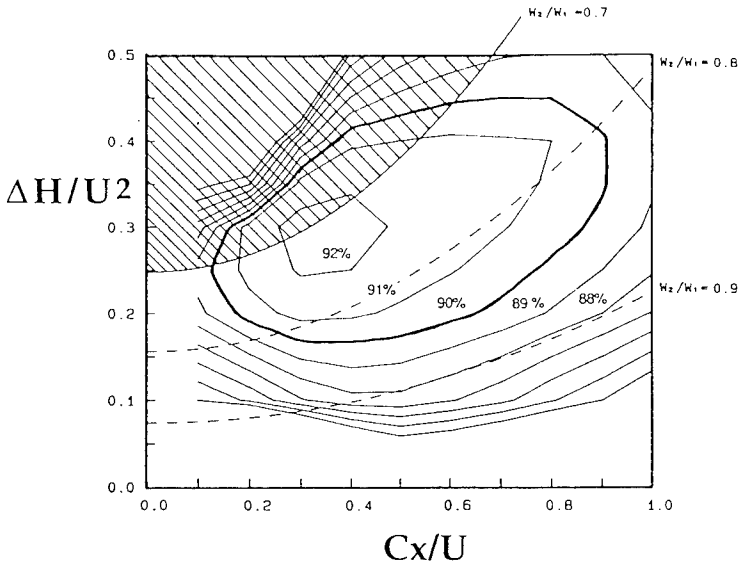

Figure 21: Smith diagram for an axial compressor stage

5.1.3 *Smith diagrams*

Design charts showing efficiency contours for a range of flow coefficients and work input coefficients, based on that for turbines first given by Smith (1965), have proved very useful for rapid design guidance in the search for optimum axial stages. The original Smith diagram was based on an analysis of measurement data, but the use of mean-line correlations allows such charts to be generated by computer.

An example of a Smith diagram for an axial compressor stage with a degree of reaction of 0.7 is given in figure 21, whereby values of the de Haller number have also been superimposed on the chart. This was generated during the design of a new middle stage for industrial axial compressors using the correlations and one-dimensional mean-line method described by Casey (1987). It should be noted that the curves given here are for fixed values of the rotor and stator space/chord ratio whereas in some other applications it would be appropriate to alter the space chord ratio with the loading level. The curves show a clear design point for peak efficiency and a drop in efficiency in all directions from this peak. The efficiency drops as the loading is increased because the increase in losses caused by a low de Haller number outweighs the additional work input.

5.2 Numerical optimisation

Given the power of computers to carry out large numbers of repetitive calculations, it is tempting to enlist the help of numerical optimisation techniques for the preliminary design process. These offer the promise of eliminating many of the tedious iterative trial-and-error calculations and replacing them with a systematic search of the design space for an optimum design. Several examples of such attempts to do this for a range of turbomachinery preliminary designs have already appeared in the recent turbomachinery literature, see, for example, Macchi (1985) and Tong and Gregory (1990) for axial turbines, Hearsey (1989) and Holt and Bassler (1991) for axial compressors and Russo et al. (1987) for radial compressors.

Many different numerical techniques exist for obtaining the optimum of a mathematically continuous multi-variable function. The majority use a form of hill-climbing in which the gradient of the function needs to be calculated to determine a search direction towards the optimum. This can be highly inefficient because the necessary derivatives are not usually directly available in turbomachinery simulation codes and need to be determined by finite difference techniques. There is also a risk that such methods search for a local optimum and do not find the true hill-top.

Recent work by Tong and Gregory (1990) has combined rule-based expert systems with genetic algorithms in an attempt to overcome these problems. Rule-based expert systems try to model the way an engineer would operate in order to eliminate designs that are not of interest. Genetic algorithms provide a systematic way of varying multiple parameters to avoid constraints or local optima. The method approximates the process of evolution in that the values of design parameters are considered as genes. A new population is generated by mutation and evolves further or becomes extinct according to its fitness, measured against a clearly defined performance measure. The gene pool can be seeded with previous good design solutions in order to reduce the computational effort.

The author is of the opinion that, for compressor preliminary design, the performance prediction methods available are not sufficiently accurate to justify the use of numerical optimisation methods. In most compressor designs it is the attainment of adequate surge margin

which determines the final design solution and our methods for prediction of surge margin are too weak for numerical optimisation to be worthwhile. The real advantage of such numerical optimisation methods is that they might point to a solution that is radically different from those previously attempted. In such cases it is likely that the correlations in use would be either outside their range of validity or constrained at the limit of their validity. This would point to the need for a critical examination of the correlations and to the need for new measurements and theory to develop them.

The example given by Tong and Gregory (1990) demonstrates this very clearly. The design of a five-stage turbine suggested by the genetic algorithm required a high value of the outer casing wall slope in the earlier stages. This was outside of the range of previous experience, but allowed the tip diameter to increase rapidly and increased the efficiency of the downstream stages.

6. GEOMETRY DEFINITION

The preliminary design process provides an initial definition of the skeletal geometry of the blading and the annulus of the turbomachine. Turbomachinery design systems are then generally based on design by analysis, whereby the blading is assessed using CFD codes and iteratively refined. During the detailed design stage the designer repeatedly adjusts the shape of the blades and flow channels until he finds a suitable geometry that combines acceptable aerodynamic performance with low stress levels and is practical and economic to manufacture. This process of continual refinement of the shape can be expensive, tedious and time consuming, since at each stage the geometrical data for the necessary aerodynamic or stress analysis must be prepared. The task is greatly simplified when a simple flexible system of geometry definition for the annulus and blading components is available. The availability of a numerical geometry definition system with appropriate interfaces also aids the transfer of data from the aerodynamicist for stress analysis and manufacture.

Traditional methods of geometry definition for turbomachinery blading involved either curve-fitting through a series of points or the use of more general polynomial expressions for the blade shapes. Curve-fitting through arrays of discrete points is fraught with problems for turbomachinery blading because of the need to model the large changes in curvature and blade surface orientation near to the leading edge. This results in inevitable oscillations in the curves that are generated. Many design systems overcome this leading edge problem by splitting the blade into four parts, whereby the leading and trailing edges are modelled as separate circular arcs or ellipses and the suction and pressure surfaces are modelled as a string of data points through which a suitable curve is fitted.

A very useful technique to obviate the need for a large number of data points to define the surface is to use a smaller number of points which are joined by piecewise continuous segments, see for example Ginder and Calvert (1987). Instead of one continuous polynomial through all the points, the points are joined by polynomials of lower degree (say, cubic curves) with no change in curvature or slope at the junction of the segments. In the design of turbomachinery blading it is often the case that the designer has a more direct relationship with the values of the blade angles than the actual blade cartesian coordinates. Because of this, most design systems are based on a definition of the blade camber line as a series of camber angles that are automatically integrated within the design system to produce the coordinates. The blade angles may be specified at a series of points and interpolated by appropriate methods.

The trend in blading geometry definition methods is to make use of techniques that have been developed for the computer-aided modelling of 3D objects, see Farin (1991). Two particular techniques have found wide application in turbomachinery - the Bezier curve and the non-uniform rational B-spline (NURBS) curve, see, for example, Smith and Merryweather (1973), Engeli et al (1978), Casey (1983) and Grein et al. (1989). Both of these techniques allow the complicated three-dimensional surface of a turbomachinery blade to be represented by a parametric surface, in which each point on the surface is associated with two parameters which range from zero to some integer. A particular pair of values of these parameters uniquely identifies any point on the actual surface.

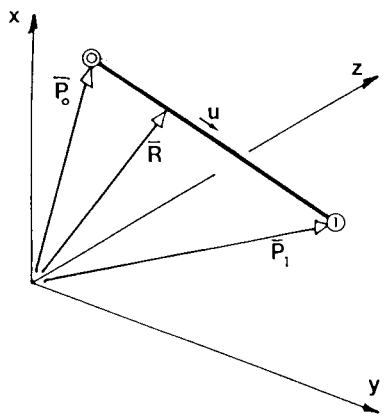

Figure 22: Bezier curve of order 1

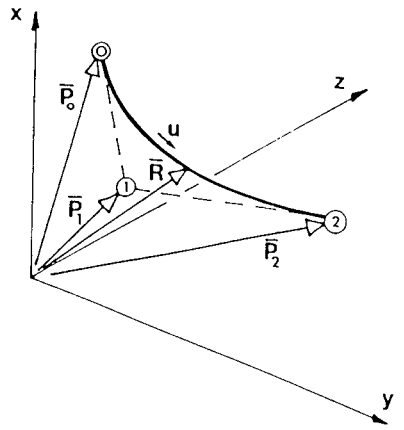

Figure 23: Bezier curve of order 2

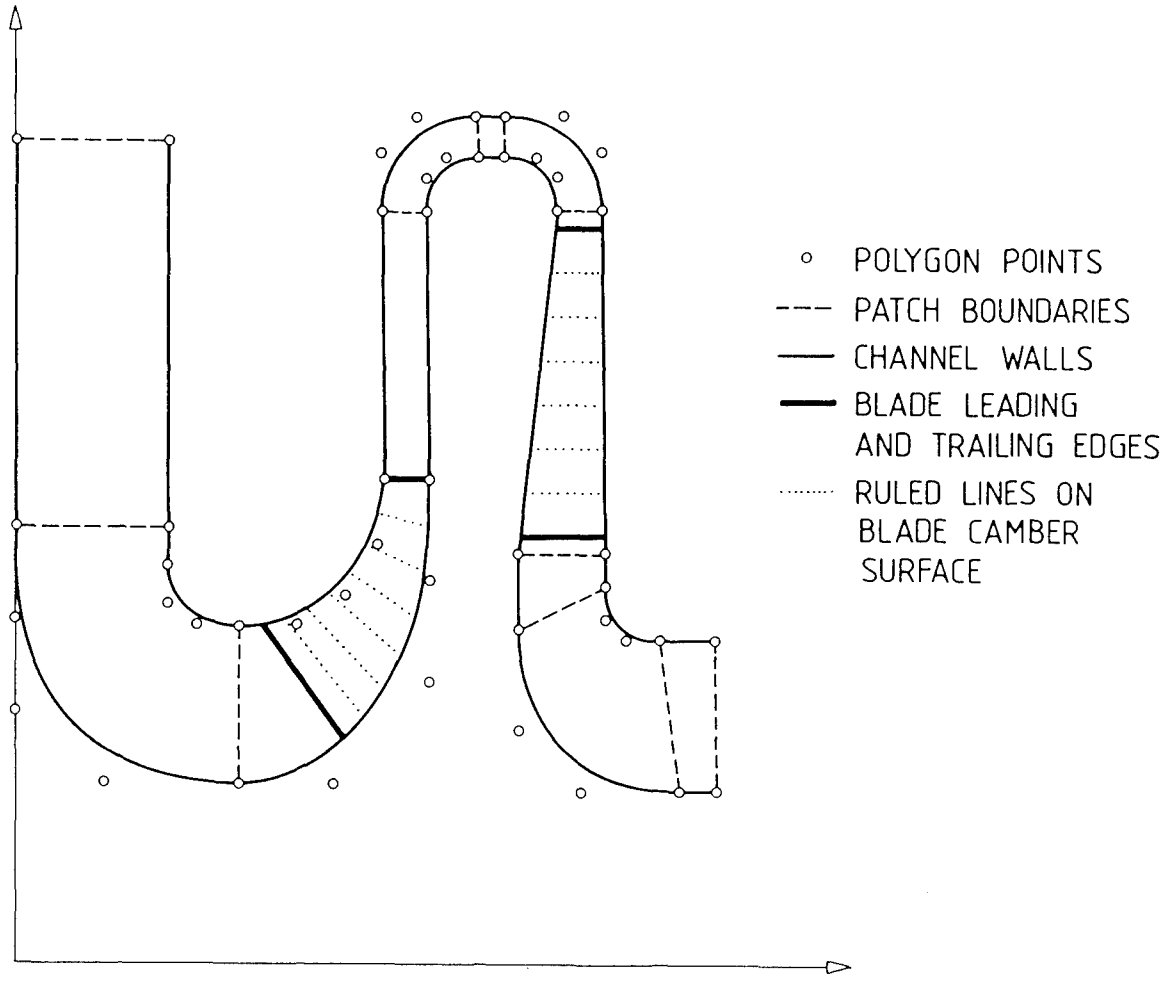

Figure 24: Radial compressor annulus defined by Bezier curves, Casey (1985)

6.1 Bezier surface

A Bezier curve is a parametric representation of a space curve. The curve is specified by the coordinates of a series of points in space of which only the first and last lie on the curve they define. The points are known as the polygon points of the curve and the figure constructed by joining these polygon points with straight lines is known as the Bezier polygon of the curve.

The simplest example is a straight line, see figure 22, defined as a Bezier curve of order 1:

$$\overline{R} = (1-u)\overline{P_0} + u\overline{P_1}$$

where R is a vector of a point on the curve and P_0 and P_1 are the vectors of the polygon points (in this case also end points) of the Bezier polygon. The parameter u is constrained to vary from 0 to 1 along the curve, and for values of u between 0 and 1 the vector R describes a straight line from point P_0 to P_1. The Bezier curve of order 2 is defined by three polygon points and can be written as:

$$\overline{R} = (1-u)^2\overline{P_0} + 2u(1-u)\overline{P_1} + u^2\overline{P_2}$$

From the example given in figure 25, it can be seen that the second polygon point does not lie on the curve but that the tangents to the curve at the end points are in the direction of this point. The Bezier curve of order 3 requires four polygon points to define it and can be written as

$$\overline{R} = (1-u)^3\overline{P_0} + 3u(1-u)^2\overline{P_1} + 3u^2(1-u)\overline{P_2} + u^3\overline{P_3}$$

From the form of these equations it can be seen that the Bezier curve is in some sense the weighted average of the polygon points defining the curve. It always goes through the first and the last points of the polygon and the direction of the start of the curve is the same as that of the line joining the first two points. The weighting functions are the Bernstein polynomials, defined as follows:

$$B_k^n(u) = \left(\tfrac{n}{k}\right)u^k(1-u)^{n-k}$$

so that the general form of the Bezier polynomial of order n requires n+1 polygon points and is given by

$$\overline{R} = \sum_{k=0}^{n} \overline{P}_k B_k^n(u)$$

These equations give the designer the ability to define a smooth curve for the annulus shape in a radial compressor, and to interactively adjust the shape by changing the position of the points. More complicated curves can be generated either by increasing the degree of the polynomial or by forming a series of individual Bezier curves. Which route offers the most flexibility depends on the application. In radial compressor

applications the use of a string of curves to define the different elements of the blading is very effective, see figure 24 from Casey (1985). In turbine profile design, both surfaces of the blade can be defined by a single curve, as shown in figure 25 from Engeli et al. (1978).

The Bezier curve can also be generalised to form a Bezier surface. The simplest example, often used to define the surface of a radial compressor vane, can be defined by a series of straight lines joining points of constant u of two adjacent Bezier curves. A second parameter, v, can be introduced which varies from 0 to 1 as one proceeds along the straight lines between these curves. Thus any point on the surface can be referred to by the values of its parametric coordinates (u,v). The three dimensional surface (x,y,z) is mapped onto a two dimensional plane by the equations. Separate Bezier surfaces can be defined for the suction surface, the pressure surface and the camber surface of the vane, as shown in figure 26.

It is of course also possible to increase the degree of the Bezier polynomial in the spanwise direction to generate arbitrary three-dimensional curved surfaces. In axial turbomachinery applications it is often the case that the individual spanwise blade sections are defined on streamsurfaces of a throughflow calculation by blade-to-blade methods. In this case it is worthwhile defining the three dimensional surface as a series of patches in the spanwise direction. Experience has shown that for axial compressor blading a parabolic variation of the shape in the spanwise direction is adequate.

6.2 Non-uniform rational B-splines (NURBS)

The Bezier curves described above have two slight drawbacks in some turbomachinery situations. Firstly, for each segment of a Bezier curve a change in the position of a single point can lead to changes in the whole curve. Secondly if the whole surface is defined as a single patch then it may require a very high order polynomial with a large increase in the computational overhead. The B-spline form of curve definition overcomes these problems at the expense of being less simple than the Bezier curve. The B-spline formulation contains the Bezier curve as a special case.

The essential difference between a B-spline and Bezier curve is that the order of the curve and the number of polygon points are independent. The interpolating functions which form the curve from the weighted average of the polygon points act on only a few adjacent polygon points. The interpolating functions are of relatively low order, typically three or four, and are non-zero over only part of the total range of the curve. There are the same number of basis interpolating functions as there are polygon points, but each one is non-zero over a different range of segments. Because of this, the shift of a single polygon point only affects the curve in its immediate neighbourhood. In addition, very complex curves can be defined with many polygon points, whilst retaining the computational speed of relatively simple low order interpolating functions. For further details, the recent literature on the topic should be consulted, Farin (1991).

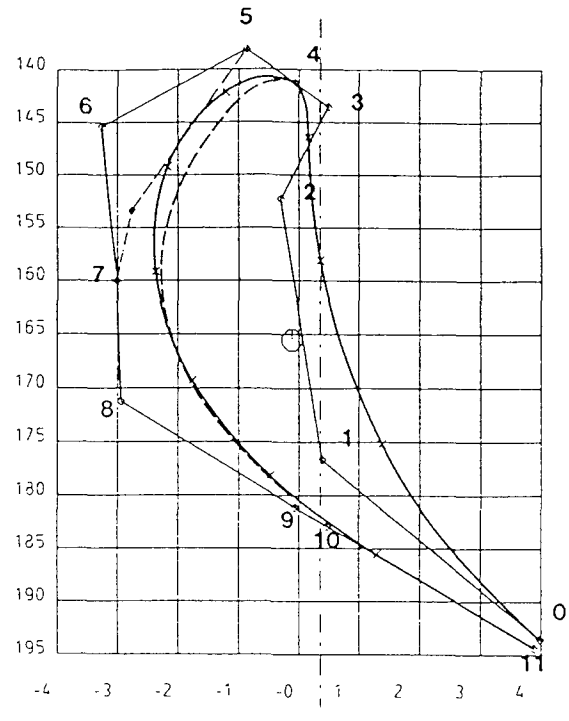

Figure 25: Turbine blade profile with each surface defined by a single Bezier curve, showing the effect of moving point 6, Engeli et al. (1978)

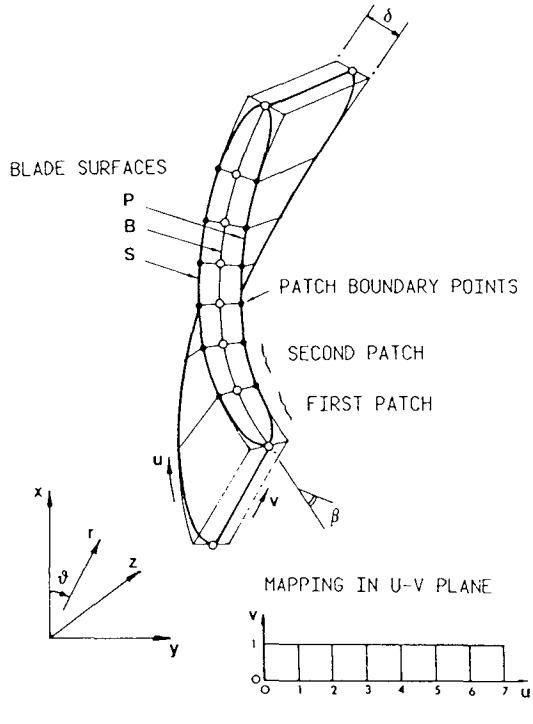

Figure 26: Bezier surfaces to define an impeller vane (suction surface (S), Pressure surface (P) and camber surface (B)).

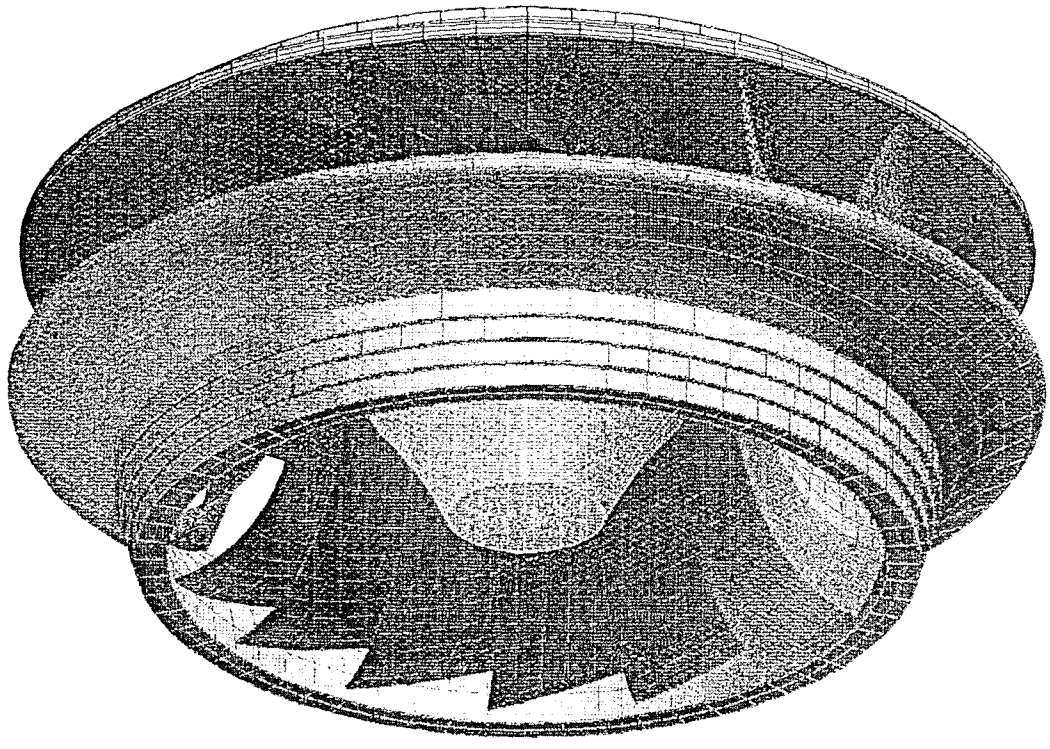

Figure 28: Francis turbine defined entirely by B-spline surfaces (Grein et al. (1989))

An example of a turbomachine geometry (a Francis turbine taken from Grein et al. (1989)) in which the total geometry comprising blades, shroud and hub has been defined by B-splines is shown in figure 29.

7. CLOSING REMARKS

This review has emphasised the crucial importance of the preliminary design process in the attainment of performance objectives for turbomachinery designs. Despite the pedestrian simplicity of the one-dimensional methods used, the preliminary design process determines within quite a narrow range the ultimate performance potential of a turbomachine. No other design phase can yield so much performance improvement with so little effort.

It is clear from the review that the status of correlations for many difficult aspects of turbomachinery flows is very inadequate. New correlations with a more physical basis are needed, especially for radial machines and for aspects of endwall flows in axial machines. In the near future CFD computations should be able to provide the basis for improvements of the correlations. It would probably be worthwhile diverting some of the enormous effort being expended on CFD validation to this end.

The use of numerical optimisation techniques combined with mean-line prediction methods is in its infancy. It is likely to become more important in the future when more accurate mean-line correlation techniques are available. Numerical geometry definition methods are also likely to become more important with the increasing use of local workstations and the trend to visualisation of the geometry and the flowfield results.

8. ACKNOWLEDGEMENT

This author is indebted to Mr. H Bantli of Sulzer Escher Wyss for information regarding B-splines, and Mr. P Wright of Rolls-Royce plc for his constructive comments on an early draft of this paper.

9. REFERENCES

Balje. O. E., 1981, *Turbomachines, a guide to design selection and theory,* Wiley.

Birdi, K., 1992, Short course on radial compressors, Lecture notes, Cranfield Institute of Technology.

Calvert, W. J., 1994, private communication.

Carter, A. D. S., 1950, "The low-speed performance of related aerofoils in cascade", Aeornautical Research Council CP29.

Casey, M. V., 1983, "A computational geometry for the blades and internal flow channels of centrifugal compressors", Trans. ASME Jnl. of Eng. for Power, Vol 105, No. 2, pp 288-295.

Casey, M. V., 1985, "The aerodynamic development of high performance radial compressor stages for industrial turbocompressors", VDI Bericht No. 572.1, *Thermische Strömungsmaschinen '85*, pp 167-181.

Casey, M. V., 1987, " A mean-line prediction method for estimating the performance characteristic of an axial compressor stage", Paper C264/87, I. Mech. E. Conference 1987-6, *Turbomachinery - Efficiency Prediction and Improvement*, Cambridge.

Casey, M. V., 1994, "The industrial use of CFD in the design of turbomachinery", AGARD Lecture series PEP LS 195, *Turbomachinery design using CFD.*

Casey, M. V., Dalbert, P., and Schurter, E., 1990, "Radial compressor stages for low flow coefficients", I. Mech. E. Fourth European Congress on *Fluid machinery for the oil, petrochemical and related industries*, The Hague, Netherlands, May 21-23, Paper C403/004.

Casey, M. V., and Hugentobler, O., 1988, "The prediction of the performance of an axial compressor stage with variable stator vane stagger angles", VDI Conference, *Thermische Strömungsmaschinen: TURBOKOMPRESSOREN im industriellen Einsatz*, 8/9 November, Essen.

Casey, M. V., and Marty, F., 1986, "Centrifugal compressors - performance at design and off-design", Proc. Institute of Refrigeration, 1985-1986. 5-1.

Cetin, M., Ucer, A. S., Hirsch, Ch., and Serovy, G. K., 1987, "Application of modified loss and deviation correlations to transonic axial compressors", AGARD Report, R-745.

Cumpsty, N. A., 1989, *Compressor aerodynamics*, Longman.

Dalbert, P., Casey, M. V., and Schurter E., 1988, "Development, testing and performance prediction of radial compressor stages for multistage industrial applications", Trans, ASME Journal of Turbomachinery, Vol. 110, No. 2, pp 283-292

Dawes, W. N., 1988, "Development of a 3D Navier-Stokes solver for application to all types of turbomachinery, ASME paper 88-GT-70.

de Haller, P., 1955, "Das Verhalten von Tragflügelgittern in Axialverdichtern und im Windkanal", VDI-Berichte, Band 3, pp 27- 31.

Denton, J. D., 1993,"Loss Mechanisms in Turbomachines", ASME Jnl of Turbomachinery, Vol. 115, October 1993, pp 621-656.

Engeli, Zollinger, Alleman, 1978, "A computer program for the design of torbomachinery blades", ASME paper 78-GT-36.

Farin, G., 1991, *Curves and surfaces for computer aided geometric design,* 3rd ed., Academic press

Freeman, C., 1985, "Effect of tip clearance flow on compressor stability and engine performance", VKI Symposium *Tip clearance effects in axial turbomachines*, Brussels.

Ginder, R. B., and Calvert, 1987, "The design of an advanced civil fan rotor", ASME Jnl. of Turbomachinery, Vol. 109, pp340-345

Göde, E. and Casey, M.V.,1988, "Stage matching in multi-stage industrial axial compressors with variable stator vane stagger angles", VDI Conference, *Thermische Strömungsmaschinen: TURBOKOMPRESSOREN in industriellem Einsatz*, Essen.

Grein, H., Scheebeli, F., and Bantli, H, 1989, "Die Modellierung dreidimensionaler Flächen, ein Werkzeug für Entwicklung und Fertigung hydraulischer Maschinen", Technischer Runschau Sulzer, Vol. 2.

Greitzer, E. M., Nikkanen, J. P., et al., 1979, " A Fundamental Criterion for the Application of Rotor Casing Treatment," ASME Journal of Engineering for Power, Vol. 101, June, pp. 237-243.

Gyarmathy, G., 1990, "An introduction to the fluid dynamic design of axial-flow turbines", IGTI course on *Fluid Dynamics of Turbomachinery*, Ames, Iowa, August 1990.

Hearsey, R. M., 1989, "Numerical optimisation of axial compressor designs", ASME paper 89-GT-14.

Herbert, M. V., 1980, "A method of centrifugal compressor performance prediction", ASME publication *Performance prediction of centrifugal pumps and compressors*, ASME gas turbine conference, New Orleans, pp 171-189.

Hirsch, Ch., and Denton, J. D., eds., 1981, "Throughflow calculations in axial turbomachines, Agard Advisory Report AGARD-AR-175.

Holt, G., and Bassler, S., 1991, "Preliminary design of axial compressors using artificial intelligence and numerical optimisation techniques", ASME paper 91-GT-334.

Howell, A. R., and Calvert, W. J., 1978, "A new stage-stacking technique for axial-flow compressor performance prediction", Trans. ASME, Jnl. Eng. for Power, Vol. 100, No. 3., pp 698-703.

Hunter, I. H., and Cumpsty, N. A., 1982 , "Casing wall boundary layer development through an isolated compressor rotor", Trans. ASME, Jnl. of Eng. for Power, Vol. 104, pp 805-818.

Japikse, D., 1985, "Assessment of single and two-zone modelling of centrifugal compressors; studies in component performance, part 3", ASME paper 85-GT-73.

Koch, C. C., 1981, "Stalling Pressure Rise Capability of Axial Flow Compressor Stages," ASME Jnl. of Eng. for Power, Vol.103, October, pp 645-655.

Koch, C. C., and Smith, L. H., Jr., 1976, "Loss Sources and Magnitudes in Axial-Flow Compressors," ASME Jnl. of Eng. for Power, Vol. 98, No.3, pp 411-424.

Lieblein, S., 1959, "Loss and Stall Analysis of Compressor Cascades.", Trans. ASME Jnl. Basic Eng., Sept., pp 387-400.

Lieblein, S., 1960, "Incidence and deviation angle correlations for compressor cascades", Trans. ASME Jnl. Basic Eng., Vol. 82, pp 575-587.

Macchi, E., 1965, "Design limits, basic parameter selection and optimisation methods in turbomachinery design", in *Thermodynamics and Fluid Dynamics of Turbomachinery*, Ed. Ucer, Stow and Hirsch, Martinus Nijhoff Publishers, pp 805-828.

Miller, D. C., and Wasdell, D. L., 1987, "Off-design prediction of compressor blade losses", I. Mech. E. Paper C279/87, I. Mech. E. Conference 1987-6, *Turbomachinery - Efficiency Prediction and Improvement*, Cambridge.

Moore, F. K., and Greitzer, E.M., 1986, "A theory of post-stall transients in axial compression systems",ASME Journal of Eng for Gas Turbines and Power, Vol 108, pp 68-76.

Pfleiderer, C., 1957, *Strömungsmaschinen*, Springer-Verlag.

Raw, J. A., and Weir, G. C., 1980, "The Prediction of off-design characteristics of axial and axial/radial compressors", SAE Paper 800628, Turbine powered executive aircraft meeting, Phoenix, Arizona.

Robbins, W. H., and Dugan, J. F., 1956, "Prediction of off-design performance of multistage compressors", in *Aerodynamic Design of Axial-Flow Compressors,* 1965, NASA SP-36, pp 297-310.

Rodgers, C., 1980, "Efficiency of centrifugal compressor impellers", Paper 22 of AGARD CP No. 282 *Centrifugal compressors, flow phenomena and performance,* Conference in Brussels May 1980.

Russo, C. J., Nicklaus, D. J., and Tong, S. S., 1987, "Initial user experience with an artificial intelligence program for the preliminary design of centrifugal compressors", ASME paper 87-GT-217.

Schobeiri, T., 1992, "One-dimensional methods for accurate prediction of off-design performance behaviour of axial turbines" ASME paper 92-GT-54.

Schobeiri, T., and Abouelkheir, M., 1992, "Row-by-row off-design performance calculation method for turbines", Journal of propulsion and power, Vol. 8, No. 4, July-Aug, pp 823-828.

Schweitzer, J. K., and Garberoglio, J. E., 1984, "Maximum Loading Capability of Axial Flow Compressors.", Jnl of Aicraft, Vol. 21, No. 8, pp 593-600.

Shepherd, D. G., 1956, *Principles of Turbomachinery*, Macmillan.

Smith, D. J. L., and Merryweather, H., 1973, "The use of analytic surfaces for the design of centrifugal impellers by computer graphics", Int, Jnl, for numerical methods in engineering, Vol. 7., pp 137-154.

Smith, L.H., Jr., 1970, "Casing Boundary Layers in Multistage Axial-Flow Compresssors," *Flow Research on Blading*, L. S. Dzung, ed., Elsevier Publishing, Amsterdam, Netherlands.

Smith, S. F., 1965, "A simple correlation of turbine efficiency", Journal of the royal aeronautical society, V0l. 69, July, pp 467-470.

Sovran, G., and Klomp, E.D, 1967, "Experimentally determined optimum geometries for rectilinear diffusers with rectangular, conical or annular cross sections", *Fluid mechanics of Internal Flow*, Elsevier

Spengler, H. 1976, *Technisches Handbuch Pumpen*, VEB Berlin.

Stone, A., 1958, "Effects of stage characteristics and matching on axial-flow compressor performance", Trans. ASME, August 1958, pages 1273-1293.

Tong, S. S., and Gregory, B. A., 1990, "Turbine preliminary design optimisation using artificial intelligence and numerical optimisation techniques", ASME paper 90-GT-146.

Van den Braembussche, 1985, "Design and optimisation of centrifugal compressors", in Ucer, A. S, Stow, P., and Hirsch, Ch., (eds) *Thermodynamic and fluid mechanics of turbomachinery*, Martinus Nijhoff.

Whitfield, A., 1989, "Preliminary design and performance prediction techniques for centrifugal compressors", Proc. Instn. Mech. Engnrs. Vol 204, pp 131-144.

Whitfield, A., and Baines, N. C., 1990, *Design of radial turbomachines,* Longman

Wiesner, F. J., 1967, "A review of slip factors for centrifugal impellers", Trans. ASME Jnl of Eng. for power, Vol 89, pp. 558-572.

Wilson, D. G., 1987, "New guidelines for the preliminary design and performance prediction of axial flow turbines", Proc Instn Mech Engrs, Vol 201, No A4, pp 279-290.

Wright, P. I., and Miller D. C., 1991, "An improved compressor performance prediction model", I. Mech. E paper C423/028.

Youngren, H. and Drela, M., 1991, Viscous/Inviscid method for preliminary design of transonic cascades", AIAA paper 91-

Zweifel, 0., 1945, "The spacing of turbomachine blading, especially with large annular deflection", Brown Boveri Review, Vol. 32, No. 12, (Baden, Switzerland)

ELEMENTS OF A MODERN TURBOMACHINERY DESIGN SYSTEM

by

Ian K. Jennions
GE Aircraft Engines
One Neumann Way, MD X409
Cincinnati, OH 45215-6301
United States

Abstract

The aerodynamic design system at GE Aircraft Engines (GEAE) consists of many parts: throughflow, secondary flow, geometry generators, blade-to-blade and fully three-dimensional (3D) analysis. This paper describes each of these elements and discusses optimization and computer architecture issues. Emphasis is placed on those areas in which the company is thought to have special capability.

Introduction

With ever increasing component efficiencies such as those achieved on the GE90 (Figure 1), the job of the turbomachinery aerodynamacist becomes more challenging and begins to take on more dimensions. Rather than designing the best vane possible, the quest is now for the best stage or multistage configuration that can operate efficiently over a wide range of flow conditions. Rather than producing the best aerodynamic design, the job now requires that the optimum design should satisfy aerodynamic, heat transfer, aeromechanical, mechanical, manufacturing, time and budget constraints simultaneously. The designer thus has to have a multidisciplinary awareness and the design systems have to complement this approach.

In order to move to a truly integrated multidisciplinary design, speed is of the essence. Speed in running individual codes, speed in looping and iterating over series of codes, speed in optimizing various design parameters and speed in being able to transmit information in a readily digestable form to other disciplines.

This paper begins by taking an historic look at the development of the main elements in the aerodynamic design system, namely the throughflow and blade-to-blade codes. It will be seen that these elements are highly linked to available computer resources, resources that today open up the possibility of great increases in designer productivity. Some of these possibilities will be explored before moving on to the design system as used at GEAE. Since designing with secondary flow has long been a part of compressor design at GEAE, special attention will be given to this area. Methods for throughflow, blade-to-blade and geometry generation, optimization strategies and links to the full 3D solvers will also be discussed.

Having built on our design system technology base for many years, the most immediate task we face in this area is one of implementing existing physical models onto ever changing computer architectures in order to increase productivity. The current technology push is in the 3D area where the underlying physics is still being explored; this is the topic of an accompanying paper (Jennions, 1994).

Historical Background

Aerodynamic designers of aircraft engines have always had a willingness to use the most up-to-date techniques to help them with their challenging jobs. Even before useful computers (1950's) such techniques as hand flux plots and electric field similarities were used to obtain information

Presented at an AGARD Lecture Series on 'Turbomachinery Design Using CFD', May to June 1994.

about the potential flow field. Hand flux plots aim to produce a graphical representaion of the streamlines through a blade row by continuously updating streamline and orthogonal positions on a diagram such as shown in Figure 2. On completion of the iteration, either when all orthogonals and streamlines are truly at right angles and aspect ratio considerations satisfied or (one suspects more commonly) when the designer was running out of time, this technique yielded the potential streamlines around the blading. The electric field simulation addressed the same situation. Blades would be cut out of metal and placed the correct pitch apart. Iron filings would be scattered between the blades and an electric potential applied between the blades causing the iron filings to align themselves with the field. By analogy between fluid flow and electric field theory (Lamb, 1932), the iron particles would describe the potential flow field around the blade.

A general scheme proposed by Wu (1952), and probably independently conceived by others, marked the way to a more analytical treatment of the full 3D flow through blade rows. In this scheme, the steady flow solution is calculated on two families of intersecting streamsurfaces: a family of blade-to-blade streamsurfaces (S1 surfaces) and a family of throughflow surfaces (S2 surfaces), as shown in Figure 3. Calculations are performed on each family of streamsurfaces but contain linkage terms, such as blade forces, to the other family. These solutions can be of any level of sophistication and by iteration a quasi-3D description of the flow field can be obtained. This technique has been elaborated on over the last 40 years and still remains the backbone of any aero design system.

The implementation of these ideas took a number of years, principally due to the lack of computer power with which to solve the equations as they had been formulated. Figure 4 shows the major events in throughflow and blade-to-blade history at GEAE over this time period, indicating the computer hardware that was being used. Each significant upgrade to our design capability can be traced back to the production of faster hardware which enabled more complex physics or numerics to be handled, giving the ever eager designer new tools with which to attack design problems.

The above analysis on its own is still not sufficiently sophisticated to address the problem of multistage compressor (or turbine) design for today's high efficiency levels. There is a built in assumption that flow remains on axisymmetric streamsurfaces as it passes through the machine, even though designers are aware that this assumption is not really valid. Secondary flows generate spanwise as well as cross-passage velocities, which convect fluid from the hub to the tip or vice versa and these can be expected to persist for some distance downstream of the blade row that generates them. Also, there is a tendency for blade boundary layer fluid to be centrifuged outward on rotor blades and moved inward on stator vanes by the prevailing static pressure field. Sweeping of the blades can also cause boundary layer cross flows.

An indication of the potential importance of this mixing in multistage compressors was observed at GEAE in the mid 1960's. At that time tests were being conducted on compressors with higher stage loadings and lower aspect ratios than had previously been common. When flow synthesis calculations were made that employed measured distributions of stagnation temperature and stagnation pressure, the deduced spanwise distributions of loss coefficient appeared to be unreasonable in the stages aft of stage 3 or stage 4; higher losses near mid-passage than near the end-walls were often implied. Since there was nothing in the blading design or operation that would cause losses to originate in this way, this strongly suggested that some of the higher temperature fluid near the end-walls was being convected to mid-passage by secondary flows. Much work has been done since this time on secondary flows and will be discussed later in the paper.

Design System

From a 1D description of the machine provided by Preliminary Design, along with the flowpath boundaries, the 2D vector diagrams and blading are laid out in the throughflow code. In essence, the throughflow is the design intent and begins the detailed design process. It is how the designer wants the machine to perform on test. The task of the rest of the detailed design system is to produce the blading to achieve the vector diagrams and efficiency levels set by this throughflow analysis.

The design systems for compressors and turbines are distinct, especially in their handling of geometry, but share many of the same tools. A bird's eye view of the system is shown in Figure 5. The process for design in each discipline is quite different, e.g. currently turbines do not use secondary flow in design; examples will be given throughout the paper to illustrate each process.

From the vector diagrams a preliminary blade shape along the throughflow streamlines is created. There are a variety of blade-to-blade codes

with a choice being made depending on the type of design. The blade-to-blade code will predict loading, exit angle and (if viscous) loss, given the blade geometry and flow conditions from the throughflow code. Some iteration with the geometry generator is needed until a blade shape satisfying throughflow and other requirements is produced. Iteration with the throughflow will also have to be performed as blade blockages, lean and flow asymmetries (the linkage terms of Wu's analysis) will affect the streamline positions and target design values.

Full 3D analysis is performed to a greater or lesser extent depending on the component. Transonic fans and turbines now place great emphasis on this part of the system, whereas multistage compressor design makes relatively little use of 3D due to the cumulative mixing effects that occur through the machine. Techniques such as those used by Adamczyk (1989) are needed for multistage compressors but are still in their infancy. 3D results can be averaged and taken back into the throughflow system to update either loss or turning throughout the blade row.

The detailed use of the design system for compressors and turbines has been described in two publications. Sullivan and Hager (1983) described the aero design and performance of the GE / NASA E^3 fan, the full scale test vehicle being shown in Figure 6. Selection of the blade shape parameters and use of the system for the fan, quarter stage booster, bypass OGV (Outlet Guide Vane) and inner OGV are all discussed. The design was conducted using many advanced technology features and improvements in design methods. Test results demonstrated aerodynamic performance that exceeded all efficiency, flow and stall margin goals. Figure 7 shows the fan performance map and how the target stall line was exceeded. For turbines, the report by Wysong et al. (1978) is a comprehensive description of an interactive system for the design of turbine airfoils. It includes turbine aerodynamics, heat transfer and mechanical design. The analytical and numerical methods in each module, and their theoretical basis, are presented in the report.

Links to other disciplines are also shown in Figure 5 where vertical placement of the other disciplines indicates the level at which data is currently extracted from the aerodynamic design system. Information regarding flowpath layout for drafting is taken from the throughflow level as is the aerodynamic data required for fan acoustics. Both manufacturing and mechanical design key off the geometry elements of the system. Aeromechanics and heat transfer take blade-to-blade flow data, or even fully 3D data, depending on the depth of analysis required.

While the above provides a background to the aero design system in use at GEAE, the following sections explore in more detail the physical processes and theoretical modelling that are present in each of the main elements. Emphasis is particularly placed on those areas where the system used at GEAE is thought to be different to those of competitors.

Throughflow

The basis of the current throughflow code is described by Smith (1966). There, an equation describing the radial variation of circumferentially averaged flow properties inside a turbomachinery blade row was derived. This equation is referred to as the Radial Equilibrium Equation (REE) expressed as:

$$\underbrace{\overline{\left(\frac{1}{\rho}\right)}\frac{\partial \overline{p}}{\partial r}}_{1} = \left(\frac{1-\overline{M}_z^2}{1-\overline{M}_m^2}\right)\left(\underbrace{\frac{\overline{C}_u^2}{r}}_{2} - \underbrace{\frac{\overline{D^2 r}}{\overline{Dz^2}}\overline{W}_z^2}_{3}\right)$$

$$+\frac{\overline{W}_r}{1-\overline{M}_m^2}\left(\overline{W}_z\left[\underbrace{\frac{\partial(r\overline{tan\varphi})}{r\partial r}}_{4} + \underbrace{\frac{1}{\lambda}\frac{\overline{D}\lambda}{\overline{D}z}}_{5}\right] - \underbrace{(\overline{\frac{1}{C_p}})(\overline{\frac{Q'}{T}})}_{6}\right)$$

$$\underbrace{+\overline{\left(\frac{1}{\rho}\right)}\left(\frac{p_s - p_p}{\theta_s - \theta_p}\right)\frac{1}{r}\left(\frac{\overline{M}_r\overline{M}_u}{1-\overline{M}_m^2} - tan\epsilon_m\right)}_{7}$$

$$\underbrace{+\frac{-G_0 + G_1 + G_2 + G_3 + G_4 + G_5}{1-\overline{M}_m^2}}_{8}$$

Term 1 is the radial pressure gradient term, the terms on the right hand side of the equation effectively telling one how this gradient is produced and, hence, how it can be controlled. Term 2 is the centripetal acceleration and is often used as the only right hand side term as a simplified form of the REE. Increasing the turning done by a blade (C_u) increases the radial pressure gradient. Term 3 is the meridional streamline curvature and will be minimal in cylindrical passages without significant three dimensional blading. Term 4 is the slope gradient term, while term 5 is the blockage gradient. Blockage can clearly be used to change the distribution of the flow through a blade row and the term gives its effect on the radial pressure gradient. Term 6 is the heat transfer term, which is negligible if the flowpath is adiabatic. Term 7

arises from the blade forces imparted on the fluid, i.e. the pressure difference across the blade, and has to come from a blade-to-blade calculation. Finally, term 8 expresses the non-uniformity of the flow in the circumferential direction. If the flow was uniform circumferentially, then these terms would be zero. Smith investigated the magnitude of these G functions in detail and found them to be negligible. Through an understanding of these terms and their actions on the flow the designer can better tailor the radial pressure gradients through a machine to meet design objectives.

Secondary Flow

For multistage machines the throughflow code forms the basis for a physical model but must be supplemented by knowledge of the mixing occuring in the machine. Adkins and Smith (1982) showed flow measurements that indicated substantial spanwise mixing of flow properties and considerable deviation in blade row turning from two-dimensional cascade theory. They put together a secondary flow model which accounted for the effects of: 1) main-stream non-free vortex flow, 2) end-wall boundary layers, 3) blade end clearances, 4) blade end shrouding, 5) blade boundary layer and wake centrifugation. The model was based on inviscid, small perturbation secondary flow theory and resulted in spanwise velocities representing mixing from each of these secondary flow sources. These velocities were then turned into a mixing coefficient that could be used in a throughflow code to mix out quantities such as total temperature, total pressure or RCu (radius times tangential velocity; work). The effects of such an analysis on profiles from high and low aspect ratio P&WA compressors are shown in Figure 8. Calculations performed without mixing show large temperature and pressure gains near the endwalls whereas those with mixing considerably flatten these profiles and result in much better agreement with the experimental data.

Gallimore and Cumpsty (1986) conducted experiments in two low-speed four-stage compressors using an ethylene tracer gas technique to trace the migration of flow through the machine. Their results showed that the dominant mechanism for spanwise mixing was random turbulent type diffusion and not the radial convection of flow properties. Further, they suggested that the results seemed fairly insensitive to the magnitude of the mixing coefficient, so that a single number appeared adequate. It should be noted that both Adkins and Smith and Gallimore and Cumpsty had arrived at a mixing coefficient to describe the spanwise mixing but they had both done so with very different underlying physical mechanisms.

Leylek and Wisler (1991) produced both experimental and numerical results to confirm that both convective and diffusive phenomena were present inside a multistage compressor. The experiments used an ethylene tracer gas technique (Wisler et al., 1987) and a 3D Navier-Stokes code in order to understand the mixing process in Stator 3 of a four stage low-speed research compressor at design point and at increased loading. Full 3D Navier-Stokes simulations of these cases aided understanding and interpretation of the experimental data as well as showing good agreement with it. Figure 9 shows experimental plots of ethylene concentration downstream of the stator, the projection of the initial injection points (upstream of the stator) onto this plane being shown by a 'X'. Three sets of contours are shown, the results from 3 different injection sites: D, G and C. When plotted as a function of radial distance from the initial injection point, the concentration profiles (Figure 10) clearly can be used to identify convection and diffusion processes. In Figure 10a, the shapes of the experimental distribution functions for Contour D reasonably approximate those for a classical type turbulent diffusion. In Figure 10b, examining the data along the major axis on the radially outward side of the injection point for Contour G, the areas of convection and diffusion are clearly shown to be of the same order of magnitude. On the radially inward side, large contour distortion occurs, which is thought to be caused by a combination of both convection and diffusion. The distribution function showing the spanwise extent of mixing for Contour C in Figure 10c also has large convective and diffusive effects present.

A further example of the use of secondary flow modelling can be found in Smith (1987) in which the aerodynamic design of the Unducted Fan (UDF, Figure 11) is described. Here, the same quasi-three-dimensional approach employed for ducted fan designs was used, consisting of a circumferentially-averaged flowfield analysis followed by cascade design that included secondary flow and sweep effects. The open-tip condition entered as a significant secondary flow contribution and the Adkins and Smith (1982) approach was extended to deal with this geometry. Blade shapes defined by this process were analyzed by a 3D Euler solver (Holmes and Tong, 1985), as the effects of viscosity were thought to be small, and final blade shape adjustments made accordingly.

Blade Geometry

Blade construction and manipulation for compressors and turbines is quite different, following design philosophies in each discipline. Compressor geometry is defined by a blade meanline and thickness distribution, following the format founded at NACA (Jacobs et al., 1933). The vector diagrams are taken from the throughflow code and with an appropriate deviation angle and choice of thickness distribution a blade is constructed. This construction is performed on the number of streamline sections for which the design is executed and, with lean and sweep considerations (Smith and Yeh, 1962), a 3D blade is generated. Leading edge geometries on components such as fans are described by parameters characterizing the droop of the leading edge and by the polynomial required to blend the leading edge geometry in with the rest of the blade. Because the blade geometry is expressed in terms of parameters, interpolation produces smoother results than working with the basic blade coordinates, especially in the leading edge region which is critical to most designs. Figure 12 shows a geometry plot for a fan tip section, showing critical areas through the passage and expected expansion lines from the leading edge region.

For turbines, the geometric description of a blade is driven by different considerations. Turbine designers need to be able to hold throat area while designing sections capable of being cooled and having reasonable trailing edge thicknesses. This is most easily achieved by treating the geometry as the surface of the blade, being described by a number of polynomial curve fits for each streamline section. Designers manipulate these curves until a desired blend of curvature continuity is achieved (Wysong et al., 1978), e.g. from the nose to the suction surface. Blade design thus proceeds as an iterative loop between this interactive geometry generator and the analysis code. Recently, however, this part of the system has been used to generate candidate blade shapes which have had different stackings applied to them before analysis with a full 3D Navier-Stokes code. A logical extension of this approach (not implemented yet) would be to interactively modify the full 3D geometry.

With the increasing use of Unigraphics as a CAD / CAM system within the company, the use of a NURBS (Non-Uniform Rational B Spline) description of the blade to be used as a 'master model' for all disciplines is being sought. The aero design system currently can produce full 3D blade descriptions in Unigraphics for complex geometric manipulation, transmittal to other disciplines (e.g. mechanical design) outside vendors or to laboratories for the creation of SLA (Stereo Lithography Apparatus) models which are becoming increasingly popular in reducing development cycle time.

Blade-to-Blade Codes

A variety of blade-to-blade solvers are currently available in the design system. They range from potential and streamline curvature methods up to fully viscous time marching solvers. The main use of the blade-to-blade codes is to ensure that the vector diagrams set by the throughflow are achievable within the bounds of blade thickness, loading and efficiencies. For example, in turbine design the suction surface diffusion is taken as a primary indicator as to the condition of the boundary layer. The blade-to-blade code solves for the suction surface velocity ratio, or diffusion factor, and the geometry is adjusted accordingly.

Most of these codes are very similar to those available in other design systems and have also been described elsewhere e.g. streamline curvature (Wysong et al., 1978) and inverse design (Drela, 1985, Giles, 1985). However, three codes (TAYLOR, AEGIS and NOVAK2D) are different enough to be worthy of mention. NOVAK2D (Holmes and Connell, 1989) is an unstructured, adaptive code and will be fully discussed in the accompanying CFD paper (Jennions, 1994), the other two codes are discussed below.

TAYLOR. The TAYLOR code (Novak and Haymann-Haber, 1982) assumes a steady, 2D, inviscid, irrotational flow and employs a fourth-order Taylor series expansion across the cascade passage. Strictly speaking, it is a channel design (not a blade design) process. In the upstream and downstream regions, the stagnation streamline shape results from the specification of zero blade thickness and zero angular momentum change. The computational process inside and outside of the blade is identical. The procedure gives solutions for subsonic, supersonic and mixed-flow conditions, although the solutions are only realistic in regions where shock free flow is possible. The code can be used in either a direct analysis mode or as an inverse design code.

Figure 13 shows the results from the code for a turbine mid-span nozzle section. The case is subsonic throughout with an inlet Mach number of 0.212. Figure 13a shows the generated blade profile with the associated Mach number contours. Figure 13b shows the surface Mach numbers, the solid line (without a scale) representing the input

pressure surface / suction surface pressure difference. Figure 14 shows a check on the code's ability by using the same case as shown in Figure 13 to compare to a streamline curvature blade-to-blade program (Novak and Hearsey, 1977). The streamline curvature code was run on the fixed geometry. The loading ($\delta P(m)$) and thickness ($t(m)$) distributions were then fed into TAYLOR with the resulting blade shape and pressure distributions shown. TAYLOR is quite close to the surface pressure distributions, the blade shape differences being almost inperceptible.

The overall objective of the TAYLOR code was to produce a conceptually simple, easy to use, preliminary design technique which fitted readily into the existing design system. For the predominant number of cascade types which occur in multistage axial compressors and turbines (i.e. subsonic, with reasonable solidity), the process appears to produce results which may well be considered better than first approximations.

AEGIS. The AEGIS (AErodynamic General Implicit Solver) code (Turner and Keith, 1985) was developed to meet requirements for fan frame flow prediction. This imposes heavy demands on any analysis code for two reasons:

1. The flow is rotational and the upstream profiles of entropy and stagnation enthalpy are a function of the flowfield solution.
2. The flowfield around the many bodies involved must be solved simultaneously, as the entire flowfield is tightly coupled.

Because of the many bodies and large size of the flowfield, an Euler solver is required which can accurately predict the flow details with few grid points per airfoil passage. These details include: (a) the flow division among the multiple strut-to-strut and strut-to-pylon passages, (b) the circumferential static pressure and mass flux distributions at the fan rotor exit plane, and (c) the effect of geometry variations such as the change in stagger angle of any given strut or the outlet guide vane circumferential spouting angle distribution. AEGIS handles the fan frame problem and also other problems of this class, including tandem blades and simple cascade flows.

The AEGIS solver is essentially a fixed grid analog of the streamline curvature method. The streamline curvature is made up of the grid curvature and one of the derivatives of velocity. This derivative is actually an unknown in the equation system along with the two velocity components. The equation system includes a finite volume form of the continuity equation, an integral form of the cross-stream momentum equation, a spline-like equation which relates the velocity with its derivative, and the boundary conditions. The streamwise momentum equation and energy equation are solved by convecting total pressure and total temperature along streamlines. This equation system is solved implicitly using Newton's method which provides for fast convergence and allows for many options in boundary condition treatment.

AEGIS has been applied to a forced response problem as reported by Chiang and Turner (1993). Figure 15 is a schematic of a set of blades along with the downstream stator vanes and struts. Based on the axial distance between the rotor and the struts, the potential disturbance from the strut reaching the rotor was expected to be minimal. However, experience has surprisingly shown that there can be a significant blade response. The stator vane and strut configuration that was analysed is shown in Figure 16, the vertical line representing the rotor trailing edge. The circumferential static pressure distribution at the rotor trailing edge was generated and Fourier decomposed as shown in Figure 17. The 6/rev component of 0.66 psi is significant enough to excite the rotor blade at resonance. Running the analysis without the vanes present gave pressure distributions as shown in Figure 18, the Fourier decomposition showing a fourfold decrease in the 6/rev strut potential disturbance - the vanes are amplifying the pressure disturbance. The stators were then restaggered (Figure 19) as suggested by the AEGIS analysis with the results shown in Figure 20; the loading on the modified stators is much more uniform from vane to vane and therefore has much less circumferential pressure variation or potential disturbance.

3D Analysis

In the past, 3D analyses have been regarded by some as a 'design check' once the design was complete. It is now, and has been for quite a while, applied on a regular basis to both compressor and turbine designs at GEAE. The current GEAE 3D Navier-Stokes turbomachinery code is called Viscous EULER due to its heritage, which dates back to the mid-1980's.

In 1985 an Euler code (Holmes and Tong, 1985) was written for GE Aircraft Engines and subsequently used in the design of the Unducted Fan (Smith, 1987). The code was then further enhanced (Cedar and Holmes, 1989) to account for boundary layers, solid bodies such as part-span

shrouds and engine splitters, and the presence of adjacent blade rows. It was used extensively in transonic fan design. Next, the viscous stress terms, viscous boundary conditions and Baldwin-Lomax turbulence model were added, followed by a novel implementation of the $k-\epsilon$ turbulence model as discussed by Turner and Jennions (1992).

These progressive steps have enabled designers to use the code at various stages of its development and hence result in a very knowledgeable user base. Current application of the code centers on its use for turbine stage calculations in order to understand the complex flows and modelling requirements. The code is coupled back into the design system as shown in Figure 5, where the 3D solution is circumferentially averaged and the quantities (work, loss, etc.) relevant to the design placed back in the throughflow solution. This enables the whole system to be run together and throughflow assumptions examined in the light of 3D results. The detailed use of this code will be discussed in an accompanying paper (Jennions, 1994) and so will not be repeated here.

Unsteady 3D simulations are still in their infancy for two main reasons. One is that the computer times required are still very high (hundreds of CRAY hours) and so they cannot be used in a design cycle (Madavan et al., 1989). It should also be noted that much of this work is for integer blade counts and the true effects of this assumption have not been explored. Secondly, there is the problem of what to do with an unsteady solution once one is obtained. As all of our previous experience has been with steady solutions, the easiest thing is to time average the unsteady results and then examine these results in relation to the steady flow results for the stage. Heat transfer is more likely than aerodynamics to benefit from such unsteady calculations due to considerations like film cooling hole placement or hot streak migration (Dorney et al., 1990).

Optimization

The above computational tools have been developed to a point where they are used routinely for new product design, such as the GE90 (Figure 1). The tools improve the accuracy of the design performance estimates and reduce the need for testing. As these tools come into wider use, two main issues need to be addressed: how to prevent human intervention from becoming a bottleneck in taking full advantage of these tools and how to preserve human design expertise. With the recent rapid reduction in the price / performance ratio for engineering workstations and advances made in technologies such as artificial intellegence (AI) the way forward to a system in which a human performs design but leaves the laborious exploration of the design space to something much more capable (but less creative) - the computer - is clear.

Tong and Gregory (1990) demonstrated such an approach using the Turbine Design and Off-Design (TDOD) program, a sophisticated preliminary design tool capable of predicting the performance of a given turbine design very accurately. TDOD uses a simple set of input criteria that describe the turbine flowpath, number of stages and work split. The designer must design the turbine with an adequate flowpath, matching all the cycle requirements of pressure, temperature and shaft speed while maintaining high performance characteristics. The laborious task of fine tuning the many parameters is tedious, iterative, time consuming and expensive. Lastly, the time given to complete such a design rarely allows for fine tuning. This is where AI, in the form of a software shell called Engineous, has helped immensely. Its basic approach is to separate problem specific information from generic design functions and then to organize them as knowledge bases. Engineous first draws on stored human knowledge to emulate a design expert and rapidly produce a good design. After this search is completed, and as time permits, Engineous automatically draws on its own set of heuristic search techniques to explore the design space.

TDOD and Engineous were used to increase the performance of an LP turbine without exceeding its present diameter or length. The results are shown in Figure 21. The designer achieved a 0.5% improvement principally by optimizing the flowpath, while Engineous optimized the flowpath, stage work split, blade count and work reaction to achieve its 0.92% improvement. The difference in turnaround time was about 10:1 (designer : Engineous) and, of course, the Engineous solution also freed up the designer while the iterations were being performed. Using Engineous allowed for greater insight into the various trade-offs of loss parameters. For instance, high wall slope (the rate at which the turbine diameter increases) leads to increased loss; on the other hand, increased tip diameter increases turbine performance. In the time allowed, the designer has very few trade-off options, Engineous can explore many. Further, by designing without constraints, turbine designers can look beyond previous experiences. Figure 22 illustrates the Engineous flowpath that is produced this way. The stage-2 outer wall flowpath has been used to 'buy' turbine diameter by speci-

fying a very steep wall slope (beyond what experience would suggest). Stage 3 performance more than compensates for the loss associated with the high wall slope, giving a further net gain of 0.1%.

A continuation of the above work using the Engineous shell and the NOVAK2D inviscid blade-to-blade code (Holmes and Connell, 1989) with the object of minimizing the downstream static pressure variation resulting from a trailing edge shock system was performed by Shelton et al. (1993). The blade shape was described using B splines and Bezier control points. Parameters familiar to designers were then chosen by a linear combination of the geometry control points. These parameters are referred to as ESPs (Engineering Significant Parameters) and, as they are familiar to the designers, allow a smaller set of design parameters to be chosen, which will accelerate the design search process. For this work a simple 1D search technique was employed. Engineous selects each ESP in turn and through increasing and / or decreasing it, given the fluids response from NOVAK2D, finds changes which show improvement. This improvement was ascertained by getting NOVAK2D to calculate the static pressure range just downstream of the trailing edge of the blade.

The results from the Engineous iteration are shown in terms of blade shape in Figure 23. for both the baseline blade and the MIDOS (MInimized DOwnstream Shock) blades designed to be tested in the Virginia Tech. transonic cascade. Results from those tests are shown in Figure 24 with the inviscid calculations for both blades. At the trailing edge of the baseline blade the suction surface Mach number is around 1.3 and as the cascade exit Mach number is 1.2, results in a strong oblique shock. Similarly, the pressure surface reaches sonic at the trailing edge tangency point, accelerates past M=1.2 and recompresses in an oblique shock to match the downstream boundary conditions. The MIDOS blade Mach number distribution is very different. Both suction and pressure surface trailing edge Mach numbers agree quite well with the downstream conditions and so very little shock structure is present.

Unfortunately, to achieve the MIDOS design, the airfoil trailing edge thickness was increased by 42% from the baseline design resulting in loss being 24% more than for the baseline. This must be weighed against the benefit of increased downstream blade row performance from shock strength reduction.

The overall approach of using an AI system inside the Engineous shell looks encouraging. Indeed it may be the only feasible way to take full advantage of the advances in CFD analysis methods. It permits the designer to focus time and energy on understanding physics and optimizing the design rather than excersizing analysis and geometry codes. This appears to be the way forward with multidisciplinary design and analysis.

Computer Architecture

Increases in computer speed from year to year are taken for granted, but when we step back and look at this speed progression (Figure 25) it is truly impressive. With further increases in chip technology and parallel processing occuring every day, tasks that seem computer intensive now, if vital to engineering needs, must be vigorously pursued in the belief that the computer power will be available in the near future. Added to this we have gone from a number of disparate operating systems to a single unifying system - UNIX. That is not to say that the transition has been smooth ("No two UNIX systems are the same!") but the objective, which is slowly being realized, is well worthwhile. The ability to operate on an HP workstation or a CRAY supercomputer as if they were the same machine overcomes an enormous amount of problems that have plagued code development and support over the years, not to mention designer ease of use. The task at hand is to use this unified operating system and available computer power to produce aero design systems that meet the needs of the designer.

While the previous sections describe the design system, each design task can involve running a number of different codes. Currently there are a couple of hundred codes in the aero design system and any detailed design job can result in running anywhere from 5 to 30 codes. Realistically, the designer is not interested in which code to run next but rather in comparing design X with design $X + 1$, these designs being expressed as the end points of a number of iterative loops. At GEAE we are currently developing two products to make this request a reality.

The first is a data base called GDS (Global Data System) for all the aero design data underlying the programs shown in Figure 5, with the exception of the 3D system which has its own data description. With the data model and dictionary for the system established, as GDS is added to the design codes they begin to look like subroutines in a large program rather than isolated programs because of the underlying common data structure. A graphics editor capable of taking any of the data in the design system viewing / modifying / deleting / adding to it and placing it back in GDS is being developed.

Having this capability, the next need is for a mechanism to automate the running of a series of codes, continue a loop until converged or give control back to a user each time around the loop.

This second product is called the Control Panel. Using PVM (Parallel Virtual Machine) for message passing between the programs and the Control Panel allows for a smooth execution of a number of codes whether they be interactive or batch in nature. This work is currently on-going but is sure to impact design cycle time significantly.

Concluding Remarks

This paper has explored the main elements of the GE Aircraft Engines turbomachinery design system. While the classical throughflow, secondary flow, geometry and blade-to-blade elements have been discussed, emphasis has been placed on those areas (secondary flow, optimization etc) where GEAE is thought to have special expertise.

The impact of CFD on the traditional design system should not be understated. Full 3D Navier-Stokes calculations are being performed on a regular basis, yielding powerful insights into complex flowfields. They are changing the way we do design and think of the design system. Progress in this area is the subject of an accompanying paper.

Acknowledgement

The author would like to thank GE Aircraft Engiones for permission to publish this paper.

References

Adamczyk, J. J., Celestina, M. L., Beach, T. A. and Barnett, M., 1989, "Simulation of Three-Dimensional Viscous Flow Within a Multistage Turbine", ASME 89-GT-152.

Adkins, G. G. and Smith, L. H., 1982, "Spanwise Mixing in Axial-Flow Turbomachines", ASME *Journal of Engineeering for Power*, Vol. 104, p97.

Cedar, R. D. and Holmes, D. G., 1989, "The Calculation of the Three-Dimensional Flow Through a Transonic Fan Including the Effects of Blade Surface Boundary Layers, Part-Span Shroud, Engine Splitter and Adjacent Blade Rows", ASME 89-GT-325.

Chiang, H-W. D. and Turner, M. G., 1993, "Compressor Blade Forced Response due to Downstream Vane-Strut Potential Interaction", ASME 93-GT-287.

Dorney, D. J., Davis, R. L., Edwards, D. E. and Madavan, N. K., 1990, "Unsteady Hot Streak Migration in a Turbine Stage", AIAA 90-2354.

Drela, M., 1985, "Two-Dimensional Transonic Aerodynamic Design and Analysis using the Euler Equations", MIT PhD Thesis.

Gallimore, S. J. and Cumpsty, N. A., 1986, "Spanwise Mixing in Multistage Axial Flow Compressors: Part I - Experimental Investigation; Part II - Throughflow Calculations Including Mixing", ASME *Journal of Turbomachinery*, Vol. 108, pp. 2-16.

Giles, M., 1985, "Newton Solution of Steady Two-Dimensional Transonic Flow", MIT GTL Report No. 186.

Holmes, D. G. and Connell, S. D., 1989, "Solution of the 2D Navier-Stokes Equations on Unstructured Adaptive Grids", AIAA 89-1932.

Holmes, D. G. and Tong S. S., 1985, "A 3-D Euler Solver for Turbomachinery Blade Rows", ASME *Journal of Engineering for Gas Turbines and Power*, 107.

Jacobs, E. A., Ward, K. E. and Pinkerton, R. M., "The Characteristics of 78 Related Airfoil Sections from Test in the Variable-Density Wind Tunnel", NACA Report No. 460.

Jennions, I.K., 1994, "The Role of CFD in the Design Process", AGARD LS-195, *Turbomachinery Design Using CFD*.

Leylek, J. H. and Wisler, D. C., 1991, "Mixing in Axial-Flow Compressores: Conclusions Drawn From Three-Dimensional Navier-Stokes Analyses and Experiments", ASME *Journal of Turbomachinery*, Vol. 113, p139.

Lamb, H., 1932, "Hydrodynamics", p. 65, Sixth Edition, Published by Dover Publications.

Madavan, N. K., Rai, M. M. and Gavali, S., 1989, "Grid Refinement Studies of Turbine Rotor-Stator Interaction", AIAA 89-0325.

Novak, R. A. and Haymann-Haber, G., 1982, "A Mixed-Flow Cascade Passage Design Procedure Based on a Power Series Expansion", ASME 82-GT-121.

Novak, R. A. and Hearsey, R. M., 1977, "A Nearly Three-Dimensional Intrablade Computing System for Turbomachinery", ASME *Journal of Fluids Engineering*, pp. 154-166.

Shelton, M. L., Gregory, B. A., Lamson, S. H., Moses, H. L., Doughty, R. L. and Kiss, T., 1993, "Optimization of a Transonic Turbine Airfoil Using Artificial Intellegence, CFD and Cascade Testing", ASME 93-GT-161.

Smith, L. H., 1966, "The Radial-Equilibrium Equation of Turbomachinery", ASME *Journal of Engineering for Power*, pp. 1-12.

Smith, L. H., 1987, "Unducted Fan Aerodynamic Design", ASME *Journal of Turbomachinery*, Vol. 109, pp. 313-324.

Smith, L. H. and Yeh, H., 1962, "Sweep and Dihedral Effects in Axial-Flow Turbomachinery", ASME *Journal of Basic Engineering*, pp. 1-14.

Sullivan, T. J. and Hager, R. D., 1983, "The Aerodynamic Design and Performance of the General Electric / NASA E^3 Fan", AIAA-83-1160.

Tong, S. S. and Gregory, B. A., 1990, "Turbine Preliminary Design Using Artificial Intellegence and Numerical Optimization Techniques", ASME 90-GT-148.

Turner, M. G. and Keith, J. S., 1985, "An Implicit Algorithm for Solving 2D Rotational Flow in an Aircraft Engine Fan Frame", AIAA 85-1534.

Wisler, D. C., Bauer, R. C. and Okiishi, T. H., 1987, "Secondary Flow, Turbulent Diffusion, and Mixing in Axial-Flow Compressors", ASME *Journal of Turbomachinery*, Vol. 109, pp. 455-482.

Wysong, R.R., Prince, T.C., Caney, R.D., Keith, J. S., Miller, W. E., Landis, D. H. and Kues, L. J., 1978, "Turbine Design System", AFAPL-TR-78-92.

Wu, C. H., 1952, "A General Theory of Three-Dimensional Flow in Subsonic and Supersonic Turbomachines of Axial-, Radial-, and Mixed-Flow Types", NACA TN 2604.

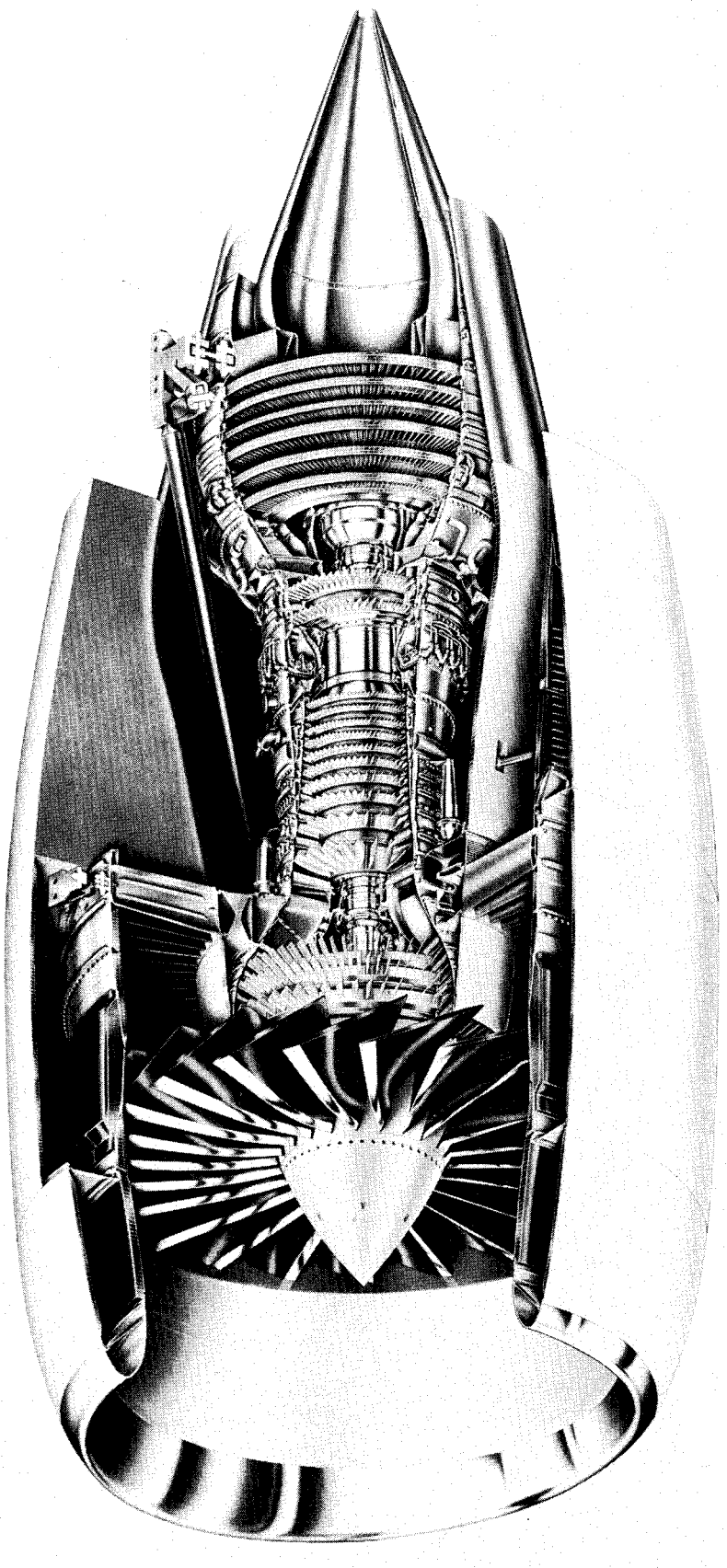

Figure 1. GE90 Engine

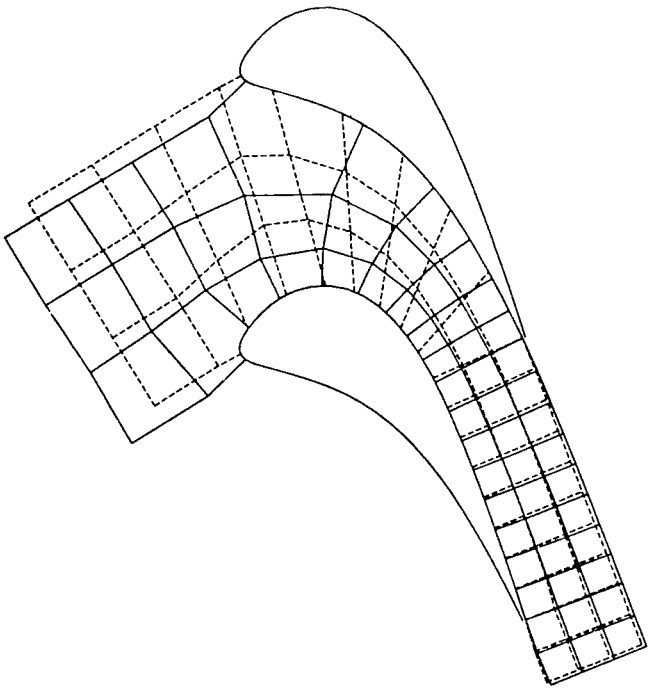

- - - Initial guess

—— Final solution

Figure 2. Hand Flux Plot for Potential Flow Solutions. Streamlines and cross-passage lines are continually adjusted for orthogonality and aspect ratio.

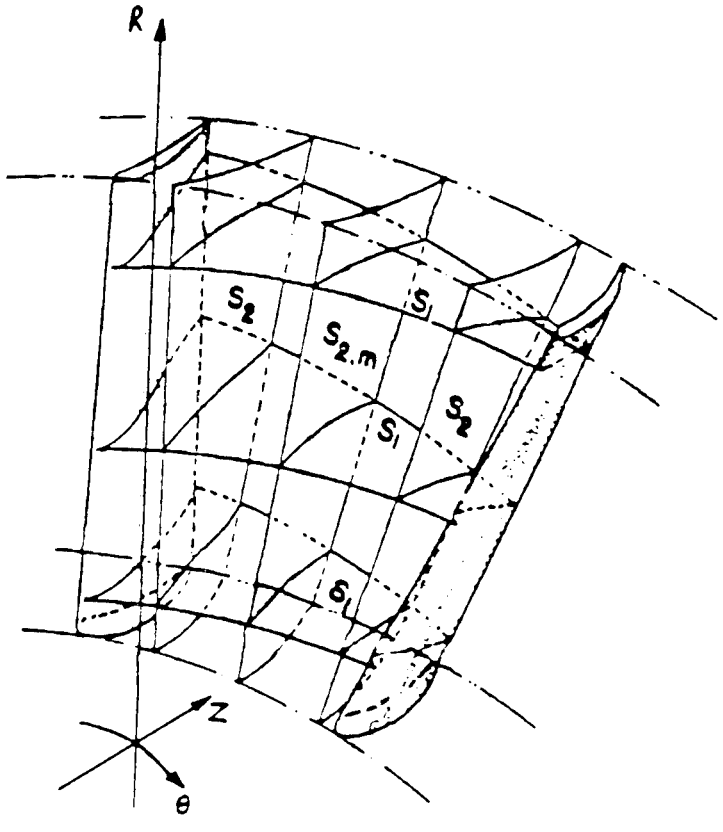

Figure 3. Intersecting Surfaces used in Turbomachinery Design.

Decade	Hardware	Throughflow Code	Blade–to–blade Codes
1950's	IBM 701	Computerized Radial Equilibrium	Hand flux plots Incompressible (panel methods)
1960's	GE625	FORTRAN, data transfer via tapes Internal stations	Subsonic (potential) or supersonic (MOC)
1970's	Honeywell time sharing	Fast convergence Non–radial stations, splitter	Transonic (streamline curvature)
1980's	VAX 11/785 CRAY XMP	Robust transonic solver	Complex geometry (splines) Inverse design, finite volume
1990's	Workstations CRAY YMP	Graphical interfaces Flexible/convenient data storage	Optimization

Figure 4. Progress of Design System Codes linked to Computer Hardware.

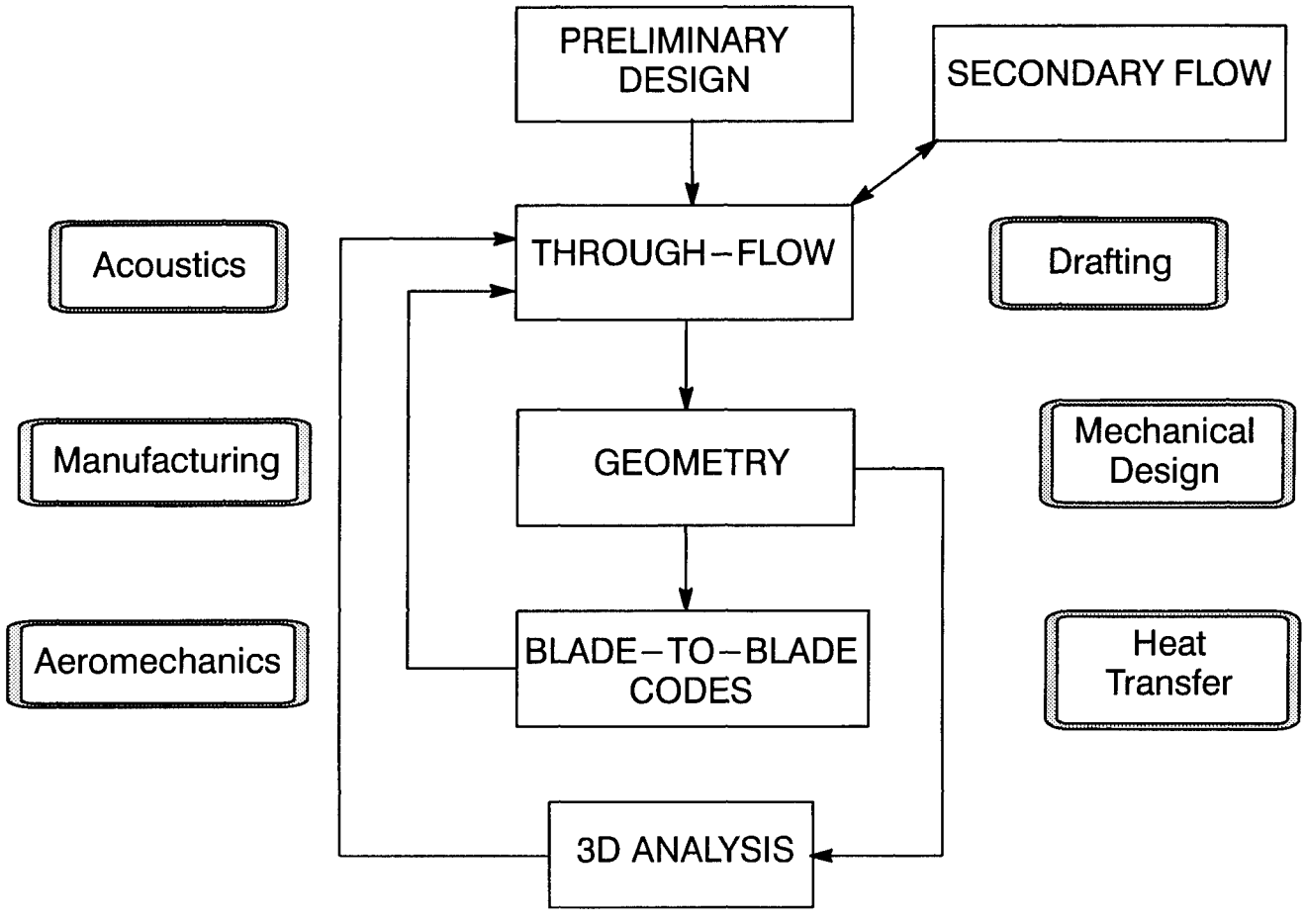

Figure 5. Turbomachinery Aerodynamic Design Process.

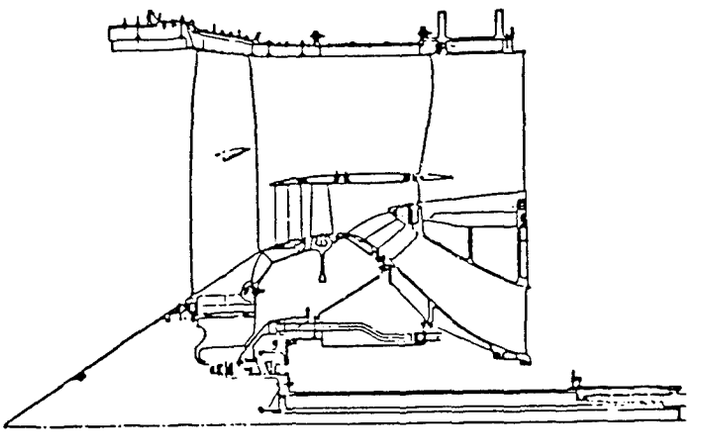

Figure 6. Full Scale E^3 Fan Test Vehicle.

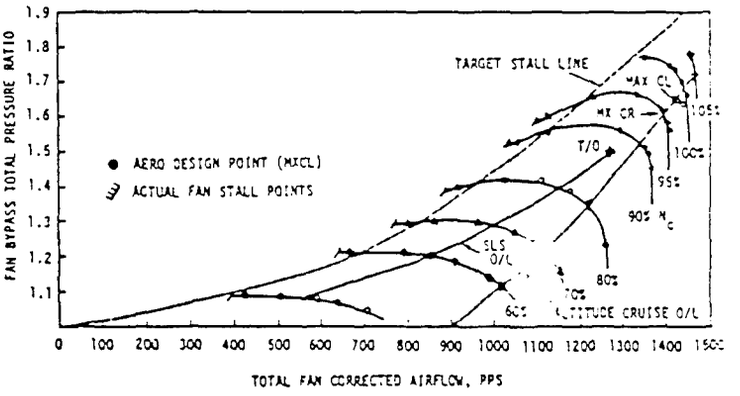

Figure 7. E^3 Fan Bypass Performance Map.

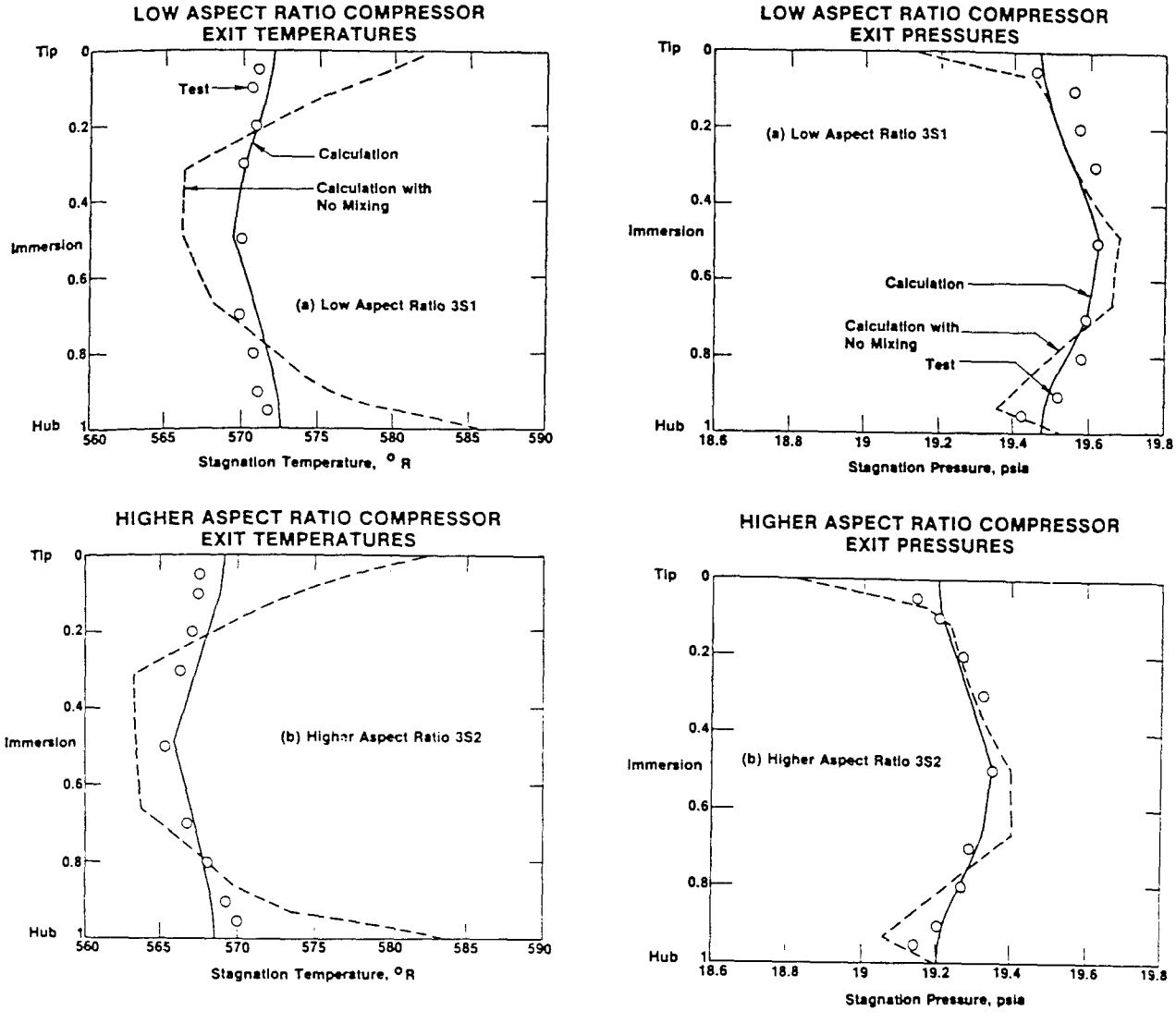

Figure 8. Exit Pressures and Temperatures from 3-stage Compressors having Different Aspect Ratios.

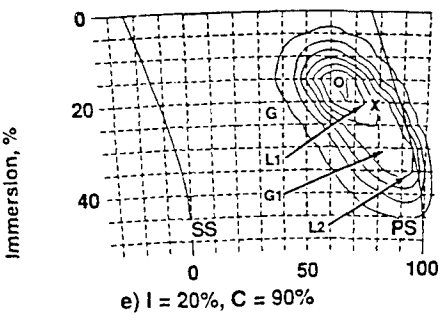

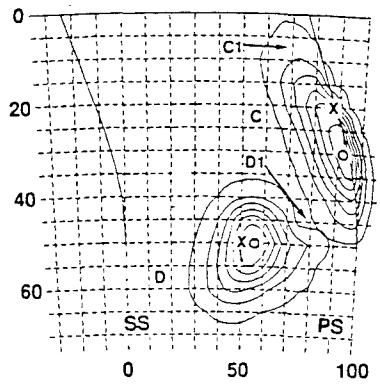

Figure 9. Ethylene Tracer Gas Measurements. Injection at stator 3 leading edge at 'X', sampling downstream at 'O', contours of max = 95%, min = 5%, δ = 15%.

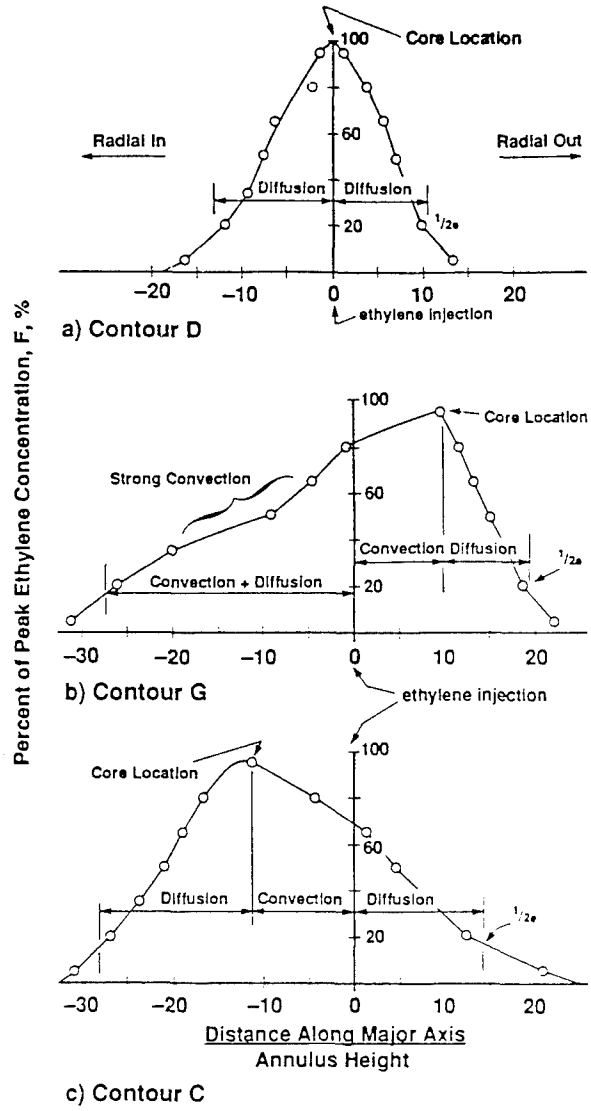

Figure 10. Ethylene Concentration as a Function of Distance from Injection Location showing Regions of Spanwise (radial) Convection and Diffusion.

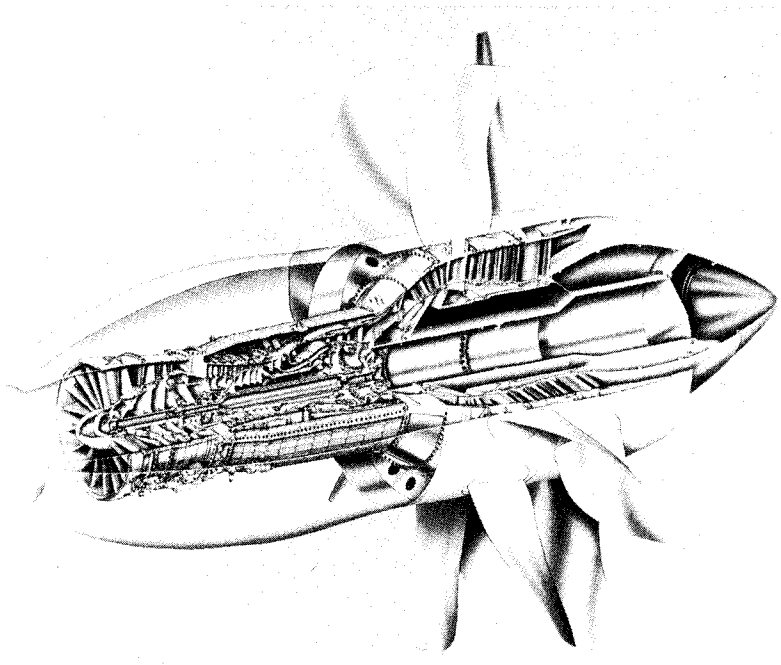

Figure 11. Unducted Fan Propulsion System.

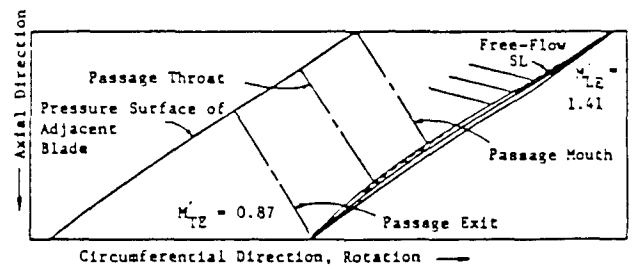

Figure 12. Fan Rotor Tip Streamline Airfoil Section.

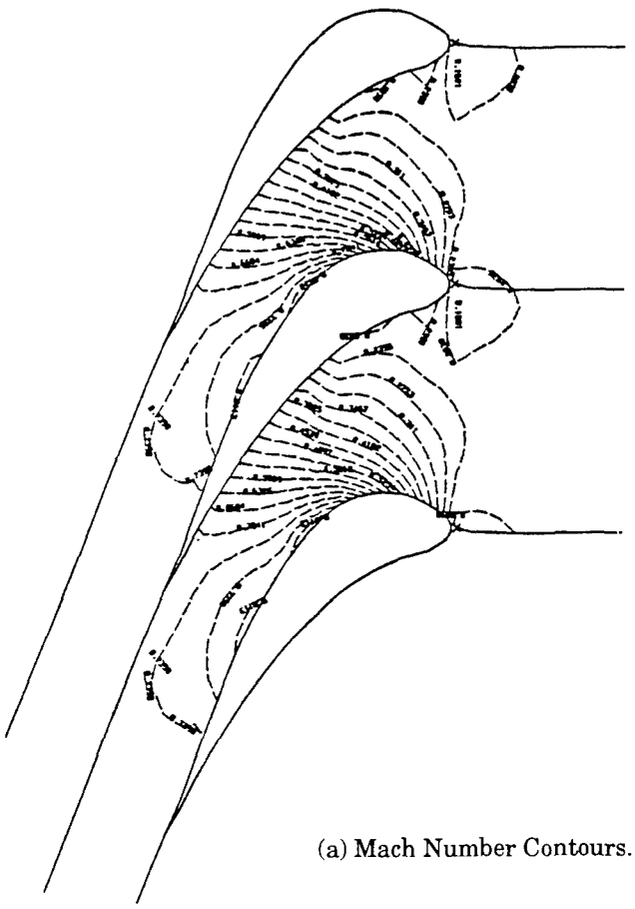

(a) Mach Number Contours.

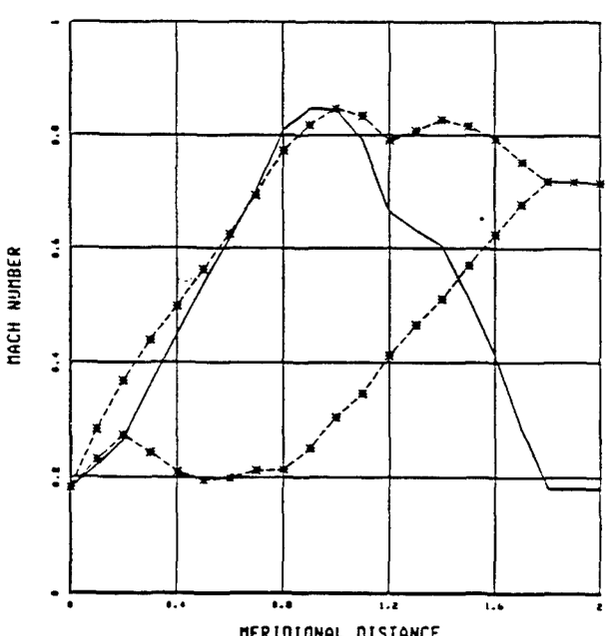

(b) Loading Distribution.

Figure 13. TAYLOR Solution for Nozzle Mid-Span Section.

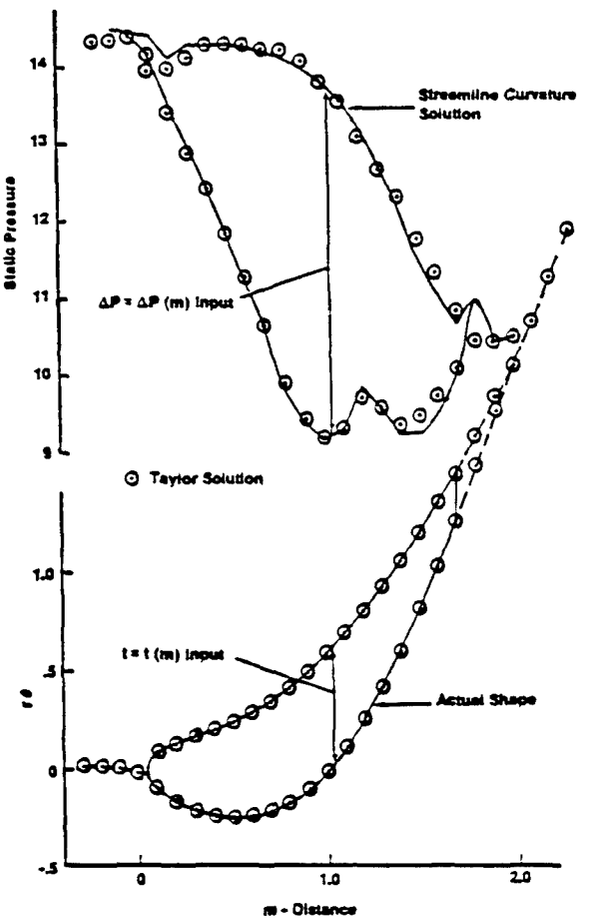

Figure 14. Comparison of TAYLOR and Streamline Curvature Results.

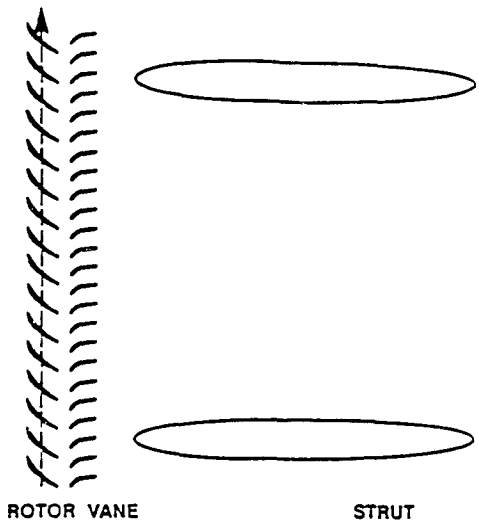

Figure 15. Schematic of Rotor with Vanes and Struts.

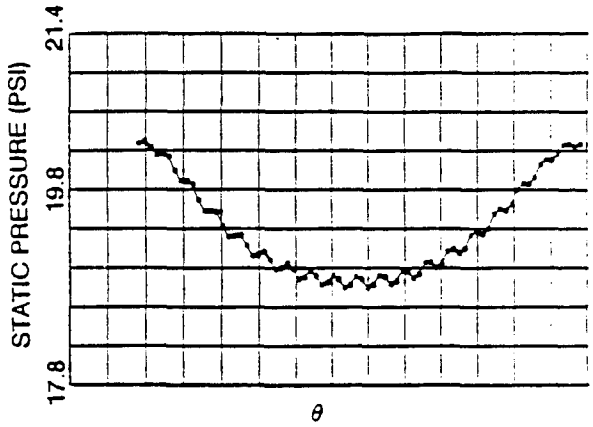

FFT		
6/Rev	12/Rev	18/Rev
0.66 psi	0.16 psi	0.05 psi

Figure 17. Rotor TE Static Pressure Distortion.

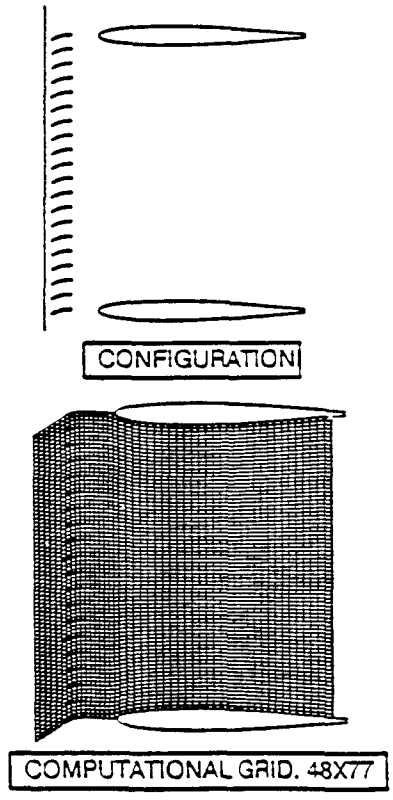

Figure 16. Vane/Strut Configuration and AEGIS Grid.

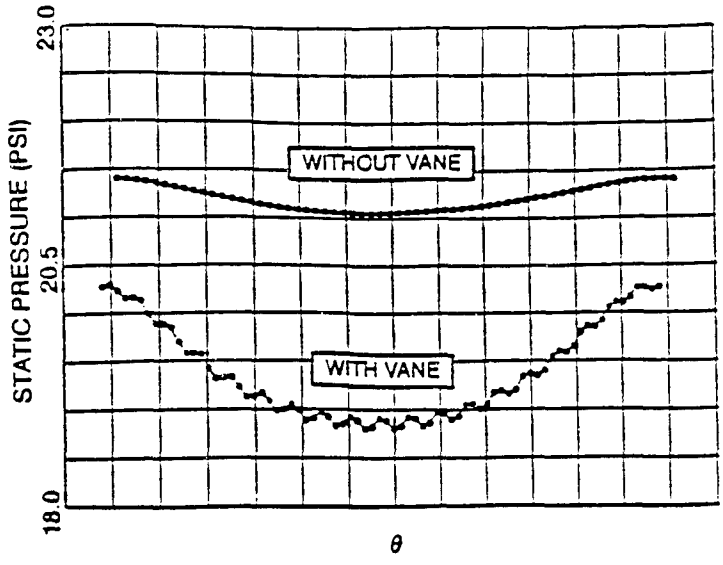

Figure 18. Rotor TE Pressures with and without Vanes.

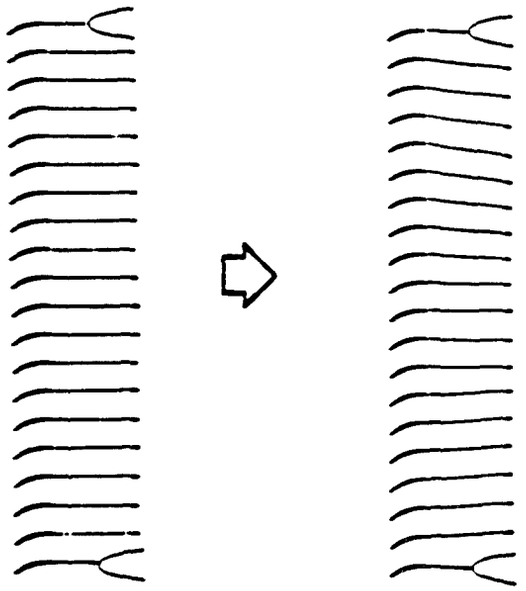

Figure 19. Baseline and Optimized Configura-tions.

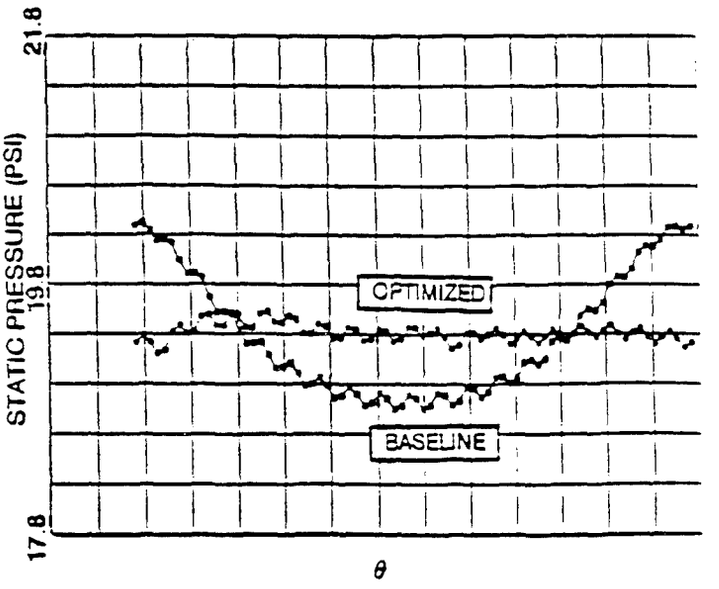

Figure 20. Baseline and Optimized Disturbances.

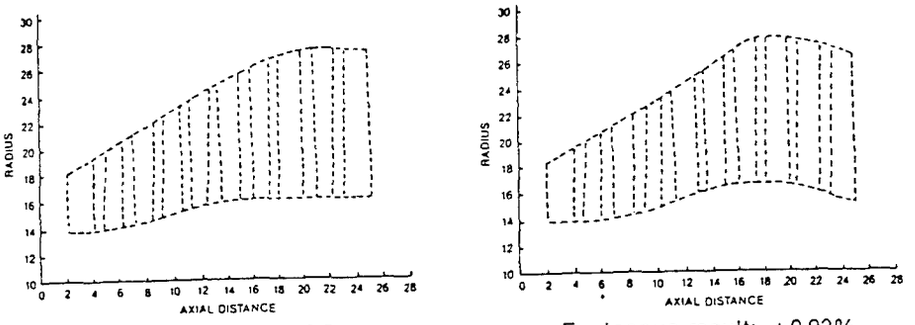

Figure 21. Multistage LP Turbines Designed by a Designer and Engineous.

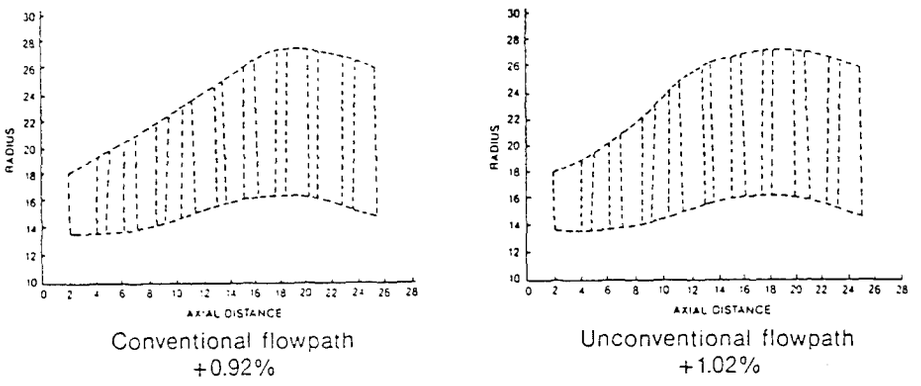

Figure 22. Multistage LP Turbines Designed by Engineous with Restricted and Unrestricted Flowpath Slopes.

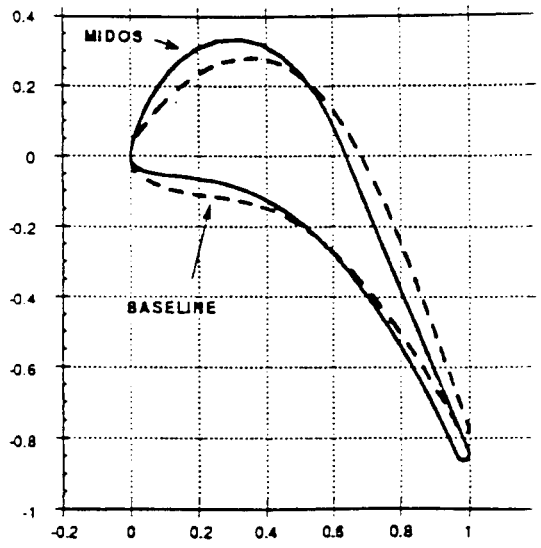

Figure 23. Cascade Blade Profiles.

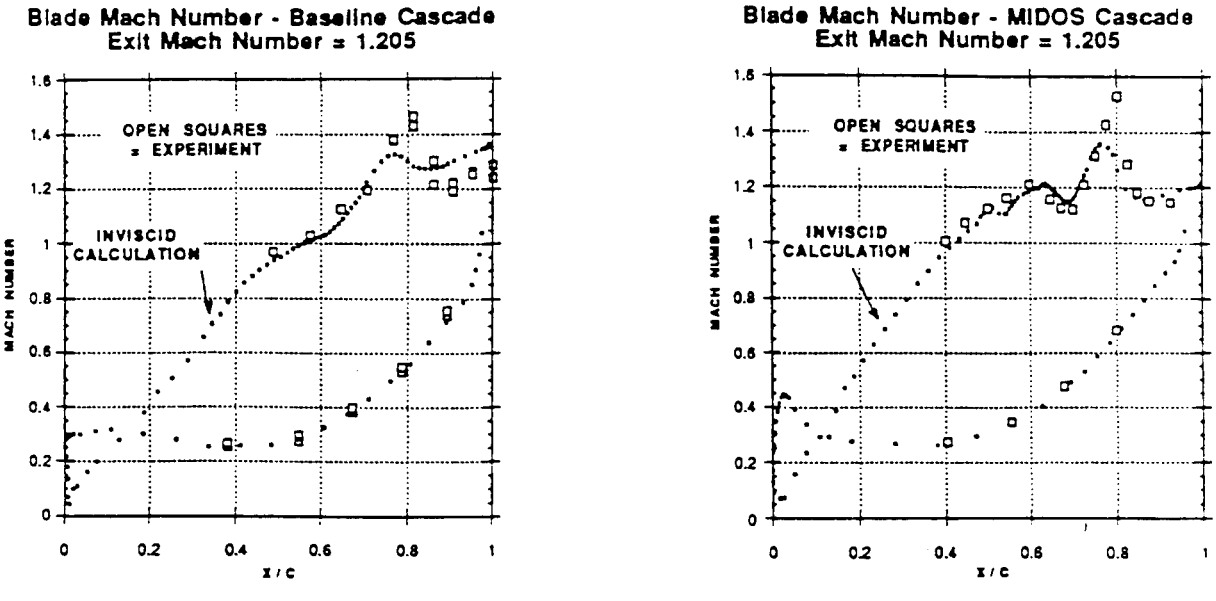

Figure 24. Blade Mach Numbers for Baseline and MIDOS Blades.

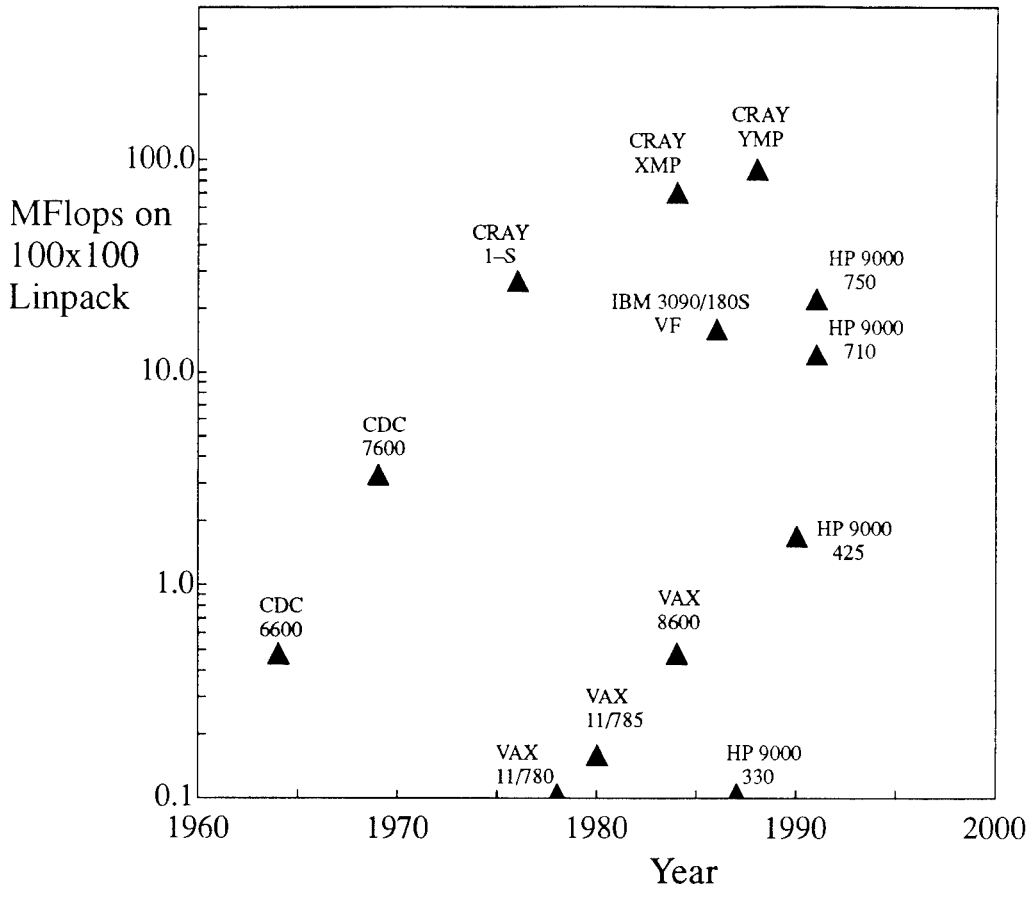

Figure 25. Computer Speeds over the Years.

DESIGNING IN THREE DIMENSIONS

by

J.D. Denton
University of Cambridge
Department of Engineering
Whittle Laboratory
Cambridge CB3 0DY
United Kingdom

SUMMARY

This lecture advocates the direct use of three-dimensional flow calculations for turbomachinery design. The limitations of the usual quasi-three dimensional approach are discussed and it is shown that fully 3D calculations overcome the modelling limitations inherent in them. Fully 3D calculations also avoid the need to iterate between throughflow and blade to blade calculations. This leads to fewer routine operations (e.g. data transfers) being needed during the design process and hence more efficient use of the designer's time.

With a flexible geometrical package, able to generate blade sections and transfer their geometry directly to a 3D data set, changes of stage geometry can be made in minutes. An outline of such a package is given. Modern 3D calculation methods, Ref(11), enable complete stage solutions, with adequate accuracy for design purposes, to be obtained in the order of 1 hour on a workstation. Hence several design iterations per day can be easily be performed for a single stage of a machine.

An example of this approach used to design a very high pressure ratio (3:1) axial fan is given and discussed.

1 INTRODUCTION

The conventional approach to turbomachine design is still basically a quasi-three dimensional (Q3D) one involving iteration between an axisymmetric throughflow calculation and blade to blade calculations on a limited number of stream surfaces. The purpose of this paper is to suggest that is is easier and faster to omit the quasi-3D blade design stage of this approach and to move straight from the throughflow calculation to a fully three dimensional (3D) flow calculation for a complete blade row, or nowadays for a complete stage. Use of this approach requires a flexible blade profile generation and stacking package that produces a 3D calculation grid directly from input data on several blade sections. However, such a package is no more difficult to produce than is one that stacks already designed 2D sections to form a 3D blade and the outline of such a blade geometrical design tool is described in Appendix 1. Limitations of computer power have restricted this approach in the past because 3D flow calculations were too expensive to run routinely and frequently. However, nowadays it is easily possible to adopt this approach on a workstation or even on a PC. Appendix 2 gives an example of this.

2. THE QUASI-THREE DIMENSIONAL APPROACH

An outline of the Q3D approach will first be given in order to discuss its limitations.

A one-dimensional meanline program may be used to establish annulus heights and mean blade angles given a specified mass flow rate, rotational speed and work for each stage. Alternatively these quantities can easily be obtained by hand calculation. This data is then fed into an axisymmetric throughflow calculation which will usually be run initially in the inverse mode. In order to complete the data for the throughflow calculation the radial distribution of work for each stage must be specified. The throughflow calculation predicts the spanwise variation of inlet and exit flow angles for all blade rows and also predicts the overall performance. Several iterations on the throughflow calculation are usually needed in order to optimise the spanwise variation of work, reaction and the hub and casing profiles.

It has long been realised (Hirsch et al, Ref 1) that the predictions of all throughflow calculations are highly dependent on the empirical data used within them. This empirical data mainly takes the form of loss and deviation correlations and, for compressors, the blockage factors. It is also accepted that if this empirical data is correct, e.g. it is provided by measurements on the machine being calculated, then the predictions of the throughflow program for the spanwise variation of velocities and flow angles are extremely good.

The completed throughflow calculation provides the required inlet and outlet angles for all blade sections and also the variation of stream tube thickness through each section. The blade sections can now be designed to accept the predicted inlet flow and to produce the required exit flow. The number of sections on which the blade row must be designed depends on how great are the spanwise variations in flow. Typically about 5 sections will be used but more may be chosen for a highly twisted row.

The blade section design is based on a Q3D blade to blade calculation which may be used in either direct or inverse mode. Inverse mode calculations are clearly most efficient in producing the required blade surface pressure distribution but must include constraints on the blade thickness and pitch:chord ratio to ensure that the blade designed is compatible with mechanical requirements and with the adjacent blade sections.

Presented at an AGARD Lecture Series on 'Turbomachinery Design Using CFD', May to June 1994.

When used in conjunction with a flexible blade geometry package (Appendix 1), analysis mode calculations can, with experience, be made to provide any required surface pressure distribution almost as quickly as an inverse calculation and it is easier to satisfy the constraints when using the analysis mode.

The blade to blade flow calculation method can be inviscid for most turbine blades but must include an allowance for boundary layer blockage for compressor blades. However, in all cases the result is critically dependent on the variation of stream surface thickness within the blade row. This must be obtained from the throughflow calculation and input to the blade to blade calculation. Fig 1 compares the calculated blade surface pressure distribution of a compressor blade with a 10% stream surface divergence with the same blade when the stream surfaces are parallel. Both calculations have the same total to static pressure ratio because this is what would be known from a throughflow calculation. The large difference between them illustrates the dominant effect of stream surface thickness. Fig 1 also shows results from a viscous calculation on the same blade and it is seen that, for this compressor blade, the effects of viscosity are too large to ignore at the design stage. The exit angle from the calculations is shown on the figures and it is clear that significantly greater blade camber would be needed to obtain the required flow turning when the effects of viscosity are included.

Having designed a sufficient number of blade sections they can now be stacked to obtain the overall blade geometry. All the calculations performed so far have completely neglected three-dimensional effects and have assumed that the stream surfaces are axisymmetric. Only in the case of a truly axial and fully free vortex design is this assumption completely valid. In almost all real blade rows three dimensional effects will be significant and these should now be checked with a fully 3D calculation. Again this should be a viscous calculation in the case of compressors. If the 3D calculation predicts significant differences from the design intent then the blade sections must be redesigned to allow for this. Since 3D inverse methods are not yet available the modification to the blade sections to allow for 3D effects must necessarily be empirical and based on the designer's judgement.

This process of Q3D blade section design, stacking and three dimensional check must be performed for all blade rows in the machine. Finally when all blade rows have been designed the throughflow calculation must be re-run in the analysis mode to check for the effects of departures from the original design intent that have been introduced through mechanical or geometrical requirements. If, for example, the throughflow calculation shows that these departures have introduced a significant amount of incidence onto some blade sections then these sections must be redesigned, checked in 3D and again checked with the throughflow calculation.

The whole process so far has been performed at one design point. The off-design performance must now be checked by at least the throughflow calculation, which must now be run in the analysis mode. For some critical blade sections more blade to blade calculations may be necessary to ensure that they do not compromise the off-design performance.

The process described in extremely labour intensive since the designer's judgement must be used at all stages. Most of the designer's time is spent transfering data between programs, loading and running programs and inspecting the output. Comparatively little time is spent in doing what the designer is trained to do, ie in exercising his judgement as to what is the best compromise between conflicting requirements. Attempts to automate the progress have been reported (Shelton et al, Ref 2) but are not yet routine. The real limitation is that only the designer can really judge when a method or a correlation has reached the limit of its validity.

3. LIMITATIONS OF THE QUASI-3D APPROACH

Quite apart from the human time and effort required by the Q3D approach, in many practical situations there are serious limitations on its accuracy . These can only be corrected after a fully 3D check has been performed on the design.

Firstly there is the sensitivity of the results to the variation of stream surface thickness as illustrated in Fig 1. This is not a fundamental limitation of the Q3D approach but it is a practical one because the stream surface thickness within a blade row can only be predicted accurately if many calculating stations are located within the blade row during the throughflow

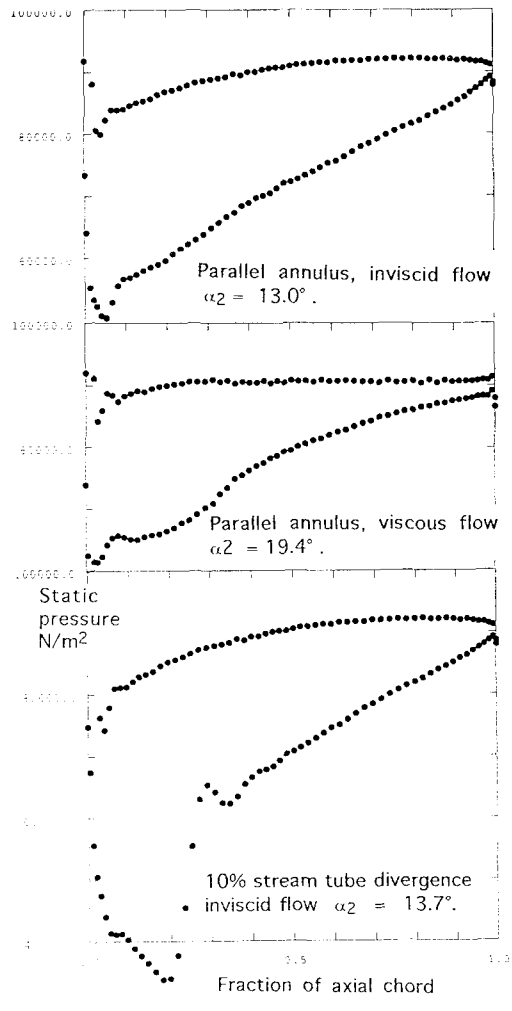

FIG. 1 Effect of stream surface thickness and viscosity on the surface pressure distribution of a compressor blade.

calculations. Very often thoughflow calculating stations will only be located at the leading and trailing edges of a blade row and a linear variaton of stream surface thickness will be assumed through the row. Even if many calculating stations are used, the blade thickness and internal flow angles at these stations must also be known accurately and used as data for the throughflow calculation. These are not available at the preliminary design stage and so, once an initial design of the blade sections has been obtained, an extra iteration is necessary to obtain more accurate values of stream surface thickness from the throughflow calculation. This extra iteration is seldom performed.

Secondly there are limitations inherent in the assumption of axisymmetric (ie untwisted) stream surfaces. Stream surface twist will occur as a result of blade sweep and blade lean as well as through streamwise vorticity.

The effects of sweep have been discussed in detail by Potts (Ref 3) who shows that they cannot be predicted by a Q3D approach. Sweep induces stream surface twist because the spanwise component of velocity tends to remain constant as the flow passes through the blade row whilst the axial velocity is increased on the suction surface and decreased on the pressure surface. This is illustrated in Fig 2. The angle of twist is greatest near mid span but its effect on blade loading is greatest near the endwalls where the stream surface twist induces a pitchwise variation in stream surface thickness. The result is that the swept forward leading edge is unloaded near the endwall and the swept back leading edge experiences an increased loading. The converse is true at the trailing edge. This is illustrated by the results of a 3D calculation shown in Fig 3

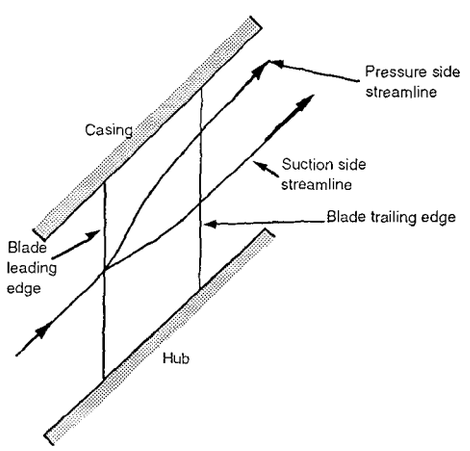

FIG 2 STREAM SURFACE TWIST INDUCED BY SWEEP.

The effects of blade lean are even stronger than those of sweep. To a first approximation they can be understood by considering that the constant pressure lines within the blade row are nearly radial with their positions determined mainly by the mid-span section, Fig 4. The pressures at the hub and casing can then be modified by moving the blade ends circumferentially without moving the mid-span section. Moving either endwall section in the direction of the positive blade to blade pressure gradient increases the pressure and reduces the velocity at that section. This is illustrated in Fig 4 which shows calculated Mach number contours within a leaned turbine blade row. The effect has been confirmed experimentally by Walker (Ref 4) and by Harrison (Ref 5).

The axial extent of the effects of lean depend on the blade aspect ratio in a manner that is discussed in detail by Walker (Ref 4). At low aspect ratios, less than unity, the effect is almost confined within the blade row that is being leaned and has little influence upstream and downstream of it. At high aspect ratios the stream surfaces are affected over a distance of the order one annulus height upstream and downstream of the leaned blade row as illustrated in Fig 5. This effect can produce a significant influence on upstream and downstream rows, so that leaning a turbine stator so that its pressure surface faces inwards can be used to increase the root reaction of the adjacent rotor blades. This effect has been extensively exploited in steam turbine design (Grant & Borthwick, Ref 6).

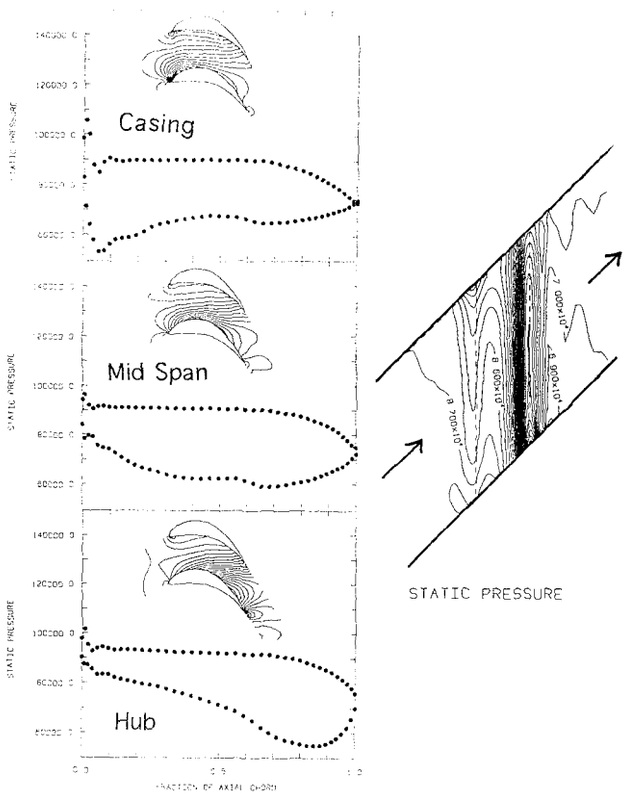

FIG. 3 Calculated effect of blade sweep on the blade surface pressure distribution.

The effects of lean arise partly through a change in stream surface thickness, induced by the lean, and partly by stream surface twist. The relative magnitudes of these two effects depends on the blade aspect ratio. The author knows of no systematic study of this but at high aspect ratio the effects are mainly due to changes of stream surface thickness. In this case it is likely they can be predicted by a throughflow calculation that includes several calculating stations within the blade row and which includes the radial blade forces induced by lean in the axisymmetric equations of motion. At low aspect ratios (say less than 2) it is likely that only a fully 3D calculation can give realistic predictions of the effects of blade lean.

Streamwise vorticity arising from secondary flows also causes stream surface twist. The effect of these on the blade loading depends on the extent of the secondary flow relative to the blade span and is only significant at low aspect ratios. The typical effect of the secondary flow is to reduce the blade loading near to the end walls

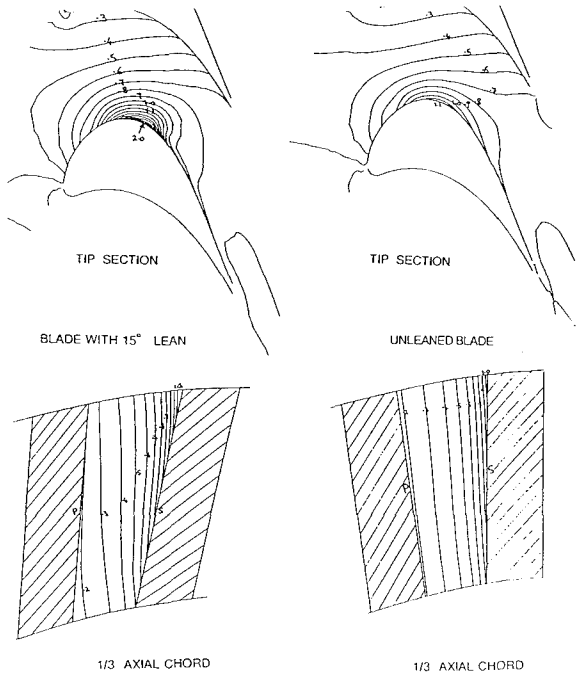

FIG 4. The effect of blade lean on the Mach number distribution in a turbine blade row.

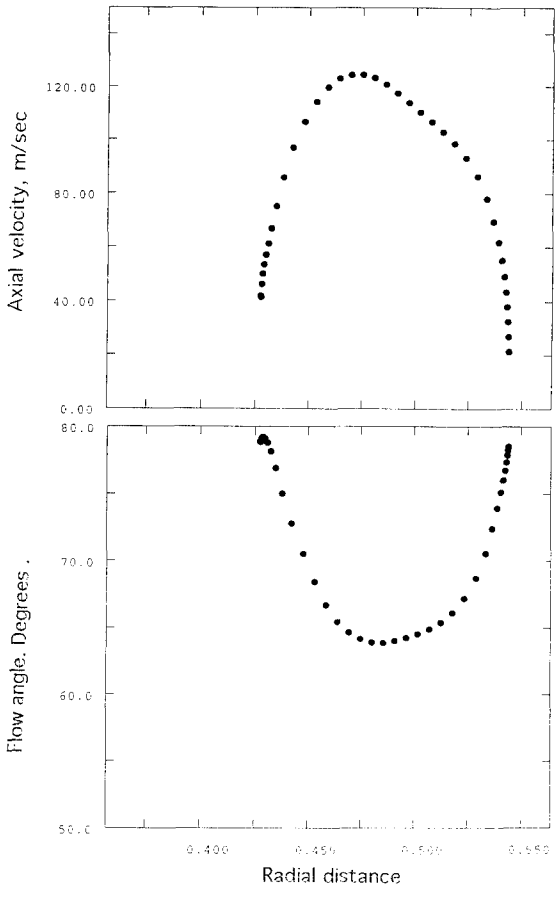

FIG 7. The effect of secondary flow on the exit angle and exit axial velocity profile of the blade of Fig 6.

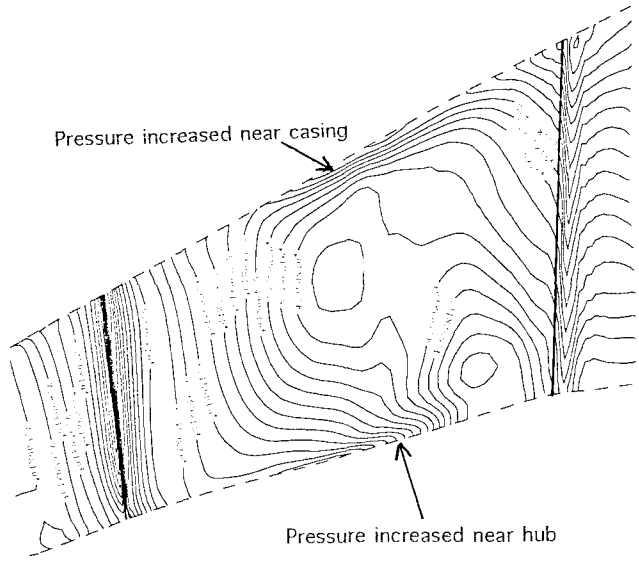

FIG 6. The effect of secondary flow on the suction surface pressure of a low aspect ratio turbine blade row.

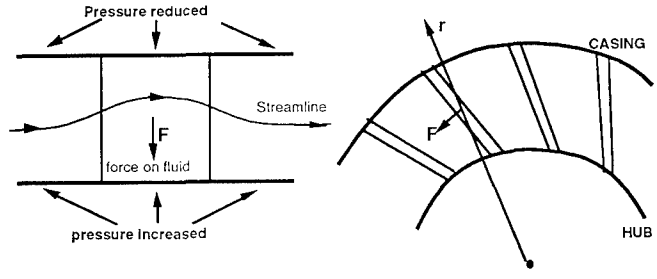

FIG 5. THE EFFECT OF BLADE LEAN

because of the increased pressure on the suction surface which is needed to deflect the secondary flow from the pitchwise to the spanwise direction. Fig 6 illustrates the calculated pressure on the suction surface of a low aspect ratio turbine blade. The regions of increased pressure near the endwalls are clearly visible. This effect is not predictable by the Q3D approach.

An even more important effect of secondary flow is its effect on the blade exit angles. This is well known to consist of overturning very close to the endwalls and a region of underturning some distance away from them. The effects of this deviation on the exit velocity profile and on the inlet angles to the next blade row can be very large. Fig 7 shows the calculated variation of exit angle and axial velocity downstream of the blade row of Fig 6. The effects of secondary flow are dominant. If this secondary deviation is included in throughflow calculations very good predictions of the exit velocity profile can be obtained as shown by Lewis (Ref 7), Fig 8. However, at the design stage this effect can only be included by correlations and these are extremely limited in accuracy. Most throughflow calculation make no attempt to model this secondary deviation, Fig 8 , and this constitutes perhaps the main limitation on the accuracy of their predictions.

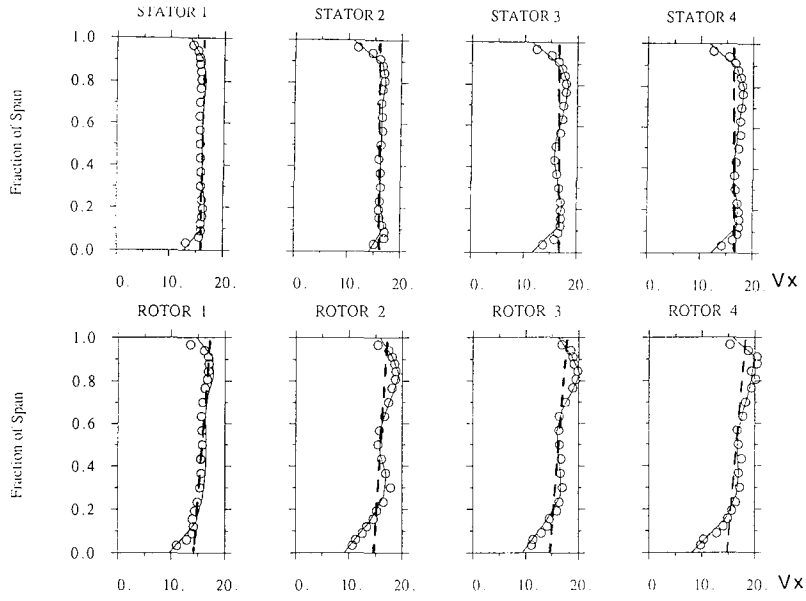

Fig 8. Measured and calculated axial velocity profiles through a 4 stage axial turbine.

oooooooooo Measured
Calculated using measured flow angles
Calculated using design flow angles.

Streamwise vorticity also arises as shed vorticity at the trailing edge of a blade row with spanwise varying circulation. It manifests itself as different spanwise velocities on the suction and pressure surfaces at the trailing edge and this in turn must be the result of stream surface twist within the blade passage. The author knows of no systematic studies of the effects of this on the blade loading.

Shock sweep, as illustrated in Fig 9, is another phenomenon that cannot be included in Q3D blade to blade calculations. Such calculations inevitably assume that the shock front is perpendicular to the stream surface and hence overestimate the shock pressure rise and loss in cases where it is swept. This is a particular problem in transonic compressors.

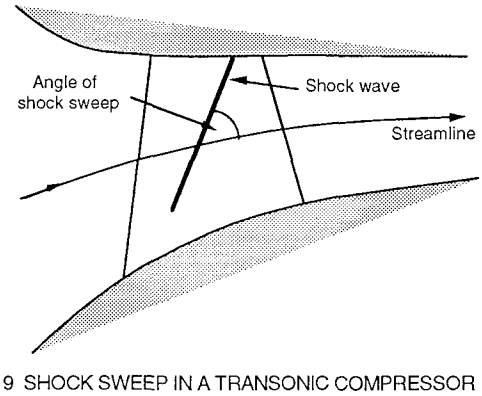

FIG. 9 SHOCK SWEEP IN A TRANSONIC COMPRESSOR

Strong spanwise migration of the suction surface boundary layer behind the shock wave is another effect that cannot be predicted by the Q3D approach.

The most serious limitation of the Q3D approach, however, is the assumption that the blade sections behave in isolation, ie that a change in the shape of one section does not affect the flow on adjacent sections. In fact there is always a "three dimensional relief' whereby if one section is changed the effect is spread out over a considerable part of the span. As a result the changes on the modified section are less than predicted by a Q3D calculation and significant changes occur on adjacent sections. The effect is brought about by local changes in stream surface thickness which are non-axisymmetric and so cannot be predicted by a Q3D approach. To illustrate this effect Fig 10 shows the pressure on the suction surface of a nominally 2D turbine blade where the mid span section has been modified by placing a "bulge" on the suction surface around mid-chord. The Figure also illustrates how the constant pressure lines remain almost radial despite the bulge. The effect on the suction surface is spread over about 25% of the span. Fig 11 shows the calculated surface pressure distribution at the section with the bulge and compares it with that calculated when the bulge was added to all spanwise sections so that blade is two-dimensional. The effect of the localised bulge on the blade loading at mid-span is about 30% less than the effect it has if it is added to all sections. The latter is what would be predicted by a Q3D calculation.

This "three-dimensional relief" is important whenever the blade geometry changes rapidly in the spanwise direction and so is especially important when features such as end-bends are used to try to control the flow near the end walls (Wadia & Beacher, Ref 8). Such features cannot be rationally designed by a Q3D approach. A consequence of this effect is that there is no point in using the Q3D approach to design a blade on a large number of different sections. If the sections are too close together then changes in geometry between adjacent sections will have much less effect on the real flow than is predicted by a Q3D method.

5. A THREE DIMENSIONAL DESIGN PROCEDURE

All of the above limitations of the Q3D approach are overcome by designing the blade row using a fully 3D calculation method. The main disadvantage of this is the lack of any inverse 3D design method that can be used to produce blades with a prescribed surface pressure distribution. However, with experience it is possible to produce any required surface pressure distribution using simple geometrical changes and calculating their effect with a direct calculation.

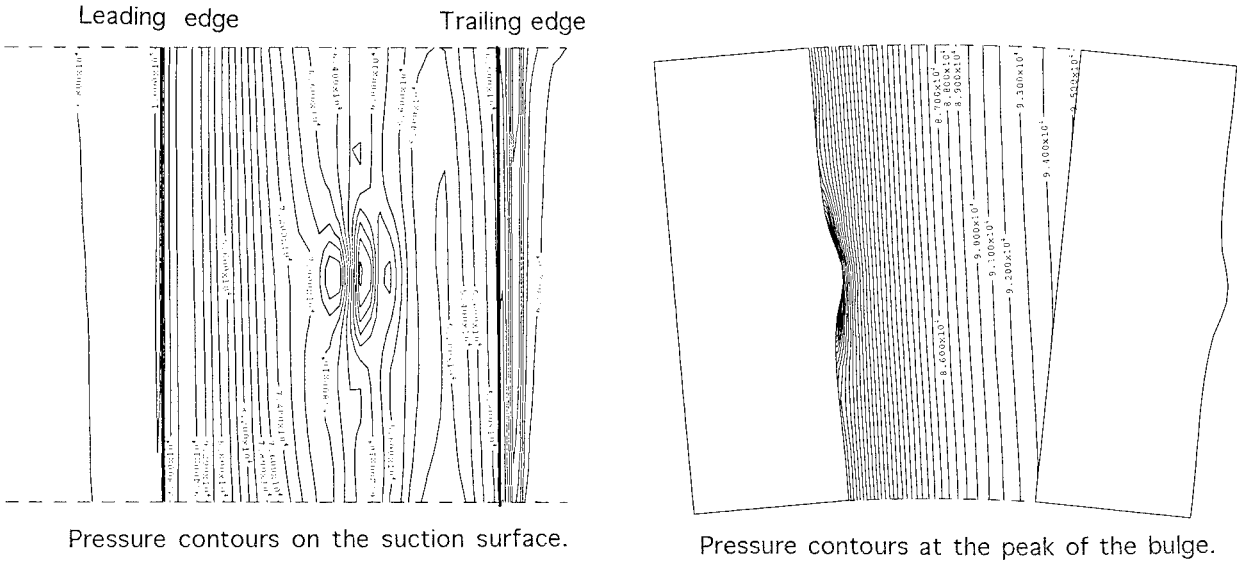

Pressure contours on the suction surface.

Pressure contours at the peak of the bulge.

FIG 10. The effects of a bulge at mid-span on the suction surface on the pressure distribution in a turbine blade row.

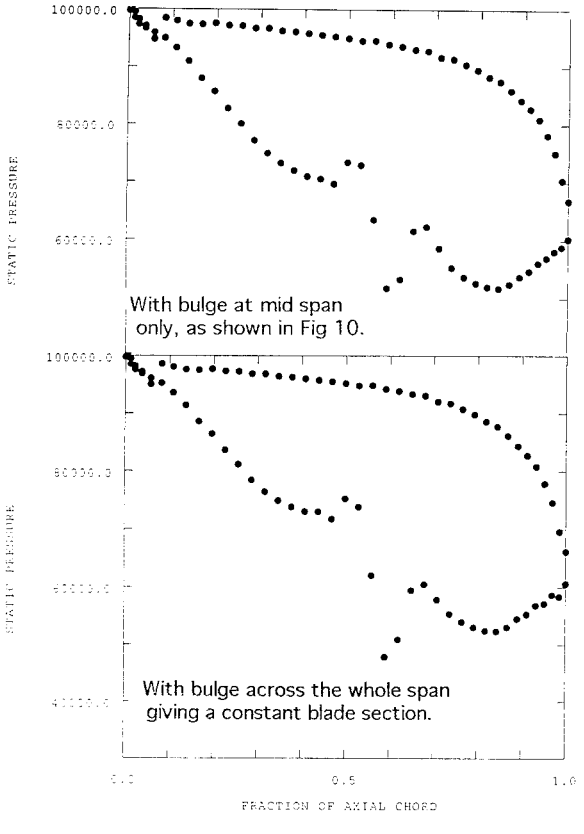

Fig 11. The pressure distribution at mid span for the blade of Fig 10.

The design process starts in exactly the same way as the Q3D one with a one-dimensional mean line calculation to predict the annulus geometry, blade speed, number of blades and mean flow angles. This is again followed by an axisymmetric throughflow calculation. The latter will provide estimates of the required inlet and exit flow angles for all blade rows, of the locations of the leading and trailing edges, of the hub and casing shapes and the streamline positions.

The designer must now decide on how many sections he wants to specify the blade geometry. This depends on the complexity of the blade row but the author's experience is that for many blade rows only three sections are necessary and even for highly twisted rows, such a transonic fans, five sections are sufficient. This is far fewer than are used by many designers. The blade shape will usually be specified on the stream surfaces predicted by the throughflow calculation but cylindrical sections can equally well be used for axial flow machines. The initial guess of the blade geometry on each section can be made in exactly the same way as in the Q3D approach but it is important that the method used to generate blade sections is fast, flexible and user-friendly, so that changes in geometry can be made very quickly. Appendix 1 gives an outline of the Author's method. At this stage the designer must make estimates of the optimum incidence and of the deviation of each section but he does not need to specify the stream surface thickness or its variation through the blade row.

This preliminary geometrical design is done for each section in turn without performing any flow calculations. The sections can now be stacked. Again great flexibility and ease of use is needed to permit changes in stacking when required, but initially the stacking will probably be simple, such as a radial centroid or a radial trailing edge. The data used to generate and stack the blade sections must be saved in a file which can be edited to change the geometry and generate a new data set whenever needed. It is very important that this can be done rapidly with a minimum

of effort on the part of the designer. In the case of the method described in Appendix 1, changes (e.g. modifying the camber line of one blade section and generation of a new 3D data set) can usually be performed in less than one minute.

The geometry of the stacked blade is now used to set up a data set for the 3D flow calculation. This must interpolate in the specified sections to generate as many mesh points as required by the calculation. It is important that this interpolation generates smooth sections with no high order "wiggles" in the geometry. The number of mesh points necessary for the 3D flow calculation at this preliminary design stage depends on the details of the 3D program being used, more points will be needed by a viscous calculation than an inviscid one. It is the author's experience is that a mesh of 19x60x19 points (22000 in total) per blade row is sufficient for a calculation with approximate allowance for viscous effects. Such a course mesh allows rapid turn round of the calculation on a modern workstation. A 3D viscous calculation should need no empirical input in the form of loss coefficients or deviation angles. Even the deviation due to secondary flow near the endwalls is well predicted by such calculations provided the correct inlet boundary layers are input to the calculation. Although the predictions of viscous losses may not be very accurate when using a course grid they are unlikely to be worse than those obtained from empirical correlations. Shock losses are remarkably well predicted even when using a course grid.

Some data on the flow properties must also be fed from the throughflow calculation to the 3D data set to be used as boundary conditions for the 3D calculation. Typically the spanwise distribution of stagnation pressure, stagnation temperature and flow angle must be specified at the inlet boundary and the static pressure distribution at the downstream boundary.

Once the process of generating a 3D data set is complete the 3D calculation can be run. Initially this can be to a very low level of convergence. The author's experience is that the broad details of the 3D flow are well established in about 1/4 of the number of iterations needed to reach the usually accepted convergence criteria. The output can then be inspected, using whatever 3D plotting package is used for visualising 3D results, and the main undesirable features of the flow can be identified. These may include high rates of diffusion, high peak suction surface velocities, strong shocks, high leading edge incidence, incorrect exit angles, etc. The overall characteristics such as mass flow rate and pressure ratio should also be checked for major departures from the design intent at this stage.

In deciding what geometrical changes to make to correc any undesirable features of the flow the designer must use his experience and ingenuity. The first features to correct will probably be the blade incidence and exit angles. These can easily be changed by changing the blade camber line angles at the leading edge and trailing edge respectively. Unless there are large flow separations present, changes in flow exit angle will follow very closely changes in the blade camber line angle at the trailing edge.

Changes in the overall mass flow can also be readily brought about at this stage. For unchoked blade rows, both turbines and compressors, with the usual boundary conditions of specified total to static pressure ratio, the mass flow rate is determined by the exit flow area, ie by $A_a \cos \alpha_2$, where A_a is the annulus area and α_2 is the exit flow angle. Hence the mass flow rate is most easily changed by changing α_2. For choked blade rows the mass flow can only be changed by changing the blade throat area. One of the advantages of 3D time-dependent flow calculation methods is that the calculation automatically finds the mass flow corresponding to the true blade throat area. This avoids the need for complex 3D throat area calculations which are based on geometrical considerations alone. Such calculations which take no account of the flow must be of limited accuracy. Some calculation methods may work with a prescribed mass flow rate rather than a prescribed pressure ratio. In this case the blade exit angle will have to be adjusted to to make the exit pressure agree with the design specification at the specified mass flow.

Having decided on a few major changes of this type the file containing the blade geometry must be edited and the necessary changes made to it. A new 3D data set can then be generated in a matter of seconds and then the 3D flow calculation can be re-run. It is preferable that the latter should restart from the previous solution because this greatly reduces the run time. With a time-dependent method the author's experience is that the major effects of any changes in geometry will be well established after about 500 time steps and so at the preliminary design stage the calculation need not be run to convergence. About four or five geometry changes and 3D runs should be necessary to get the broad details of the flow correct in this way.

Once the overall flow pattern is reasonably well established the detailed blade surface pressure distributions can be considered. In the absence of an inverse 3D method these must be corrected by iteration using the designer's experience to decide on the direction of the changes. The dominating rule is that increasing surface curvature, in the sense of convex surface curvature being positive, will always increase the surface velocity and vice-versa. This rule applies equally in subsonic and supersonic flow. The change in surface curvature may be brought about either by changes in thickness or by changes in camber. The latter are generally more effective but must necessarily affect both blade surfaces. The curvature of the hub and casing way be changed in a similar way and this can have a powerful influence on the flow near the end walls. Changes in blade thickness will change the mean flow velocity across the passage as well as the local value and may affect the throat area.

A second way in which the designer can influence the blade loading is through the blade stacking. Here the main rule is that if only a part of the blade is moved tangentially the pressure field within the row will scarcely change and the section that is moved will tend to take up the pressure distribution that previously prevailed at its new position. Thus moving a section in the direction of the prevailing positive pressure gradient will raise the pressure and lower the velocity on that section. This rule may be used to decide on the effects of endbends and blade lean on the surface pressure distribution. The designer must still use his own judgement of what are good and bad pressure distributions but the predictions of loss obtained from a 3D viscous calculation should help him in this.

After the initial design has been completed using a course grid 3D flow calculation it will usually be necessary to run a fine grid calculation (of order

100000 points) in order to predict the details of viscous effects more accurately. For a rotor or a stage design it will then be possible to predict the efficiency. The result will probably not be of great accuracy because of the limitations of current transition and turbulence modelling. However, at least the trends should be predicted correctly. The author, Ref(12), is continually amazed by how realistic are the predictions of efficiency from course grid calculations using a very crude turbulence model and believes that many loss mechanisms in turbomachines are not dependent on the accurate modelling of viscous effects. For some blade rows it will be necessary to include tip clearance in the calculations since this can greatly influence the flow (Appendix 2) and this will require even more mesh points to be used. Off-design calculations can also be run at this stage if desired, leading to a complete prediction of the machine characteristic.

The number of geometry changes and 3D flow calculations that will be needed to obtain a satisfactory blade row depends on the complexity of the flow and on the time available for the process. Like any other iterative procedure one has to define a convergence criterion for the design. This should be when further efforts on the part of the designer produce changes that are worth less than the cost of his time. Only the designer himself can judge when this point has been reached. The number of 3D calculations used to reach this point may be only about 10 for a nearly two-dimensional blade row up to over 50 for a transonic fan stage. For the complex and aggressive fan stage design described in Appendix 2 about 60 3D flow calculations were performed. If started from a previous solution each course grid calculation takes about 1/2 hour on a modern workstation (or about 3 hours on a PC). The time needed to inspect the results from a calculation, decide on the necessary changes, edit the blade geometry file and generate a new 3D data set is at most 1/2 hour (much less in many cases) and so at least 5 design iterations can be performed per day. Hence the minimum time needed to produce a design ranges from about 2 days for a simple blade row to about 10 days for a complex stage design.

However, it is always advantageous to allow the designer more time to think about the implications of the currently predicted flow pattern before deciding on changes to it. This can be done whilst he is relaxing or working on other tasks and so the author would suggest that about two design changes per day, rather than the maximum number that are achievable, are optimum in respect of the overall use of the designer's time.

6. CONCLUSIONS

The conventional Q3D approach to turbomachinery design has been in use for around 20 years. The next stage in the evolution of the design process will inevitably be the inclusion of more accurate flow calculation methods both as regards three-dimensional effects and viscous effects. It is shown in this paper that it is possible to omit the Q3D blade to blade calculation stage of the current design process and use fully 3D flow calculations to refine the blade shapes. This can now be done for complete stages or even for several stages together. The direct use of 3D methods avoids most of the limitations of Q3D methods and is actually less demanding on the designer's time than is the Q3D approach. An important advantage is that the understanding of the flow behaviour obtained from a 3D design approach is considerably greater than that obtained from the Q3D approach.

The accurate prediction of viscous effects is still not possible and is unlikely to become so for a long time to come. Hence there remains considerable scope for the designer to use his experience and judgement in deciding what is the optimum flow distribution to satisfy his requirements.

REFERENCES

1. Hirsch, Ch, & Denton, J.D., eds., Throughflow Calculations in Axial Turbomachines. AGARD AR175, 1981.

2. Shelton, M.L. Gregory, B.A., Lamson, S.H,. Moses, H.L., Doughty, R.L.& Kiss,T. Optimisation of a transonic turbine aerofoil using artificial intelligence, CFD and cascade testing. ASME paper 93-GT-161. 1993.

3. Potts, I. The importance of S1 stream surface twist in the analysis of inviscid flow through swept linear turbine cascades. I Mech E. paper C258/87. 1987.

4. Walker, P.J. Blade lean in axial turbines: model turbine measurements and simulation by novel numerical method. Ph.D. thesis. Cambridge Univ. 1987.

5. Harrison, S. The influence of blade stacking on turbine losses. Ph D. thesis . Cambridge University, 1989.

6. Grant, J. & Bothwick, D. Fully three dimensional inviscid flow calculations for the final stage of a large low pressure steam turbine. I.Mech. E. paper C281/87. 1987.

7. Lewis, k.L . An investigation into the aerodynamics of shrouded multistage turbines. Ph D thesis. Cambridge University, 1993.

8. Wadia, A.R. & Beacher, B.F. Three dimensional relief in turbomachinery blading. ASME paper 89-GT-151.1989.

9. Wennerstrom, A. J. Experimental study of a high throughflow transonic axial compressor stage. Trans ASME . Vol106, July 1994.

10. Wennerstrom, A. J. & Buzzell, W.A. Redesign of a rotor for a1500 ft/sec transonic, high throughflow single stage axial flow compressor with low hub/tip ratio. AFAPL-TR-79-2078. 1979.

11. Denton, J.D. The calculation of three dimensional viscous flow through multistage turbomachines. ASME paper 90-GT-19. 1990.

12. Denton, J.D. Loss mechanisms in turbomachines. ASME J. Turbomachinery. Vol 115, No 4. Oct 1993.

APPENDIX 1 A BLADE GENERATION AND STACKING METHOD

The blade generation and stacking package used by the author is described in this Appendix. The objectives are to be able to generate blade shapes of any degree of complexity from a minimum of geometrical input. At present the method is only suitable for predominantly axial flow machines with meridional pitch angles up to about 45° but it could easily be extended to design mixed or purely radial flow machines.

The blade sections are first designed as two-dimensional sections on cylindrical surfaces (hence the current limitation to axial flow machines). Each of these sections is associated with a stream surface whose geometry (axial and radial coordinates) is obtained from the throughflow calculation. The inner one of these surfaces must be the hub and the outer one the casing of the machine and any number of stream surfaces can be used between them.

The blade section is specified via its camber line and tangential thickness distribution. The camber line is input as multiple parabolic arcs, mainly because this leads to the simplest equations. The camber line angle α_c is input at an arbitrary number of fractions of axial chord and the slope ($dy/dx = \tan \alpha_c$) is assumed to vary linearly between the points where it is input, if slopes s_1 and s_2 are specified at axial positions x_1 and x_2 then

$$\frac{dy}{dx} = s_1 + \frac{(s_2-s_1)}{(x_2-x_1)} \quad (x-x_1)$$

Which is easily integrated to obtain the shape of the camber line in the region between x_1 and x_2. Typically the slope must be input at about 6 positions to obtain the required degree of control over the camber line shape. There may be discontinuities of curvature but not of slope at the points where the slope is specified.

The blade tangential thickness distribution is specified via the maximum thickness/chord ratio, the axial position of maximum thickness, the leading and trailing edge thicknesses and an exponent p that determines the shape of the curve. The equations used are

$$TK = TKLE + \frac{TKTE-TKLE}{XTE-XLE} (X-XLE) + T$$

Where T is given by

$$T = TKMAX\left[1 - \{ABS(2\ XT-1)\}^P\right]$$

$$XT = \left(\frac{X-XLE}{XTE-XLE}\right)^k$$

$$k = Log(0.5)/Log\left(\frac{XTMAX-XLE}{XTE-XLE}\right)$$

The exponent p determines the shape of the thickness distribution such that p =1 gives a wedge, p = 2 gives a parabolic thickness and higher values of p give more and more blunt distributions. A value p = 2 is most commonly used. In all cases the thickness distribution is transformed using the exponent k so that the maximum thickness occurs at XTMAX. Fig A1.1 shows some of the thickness distributions that can be obtained using these equations.

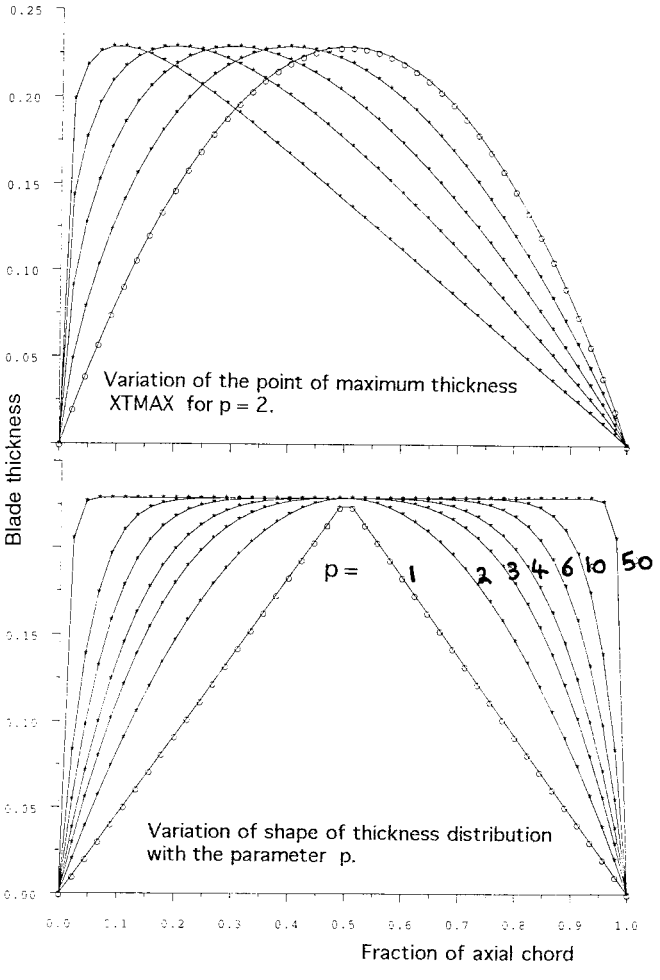

FIG A1.1 Blade thickness distributions obtainable from the equations.

The above equations lead to blunt leading edges and trailing edges with thickness TKLE and TKTE, these are then modified over prescribed fractions of the chord to form elliptic leading and trailing edges The blade suction and pressure surfaces are now formed by adding half the tangential thickness above and below the camber line. The tangential thickness is preferred because there is no possibility of the points crossing as there would be if the perpendicular thickness was used. The completed 2D blade is then viewed on the screen to decide if it is acceptable. Fig A1.2 shows some examples of blades designed using this method.

After producing a suitable blade shape on the cylindrical surface it is then projected onto the stream surface. The basis of this projection is to make

$\frac{dy}{dx}$ in the 2D surface = $r \frac{d\theta}{dx}$ on the stream surface

so that $\left(\frac{d\ r\theta}{dx}\right)_{ss} = \left(\frac{dy}{dx}\right)_{2D} + \theta\left(\frac{dr}{dx}\right)_{ss}$

or integrating with respect to x along the stream surface

$$r\theta = y)_{2D} + \int \theta\ dr$$

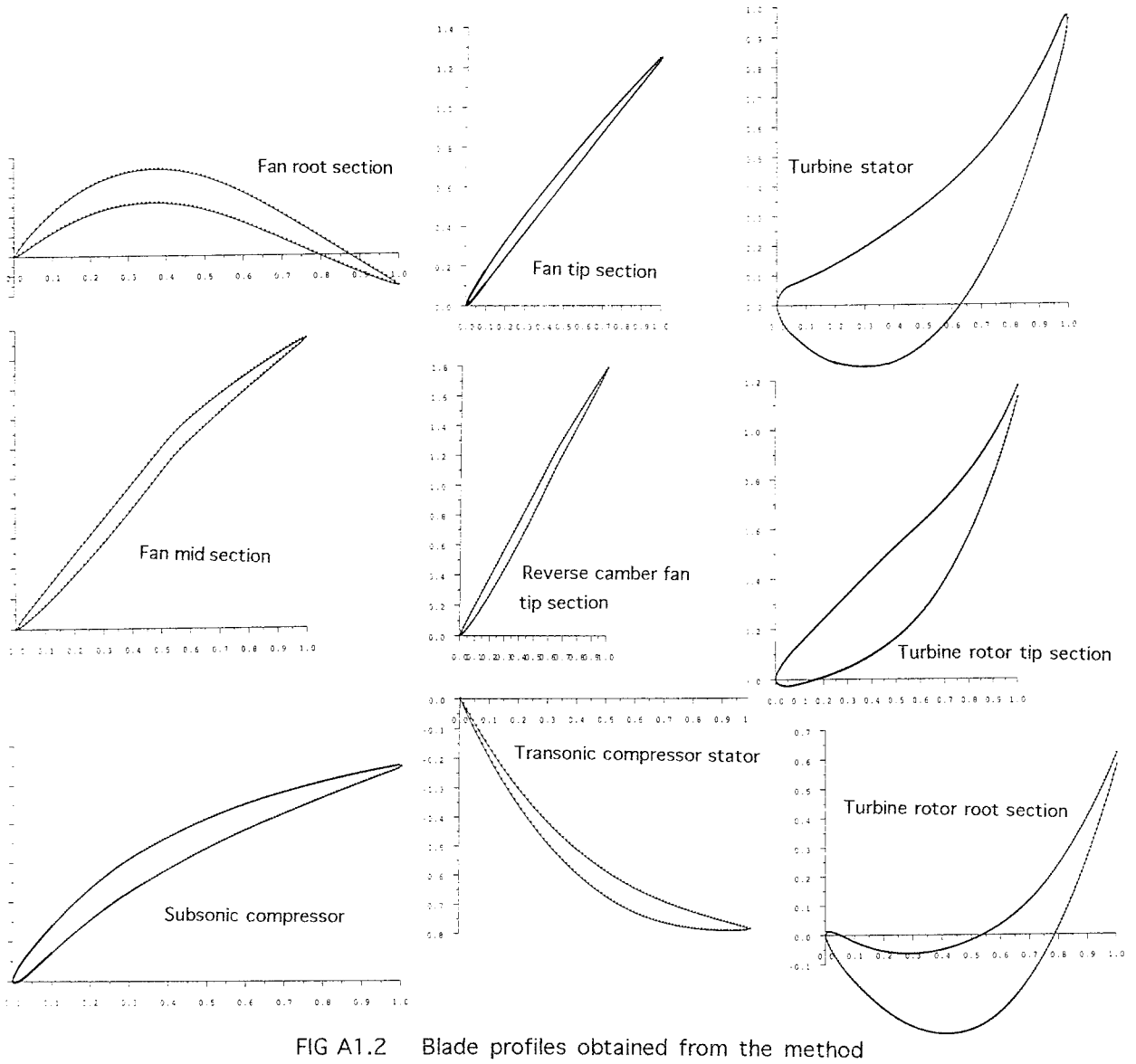

FIG A1.2 Blade profiles obtained from the method

The value of dy/dx is obtained from the 2D section and the above equation is solved by integrating numerically to obtain the value of $r\theta$ that is needed to specify the blade shape on the stream surface. At this stage the angle θ is taken to be zero at the centroid of the section.

The axial positions of the leading edge and trailing edge are specified by the throughflow calculation and the blade is scaled and shifted to fit between these points on the stream surface. The circumferential position of the blade is initially determined by placing its centroid on the axis $\theta = 0$ but it may then be shifted circumferentially through any specified distance in order to change the stacking axis.

Once the blade section has been fitted to the stream surface and stacked its coordinates are stored as the axial, radial and circumferential ($r\theta$) positions of points on the blade surface. An interpolation in these coordinates is then used to obtain the data input required by the 3D flow calculation and this is written to the input file for the latter.

This is done for as many stream surfaces as are felt necessary to specify the blade geometry. It has not yet been found necessary to use more than 5 surfaces.

The above process can be repeated, within the same data set, for any number of blade rows so as to generate a data set for a 3D stage or multistage calculation.

To complete the data set for the 3D flow calculation the distributions of inlet stagnation pressure, temperature and flow angle and the exit static pressure are taken from the throughflow calculation and the values on the 3D grid are obtained by interpolating in these. The number of blades, rotational speed, Reynolds number, gas properties, etc, must also be transferred. Default values of all other parameters required by the 3D flow calculation are built in to the blade generation program and fed to the 3D data set. Thus on completion of the blade design and stacking program a data set for the 3D flow calculation is complete and ready to run.

Once an initial data set for the blade generation and stacking programme has been built up it in this way it can be edited to change any required blade section or flow parameter very quickly, usually the required changes can be made in less than 1 minute and a new 3D data set is then generated in a further few seconds.

APPENDIX 2 THE DESIGN OF A 3:1 PRESSURE RATIO AXIAL FAN STAGE

As an example of the use of the method of design described in this lecture a design exercise was performed with the target of designing an axial flow fan stage (two blade rows) with a tip speed of 533.4 m/s (1750 ft/s) a stagnation pressure ratio of 3:1 and an axial Mach number at the rotor inlet face of 0.75. This is a higher pressure ratio than has been reported in the literature for any purely axial flow stage. The compressor designed and tested by Wennerstrom (Ref 9) had a tip speed of 1500 ft/s , a stagnation pressure ratio of 2.1 and an axial Mach number of 0.56. Wennerstrom's design procedure is well documented by Wennerstrom & Buzzell (Ref10) .

With a casing radius of 0.1 m and a radius ratio of 0.3 at inlet the mass flow corresponding to a mean axial Mach number of 0.75 at the rotor inlet face is 6.1 kg/s. This was the design target. The design can be scaled to different mass flow rates if required. A target total to total efficiency of 85% was guessed.

The reason for this choice of machine as a design exercise was because it represents a machine of great technical interest, at the forefront of aerodynamic and materials technology, for which 3D effects are expected to be very strong. These effects include such features as blade and shock sweep, blade lean, large variations in stream surface thickness and radial migration of the boundary layers, which cannot be calculated correctly by the Q3D approach. The author had no previous experience of designing a machine like this but has designed several conventional transonic fans with pressure ratios between 1.4 and 1.8 . The design process was documented and is outlined below. All the course grid flow calculations were performed on a 50 MHz 486 PC using the author's 3D multistage viscous code. Denton (Ref 11).

Initially a hand calculation was performed, using a guessed efficiency of 85%, to calculate the annulus area ratio between inlet and exit of the fan. Because the machine was to be a fan the frontal area must be as small as possible and the tip radius should not increase through the stage. This ruled out the use of a mixed flow compressor which would have been much easier to design. The hub to casing radius ratio at rotor inlet was chosen as 0.3 to give as high a frontal area as possible for a limited casing radius. To maintain a high blade speed over as much of the span as possible the casing radius was held constant and the hub radius strongly flared outwards to reduce the annulus area and to maintain approximately constant axial velocity. This has the advantage of making the hub behave like a mixed flow compressor. To relieve the loading on the stator blades some swirl was left in the flow leaving the stator, this was chosen vary from 20° at the hub to 10° at the casing.

An initial sketch of the annulus line was made by hand and used to prepare data for a throughflow calculation. The latter was run in the design mode with the loss coefficients first guessed and then adjusted to obtain an efficiency of about 85%.

Initially the throughflow program would not pass the design mass flow because the annulus choked at rotor inlet. This was found to be a result of the high streamline curvature at inlet leading to axially

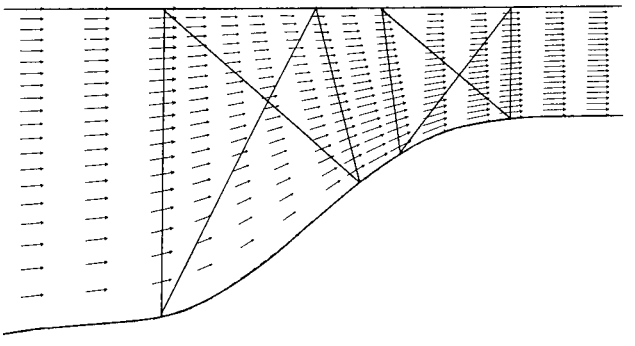

FIG A2.1 Streamlines and velocity vectors from the preliminary throughflow calculation.

supersonic flow near the casing. Reducing the hub curvature overcame this problem and enabled throughflow solutions with the required mass flow to be obtained. Viewing these showed that the streamlines were not smooth, due to insufficient calculating planes, and so more planes were added and the hub coordinates smoothed to obtain an acceptable solution. The annulus line, streamlines and velocity vectors corresponding to this are shown in Fig A2.1.

The results from the throughflow calculation were now used to prepare an data set for the 3D blade generation program. This required about 1 hour using manual data input on only 3 blade sections. The blade generation program was then run to prepare a data set for the 3D flow calculation. This requires negligible CPU time. Initially the 3D calculation refused to run due to an error in the data which took about 1 hour to locate and to correct.

The 3D flow calculation was first run for only 10 steps to produce a plotting file from which the grid and blade sections could be seen on the screen. The hub camber was increased and more grid points added between stator and rotor as a result of this inspection.

The 3D calculation was then run for 1000 steps by which time it had nearly converged. This required about 2.5 hours on the PC. The predicted stagnation pressure ratio was about 2.85 but the mass flow was 10% down on specification and the efficiency was low. Viewing of the output on the screen showed that the rotor was unstarted with a very strong shock in front of its leading edge. Several geometrical modifications and further 3D runs were tried to overcome this problem, but without success, the rotor would not swallow the shock. Since it was not certain whether the problem was in the rotor or due to too little stator throat area it was decided to run rotor alone to see if it would swallow the shock at low back pressure without the stator present.

The blade geometry package was made to produce a data set for the rotor alone . This did swallow the shock at low back pressures. Several geometrical changes and 3D flow calculations were performed on this to achieve a mass flow of 6.3 kg/s at near design pressure ratio. The rotor tip section, for which the relative inlet Mach number is about 1.8, was found to need considerable reverse curvature to keep the surface Mach number and shock strength to acceptable levels.

This rotor was then combined with the original stator. Again the rotor would not start. The problem was clearly in the stator and so the number of stator blades

was increased to 30 (from 20) and their thickness reduced. The stage exit pressure was reduced to 2 bar, well below the design value of 2.5 bar, and the calculation restarted. The rotor now swallowed the shock and the stage ran at something like its design condition, giving a mass flow of 6.11 kg/s with an efficiency of 81% but with a low pressure ratio because of the low exit pressure. There was a strong shock in the stators at this condition.

Having obtained a design that was achieving something like its specified flow a total of about 20 different 3D runs were made with many minor changes to the geometry. These included: Adjusting the tip section to have a kink about 0.6 chord where the shock meets the suction surface. Increasing the rotor leading edge camber at the hub. Increasing the stator inlet angle at the tip. Increased rotor tip exit angle. Adding reverse camber at the rotor hub near the trailing edge. Adding reverse leading edge camber on the rotor mid section. Changing the tip stagger to reduce the mass flow. The axial chord at the rotor tip was also changed to increase the solidity. After these changes the calculation predicted a mass flow of 6.02 kg/s at a pressure ratio of 2.85 with efficiency of 88%.

All the designs calculated so far had only 3 input blade sections. Two more sections at about 25% and 75% span were added to the geometry data set, requiring about 1/2 hour of manual input, and a new blade was generated. At first the flow would again not start but this was soon found to be due to an error introduced in the stator axial position which was reducing the stator throat area. Once corrected the design gave a reasonable flow pattern but the rotor trailing edge was found to be kinked about mid-span when viewed along the machine axis. This was corrected by reducing the rotor camber at mid-span and increasing it at 3/4 span to obtain a smooth trailing edge. When viewed along the axis the rotor suction surface is leaned strongly inwards near the hub. This is not good for the flow, increasing the suction surface velocity near the hub, but is an inevitable consequence of the high twist on the rotor.

Many small adjustments were next made over about 10 3D runs. The rotor hub and 1/4 span sections were increased in thickness because they looked rather weak. The tip and 3/4 span sections were then unstaggered by 1° to restore the mass flow. The maximum thickness point was moved forward at the rotor tip and at 3/4 span in order to generate a wedge shaped leading edge and stronger bow shock. The hub curvature was increased at the stator trailing edge to lower the pressure and reduce the size of the hub corner separation in the stator. The back pressure was increased to 2.4 bar as the design improved so as to achieve a near design pressure ratio. This caused increased incidence onto the stators and so their inlet angle was increased by 2° over the whole span to better accommodate the flow near the design point.

All the designs produced so far had a velocity peak at about 75% axial chord on and near the rotor hub, leading to very strong diffusion towards the rotor trailing edge. No changes to the blade shape at the hub, including reverse camber, seemed to cure this and inspection of the pressure distribution on the whole suction surface suggested that it was due to the hub meridional profile. The hub profile within and immediately downstream of the rotor was redrawn to have concave upwards curvature over the rear of the rotor. The rotor hub exit radius was reduced from 0.06 to 0.058m to

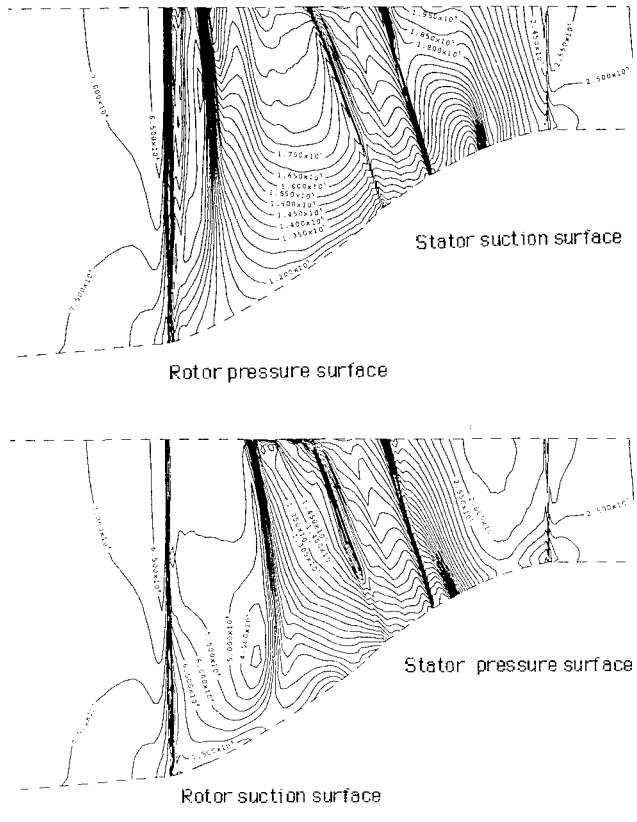

Fig A2.2 Meridional view of the stage with static pressure contours on the blade surfaces.

accommodate this and also to increase the rotor exit area since increases of flow area downstream of the rotor throat help to increase the operating range. The 3D solution showed that this greatly improved the rotor hub pressure distribution but the increase in annulus area at rotor trailing edge increased the swirl into the stators. The stator inlet angle was increased near the tip to accommodate this. The flow now looked quite acceptable so the exit pressure was increased to 2.5 bar at which condition the calculation predicted a pressure ratio of 3.1 at a mass flow of 6.22 kg/s with an efficiency of 86% .

The design was now considered acceptable at the design point. Fig A2.2 shows the meridional view of the final geometry with pressure contours on the blade surfaces. Fig A2.3 shows the Mach number contours near the hub, mid-span and casing and gives an idea of the blade profiles developed. Fig A2.5 shows the associated blade surface pressure distributions.

All sections outboard of mid span had reverse camber over the upstream part of the chord and a sharp "kink" around mid-chord to try to cancel the shock reflection. This is only partly successful because the shock is always strong enough to separate the boundary layer, leading to a thick separated boundary layer behind the "kink". The fluid in this separated region centrifuges outwards and accumulates near the tip. The large wake predicted at the rotor tip, Fig A2.4, is due to this accumulation. This loss core is analogous to the wake of a centrifugal compressor and may be a fundamental limitation on the performance of very high speed axial compressors.

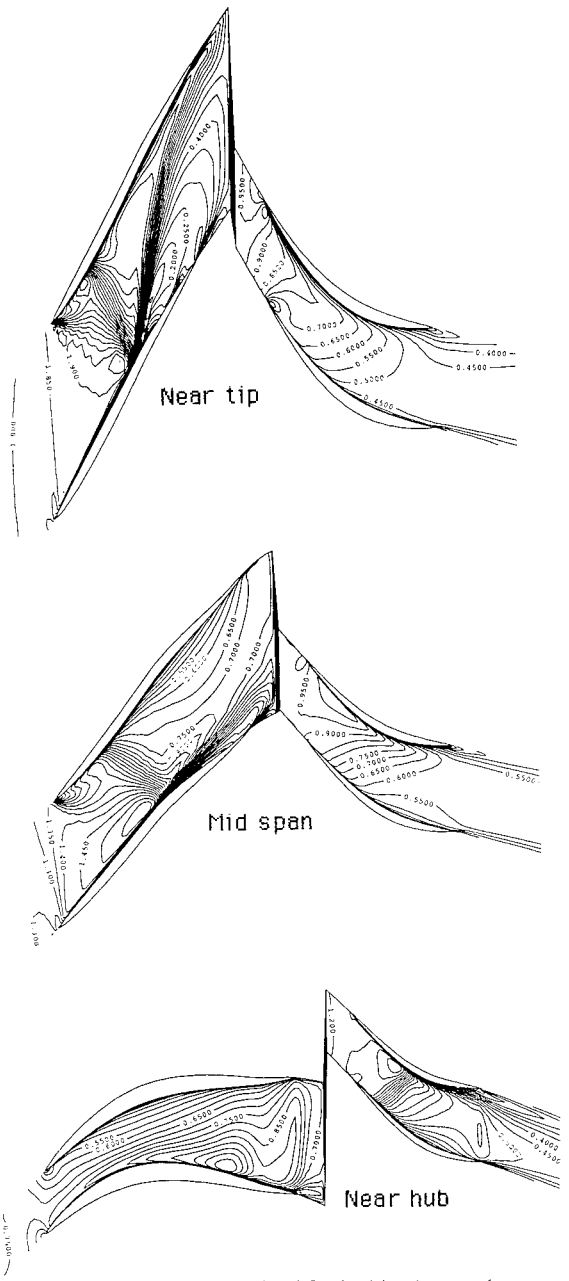

Fig A2.3 Blade to blade Mach number contours at the design point.

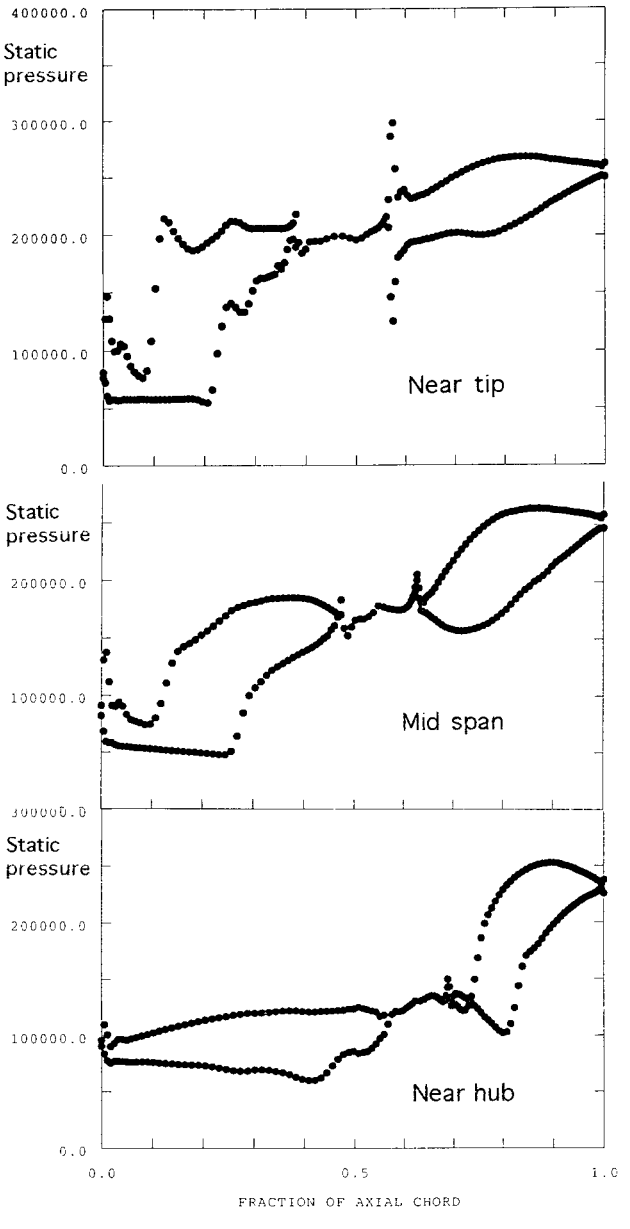

Fig A2.5 Blade surface pressure distributions at the design point.

A few calculations were performed with a finer mesh, 28x164x28 points, and these gave very similar results to the course grid calculations.

The stage has virtually no operating range of mass flow because the rotor remains choked, the mass flow of 6.2 kg/s is slightly above the design target. Because the mass flow does not change the stagnation pressure ratio and total to total efficiency are plotted in Fig A2.6 against the downstream static pressure (which was varied to control the operating point), rather than as is usual against the mass flow. The stator is also choked at low back pressures and most of the changes in pressure ratio and efficiency are due to the changing shock position and losses in the stator. Once the stator unchokes the rotor can stand very little further increase in pressure ratio. This is an inevitable consequence of the large annulus convergence required through the rotor which leads to very little area increase behind the throat. Such an area increase is necessary to stabilise a passage shock. When the rotor stalls the mass flow and efficiency drop very suddenly as the shock moves upstream of the leading edge.

In order to check the performance a fine grid calculation with 33x165x33 points, was run including tip clearance on the rotor. The clearance used was 0.5% of blade span. Tip clearance has a large effect on the flow near the tip but little effect inboard of about 75% span. This is shown in Fig A2.7. The blade Mach number distributions at mid-span and near the hub are almost identical to those from the course grid calculation. The predicted efficiency, mass flow rate and pressure ratio at the design point were not significantly affected by the tip clearance.

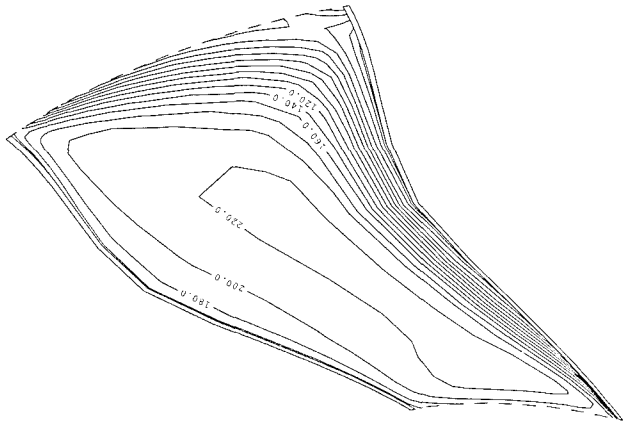

Fig A2.4 Contours of axial velocity at the rotor trailing edge showing the concentration of low velocity flow near the casing.

The above process required about 60 runs of the 3D flow calculation program, excluding those used to generate the overall characteristics. This involved about 150 hours of CPU time on a PC, equivalent to about 30 hours on a modern workstation. The author spent a total of 5 weeks working perhaps 1/4 time on this problem, equivalent to about 1.5 weeks full time work. This should not be taken to imply that a design could be produced in 1.5 weeks full time work. Part-time working on such a problem is advantageous in that it provides time to think between design iterations.

The conclusion of the exercise is that the design targets were achieved in theory but that such a machine has virtually no operating range of mass flow. The predicted flow pattern and performance were not significantly changed by using a much finer mesh than that used for the design process. An extremely important aspect of the exercise is that the designer learned a great deal about the flow behaviour in such high speed compressors and will be in a position to produce a better design more quickly next time. It is considered that the understanding of the flow obtained is much greater than would have been obtained from a Q3D design process and this is a very important advantage of the fully 3D approach.

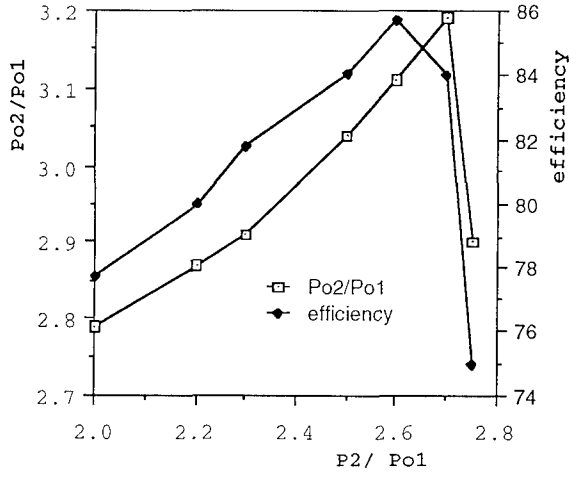

FIG A2.6 PREDICTED FAN CHARACTERISTIC

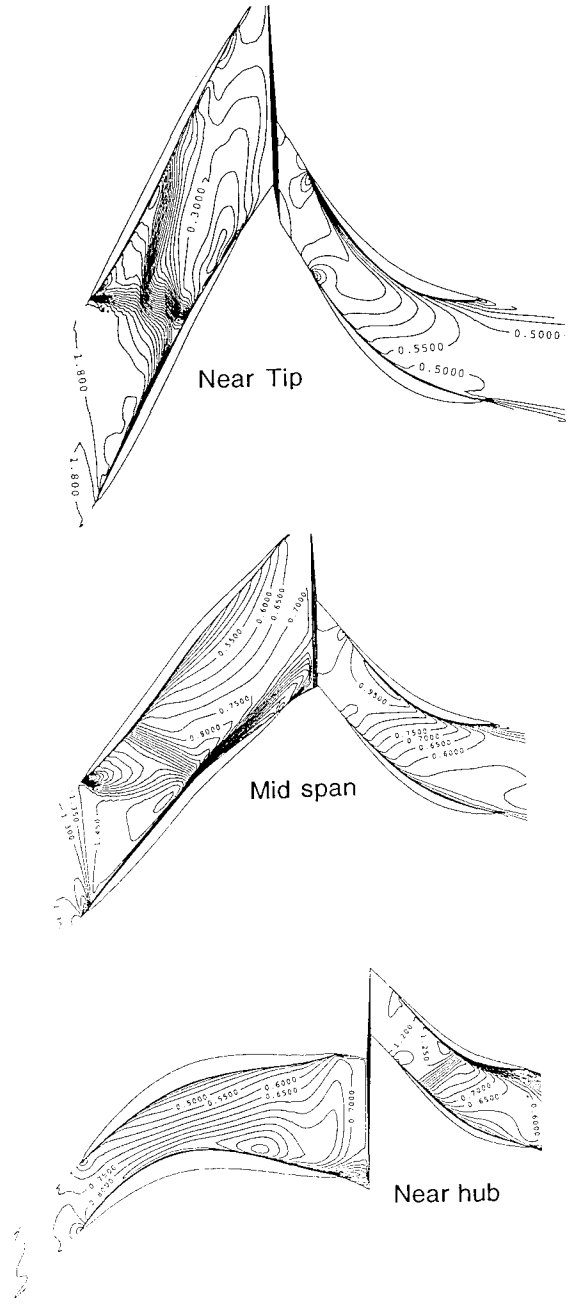

Fig A2.7 Mach number contours from a fine grid solution (33 x 165 x 33) with tip clearance, at the design point.

CFD METHODOLOGY AND VALIDATION FOR TURBOMACHINERY FLOWS

Ch. HIRSCH
Dept. Fluid Mechanics, Vrije Universiteit Brussel
Pleinlaan 2, 1050 Brussels, Belgium

ABSTRACT

The essential problem today, in the application of 3D Navier-Stokes simulations to the design and analysis of turbomachinery components, is the validation of the numerical approximation and of the physical models, in particular the turbulence modeling. Although most of the complex 3D flow phenomena occurring in turbomachinery bladings can be captured with relatively coarse meshes, many detailed flow features are dependent on mesh size, on the turbulence and transition models.

A brief review of the present state of the art of CFD methodology is given with emphasis on quality and accuracy of numerical approximations related to viscous flow computations. Considerations related to the mesh influence on solution accuracy are stressed. The basic problems of turbulence and transition modelling are discussed next, with a short summary of the main turbulence models and their applications to representative turbomachinery flows. Validations of present turbulence models indicate that none of the available turbulence models is able to predict all the detailed flow behavior in complex flow interactions. In order to identify the phenomena that can be captured on coarser meshes a detailed understanding of the complex 3D flow in compressor and turbines is necessary. Examples of global validations for different flow configurations, representative of compressor and turbine aerodynamics are presented, including secondary and tip clearance flows.

NOMENCLATURE

a	convection velocity or wave speed
$\vec{A}$	jacobian of flux vector, with components A,B,C
c	speed of sound
c_p	specific heat at constant pressure
c_v	specific heat at constant volume
d	artificial dissipation function
e	internal energy per unit mass
E	total energy per unit volume
f	scalar flux function
f^*	numerical flux function
f_e	external force
$\vec{F}$	flux vector with components f,g,h
h	enthalpy per unit mass
H	stagnation enthalpy per unit mass
I	rothalpy
k	coefficient of thermal conductivity
k	wave number, turbulent kinetic energy
M	Mach number
n	normal distance
p	pressure
Pr	Prandtl number
q_H	external heat sources
Q	source term
r	gas constant per unit mass
R	residual of iterative scheme
Re	Reynolds number
s	entropy per unit mass
$\vec{S}$	surface vector
t	time
T	temperature
U	column-vector of conservative variables
$\vec{v}$	velocity vector
W_f	work of external forces
x,y,z	cartesian coordinates
Greek	**symbols**
γ	specific heat ratio
$\bar{\delta}$	central-difference operator: $\bar{\delta} u_i = (u_{i+1} - u_{i-1})/2$
Δt	time step
$\Delta x, \Delta y$	spatial mesh size in x and y directions
ε	turbulence dissipation rate
$\lambda(A)$	eigenvalue of matrix A
Λ	diagonal matrix of eigenvalues
μ	coefficient of dynamic viscosity
ρ	density
σ	Courant number
$\bar{\bar{\tau}}$	viscous and turbulent shear stress tensor
$\bar{\bar{\tau}}_R$	Reynolds stress tensor
ν	kinematic viscosity
Ω	volume

TABLE of CONTENT

Presented at an AGARD Lecture Series on 'Turbomachinery Design Using CFD', May to June 1994.

1. INTRODUCTION

The algorithmic methodology of Computational Fluid Dynamics –CFD– has reached, since the mid-eighties, a mature stage enabling to perform reliable numerical simulations of perfect or viscous/turbulent flow models.

Coupled to efficient convergence acceleration techniques, such as multigrid methods, the impressive progress in computer hardware performance has led to the present ability to perform flow simulations with meshes of the order of 100,000 points, in CPU times of the order of one to two hours on workstations, that is minutes of supercomputer time. As a consequence, advanced CFD simulations can be used today at various stages in the design process.

The essential problem is therefore to ensure the reliability of the predictive capability of the simulations, taken into account the numerical factors and the uncertainties of the physical models associated to turbulence, transition, combustion and other physical effects. Other factors affect the outcome of turbomachinery CFD computations, such as the influence of the flow distribution at the inlet of blade rows, tip clearance and cooling flows, unsteady components associated to rotor-stator interactions in multistage environments, to mention the most important ones. Hence, although the exact CFD prediction of all aspects of experimental data might still be somewhere ahead of us, the validation of CFD computations is an essential task, in particular the determination of the range of validity of simulations with varying levels of mesh refinements, from 50,000 to many hundred thousands, and with the present state of turbulence and transition modelling.

In order to guide the reader in the process of distinguishing numerical factors from physical factors, we will discuss the most important elements of present CFD algorithms and the influence of numerical schemes and mesh properties on the computed accuracy. Also, to make clear the requirements on the CFD simulations, the present understanding of the complex 3D flow structure in compressors and turbine blade rows is summarized and representative computations will be discussed. Large references will be made to the 77th PEP Symposium on **"CFD for Propulsion Applications"**, (AGARD CP-510), held in May 1991, where the main focus was on validation of numerical accuracy and of physical models, essentially turbulence and transition modelling.

Since the most important physical models refer to turbulence, a brief review of the most widely used turbulence models and their limitations are presented.

Several examples of computations, taken from our own experience as well as from the literature are presented with various mesh levels and turbulence models, for turbine and compressor blade rows.

2. REVIEW OF CFD METHODOLOGY

In this section we present a short summary of the most important numerical schemes available today, as they result from the algorithmic developments of the last 30, or more, years. We will refer the reader to a selected number of original reference papers and to Hirsch (1988), (1990) for a general presentation of CFD techniques.

We consider the Reynolds Averaged Navier-Stokes (NS) equations as the basic physical model, expressing the conservation laws for mass, momentum and energy and written in conservation form

$$\frac{\partial}{\partial t}\begin{vmatrix}\rho\\ \rho\vec{v}\\ \rho E\end{vmatrix}+\vec{\nabla}\cdot\begin{vmatrix}\rho\vec{v}\\ \rho\vec{v}\otimes\vec{v}+p\,\overline{\overline{I}}-\overline{\overline{\tau}}\\ \rho\vec{v}H-\overline{\overline{\tau}}\cdot\vec{v}-k\vec{\nabla}T\end{vmatrix}=\begin{vmatrix}0\\ \rho\vec{f}_e\\ W_f+q_H\end{vmatrix}$$

or in condensed form

$$\frac{\partial U}{\partial t}+\vec{\nabla}\cdot\vec{F}=Q \qquad (2.1)$$

The time dependent N-S equations are hyperbolic-parabolic in space-time while the stationary NS equations are of mixed type in space, that is elliptic-parabolic for subsonic flows and hyperbolic-parabolic for supersonic flows. The physical interpretation of these properties are of great importance for the choice of a numerical scheme, since an hyperbolic system is dominated by wave propagation (or convection) effects, an elliptic system describes diffusion phenomena, while a parabolic system is associated with damped propagation effects. Note that for high Reynolds number flows, the system of conservation equations is convection dominated in most of the flow region.

2.1. SPACE DISCRETIZATION METHODS

The discretization of the space gradients of the fluxes can be performed by finite difference methods (only on structured meshes) or by finite element (Galerkin or Petrov-Galerkin) or finite volume methods, the last two techniques being applicable to structured as well as unstructured meshes.

Although the finite element approach is certainly the most general one, the finite volume method, which can be considered as a subset of a Galerkin method, is a most widely used technique, because of its generality, flexibility and straightforward interpretation as the direct discretization of the integral form of the conservation equations on a mesh volume cell.

2.1.1. Conservative scheme and numerical flux

The integral form of the conservation laws is written for an arbitrary volume Ω, bounded by the control surface S

$$\frac{\partial}{\partial t}\int_\Omega U\,d\Omega+\oint_S\vec{F}\cdot d\vec{S}=\int_\Omega Q\,d\Omega \qquad (2.2)$$

Integrating from $t=n\Delta t$ to $(n+1)\Delta t$ for Ω selected as a control volume associated to a node or cell J, fig.1,

$$\int_{\Omega_J}U^{n+1}\,d\Omega=\int_{\Omega_J}U^{n}\,d\Omega-\sum_{\text{sides}}\int_n^{n+1}\vec{F}\cdot\Delta\vec{S}\,dt+\int_n^{n+1}dt\int_{\Omega_J}Q\,d\Omega$$

The conservative discretization defines the cell-averaged conservative variable $\overline{U}_J^n$ at time $n\Delta t$ and the numerical flux $\vec{F}^*$ over each side, together with the cell-averaged sources $\overline{Q}_J^*$, via

$$\overline{U}_J^{n+1}\,\Omega_J=\overline{U}_J^{n}\,\Omega_J-\Delta t\sum_{\text{sides}}\left[\vec{F}^*\cdot\Delta\vec{S}\right]+\Delta t\;\overline{Q}_J^*\,\Omega_J \qquad (2.3)$$

This is an exact relation for the time evolution of the averaged conservative variables $\overline{U}_J^n$ over cell J. It is important to observe that there is no mesh point associated to $\overline{U}_J^n$ which is attached only to cell J.

The numerical flux identifies therefore a scheme by the way it approximates the time-averaged physical flux along each cell face. In order to fulfil conservativity at the discretized level, the estimation of the numerical flux at a given cell face must be independent of the cell to which the face belongs.

The space discretization is therefore completely defined by its numerical flux, leaving open the choice of the time integration. A general numerical scheme can then be defined as a system of ordinary differential equations in time by, removing the overbars on the variables U_J,

$$\frac{dU_J}{dt}\Omega_J = -\sum_{sides}\left[\vec{F}^{\,*}\cdot\Delta\vec{S}\right] \equiv -\Omega_J R_J \qquad (2.4)$$

or in a one-dimensional form

$$\frac{dU_i}{dt} = -\frac{1}{\Delta x}\left(f^*_{i+1/2} - f^*_{i-1/2}\right) \equiv -R_i \qquad (2.5)$$

Note that the form (2.3) includes also coupled space-time discretizations, depending on the definition of the numerical flux.

2.1.2. Central schemes with combined space-time discretizations

The Lax-Wendroff (1960), (1964) family of schemes, and their Predictor-Corrector nonlinear variants, e.g. the MacCormack scheme (1969), (1971), were the reference schemes in the 70's and early 80's. Their importance comes from the fact that the Lax–Wendroff (L–W) scheme is the unique second order central explicit scheme for the one-dimensional linear convection equation on a three point support, and plays an essential role as guideline for all schemes attempting to improve certain of its deficiencies. The essential property of the Lax-Wendroff schemes lies in the combination of time and space discretizations, whereby the numerical flux depends on the time step. This is required in order to achieve second order accuracy with an explicit time integration and the Lax-Wendroff schemes are therefore the simplest explicit schemes of second order accuracy in space and time.

Many extension of the L–W schemes can be defined for nonlinear fluxes, even in one dimension. They all reduce to the same linear form and are generally structured as predictor-corrector algorithms with an explicit time integration. The numerous variants of the Lax-Wendroff scheme differ in the treatment of the non-linearities and in their multidimensional aspects, but reduce to the same linearized, one-dimensional form. The popularity of these schemes, and in particular the two step version of MacCormack (1969), was due to their second order accuracy and simplicity, although their behaviour around discontinuities is not fully satisfactory. One drawback, and part of the ground for the present loss in popularity of these schemes, is connected to the fact that for steady state problems the numerical solution depends upon the non-physical time step applied to reach the steady state. This is however more of a conceptual weakness, since the associated error is of the order of the truncation error, but in addition, more recent approaches, based on separate space and time integrations, lead also to better convergence performances.

The Lax-Wendroff numerical flux can be defined in various, linearly equivalent, ways but having different non-linear forms

$$f^*_{i+1/2} = \frac{1}{2}\left(f_i + f_{i+1}\right) - \frac{\Delta t}{2\Delta x} A_{i+1/2}\left(f_{i+1} - f_i\right) \qquad (2.6)$$

written here in a one-dimensional form. Alternative formulations, based on Roe's Jacobian matrix, are defined by

$$A_{i+1/2} = \begin{cases} \dfrac{f_i - f_{i+1}}{U_i - U_{i+1}} & \text{if} \quad U_i \neq U_{i+1} \\ A(U_i) & \text{if} \quad U_i = U_{i+1} \end{cases}$$

$$f^*_{i+1/2} = \frac{1}{2}\left(f_i + f_{i+1}\right) - \frac{\Delta t}{2\Delta x} A^2_{i+1/2}\left(U_{i+1} - U_i\right)$$

These schemes still need additional dissipation terms to remove shock oscillations.

In the field of turbomachinery, several well-known programs have been developed based on the Lax-Wendroff approach. In particular, the 2D time marching method of P.Mc Donald (1971) was based on a modified Lax-Friedrichs scheme, with 'corrected viscosity' enabling to come close to second order accuracy at steady state convergence. Note that Mc Donald (1971) is probably the first application of a finite volume method to the Euler equations. Another scheme for the Euler equations has been developed along similar lines by Denton (1975), (1982) and has been widely used in the field of internal turbomachinery flows. The method of Ni(1982) is the first multigrid application to the 2D Euler equations and is based on a reformulation of the standard L–W scheme, applied to cascade flows. It has been extended to 3D flows by Koeck (1985) for external aerodynamics. The MacCormack scheme has been applied by Veuillot and Meauze (1985) to various single and multistage configurations; see also Fourmaux and Le Meur (1987).

2.1.3. Central schemes with separate space and time discretization

In this approach the physical flux is discretized centrally as

$$\left[\vec{F}\cdot\Delta\vec{S}\right]_{i+1/2} = \frac{1}{2}\left[\vec{F}_i + \vec{F}_{i+1}\right]\cdot\Delta\vec{S} \qquad (2.7)$$

This choice for the numerical flux does not lead to stable schemes, since there is not enough numerical dissipation. Therefore artificial dissipation terms are required in order to remove the odd-even oscillations due to the central discretization (high frequency oscillations) and to provide shock capturing without oscillations. The most current formulation, following Jameson et al. (1981), Jameson (1982), is formed by the sum of a second order term with nonlinear coefficients for shock capturing and a linear fourth order term for background oscillations.

The numerical flux takes the form

$$\vec{F}^{\,*}_{i+1/2}\cdot\Delta\vec{S} = \frac{1}{2}\left(\vec{F}_i + \vec{F}_{i+1}\right)\cdot\Delta\vec{S} - d_{i+1/2} \qquad (2.8)$$

where Jameson's artificial dissipation (1D form) terms are defined by

$$d^J_{i+1/2} = \varepsilon^{(2)}_{i+1/2}\left(u_{i+1} - u_i\right) -$$

$$-\varepsilon^{(4)}_{i+1/2}\left[\left(u_{i+2} - u_{i+1}\right) - 2\left(u_{i+1} - u_i\right) + \left(u_i - u_{i-1}\right)\right]$$

$$\varepsilon^{(2)} = \kappa^{(2)}|a|\nu \qquad \varepsilon^{(4)} = \mathrm{Max}\left[0, \left(\kappa^{(4)}|a| - \varepsilon^{(2)}\right)\right]$$

with the pressure sensors

$$\nu_i = \frac{\left| p_{i+1} - 2p_i + p_{i-1} \right|}{p_{i+1} + 2p_i + p_{i-1}}$$

For Navier-Stokes equations, the viscous dissipation is not sufficient at the scale of the mesh, at least for high Reynolds number flows, to provide enough physical damping. Therefore, the artificial dissipation terms remain necessary even for N-S computations. The difficulty encountered with this approach is that the solution and convergence can be strongly dependent on the coefficients.

This is today one of the most widely used approaches, either with explicit or implicit time integrations.

2.1.4. The upwind approach

Upwind methods aim at introducing informations, at the level of the discretization, taken from the physical properties of the system of conservation laws, in particular for the inviscid convective fluxes. Since the system of Euler equations is hyperbolic, that is dominated by propagation properties, one can distinguish two levels of upwind approaches:

First level: One takes into account the directional properties in function of the sign of the wave propagation speed. This leads to the Flux Vector Splitting schemes of Steger-Warming (1981), Van Leer (1982), where the inviscid fluxes are separated according to the direction of propagation of the associated waves, obtained from the sign of the eigenvalues of the Jacobians of the flux vectors.

Separating the jacobian matrix A into $A=A^+ + A^-$, the positive and negative flux components are obtained from the property of homogeneity of the inviscid fluxes, as

$$f = A\,U \quad \text{and} \quad f^{\pm} = A^{\pm} U$$

The positive flux component is discretized by a backward (upwind) difference, and the negative component by a forward difference, leading to the associated numerical flux for the first order upwind scheme

$$\begin{aligned} f^*_{i+1/2} &= f^+_i + f^-_{i+1} \\ &\cong \frac{1}{2}(f_i + f_{i+1}) - \frac{1}{2}\left|A\right|_{i+1/2}(U_{i+1} - U_i) \end{aligned} \qquad (2.9)$$

The second equation is an approximation, valid to first order accuracy, representing the upwind scheme as a central scheme plus dissipation terms, in the same line as equ. (2.8).

Second level: Here one takes into account properties of exact solutions of the system of Euler equations, namely the solution of the Riemann problem. This was introduced by Godunov and extended to second order by Van Leer (1979). The basic first order Godunov method involves three steps i) Define a piecewise constant approximation at $t=n\Delta t$; ii) Solve the local Riemann problem at the interface between two cells; iii) Average the new solution after time step Δt.

The approach in use today is based on approximate Riemann solvers, Roe (1981), Osher (1982), which are less costly than the exact solutions of the Riemann problem. Roe's scheme, also called flux difference splitting (FDS) is based on the following definition:

Find a matrix $\bar{\bar{A}}$ which satisfies exactly

$$f_{i+1} - f_i = \bar{\bar{A}}(U_i, U_{i+1})(U_{i+1} - U_i) \qquad (2.10)$$

combining conservativity and wave decomposition. The numerical flux is defined exactly for the first order FDS scheme by

$$f^*_{i+1/2} = \frac{1}{2}(f_i + f_{i+1}) - \frac{1}{2}\left|\bar{\bar{A}}\right|_{i+1/2}(U_{i+1} - U_i) \qquad (2.11)$$

The extension to second order requires a series of non trivial steps. They are based on the replacement of the piecewise constant approximation by piecewise linear solutions, following Van Leer (1979). For nonlinear problems an alternative is flux extrapolation instead of the above variable (so-called MUSCL) approximation.

However, the second order upwind schemes do not prevent oscillations around shocks and measures have to be taken to avoid the creation of unwanted numerical oscillations. The only way to combine second order accuracy with monotonicity is the introduction of nonlinear components in the schemes. This has led to the introduction of limiters, to control and limit the solution gradients, preventing the appearance of oscillations. The most popular formulation is based on the concept of Total Variation Diminishing (TVD) schemes, introduced by Harten (1983), (1984). In order to obtain a second order TVD scheme, it is necessary to write the scheme as a first order, monotone contribution plus additional terms. These additional terms are then restricted, in a non-linear way, such as to satisfy the TVD conditions. The introduction of limiters, leading to nonlinear schemes is a major achievement of CFD research of the 1980's.

2.1.5. Unified formulation of central and upwind schemes

The formulation of second order upwind schemes based on flux extrapolation instead of variable extrapolation, allows to express all numerical fluxes as a sum of the centred physical flux plus additional terms, equ. (2.8), which act as dissipation terms. From this point of view, an upwind TVD scheme can be seen as a rational way to derive appropriate dissipation terms. As example, one possible extension of the first order FDS scheme (2.11) is given by the 'Symmetric' TVD scheme, Yee (!985), (1987)

$$f^*_{i+1/2} = \frac{1}{2}(f_i + f_{i+1}) - \frac{\beta}{2}\left[1 - Q\left|\bar{\bar{A}}\right|\right]_{i+1/2}(U_{i+1} - U_i) \qquad (2.12)$$

with $\beta>1$ for the scheme to be TVD and where Q is a limiter function depending on ratio's of gradients of the solution.

A large number of options are available in the literature for the choice of dissipation terms, from central to various upwind TVD forms, giving all nearly identical results on fine enough meshes, for inviscid flows, certainly in the subsonic, transonic to low supersonic range, as encountered in turbomachinery flows.

2.2. TIME INTEGRATION METHODS

For separate space and time discretizations a choice can be made between explicit multistage schemes or implicit multistep (relaxation) schemes. The general family of Runge-Kutta (R–K) methods for the semi-discretized scheme

$$\frac{dU}{dt} = -R$$

is defined by, for k-stages

$$\begin{aligned} U^{(1)} &= U^n \\ U^{(2)} &= U^n - \alpha_1 \Delta t\, R^{(1)} \\ &\cdots \\ U^{(k)} &= U^n - \alpha_k \Delta t\, R^{(k-1)} \\ U^{n+1} &= U^n - \Delta t \sum_{j=1}^{k} \beta_j R^{(j)} \end{aligned} \qquad (2.13)$$

The stability region can be extended to CFL=(k–1) while the α-coefficients can be optimized for optimum damping properties. The R–K methods are very frequently applied today, in combination with a variety of convergence acceleration techniques.

The implicit multistep (relaxation) schemes, have been introduced by Beam and Warming (1978) and a simplified form is given by the one parameter (θ) family

$$U^{n+1} = U^n - \Delta t\left[\theta R^{n+1} + (1-\theta) R^n\right] \qquad (2.14)$$

with appropriate linearization of the residual at time (n+1). This introduces jacobian matrices in the left hand side and the necessity to apply efficient solution algorithms for the algebraic system. The original Beam and Warming method introduced an approximate dimensional factorization of the implicit operators leading to block tridiagonal systems.

$$\left[1+\theta\,\Delta t\,\overline{\delta_x}\,A^n\right]\left[1+\theta\,\Delta t\,\overline{\delta_y}\,B^n\right]\Delta U^n = -\Delta t\,R^n \qquad (2.15)$$

Although unconditionally unstable for the 3D Euler equations, the method provides good results for both Euler and Navier-Stokes equations, in presence of the indispensable dissipation terms.

Applying concepts from the upwind methodology, one can replace the central difference of AΔU by an upwind discretization.

$$\overline{\delta}_x A^n \Rightarrow \delta_x^- A^+ + \delta_x^+ A^-$$

The resulting system can be made diagonal dominant, which allows a variety of relaxation techniques, such as point, line over-relaxations to be applied to the time marching problems. Other techniques, such as LU decompositions are also applied and a large variety of options are available and can be optimized for maximum damping properties.

At the PEP 77th Symposium on **"CFD for Propulsion Applications"**, AGARD CP-510 (1991), an overview of a large number of turbomachinery codes were presented. Applications of the Jameson-type code based on central space discretizations, artificial dissipation and explicit, R–K type time integrations was reported by Gerolymos (Paper 11) , Sehra et al (Paper 13) , Chima (Paper 21), Birtch and Kitchen (Paper 25). Other codes based on this approach have been developed by Arnone, Liou and Povinelli (1991), Jennions and Turner (1992). The codes developed by Dawes (1986), (1988) are based on a similar approach but with a simplified combination of a two stage R-K scheme with implicit residual smoothing.

Flux difference splitting, with implicit time integration based on a Beam and Warming approximate factorisation, is applied by Dorney and Davis (1991) and by Dutoya et al (Paper 29), although these codes can differ strongly by their practical implementation. The codes developed by Escande and Cambier (Paper 14) and Lemeur (Paper 23) at ONERA are based on a Lax-Wendroff two step scheme with artificial dissipation. In the code of Hirsch et al (1991) a unified formulation of central and upwind schemes is introduced, by a choice of different dissipation expressions, whereby all the schemes are written as central fluxes plus additional terms. Similarly, both explicit and implicit time integrations can be applied as different options for a multigrid smoother.

2.3. PRESSURE CORRECTION METHODS

Pressure correction methods form a different family of schemes, which were originally developed for incompressible flows. The methods falling in this class can be applied to the stationary as well as to the time dependent incompressible flow equations. They consist of a basic iterative procedure between the velocity and the pressure fields, through the solution of a Poisson equation for the pressure. In this approach, the discretized continuity equation is transformed into an equation for the pressure by introducing the unknown velocities taken from the discretized momentum equations. The most current formulations are variants of the method introduced by Patankar and Spalding (1972), known as the SIMPLE algorithm, see also Patankar (1980). The method can be summarized as follows: for an initial approximation of the pressure, the momentum equation can be solved to determine the velocity field. The obtained velocity field does not satisfy the divergence free, continuity equation and has therefore to be corrected. Since this correction has an impact on the pressure field, a related pressure correction is defined, obtained by expressing that the corrected velocity satisfies the continuity equation. This leads to a Poisson equation for the pressure correction. The pressure correction method has been extended to handle compressible and transonic flows, see for instance Hah (1984), (1987b), Moore and Moore (1989) for turbomachinery applications.

In AGARD CP-510 (1991), various authors reported interesting results with this approach. Moore and Moore (Paper 4) presented a fully elliptic formulation applied to a turbine blade row with tip clearance. This code is based on an original, multidimensional upwind definition of control volumes, leading to a scheme with reduced cross-diffusion and hence, improved spatial accuracy. Additional validation tests of this code are reported by Cleak and al (Paper 8). Another code, based on a staggered mesh, SIMPLE-type, fully elliptic algorithm, is applied by Abou Haidar et al (Paper 34) for an interesting comparison of different turbulent models in S-bends. The code makes use of a quadratic, upwind discretization of the convection terms. Fotea et al (Paper 35) , on the other hand, rely on a parabolized Navier–Stokes approximation for duct flow computations, while Rachner (Paper 37) applies a non-staggered grid formulation, coupled to a zonal approach, with a particular attention to the pressure–velocity decoupling problem. This paper contains a detailed investigation of the numerical accuracy of various boundary treatments at solid walls and at zonal interfaces. A very similar approach is followed by Coelho and Pereira (Paper 30). All these codes are applied to incompressible flows, with the exception of Hah (Paper 10) who applies his code to a transonic compressor rotor, including tip clearance.

2.4. CONVERGENCE ACCELERATION AND MULTIGRID TECHNIQUES

The practical application of CFD simulations in the design environment requires accurate, but also efficient algorithms in terms of overall CPU times, for reasons of cost and turnaround time of a computation.

Implicit methods which are linearly unconditionally stable and allow in principle to apply high CFL values, can be made to converge very rapidly, in hundreds of time steps, instead of many thousand time steps for standard R–K or L–W methods. However, this requires efficient solvers for the coupled algebraic systems of the implicit operators. Iterative, relaxation methods are generally not efficient enough and the development of more sophisticated methods is an area of current research.

Within the framework of explicit methods, various techniques are currently applied for steady state computations, such as local time stepping, the addition of an implicit residual smoothing step to the explicit multistage R–K, leading to computations with CFL values of the order of 6-7 with four or five stages.

The most general and most efficient acceleration technique is the multigrid method, which can be applied for structured as well as unstructured meshes to the multidimensional Eu-

ler and Navier-Stokes equations. The basic methodology consists of the following steps: i) Time advancing the solution with the convergence operator tuned for maximal damping properties in the high frequency range of the error spectrum. This operator can be considered as a 'smoother' and both R–K multistage or implicit relaxation methods can be applied; ii) Transfer the corrections on a coarser grid; iii) Solve the corrected problem on the coarser grid, damping the high frequencies on that grid; iv) Transfer the corrections back to the fine grid. A variety of strategies can be applied and the choice of best smoother may also depend on the computer architecture. A representative example of efficient computation can be found in Arnone, Liou and Povinelli (1991), Arnone (1993), for a central scheme and R–K time stepping. Calculations of the NASA transonic rotor 67, with near to 330,000 points, require close to 200 cycles for four orders of residual reduction and about 35 minutes on the NASA Lewis RC CRAY Y-MP computer.

3. ACCURACY OF SCHEMES AND GRID DEPENDENCE

Although Navier–Stokes computations are currently becoming the most widely applied approach to practical flow simulations, a certain number of difficulties have still to be considered, in order to achieve fast and accurate computational results. A most important item deals with the question of the numerical errors in viscous solutions, as generated by various schemes and grids.

3.1. VISCOUS RESOLUTION OF VARIOUS SCHEMES

It can be considered today that all second order schemes will produce nearly identical results on fine enough meshes, certainly for Euler flow calculations and, at a higher degree of mesh resolution, for N–S computations. However, on coarser grids more significant differences can appear, reflecting the ways different schemes treat their numerical dissipation. But even on fine meshes, there appears to be more important differences for viscous flows. In particular, it is known that the dissipation of standard flux vector splitting schemes, such as the Steger-Warming or Van Leer flux splitting schemes, has to be carefully monitored to avoid excessive drag predictions because of too much numerical dissipation in the viscous regions.

To show the influence of the space discretization (upwind, central) and the mesh quality (stretching method, number of points in the boundary layer) on accuracy, a subsonic flat plate problem, both for laminar and turbulent flows, is considered at a high Reynolds number of 10.5×10^6 per meter and a free stream Mach number (M_∞) of 0.35. The turbulent viscosity is calculated by using an algebraic Baldwin-Lomax model. A 4-level MG procedure, using a V-cycle sawtooth with a 5 stage Runge-Kutta scheme is applied to compute the flow. A central difference scheme, using a fourth order scalar artificial dissipation model with a modification for high-aspect ratios, and a second order symmetric TVD scheme, with a Van Leer limiter, are used to discretize the convective fluxes. To accelerate the convergence a local time step and implicit residual smoothing are used, allowing CFL=7 for the central scheme and CFL=4 for the upwind calculations. At the inlet the total pressure, the total temperature and the flow angle are imposed and the Mach number is extrapolated from the inner flow field. The pressure is specified at the upper and downstream boundaries, and the other variables are extrapolated. The solid wall is treated as an adiabatic wall and a no-slip condition is enforced.

For the laminar calculation a mesh containing 41x81 cells, in the x and y directions respectively is used. The grid is parabolically stretched in X-direction (PX), with an exponential stretching in the Y-direction (EY), resulting in a maximum aspect ratio of about 1900. Results are also presented for a coarse mesh (21x41,c) and a very coarse mesh (11x21,vc) obtained from the finer one by taking out every other point. The grids used for the turbulent calculations contain 41x81 cells. Results are presented on a uniform mesh (UX) and on a parabolically stretched mesh (PX) in X-direction. In the Y-direction an exponential and a parabolic stretching procedure is applied, resp. EY and PY resulting in a maximum aspect ratio of 4000 (UX) or 7900 (PX). The y^+ value of the first point is about 0.45 and there are at least 8 points with y^+ value less than 10 for the exponential mesh and at least 3 points for the parabolic one.

Influence of the discretization scheme

For the laminar case the velocity and the skin-friction profiles calculated with an upwind and a central scheme are shown in figures 2 and 3. The agreement of the velocity profile with the Blasius solution is very good for the upwind calculation on both the fine and the coarse grids (with resp. 50 and 25 points in the boundary layer). The central scheme gives reasonable results on a fine grid, but rather poor results on the coarse mesh. On a very coarse mesh, with only 12 points in the boundary layer, the accuracy of the upwind scheme is better than the central scheme on the coarse grid. The difference between a central and an upwind calculation is also seen in the skin-friction profile (fig.3). The results obtained with both schemes on the fine mesh are nearly identical, but on the coarse and very coarse grids the upwind scheme remains very good, while the central scheme shows a lack of accuracy, indicating too much dissipation in the viscous layer. This has also been reported elsewhere by Allmaras (1992). Recent work by Jameson and coworkers, Jameson (1993), Tatsumi, Martinelli, Jameson (1994) demonstrate that introducing some forms of limiting on the fourth order dissipation terms cures the problem, leading to the same accuracy as upwind schemes.

Similar results are also obtained with the turbulent calculations. The velocity profiles, in the non-dimensional turbulent quantities y^+ and u^+, show a good agreement with the empirical law of Musker for the results on all the meshes for the upwind scheme, while the central scheme leads to a loss of accuracy on coarser meshes (fig.4). The skin friction variations are in good agreement with the empirical profile of Nikuradse for the coarse and the fine mesh (fig.5), although the results for the central scheme are somewhat different, because there is no stretching used in X-direction. For the very coarse grids both schemes show similar differences from the reference, probably due to the fact that the first point is further from the wall ($y^+ \cong 2.5$).

The influence of the stretching method in the near wall region is investigated by comparing the exponential (PX/EY) and the parabolic fine (PX/PY) (41x81) meshes, combined with upwind and central discretization schemes. As seen from figures 6 and 7, the parabolic mesh leads to an innacurate result for the central scheme, which seems more sensitive to the spacing of the near-wall cells. The profiles of velocity and skin-friction on the exponential mesh are nearly identical for the upwind and the central calculations. These comparisons indicate that the critical parameter, for the central scheme, is the clustering of mesh points near the wall. The exponential mesh has a linear distribution in (log y), while the parabolic mesh has a spacing increasing as y^2, which clearly is not a good choice.

The problem of excesssive numerical dissipation becomes particularly severe in unsteady flows, were time accuracy is strongly dependent on space accuracy. When the relevant space and time scales of the computed flow are large compared to the step sizes, the computed solutions are reliable with most of the current methods, provided sufficient space resolution is applied. However, with spontaneous, self-induced flow unsteadiness, such as the Von Karman street behind a cylinder at high Reynolds numbers, the separating vortices are created out of the very small vortices formed at

the solid wall surface and subsequently growing in time. Since the numerical dissipation acts as a filter on the small scales, the time development of the flow will be very sensitive to mesh configurations and to the numerical scheme. This is illustrated by figure 8, taken from Hänel (1991), which shows the influence of mesh configuration and numerical dissipation for a central scheme on the time evolution of the laminar vortex street around a circular cylinder. The figure shows the time history of the lift coefficient, for different grid stretchings. Particularly interesting is the non-zero average lift coefficient when a tangential stretching is introduced, fig. 8a, revealing a non-symmetrical development of the vortex street. This effect disappears on a circumferentially uniform mesh, but a very strong dependence of the value of the fourth order numerical dissipation is clearly seen. Similar dependencies have been reported on other geometries and with other schemes. This creates a major difficulty for the computation of unsteady flows, particularly in 3D and in presence of geometrical complexities. At present, there is no known solution to these difficulties, unless use is made of excessive, and probably prohibitive, fine meshes. It has to be mentioned however, that these problems might be slightly less severe in turbulent flows because of the higher value of the physical dissipation generated by turbulence.

3.2. MESH QUALITY AND MESH REFINEMENT

All available experience in CFD applications indicates that the mesh definition and quality has a considerable influence on accuracy and convergence properties. Although uniformity of a mesh is always to be recommended, geometrical and modelling constraints makes it often difficult to achieve this desired objective. The question of mesh aspect ratio in viscous layers has already been discussed in the previous sections, and we will discuss here the problems of mesh skewness and refinement.

3.2.1.Influence of mesh skewness

In turbomachinery bladings with high stagger or high turning, the courant practice of H or C-meshes with periodic boundaries leads to highly skewed meshes. This has detrimental effects on the accuracy of the computed flow, as can be seen for instance from the calculations of Horton, Harasgama and Chana (1991), who compare results on four different H-meshes of a nozzle guide vane with high exit angle, figure 9. A considerable mesh influence is observed at these relative coarse meshes; meshes 1 and 2 having 55625 nodes, while meshes 3 and 4 have 129591 mesh points. Figure 10 compares Mach number distributions in the trailing edge region for meshes 2 and 4, where clearly, the Mach isolines carry over traces from the mesh discontinuities. Figure 11 shows the mesh sensitivity of the computed total pressure losses, revealing the amount of numerical dissipation of the coarse meshes. In addition, the total pressure contours at the exit plane for the four meshes under consideration, not shown here, reveal differences larger than the variations resulting from different turbulence models. Additional examples of the inability of sheared meshes to capture the details of the flow field, particularly at shear angles of 70º or higher, can be found in Turner et al (1993). In addition, it is our experience that refining highly skewed meshes leads also to increasing convergence difficulties. The remedy to this undesirable situation is to generate either unstructured meshes or structured, nearly orthogonal meshes, such as in figure 12, where the periodicity of points on the periodic boundaries has to be imposed via extrapolations of variables or fluxes.

3.2.2.Mesh refinement

Defining the level of mesh refinement necessary to ensure a mesh independent numerical solution is a difficult and costly task, particularly in 3D. It depends on many factors, such as geometrical configuration, flow properties (presence of viscous regions, shocks, separation, possible unsteadiness,...), mesh, numerical scheme, turbulence models. Despite the inherent difficulty of this task, it is nevertheless essential in order to be able to validate turbulence models in a non-ambiguous way. The fact that most of the turbulence model validations presented in the literature for 3D turbomachinery flows do not demonstrate mesh independent results, contributes largely to the uncertainties concerning the degree of validity of various turbulence model formulations.

An interesting example of the degree of refinement necessary to achieve grid independence, as well as loss predictions with negligible contributions from numerical dissipation, is provided by Arnone and Swanson (1993), for the 2D computation of a transonic turbine section tested extensively by C. Sieverding at VKI and by Kiock et al (1986) at four European wind tunnels, see Sieverding (1990). Applying a central scheme with artificial dissipation, multigrid acceleration and a Baldwin-Lomax algebraic turbulence model, Arnone and Swanson (1993) compare results between three mesh levels of respectively 193x25, 365x33 and 769x65 points. The C-meshes are carefully designed, with non-periodic quasi orthogonal lines to minimize mesh skewness, as seen in figure 12, for the medium mesh, where the first mesh line is at a distance of the order of $y^+ \approx 1$, corresponding to 5.10^{-5} chord. For the coarsest mesh this distance is multiplied by two and halved for the finest mesh. Figure 13 shows the isentropic Mach number distributions obtained with the finest mesh, in comparison with the experimental data, while figure 14 shows the Mach contours at four values of the back pressure. These distributions remain practically the same for the three mesh levels, with the exception of the case at $M_{2is}=1.0$, where more points are needed to capture the weak interaction of the trailing edge shock and the suction surface boundary layer. However, wall pressure distributions are not very sensitive quantities for the assessment of Navier-Stokes simulations and skin-friction data are indeed more severe indicators. Figure 15 shows the effect of the y+-values of the first mesh line on skin-friction, as obtained on the fine mesh. Although this mesh is extremely fine (close to 50000 points) there is still a detectable effect, which does not appear to have an influence on the calculated losses which are in excellent agreement with the experimental data. Unfortunately, the authors do not show similar plots on the two other meshes, but one can only guess that this effect would be amplified. This is confirmed by figure 16, displaying the calculated loss coefficients in function of the inverse of the number of mesh points. The highest transonic case M2is=1.2, is apparently less sensitive to the mesh levels, probably since the losses are dominated by the shock losses, which are well captured on the three meshes. For the other cases, where boundary layer losses are increasingly important, the influence of the numerically generated losses becomes significant, with the highest mesh dependence for the subsonic case M2is=0.81. The authors' conclusion is that the medium grid provides enough resolution for engineering applications, that is roughly 12705 points would be needed for a two-dimensional blade section.

Similar conclusions have been reached by Dorney and Davis (1991), investigating heat transfer and loss prediction on a 3D subsonic turbine blade (the Langston cascade). Their code is based on flux difference splitting, with implicit time integration and a Beam and Warming approximate factorisation. A Baldwin–Lomax turbulence model is applied, with fixed positions of transition. The heat transfer data clearly indicate that the accuracy of the predictions is very strongly dependent on a reliable estimation of transition. In order to get close to the experimental data, the

onset of transition was varied spanwise, with fully turbulent end-walls and mid-span transition at 20% chord on the suction surface. Systematic studies of 2D turbine blade sections with a combined O-H overlaid grid, figure 17, indicate that grid independent solutions and heat transfer data where obtained with meshes of close to 10,000 points (O-131x61 + H-71x21) with a first mesh point spacing of 2.10-5 chord corresponding to y+=0.06. Very low value of y+ (<1) seem to be essential for accurate heat transfer estimations. For the 3D computations Dorney and Davis compare mesh densities with (O-101x31 + H-70x31) in the blade-to-blade planes and a number of spanwise sections ranging from 25 to 91 over half the span with various levels of clustering. The endwall y+ values range from 7 to 0.3 for the finest mesh, which has over 480,000 points, while the coarsest mesh has 132,000 points. Figure 18 and Table 1 show the influence of mesh point densities on overall (18a) and on spanwise distributions of loss (18b) and exit angle (18c). The authors conclude that mesh independent solutions require over 950,000 points full-span, while the remaining discrepancies in capturing the details of the secondary flow on this fine mesh are attributed to the limitations of the Baldwin-Lomax turbulence model. Unfortunately, no mesh dependence of the heat transfer predictions are shown. However, the authors refer to the underestimation of the wake heat transfer due to the insufficient wake resolution provided by the O-mesh, although each blade-to-blade section has only half the points estimated for a mesh independent 2D solution.

Are 50,000 mesh points sufficient for 2D computations?

Although the results of Arnone and Swanson (1993) with their finest mesh of 50,000 points show fine details, such as the separated trailing edge flow, figure 19, one might wonder if this is still enough to capture all the physical phenomena. Figure 20, from Detemple-Laake (1991) shows Schlieren pictures from mid-span turbine sections at 50° and 65° incidence at subsonic, sonic and supersonic exit Mach numbers (the design incidence being 40°). A close view on the wakes indicates the presence of an unsteady vortex shedding, which could affect the local heat transfer, the trailing edge shocks and contribute to additional unsteadiness to the rotor-stator interaction. Although this spontaneous unsteadiness remains local, it clearly requires extremely fine meshes near the trailing edge region, since the very fine mesh of figure 19, does not seem sufficient to capture this unsteadiness.

3.3. ENGINEERING REQUIREMENTS FOR CFD APPLICATIONS

From the available experience today, one can derive a certain number of requirements and recommendations for reliable CFD computations. Independently of the selected schemes, all methods should

- be at least second order accurate in space, first order schemes generating far too much diffusion
- be tested for convergence to machine accuracy for simplified, representative problems of the type of configurations currently analysed
- be able to detect spontaneous flow unsteadiness, such as unsteady separation or vortex shading phenomena. This is an important aspect of CFD simulations, since most of the separated flow configurations are unsteady, and it is of great importance to be able to detect, for instance, stalling incidences on turbomachinery blade rows.

In addition severe requirements are to be set on the mesh quality, in order to minimize truncation errors and maximize convergence rates. Various type of structured meshes can be applied, H, O, C or/and various combinations of them, or unstructured meshes can be selected and several examples will be given in the following. But in all cases, mesh quality will greatly influence accuracy and convergence. It is therefore recommended to

- ensure smooth meshes, able to recognize flow structures, and avoid discontinuities in the sizes of adjacent cells. For instance, an O-mesh might not be suitable for accurate wake flows where a H or C-mesh would be better adapted.
- avoid highly skewed cells which have a devastating effect on accuracy. Nearly orthogonal cells will always be favourable for accuracy and will reduce numerical dissipation. This will require non-periodic meshes when dealing with highly staggered compressor, or highly cambered turbine blade rows.
- ensure, whenever possible that the obtained solution is grid independent. This requires computations on successive finer meshes, having also good regularity properties, and may not be always feasible for reasons of time and/or cost. Very efficient codes are essential in order to be able to perform large scale computations on a routine basis.

Several ingredients of efficient codes are still the subject of current research, in particular

- in viscous computations, high cell aspect ratios are unavoidable, and experience indicates that this can have a deteriorating effect on convergence rates. The control of the interaction between multigrid and cell aspect ratio has still to be better understood.
- Mesh adaption is a main source of potential gains in accuracy and computational performance. Unstructured meshes are particularly well suited for effective mesh adaption, see for instance Dawes (1991). A great deal of research is required for the optimization of adaption criteria, such as 'activity' or 'error' detectors, and effective mesh generation systems, particularly in 3D. So more that the best detectors might depend on the type of problem (shear layer, shock, local gradients,..)
- the control of the complex interactions between components such as mesh, solver, turbulence models, etc..

Engineering CFD is also characterized by the need for the integration of efficient mesh generators and graphic flow visualisation systems, with high degrees of interactivity, see for instance Hirsch et al (1991).

4. TURBULENCE MODELS

We consider here that the best adapted formulation, for engineering calculations, is the Reynolds Averaged Navier-Stokes model (RANS), since any higher model will require some form of direct simulation, which cannot be considered for current industrial applications, at least within the foreseeable future.

A large variety of turbulence models are available, ranging from simple algebraic models to the system of transport equations for the Reynolds stresses, and within each family a still larger number of variants can be applied, either based on different assumptions or on different empirical data. The turbulence models form the most critical parts in a practical code, since none of the available models has a universal validity, all of them being based on some degree of empiricism. Hence the calculated flow field, at least in complex flow situations, can be strongly dependent on the selected model and careful validation is necessary.

The problem of adequate turbulence models, including prediction capabilities for laminar-turbulent transition, influences of curvature, rotation, buoyancy forces, separated regions, heat transfer, combustion processes, etc., is a major item of present day research and likely to remain so for some time. Hence, although some general trends and methods are widely applied, such as the k-ε model, this field is in

constant evolution and evaluation, especially for complex flow systems.

The algebraic models and one or two transport equation models are based on an eddy viscosity hypothesis, assuming the turbulent stresses proportional to the main flow strain rate, with isotropic turbulence exchanges similar to the molecular viscosity. This can lead to inconsistencies, in particular in the vicinity of separation or reattachment points. In addition, the algebraic models are not able to take into account the transport and diffusion of turbulence and therefore history effects can not be simulated. These deficiencies will mainly appear in recirculating or separated flows, where the anisotropy of the turbulence plays a more significant role. However, despite these deficiencies, the algebraic and k-ε models offe ra wide range of applications, since the anisotropy effects are not always dominating.

4.1. BALDWIN-LOMAX MODEL

The Baldwin-Lomax (1978) model is widely used in external as well as in internal aerodynamics and is constructed as an improved version of the Cebeci-Smith (1974) model.

The turbulent boundary layer is considered to be formed by two regions, an inner and an outer region, with different expressions for the eddy viscosity coefficient. The inner region, of the order of 10 to 20% of the boundary layer thickness, is the region of validity of the law of the wall. In the inner region the albebraic model evaluates μ_T through the mixing length by the following steps, following the presentation of Cebeci and Bradshaw (1984)

$$\mu_T^{(i)} = \rho\, l^2\, |\nabla \times \vec{v}|\, \Gamma \cdot \Gamma_{tr} \qquad (4.1)$$

where Γ is the intermittency factor, accounting for the fact that the turbulence becomes intermittent as the edge of the boundary layer is approached, being turbulent only for a fraction Γ of the time. The other intermittency factor Γtr takes into account the effects of transition.

In a two dimensional boundary layer along a surface aligned with the x-axis and with normal direction y, the vorticity in equation (4.1) reduces to the shear $\partial u/\partial y$. Representative models for the mixing length are given by the classical representation of Prandtl $l=\chi y$, corrected by Van Driest (1956) in order to include also the transition region between the linear velocity law, $u+=y+$, in the viscous sublayer and the logarithmic region,

$$l = \chi\, y\, (1 - e^{-y+/A}) \qquad (4.2)$$

where χ= 0.41 is the Von Karman constant; the parameter A has been calibrated with boundary layer data to be A = 26.

The outer eddy viscosity coefficient is defined by the following relation,

$$\mu_T^{(e)} = \rho\, \alpha\, C_{cp}\, F_w \cdot \Gamma \qquad (4.3)$$

where α=0.0168 and the function F_w is given by the smallest of the following two values

$$F_w = \text{or} \quad \begin{matrix} y_{max}\, F_{max} \\ C_{wk}\, y_{max}\, \dfrac{u_{dif}^2}{F_{max}} \end{matrix} \qquad (4.4)$$

The values y_{max} and F_{max} are obtained from

$$F(y) = y \left| 1 - \exp\left(-\frac{y^+}{A}\right) \right| \frac{\partial u}{\partial y} \qquad (4.5)$$

and y_{max} is the value where the function F attains its maximum value F_{max} .

The quantity u_{dif} is a velocity scale equal to the difference between the maximum and minimum velocity inside the shear layer. This applies to wakes as well as to boundary layers and u_{dif} is equal to u_e in the latter case. The intermittency factor Γ is given by

$$\Gamma = \frac{1}{1 + 5.5 \left[C_k \cdot y / y_{max} \right]^6} \qquad (4.6)$$

The Baldwin–Lomax model has the following constants

$$C_{cp} = 1.6 \quad , \quad C_k = 0.3 \quad \text{and} \quad C_{wk} = 0.25$$

although other values have been applied. An interesting extension by Granville (1987) introduces some effects of pressure gradients in the first two coefficients. The switching from the inner to the outer value of the eddy viscosity occurs at the position y_c where the inner value becomes equal to the outer value.

Experience shows that the predicted flow can be quite sensitive to the value of the parameter C_{wk}, particularly in presence of strong shock-boundary layer interactions, as discussed in the section 4.5. Many authors have applied this model with varying values of the other coefficients, Visbal and Knight (1983), York and Knight (1985) or/and with different wall treatments, Turner and Jennions (1992). It can be considered that algebraic models provide acceptable accuarcy for well-behaved, attached shear layers.

4.2. TWO EQUATION k-ε MODELS

A variety of two equation models have been developed, which can be considered as variants of the more popular one, namely the k–ε model Launder and Spalding (1972), defined by transport equations for the turbulent kinetic energy and dissipation rate. Two forms of models are available, the 'Standard' model and the 'Low-Reynolds Number' model. The 'Standard' model does not apply to the near-wall region and requires the addition of either a 'wall function', or an additional near-wall model. It is less demanding in terms of mesh resolution, since the first mesh points above the walls may be situated at values of y^+ below 300. The 'Standard' model corresponds to D=E=0 and to the functions $f_\mu=f_1=f_2=1$ in Table 2. The 'Low-Reynolds Number' models aim at describing the turbulent behaviour over the whole viscous layer, down to the wall. They require first mesh point distances y^+ of the order or below 1.

The various 'Low-Reynolds Number' models rely on the Prandtl-Kolmogorov relation for the turbulent eddy viscosity, with

$$\nu_T = C_\mu\, f_\mu\, \frac{k^2}{\tilde{\varepsilon}} \qquad \varepsilon = \tilde{\varepsilon} - D \qquad (4.7)$$

The term D is introduced in order to apply a boundary condition $\tilde{\varepsilon}=0$. The various terms of the turbulent kinetic energy equation can be modeled, as follows

$$\frac{\partial(\rho k)}{\partial t} + \nabla \cdot (\rho\, \vec{v}\, k) = \nabla \cdot (\mu_k\, \nabla k) + (\bar{\bar{\tau}}_R \cdot \nabla)\vec{v} - \rho\tilde{\varepsilon} - \rho D \qquad (4.8)$$

The first term on the right hand side is a diffusion term, while the second term, denoted by P, is the production of turbulent energy by the work of the main flow against the Reynolds stresses. The third term is the dissipation contribution. An equation of similar nature is assumed for the dissipation rate

$$\frac{\partial(\rho\tilde{\varepsilon})}{\partial t} + \nabla \cdot (\rho \vec{v} \tilde{\varepsilon}) = \nabla \cdot (\mu_\varepsilon \nabla \tilde{\varepsilon}) + \frac{\tilde{\varepsilon}}{k} \left[C_{\varepsilon 1} P f_1 - C_{\varepsilon 2} \rho \tilde{\varepsilon} f_2 \right] + E \qquad (4.9)$$

where P is the production term of the k equation.

The eddy diffusivities μ_k and μ_ε associated with the kinetic energy and dissipation equations respectively, are defined by

$$\mu_k = \mu + \frac{\mu_T}{\sigma_k} \qquad \text{and} \qquad \mu_\varepsilon = \mu + \frac{\mu_T}{\sigma_\varepsilon}$$

The terms E, f_1, f_2, f_μ are additional terms introduced in order to obtain better agreements in specific flow situations and to provide a low reynolds number behavior near the walls. A few of the many versions of the k-ε models are summarized in Table 2, from Biswas and Fukuyama (1993), with the variants of Launder-Sharma (L-S), Lam-Bremhorst (L-B), Nagano-Tagawa (N-T), Kasagi-Sikasomo (K-S).

The two equation models are being applied to a large variety of flow situations in turbomachines, the first attempts having been pioneered by Hah (1987a), and they present an acceptable compromise between economy of calculations and range of validity, although they appear still insufficient for complex separated flows, heat transfer, combustion.

4.3. OTHER MODELS

Reynolds stress models allow to take into account anisotropy and additional effects, such as curvature and rotation, and seem to give slightly better predictions for shock boundary layer interactions. Although they still suffer from many limitations and lead to a significant increase in computer time, their application for turbomachinery flows might provide more reliable turbulence modelling in the future. For instance, Abou Haidar, Iacovides and Launder (CP-510, Paper 34) compare different turbulence models for the flow in a circular sectioned S-duct. An algebraic Reynolds stress model is applied, with various near wall corrections such as one and two equation models, on a grid of 117800 mesh points. The main conclusion of the authors is that full second moment closure equations over the complete cross-section might be required for highly accurate simulations. Similar trends are suggested by Lien and Leschziner (1993) for the accurate representation of shock-boundary layer interactions.

4.4. LAMINAR-TURBULENT TRANSITION

A particular important and difficult problem is connected to the prediction of laminar-turbulent transition. Very few reliable criteria have been developed, although a poor prediction of transition can have dramatic effects on calculated results, particularly with shock induced separations. A spectacular example is provided by the calculations of Nakahashi et al.(1987) of the two-dimensional flow in a turbine cascade, with a Baldwin-Lomax turbulence model and a simple transition criteria based on the maximum eddy viscosity becoming higher than an imposed value. Figure 21a shows the computed density lines with transition prediction at the point indicated by a triangle on the suction surface. The transition is predicted at the point of impingement of the shock, inducing a small turbulent separation. Figure 21b correspond to an assumed laminar flow and shows a massive separation due to the shock-boundary layer interaction, the computed flow on the suction side becoming unsteady. Comparing to the Schlieren picture in fig. 21c it is seen that the turbulent calculation, provides an excellent agreement. However for the same cascade at a higher exit Mach number of 1.43 and 20° negative incidence to the design value of 60°, the turbulent calculations do not indicate separation, while the experiments are in good agreement with the laminar data as seen from figure 22. In this case, the innacurate transition prediction led to the strongly innacurate flow field of figure 22a. Hence it can be considered that whatever the numerical qualities of a Navier-Stokes code, its results will be strongly dependent on the transition prediction model.

This uttermost important topic requires still considerable research. Earlier attemps to model transition with semi-empirical additions to algebraic models are described in Sharma (1987), Sharma and Syed (1991). A recent account on transition predictions on a variety of basic test cases, based on "Low Reynolds Number" variants of k-ε models, can be found in Savill (1992), (1993). Applications of the same approach to turbine heat transfer predictions are reported in Hah (1989), Biswas and Fukuyama (1993) and to unsteady flows in Cho et al (1992).

4.5. TURBULENCE VALIDATIONS

Various turbulence models are being applied in turbomachinery applications. Although significant differences can be observed, more work is still required to separate mesh influences from modeling effects, since few computations are presented with convincing mesh independence of the results.

Several systematic comparisons are available in the literature, where different models have been compared on the same meshes with the same codes. Figure 23, from Dawes (1990), shows a comparison of the loss distribution in a cross plane situated 42% chord downstream of a turbine blade row of 54° exit angle, calculated on a H-mesh of 107x33x33=116253 points, with a first mesh point at a y^+ value below 5. The transport equation is a one equation model for the turbulent kinetic energy following Birch (1987). The laminar calculation leads to massive separation and there is no clear advantage between the Baldwin-Lomax and the transport equation models, although the latter appeared to give a better prediction of separation bubbles.

As pointed out by Dawes (1990), the loss levels predicted by various turbulence models are very close to each other, mainly because the major loss contribution occurs in the near wall region, with nearly 90% being produced in the laminar sublayer and the log--region. Both families of models predict similar levels of eddy viscosity, as a consequence of the fact that they are based on local equilibrium assumptions and are tuned to reproduce the logarithmic velocity distribution. Hence the essential point is to ensure that the mesh allows the inner turbulent viscosity to be appropriately captured in the numerical simulation.

Simulations have been performed by Matsuo (1991) on a subsonic turbine blade row on a 146x71x51=528,666 points, comparing laminar, Baldwin-Lomax and a k-ε model. Despite the fine mesh, discrepancies still remain with the experimental data, where the predicted secondary vortex core is too close to the end-wall with all the cases. Nevertheless, the author concludes that the k-ε model leads to a better prediction of the separated region.

Turner and Jennions (1992) reach similar conclusions from comparisons between three versions of the Baldwin-Lomax model and two versions of the 'standard' k-ε model on the computed flow in a transonic compressor. The local flow pattern at rotor tip is dominated by the interaction between the tip leakage vortex and the leading edge shock. The calculations performed on a 97x49x37=175,861 points, with 4 spanwise points in the tip clearance region and a first y^+ value on the average around 100, are shown in figure 24 for the tip section. The standard Baldwin-Lomax model predicts a strong normal shock due to an underestimation of the viscous shear layers, as a consequence of the high y^+ value. The k-ε model clearly provides a better representation of the shock position and strength.

A detailed investigation of turbulence models for shock-boundary layer interactions has been performed in the EUROVAL project, Haase et al (1993). In this project many groups calculated the same test cases, for instance a shock-boundary layer interaction inside a channel, known as the ONERA 'bump', with different turbulence models, but on the same mesh. This test case presents data in two different

configurations, case A involving a weak shock-boundary layer interaction with no separation and case C with a stronger interaction and separation. All the computations, by 6 different groups were done on the same grids of 193x65=12545 points for case A and 193x97=18721 points for case C, which were shown to yield mesh independent results.

The conclusions from test case A, not shown here, can be summarised as follows. In the absence of shock induced separation, the majority of models behave satisfactorily, including algebraic models, when properly calibrated. The standard value of C_{wk}=0.25 gives a too severe interaction, leading to separation at the foot of the shock, while values of 0.5 to 1 give better agreement with the data. This is confirmed by other test cases, see for instance Chima, Giel and Boyle (1993), where a value of C_{wk}=0.825 is recommended. The Granville corrections perform very well, as do the k-ε models, although the sensitivity to the shock is underestimated, indicating too much turbulent mixing. The Johnson-King (JK) model displays serious weaknesses in these near equilibrium conditions, showing an excessive sensibility to the shock with premature separation and excessive displacement thickness. The Reynolds stress models show also an over-sensibility to the shock, although to a lesser degree than the JK model. All the transport models show a too low rate of recovery of the boundary layer after the shock, which might connected to the behaviour of the dissipation equation.

A comparison of different calculations for Case C is shown in figure 25. The BL results do not show the λ-shock structure, which is seen for the Granville corrections and for the JK and Reynolds stress models. With the standard value of C_{wk}=0.25, the BL models produce a stronger shock boundary layer interaction, without generating the λ-shock structure. On the other hand, the k-ε models show a weaker interaction. As can also be seen from figure 26, showing the Mach number distribution on the lower wall, the plateau associated with separation is not captured by the current BL model implementations, nor by the k-ε models. Better results are obtained with the JK and Reynolds stress models. The displacement and momentum thicknesses, are under predicted with the BL models, while the other models give better agreement with the data, although none of the models captures the post shock level of the boundary layer thickness. With regard to the velocity profiles, figure 27, at the foot of the shock the BL models miss completely the interaction, which is somewhat better predicted with other models, although all models give an insufficient rate of recovery. However, further downstream, x/L=1.5, all models predict correctly the velocity profiles. On the other hand, the shear stresses are underestimated by all models downstream of the shock. In conclusion, none of the models appear to provide an accurate prediction of the strong shock-boundary layer interaction. It has to be added that the downstream pressure necessary to predict, in 2D, the correct shock position differs from the experimental value, indicating the presence of 3D effects.

It is of interest to observe that different programs with the same turbulence models gave practically the same results, providing additional confidence in the objective analysis of the behaviour of the Tu-models. However, in general many parameters influence the output of a computation, mesh definition close to the walls, implementation details of the models, choice of model constants, boundary conditions.

Other turbulence validation studies, for instance Leschziner and Launder (1993), indicate for a test case of an impinging jet on a plate, including heat transfer data, that none of the turbulence models provides accurate predictions of the turbulence intensities along the stagnation streamline. This is crucial for the correct overall flow behaviour. It appears that the linear eddy viscosity stress-strain relation causes excessive levels of k, eddy viscosity and Nusselt numbers. Even current Reynolds stress models do only slightly better than the simpler two equation models. It appears therefore that a particular research effort is to be done to improve the behaviour of turbulence models, particularly on basic test cases, representing essential physical phenomena.

5. CODE VALIDATIONS

The problem of code validation for turbomachinery flows is essentially connected to complex geometries, including tip clearance, boundary conditions particularly in multistage environments, turbulence models, transition, combustion real gas models. Although simulations of the complex flow field can provide a wealth of information on the flow structure, none of the computations found in the literature today are able to predict accurately all the flow details, even if the grid is fine enough. This is connected to the present deficiencies of turbulence and transition models.

However, many flow features do not depend on the exact evaluation of the Reynolds stresses, being dominated either by inviscid effects, such as secondary or tip clearance flows, or depending essentially on the presence of shear more than on its magnitude, such as the formation of horseshoe or tip vortices. These phenomena can therefore be captured even with relatively coarse meshes, without guarantying an accurate description of the fine details. For instance, most features of the tip leakage flow can be captured by as little as 4 to 6 points over the clearance gap, see figure 24, but it is our experience that more than 11 points are needed to approach the correct intensity of the tip leakage vortex and to capture the secondary tip vortex, Kang and Hirsch (1994), as will be discussed in section 5.3. With regard to losses, overall values can be made largely independent of the turbulence models, provided the inner layer eddy viscosity is correctly captured, as shown by Dawes (1990). At the level of turbulence models, although turbulence is essentially three-dimensional and anisotropic, the 'isotropic' algebraic and k-ε models do capture many flow features which are largely insensitive to the anisotropy of turbulence. On the other hand, separated flows, heat transfer, shock boundary layer interactions, are known to be extremely sensitive to the turbulence structure, including of course transition. Since these effects can influence strongly, or even dominate some of the turbomachinery flow features, it is essential to develop a good understanding of the underlying physical phenomena, in order to define guidelines for the required level of simulation. In particular, it is of essential importance to evaluate if and when these effects remain local or influence wider regions of the flow domain.

The process of validation itself has therefore to be clearly defined. It is obvious that a surface pressure distribution is a weak validation criterion for Navier-Stokes computations; while wall stresses, drag, boundary layer velocity profiles, Reynolds stresses, temperature profiles, heat transfer coefficients are basically more severe tests for accurate Navier-Stokes simulations. These data are difficult and costly to obtain in experimental tests, but it is essential that a major effort in this direction be undertaken. Many codes are used in research and design environments with a low number of mesh points, far from the level ensuring mesh independence. Comparisons of the output of these computations with experimental data will be able to show most of the essential physics of the flow, but will generally miss finer details. Validations at this level depend on a mixture of numerical effects and turbulence modelling and we prefer to consider them as 'calibrations' or 'Industrial'-type validations, keeping 'validations' for the evaluation of physical models, free of numerical effects. This situation is very representative of a current trend in the design process, where

full 3D Navier-Stokes calculations are performed on complex configurations such as splittered rotors, full stages, with rather coarse meshes, of the order of 50000-100000. The clear objective being to identify trends and signs of variations of selected global quantities such as overall losses or pitch averaged flow properties, with modified design parameters, more than to simulate all the flow details. The paper by Sehra, Abolfadl and Zedan (AGARD CP-510, Paper 13) is most representative of this situation. Computations on transonic compressors, or high work turbines, are reported with meshes of 80,000 points, identifying the most salient flow features and with reasonably good quantitative predictions of pitch averaged flow quantities. Another 'industrial' oriented application has been presented by Vogel (AGARD CP-510, Paper 7), were combined flow and blade heat conduction computations with coolant injection, are applied to film cooled gas turbine blades. Birtch and Kitchen (AGARD CP-510, Paper 25) present calculations of a 3D intake, typical of a modern high bypass ratio engine in an underwing, twin-jet installation. The calculations are performed with a Prandtl mixing length turbulence model and 47450 mesh points. The authors recognise that a higher grid resolution and more adequate turbulence models are necessary in order to capture accurately the details of this complex flow, which is dominated by shock-boundary layer interactions.

5.1. 3D FLOWS IN TURBINE BLADES

Much progress on understanding the three-dimensional viscous flow phenomena in a single blade row with or without tip clearance has been made in recent years from advanced experimental and numerical research.

Figure 28 shows a schematic flow structure in a turbine cascade as proposed recently by Chen and Goldstein (1991). Associated with all the vortices, a high loss and high turbulence intensity core normally exists. The incoming boundary layer on the end-wall starts to roll up to form the horseshoe vortex. Ahead of the leading edge, S_1-S_2 is the separation line and the two legs of the horseshoe vortex are marked as vortices Vsh and Vph. The leading edge corner vortex shown in the figure is the secondary vortex, being induced by the horseshoe vortex and rotating in an opposite sense to it. Separating from the leading edge, the suction and pressure side corner vortices are marked as V_{sLc} and V_{pLc}, respectively. When both the suction side leading edge corner vortex and the horseshoe vortex enter the passage, they experience a strong transverse pressure gradient, keeping them close to the suction surface. As the suction side horseshoe vortex travels along the suction surface towards the trailing edge, it moves away from the end-wall (separation line S_1) towards the midspan. As to the leading edge corner vortex, after it is forced toward the suction surface, its path is not easily traced. When the separation line of the leading edge vortex approaches the suction surface at points S_1 and S_2, two very small vortices in the corner may be produced, marked as V_{sc1} and V_{sc2}. Over the pressure surface, the flow is relatively simpler. In the pressure side corner, a pressure side corner vortex (V_{pc}) may be formed due to the down flow on the pressure surface.

The pressure side leg of the horseshoe vortex (V_{ph}) moves towards the suction surface of the adjacent blade. During this transverse motion, it becomes a major component of the passage vortex (V_p) entraining fluid from the end-wall boundary layer. After the passage vortex reaches the suction surface of the adjacent blade, it moves away from the end-wall (S_2) towards the midspan as it travels along the suction surface towards the trailing edge. Figure 28b shows the 2D boundary layer in the mid-span region, while figure 28c identifies the various flow regions on the suction surface. S_{Vsh} and S_{Vp} are the separation lines created by the horseshoe vortex and the passage vortex on the suction side. Between these two separation lines, a reattachment line R_{Vsh} /R_{Vp} is observed, defining the region A. These separation lines encounter the 2D separation bubble delimited by the lines S_{2D} and R_{2D}. The lines R_{Vsc1} and R_{Vsc2} are associated with the suction side corner vortices V_{sc1} and V_{sc2}.

Many of these flow features can be seen from figure 29, (associated to figure 20) from Detemple-Laake (1991). The 50° incidence case shows also the laminar separated region followed by turbulent re-attachment, close to the trailing edge in the central part of the blade (design incidence is 40°). In the supersonic case (top right figure), this laminar separation/turbulent re-attachment, is induced by the shock. The oil flow patterns close to the leading edge at the higher incidence of 65° (bottom figures) show that this laminar separation followed by turbulent re-attachment has moved strongly upstream, and is created by the strong local acceleration followed by a small shock at the leading edge, as seen from figure 20. Comparing the top and middle figures, it is also seen that a higher incidence leads to a stronger uplift of the passage vortex separation/re-attachment line on the suction surface, increasing the spanwise migration of the end-wall low energy fluid along the suction surface. It is of importance to note that the intense secondary flow in turbine passages appears to be of sufficient strength to prevent separation of the suction surface boundary layer near the endwall, although separation is present in the two-dimensional sections.

As seen from figure 30, from Dorney and Davis (1991), (see also fig. 18) calculations applied to the Langston cascade, predict well the end-wall limiting streamline pattern (Fig.30a), where the saddle point indicates the formation of the horseshoe vortex. In the contours of the predicted Stanton number (Fig30b), a region of increased heat transfer around the leading edge can be found, caused by the motion of the horseshoe vortex. Fig. 30c shows the predicted limiting streamlines along the suction surface, compared to the visualizations.

Although these calculations, performed with a fine mesh, capture most of the features, it is seen from figure 18 that the detailed near wall flow properties, influenced by the corner vortices, are not well represented.

Durham turbine cascade

A challenging test case is given by the Durham turbine cascade of Gregory-Smith and Cleak (1992), which is dominated by transitional flows. This cascade is used as one of the test cases in the annual Workshop on '3D Turbomachinery Flow Prediction' organised by the ERCOFTAC Special Interest Group on Turbomachines, Gregory-Smith (1993).

In order to illustrate aspects of mesh influence and typical questions raised in validating this test case, we show some results at different grid levels for Navier-Stokes and Euler solutions. Comparisons with the experiments are made for total pressure loss and flow angle. The calculations are performed with a central scheme, a V-cycle multigrid with a five-stage Runge-Kutta scheme and implicit residual smoothing, allowing a constant CFL number of 7.0. The residuals reach machine accuracy in about 300 iterations on a single precision workstation. The exit angle is 67.8° and a periodic H-mesh is used, with 121x49x33 =195657 points, in the axial, blade to blade and spanwise directions, for the fine mesh, while the coarser mesh has 61x25x25 =38125 points. This leads to a sheared mesh, with the weaknesses discussed earlier. The algebraic turbulence model of Baldwin-Lomax is selected without transition criteria.

Qualitative visualisation of the complex 3D flow patterns are shown in figure 31, where the horseshoe and corner vortices can be identified.

In order to quantify the numerical dissipation on the coarse mesh and to identify the inviscid components of the secondary flows, an Euler calculation is performed with the experimental inlet total pressure profile. Hence, the secondary flow, or passage vortex is reproduced, but a wide wake is predicted even without physical viscosity, as seen from figure 32. This figure compares the secondary flow and total pressure losses for the coarse mesh Euler solutions and the NS solutions on the two meshes, with the experimental data at section 10, about 50% axial chord downstream of the trailing edge. Note that the experimental data are plotted over more than one pitch spacing. It is seen that the secondary flow pattern of the coarse Euler and NS results are nearly the same, while the fine mesh results provide more details. However, as seen from the pitch averaged flow angle and loss distributions, figure 33, the overturning close to the wall is over predicted. Figures 33b and c, compare the loss levels, showing the high numerical dissipation on the coarse level, while the fine mesh losses, although reduced, are also too high. This is due to the sheared H-mesh, leading to too much wake diffusion, and to insufficient grid resolution. It is seen that the averaged losses show a similar distribution between the Euler solution and the experiment, where the higher values around 12% to 25% span relate to the core of the passage vortex.

Results with similar levels of discrepancy between computations and experiments, were obtained by other authors at the above mentioned Workshops, applying various codes and turbulence models, on coarse or fine meshes. It has to be added that the flow in this turbine is strongly influenced by transition, which makes it an extremely difficult test case. Cleak, Gregory-Smith and Birch (AGARD CP510, Paper 8) present an analysis of the mesh and turbulence model effects with different assumptions concerning fixed regions of laminar and turbulent flows. Very large effects were observed with varying turbulence models and regions of transition.

5.2. 3D FLOWS IN COMPRESSOR BLADES

Three-dimensional flow patterns in axial compressors show many common points with turbine flows, but also significant differences. Schulz and Gallus (1988, 1990) have reported extensive flow visualisations of the flow in an annular compressor cascade (without clearance), over a wide range of incidences. The most striking feature is the region of the separation flow near the hub end-wall and the blade suction side. Figure 34 shows the schematic explanation of the flow structure and proposed topology of the hub corner stall. Since the separation region is closed off from the main flow by limiting streamlines at the hub and on the blade suction surface, it is anticipated that a ring vortex is formed joining the blade suction surface and the hub somewhere near the blade trailing edge. The separation region near the hub extends in size with increasing angle of attack. There appears to be a large amount of radial outflow on the vane surface within and outside of the separation region. A region of back flow is also visible within the separated flow region on the suction surface and on the hub. Some of the back flow originates in the pressure surface boundary layer, turns around the trailing edge and moves upstream slightly upstream. On the hub wall, the flow moves upstream into the separation region, joining the back flow and generating a vortex with clockwise orientation.

This is also confirmed from the experimental and numerical analysis of the 3D viscous flow in a linear compressor cascade, with and without tip clearance, Kang and Hirsch (1991, 1992a,b, 1993a,b). Figure 35 shows a schematic structure of the 3D flow over the passage and within a tip gap. The 3D viscous flow exhibits a very complex structure, characterised by various concentrated vortices. Around the leading edge on the end-wall, a horseshoe vortex (HV) is formed. The suction side leg (HVs) disappears in the suction side corner within a short distance due to viscous dissipation. The pressure side leg (HVp), however, is merged with the passage vortex (PV) in its downstream evolution due to their same rotation sense.

The most complex phenomena occur in the suction side corner close to the trailing edge. In the extreme corner, there is a small size separation region, bounded by two separation lines issued from the saddle point Sc and terminated at node points Ncb and Ncw on the blade surface and the end-wall respectively. This separation region, or separation bubble, was only observed in the pain-trace visualisation process and seems to be unsteady.

Behind the cascade, the remarkable nature of the flow in the wake region is dominated by a concentrated shed vortex (CSV). This vortex, with an opposite sense to the passage vortex, is believed to be originated from a spiral node Nc on the suction surface near the trailing edge. Very close to the end-wall, there is a corner vortex (CV) which is much smaller and is believed to originate behind the trailing edge. On the tip side, except the presence of the passage vortex (PV), the flow is complicated by the tip leakage flow and the tip leakage vortex (TLV). The new flow phenomena around the tip are the tip separation vortex (TSV) and the tip secondary vortex (TS). The former is the so-called vena contracta identified by Rains (1954) and others. The sense of the TSV is the same as the TLV but opposite to the SV.

Computations performed on this cascade with a Baldwin-Lomax model on a grid of 97x41x33=131,241 points, or its one level coarser 49x21x17=17,493 points, confirm these structures and also demonstrate that many of these can also be captured on the coarse mesh. The paint-trace visualisations on the end-wall at design and off-design conditions are presented in Fig.36, compared with the calculations. A saddle point in front of the leading edge indicates the formation of a horseshoe vortex. Figure 37a shows the limiting streamlines on end-wall and suction surface, from which the corner separation and trailing edge separation can be seen. Figure 37b shows a view from downstream of the cascade on part of the calculated streamlines inside and behind the passage at both design and off-design conditions. The black streamlines, coming from upstream of the cascade, turn towards the suction side corner with convergence. In this corner, they turn first backwards and rise up along the suction surface, and then turn back to the mainstream direction. In the downstream region they form the concentrated shed vortex (CSV). The white streamlines rise up under the black streamlines straight towards midspan. They form the trailing edge separation vortex. A traverse section behind the cascade, about 46% chord behind the cascade, is also presented in the figures with cross velocity vector lines. The existence of passage vortex (PV) and concentrated shed vortex (CSV) can be easily identified from the nodes in the surface streamline pattern.

NASA Rotor 67

An interesting test case, computed by several groups, is the transonic NASA rotor 67, documented in Fottner (1990). We compare here four calculations with the experimental data. Chima (AGARD CP-510, Paper 21) applies a Baldwin–Lomax algebraic model, with a periodic C-grid of 185x40x45= 362,600 points and no points in the clearance gap. This fine mesh calculation allows the identification, through particle traces, of regions of separation at the leading edge and at the trailing edge, figure 38, too small to have been seen in the experimental laser data and similar to the CSV vortex of figure 35. These structures are also observed by Jennions and Turner (1992) on a non-periodic grid of 137x49x49=328,937 points (4 radial points in the clearance gap) with a k-ε turbulence model with wall functions. Arnone (1993) applies a similar non-periodic, nearly

orthogonal grid of 137x49x49 = 328,937 points (4 radial points in the clearance gap) with a Baldwin–Lomax algebraic model. These three codes are based on central schemes with artificial viscosity and Runge-Kutta time stepping. The calculations of Weber and Delaney (1991) are performed with a periodic O-grid and nearly orthogonal lines. A comparison with a C-grid having lines parallel to the pitchwise direction shows a poor shock resolution for the high stagger blade sections, because of the high sheared mesh cells. The mesh is 199x31x61= 376309 points, without points in the clearance gap. The scheme is based on central discretization and an implicit, approximate factorisation time integration. The Baldwin-Lomax turbulence model is applied.

Figure 39 compares the performance curves from the first three calculations. The results of Chima overpredict somewhat the efficiency and the pressure ratio, probably due to the absence of tip clearance in the computation, while all authors underestimate the shocking mass flow by 1 to 1.5%. Blade section iso-Mach plots are shown on the next figures 40 and 41, respectively at near-peak-efficiency and near-stall conditions. All computations reproduce the main features of the experimental observations, with regard to shock structure and position. However, more detailed blade-to-blade distributions, only shown by Chima, indicate large differences with the observed data, such as Mach number level, thickness and position of wakes.

Many factors make very detailed validations in rotating blade rows, even isolated rotors, difficult. Since the four computations predict quite accurately averaged total pressure spanwise distributions, differences in mass flow lead to significant differences in flow angles, which will affect the detailed blade-to-blade distributions. Moreover the experimental data are influenced, in addition to the measurement errors, by small inlet flow distortions, by blade deformation and varying clearance during rotation. On the side of the computations, turbulence models will affect greatly the predicted shock-boundary layer interaction and the downstream boundary layer thickness can then strongly influence the blockage and flow distribution in the compressor blades. Stall in modern fan rotors often originates in the tip region due to the interaction between the tip leakage vortex and the in-passage shock system, as shown by Adamczyk et al. (1993). They showed that this interaction plays a major role in determining the fan flow range and therefore sufficient resolution is required in the clearance gap in order to capture the correct strength of the tip leakage and separation vortices, although main parts of this interaction can be captured with as little as four radial points in the gap. This can be seen on figure 24 and on similar results in Jennions and Turner (1992), indicating that important parts of the clearance flow is of inviscid nature.

5.3. LEAKAGE FLOW MODELS

The recognition of the importance of tip clearance on turbine and compressor flows is being expressed by a growing research effort, both experimentally and computationally. Many papers have appeared recently and, although it is not the place here to enter into a detailed discussion of tip leakage flow properties, some points related to validations are in order.

Main components of the tip leakage flow, in turbines and compressors, are pressure dominated and hence can be approached in an inviscid way, implying that even coarse meshes in a clearance gap will provide a valid representation, see for instance Chen et al (1991).

Tip leakage losses generally have three distinct components: i) Reduction in blade force and work done, due to the leakage flow passing over the blade tip essentially without being turned; ii) losses produced inside the gap due to the shear stress and mixing following the vena contracta; iii) mixing of the leakage flow with the passage vortex. Although significant differences can be identified between compressor and turbine clearance flows, due to the opposite direction of relative motion between blade and end-wall and to the generally thinner compressor blades, mixing losses can be captured by coarse meshes, since they result from global energy and momentum conservation, more than from the details of the turbulence. This raises the question of the resolution necessary in tip clearance flow simulations. As will be shown in the following, in order to capture the intensity of the tip leakage and separation vortices and their interaction with the main flow, fine enough meshes, at least 11 radial mesh points over the gap, are necessary.

A detailed evaluation, based on Kang and Hirsch (1992a,b), (1993a), (1994) is summarised here, in relation with the above description of the multiple vortex structure around the blade tip. Two different periodic H-grids were used, the fine mesh has 97x41x45 points in the blade passage and 97x13x13 in the gap, for a total of 195,358 points; while the coarse mesh has 49x21x37 points in the blade passage and 49x13x17 in the gap. In both meshes, there are 13 O-lines leading to 25 points across the blade profile in the gap. Over the gap, however, there are 17 points for the coarse mesh and 13 points for the fine mesh. Hence, it was expected that the fine mesh would produce high accuracy inside the passage, but the coarse one would show more details of the gap flow.

The predicted limiting streamline patterns are shown in figs.42 and 43 at the off-design condition, compared with the experimental observations. It is seen from fig.42b, calculated with the coarse mesh, that the calculations predict the observed endwall flow, such as the reattachment line in the pressure side and the separation line of the tip leakage vortex in the suction side. However, the predicted separation line in Fig.42b is closer to the mid passage downstream of the mid chord than in the experiments. At the trailing edge, for example, the separation line in fig.42a is located at about 26% pitch from the suction side, compared to 36% pitch in fig.42b. No apparent difference was found from the endwall flow patterns between the fine and coarse mesh calculations. Figure 43 presents the predicted limiting streamline patterns on the tip surface at the design and off-design conditions, compared with the ink-trace visualisation of the blade tip. It is seen that the main features of the flow, observed in the visualisation, are reproduced in fig.43b,c and d with both meshes. The reattachment line of the tip separation vortex coincides well with the experiments. It is located near the mean line of the blade profile and disappears at about 70%c downstream of the leading edge in the coarse mesh case (more points over the tip gap). With the fine mesh (less points over the gap), however, the reattachment line is closer to the pressure side edge and disappears near the trailing edge. With a decreasing inlet flow angle, this line (fig.43d) tends to shift towards the pressure side, which implies a reduction of the tip separation vortex core. It is also observed from the calculations that the separation line of the tip separation vortex is not along the pressure side edge but a short distance inside the gap entrance. Figure 44 shows the predicted flow structure around the tip and near the trailing edge with the coarse mesh. It includes the tip separation vortex, the tip leakage vortex and the trailing edge separation vortex. The streamlines, indicated in the figure as tip leakage flow, pass through the midgap of the pressure side. However, the tip secondary vortex of fig.35 is not confirmed in this calculation but is well reproduced in the fine mesh calculation. Comparing the fine and coarse mesh computations, there is almost no difference in midspan pressures. But difference do exists close to the tip. The fine mesh predicts better the unloading in the leading edge region, even though the downstream reloading is still

under predicted. The difference of endwall static pressures between the fine and coarse mesh computation can also be found from fig.45, which shows the static pressure isolines at the off-design condition. Due to the tip leakage vortex motion, the contours of wall static pressure just under the vortex core should exhibit a pressure dip. It is seen clearly that the pressure dip is predicted with the fine mesh calculation but not with the coarse mesh. Under the blade, however, the pressure dip related to the tip separation vortex is well predicted in both meshes.

Figure 46 shows a comparison of the vector lines of secondary flow velocity in selected traverse (S_3) planes, in which S_3 plane No.2 is at the leading edge and S_3 plane No.11 is located at 1% chord before the trailing edge. The secondary flow vectors are obtained by projecting the velocities on the plane normal to the flow direction at midspan at the same pitch coordinate. The spiral nodes occurring in the planes denote respectively the horseshoe vortex (HV), passage vortex (PV), and tip leakage vortex (LTV). Since the clearance allows fluid to pass through the gap, a leading edge horseshoe vortex may be weakened or even not occur, especially when the clearance is large. At the present condition, of 2.0% clearance, one can see a node of the suction side horseshoe vortex (HV_S) from the experimental results (fig.46a) in the suction side of plane No.1 (7.5%c upstream of the leading edge). In the calculations, both pressure and suction side legs of the horseshoe vortex can be seen from the secondary flow field, denoted as HV_P and HV_S respectively in fig.46b and c. The suction side leg dissipates with its stretching into the passage due to both the fluid viscosity and the traverse pressure gradient, and completely disappears at about 11% chord (S_3 plane No.3, or I=41 in fig.46c) downstream of the leading edge. The apparent rotation of the tip leakage vortex starts from about S_3 plane No.5 (32% chord), which compares well with the experimental results. However, the fine mesh calculations predict well the TLV and PV vortices downstream of the cascade. The secondary vortex (SV) around the suction side tip deduced from experiments is well reproduced in the fine mesh calculation, as seen from fig.46c for details in the suction side corner of section I=51 (around mid chord) and I=69 (near the trailing edge). This small size vortex starts before S_3 No.5 and evolves towards downstream along the tip suction side. Near the trailing edge, it wraps round the tip leakage vortex (TLV). The interaction between the tip leakage vortex and the secondary vortex (SV) may cause some instability, since the convergence history of residuals indicates the appearance of some unsteadiness.

All the flow features are captured on the coarse mesh, but the tip leakage vortex (TLV) and the passage vortex (PV) dissipate progressively towards the cascade exit on this coarse mesh, but their intensity is still mesh dependent, since the tip leakage flow is underestimated, which may be attributed to insufficient mesh resolution and/or to the simple turbulence model. More details are to be found in Kang and Hirsch (1994).

6. CONCLUSIONS

The present CFD capability is able to predict the complexity of 3D flows in compressors and turbines, including tip clearance effects, but one is still far away from a reliable representation of all the fine details of turbomachinery flows.

- The analysis of today's CFD methodology shows that reliable and efficient methods are available and that all second order codes will provide similar results on fine enough meshes. Although various schemes react differently on coarse meshes, due to their different numerical dissipation, these aspects of mesh resolution can be evaluated on reference test cases.

- Criteria for mesh quality can be defined and highly sheared meshes are recognised as major sources of loss of accuracy.

- A key issue is connected to turbulence and transition modelling. Although simple attached turbulent flows can be accurately predicted with current models, the complex flows encountered in turbomachinery require more reliable and general models. The importance of transition for separation, heat transfer, shock-boundary layer interactions, a.o., cannot be overstated. Nor can the recognition of the urgent need for engineering guidelines for transition criteria.

- The mesh resolution needed for reliable estimations of losses and turbulence are rather severe and require mesh points close enough to the walls, in order to resolve the inner eddy viscosity.

- Predictions of all flow details need very fine meshes and better turbulence models.

- Validation of turbomachinery flows is also made difficult due to uncertainties in experimental data, lack of simultaneous matching of calculated and measured pressure ratios and mass flows, boundary conditions particularly in multistage environments, blade geometry variations during rotation, tip clearance geometry.

- In order to evaluate the level of validation on coarse meshes, a good understanding of the complex 3D flows in compressors and turbines is necessary. This allows to identify the phenomena of basically inviscid origin, such as parts of the secondary and tip leakage flows; those depending on overall conservation laws, such as mixing effects on global losses; and those depending on the fine details of the turbulence structure.

The present experience on turbomachinery CFD validation shows that

- the overall 3D flow structure can be globally reproduced with coarse meshes of the order of 50,000 to 100,000 points, including the tip clearance gap. This allows the systematic use, at the design level, of coarse mesh computations of 3D turbulent Navier–Stokes flows, with the main objective of identifying general trends on global quantities such as losses.

- the current level of fine mesh calculations, with 200,000 to 300,000 points may still not be fine enough to ensure mesh independence and to reproduce quantitatively all the details of the flow.

- there is a great need for further research in turbulence and transition models, with sufficient generality as to cover most of the turbomachinery phenomena. A consistent effort has to be done on reference test cases for turbulence validation of the elementary physical phenomena.

Finally, a continuous effort on global turbomachinery validation should be pursued, in order to develop a better knowledge for the efficient use of CFD tools in turbomachinery design. This requires a coordinated effort between research and industry in the exchange and comparisons of test case computations, and a strong interaction between experimentalists and CFD specialists.

7. REFERENCES

Adamczyk J. J., Celestina M. L., Greitzer E. M. (1993). "The Role of Tip Clearance in High-Speed Fan Stall" Transactions of the ASME, J. of Turbomachinery, Vol.115, pp.28-39.

AGARD (1991). Proc. 77th Propulsion and Energetics Panel Symposium on CFD Techniques for Propulsion Applications, AGARD CP 510.

Allmaras S. (1992). "Contamination Of Laminar Boundary Layers By Artificial Dissipation In Navier-Tokes Solutions", Proc.Conf. on Numerical Methods in Fluid Dynamics, Ed. W.K. Morton, Reading, UK.

Arnone A., Liou M., Povinelli L. (1991). "Multigrid Calcualations Of Three-Dimensional Viscous Cascade Flows", Aiaa Paper 91-3238, NASA TM 105257, ICOMP-91-18.

Arnone A. (1993). "Viscous Analysis Of Three-Dimensional Flows Using A Multigrid Method", NASA TM 106266, ICOMP-93-25.
Baldwin, B.; Lomax, H. (1978). "Thin Layer Approximation and Algebraic Model for Separated Turbulent Flow". AIAA Paper 78-0257, AIAA 16th Aerospace Sciences Meeting.
Beam R.M., Warming R.F. (1978). "An Implicit Factored Scheme For The Compressible Navier-Stokes Equations". AIAA Journal, Vol. 16, pp. 393-402.
Birch N.T. (1987). "Navier-Stokes Predictions of Transition, Loss and Heat Transfer in a Turbine Casscade", ASME Paper 87-GT-22.
Biswas D., Fukuyama Y. (1993). "Calculation of Transitional Boundary Layers with an Improved Low-Reynolds Number Version of the k-e Turbulence Model", ASME Paper 93-GT-73.
Cebeci T., Bradshaw P. (1984) Physical and Computational Aspects of Convective Heat Transfer, Springer Verlag, New York.
Cebeci T., Smith A.M.O. (1974). Analysis of Turbulent Boundary Layers. Academic Press, New York.
Chen, P. H., and Goldstein, R. J., (1991). "Convective Transport Phenomena on the Suction Surface of a Turbine Blade Including the Influence of Secondary Flows Near the Endwall", ASME Paper No.91-GT-35.
Chen, T. G. Greitzer, M. E. Tan C. S. Marble, F. E. (1991). "Similarity Analysis of Compressor Tip Clearance Flow Structure," ASME J. of Turbomachinery, Vol.113, pp.260-271.
Chima R.V., Giel P.W., Boyle R.J. (1993). "An Algebraic Turbulence Model for Three-Dimensional Viscous Flows", NASA TM 105931.
Cho N.H., Liu X., Rodi W., Schönung B. (1992). "Calculation of Wake-Induced Unsteady Flow in a Turbine Cascade", ASME Paper 92-GT-306.
Dawes W.N. (1986). "A Pre-Processed Implicit Algorithm For 3D Viscous Compressible Flows". In Proc. 6th GAMM Conference On Numerical Methods In Fluid Dynamics, D. Rues, W.Kordulla, Eds, Notes On Numerical Fluid Mechanics, Vol.13, pp.70-77, Vieweg, Braunschweig
Dawes W.N. (1988). "Development Of A 3D Navier-Stokes Solver For Applicatopns To All Types Of Turbomachinery" ASME Paper 88-Gt-70
Dawes W.N. (1991). " The Development Of A Solution Adaptive 3D Navier-Stokes Solver For Turbomachinery", AIAA Paper 91-2469, AIAA/SAE/ASME/ASEE 27th Joint Propulsion Conference
Denton J. (1975). "A Time Marching Method For Two And Three Dimensional Blade To Blade Flows". Aeronautical Research Council, R & M 3795.
Denton J. (1982). "An Improved Time Marching Method For Turbomachinery Flow Calculations". In Numerical Methods In Aeronautical Fluid Dynamics, P.L. Roe Ed. Academic Press, London.
Dorney D., Davis R. (1991). "Navier-Stokes Analysis of Turbine Blade Heat Transfer and Performance", Proc. 77th PEP Symposium on CFD Techniques for Propulsion Applications, AGARD CP 510. See also Transactions of the ASME, J. of Turbomachinery, Vol.114, pp.795-806.
Fottner L., Ed. (1990). Test Cases for Computation of Internal Flows in Aero Engine Components, AGARD-AR-275.
Fourmaux A., Le Meur A. (1987). "Computation Of Unsteady Pheenomena In Transonic Turbines And Compressors". Onera Report TP 131, Onera, France
Granville P.S. (1987). "Baldwin-Lomax Factors for Turbulent Boundary Layers in Pressure Gradients". AIAA Journal, Vol.25, pp.1624-1627.
Gregory-Smith, D. G., Cleak, J. G. E., (1992). "Secondary Flow Measurements in a Turbine Cascade with High Inlet Turbulence," ASME J. of Turbomachinery, Vol.114, pp.173-183.
Gregory-Smith D. G. (1993). "The ERCOFTAC Seminar and Workshop on 3D Turbomachinery Flow Prediction, December 1992", ASME Paper 93-GT-423.
Haase W. et al. Eds (1993). EUROVAL-A European Initiative on Validation of CFD Codes, Notes on Numerical Fluid Dynamics , Vol. 42, Vieweg Verlag.
Hah C. (1984). "A Navier-Stokes Analysis Of Three-Dimensional Turbulent Flows Inside Turbine Blade Rows At Design And Off-Design Conditions". Trans.ASME, Journal of Engineering for Gas Turbines and Power, Vol.106, pp.421-429.
Hah C. (1987a). "Numerical Solution of Three-Dimensional Flows for Modern Gas Turbine Components", ASME Paper 87-GT-84.
Hah C. (1987b). "Calculation of Three-Dimensional Viscous Flows in Turbomachines with an Implicit Relaxation Method", AIAA Journal of Propulsion and Power, Vol. 3, pp.415-422.
Harten A. (1983). "High Resolution Schemes For Hyperbolic Conservation Laws". Journal Of Computational Physics, Vol. 49, pp. 357-393.
Hänel D. (1991). "Computational Techniques for Solving the Navier-Stokes Equations", Proc. 77th Propulsion and Energetics Panel Symposium on CFD Techniques for Propulsion Applications, AGARD CP 510.
Harten A. (1984). "On A Class Of High Resolution Total Variation Stable Finite Difference Schemes". Siam Journal of Numerical Analysis, Vol. 21, pp. 1-23.
Hirsch Ch. (1988). Numerical Computation Of Internal And External Flows. Vol.1: Fundamentals Of Numerical Discretization. J. Wiley & Sons, Chichester .
Hirsch Ch. (1990). Numerical Computation Of Internal And External Flows. Vol.2: Computational Methods For Inviscid And Viscous Flows. J. Wiley & Sons, Chichester.
Hirsch, Ch., Lacor, C., Dener, C., And Vucinic, D., (1991), "An Intergrated CFD System For 3D Turbomachinery Applications", Proc. 77th PEP Symposium on CFD Techniques for Propulsion Applications, AGARD CP 510.
Horton G., Harasgama S., Chana K. (1991). "Prediction and Measurements of 3D Viscous Flows in a Transonic Turbine Nozzle Guide Vane Row", Proc. 77th PEP Symposium on CFD Techniques for Propulsion Applications, AGARD CP 510.
Jameson A., Schmidt W., Turkel E. (1981). "Numerical Simulation Of The Euler Equations By Finite Volume Methods Using Runge-Kutta Time Stepping Schemes". AIAA Paper 81-1259 - AIAA 5th Computational Fluid Dynamics Conference.
Jameson A. (1982). "Transonic Aerofoil Calculations Using The Euler Equations". In Numerical Methods In Aeronautical Fluid Dynamics , P.L.Roe, Ed., Academic Press, New York.
Jameson A. (1993). "Artificial Diffusion, Upwind Biasing, Limiters and their Effect on Accuracy and Multigrid Convergence in Transonic and Hypersonic Flows", AIAA Paper 93-3359 - AIAA 11th Computational Fluid Dynamics Conference.
Jennions I.K., Turner M.J. (1992). "Three-Dimensional Navier-Stokes Computations of Transonic Fan Flow Using an Explicit Flow Solver and an Implicit k-ε Solver", ASME Paper 92-GT-309.
Kang, S., Hirsch, Ch., (1991). "Three Dimensional Flows in a Linear Compressor Cascade at Design Conditions," ASME paper No.91-GT-114.
Kang, S., Hirsch, Ch., (1992a). "Experimental Study on the Three Dimensional Flow within a Compressor Cascade with Tip Clearance: Part I -- Velocity and Pressure Fields," ASME paper No.92-GT-215.
Kang, S., Hirsch, Ch., (1992b). "Experimental Study on the Three Dimensional Flow within a Compressor Cascade with Tip Clearance: Part II -- The Tip Vortex," ASME paper No.92-GT-432.
Kang. S., Hirsch, Ch.. (1993a). "Tip Leakage Flow in a Linear Compressor Cascade", ASME Paper GT-93-303.
Kang. S., Hirsch, Ch.. (1993b). "The Three Dimensional Flow in a Compressor cascade at Design and Off-Design Conditions", Proceeding of 2nd ISAIF, Prague.
Kang. S., Hirsch, Ch.. (1994). "Numerical Simulation of 3D Viscous Flow in a Linear Compressor Cascade with Tip Leakage", ASME Paper GT-94- .To be published
Kiock R., Lehthaus F., Baines N. Sieverding C. (1986). "The Transonic Flow Through a Plane Turbine Cascade as Measured in Four European Wind Tunnels", ASME Journal of Engineering for Gas Turbines and Power, Vol 108, pp.277-284.

Koeck C. (1985). "Computation Of Three-Dimensional Flow Using The Euler Equations And A Multiple-Grid Scheme". Int. Journal For Numerical Methods In Fluids, Vol. 5, pp. 483-500.
Launder, B.E., Spalding B. (1972). **Mathematical Models of Turbulence**. Academic Press, New York.
Lax P.D., Wendroff B. (1960). "Systems Of Conservation Laws". Comm. Pure And Applied Mathematics, Vol. 13, pp. 217-237.
Lax P.D., Wendroff B. (1964). "Difference Schemes For Hyperbolic Equations With High Order Of Accuracy". Comm. Pure And Appl. Math., Vol. 17, pp. 381-398.
Lerat A. (1979). "Une Classe De Schémas Aux Différences Implicites Pour Les Systêmes Hyperboliques De Lois De Conservation". Comptes Rendus Acad. Sciences, Paris, Vol. A288, pp. 1033-1036.
Lerat,A. (1985), " Implicit Methods of Second Order Accuracy For The Euler Equations". AIAA Journal, Vol. 23, pp.33-40.
Leschziner M.A., Launder B.E., Eds (1993). Proceedings of the 2nd ERCOFTAC–IAHR Workshop on Refined Flow Modelling, Univ. of Manchester,UK.
Lien F-S., Leschziner M.A. (1993). "A Pressure-Velocity Solution Strategy for Compresible Flow and its Application to Shock/Boundary Layer Interaction Using Second–Moment Turbulence Closure", Trans.ASME, Journal of Fluids Engineering, Vol.115, pp.717-725.
Maccormack R.W. (1969). "The Effect Of Viscosity In Hypervelocity Impact Cratering". AIAA Paper 69-354.
Maccormack R.W. (1971). "Numerical Solution Of The Interaction Of A Shock Wave With A Laminar Boundary Layer". Proc. Second International Conference On Numerical Methods In Fluid Dynamics, pp. 151-163, Lecture Notes In Physics, Vol. 8, Springer, Berlin.
Matsuo Y. (1991). "Computations of Three-Dimensional Viscous Flows in Turbomachinery Cascades", AIAA/SAE/ASME/ASEE 27th Joint Propulsion Conference, AIAA–91-2237.
Mc Donald P.W. (1971). "The Computation of Transonic Flow Through Two-Dimensional Gas Turbine Cascades". ASME Paper 71-Gt-89.
Moore, J., Moore, G. J., (1989). "Shock Capturing And Loss Predictions For Transonic Turbine Blades Using A Pressure Correction Method", 27xth ISABE Meeting, Athens.
Nakahashi K., Nozaki O., Kikuchi K. Tamura A. (1987). "Navier-Stokes Computations of Two- And Three-Dimensional Cascade Flow Fields". AIAA-Paper 87-1315, AIAA 19th Fluid Dynamics, Plasma Dynamics and Lasers Conference.
Ni R.N. (1982), "A Multiple Grid Scheme For Solving The Euler Equations". AIAA Journal, Vol.20, pp. 1565-1571.
Osher S. (1982). "Shock Modelling In Aeronautics". In Numerical Methods For Fluid Dynamics. Ed. by K.W.Morton And M.J.Baines, Academic Press, London, pp.179-218.
Patankar S.V., Spalding D.B. (1972). "A Calcualtion Procedure For Heat,Mass And Momentum Transfer In Three-Dimensional Parabolic Flows". Int. Jour. Heat Mass Transfer, Vol.15, pp. 1787-1806.
Patankar S.V. (1980). "Numerical Heat Transfer And Fluid Flow". Hemisphere Publ. Co./ Mc Graw Hill, New York
Roe P.L.(1981). "Approximate Riemann Solvers, Parameter Vectors And Difference Schemes", Journal of Computational Physics, Vol. 43, pp. 357-372.
Savill M. (1992). "Evaluating Turbulence Predictions of Transition– an ERCOFTAC SIG Project", in Advances in Turbulence, F. Nieuwstadt Ed., Kluwer Acad. Publ., pp.555.
Savill M. (1993). "Further Progress in the Turbulence Modelling of By-Pass Transition", in Engineering Turbulence Modelling and Experiments, W. Rodi, F. Martelli, Eds, Elsevier Publ., pp.583.
Sharma O.P. (1987). "Momentum and Thermal Boundary Layer Development on Turbine Airfoil Suction Surfaces", AIAA Paper 87-1918.
Sharma O.P., Syed S.A. (1991). "Turbulence Modelling in Gas Turbine Design and Analysis", AIAA 29st Aerospace Sciences Meeting, Reno - AIAA Paper 91–0514.
Sieverding, C.H., (1990). "Experimental Test Cases for Turbines" in Test Cases for Computation of Internal Flows in Aero Engine Components, L. Fottner Ed., AGARD-AR-275.
Schulz H.D., Gallus H.E.(1988). "Experimental Investigation of the Three-Dimensional Flow in an Annular Compressor Cascade", ASME Paper 88-GT-201.
Steger J.L., Warming R.F. (1981). "Flux Vector Splitting Of The Inviscid Gas-Dynamic Equations With Applications To Finite Difference Methods". Journal Computational Physics, Vol. 40, pp. 263-293.
Tatsumi S., Martinelli L., Jameson A.(1994). "Design, Implementation and Validation of Flux Limited Schemes for the Solution of the Compressible Navier-Stokes Equations", AIAA Paper 94-0647 - AIAA 32nd Aerospace Sciences Meeting.
Turner M.J., Jennions I.K. (1992). "An Investigation of Turbulence Modelling in Transonic Fans Including a Novel Implementation of an Implicit k-ε Turbulence Model", ASME Paper 92-GT-308.
Turner M., Liang T., Beauchamp P., Jennions I. (1993). "The Use of Orthogonal Grids in Turbine CFD Computations", ASME Paper 93-GT-38.
Van Leer B.(1979). "Towards The Ultimate Conservative Difference Scheme. V. A Second Order Sequel To Godunov's Method". Journal of Computational Physics, Vol. 32, pp. 101-136.
Van Leer B. (1982). "Flux Vector Splitting for the Euler Equations". Proc. 8th Int. Conf. on Numerical Methods in Fluid Dynamics; Lecture Notes In Physics, Vol.170, pp.507-512, Springer Verlag.
Veuillot J.P., Meauze G. (1985). "A 3D Euler Method for Internal Transonic Flow Computations with a Multi-Domain Approach", AGARD-LS-140.
Visbal, M.; Knight, D. (1983). "Evaluation of the Baldwin-Lomax Turbulence Model for Two-Dimensional Shock Wave Boundary Layer Interactions". AIAA Paper 83-1697, AIAA 16th Fluid and Plasma Dynamics Conference.
Yee H.C. (1985). "On Symmetric And Upwind Tvd Schemes", Proc.6th GAMM Conf. On Numerical Methods In Fluid Mechanics, pp. 399-407, Vieweg, Braunschweig
Yee H.C. (1987). "Construction Of Explicit And Implicit Symmetric Tvd Schemes And Their Applications", Journal Of Computational Physics, Vol. 68, pp. 151-179.
York B., Knight D. (1985). "Calculation of Two-Dimensional turbulent boundary layers using the Baldwin-Lomax model". AIAA Journal, Vol.23, pp.1849-1850.

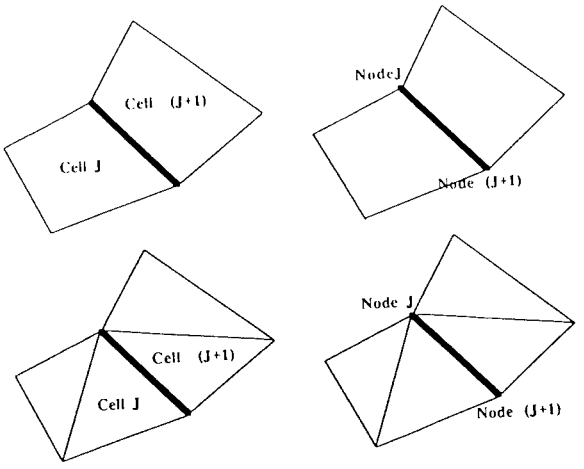

Figure 1: Cell centered and cell vertex configurations for structured and unstructured meshes.

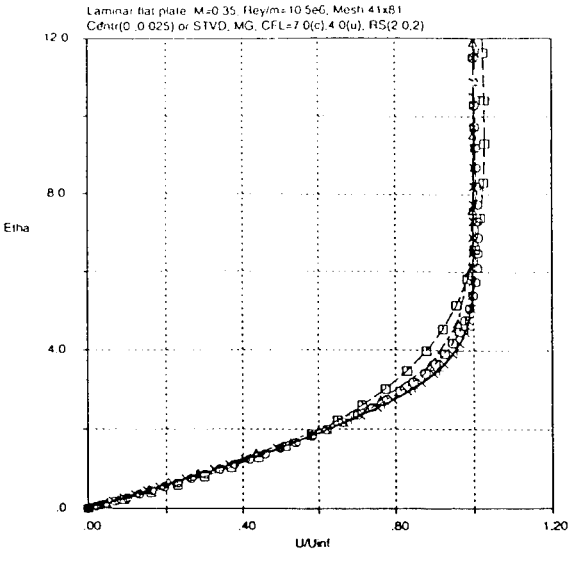

Figure 2: Comparison of laminar profiles with upwind (U) and central schemes (C) on different meshes.

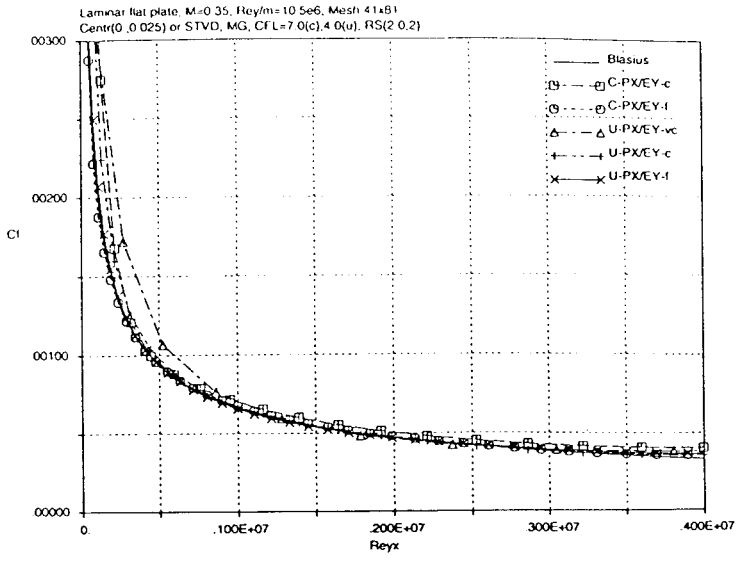

Figure 3: Comparison of laminar skin friction with upwind (U) and central schemes (C) on different meshes.

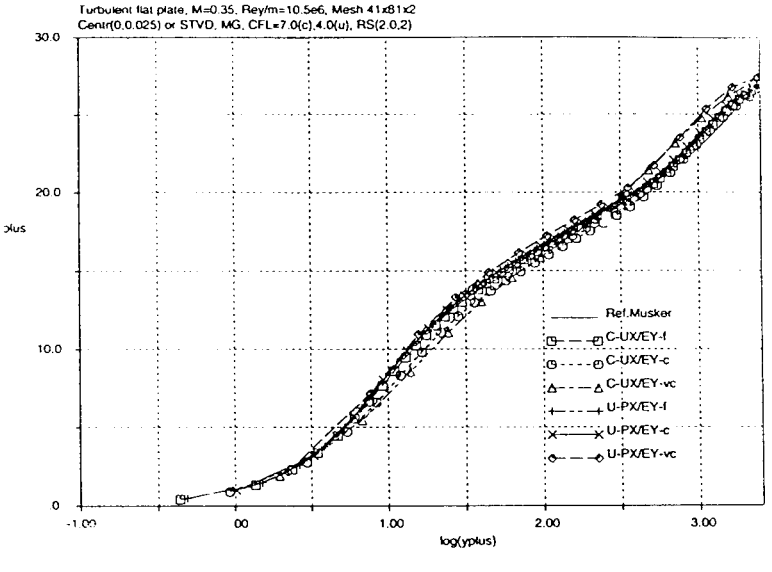

Figure 4: Comparison of turbulent profiles with upwind (U) and central schemes (C) on different meshes.

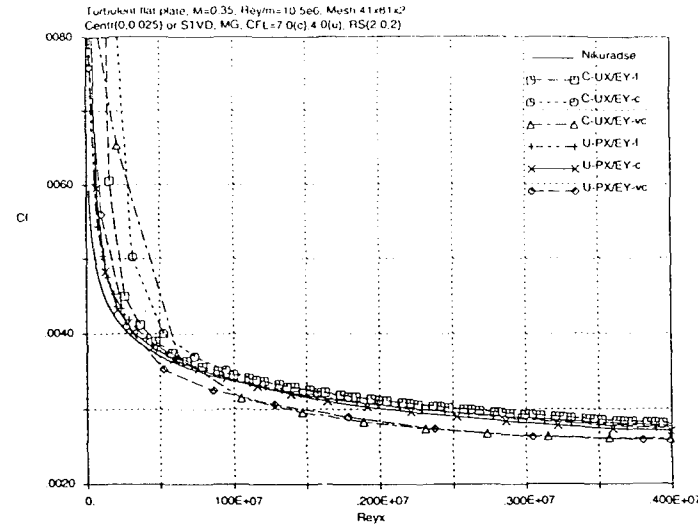

Figure 5: Comparison of turbulent skin friction with upwind (U) and central schemes (C) on different meshes.

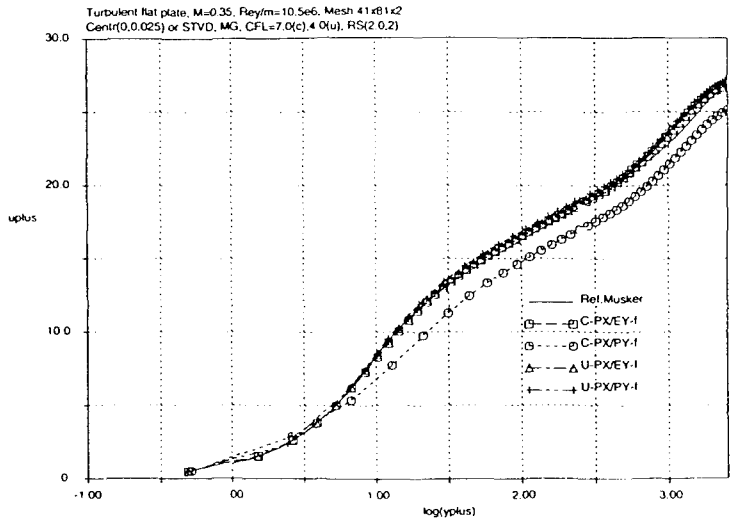

Figure 6: Comparison of turbulent profiles with upwind (U) and central schemes (C) on different meshes.

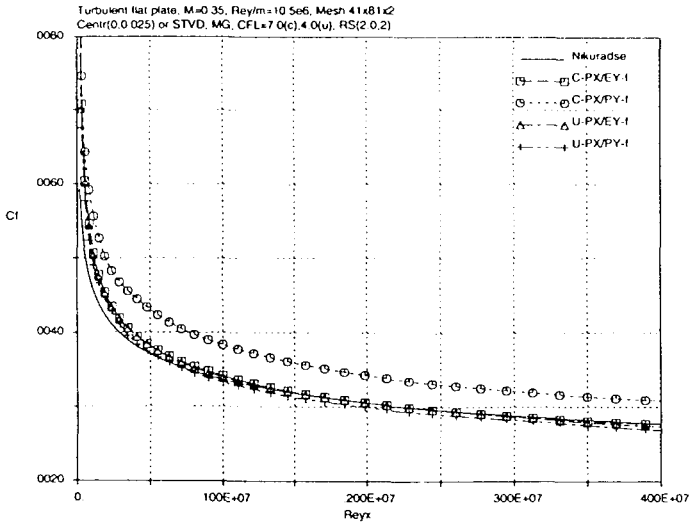

Figure 7: Comparison of turbulent skin friction with upwind (U) and central schemes (C) on different meshes.

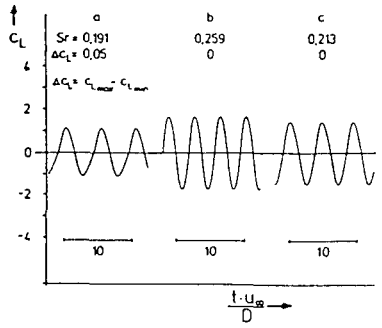

Time histories of the lift for unsteady flow around a circular cylinder, Re=3000, Ma=0.3, 177x113 grid points.
a) grid stretched in cirumferential direction, coefficient of fourth order damping $\epsilon^{(4)} = 1/256$
b) grid equidistant in cirumferential direction, coefficient of fourth order damping $\epsilon^{(4)} = 1/256$
c) grid equidistant in cirumferential direction, coefficient of fourth order damping $\epsilon^{(4)} = 1/32$

Figure 8: from Hänel (1991)

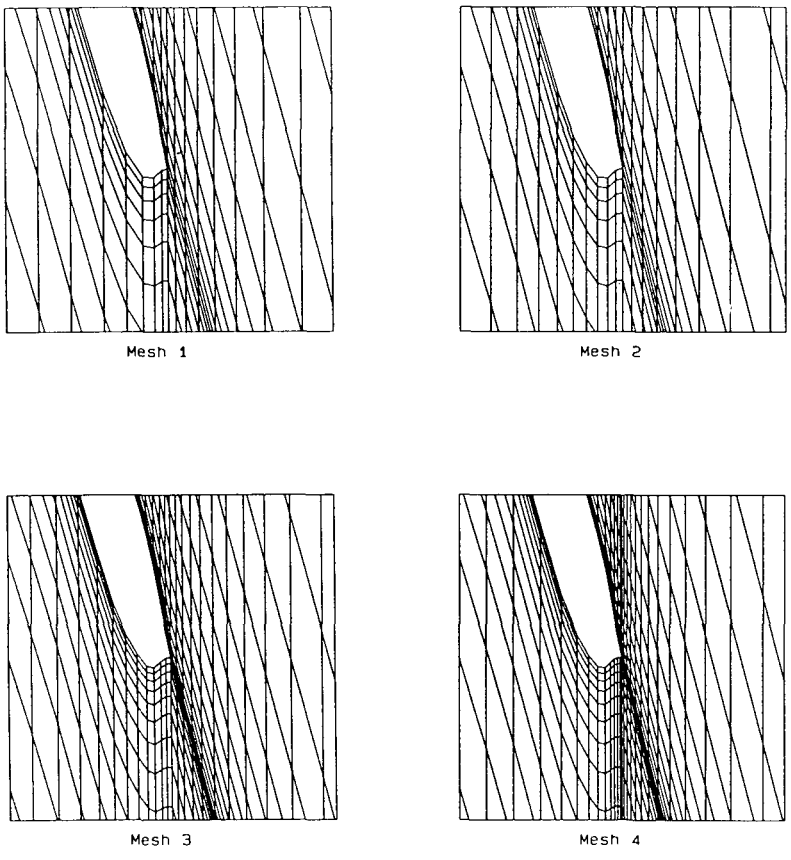

Figure 9: Details of mesh near trailing edge; from Horton et al. (1991).

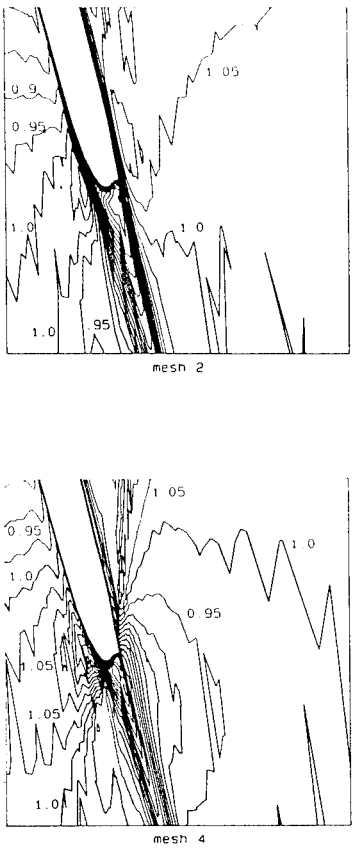

Figure 10: Contours of Mach number near trailing edge; from Horton et al. (1991).

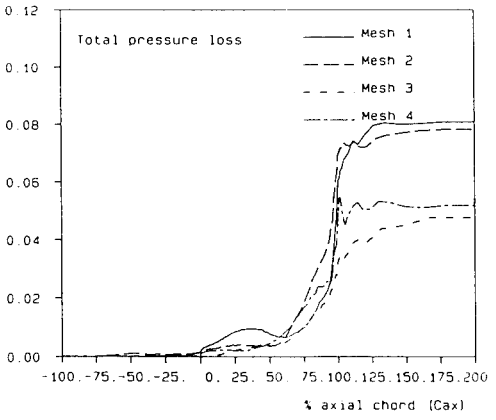

Figure 11: Development of total pressure loss with different meshes; from Horton et al. (1991).

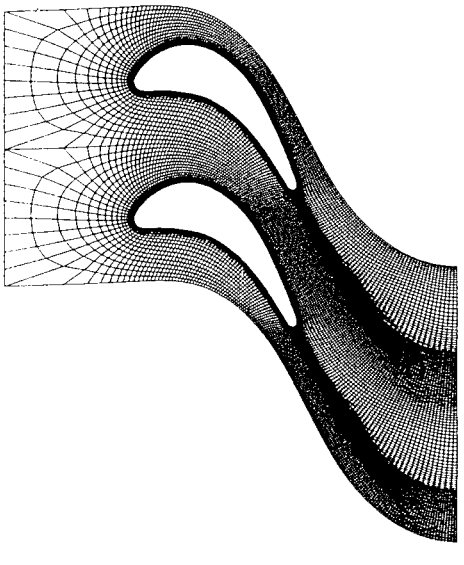

Figure 12: A 385 x 33 nonperiodic C-type grid for the VKI LS59 rotor blade.
from Arnone and Swanson (1993)

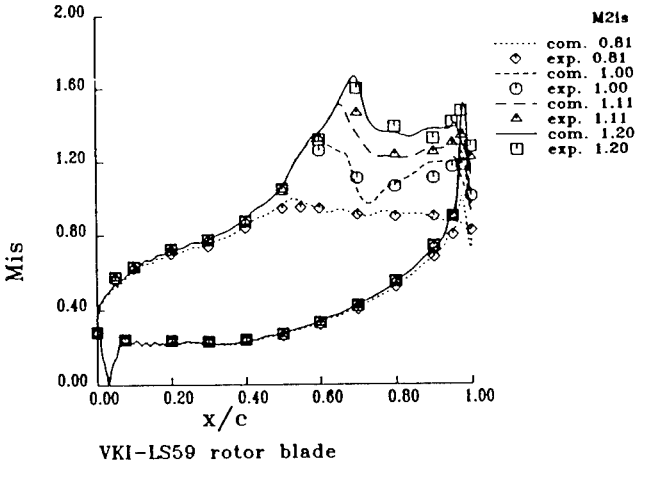

Figure 13: Isentropic Mach number distribution for different values of M_{2is} (769 x 65 grid)
from Arnone and Swanson (1993)

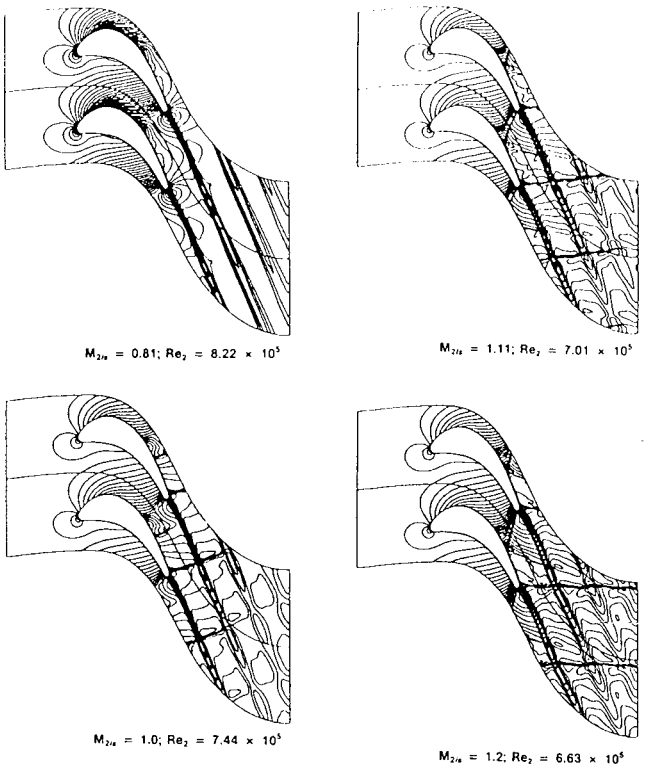

Figure 14: Mach number contours for turbine blade cascade (769 x 65 grid) from Arnone and Swanson (1993)

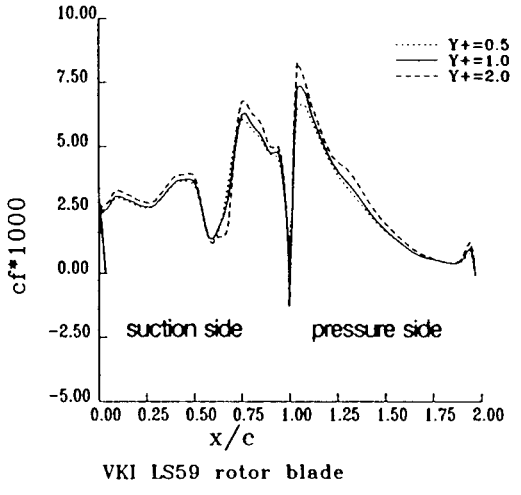

Figure 15: Effect of Y^+ on skin-friction distribution (M_{2is} = 0.81) from Arnone and Swanson (1993)

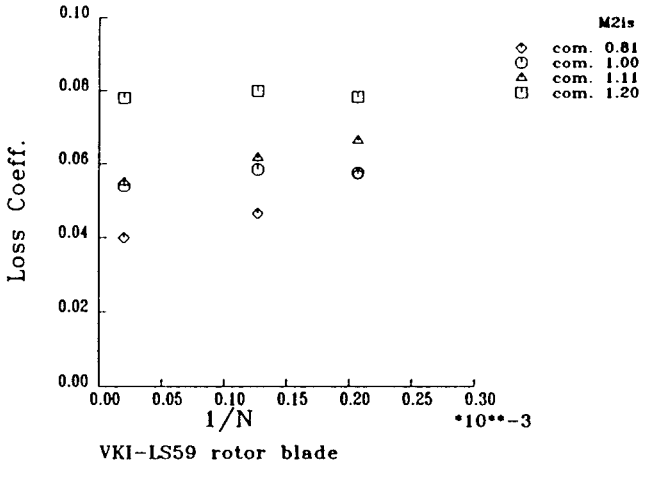

Figure 16: Variation of loss coefficient with reciprocal of number of mesh points. from Arnone and Swanson (1993)

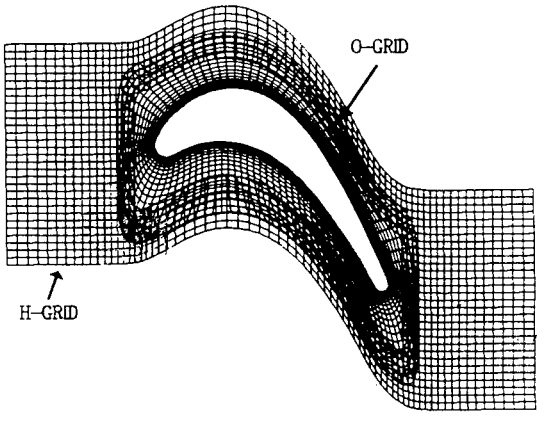

Figure 17: Blade-to-blade computational grid for Langston cascade.
from Dorney and Davis (1991)

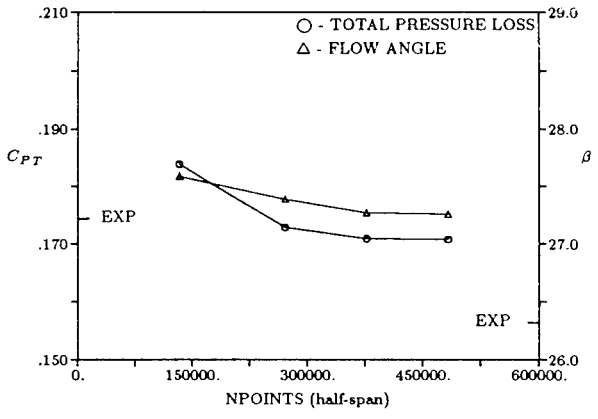

Exit flow angle and total pressure loss as a function of grid point density

a

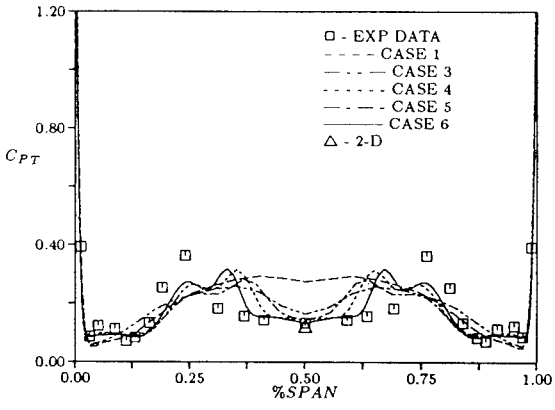

Gap-averaged total pressure coefficient distributions

b

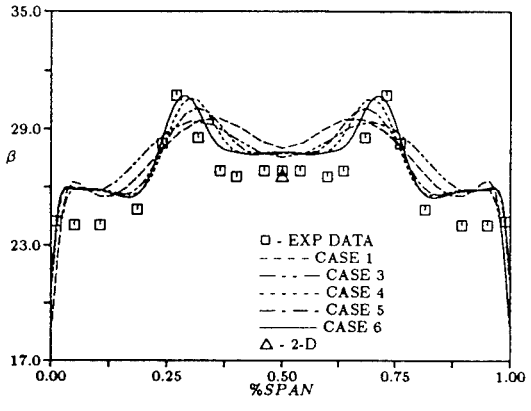

Gap-averaged flow angle distributions

c

Figure 18 : Loss and angle distributions in function of grid point density. from Dorney and Davis (1991)

Table 1 : Grid refinement study
from Dorney and Davis (1991)

Case	Grid Density stream×tang×span	Δy_{blade} (y^+)	$\Delta y_{endwall}$ (y^+)	Profile $\Delta P_T/P_{T_1}$	Total $\Delta P_T/P_{T_1}$	Profile β_2	Total β_2	Trns
1	H-70 × 31 × 25	0.00100	0.00300	0.20846	0.19065	27.96	27.34	yes
	O-101 × 31 × 25	(4.260)	(7.430)					
2	H-70 × 31 × 25	0.00010	0.00100	0.16102	0.18373	27.49	27.36	no
	O-101 × 31 × 25	(0.384)	(2.920)					
3	H-70 × 31 × 25	0.00010	0.00100	0.16100	0.18372	27.49	27.58	yes
	O-101 × 31 × 25	(0.379)	(2.781)					
4	H-70 × 31 × 51	0.00010	0.00010	0.14575	0.17271	27.67	27.38	yes
	O-101 × 31 × 51	(0.360)	(0.266)					
5	H-70 × 31 × 71	0.00010	0.00010	0.13898	0.17075	27.73	27.26	yes
	O-101 × 31 × 71	(0.351)	(0.266)					
6	H-70 × 31 × 91	0.00010	0.00010	0.13051	0.17064	27.75	27.25	yes
	O-101 × 31 × 91							
2-D	O-131 × 61	0.00002	—	0.12030	—	26.58		yes
	H-71 × 21	(0.059)	—					
EXPT	—	—	—	0.13000	0.17437	26.80	26.32	—

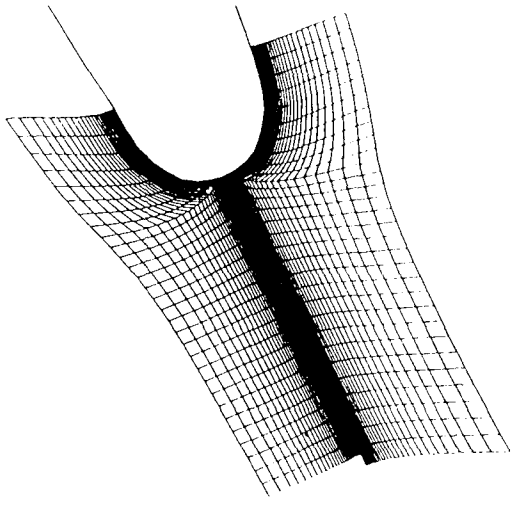

Figure 19a: Blowup of trailing edge (769 x 65 grid) ; from Arnone and Swanson (1993)

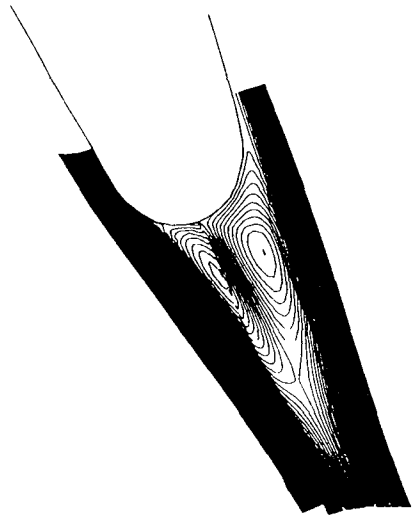

Figure 19b: Streamfunction contours (M_{2is} = 1.0); from Arnone and Swanson (1993)

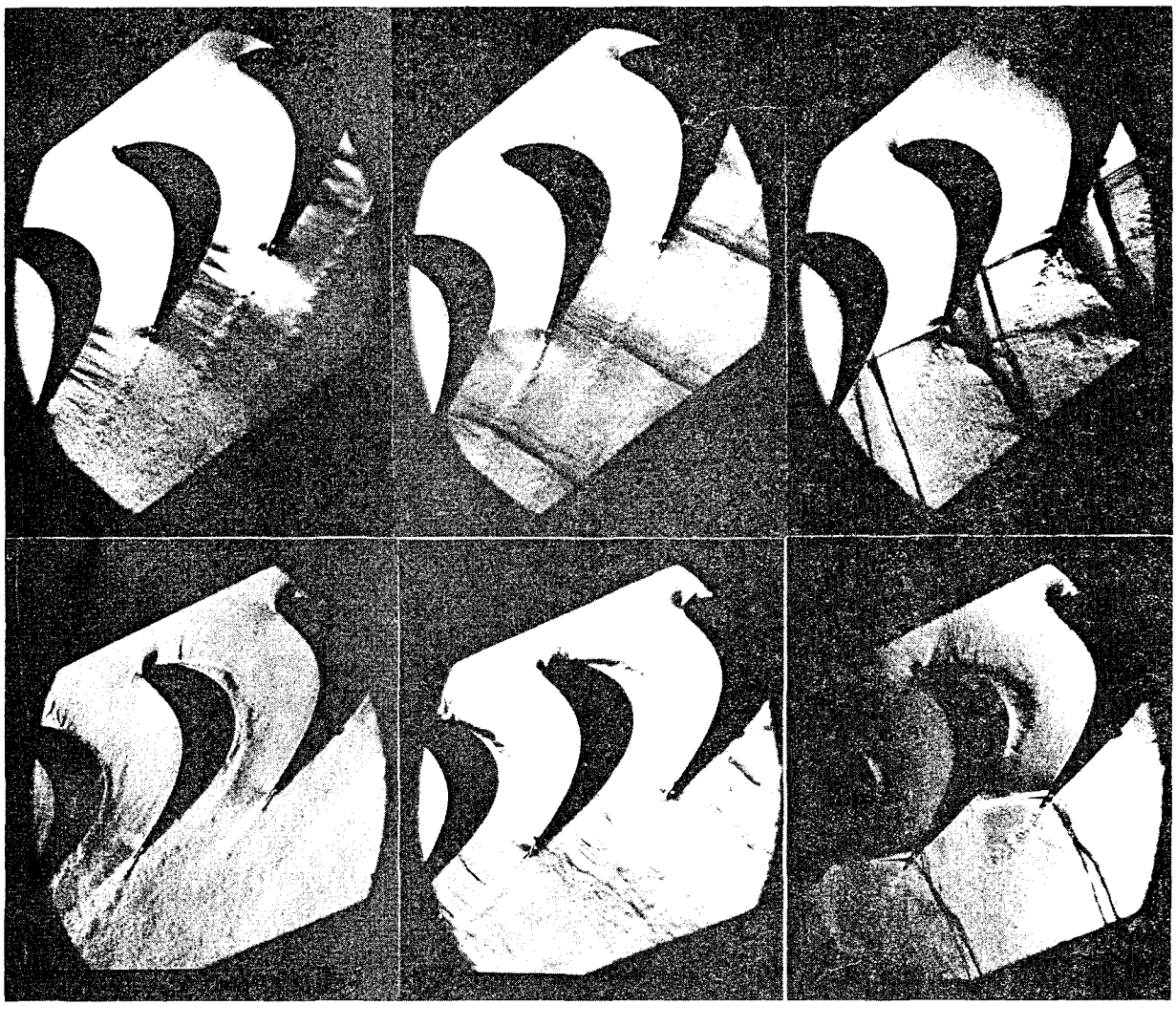

Figure 20 : Schlieren pictures β_1=140° (top), β_1=155° (bottom):subsonic case (left) sonic case (mid.), supersonic case (right).
from Detemple - Laake (1991)

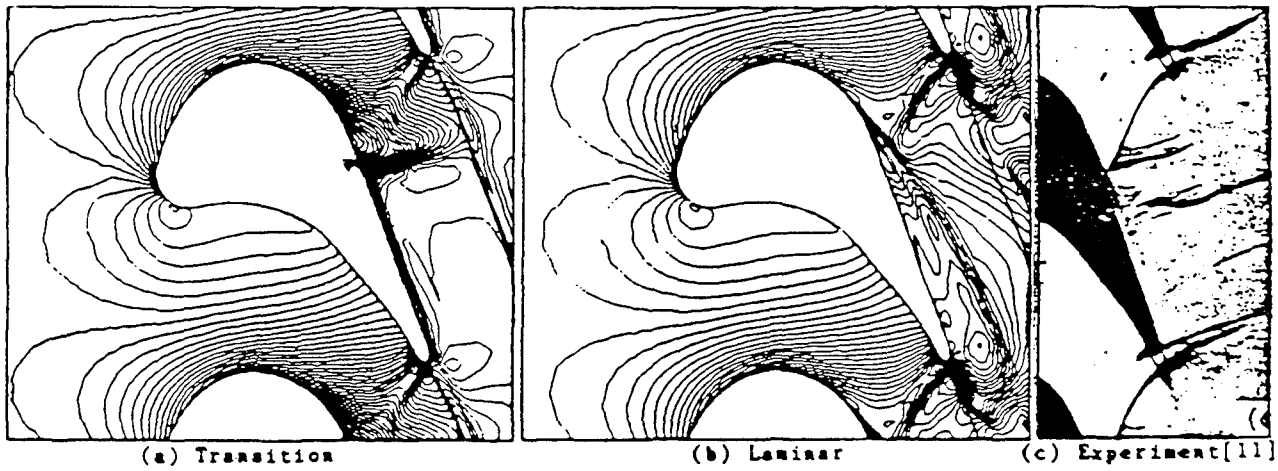

Figure 21 : Computed density contours and Schlieren photograph for a high-turning transonic turbine cascade at M_{2th}=0.91, α_1=60° and Re_2=8.6x10^6
from Nakahashi et al. (1987)

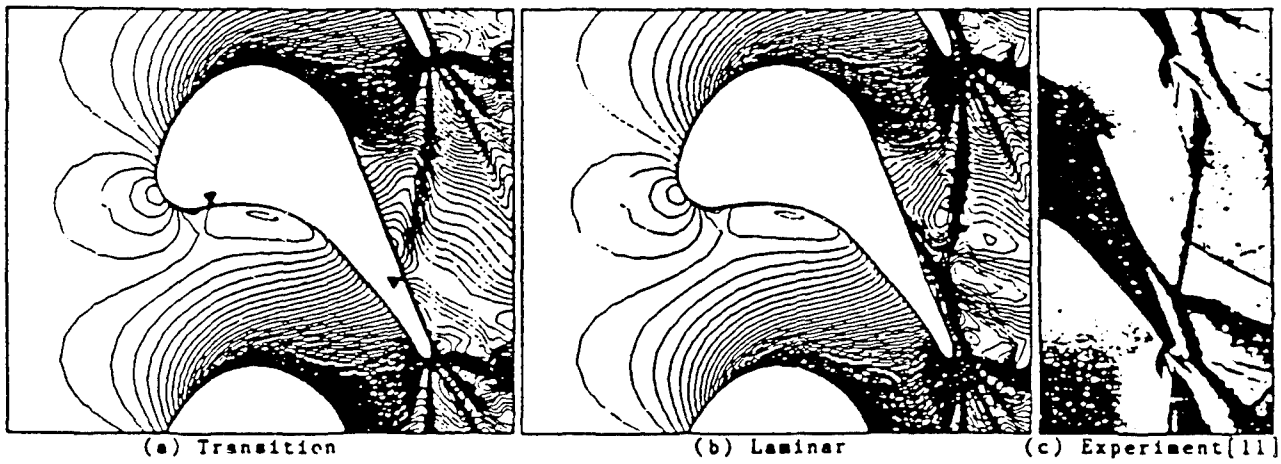

Figure 22 : Computed density contours and Schlieren photograph for a high-turning transonic turbine cascade at M_{2th}=1.43, α_1=40° and Re_2=8.6x10^6
from Nakahashi et al. (1987)

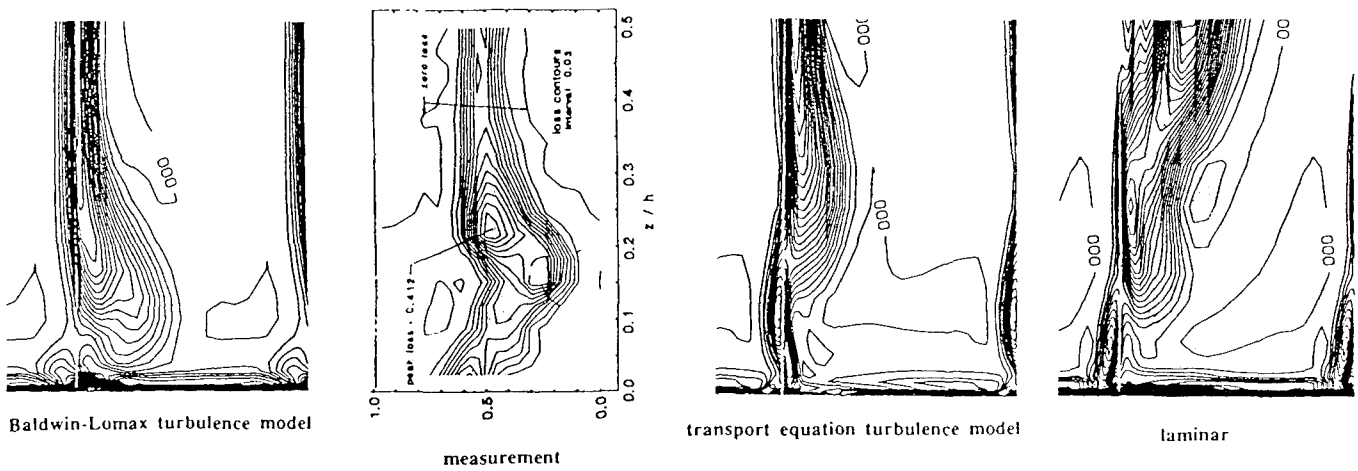

Figure 23 : Comparison of predicted loss coefficient (interval 0.035) with measurement (interval 0.030) in a cross-flow plane at 142% axial chord.
from Dawes (1990)

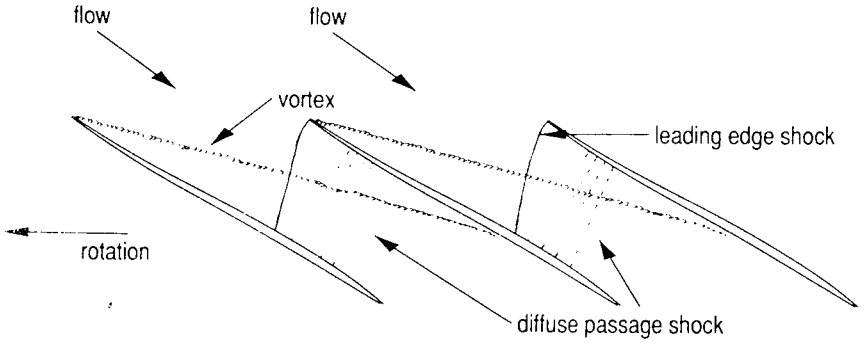

a) Schematic.

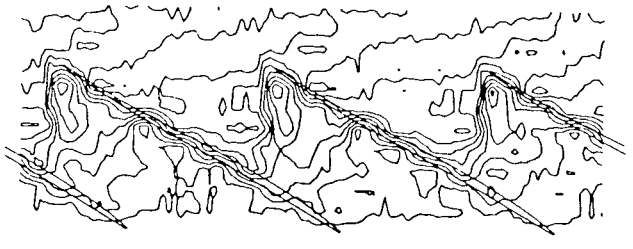

b) Experiment.

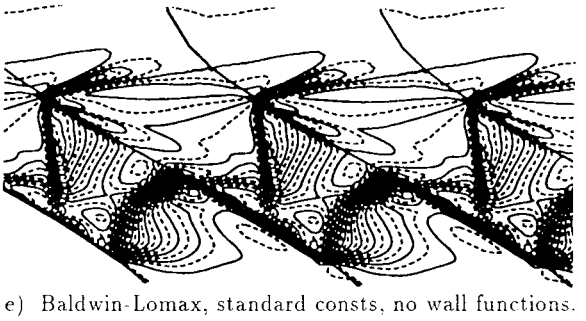

e) Baldwin-Lomax, standard consts, no wall functions.

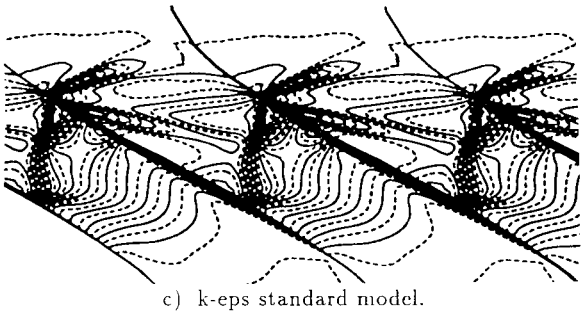

c) k-eps standard model.

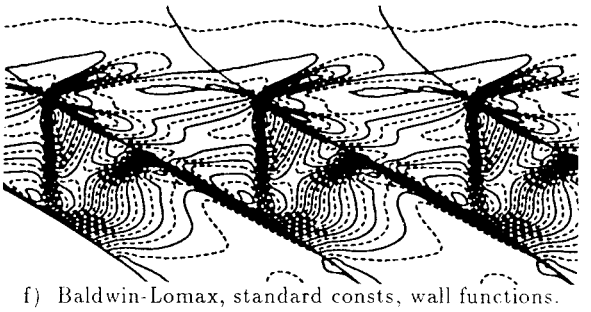

f) Baldwin-Lomax, standard consts, wall functions.

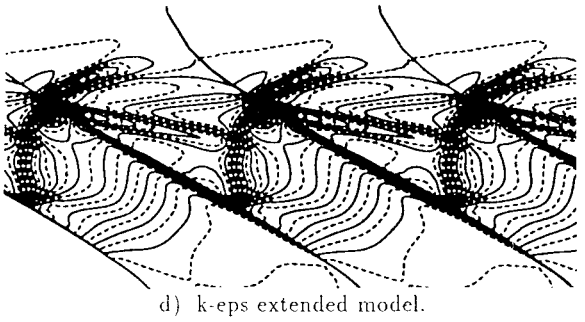

d) k-eps extended model.

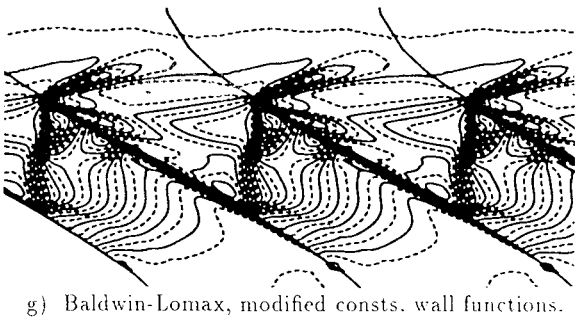

g) Baldwin-Lomax, modified consts, wall functions.

Figure 24 : The casing static pressure contours comparing five numerical results with experimental Kulite measurements. The numerical contour intervals are 0.5 psi. from Turner and Jennions (1992).

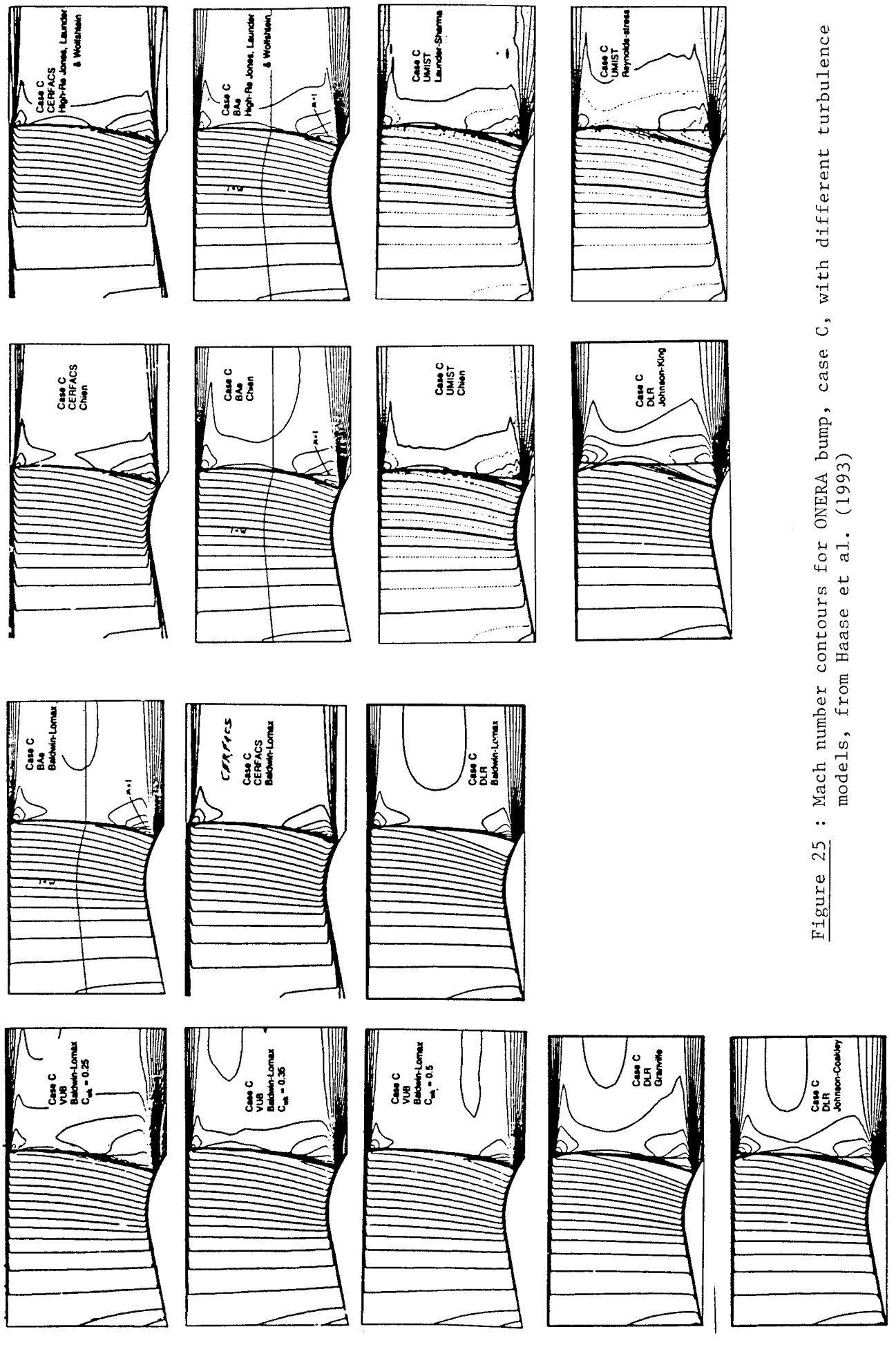

Figure 25 : Mach number contours for ONERA bump, case C, with different turbulence models, from Haase et al. (1993)

Table 2. Constants and functions for the k-ε group of models

Model	C_μ	$C_{\varepsilon 1}$	$C_{\varepsilon 2}$	σ_k	σ_ε	f_μ	f_1	f_2	D	E	ε_w - B.C.
L-S	0.09	1.44	1.92	1.0	1.3	$\exp[\frac{-3.4}{(1+R_t/50)^2}]$	1.0	$1-0.3\exp(-R_t^2)$	$2\nu(\frac{\partial\sqrt{k}}{\partial y})^2$	$2\nu\nu_t(\frac{\partial^2 U}{\partial y^2})^2$	0
L-B	0.09	1.44	1.92	1.0	1.3	$[1-\exp(-0.016R_y)]^2 \times(1+\frac{19.5}{R_y})$	$1+(0.05/f_\mu)^3$	$1-\exp(-R_t^2)$	0	0	$\frac{\partial\varepsilon}{\partial y}=0$
N-T	0.09	1.45	1.90	1.4	1.3	$[1-\exp(-\frac{y^+}{26})]^2 \times(1+\frac{4.1}{R_t^{0.75}})$	1.0	$[1-0.3\exp[-(\frac{R_t}{6.5})^2]] \times[1-\exp(-\frac{y^+}{6})]^2$	0	0	$\nu\frac{\partial^2 k}{\partial y^2}$
K-S	0.09	1.32	1.80	1.4	1.3	$[1+(\frac{13.5}{R_t})\exp(-R_t^{0.25})] \times[1-\exp[-\frac{R_\ell}{150}-(\frac{R_\ell}{25})^2]]$	1.0	$[1-2/9\exp[-(\frac{R_t}{6})^2]] \times[1-\exp(-\frac{R_\ell}{3.7})]^2$	0	0	$\nu\frac{\partial^2 k}{\partial y^2}$
Present	0.09	1.46	1.90	1.4	1.3	$[1-\exp(-\frac{R_t}{150})] \times(1+\frac{18.5}{R_t})$	$1+0.3\exp[-(\frac{R_t}{50})^2]$	$[1-0.3\exp[-(\frac{R_t}{6.5})^2]] \times[1-\exp(-\frac{R_y}{10})]$	0	0	$\frac{\partial\varepsilon}{\partial y}=0$

$R_t=\frac{k^2}{\nu\varepsilon}$; $R_y=\frac{\sqrt{k}\,y}{\nu}$; $y^+=\frac{U_\tau y}{\nu}$; $R_\ell=y/(\nu^3/\varepsilon)^{0.25}$ from Biswas and Fukuyama (1993)

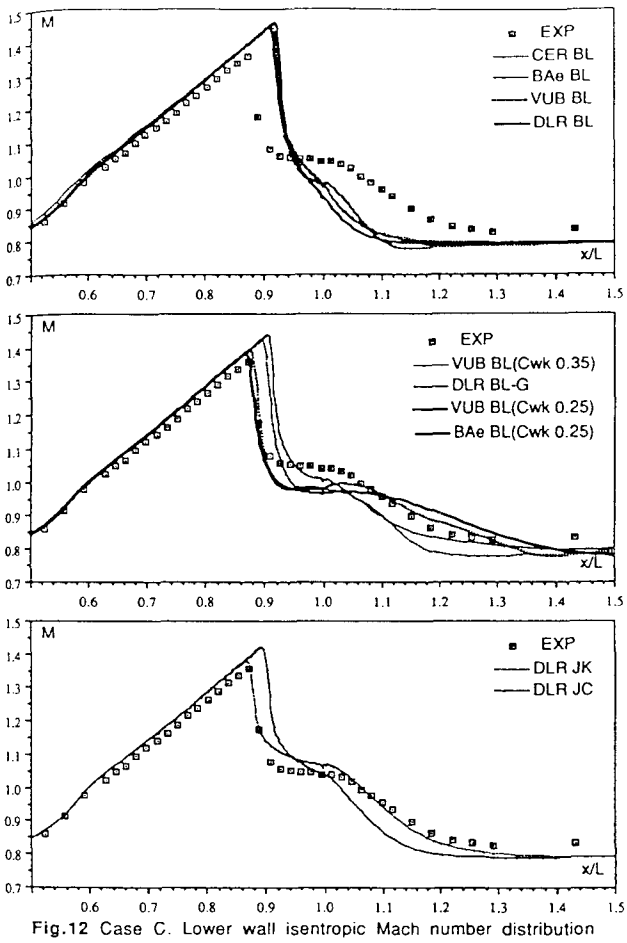

Fig.12 Case C. Lower wall isentropic Mach number distribution

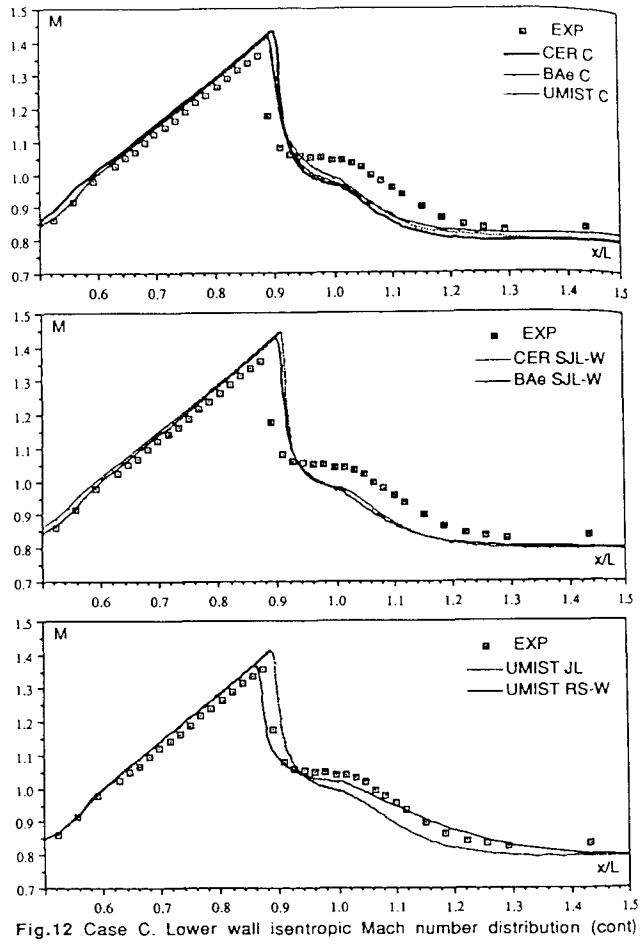

Fig.12 Case C. Lower wall isentropic Mach number distribution (cont)

Figure 26 : Lower wall isentropic Mach number for ONERA bump, case C, with different turbulence models, from Haase et al. (1993)

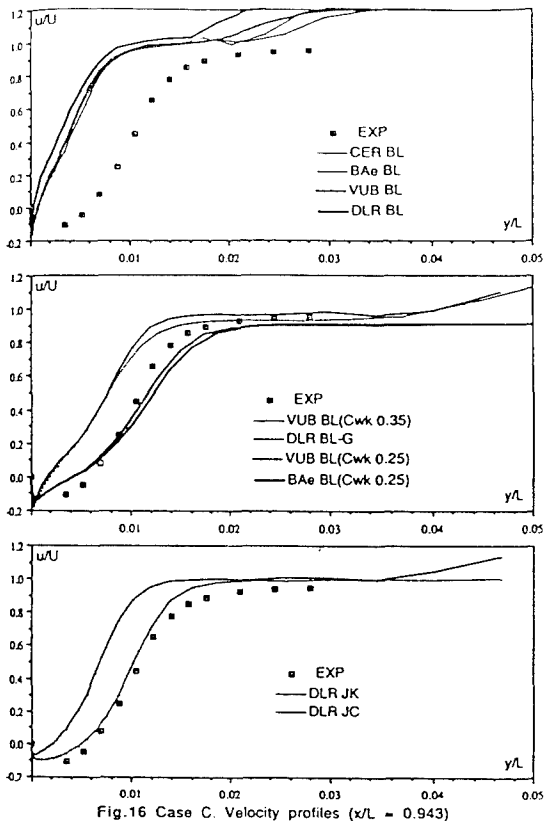

Fig.16 Case C. Velocity profiles (x/L = 0.943)

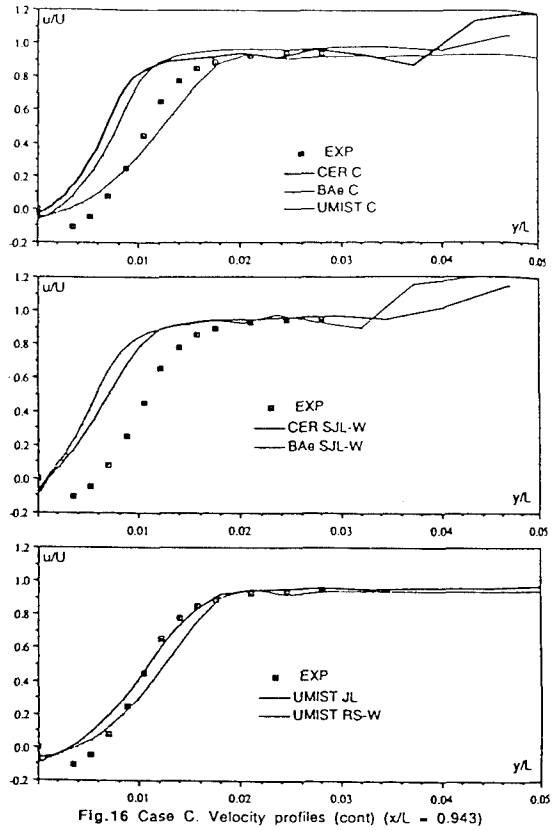

Fig.16 Case C. Velocity profiles (cont) (x/L = 0.943)

(a)

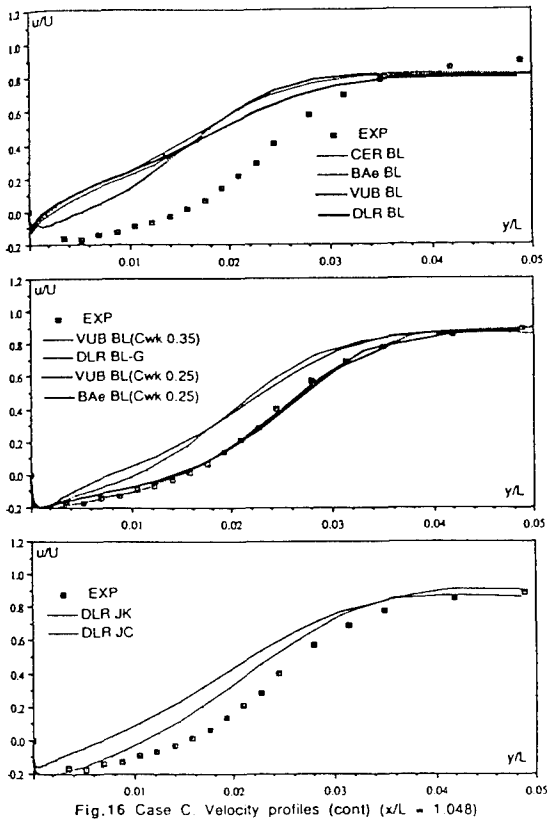

Fig.16 Case C. Velocity profiles (cont) (x/L = 1.048)

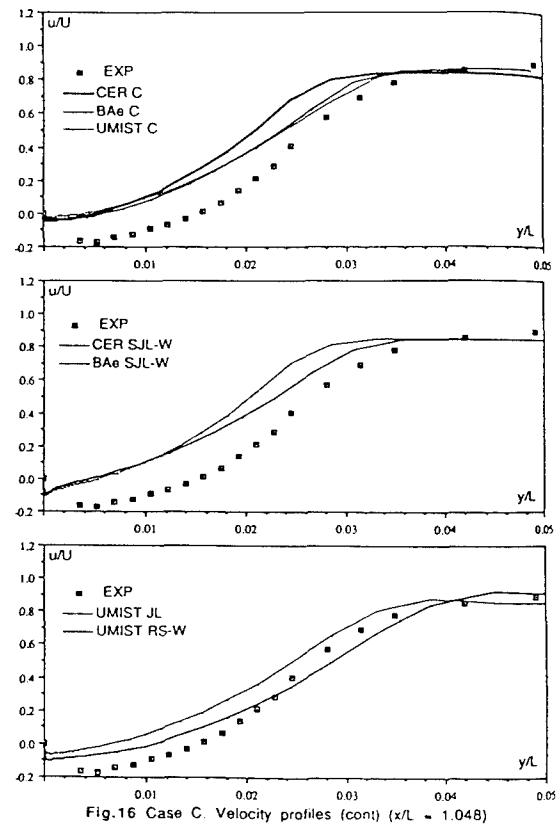

Fig.16 Case C. Velocity profiles (cont) (x/L = 1.048)

(b)

Figure 27 : Velocity profiles for ONERA bump, case C, with different turbulence models, from Haase et al. (1993)
(a) at x/L=0.943
(b) at x/L=1.048

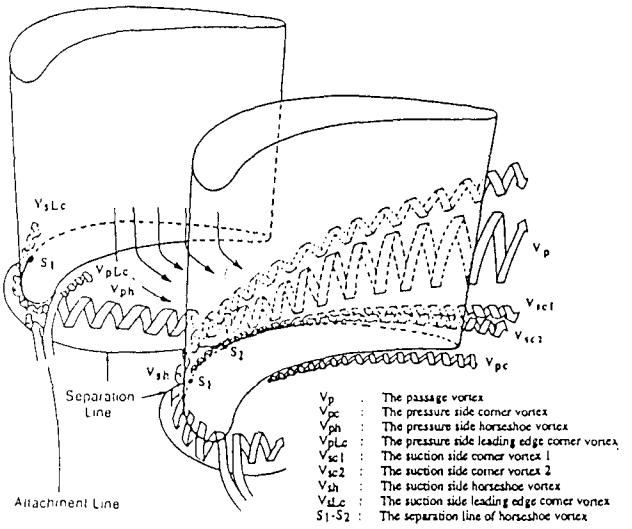

(a) Diagrams of turbine blade vortices

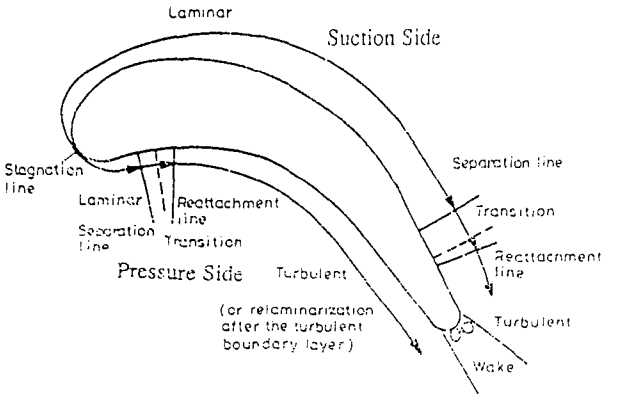

(b) Boundary layer over a turbine blade in the two-dimensional region

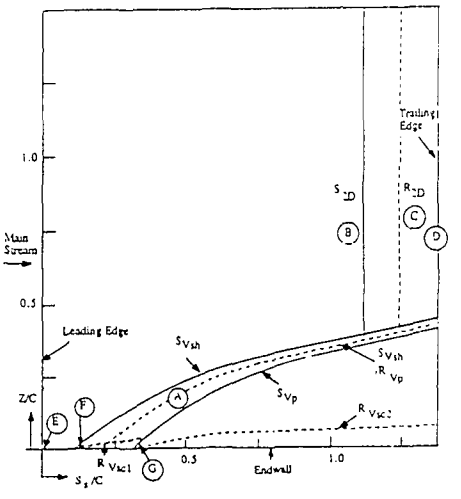

(c) Limiting streamline pattern on the suction surface of the test blade

Figure 28 : from Chen and Goldstein (1991)

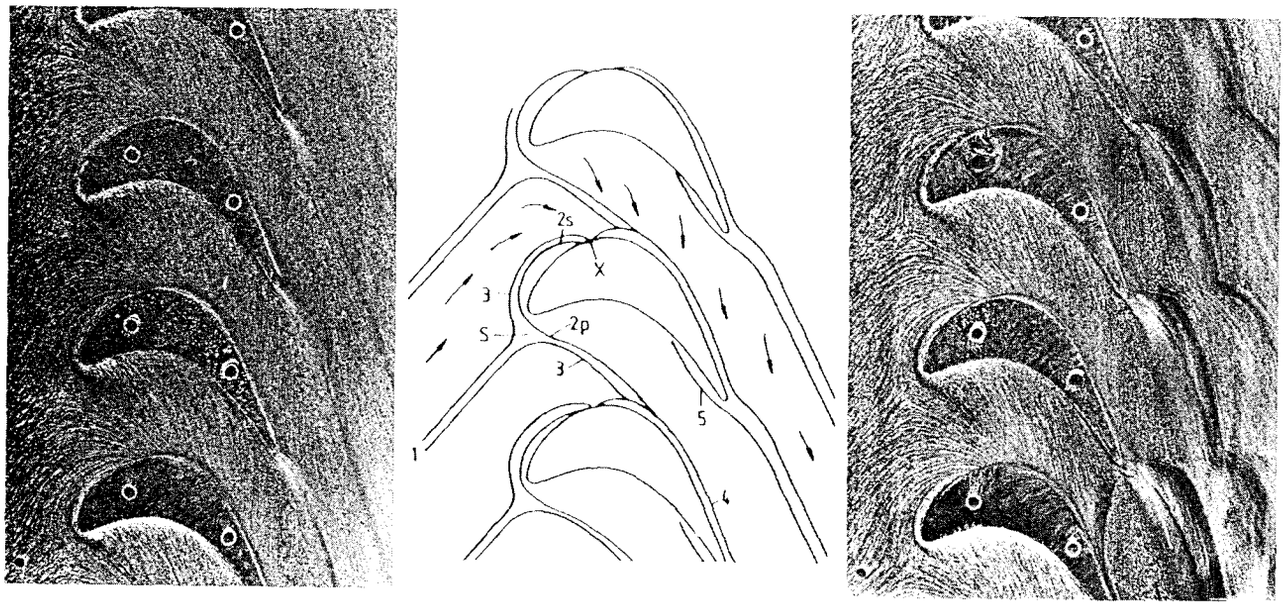

(a) Surface oil flow patterns on the side wall: subsonic case (left), supersonic case (right)

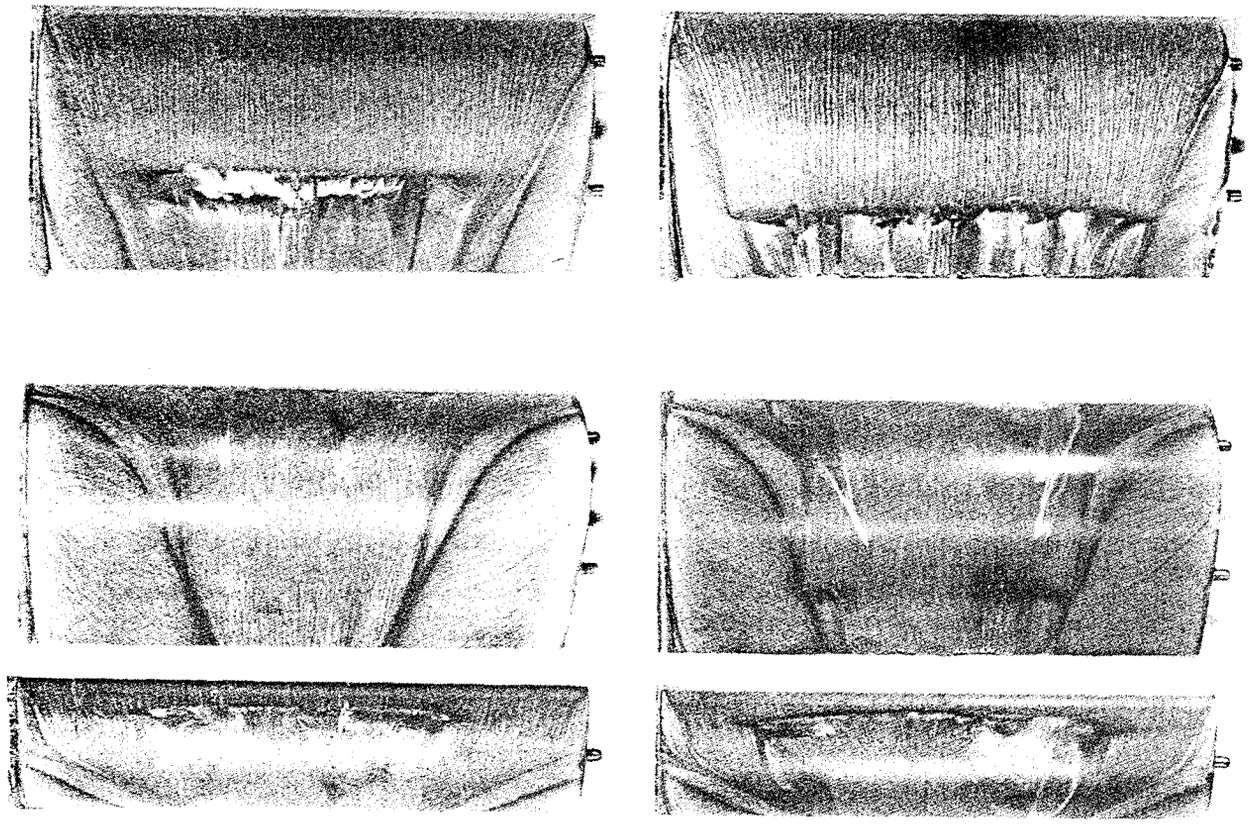

(b) Surface oil flow patterns on the suction surface: $\beta_1 = 140°$(top), $\beta_1 = 155°$ (bottom); subsonic case (left), supersonic case (right)

Figure 29 : from Detemple - Laake (1991)

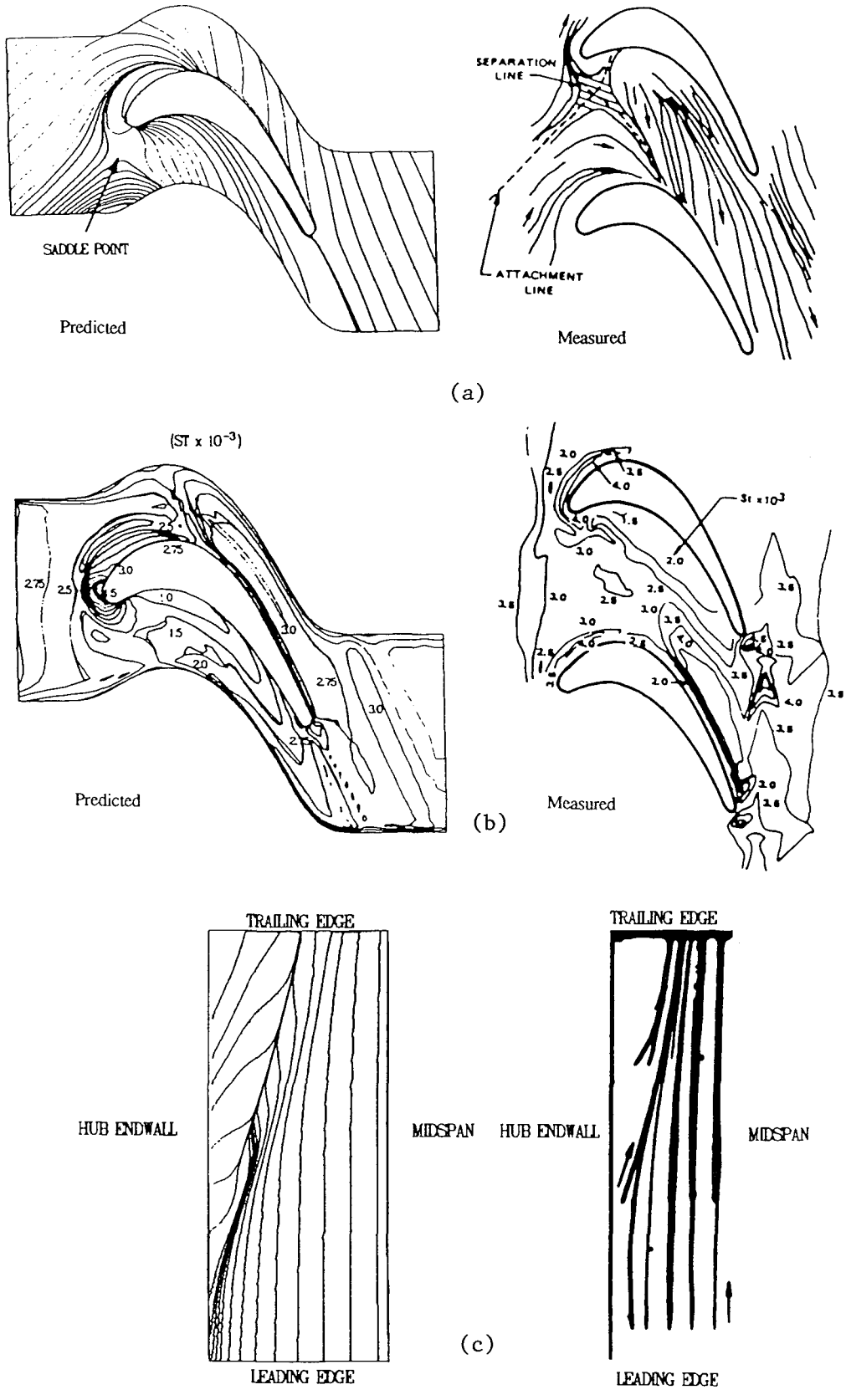

Figure 30 : Predicted turbine endwall flow, compared with the experiments.
a) limiting streamlines and
b) Stanton number contours,
c) Predicted and experimental suction surface limiting streamlines.
from Dorney and Davis (1992)

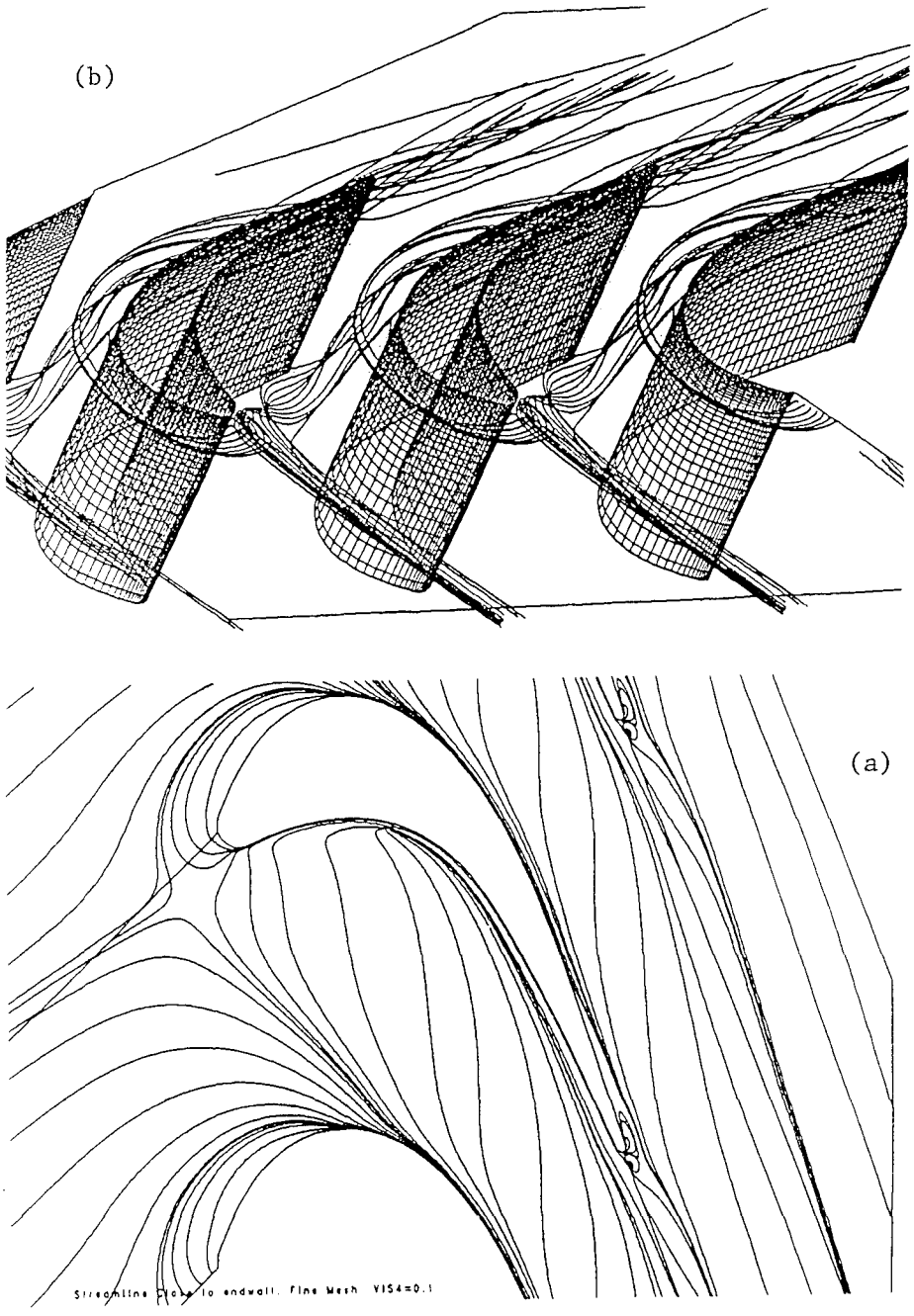

Figure 31 : Computed limiting streamlines on end-wall (a) and horseshoe and corner vortices (b), for the Durham turbine cascade.

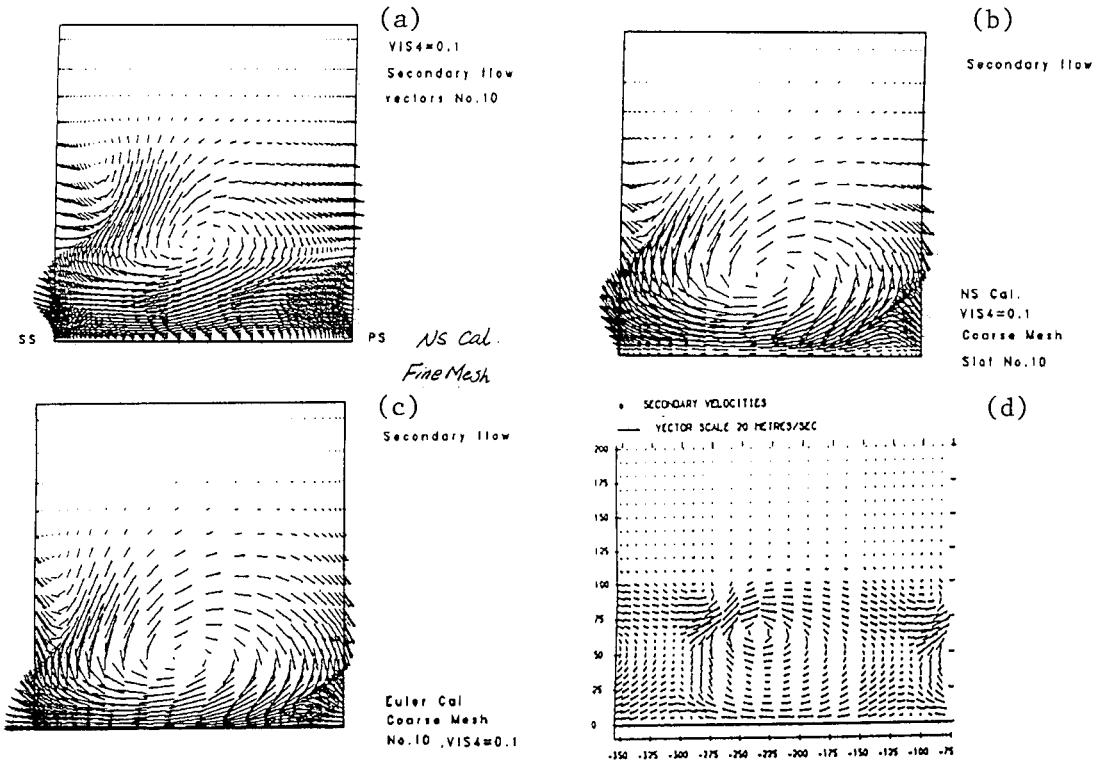

Figure 32: Computed secondary flows for the Durham turbine cascade. a):Euler solution on coarse mesh; b):Navier-Stokes solution on coarse mesh; c):Navier-Stokes solution on fine mesh; d):Experimental secondary flow pattern.

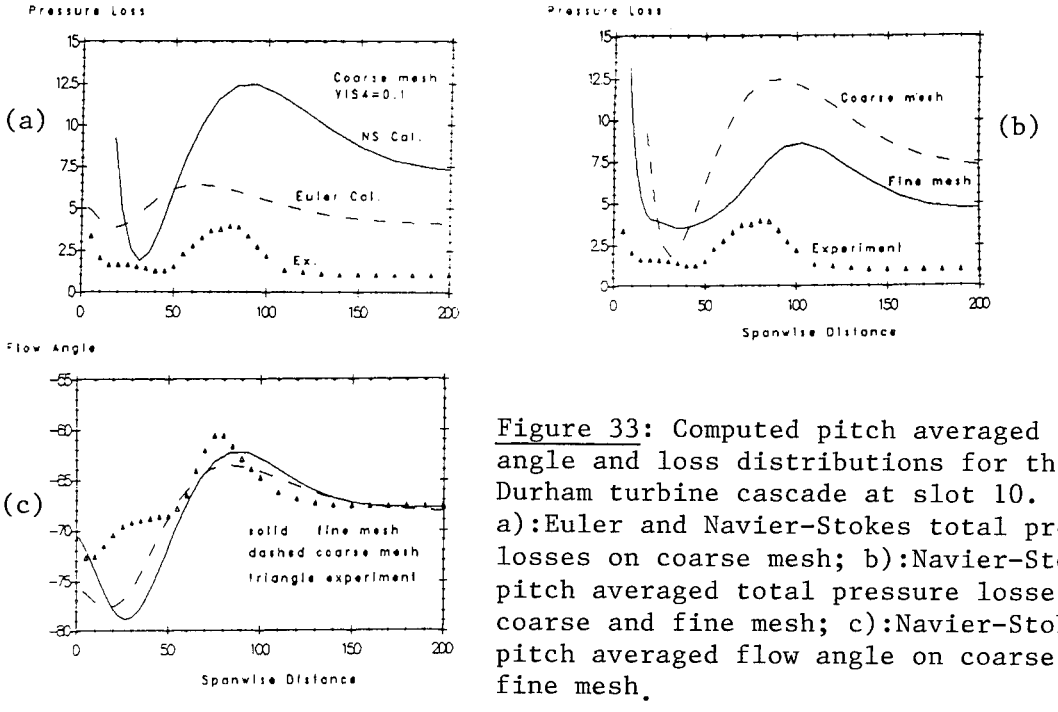

Figure 33: Computed pitch averaged flow angle and loss distributions for the Durham turbine cascade at slot 10. a):Euler and Navier-Stokes total pressure losses on coarse mesh; b):Navier-Stokes pitch averaged total pressure losses on coarse and fine mesh; c):Navier-Stokes pitch averaged flow angle on coarse and fine mesh.

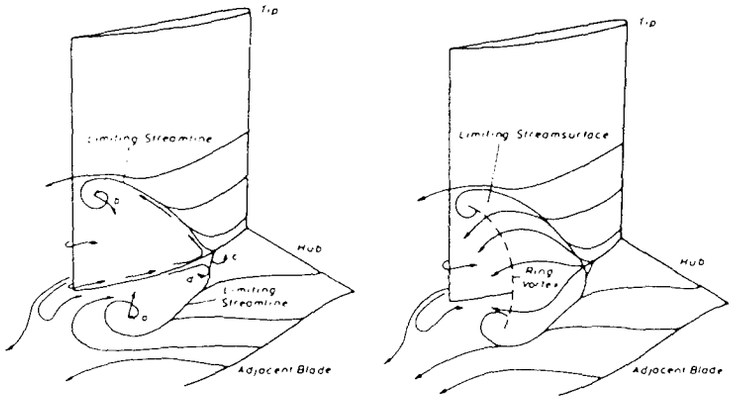

Figure 34: Flow structure in the suction side corner of a compressor rotor; from Schulz and Gallus (1988 and 1990).

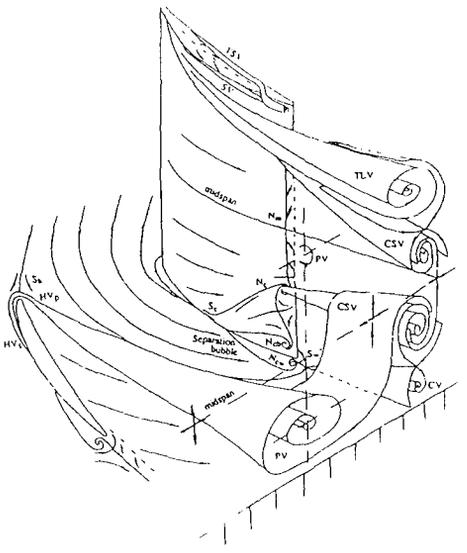

Figure 35: Schematic structure of secondary flows in linear compressor cascade. from Kang and Hirsch (1993a)

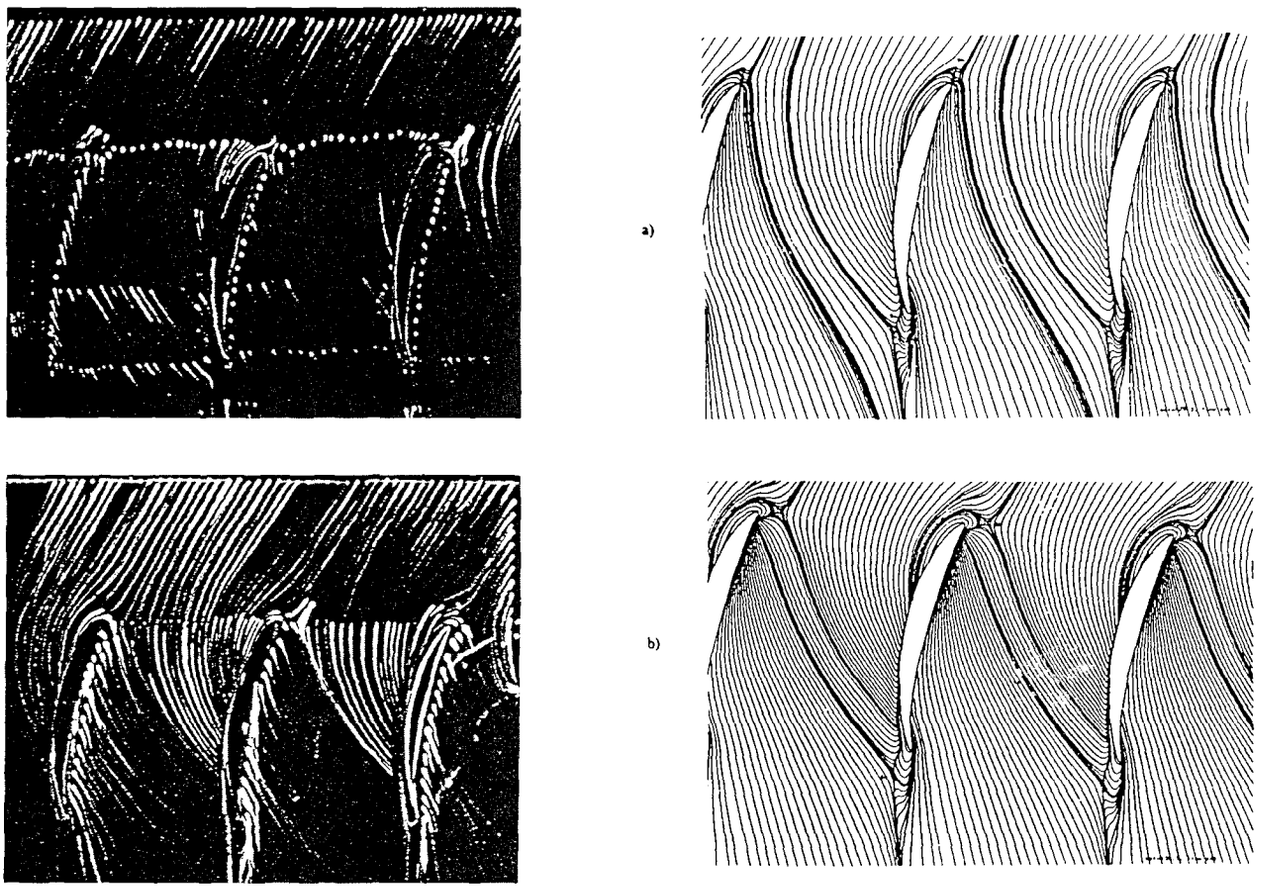

Figure 36 : Paint-trace visualization and predicted limiting streamlines and endwall at design (a) and off-design condition (b).

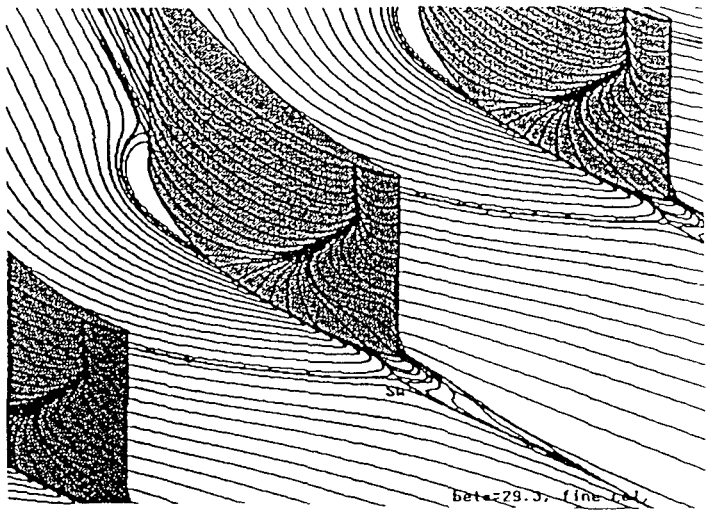

Figure 37a: Calculated streamline pattern on the surfaces near the endwall and the suction surface at design condition.

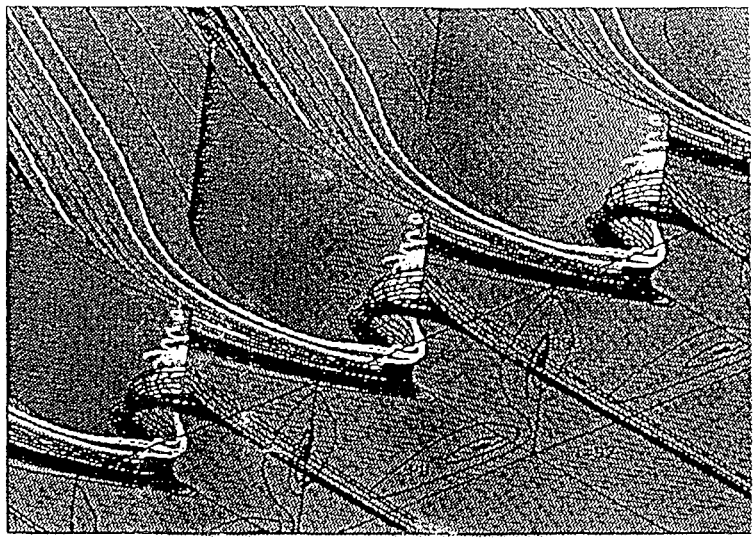

Figure 37b: Streamlines calculated at design condition, with the section streamline pattern in a section at about 46%c behind the exit. The streamlines pass through a common line which is located near the centre of the trailing edge separation vortex at midspan.

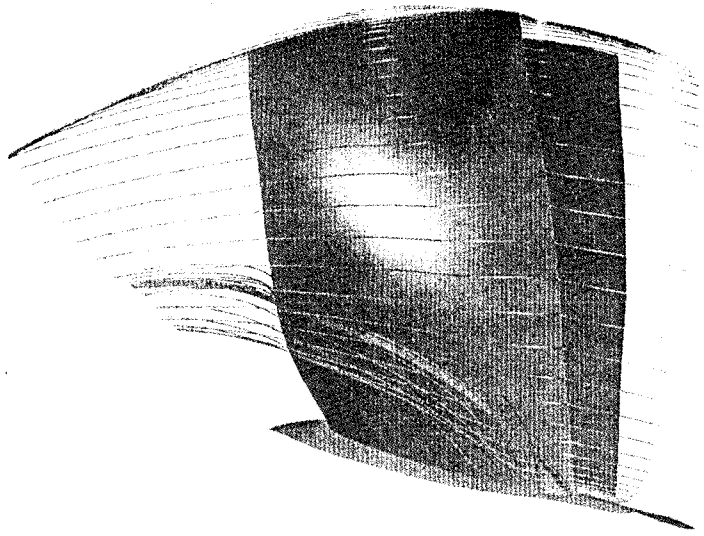

(a)

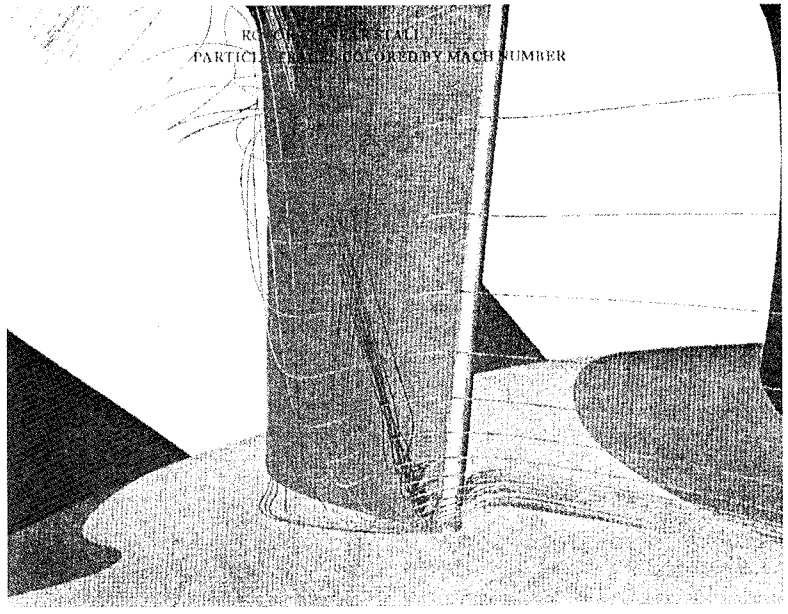

(b)

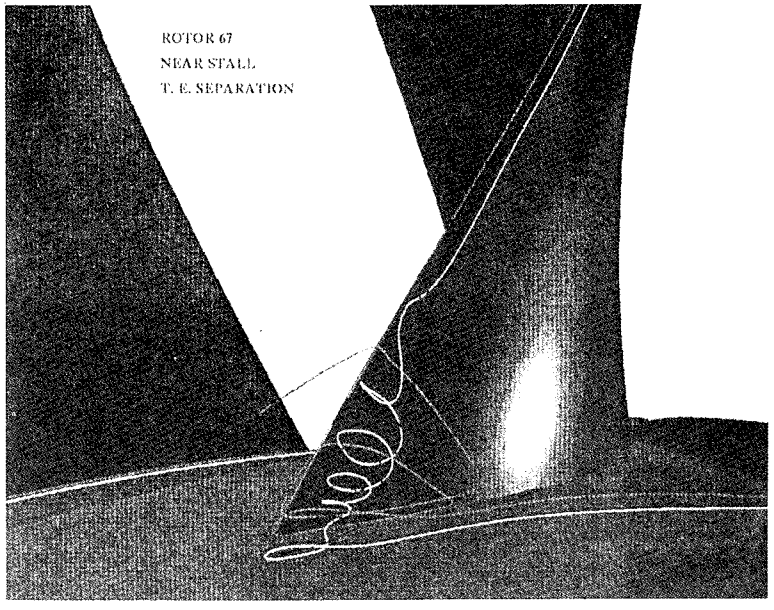

(c)

Figure 38: Computed particle traces, near stall. a) Suction surface overview; b) leading edge enlargement looking downstream; c) trailing edge enlargement looking upstream; from Chima (1991).

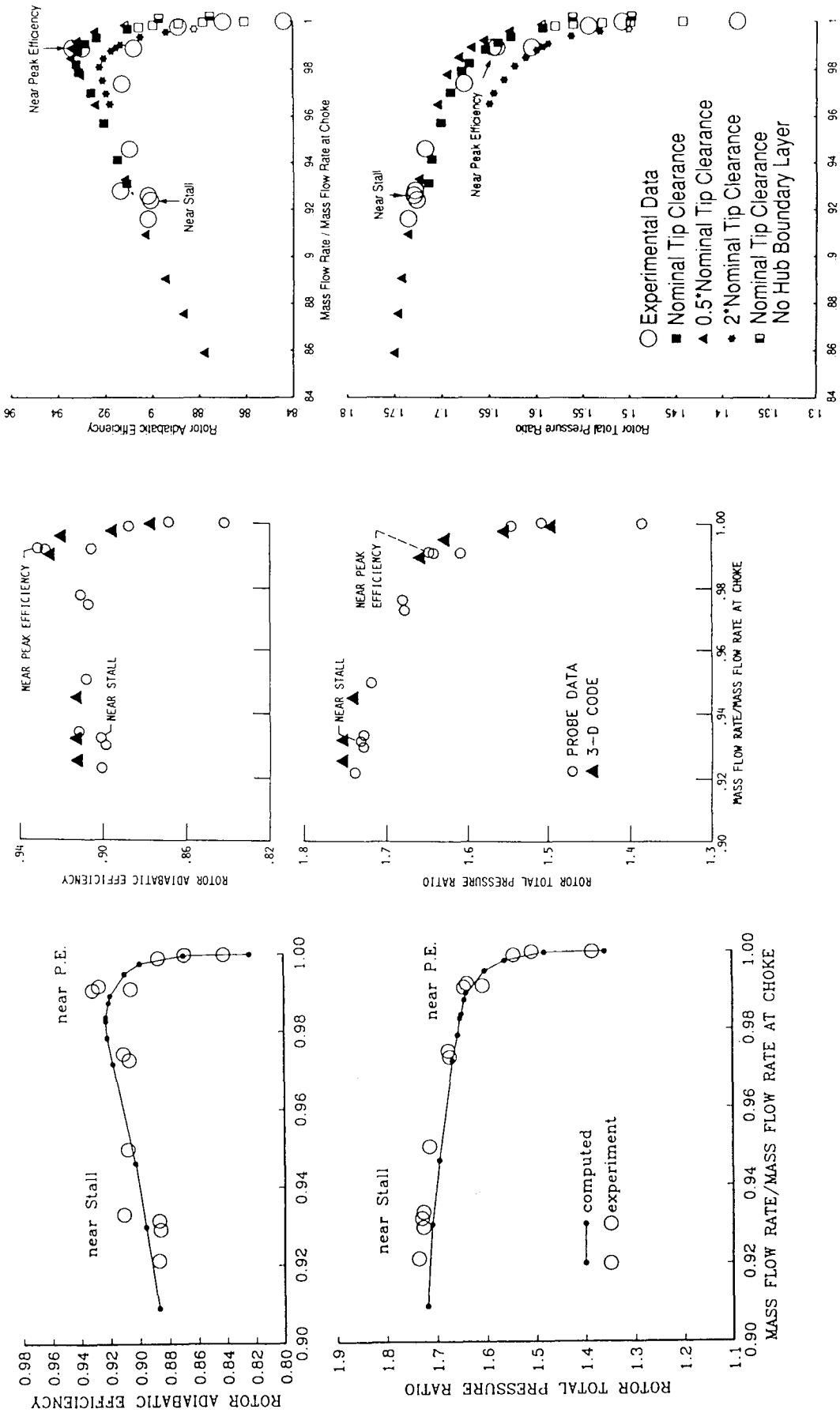

(a) from Arnone (1993)

(b) from Chima (1991)

(c) from Jennions & Turner (1992)

Figure 39 : Comparison of computed and measured adiabatic efficiency and total pressure ratio characteristic at 100 percent speed, for NASA Rotor 67.

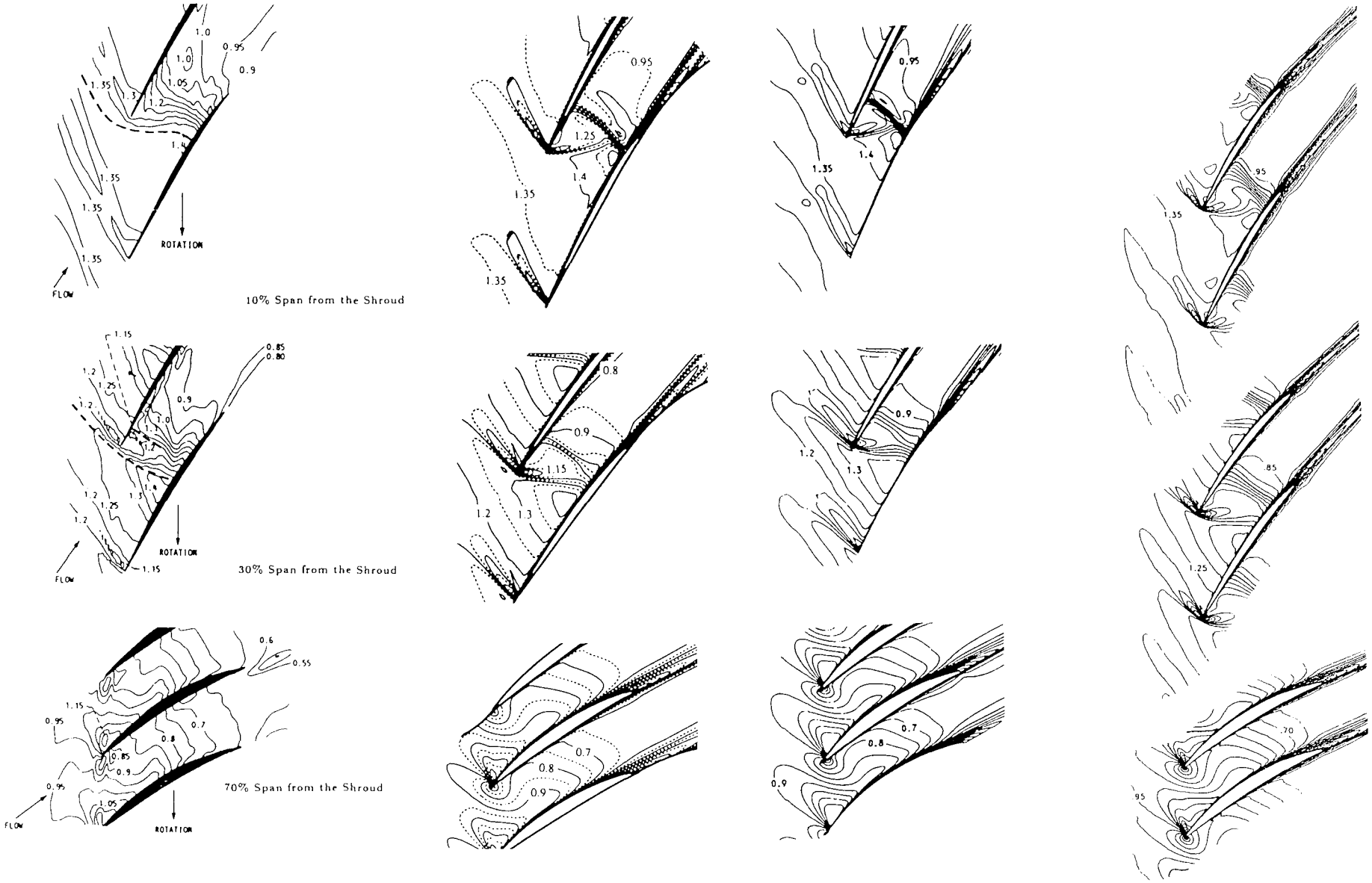

Figure 40 : Blade section iso-Mach plots at near-peak-efficiency for NASA Rotor 67

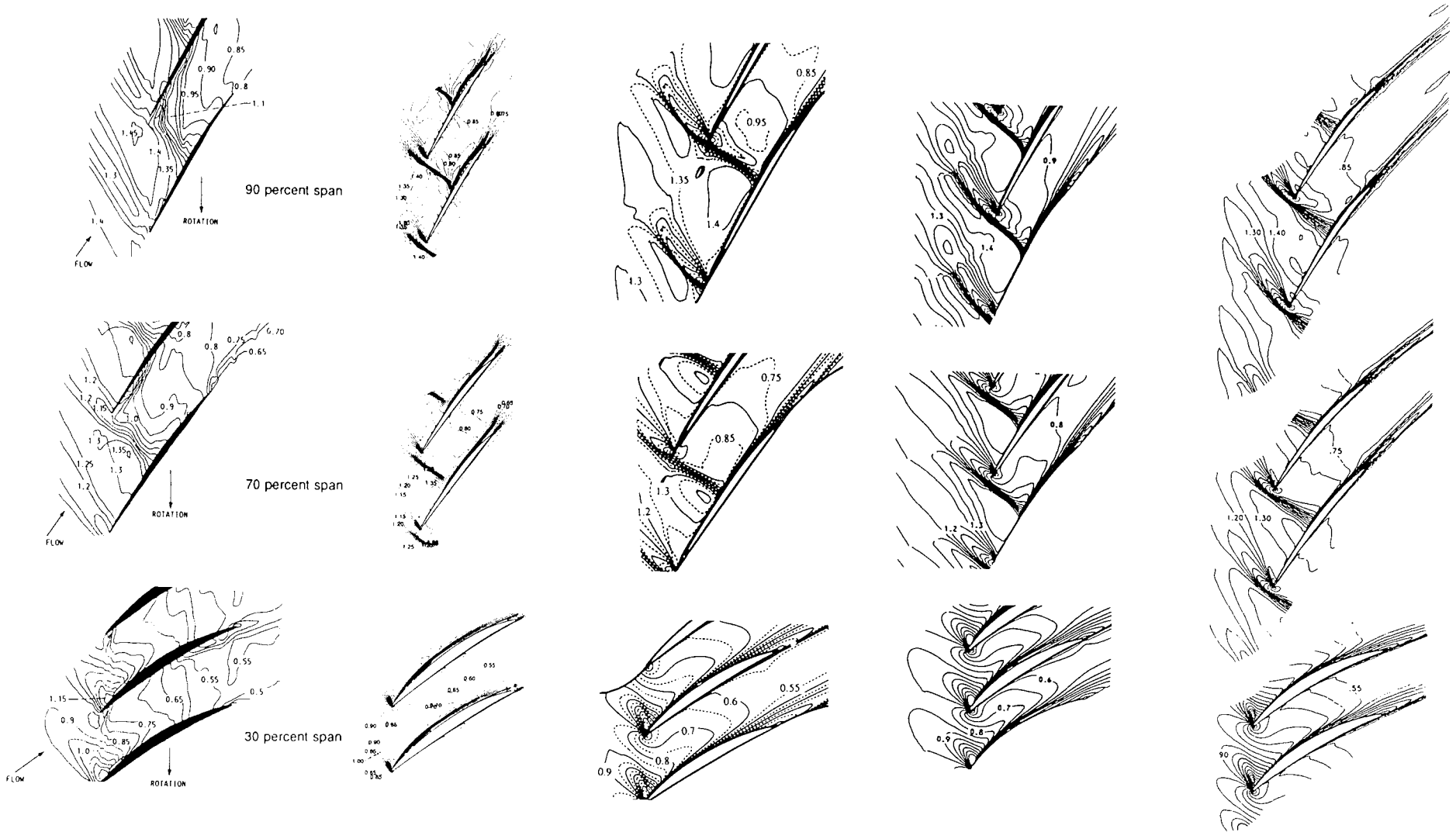

Measured

Calculated from Weber and Delaney (1991)

Calculated from Jennions & Turner (1992)

Calculated from Arnone (1993)

Calculated from Chima (1991)

Figure 41 : Blade section iso-Mach plots at near-stall conditions for NASA Rotor 67

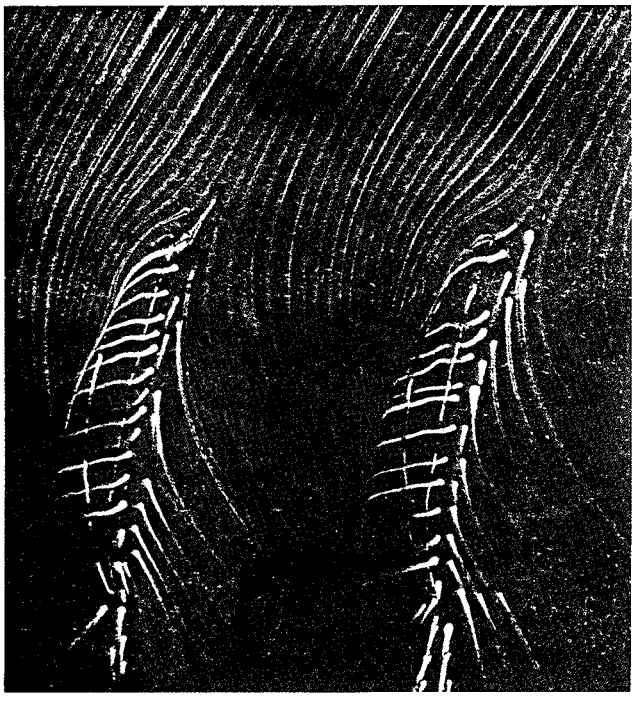

a)

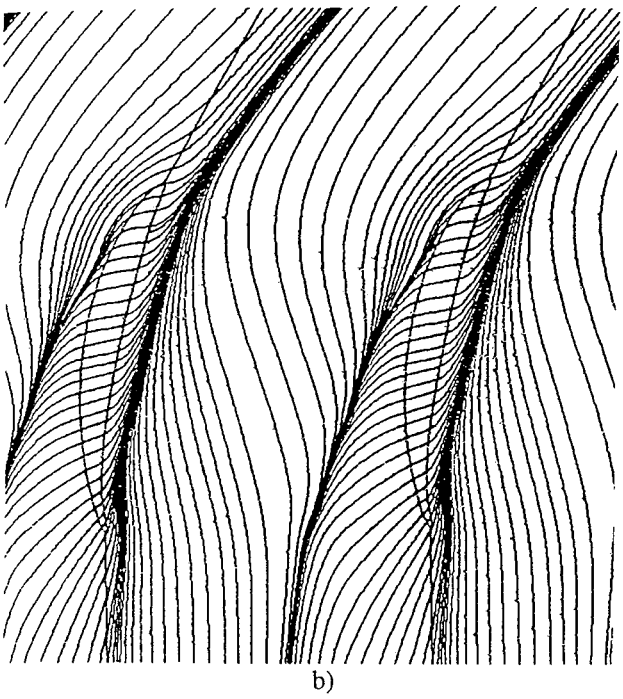

b)

Figure 42: a) Paint-trace visualization and b) limiting streamlines on the endwall, predicted with coarse mesh, at the off-design condition.

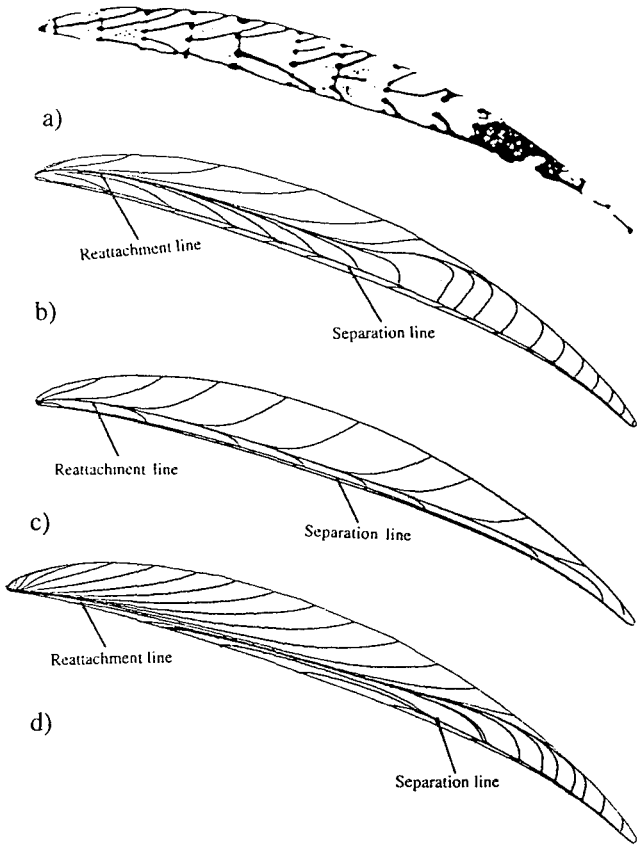

Figure 43: a) ink-trace visualization on tip surface. b), c) and d) calculated limiting streamlines on the tip surface. b) coarse mesh (17 points over the gap) at off-design condition; c) fine mesh (13 points over the gap) at off-design condition; d) coarse mesh (17 points over the gap) at design condition.

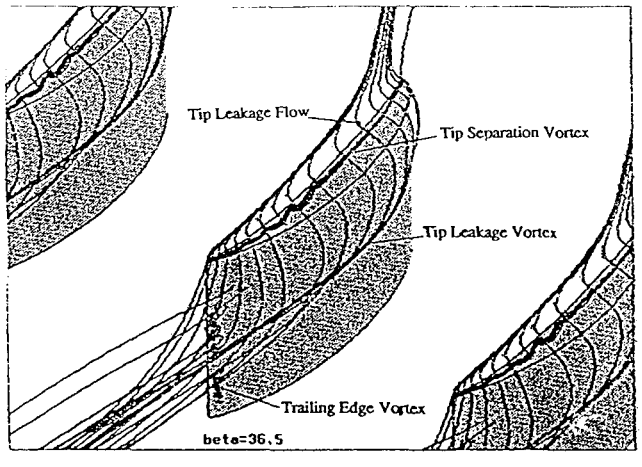

Figure 44: Streamline pattern around the tip and trailing edge over half span at off-design condition, calculated with coarse mesh.

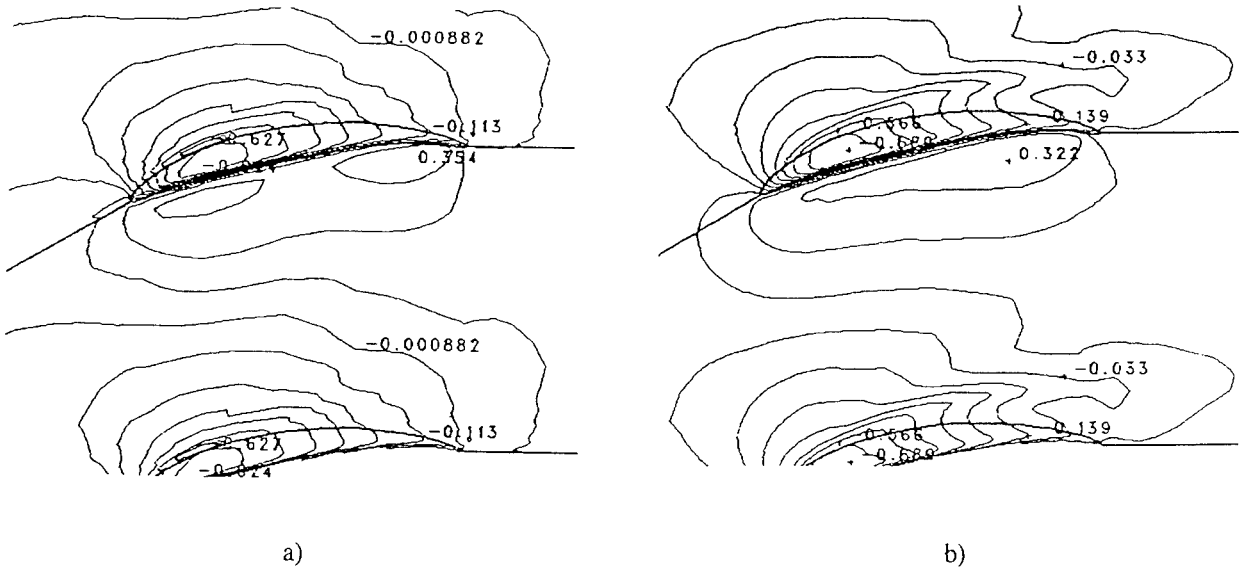

Figure 45: Contours of static pressure on the endwall, calculated with a) coarse and b) fine meshes.

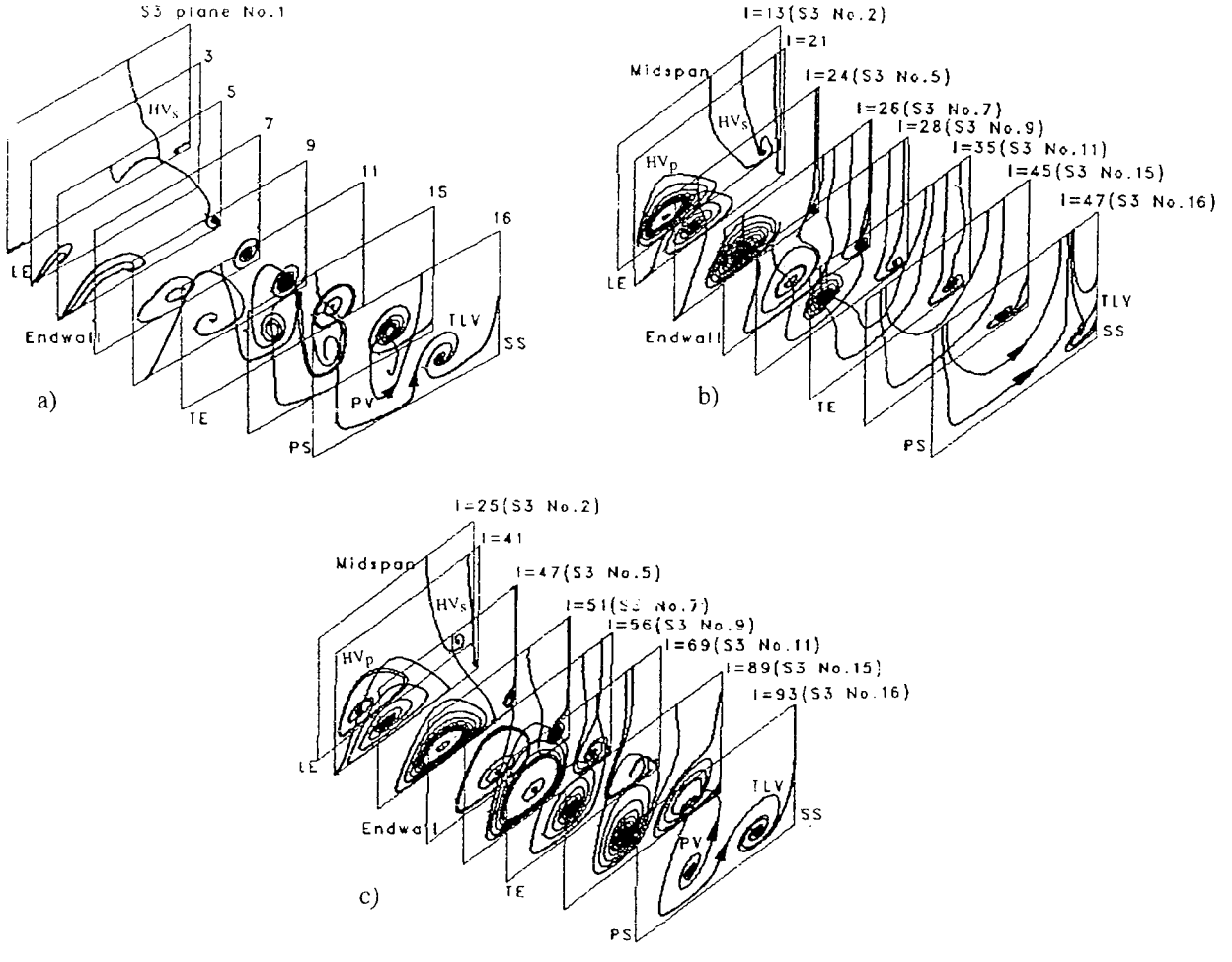

Figure 46: Comparison of secondary flow vector lines, a) experimental, b) computational with coarse mesh, and c) computational with fine mesh at off-design condition.

UNSTEADY FLOWS IN TURBINES – IMPACT ON DESIGN PROCEDURE

by

O.P. Sharma, R.H. Ni and **S.Tanrikut**
Pratt & Whitney
400 Main Street M/S 163-01
East Hartford, Connecticut 06108
United States

The impact of recent research activities in unsteady flows and flow simulation methods used in the turbine design process are outlined. Results from a number of experimental investigations are described to quantify the effect of unsteadiness on the time-averaged flows in turbines. Results from numerical simulations, obtained by using 3-D unsteady Computational Fluid Dynamics (CFD) codes, are also shown to indicate that some of the unsteady flow features can be fairly accurately predicted. An overall discussion is presented to distinguish flow parameters that can be modeled with existing steady CFD codes, from those that require unsteady codes.

1.0 INTRODUCTION

Although the importance of periodic unsteadiness, induced by relative movements of adjacent airfoil rows in turbomachinery, has long been acknowledged by design engineers; the unavailability of established prediction methods has precluded an explicit impact on the hardware design. The effects of periodic unsteadiness, until recently, were accounted for through empiricism in correlations and criteria used in design procedures. Application of these procedures often yield non-optimal designs requiring expensive and time consuming development programs. Work has been done over the past fifteen years to develop simple procedures to account for these unsteady flow effects as discussed below.

Experimental programs have been conducted to investigate the impact of periodic unsteadiness on the loss and heat load generation mechanisms in turbines. Highlights from these experiments indicate that losses and heat load in an unsteady flow environment are larger than those measured for the same airfoils in a steady flow environment as shown in Figure 1 (Ref. 1, 2, 3 & 4). Simple models (Ref. 3, 4 & 5) are available to account for the effects of upstream wake induced unsteadiness on the performance of the downstream airfoil. The model proposed in Ref. 6 showed that the change in the profile losses of an airfoil in an unsteady environment can be related to the "Reduced Frequency" as given in Figure 2. Reduced frequency in this figure is defined as a ratio of the "flow change period" (relative speed / pitch of the upstream airfoil row) to the "flow interaction period" (axial velocity / axial chord of the downstream airfoil). In addition to providing a good estimate of profile losses for an embedded row of a multistage turbine, the correlation shown in the above figure can also be used to calculate time averaged boundary layer properties including heat transfer as shown in Figure 3. These calculations were conducted by assuming an increased level of intermittency factor in the airfoil suction surface boundary layer; the net increase in the intermittency factor is deduced from correlation shown in Figure 2.

Different models have been proposed (Ref. 7, 8 & 9) to account for effect of periodic unsteadiness on the airfoil boundary layer characteristics through modification of the transition behavior, but results from these models are not found to be much different than those shown in Figure 3. All of these models predict increase in both loss and heat load for downstream airfoils in the unsteady environment, provided the airfoils have attached boundary layers for steady incoming flows. In situations such as low Reynolds number operating conditions, where airfoils have extended regions of separated laminar flows (Figure 4), interaction from upstream wakes can result in lower losses in an unsteady environment relative to the steady flow operating conditions. No model is available to predict the behavior of airfoils operating at low Reynolds numbers.

It should be pointed out here that measured airfoil surface static pressure data in the above experiments could be well predicted by using steady flow codes indicating that periodic unsteadiness has an insignificant effect on the airfoil loadings. Results shown in Figure 3 were obtained by using time averaged experimental data for the airfoil loadings which demonstrates that if airfoil loadings do not get affected by unsteadiness, fair estimates of time averaged profile losses and heat loads can be obtained. Experience indicates that periodic unsteadiness has a relatively small effect on time averaged loadings for turbines operating with moderate axial spacing between adjacent airfoils and operating at subsonic speeds.

Presented at an AGARD Lecture Series on 'Turbomachinery Design Using CFD', May to June 1994.

Recent calculations (Ref. 10), conducted by using an unsteady Reynolds Averaged Navier Stokes (RANS) code for the mean section of the first stage of a transonic turbine, indicate that time averaged loadings on upstream stator are strongly affected by the axial gap between stator and the rotor. These results, plotted in Figure 5, clearly show that the time-averaged diffusion on the stator is significantly reduced as the axial gap between the airfoil rows is increased. Experimental verification of this numerical result is needed to enhance confidence in the predictive capabilities of the CFD code. The predicted time-averaged loadings for the above stator at the largest axial gaps were found to be quite close to those predicted by using steady CFD codes currently used in the Pratt & Whitney (P&W) design system.

The above result shows limitations of the current prediction methods in accounting for the effects of periodic unsteadiness on airfoil loadings which affects both performance and heat transfer coefficient distributions.

The main focus of this paper is to identify flow situations which can be adequately predicted by CFD codes used in the current design process and those flow situations which cannot be well predicted. This paper also points out research work required to enhance the predictive capabilities of the current CFD codes to model these flow situations.

In the next section, the results obtained from analyzing data from a number of experimental turbine programs are described first in order to provide an improved understanding of the flow physics. The impact of upstream wakes, hot streaks and secondary flow vortices on the performance, heat load and flow distribution through downstream airfoil rows are also discussed.

Advancements made in the flow simulation capabilities for multistage turbines through the use of unsteady CFD codes are discussed in Section 3. It is shown that these unsteady codes provide realistic predictions of flow features through multistage turbines by using relatively simple models for the effect of viscosity.

Implications of the information discussed in the paper are discussed in Section 4. A clarification on situations where steady and unsteady CFD codes are needed in the design process are given in that section.

Conclusions from the work are outlined in Section 5.

2.0 UNSTEADY FLOW EFFECTS IN TURBINES - EXPERIMENTAL DATA

All airfoil rows in turbines encounter both spatial and temporal flow distortions generated by upstream airfoil rows and combustors resulting in unsteady flows. Flow in the first rotor passage is influenced by temporal distortions from adjacent stators. These temporal distortions consist of wakes and vortices from upstream stators and potential waves from both the upstream and the downstream stators. Flow in the second stator is affected not only by the temporal distortions generated by the adjacent rotor airfoils but also by the spatial distortions generated by the first stator. The effects of temporal distortions, termed as "Upstream Row Induced Effects", are discussed in Section 2.1. The effects of spatial distortions, termed as "Upstream Stage Induced Effects" are discussed in Section 2.2.

2.1 Upstream Row Induced Effects

The circumferential variation in velocity field downstream of the first stators for turbines are normally generated by the drag on the airfoil and endwall surfaces which causes a reduced velocities and increased turbulence. For airfoil rows downstream of a combustor, high velocity jets are found to exist due to large circumferential gradients in temperature. The effects of these upstream velocity variations can be simply illustrated through the use of velocity triangles (Figure 6 (Ref. 11 & 12)). This figure shows that the low velocity fluid has a slip velocity towards the suction side of the downstream airfoil (for the compressor, the slip velocity is towards the pressure side) indicating that the high turbulence, low velocity fluid from the upstream airfoil wake will migrate towards the suction side of the airfoil. In a similar manner high velocity (high temperature) fluid will migrate towards the pressure side of the downstream airfoil. This preferential migration of fluid particles has three effects:

i) Alterations in the boundary layer characteristics of the airfoil through its effect on the transition process. This effect is reasonably well accounted for in the turbine design process as outlined above.

ii) Variation in the secondary flow generation for downstream passages.

iii) Redistribution of stagnation enthalpy.

Detailed discussions on the second and the third effects are given below.

2.1.1 Effect of Upstream Wakes on Secondary Flows

Total pressure loss data (Ref. 13), obtained by using high response probes in the United Technologies Research Center (UTRC) Large Scale Rotating Rig (LSRR), for the rotor as it passes through the upstream stator flow field are shown in Figure 7. This figure

shows contour plots of relative total pressure coefficient upstream and downstream of the rotor passage. In this figure, the residence time of the fluid particles in the rotor passage is accounted for in such a manner that the exit flow field corresponds to the given inlet flow field. Large variations in the rotor exit flow structures are seen in the figure for three different inlet conditions. These inlet conditions correspond to different positions of the upstream stators relative to the rotor passage. When the inlet flow is circumferentially uniform due to the rotor passage positioned between two adjacent stator wakes, the exit flow field shows three distinct vortices as shown in Figure 7a. The vortices are due to the hub and tip secondary flows and the tip leakage effects. Without the tip leakage vortex, the flow field shown in Figure 7a is similar to the one expected for this airfoil in a steady cascade environment. As the rotor passes through the upstream stator flow field, the tip leakage vortex shows little variation (Figures 7a - 7c) indicating that the leakage phenomenon is not influenced by upstream circumferential distortions. The hub secondary flow vortex shows the largest variation transforming from a distinct structure in Figure 7a to a diffused structure in Figure 7b, and becoming almost non-existent in Figure 7c. The overall variation in the size of the tip secondary flow vortex is smaller than that of the hub vortex but larger than the leakage vortex. Figure 7c. This indicates that the secondary flow generation mechanisms, especially at the hub, are strongly influenced by the upstream circumferential distortions such as wakes.

The periodic oscillation in the size and strength of the secondary flow vortices observed in this experimental investigation indicates almost 40% variation in the secondary flow losses for the rotor passage. These data indicate that there is a potential to reduce secondary flow losses by manipulating the secondary flow vortices.

2.1.2 Effect of Upstream Temperature Streaks

Heat loads on turbine rotors are also affected by migration of hot and cold air from the upstream stator and the combustor. Experimental data acquired in an engine indicates that pressure and suction sides of an airfoil can operate at fairly different temperatures, results plotted in Figure 8 show that the differences can be on the order of 250 degrees F. Extensive work has been done over the past 10 years to highlight physical mechanisms responsible for this segregation of hot and cold air in turbine rotors and it is discussed here.

Results from an experimental investigation, conducted to quantify the influence of burner induced hot streaks on segregation of hot and cold air in turbine rotors, are discussed.

In this investigation, experimental data were acquired in the UTRC LSRR by introducing temperature streaks at inlet to the first stator (Figure 9). Two types of temperature profiles were generated upstream of the first stator, these being:

i) Hot streak with a circular pipe to yield a temperature profile both in the radial and the circumferential direction, some of the results from this investigation were reported in Ref. 4 & 11. Data were acquired for two different flow coefficients by restaggering the stator and by increasing the speed of the rotor to maintain design incidence angle on the rotor airfoil.

ii) Hot streak with a rectangular nozzle to yield a radially uniform profile that had temperature gradients in the circumferential direction, this experiment was conducted for the lower flow coefficient only.

The hot air in these experiments was seeded with CO2 to facilitate measurement of its migration in the turbine by using a sniffing technique discussed in Ref. 11. The temperature pattern at the exit of the first stator for this test are given in Figure 9b which indicates little mixing in the stator passage demonstrating the Munk and Prim principle (Ref. 14). Measured concentration of CO2 on the rotor airfoil surfaces from the nozzle (rectangular) experiment are shown in Figure 10. This figure shows higher levels of CO2 on the rotor airfoil pressure side than on the suction side. These results, obtained with a radially uniform inlet profile (Figure 9c), clearly demonstrate that the segregation of the hot and cold air in turbine rotors is mainly driven by two-dimensional mechanisms. Experimental data acquired on the rotor, with incoming hot streak generated by the circular pipe, are shown in Figure 11 for two different flow coefficients. These data indicate that the rotor pressure side temperature is higher for the lower flow coefficient configuration.

Extrapolation of these data to an actual engine environment indicate that pressure sides of first rotors can operate anywhere between 100-700°F higher temperatures than the suction sides. These temperature differences can cause significant durability problems for airfoils and endwalls. Large amounts of cooling air are required to accommodate these temperature levels resulting in reduced efficiency of the cycle and substantial detrimental effects on the specific fuel consumption of the engine.

2.2 Upstream Stage Induced Effects

Substantial variations in flow quantities are measured downstream of a stage at stations where the second stage airfoils are normally located. Indexing of second

stage airfoils relative to these incoming distortions can have a significant impact on the overall performance of the machine as discussed below.

The performance of the Alternate Turbopump Development (ATD) Turbine Test Article was evaluated at NASA MSFC during 1991 (Ref 15). Turbine efficiency counters measured downstream on the second stage (Figure 12) showed a 2 cycle pattern on top of a 54 cycle pattern, the latter corresponds to the second stator airfoil count. The 2 cycle pattern showing a +/- 0.5% in the overall turbine efficiency was found to be due to the interaction between the first and second stators where the wake fluid from the first stator impinges at different locations on the second stator. With airfoil counts for the first and the second vanes of 52 and 54 respectively, a 2 cycle pattern will exist over the full annulus as indicated in Figure 12.

Experiments were conducted to assess the impact of indexing on the overall turbine performance and to establish whether this concept can be exploited for engine application. Hardware was built to allow indexing of the two stators as shown in Figure 13. Both temperature and torque were measured to define the efficiency. Flowfield data were acquired over the full annulus. Results from these experiments (Ref. 16) clearly indicate that the performance of the turbine can be optimized by appropriately indexing first and second stator airfoils as shown in Figures 14 & 15. Experimental data acquired over the range of incidence angles also showed large change in performance due the indexing effects.

The above results indicate a knowledge of the shapes and locations of wakes from upstream stage airfoils are required to optimize the design of downstream stage airfoils.

3.0 UNSTEADY FLOW EFFECTS IN TURBINES - NUMERICAL SIMULATIONS

Significant progress has been made over the past twenty years in developing flow prediction systems based on CFD codes. The application of these CFD codes in the turbine design process is shown in Figure 16, where the inter-relationships of the CFD codes with the conventional design procedures is illustrated. The main contribution from CFD has come through the use of multi-stage analysis capability. Three different approaches are available to compute time-averaged flows through multistage machines.

(i) In the first approach, flow through each airfoil row in the machine is calculated for a specified circumferencially uniform inlet and an average exit boundary conditions. These boundary conditions were initially obtained from predicted or "data matched" streamline curvature methods. Subsequently these boundary conditions were deduced from circumferencially averaged mean flow quantities obtained from computations for adjacent airfoil rows. This approach (Ref. 17 - 20), known as the "Mixing Plane" approach, was extensively used during the 1980's to establish spanwise distributions of airfoil loadings and flow profiles, an example of this is shown in Figure 17. This approach relies on the solution of equations governing the conservation of mass, momentum and energy, while the impact of periodic unsteadiness represented by "apparent stress" like terms is neglected. The effect of periodic unsteadiness has, therefore, not been accounted for in this approach.

(ii) The second approach, termed as the "Average Passage" approach, was developed (Ref 21), to accurately simulate time-averaged flows through multistage machines. The effects of adjacent airfoil rows in this approach is accounted for through the use of body forces and "apparent stresses". Reliable models are not yet available to account for circumferencial variation of "apparent stresses". These are currently assumed to be constant in the circumferencial direction. "Average Passage" approach has the potential to yield more accurate estimates of flow through multistage machines at off-design conditions than the "Mixing-Plane" approach. Significant work is, however, needed towards the development of physics based models to account for the radial and circumferencial variations of "apparent stresses" to enhance the predictive capabilities of codes based on the "Average-Passage" approach. It should be pointed out here that in a number of situations flow may need to be computed over more than one airfoil passage in the machine, this may require simulation of flow over the most pertinent circumferential dimension that includes multiple airfoil passages. This would require minor modifications to both "Mixing-Plane" and "Average-Passage" approaches, this point is further discussed in Section 3.2.

(iii) Unsteady flow computations are conducted in the third approach utilizing either Euler (Ref. 22 & 23) or RANS (Ref. 24 - 27) codes. These computations, conducted for an actual airfoil count yield, very accurate results for the time averaged flows. Simulations of actual airfoil count in a multistage environment requires much larger resources at least for the execution of RANS codes. The

Euler codes, with approximate airfoil counts and with relatively coarse grids, have been extensively used in conducting design optimization studies. The application of RANS codes has, to date, been limited to conducting numerical experiments to highlight pertinent flow physics and to guide further numerical or physical experiments. Numerical experiments recently conducted with unsteady RANS codes are providing information which indicates that their application to the design process needs to be accelerated as discussed below.

One of the corner-stones of the design process is the ability to predict airfoil surface static pressure distributions which provide information about work, losses and heat loads. Once the pressure distribution is known, design criteria and boundary layer calculation methods are used to select a 'good' performing airfoil section. The main reason why Euler flow solvers were so easy to incorporate into the design process was that these produced reliable predictions of airfoil surface static pressure distributions in cascades and in multistage rotating rig environments; this gained the confidence of design engineers. Initial positive results (Ref. 28 & 29) from the application of these codes encouraged turbine design engineers to look for further improvements in durability and performance through the use of more advanced codes.

Unsteady flow simulations of the UTRC LSRR model turbine provide improved insight into the effects of upstream wakes and hot streaks on flow development. These simulations (Ref 22 & 30) were conducted for the single and 1&1/2 stages by using a 3-D unsteady multistage Euler code. Airfoil count in these simulations contained 3 first stators ,4 rotors and 4 second stators (instead of 22 first stator 28 rotor and 28 second stator airfoils) in order to contain computer requirements. Two sets of simulations were conducted; one with a uniform upstream total temperature profile (single stage) to simulate the flow conditions from Ref. 13 and other with an upstream temperature streak (1&1/2 stage) to simulate flow conditions from Ref. 11. Wall shear stress model (Ref. 31) was used in this code to simulate the viscous flow effects. The tip leakage flow was not modeled in these calculations. The results from these simulations are discussed below.

3.1 Effect of Upstream Wakes on Rotor Secondary Flows

The computational mesh used in this single stage simulation for the UTRC LSRR (Ref. 22) is shown in Figure 18a. A total of 70,000 grid points were used in the axial, radial and tangential direction to simulate the flow field. The time-accurate solver and the interpolation method at the interface were used to obtain the unsteady periodic solution in time. Convergence was obtained at about 20,000 time steps or six rotor cycles (rotor moving past one stator airfoil pitch) requiring about 10 CPU hours on a CRAY XMP computer for each simulation. Calculated time averaged loading on the stator and the rotor airfoils from both simulations are compared to the experimental data in Figure 18b at three spanwise locations. The experimental data are shown to be in good agreement with the predictions. It should also be pointed out that these predictions are almost identical to the predictions obtained by the steady multistage code (Ref. 17), indicating that unsteadiness has relatively little effect on loadings on airfoil surfaces in a multistage environment represented by the UTRC LSRR.

The effects of upstream wakes on the secondary flow generation on the downstream rotor can be deduced through the review of unsteady total pressure contours downstream of the rotor from the simulation conducted with a uniform upstream total temperature profile. Contour plots of the computed instantaneous relative total pressure coefficients downstream of rotor together with the 3-stator-4-rotor configuration are shown in Figure 19a which indicate a strong effect of unsteadiness on the rotor flow field. Organized flow structures pointed out in this figure indicate the existence of different secondary flow vortices in each rotor airfoil passage. The secondary flow vortices in the tip region are similar in all four rotor passages which indicate that circumferential distortions generated by the upstream stator have relatively little effect on the flow in the tip region. Significant passage-to-passage variations in the flow structures are observed in the root region. In particular, there are substantial reductions in the strength of the root secondary flow vortex as the rotor moves past the stator airfoils. This periodic disappearance of the root secondary flow vortex is in excellent agreement with experimental data (Ref 13), as shown in Figure 19b. The comparison indicates that the unsteady flow simulation using a Euler code successfully predicts the unsteady and distorted flow features observed in the experimental data with primitive modeling of viscous effects.

Results from this numerical study clearly demonstrate that Euler codes can be used to obtain first order effects of flow unsteadiness in turbines.

3.2 Hot Streak Migration Through a 1-1/2 Stage Turbine

The 3D hot streak simulation was conducted by using 1 hot streak, 3 first-stator, 4 rotor, and 4 second-stator passage flow configuration. Four views of the isotherm of one hot streak for the simulation are shown in Figure 20. It should be pointed out that one hot streak is

located in every third first stator passage; only one is shown in the figure for clarity. A complex interaction of the hot streak with the rotor and the second stator is illustrated in this figure. The hot streak is injected at inlet to the first stator in-between the two airfoils and it is found to convects through the first stator passage without any perturbation. The hot streak then enters the rotor passages, where it is chopped up by the passing rotor airfoils. The remains of the hot streak out of the rotor passages enter the second stator airfoil passages in distinct periodic pulses.

The calculated time-averaged temperature distributions in four rotor passages is shown in Figure 21. Note that each of the four rotor passages have identical time-averaged solutions, since each rotor sees, over a periodic cycle, the identical inlet and exit boundary conditions. The hot gas tends to migrate toward the rotor pressure side (temperature segregation) and rotor passage secondary flow transports the hot gas radially over the pressure surface and then over the endwalls (three-dimensional convection). Simultaneously, the hot gas on the rotor suction side appears to lift off the surface with increasing axial distance. An important observation from this figure is that maximum time-averaged temperatures downstream of the rotor leading edge are higher than time-averaged maximum gas temperatures forward of the leading edge. These higher-than-inlet time-averaged temperatures are an indicator of long residence time of the segregated hot gas in the rotor passage.

A comparison of the temperature distribution in the rotor passage obtained from time-averaged results from the unsteady simulations to those obtained from steady multistage ("Mixing-Plane") simulations are shown in Figure 22 as contour plots at given axial locations. This figure clearly shows that maximum temperature from the steady multistage code is significantly lower than that obtained from the time-averaged results from the unsteady code. This result demonstrates that time-averaged temperature on the rotor airfoil surfaces is strongly affected by periodic unsteadiness induced by combustor generated hot streaks. Conventional design procedures rely on axisymmetric rotor inlet temperature to define the heat load on rotor airfoils, this has historically resulted in underestimation of airfoil pressure surface temperatures and inaccurate estimates of cooling air requirements. The present work indicates that unsteady Euler code can be used to provide a more accurate estimate of the gas temperature near the airfoil surface, which should result in a better cooling air estimate in the design process.

Two numerical experiments were conducted (Ref. 32) for the UTRC 1&1/2 stage LSRR to assess the degree of complexity needed to model the effect of hot streak migration by using steady multistage Euler codes. Since the flow in this problem is periodic over 3 first stator passages, the simulation needed to be conducted by using an "Average-Period" approach by utilizing 3 first stator, 4 rotor and 4 second stator passages. In addition, the effects of periodic unsteadiness were accounted for through the use of "apparent stresses". Distributions of "apparent stresses" were computed in the entire computational domain from the unsteady flow simulations discussed above. Circumferential averaged values of these stresses termed as "axisymmetric apparent stresses" were used in the first numerical experiment, while the three dimensional distribution of stresses (non-axisymmetric) were used in the second experiment. Results from these numerical experiments are shown in Figure 23 as contours of relative total temperature at various axial stations in the rotor passage. These results clearly show that axisymmetric stresses are insufficient to explain segregation of hot and cold air in rotor passages. Results obtained by using non-axisymmetric stresses are, however, in excellent agreement with those obtained from unsteady simulations (Figure 21).

Time-averaged temperatures in four second stator passages are shown in Figure 24. A number of observations can be made from the numerical results shown in this figure:

i) Hot gas in the second stator passage is found to be confined to a small region of the entire 4-stator flow solution domain. This is in contrast to the results obtained for the rotor passages, which had identical time-averaged temperature fields.

ii) The maximum time-averaged temperature levels in the second stator passage are significantly higher than in rotor passage. This is mainly because the hot gas in the second stator passage is confined to a small region of the entire 4- stator flow solution regime.

iii) The maximum downstream time-averaged temperatures are not higher than maximum time- averaged temperatures at the second stator inlet. This is opposite of what was observed in the time averaged rotor flow field and indicates that hot gas in not lingering in time on the second stator surfaces.

iv) There are no obvious signs of temperature segregation in the second stator passage, the hot gas does not have a tendency of preferential migration to either the pressure or the suction surface.

Figure 24 also shows that the hot streak has been split as it reaches the leading edge of a second stator airfoil.

The hot gas that splits to the pressure side in Passage 2 stays attached to the pressure surface, migrating radially along the surface toward the endwalls with increasing axial distance. This radial migration of the hot gas is similar to that observed on the rotor pressure side (Figure 21) and indicates transport with classical secondary flows generated in the stator passage. The hot gas that splits toward the suction side (in Passage 1 of Figure 24) stays attached to the suction surface where it spreads radially toward both inner and outer endwalls with increasing axial distance. This radial spreading on the suction side is opposite to the behavior on the rotor (see Figure 21) where the hot gas on the rotor suction side migrated radially toward the midspan, transported by the secondary flow endwall vortices generated in the rotor passage. The suction surface hot gas in Figure 24 is apparently being transported radially toward both endwalls by vortices near the suction sides for which analogous vortices did not appear in the rotor passage.

The second stator passages apparently contain four primary vortices as shown by the radial velocity component contours in Figure 25 at a planar cut of passage 1 near the airfoil trailing edge. The mechanism believed to be causing the two extra suction side vortices is the interaction of vortices generated in the rotor passage with the downstream second stator. Figure 25 also shows the radial velocity component at the trailing edge plane of the upstream rotor. There appear to be only two primary vortices in the rotor passage, which are the classical counter-rotating endwall vortices generated in the rotor passage.

To further illustrate the differences between rotor and second stator secondary flow, the streamlines on the rotor and second stator airfoil surfaces are shown in Figure 26. Both rotor and second stator pressure sides show streamlines bending toward the endwalls with increasing axial distance from the leading edge, consistent with the existence of classical endwall secondary flow vortices on the pressure sides. However, on the suction sides, the streamlines for the rotor bend toward the midspan region and the streamlines for the second stator bend toward the endwalls. This observation is consistent with the existence of two primary vortices in the rotor and four in the second stator.

Figure 27 shows total temperature contours at five axial planes in the second stator passage obtained from:

i) time-averaged results from the unsteady Euler code

ii) steady multistage ("Mixing-Plane") code

iii) steady multistage ("Average-Period") code where the effects of periodic unsteadiness are accounted for through non-axisymmetric distribution of "apparent stress".

The above figure illustrates that results obtained from the "Average-Period" approach are almost identical with those obtained from the unsteady code. Results obtained from the "Mixing-Plane" approach are, however, much different than those obtained from the unsteady code. This comparison indicates that current steady multistage codes ,which solve for the flow through an average passage using either the "Mixing-Plane" or the "Average-Passage" approach, are insufficient to describe flow features having circumferential length scales larger than one airfoil passage. An "Average-Period" approach is required to describe these flows, in addition, the effects of periodic unsteadiness need to be accounted for through three-dimensional distributions of "apparent stresses".

4.0 IMPLICATIONS OF RESULTS

Results from both experimental data and unsteady numerical simulations indicate that time-averaged loadings at subsonic Mach # on airfoil surfaces (and endwalls), in turbines with moderate axial gaps between adjacent airfoil rows, are not influenced by unsteadiness even in the presence of temperature streaks. Airfoil loadings are, however, affected by potential waves in turbines with small axial gaps between adjacent airfoil rows. Non-reflecting boundary conditions suggested in Ref. 33 allow this effect to be accurately accounted for in multistage steady CFD codes with "Mixing-Plane" approach.

Pressure sides of turbine rotors operate at higher temperatures than the suction sides in the presence of circumferentially non-uniform temperature profiles. Currently available steady multistage CFD codes do not predict this phenomenon. Unsteady multistage Euler codes can predict this flow phenomenon, computational resources have recently become available to allow the application of these codes in the turbine design process. Unsteady Euler codes by themselves are, however, not sufficient to provide accurate estimates of heat loads since viscous regions on airfoil surfaces also contribute towards establishing magnitudes of heat loads on airfoil surfaces. A viable technique may, therefore, be to utilize a multistage steady RANS code based on the "Average-Period" approach discussed in Section 3.2. Effects of periodic unsteadiness in this code may be accounted for through the use of "apparent stresses" computed from numerical simulations conducted by using the unsteady Euler code. Further work is needed to demonstrate the accuracy of utilizing this technique in the turbine design process.

Circumferential distortions generated by viscous flow mechanisms in first stage airfoils have a significant effect on the performance of second stage airfoils as

discussed in Section 2.2. Significant improvements in the performance of multistage turbines may be achieved by indexing first and second stage airfoils. An improved physical understanding of the loss generation mechanisms is, however, needed to allow its routine application in the design process. Numerical simulations by utilizing unsteady and/or "Average-Period" RANS codes should be able to provide this insight.

5.0 CONCLUSIONS

Following conclusions are drawn from the above discussions presented in the paper:

Three dimensional steady multistage flow prediction codes provide accurate estimates of loadings for airfoil rows even in the presence of periodic unsteadiness and temperature distortions.

Turbine inlet circumferential temperature distortions result in hotter pressure sides and colder suction sides for rotor airfoils. This phenomenon is not predicted by the steady multistage codes which are currently used in turbine design procedure. Unsteady multistage Euler codes together with RANS codes based on "Average-Period" approach are needed to provide accurate estimates of heat loads in a realistic turbine flow environment.

Efficiency of multistage turbines can be improved by indexing first and second stage airfoils. Improved understanding of the loss generation mechanisms is, however, needed to apply these concepts in a routine manner.

Continued development of unsteady RANS codes are needed to provide accurate estimates of heat loads and losses in realistic turbine environments.

ACKNOWLEDGEMENTS

The authors wish to thank Pratt & Whitney management for their permission for publishing this paper. The authors are grateful to Mr. L.L.Coons and Dr. G.F.Pickett for their encouragement and support during this research project. The authors would also like to acknowledge the technical support provided by Gary Stetson, Ron Takahashi, Diane McGrath, Brent Staubach, Frank Huber and Dean Johnson.

REFERENCES

1. Hodson, H. P., 1983, "The Development of Unsteady Boundary Layers in the Rotor of an Axial-Flow Turbine, "AGARD Proceedings No. 351, Viscous Effects in Turbomachines.

2. Blair, M. F., Dring, R. P. and Joslyn, H. D., "The Effects of Turbulence and Stator-Rotor Interactions on turbine Heat Transfer Part I, Design Operating Conditions", ASME Paper #88-GT-125, 1988.

3. Doorley, D. J., Oldfield, M. L. G. and Scrivener, C. T.J., "Wake Passing in a Turbine Rotor Cascade," AGARD CP-390, Paper No. 7, Bergen, Norway.

4. Sharma, O. P., Pickett, G. F. and Ni, R. H., "Assessment of Unsteady Flows in Turbines", ASME Paper #90-GT-150, 1990.

5. Speidel, L., "Beeinflussung der laminaren Grezschicht durch periodische Strorungen der Zustromung", Z. Flugwiss. 9 (1957) 5.

6. Sharma, O. P., Renaud, E., Butler, T. L., Milsaps, K., Dring, R. P., and Joslyn, H. D., "Rotor-Stator Interaction in Multistage Axial-Turbines," AIAA Paper #88-3013, 1988.

7. Scholz, N., "Aerodynamics of Cascades," AGARD-AG-220, 1977.

8. R. E. Mayle and Dullenkopfk,K. "A Theory for Wake-Induced Transition ", ASME Paper #89-GT-57, 1989.

9. Hodson, H. P., Addison, J. S. and Shepherdson, C. A., "Models for Unsteady Wake-Induced Transition in Axial Turbomachines", J. Physics III, France 2 (1992), pp 545-574.

10.Rangwalla, A. A., Madavan, N. K., and Johnson P. D., "Application of Unsteady Navier Stokes Solver to Transonic Turbine Design," AIAA Paper #2468, 1991.

11. Butler, T. L., Sharma, O. P., Joslyn, H. D., and Dring, R. P., 1989, "Redistribution of an Inlet Temperature distortion in an Axial Flow Turbine Stage,: Journal of Propulsion and Power, Vol. 5, pp.64-71.

12. Kerrebrock, J.L., and Mikolajczak, A.A., "Intra Stator Transport of Rotor Wakes and Its Effect on Compressor Performance," ASME Journal of Engineering for Power, Oct. 1970, pp. 359-370.

13.Sharma, O. P., Butler, T. L., Joslyn, H. D., and Dring,R. P., "Three - Dimensional Unsteady Flow in an Axial Flow Turbine," Journal of Propul- sion and Power, Vol. 1, No. 1, Jan-Feb. 1985.

14.Munk, M., and Prim., R. C., "On the Multiplicity of Steady Gas Flows Having the Same Streamline Pattern," Proceedings of the National Academy of Sciences, U.S. Vol. 33, 1947.

15. Gaddis, S.W., Hudson, S.T. and Johnson, P.D.,"Cold Flow Testing of the Space Shuttle Main Engine Alternate Turbopump Development High Pressure Fuel Turbine Model", ASME Paper # 92-GT-280, 1992.

16. Huber, F.W., Johnson, P.D., Sharma, O.P., Staubach, J.B. and Gaddis, S.W., "Experimental Investigation of Vane Wake Clocking Effects on Turbine Performance", Paper to be presented at the 1994 IGTI Meeting.

17.Ni, R-H and Bogoian, J. C., "Prediction of 3D Multistage Turbine Flo w Field Using a Multiple-Grid Euler Solvers:, AIAA Paper #89-0203, 1989.

18.Denton, J., "Calculation of Three-Dimensional Viscous Flows Through Multistage turbine;, ASME Paper # 90-GT-19, 1990.

19.Dawes, W. N., "A Comparison of Zero and One Equation Turbulence Modeling for Turbomachinery Calculations", ASME Paper #90-GT-303, 1990.

20.Dawes, W. N., "Towards Improved Throughflow Capability: The Use of 3D Viscous Flow Solvers in Multistage Environment", ASME Paper 90-GT-18, 1990.

21. Adamczyk, J. J., "Model Equation for Simulating Flows in Multistage Turbomachinery," ASME Paper 85-GT-226, 1985.

22. Ni, R. H., Sharma, O. P., Takahashi, R, and Bogoian, J., "3D Unsteady Flow Simulation Through a Turbine Stage," Paper presented in the 1989 Australian Aeronautical Conference - Research and Technology - The Next Decade, Melbourne, Australia, Oct. 1989.

23. Ni, R. H. and Sharma, O. P.,"Using 3D Euler Flow Simulations to Assess Effects of Periodic Unsteady Flow through Turbines," AIAA Paper 90-2357.

24. Rai, M. M., "Three Dimensional Navier-Stokes Simulations of Turbine Rotor-Stator Interactions", Journal of Propulsion and Power, Vol. 5, No. 3, pp. 307-319, 1989 25. Rai, M. M. and Madavan, N.K., 1988, "Multi Airfoil Navier Stokes
Simulations of Turbine Rotor-Stator Interaction," Journal of Propulsion and Power, Vol. 5, No. 3, pp. 307-319.

26. Rao, K. and Delaney, R., "Investigation of Unsteady Flo Through Transonic Turbine Stage - Part 1: Analysis," AIAA Paper #90-2408, 1990.

27. Gundy-Burlet, K. L., "Computations of Unsteady Multistage Compressors Flows in a Workstation Environment," ASME Paper #91-GT-336, 1991.

28. Huber, F.W. and Ni, R-H.,"Application of A Multistage 3D Euler Solver To the Design of Turbines for Advanced Propulsion Systems," AIAA Paper 89-2578.

29. Huber, F. W., Rowey, R. J., and Ni, R-H, "Application of 3D Flow Computation to Gas Turbine Aerodynamic Design," AIAA-85-1216, 1985.

30. Takahashi, R., and Ni, R.H., "Unsteady Hot Streak Simulation Through 1-1/2 Stage Turbine", AIAA Paper # 91-3382, 1991.

31. Denton, J. D.,"The Use of a Distributed Body Force to Simulate Viscous Flow in 3D flow Calculations" ASME Paper 86- GT-144.

32. McGrath D.L., Sharma, O.P., Ni, R.H., Takahashi, R.T., Stetson, G.M. and Staubach, J.B., "Accurate Simulations of Flow Through Multistage Turbomachines by using 3D Steady CFD Codes", Paper to be presented at 1994 AIAA Joint Propulsion Meeting.

33. Giles, M.B., "Stator-Rotor Interaction in a Transonic Turbine", AIAA Paper# 88-3093, 1988.

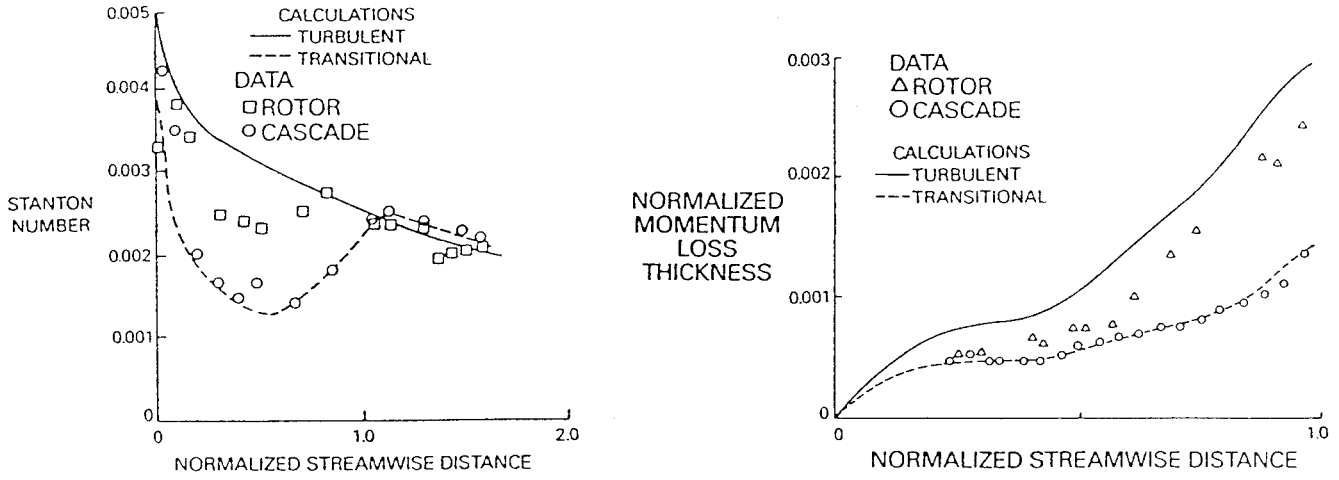

Figure 1. Measured streamwise distribution of time-averaged Stanton number of Blair et al. [2] and Sharma et al. [6] and boundary layer thickness of Hodson [1] show larger values in an unsteady environment than in a steady cascade configuration.

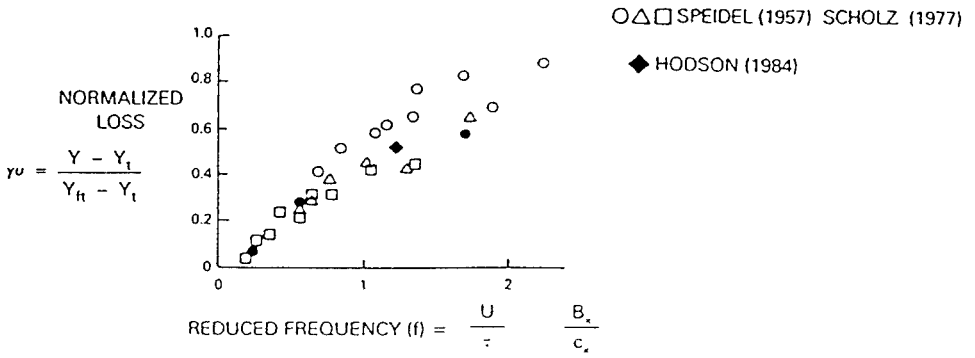

Figure 2. Additional time-averaged loss (γ_u) generated due to unsteadiness induced by upstream wakes can be related to reduced frequency (f) [6].

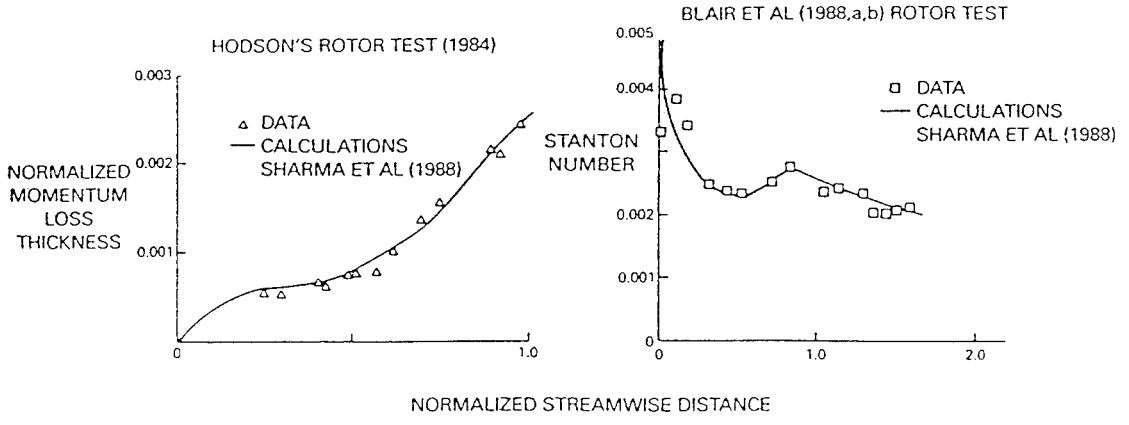

Figure 3. Sharma [6] model yields good estimates of time averaged momentum loss thickness and Stanton numbers from data acquired in an unsteady flow environment.

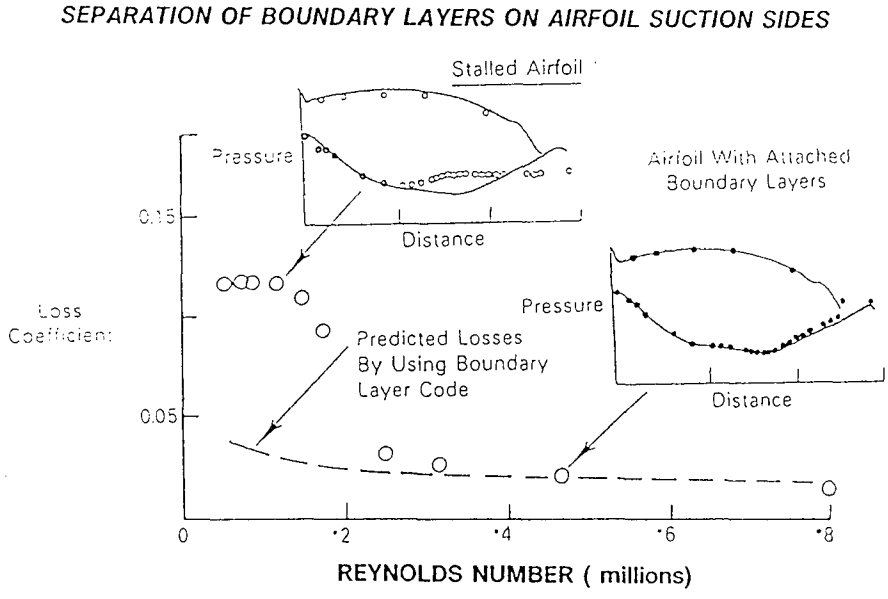

Figure 4. High loss levels measured for airfoils at low Reynolds numbers. Boundary layer flow separation evident on airfoil suction surfaces.

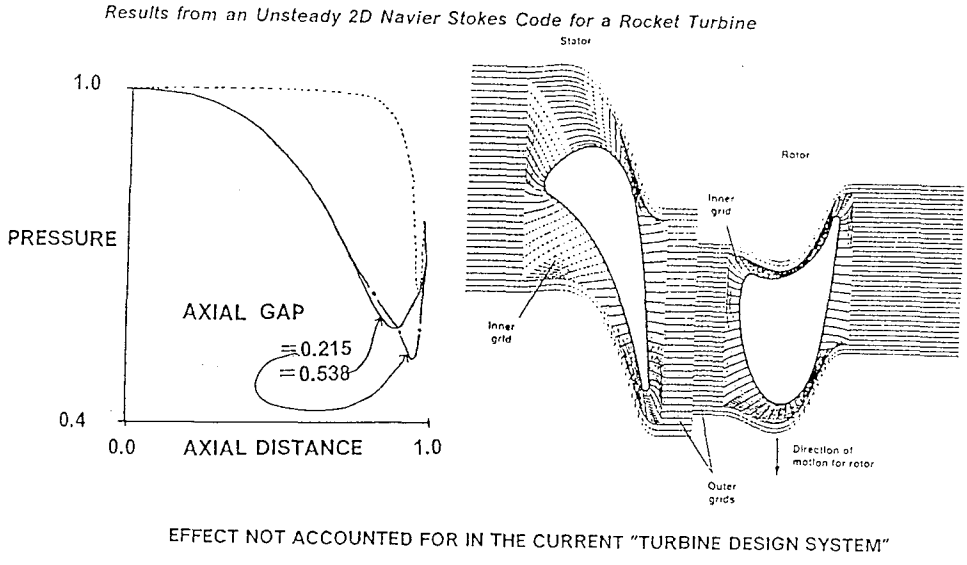

Figure 5. Diffusion on the upstream airfoil affected by axial gap between rows. Effect not accounted for in classical "design systems".

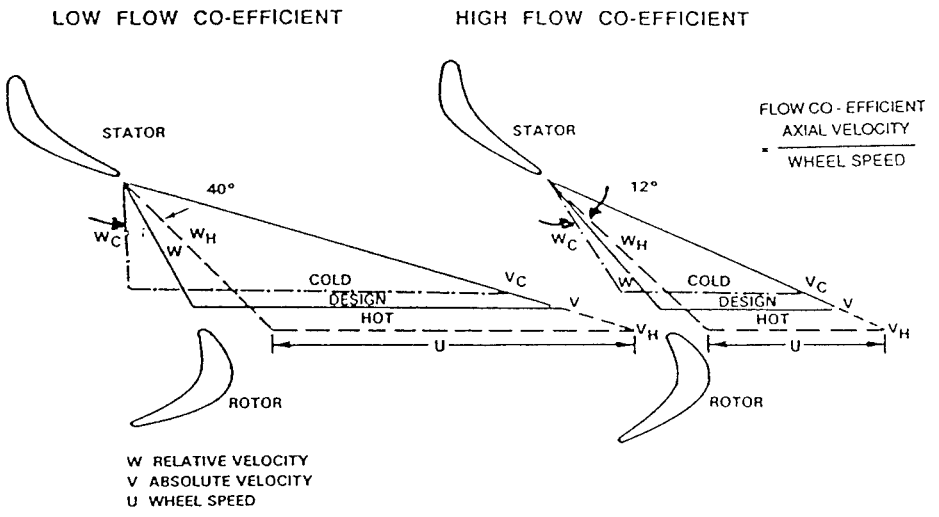

Figure 6. Rotor inlet gas temperature distortion causes large variation in blade incidence angle. Simple calculations conducted for hot-to-cold temperature ratio of 1.7 indicates incidence angle variation of 12 and 40 degrees for typical high and low flow coefficient configurations respectively.

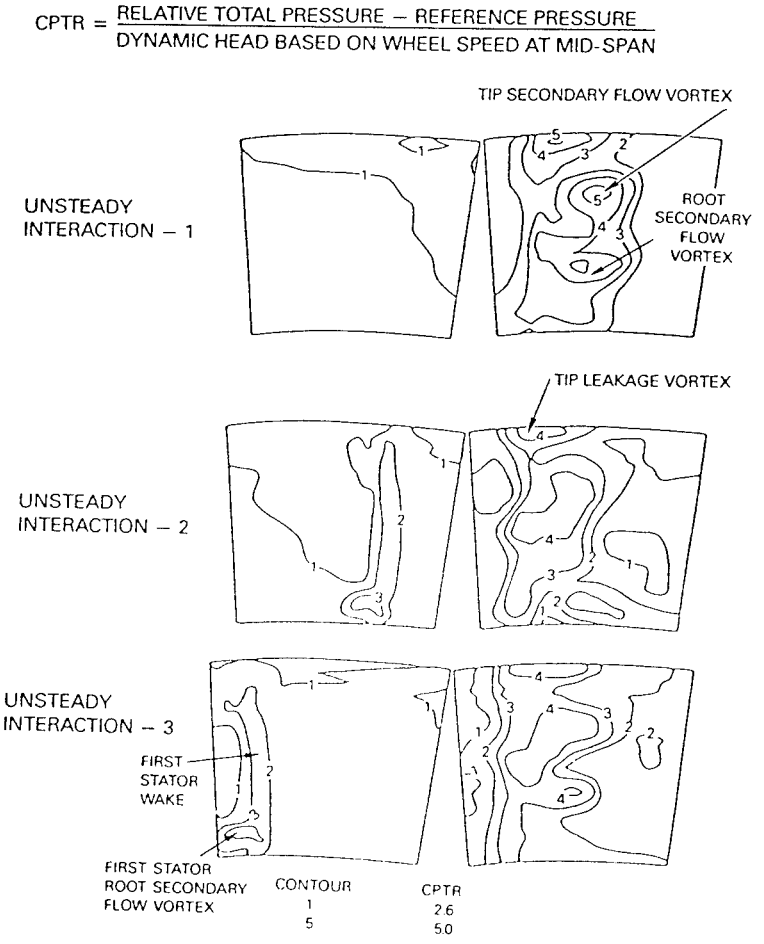

Figure 7. Total pressure loss contours and gap averaged profiles at inlet and exit of the rotor in relative frame indicating the influence of unsteadiness.

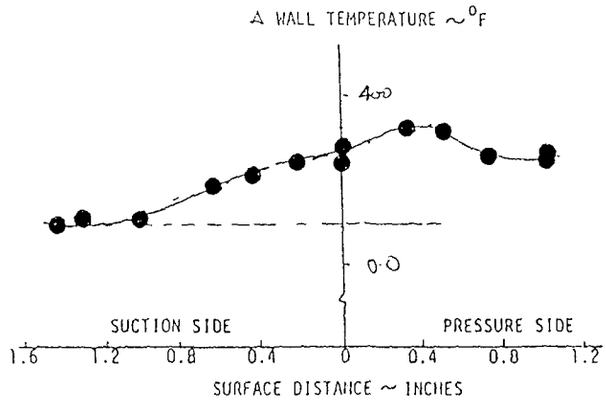

Δ *TEMPERATURE ON THE TWO SIDES OF THE AIRFOIL* = = 250°F

Figure 8. Hotter pressure sides indicated in turbine rotors. Temperature difference between pressure and suction surfaces of 250 F observed.

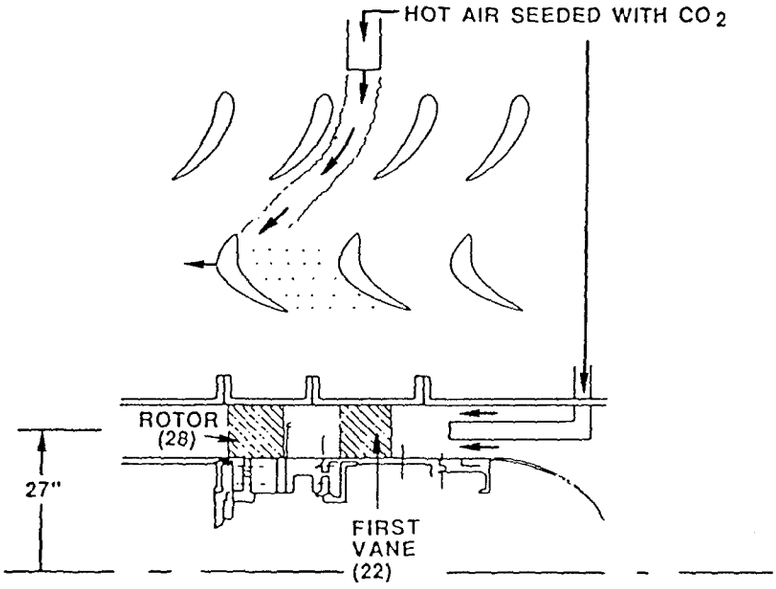

Figure 9a. Schematic of the experimental apparatus used to simulate the redistribution of hot-streak in the turbine rotor [11].

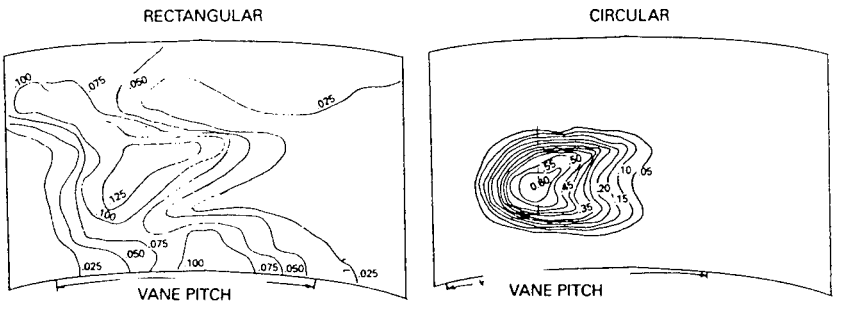

Figure 9b. Contour plots of normalized CO_2 concentration downstream of the first stator in the UTRC LSRR obtained with a circular and rectangular hot streaks - high values indicate high temperatures.

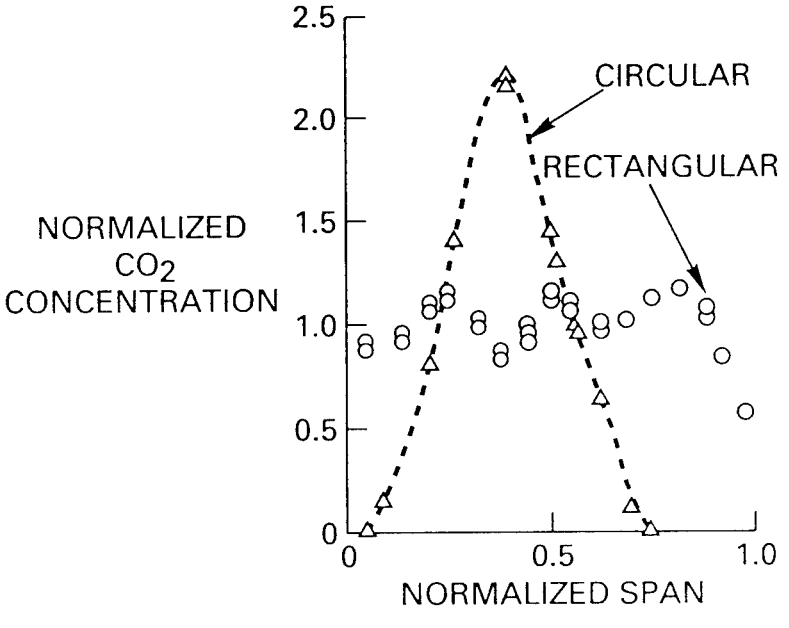

Figure 9c. Spanwise distribution of normalized CO_2 concentration profiles (indicators of temperatures) measured in the rotor frame for the circular and rectangular hot streaks.

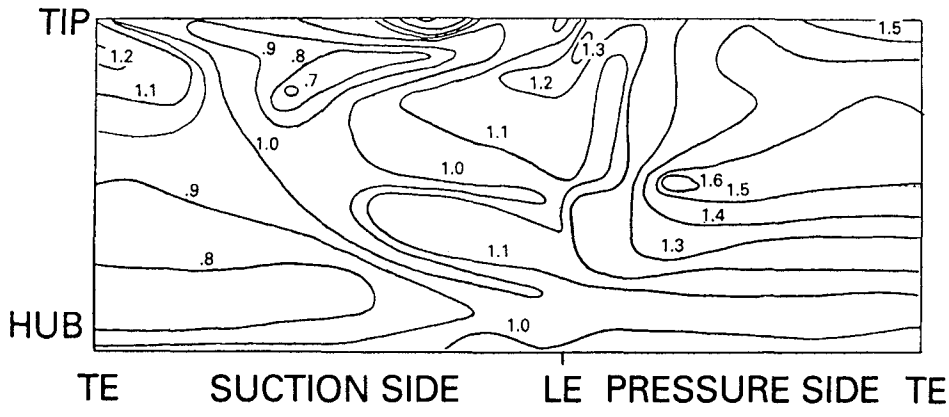

Figure 10. Larger time-averaged CO_2 concentration (temperature) measured on the pressure side of rotor airfoil relative to the suction side indicates segregation of hot and cold air.

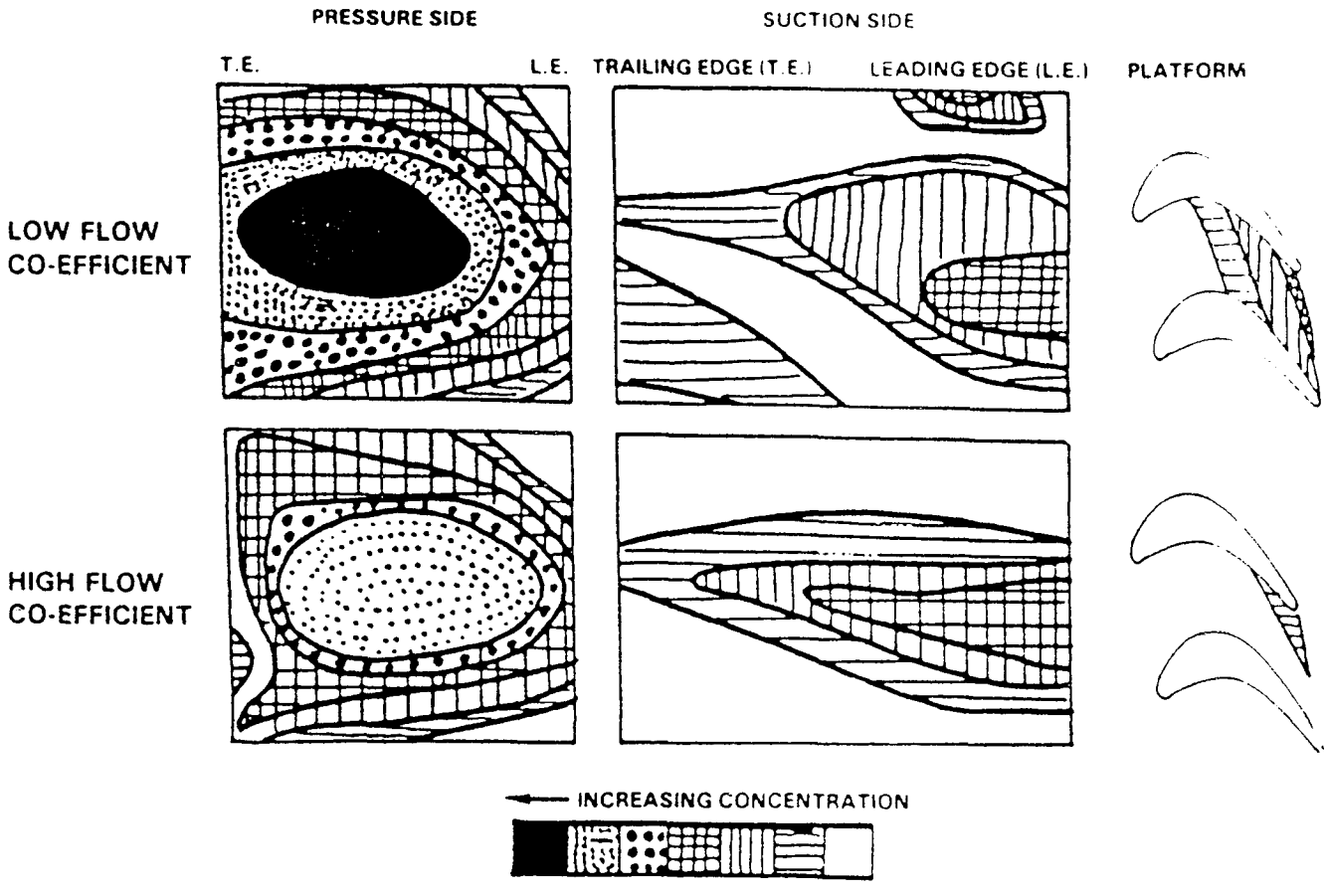

Figure 11. Effect of inlet temperature distortion can be reduced by increasing the flow coefficient.

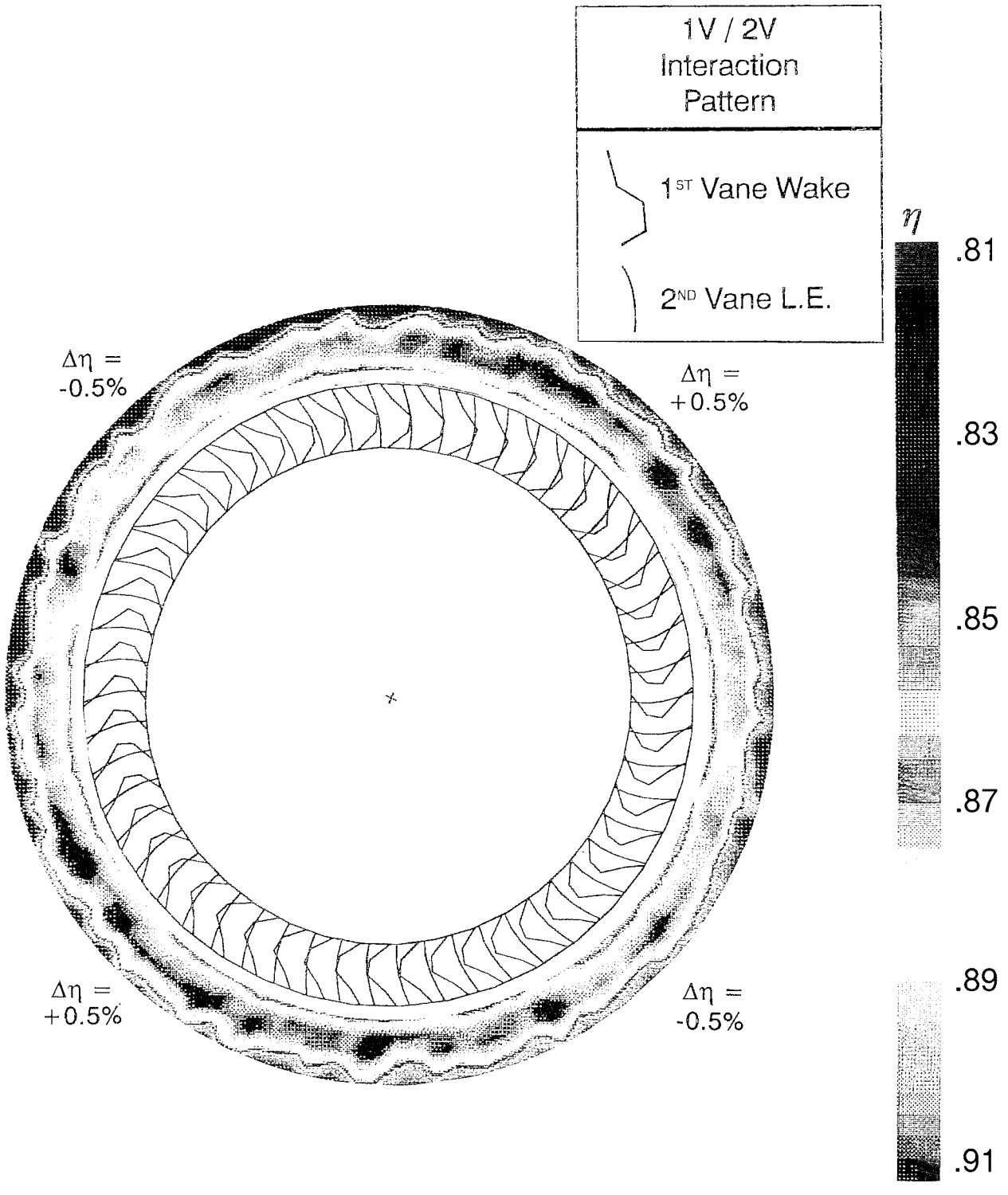

Figure 12. Original Alternate Turbopump Design (ATD) Turbine Test Article (TTA) measured efficiency contours.

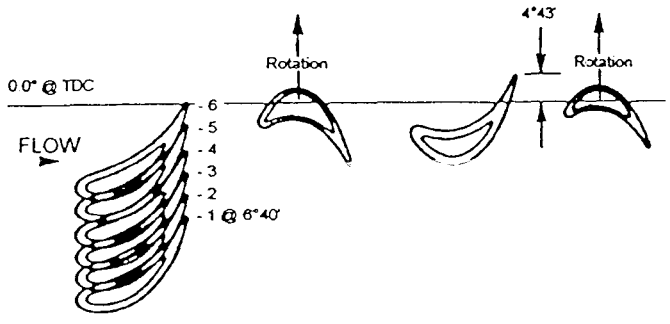

Vane Position	1	2	3	4	5	6
Circ Location	6° 40'	5°20'	4°0'	2°40'	1°20'	6°40'

Figure 13. ATD TTA first vane clocking positions.

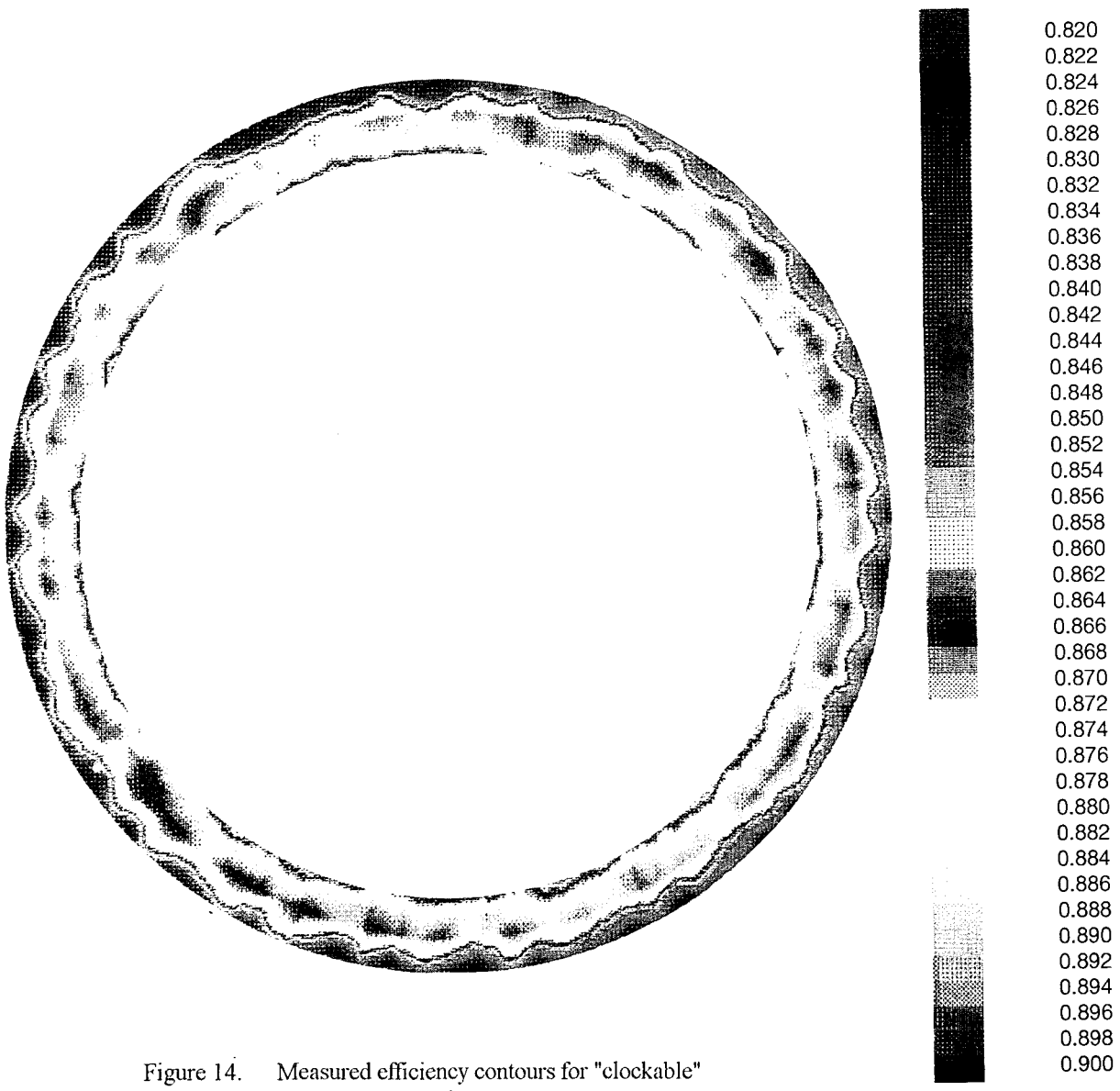

Figure 14. Measured efficiency contours for "clockable" turbine configuration.

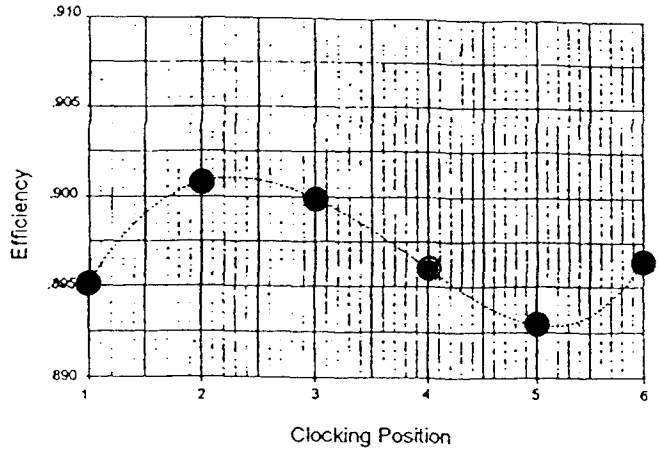

Figure 15a. Efficiency as a function of clocking position at midspan clearly indicates a minimum and a maximum.

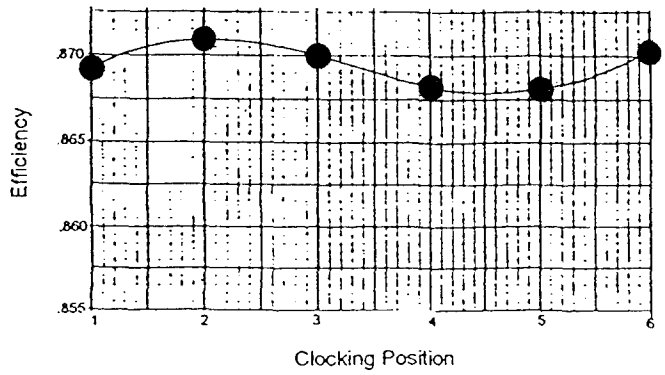

Figure 15b. Overall efficiency as a function of clocking position also indicates a minimum and a maximum.

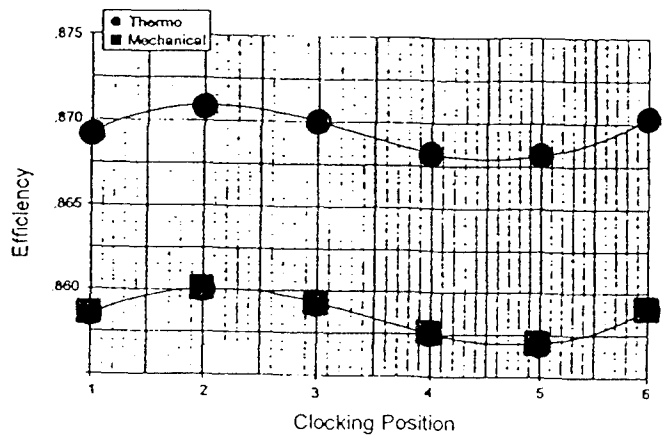

Figure 15c. Both thermodynamic and mechanical measurement of turbine efficiency in the ATD TTA confirm clocking effects and magnitude of variation.

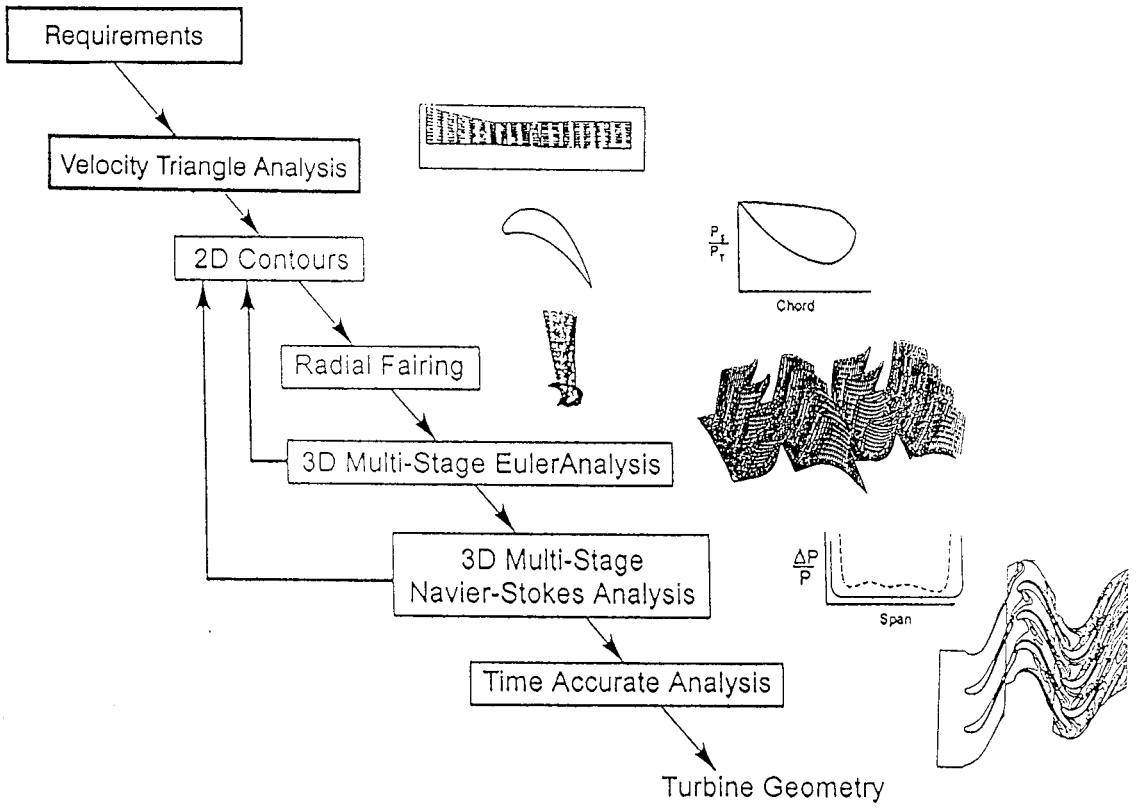

Figure 16. Current turbine design practices are based on steady CFD codes.

ELEVATION VIEW OF A TWO-STAGE HIGH PRESSURE TURBINE RIG.

COMPUTATIONAL BOUNDARIES FOR THE MULTI-STAGE FLOW SIMULATION.

COMPUTATIONAL MESH USED FOR THE TWO-STAGE TURBINE FLOW SIMULATION.

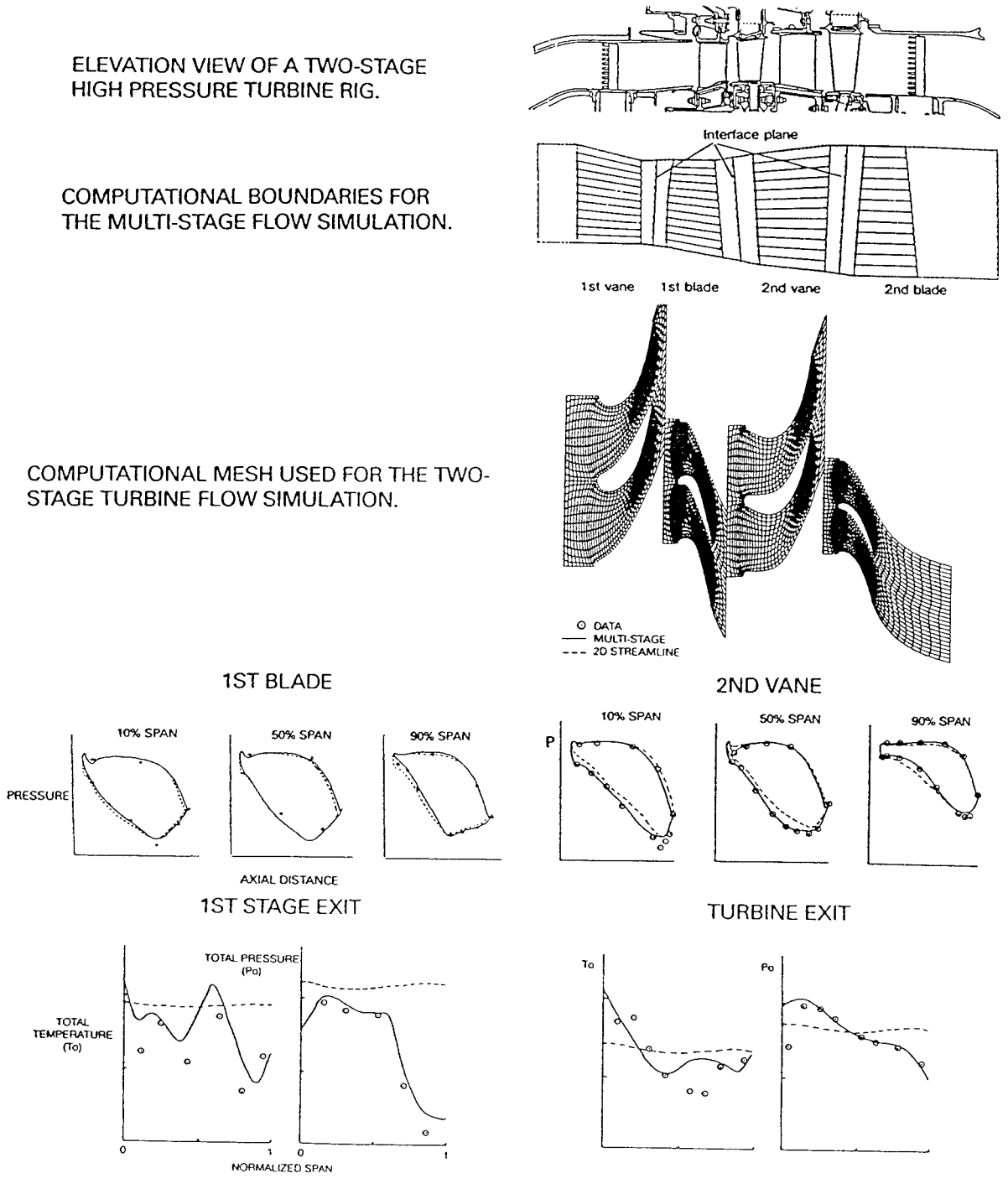

Figure 17. 3D steady multistage Euler code of Ni and Bogoian [17] provides accurate estimates of airfoil loadings and total pressure as well as total temperature profiles in multistage turbines.

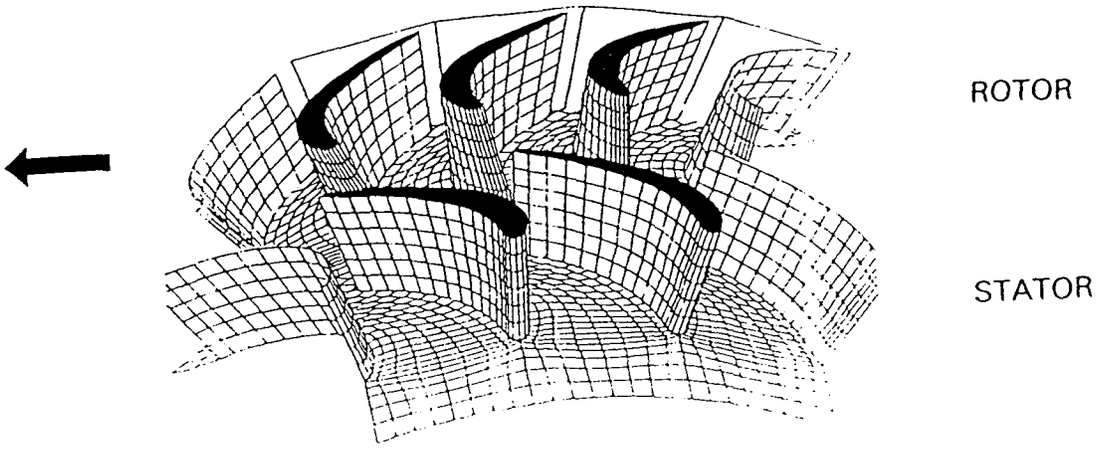

Figure 18a. Computational mesh of Ni and Bogoian [17] for the UTRC Large Scale Rotating Rig (LSRR).

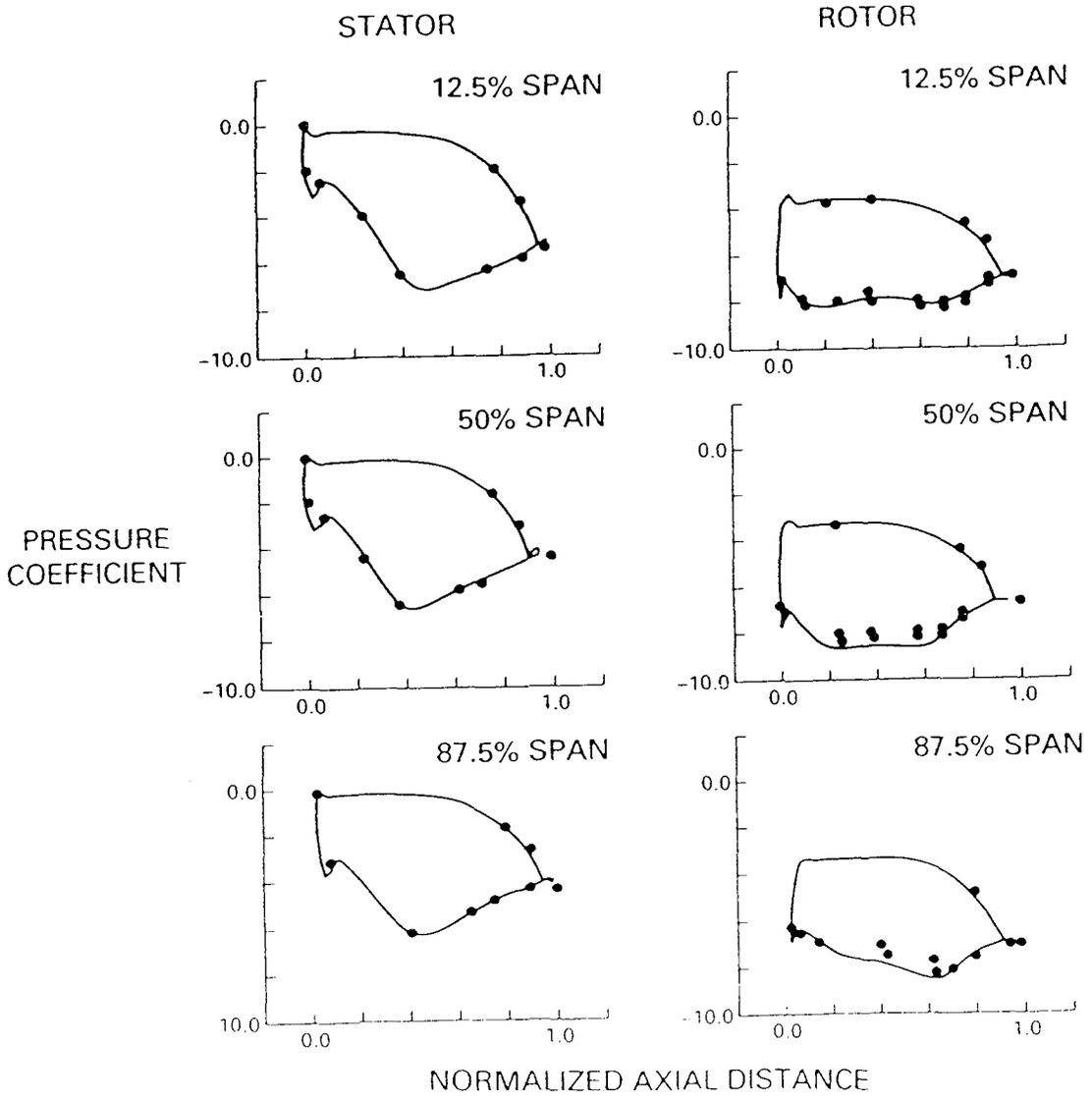

Figure 18b. Predicted time-averaged pressure distributions from the 3D Euler code of Ni and Bogoian [17] show good agreement with measured data for the LSRR first stage. Both steady and unsteady multistage codes yield similar results for loadings.

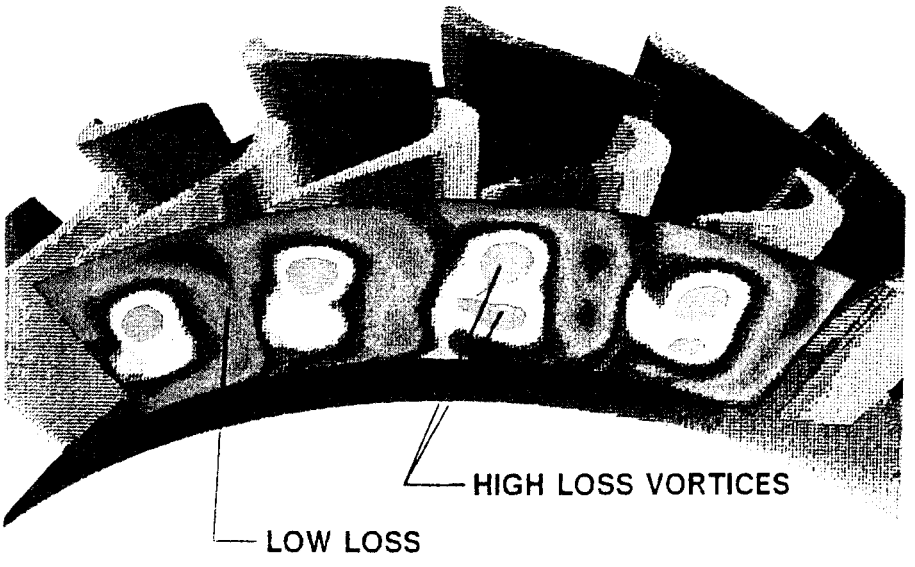

NUMERICAL SOLUTION ANIMATED

Relative Total Pressure Loss at Rotor Exit

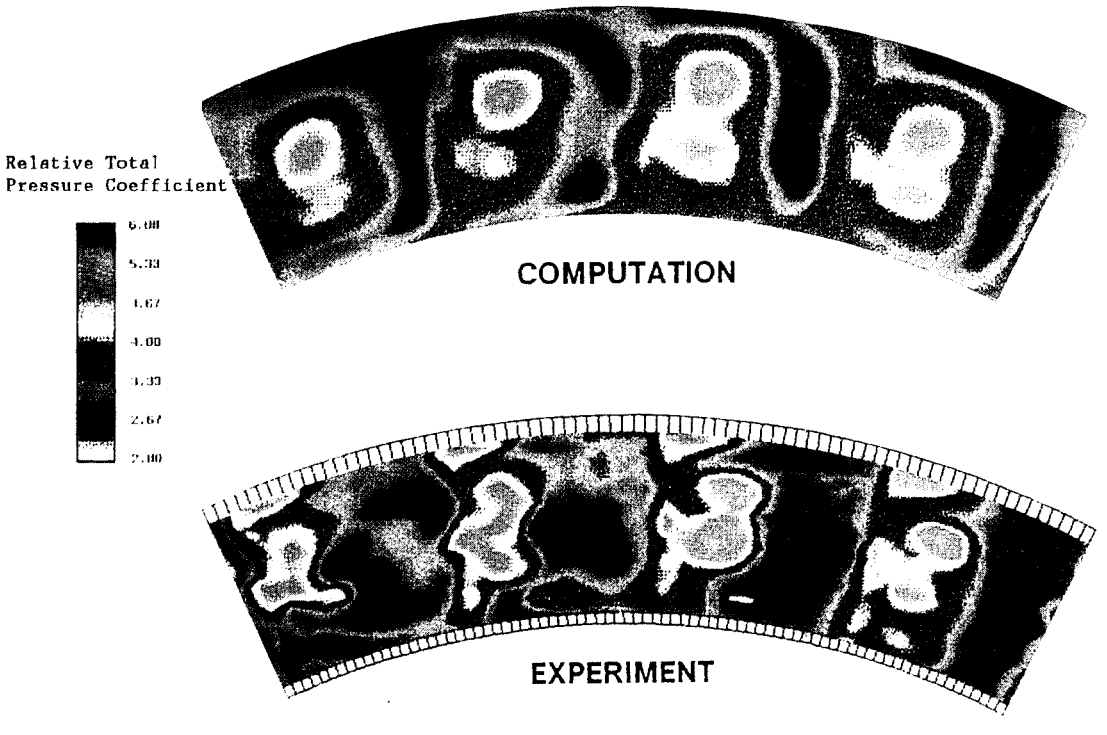

Figure 19. Relative total pressure loss at exit of rotor; (a) location of data plane, and (b) periodic disappearance of root secondary flow vortex is in agreement with experimental data.

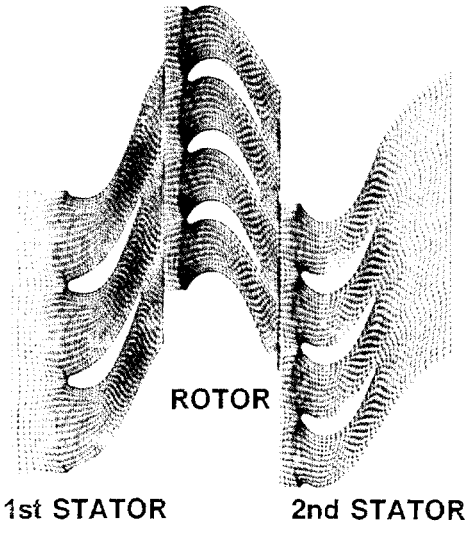

Computational mesh at midspan for 1-1/2 stage simulation.

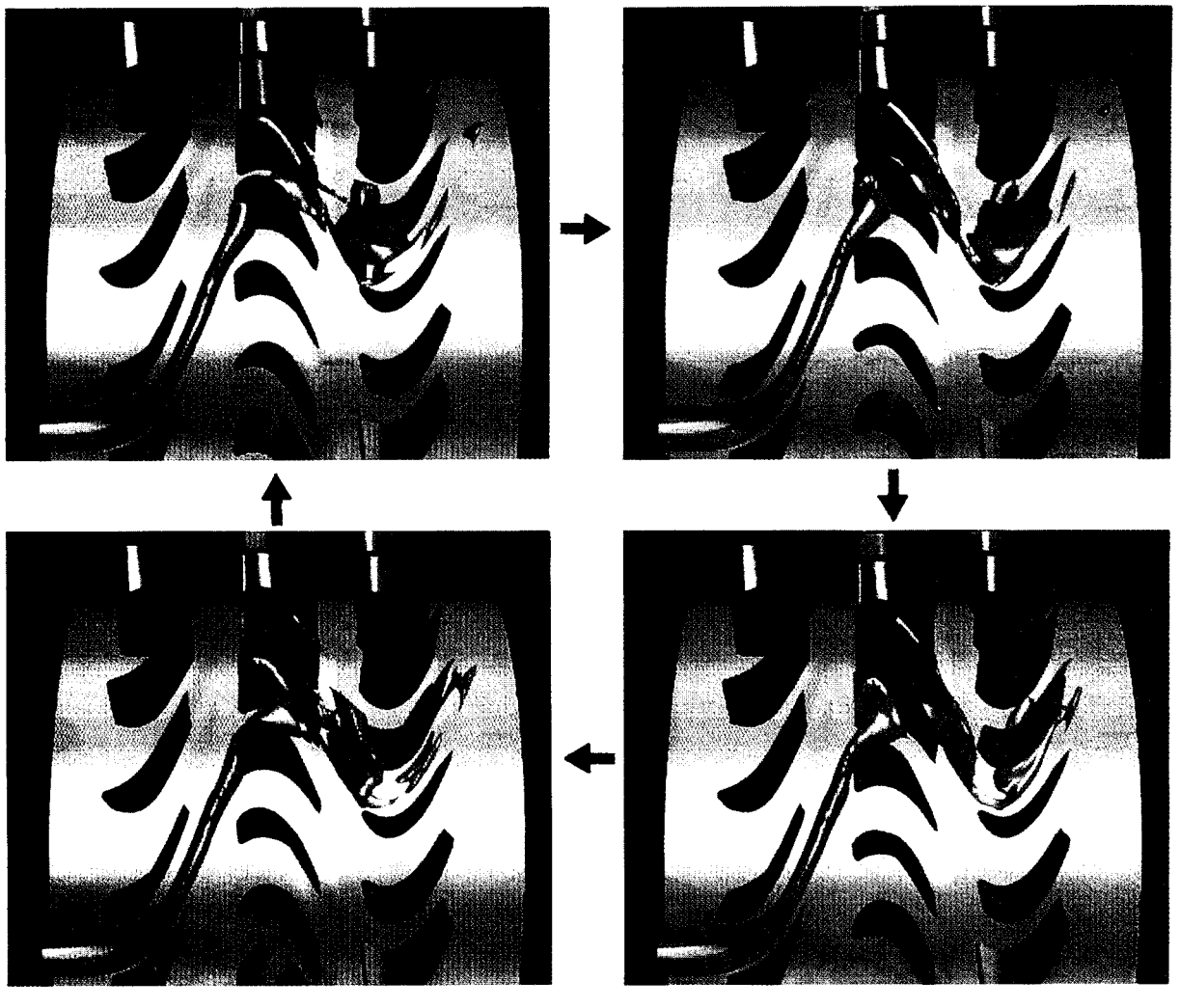

Figure 20. Four snapshots in time of an isotherm of one hot jet in 1½ stage flow simulation.

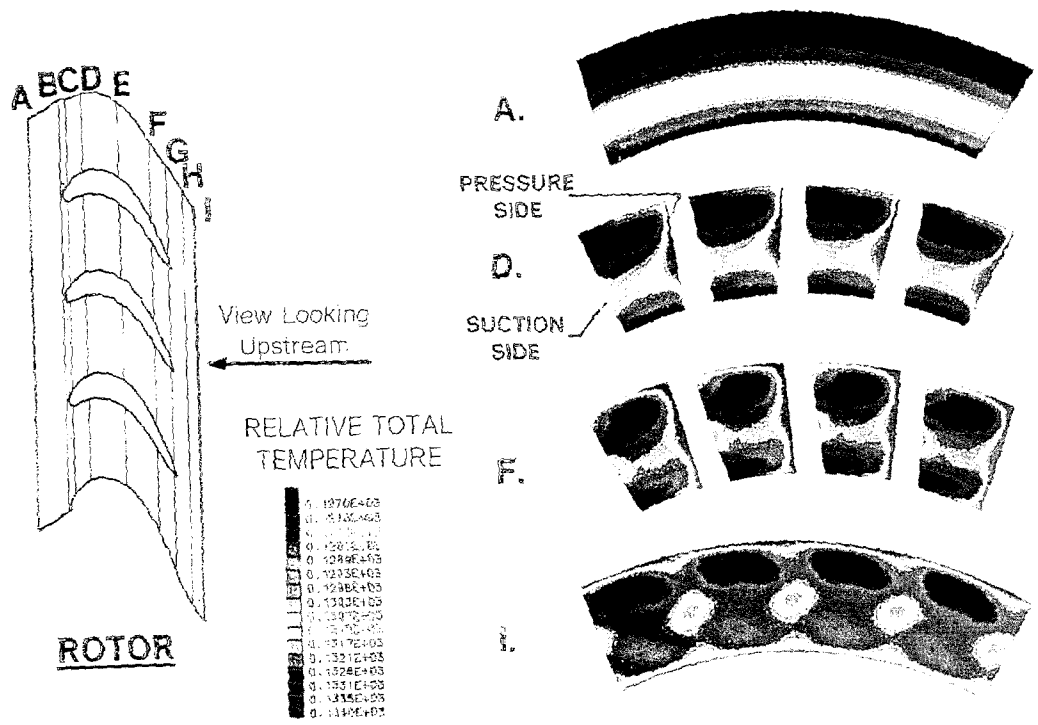

Figure 21. Time-averaged temperature in four rotor passages shows the hot jet segregation and migration.

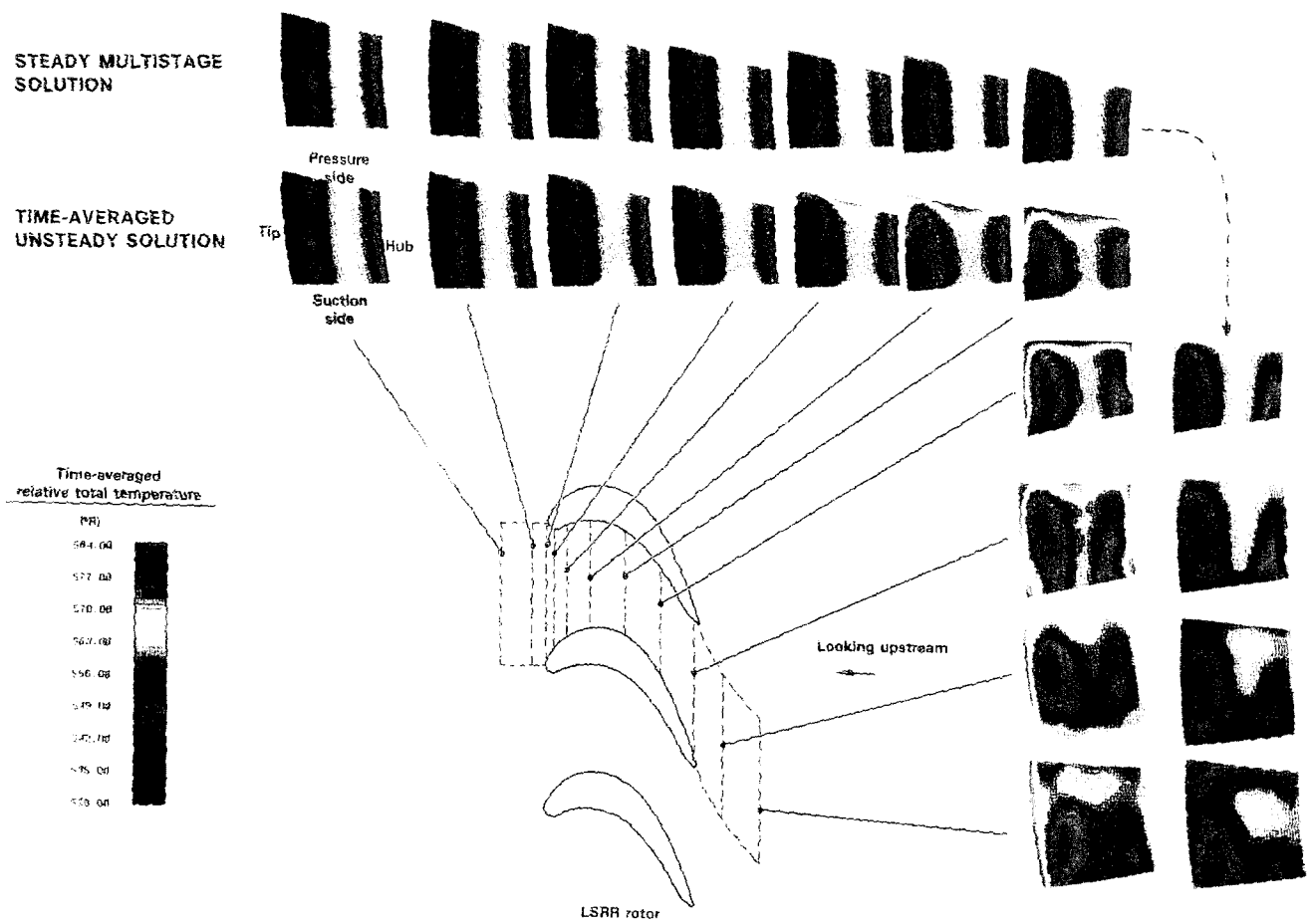

Figure 22. The maximum temperature from steady solution is significantly lower than that from time-averaged unsteady solution.

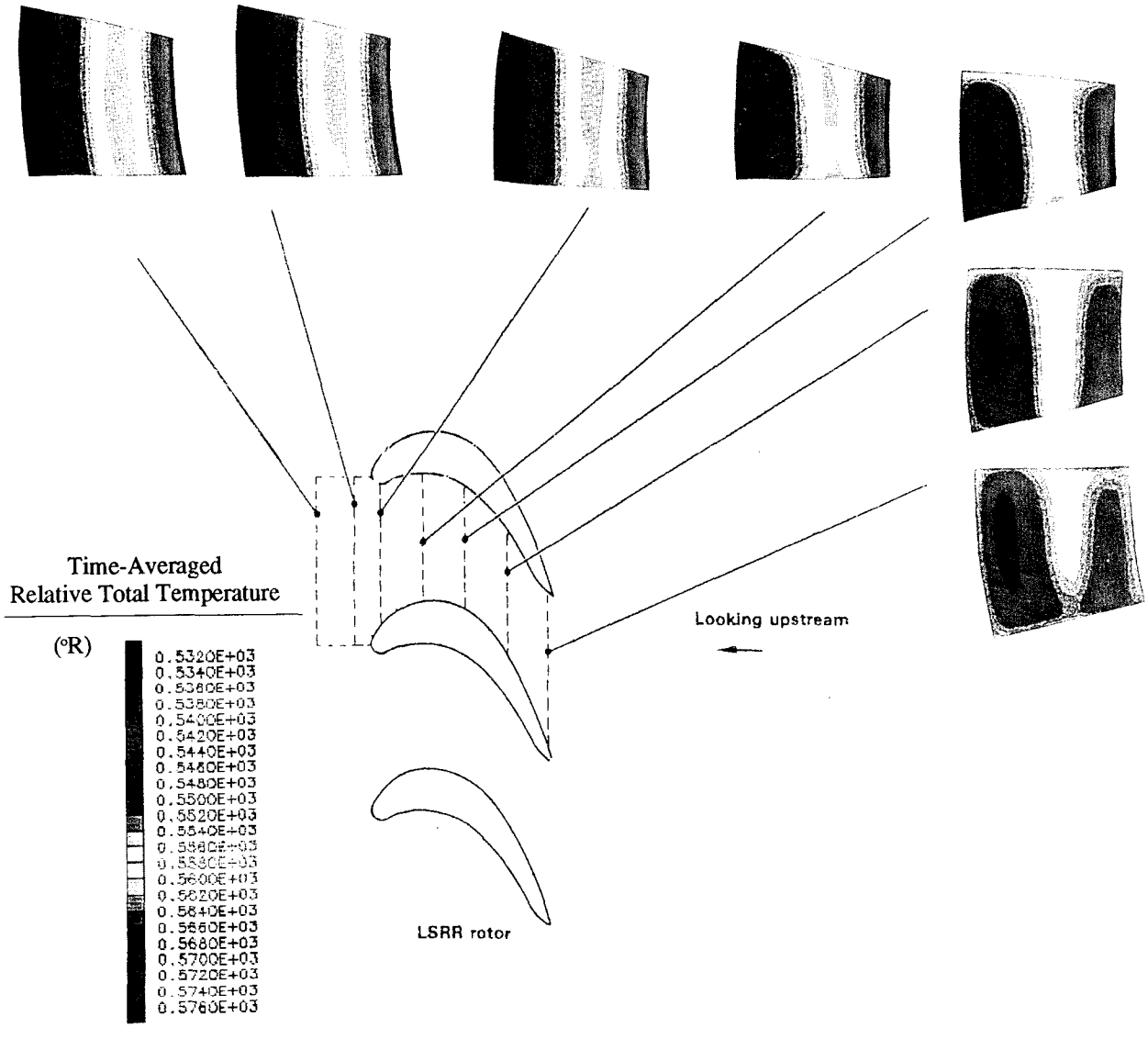

Figure 23. Segregation of hot and cold air is not predicted by "average passage" code. Relative total temperature contours in the rotor passage in same view as given in Figure 22.

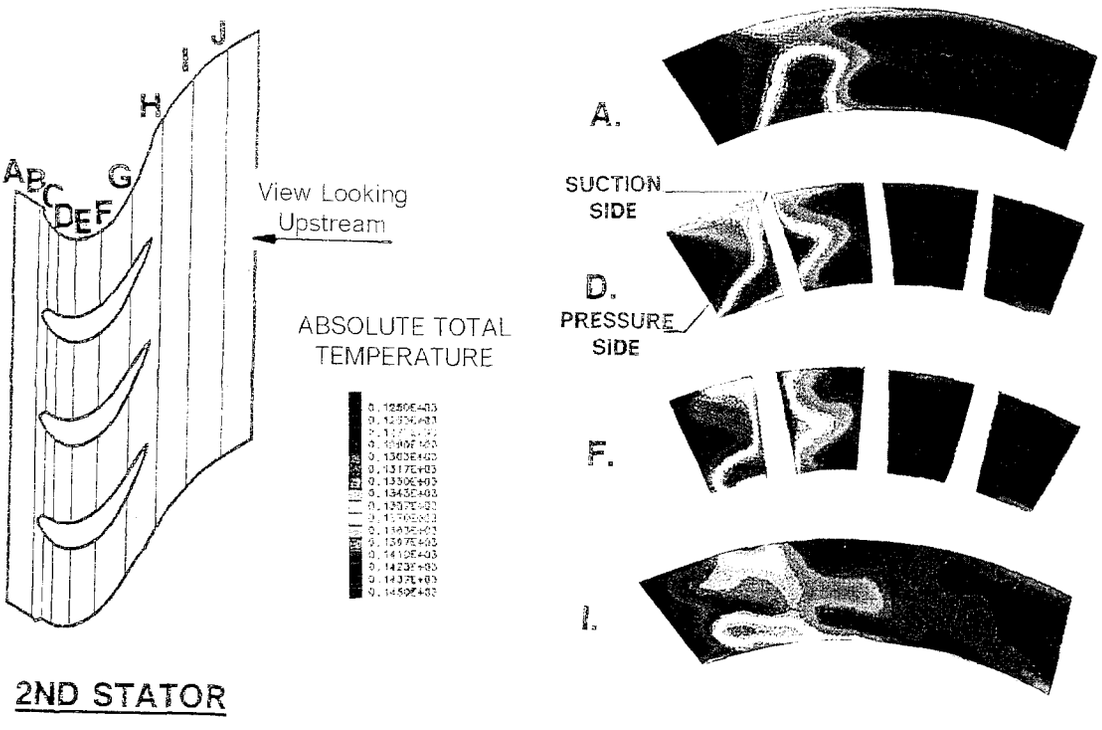

Figure 24. Time-averaged temperature in the four second stator passages shows that hot gas is confined to a small region.

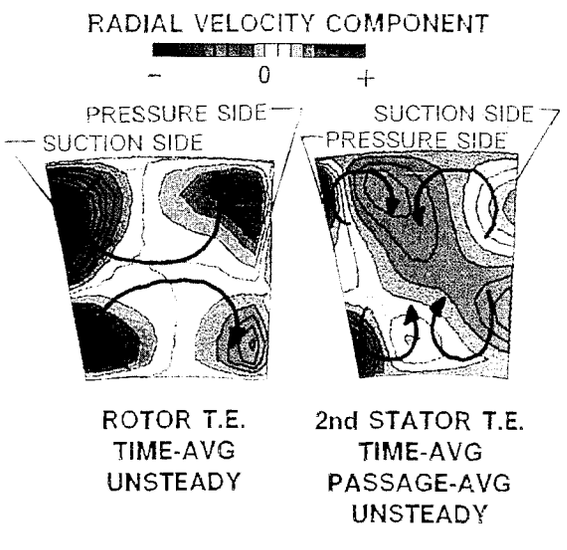

Figure 25. Time-averaged radial velocity contours show that there are four vortices in the second stator passage and two vortices in the rotor passage.

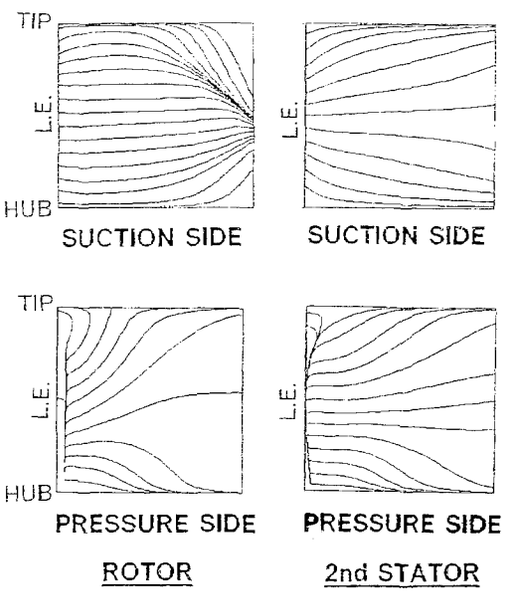

Figure 26. Streamlines on the rotor suction side converge to midspan at trailing edge, whereas the second stator suction side streamlines diverge toward the endwalls.

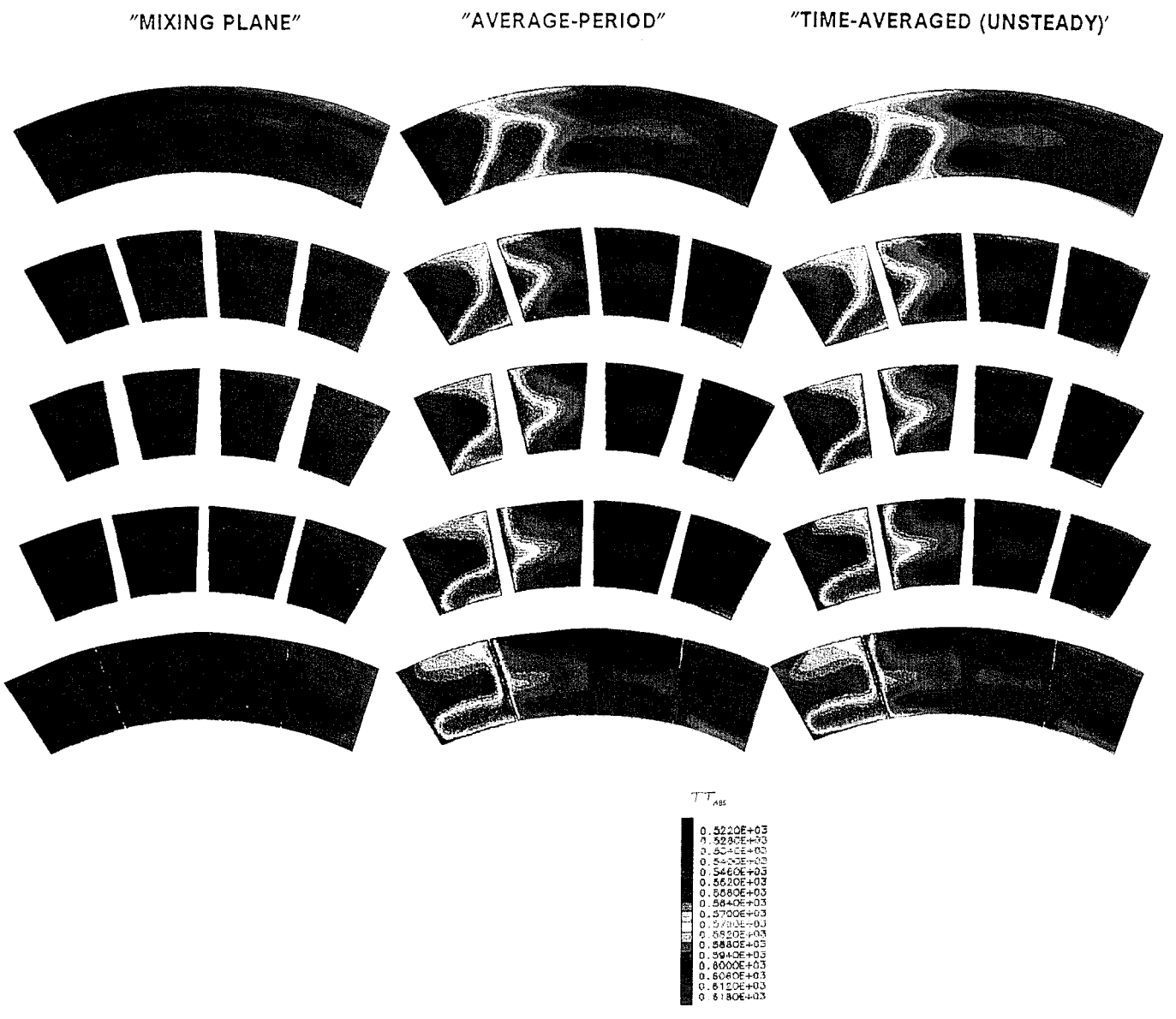

Figure 27. Computed temperature distributions in the UTRC LSRR second stator.

THE INDUSTRIAL USE OF CFD IN THE DESIGN OF TURBOMACHINERY

M. V. Casey
Fluid Dynamics Laboratory
Sulzer Innotec AG
CH-8401, Winterthur
Switzerland

1. SUMMARY

The numerical simulation of the internal flowfield now plays a major role in all turbomachinery aerodynamic designs, from aero-engines to hydraulic turbines and pumps. With the help of CFD codes an experienced designer is able to produce more adventurous, better engineered and more clearly understood designs more rapidly at lower cost.

This paper reviews the use of CFD as an engineering tool in modern turbomachinery design from the standpoint of a turbomachinery designer. Particular attention is given to the current limitations with regard to performance prediction. The necessary engineering criteria used by turbomachinery designers to overcome these limitations and to assess the weak points of their designs using CFD flowfield computations are discussed. Examples of the application of these general aerodynamic design criteria to most classes of turbomachines using a variety of different CFD codes are given.

2. INTRODUCTION

The use of Computational Fluid Dynamics (CFD) has completely revolutionised the aerodynamic design process for turbomachinery blading over the last two decades. The change in blading design techniques has been driven by the continual improvements in numerical simulations. These improvements have generated crucial competitive advantages for those companies using the most advanced methods. The key commercial advantages arising from the use of CFD in blading design are:

- More accurate prediction of turbomachinery flow behaviour is possible. This means that more adventurous designs which are outside the range of previous experience can be attempted with less risk.
- New designs can get closer to the natural physical limits controlling fluid dynamic behaviour (flow separation, cavitation and choking). This enables higher aerodynamic loadings and flow capacity to be achieved, which in turn cuts down the number, size and weight - and therefore the cost - of the components involved.
- Where CFD is used in conjunction with modern graphical visualisation techniques the designer can achieve a better understanding of the flowfield. This should then lead to designs with reduced aerodynamic losses and improved performance.
- Shorter development times are possible, as some of the necessary parameter studies can be made numerically without having to use experimental rigs and prototypes.

These advantages justified the high expense of the initial development and validation of CFD methods for improved blading design in the highly competitive aero-engine gas turbine industry. The methods developed have now reached a level of maturity where their use has been expanded to cover all turbomachines from pumps to steam turbines: nowadays the most competitive performance is offered by those turbomachinery manufacturers with CFD fully integrated into the design system (figure 1).

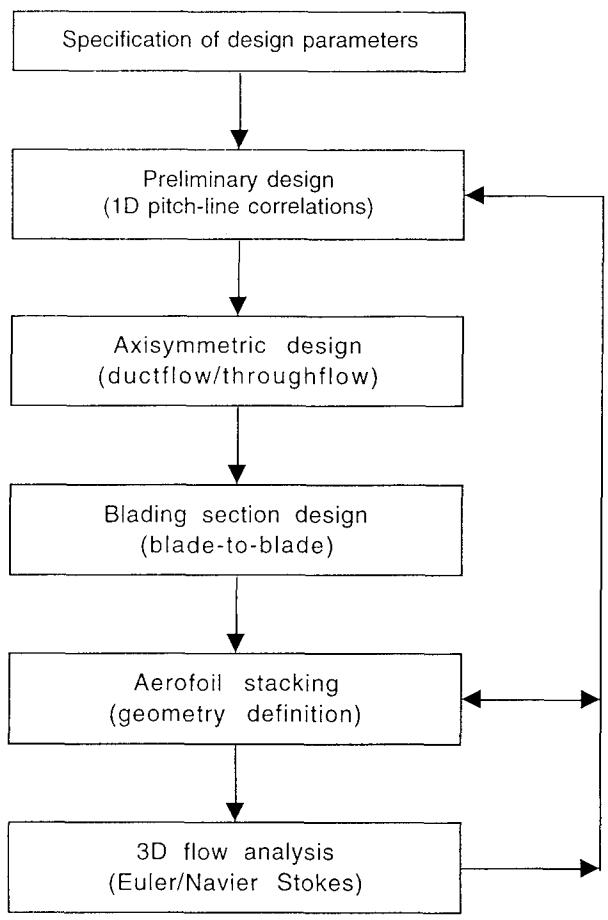

Figure 1: Typical turbomachinery aerodynamic design system

Presented at an AGARD Lecture Series on 'Turbomachinery Design Using CFD', May to June 1994.

Despite the steady advances in fully 3D Navier-Stokes methods, the bulk of the routine aerodynamic design work for turbomachinery designs is still carried out with simpler methods. Typically, an axisymmetric throughflow (S2) calculation is used to define the mean hub-to-tip flow and several blade-to-blade (S1) computations are carried out across the span to specify the complete three-dimensional blade. These two-dimensional calculations define the machine in terms of annulus shape, number of stages, and spanwise distribution of flow, thus providing the designer with essential information on flow angles, incidence, blade loading, Mach number levels, blade profile surface velocity distribution and, in some cases, blade boundary layer behaviour.

Sophisticated coupled S1-S2 solution systems have also been developed. These are able to predict the performance of multistage turbomachinery through fine tuning of the empirical input to match experimental data. The S1-S2 methods generally work well if the flow is reasonably well-behaved and follows meridional streamsurfaces. In some turbine applications, however, 3D Euler solvers have been found entirely satisfactory (because of the thin boundary layers) and are used instead of S1-S2 calculations. In radial compressor applications a simplified S1-S2 system is often used, in which the mean camber line is taken to represent the S2 stream surface and in which the variation in the blade-to-blade flow is taken to be linear.

Advanced 3D Navier-Stokes codes are increasingly being applied to assess certain aspects of the design of individual blade rows and to suggest further refinements in the blade stacking and the aerofoil design, especially in the end wall region. Initially their use was reserved for a check of the flowfield of designs relying on other methods, but, increasingly, they now form part of the iterative design process. The 3D methods provide informative flowfield detail in aspects such as spanwise flows caused by radial components of blade forces, shock structure and choking in transonic machines, leakage flows and clearance vortices, secondary flows and 3D flow separation such as corner stall. The 3D computations also allow the details of particle paths through the blade rows to be determined and can be used to optimise geometries to avoid dirt ingestion and abrasion. The accurate prediction of the 3D pressure field is also of great assistance in avoiding cavitation in hydraulic machines and in determining the gas loads for blade stressing calculations.

Multistage 3D Navier-Stokes calculations have been developed to the stage where they are also already being applied in design. The advantage of these over single blade row calculations is that they take into account the important interactions between adjacent blade rows. Unsteady periodic turbomachinery calculations have also been developed but are not considered in any detail in this review, as they are not yet a normal design tool in the turbomachinery industry.

Despite the enormous progress made in CFD algorithms, the real flow physics within a turbomachinery blade row remains much more complex than that which can be computed with the current generation of design codes. For example, the real flow exhibits strong pressure gradients that are outside the range of accuracy of most of the turbulence models in use; the real flow includes unsteadiness from the wakes and tip clearance vortices of upstream blade rows, and it often involves unsteady three-dimensional flow separation. As a result of this, the current generation of 3D design codes cannot accurately predict the absolute performance levels of a turbomachine, especially at off-design operating points.

The predictive accuracy of current CFD methods is certainly adequate to eliminate poor quality blading concepts on the basis of performance predictions alone, without the need for extensive rig testing. In most turbomachinery applications, however, the level of technical development is already at such a highly advanced state that a possible efficiency improvement of 0.5% is extremely significant. The engineering accuracy of CFD predictions of performance at the design point is, at very best, around $\pm$ 2% for efficiency if one takes into account uncertainty in the geometry and measurement errors. This can be reduced to around $\pm$1% if the method has first been calibrated on a previous design. At off-design operating points the errors are substantially larger than this.

This level of accuracy is insufficient to allow a designer to rely entirely on performance predictions to screen competing designs. Instead, the designer must rely on a critical examination of the CFD flowfield predictions to assess weak aspects of the design. This process involves a careful assessment of a range of engineering design criteria which link the calculated flowfield with the possible sources of loss and the experience obtained from previous designs to quantify the expected performance. For the best results it is essential for the designer to know the limitations of the methods being used, as well as to have previous experience of their use.

This paper reviews some of the current limitations of CFD methods from the standpoint of a turbomachinery designer. The engineering criteria used to evaluate the CFD flowfield predictions during the design process are discussed, whereby examples are chosen from a wide class of turbomachinery geometries using a variety of CFD codes.

3. THE LIMITATIONS OF CFD IN TURBOMACHINERY DESIGN

The user of any engineering design method needs at least a rough idea of its limitations, the sources of error and of the accuracy of the method, in order to avoid wasting time on details that are outside the applicable range of the method. As pointed out by Ferziger (1993), CFD errors fall into two categories, those that arise because the equations being solved are only approximations of the real flow physics and those that are due to numerical errors. In most turbomachinery CFD problems the former types of error outweigh the latter. The discussion that follows emphasises the general limitations and sources of error in CFD methods for turbomachinery aerodynamic design.

To set the scene for this discussion, it is worthwhile noting that the prediction of turbomachinery losses is fraught with difficulty (see Denton (1993)), and is certainly more problematic than the prediction of the drag of bodies immersed in an external flow. A fairly recent review of drag prediction with CFD in external flows, AGARD AR 256 (1988), concluded that "accurate and consistent computation through CFD of absolute drag levels for complex configurations is, not surprisingly, beyond reach for a considerable time to come".

3.1 Blade-to-blade computations (S1 codes)

Q3D blade-to-blade computations have been in routine industrial use for the optimisation of blade profile design for many years, going back to the early popular streamline curvature blade-to-blade code of Katsanis (1965). The Q3D design codes that are most widely used in industry today are coupled inviscid-viscous interaction methods, for example, those described by Calvert (1982), Stow (1985), Barnett et al. (1991) and Youngren and Drela (1991). Coupled inviscid-viscous interaction methods offer the designer the best compromise between computational efficiency and accuracy in calculating the Mach number distribution and boundary layer development on the blading surfaces. Several sophisticated coupling techniques have been developed to allow such methods to cope with the strong interactions between the viscous and inviscid flows which can occur in shock-boundary layer interaction and flow separation. The fastest of these methods employ integral boundary layer equations for the boundary layer and wake development, making use of the extensive development of such methods and the large data-base available from external aerofoil flows.

Being two-dimensional, inviscid-viscous interaction methods can be applied on very fine meshes to obtain good resolution of important flow details. This makes them particularly popular in design because, as they tend to run quickly, the designer can look at more cases, thus expanding the design space that can be examined in the time available. Although several Q3D Navier-Stokes solvers have been developed for blade-to-blade calculations, these methods have not yet found much favour with designers, since they tend to be less efficient in terms of computer usage, and the limitations of the turbulence models for prediction of transition and of flow separation in adverse pressure gradients (see discussion below) are more severe.

The accuracy of the performance prediction of Q3D blade-to-blade methods is nevertheless quite limited. Calvert (1991) gives the following estimates of accuracy for his method, as applied to transonic compressor cascade operating points below stalling incidence:

- choking/unique incidence and deviation angles ± 1°
- static pressure rise ±4%
- total loss coefficient (as fraction of inlet head!) ±2%

These values include experimental errors, and some transonic cases where the loss coefficients were about 10% of inlet dynamic head, and so are likely to be pessimistic for subsonic cascades with attached flow. The design loss coefficient of a well-designed compressor cascade with no turbulent separation is about 2% of the inlet dynamic head, and the error in loss prediction is probably at best about ±10% of its value. Denton (1993) is slightly more pessimistic and quotes an accuracy of ±20% for the loss calculation of a two-dimensional cascade at design point for the best available methods. Other authors are not more accurate, just not as honest! Nevertheless it is clear that the accuracy of the performance prediction of such methods is barely adequate for the predicted losses to be used in this direct way as an engineering design tool to select an optimised design. At off-design operating points all the methods are substantially less accurate and the performance prediction problems are more severe.

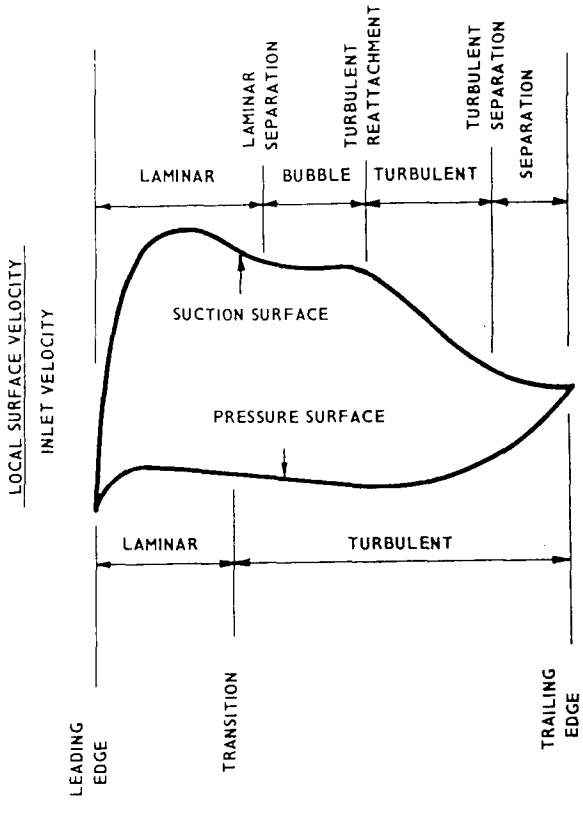

Figure 2: Possible boundary layer development on a compressor blade surface

The main causes of these inaccuracies are the inadequacies of the viscous modelling, that is the prediction of laminar boundary layer separation, laminar separation bubble, laminar to turbulent transition, the turbulent boundary layer, turbulent boundary layer separation, relaminarisation and shock-boundary layer interaction (see figure 2). An accurate prediction of transition from laminar to turbulent flow is essential for accurate loss prediction as it determines the extent of the turbulent boundary layer and hence the loss production on the blade section. The complex nature of the many modes of transition in a steady flow make accurate predictions of the transition region somewhat difficult, Mayle (1991). Natural transition from the growth of Tollmien-Schlichting instabilities in the laminar boundary layer is probably somewhat academic for the high turbulence levels in turbomachinery. Bypass transition in a flow with high free-stream turbulence levels, or separated-flow transition following laminar separation close to the leading edge, are almost always the dominant types that

occur in turbomachinery flows. Most transition prediction methods used in design codes do not take all of these types of transition into account, and usually assume that transition takes place at a single point along the blade surface. Those that do consider the more complicated modes of transition require extensive empirical data, especially for the effect of free-stream turbulence on bypass transition.

Accurate prediction of the turbulent boundary layer is also important in determining the losses. The turbulent boundary layer contributes both to the base drag effect of the trailing edge and the boundary layer blockage which affects the wake mixing loss. The application of boundary layer methods derived from those in use on external aerofoils may lead to errors because of the neglect of high free-stream turbulence. This affects the calculated initial thickness of the turbulent boundary layer through the position of transition which, in turn, controls the rate of growth of the boundary layer momentum thickness via the momentum integral equation. The entrainment and growth of a turbulent boundary layer in a highly turbulent free-stream flow is also likely to be more rapid than that in a low turbulence flow.

A further important factor which must be taken into account is that Q3D design calculations are made without consideration of the influence of the unsteady effects caused by the close proximity of the adjacent blade rows: it has been known for some time that blades behave differently in a machine environment than when they are considered in isolated cascades. The real flow is periodically unsteady, which means that the steady calculation of boundary layers is of limited value in a flow where the boundary layers are periodically disturbed by wakes from upstream blade rows. The moving wakes can have a profound effect on the boundary layer development and lead to substantial alterations, causing early transition in turbines, Hodson (1984), and temporarily eliminating laminar separation bubbles in compressors, Dong and Cumpsty (1990).

As if this were not enough, the real flow does not necessarily follow the meridional stream surfaces assumed in a Q3D method, but may have a strong spanwise component. The spanwise flow may occur in the mainstream (due to stream surface twist), in the blade surface boundary layers (due to secondary flows) or close to the endwalls (due to endwall boundary layer separation and secondary flows). The Q3D methods will be reasonably accurate when the real flow is nearly 2D; the problem comes if the flow does not do what the designer intended and has significant spanwise velocity components. This effectively limits the range of applicability of Q3D methods to well-designed axial machines operating close to their design point. Thus even with a perfect CFD code for calculating the steady viscous flow on a Q3D stream surface the designer should be sceptical about the absolute accuracy of its performance predictions for a real machine.

The ultimate goal of the Q3D calculation is to allow the designer to achieve an optimal cascade design over the entire operating range of the cascade. His main interest is to select a blade profile that achieves the flow turning in the throughflow calculation with the lowest losses. Of particular interest to the compressor designer is the prediction of the "stalling" incidence at which the rapid increase in loss occurs. Both the turbine and the compressor designer are also interested in the accurate prediction of the choking mass flow and the incidence for choking.

Despite the fact that they are not yet able to predict either the losses or the flow range with absolute accuracy, the Q3D blade-to-blade methods remain the engineering basis of the optimisation of blade shape at the design point. This optimisation relies not only on the predicted performance but also on an engineering assessment of the velocity distribution, the loading distribution, adverse pressure gradients, shock position, transition position and boundary layer loading.

Inverse design methods have also been developed for the two-dimensional blade-to-blade flow. With these, the designer is able to specify the pressure distribution or Mach number distribution he considers to be optimum and the blade shape is generated by the code. A problem with early versions of these methods was that they were unable to take into account various mechanical constraints, such as blade thickness and the thickness of the leading and trailing edges. Semi-inverse methods have been developed which allow the designer to specify the blade shape over part of the surface and Mach number distribution over other parts.

3.2 Throughflow computations (S2 codes)

The meridional throughflow methods (based on a nominally axisymmetric flow in the hub-casing plane) which are still widely used in design make use of the streamline curvature technique. Axial turbomachinery calculations often make use of a "ductflow" method which has calculating stations only at the leading and trailing edges of blade rows, see for example the compressor in figure 3. Intra-blade calculating stations are needed in transonic blade rows, as used in the fan of figure 3, and are also used in radial impeller methods, as shown in figure 4.

The use of finer grids with more intra-blade stations is restricted in streamline curvature codes by the effect of the grid aspect ratio on numerical stability. More sophisticated numerical methods with more refined grids have, however, not found favour in design applications because the limit on accuracy of throughflow codes is not usually related to the numerical modelling used. The main limitation on their effectiveness is largely due to poor estimates of the effects of the boundary layer on the inner and outer casing walls. These effects include blockage and losses from the endwall boundary layers (especially in compressors), skew caused by the transfer from a stationary to a rotating frame, and more complicated 3D effects, such as secondary flow, corner separation and tip clearance flow, which cannot be captured in a Q3D method. Some recent developments of throughflow methods have attempted to overcome some of these difficulties by incorporating the endwall boundary layers and the mixing caused by

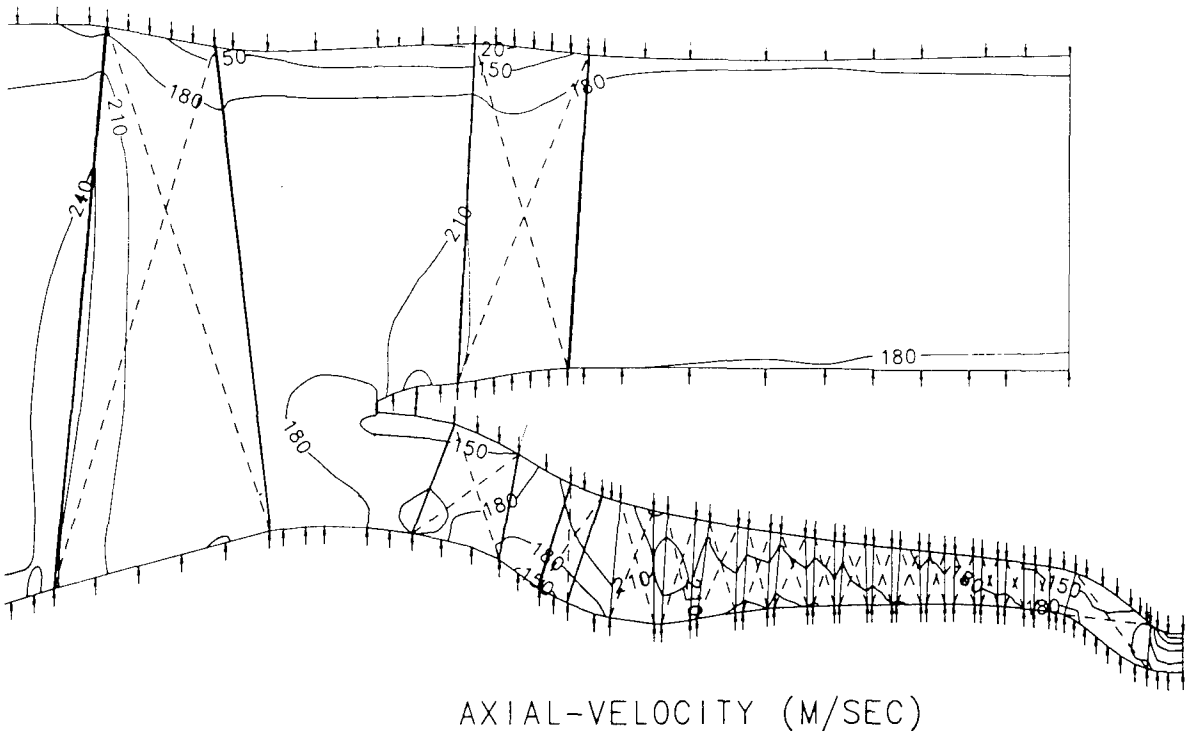

Figure 3: Axial compressor and fan throughflow calculation showing axial velocity contours, (the arrows along the annulus show the location of the quasi-orthogonal calculating stations).

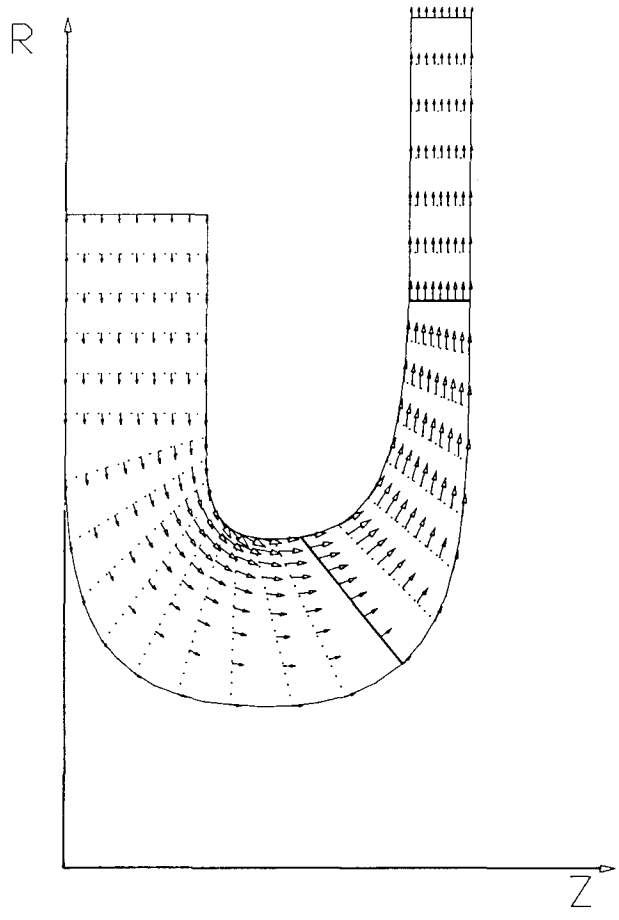

Figure 4: Radial impeller throughflow calculation, showing meridional velocity vectors along streamlines and quasi-orthogonal calculating stations (dotted lines), Casey (1985)

spanwise flows into these models, for example, Howard and Gallimore (1992) and Dunham (1993).

Nevertheless, throughflow methods still require extensive empirical data on blockage, losses and flow turning, and the distribution of these through the machine. The accuracy of the calculation is determined by the precision with which this data can be specified. In compressor calculations it is the specification of blockage which is crucial, and in turbine calculations it is the specification of the change in angular momentum.

The most effective use of throughflow methods for the design of turbomachinery is found when the empirical data on losses, turning and blockage is adjusted to match the measured performance of a machine similar to that being designed. Since most turbomachinery manufacturers design new machines as developments of those already in production, and thus do not need to start from scratch, it is generally not a problem to find a similar machine. The blockage and loss adjustment can be limited to those aspects which are not susceptible of prediction by a blade-to-blade calculation. For example, in a compressor calculation the blade profile loss and turning can be taken from a blade-to-blade calculation, such that only the endwall blockage and endwall loss need to be provided as empirical data. The empiricism provides the designer with a useful tool for fine tuning his predictions to match the available experimental data. Having matched the measured performance of a machine with a throughflow calculation, it is then possible to identify ways in which the machine can be improved by examination of fluid dynamic aspects of the predicted flowfield. By carrying out a fine-tuning of empirical coefficients in this way it is possible for such methods to

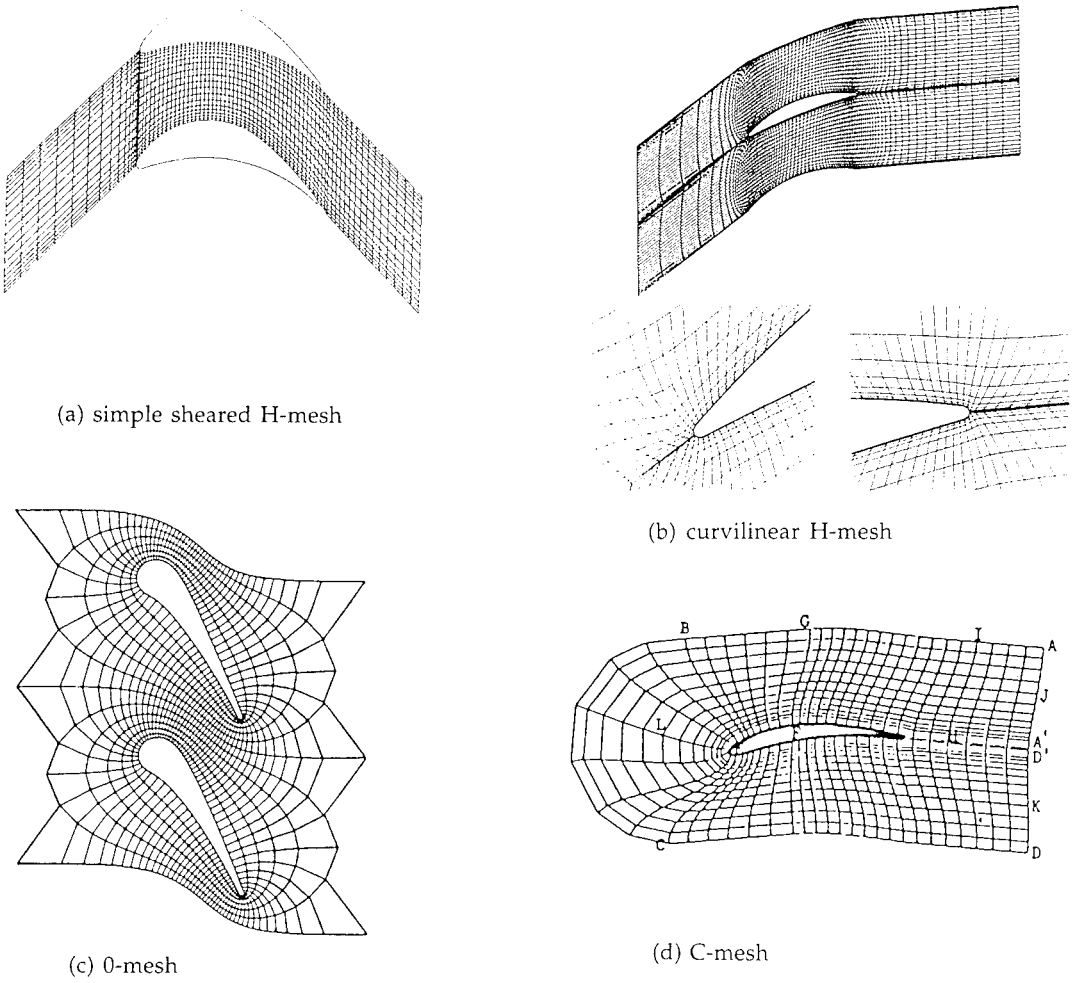

(a) simple sheared H-mesh

(b) curvilinear H-mesh

(c) 0-mesh

(d) C-mesh

Figure 5: Types of grid in use for turbomachinery CFD design calculations
(a) simple sheared H-mesh (b) curvilinear H-mesh
(c) 0-mesh (d) C-mesh

be applied (with some success) to the performance estimation of multistage compressors.

In cases where the empirical data on loss and turning of the blade sections and on endwall losses and blockage are inadequate, the calculated pressure ratios and work input are unlikely to be correct. Nevertheless, the throughflow calculation still provides the designer with an idealised impression of the flow through the machine, from which he can estimate the loading and incidence and on which he can base the design of blading to meet the throughflow conditions.

3.3 Euler/Navier-Stokes computations (3D)

There are a number of errors and limitations associated with 3D Navier-Stokes design computations of which the turbomachinery designer needs to be aware. These can be classified into four groups related to:

- the numerical scheme (discretisation, grid density and orthogonality, artificial dissipation, convergence),
- the boundary conditions,
- the capability of the turbulence model,
- the neglect of blade-passage periodic unsteadiness.

The errors related to the discretisation of the numerical scheme and the orthogonality of the grid have become less significant as, with modern computing power, they can be reduced by the use of a sufficiently fine grid. Although standard methods are available for estimating the numerical errors (see Ferziger (1993)), these are seldom applied. Some popular codes (for example Denton (1982) and Dawes (1988)) retain a simple sheared H-grid, with circumferential blade-to-blade grid lines. The advantages of this are that the grid lines conveniently fit the quasi-orthogonal planes in the throughflow calculation and that they require fewer equations to be solved. It is known, however, that more accurate predictions, especially at the leading edge of highly staggered blade rows, are possible with boundary orthogonal curvilinear H-grids or O- and C-grids (see figure 5). Unstructured grids and structured grids with local refinement are also possible (see figure 6). The recent development of solution adaptive unstructured grids (for example, Dawes (1991)) shows potential for eliminating some of the grid dependency of current codes.

A very important practical consideration for a designer is

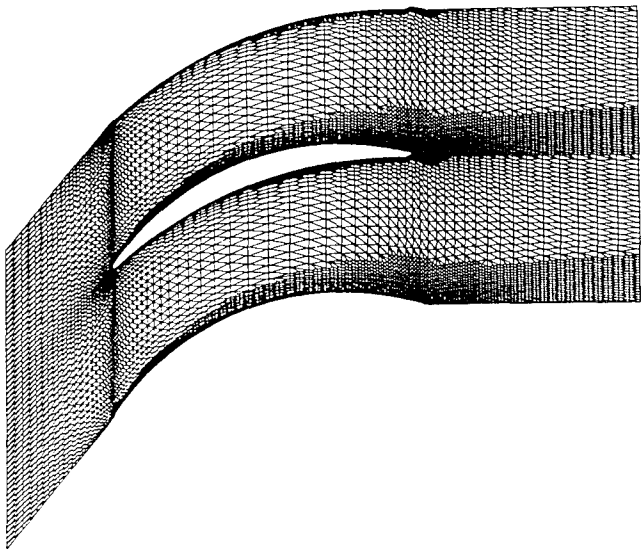

Figure 6: Unstructured solution-adapted mesh, Dawes (1993)

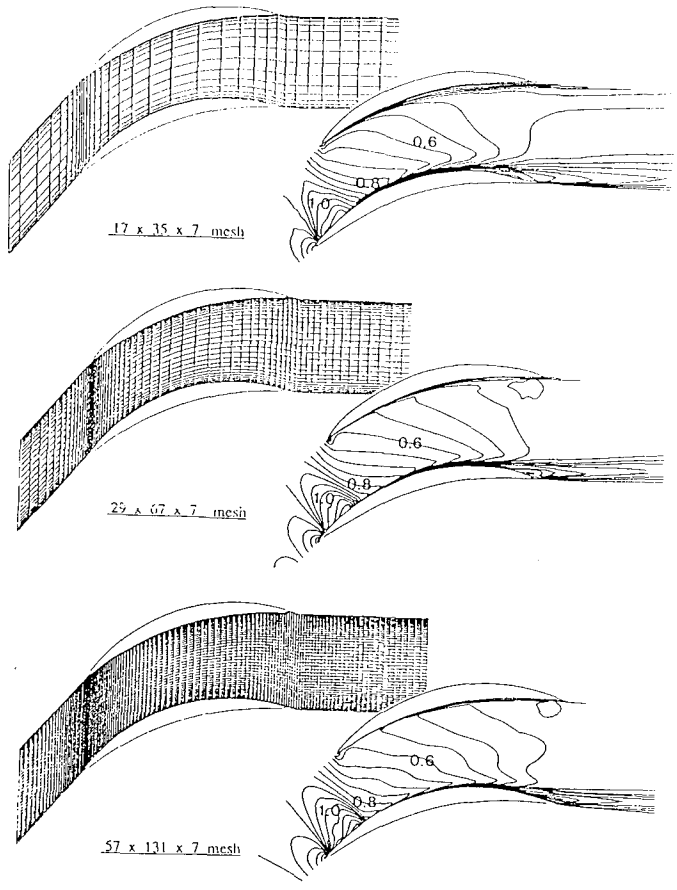

Figure 7: Effect of grid refinement on Dawes code results

that a 3D Navier-Stokes flowfield calculation with a very fine grid is usually too expensive and cumbersome for the bulk of the design process, requiring hours of cpu time for a single solution of one blade row. Because of this most turbomachinery design is carried out on a calculating grid that is probably too coarse for the results to be considered to be entirely grid independent. For this reason most designers do not change the fineness of the mesh from one design to another, since the experience gained on a coarse mesh cannot always be transferred to a finer mesh. The objective is usually to design a good turbomachine and not to generate the best CFD computation!

A good example of grid dependency has been given by Dawes (1990), see figure 7, where he has demonstrated the effect of succesive mesh refinements in the blade-to-blade and axial directions on the performance of his code for an axial compressor blade section. The change in blade-to-blade grid from 17x35x7 = 4165 to 29x67x7 = 13601, and then to 57x131x7 = 52269 (blade-to-blade x axial x spanwise) causes successive improvements in the shock capture and wake definition. It is interesting that the coarsest grid provides the best prediction of the measured loss coefficient (!). This is purely fortuitous but clearly shows that the performance predictions are limited by the turbulence modelling and transition prediction and not by numerical errors. Fortunately most of the code developers are also faced with the problem of computer capacity and have tuned and adjusted the empirical dissipation coefficients of their codes for use on relatively coarse grids. Dawes recommends that with his BTOB code (Dawes (1988)) the grid should be sufficiently fine close to solid walls such that the empirical wall functions of the turbulence models are avoided. Other types of turbulence model, for example, the standard k-ε model or low Reynolds number k-ε models, have different requirements in this respect.

The designer needs to be aware that numerical errors and the artificial losses generated by the algorithms can also effectively lead to a computation being for a slightly different operating point than that specified. Most time-marching codes, for example, require the specification of inlet total pressure and outlet static pressure to define the operating point. Runs with different levels of grid refinement cause predicted losses and blockage in boundary layers to change which can lead to a change in the mass flow and Mach number for a specified pressure ratio. In calculations of choked compressor blade rows this can lead to a different estimate of the maximum flow capacity.

An additional problem in multistage turbomachinery calculations is the specification of appropriate boundary conditions on the upstream plane. A calculation of a single blade row of an axial machine using an upstream inflow boundary about half an axial chord upstream of the blade row, would place the upstream boundary of the computational domain within an upstream cascade; consequently artificial boundary conditions need to be imposed. In both multistage compressors and turbines, the interaction between adjacent blade rows can be quite strong so that a blade row considered in isolation will perform differently to one in the machine environment. Elementary throughflow calculations take such interactions into account in the mean axisymmetric solution, whereas 3D simulations of isolated blade rows neglect these effects! Multistage 3D computations have been developed to eliminate these problems, Denton (1992) and Dawes (1992). These operate by assuming

steady flow relative to each individual blade row with suitable mixing planes between each row. These techniques are, however, also approximate and the accuracy and limitations of the circumferential averaging techniques at the mixing plane between moving and stationary blade rows has not yet been extensively studied. Both Dawes (1992) and Adamczyk (1989) have proposed a promising alternative to the mixing plane approach in which the blade rows adjacent to that being studied are modelled by axisymmetric body forces.

Most of the turbomachinery CFD community currently uses either the well-known Baldwin-Lomax mixing length model or the two-equation k-ε model as the basis for the prediction of the turbulent shear stresses. Neither of these turbulence models are adequate for the complex flow with high adverse pressure gradients found in compressors and highly loaded turbine blading. More advanced turbulence models do exist, but few have yet been fully tried and tested in the turbomachinery environment. The turbulence research community has not yet come up with any real recommendations for the best turbulence models for turbomachinery flows, nor do any recommendations appear to be on the horizon.

It is well-known that the k-ε model gives a poor prediction of boundary layer parameters in adverse pressure gradients. Numerous test cases demonstrate this, see, for example, figure 8 taken from Wilcox (1993). In an adverse pressure gradient, the k-ε model predicts that the flows are further from separation than the measurements. This can be quite dangerous for turbomachinery designers as the predictions tend to separate later than the real boundary layer flow and give the impression that the design is safer than it really is. To improve this situation the k-ε model is often used in the outer part of the boundary layer and in the bulk of the flow, but a conventional mixing length model is used close to the surface (Rhie et al. (1993)).

As discussed above (section 3.1) many of the limitations in loss prediction are related to the prediction of transition; none of the current turbulence models in use in 3D codes are adequate for this and all of these models provide considerably less resolution than the 2D methods available. Despite these problems, the three-dimensional visualisation of the blade row flowfield available from CFD calculations is of enormous importance to the designer in his assessment of a design, as discussed below.

4. CFD AERODYNAMIC DESIGN RULES

Because of the limitations of CFD methods for performance prediction outlined above, the experienced designer does not rely on their absolute accuracy but uses the performance predictions only in a comparitive sense. Typically he first calculates the performance of a geometry for which test data is available to calibrate the code. He then compares these results with the predictions for a new design and, in a commonly used jargon, he makes use of only the "deltas" in performance relative to his calibrated test case. This process is more accurate than when the absolute performance values predicted by the code are used, but is still not necessarily accurate enough for reliable engineering design.

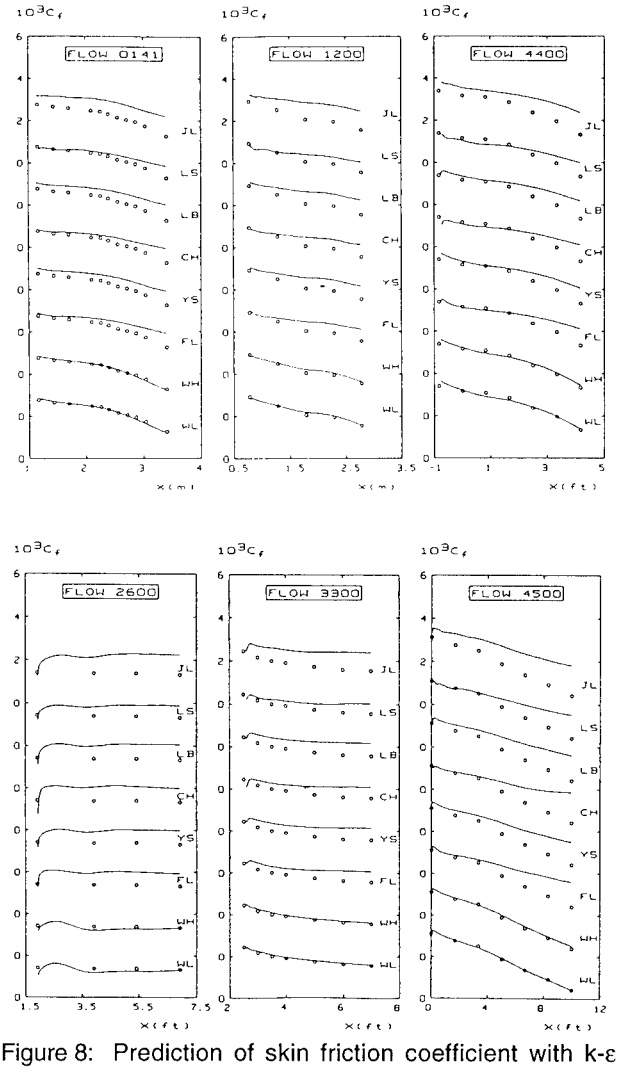

Figure 8: Prediction of skin friction coefficient with k-ε boundary layer prediction methods in an adverse pressure gradient.

JL, LS, LB, CH, YS, and FL are k-ε methods, and WH and WL are k-ω methods, see Wilcox (1993).
FLOW 0141, 1200, 4400, 2600, 3300 and 4500 are test cases from the AFOSR-HTTM Stanford conference on complex turbulent flows Kline (1981)

The CFD predictions of the flow field are, however, of utmost importance to the designer since they allow him to make an assessment of the weak points in the flow, through examination of various aerodynamic criteria relating to incidence levels, loading parameters, velocity distributions and boundary layer development. These criteria enable the designer to quantify the performance of the machine based on his understanding of the sources of loss in the flow and their probable magnitude. The CFD flowfield predictions also need to be calibrated against good quality test data, so that a new design can be compared with the best experience available from research and development tests on similar machines.

The key aerodynamic aspects of the CFD flowfield predictions used by the designer to assess and improve the quality of a turbomachinery blading design are summarised below, and a checklist is given in figure 9. It should be noted that the requirements of these key items may often conflict with each other, so that compromises and experience are generally needed.

4.1 Avoid poor incidence onto blading

It is crucially important in compressors (less so in turbines) to ensure that the blade rows operate close to the incidence which minimises their losses (not necessarily zero incidence) and with a sufficient margin from the "stalling" and "choking" incidences at which losses begin to rise above twice their minimum value. Although CFD computations are not yet able to predict the operating range of a cascade, they allow the flow incidence to be checked across the span of the blade (radial matching) and through the machine (axial matching) at various operating points. The selection of incidence at the design point may require some degree of compromise, and may even require the application of variable geometry, if the turbomachine operates over a range of speeds or with variable flow capacity.

Particular attention needs to be paid to the incidence in those regions of the blades influenced by the annulus wall boundary layers, but it is not essential in these regions to adapt the leading edge so that it exactly matches the flow direction, Wadia and Beacher (1989), see section 5.2 below. In supersonic flows, the designer may not have much choice in the selection of the incidence at the design point, as this is often determined by the "unique incidence" condition, see section 5.3 below.

Examination of the effective incidence onto the blading provides a very reliable indicator of any possible increased losses which, due to limitations in numerical resolution of the leading edge and inadequate viscous modelling, may not be accurately predicted by a CFD method. For those CFD methods with high resolution of the leading edge flow, the acceleration of the flow from the leading edge stagnation point onto the suction and pressure surfaces (giving leading edge spikes) may provide a good indication of quality of the leading edge loading and the incidence. Highly unequal spikes at the leading edge would suggest that the leading edge is not well adapted to the inlet flow. It is interesting to note that even during the early phases of the use of CFD for blade optimisation it was realised that examination of the velocity distribution could indicate optimum incidence, Dodge (1973)

4.2 Reduce friction on wetted surfaces

Friction losses can be reduced in a number of ways: by selecting the minimum number of blades (compatible with the loading considerations), by choosing the lowest possible velocity levels (compatible with the need to reduce the size of the machine), and by choosing large flow channels of maximum hydraulic diameter (low hub/tip ratio). In radial compressors, splitter vanes are used to reduce the blockage and Mach number at the impeller inlet; these also reduce the wetted area that would be associated with full length blades.

In turbines with accelerated flow it is often possible to reduce friction losses further by having extensive regions of laminar flow in the favourable pressure gradients. As noted above, the prediction of transition from laminar to turbulent flow in CFD computations is not generally reliable in the highly unsteady turbomachinery environment. Even if the code being used has an in-built boundary layer calculation the experienced turbine designer is unlikely to rely entirely on the CFD prediction of transition, but will examine the predicted velocity distribution to ensure that the region of favourable pressure gradient is as large as possible.

4.3 Avoid kinetic energy loss

There are a number of potential sources of unwanted kinetic energy loss: spanwise velocities induced by secondary flows, spanwise velocities caused by blade loading and shed vorticity effects, leakage jets caused by clearance gaps at the end of blades and over blade shrouds, and leaving losses and swirl at the exit of a turbomachine. In some instances these may not be large enough to make a big contribution to the losses. In others, it may be worthwhile retaining some kinetic energy as swirl in the downstream flow from the machine, since this can sometimes improve the performance of a downstream component (in the annular diffuser downstream of an axial compressor, for example). In most cases, however, it is advisable to minimise the kinetic energy in these flows.

4.4 Avoid flow separation

The mixing of a separated flow with the relatively healthy mainstream flow inevitably gives rise to some mixing losses, see Denton (1993). In addition to causing unwanted losses, the separation region may be a source of vortex shedding which will cause possible blade vibration and excitement in adjacent blade rows. The large wakes from a separated blade row may also lead to high incidence onto the downstream blade rows. The CFD calculations need to be examined for evidence of separated flow and nearness to separation, both at the design point and at off-design operating points.

Stratford (1959) found that the best method for cutting down the risk of boundary layer separation is to avoid large flow decelerations in regions where the boundary layers are already thick. If this strategy is applied, the turbulent boundary layer is usually highly loaded at the beginning of the adverse pressure gradient. For a successful design, transition must be completed before the boundary layer experiences the strong adverse pressure gradient, otherwise the laminar boundary layer will separate. Again the predicted position of transition may be a crucial aspect of the CFD calculation.

4.5 Provide a uniform distribution of flow onto downstream blade rows.

The uncritical optimisation of the performance of an individual blade row may lead to an unhomogenous distribution of flow and incidence onto the downstream blade rows, with an associated performance penalty. In radial compressor design, for example, the performance of the diffuser blading is crucially dependent on the uniformity of the impeller outlet flow. In transonic turbine design, the reduction in the strength of the downstream shock wave can be expected to result in a performance improvement for the downstream blade row. In the design of high bypass ratio fans for civil aero-engines, any flow separation causing flow distortion in the hub region of the fan may, because of its proximity to the compressor inlet duct (see figure 3), lead to a

- Avoid poor incidence onto blading
  - axial matching
  - radial matching
- Reduce friction on wetted surfaces
  - large hydraulic diameter
  - low hub/tip ratio
  - low velocities / laminar flow
  - as few blades as possible
- Avoid kinetic energy loss
  - leaving loss
  - clearance flow
  - secondary flow
- Avoid flow separation
  - mixing loss
  - vortex shedding
- Avoid unnecessary acceleration / deceleration
  - thin blades
  - low curvature
- Check established blade loading criteria
  - De Haller number
  - Lieblein Diffusion factor
  - Zweifel number
- Match flowfield to that on similar successful designs
- Use performance predictions in a comparitive sense only (compare "deltas")
- Provide a uniform distribution of flow onto downstream blade rows
- Minimise the pre-shock Mach number in transonic / supersonic flow
- Achieve a smooth and consistent variation of parameters
- Design close to where the machine will operate
- Examine key sensitivities
  - Off-design
  - Reynolds number
  - Transition and Turbulence
  - Tolerances (clearance)
  - Asymmetry
  - Numerical parameters
- Avoid "point optimisations" in favour of robust designs
- Use different codes for different flow details

Figure 9: Checklist of general turbomachineryaerodynamic design criteria for use with CFD predictions

strong unwanted inlet disturbance to the flow in the core compressor.

4.6 Check established blade loading criteria

The quest for improved levels of performance has led to increased blade loadings in both compressors and turbines. It is tempting for designers to rely increasingly on CFD computations to estimate the risk of flow separation and increased losses from higher blade loadings. However, these methods are not in themselves adequate to ensure that higher blade loading levels are acceptable. The best use of the CFD methods is to compare the blade loading levels of a new design to those of similar designs for which test data are available. In this process the many well-established classical blade loading parameters for compressors and turbines should be checked (for example, De Haller number, Lieblein Diffusion factor, Zweifel number) and compared to values that have proved acceptable in earlier tests of similar machinery with similar clearance levels. It is asking for trouble to ignore the enormous wealth of experience encapsulated in the simple blade loading criteria developed by the early giants of the business.

4.7 Avoid any unnecessary acceleration and deceleration

The entropy production in the flow is roughly proportional to the cube of the local velocity, Denton (1993); this makes it essential to avoid unnecessary acceleration and to keep velocity levels low. If the flow has been unnecessarily accelerated it must then be decelerated again. This may cause flow separation, a further possible source of loss. The key to reducing the risk of unnecessary acceleration and deceleration in compressor blade rows is to use blades which are as thin as possible, to ensure that they have thin leading edges operating at at low incidence, and to avoid unnecessary flow curvature.

No universally valid criteria can be given as to what the optimal velocity distribution, with the minimum amount of unnecessary acceleration and deceleration, from a CFD calculation is. The best engineering design processes make use of CFD to predict the velocity distribution of a blade row whose performance has already been demonstrated in research and development rig tests. The predicted velocity distribution of a new design is then matched to this.

4.8 Minimise the pre-shock Mach number in transonic/supersonic flow

In order to reduce the strength of shocks and the risk of separated boundary layers in shock-boundary layer interaction, the pre-shock Mach numbers should be examined and, if possible, reduced. In supersonic flow this can be done using precompression or reverse camber, see section 5.3 below.

4.9 Achieve a smooth and consistent variation of parameters

It is important to ascertain that there is a smooth and consistent variation of parameters across the span and through the machine. For example, Q3D blade-to-blade calculations of adjacent sections across the span should not show discontinuities in loading, shock position, incidence and so on. The CFD calculations may allow this but the real flow is not likely to. Simple plots of the major geometrical and aerodynamic parameters across the span and through the machine often identify unwanted irregularities that the CFD codes may have missed!

4.10 Design close to normal operating point

The turbomachine design point should be close to where the machine will normally operate and any sensitivity to changes in the design point and design conditions should always be critically examined. It may be worthwhile to employ several clearly defined "design" points where the requirements are clearly understood. For example, the main design point might be the normal operating point where peak efficiency is of paramount importance. A second point might be a part-speed operating point where the attainment of sufficient surge margin would be critical. A third point might be a highly loaded condition where it would be crucial that the machine could pass the required mass flow. The examination of the flow conditions at all three points would clarify the compromises made in the attainment of the objectives, and provide guidance should a redesign be necessary.

4.11 Examine key sensitivities

The key sensitivities are off-design operation, possible changes in duty over the life of the machine (growth), Reynolds number (due to changes in altitude of an aero-engine), manufacturing tolerances (such as tip clearance gaps), untwist of blades due to centrifugal and gas loads, and asymmetry due to the presence of struts, pylons, and asymmetric inlets and outlets.

It is important to be aware of the sensitivity of the CFD method being used to the assumptions made. In 3D CFD calculations, for example, the fineness of the grid and the many numerical smoothing and convergence parameters are often an issue. In Q3D blade-to-blade calculations, the results may be sensitive to the location of transition, the specified turbulence level and the Reynolds number. In throughflow calculations, the main sensitivity is with respect to the empirical input of blockage, turning and losses.

Should a design appear to be extremely sensitive to any of these factors it may be worthwhile to renogotiate the design point and it is certainly worthwhile to reexamine the basis of the preliminary design.

4.12 Avoid "point optimisations" in favour of robust designs

A mistake that is very often made is to carry out a superb optimisation of a design for a single point operation with a single CFD code, without recognising that most of the data required for the optimisation and the accuracy of the computation are unlikely to be accurate enough to justify this. A robust design should avoid extremes of optimisation which might be over-sensitive either to the accuracy of the prediction method or to the precise operating condition. Computer-based optimisation techniques have not yet found much application in turbomachinery design, precisely because the optimisation is not straightforward and requires considerable engineering art and experience as well as engineering science.

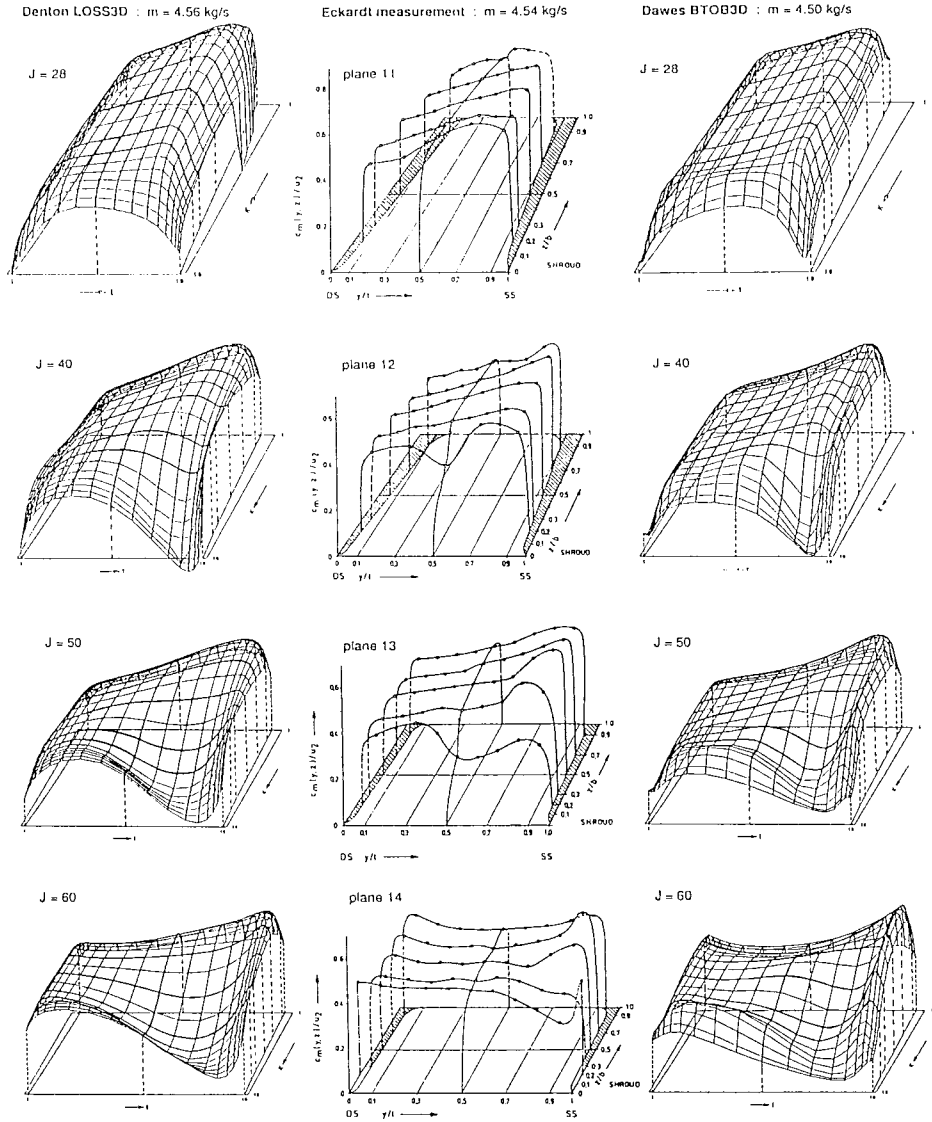

Figure 11: Comparison of 3D CFD impeller flowfield calculations with measurements, Casey et al. (1992).

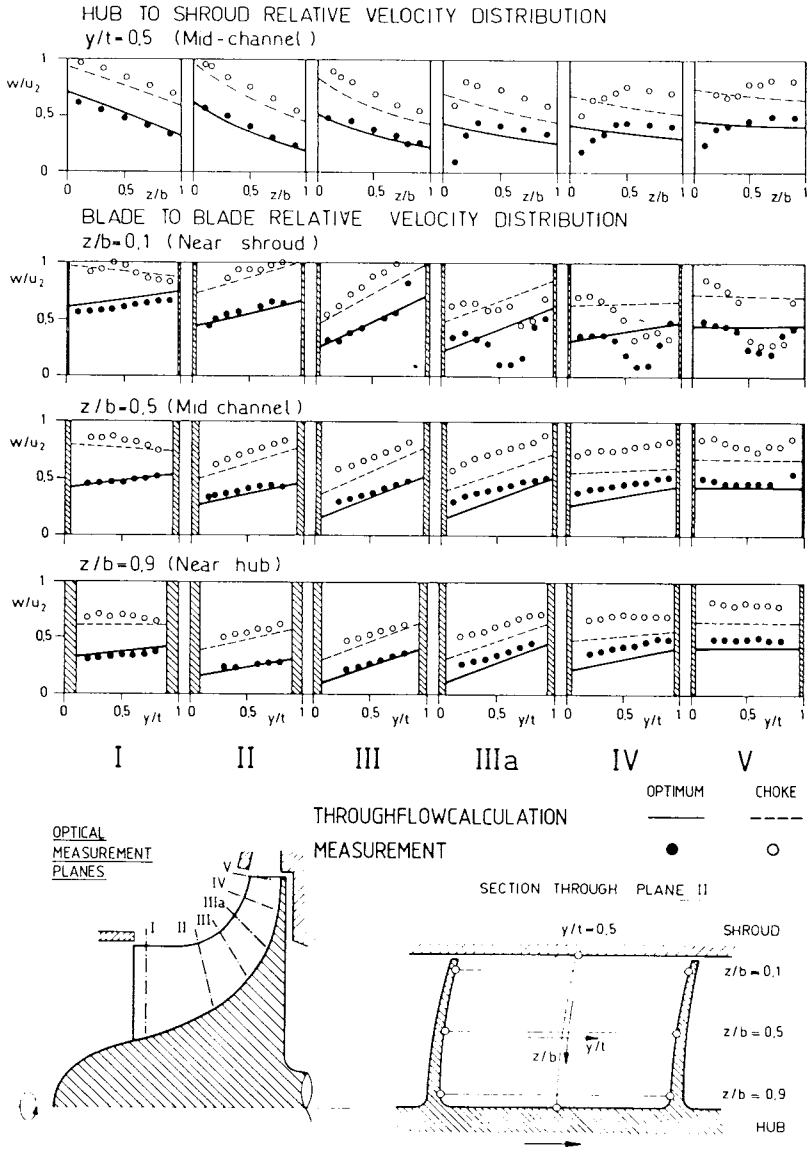

Figure 10: Comparison of impeller throughflow calculations with measurements of Eckardt (1980), Casey (1985).

4.13 Use different codes for different flow details

The prediction method used should not be based on its universal applicability, but on its ability to resolve the relevant flow characteristics. No single method is likely to be best for all problems and a combination of methods should be used to highlight different flow features. For example, a Q3D inviscid blade-to-blade calculation can be used for leading edge flow detail, a viscous-inviscid method to predict boundary layer development and a 3D method for secondary flows and tip clearance flows.

5. TURBOMACHINERY AERODYNAMIC DESIGN EXAMPLES

In this section some examples of the use of the above engineering rules for different types of turbomachinery design are given. The examples are taken from a range of turbomachines for which a wide variety of CFD methods have been used. Inevitably, there are fewer examples given for turbine flows, as the author's personal design experience has been mainly confined to compressor flows.

5.1 Radial compressor design

One of the most successful applications of modern 3D CFD codes is in the design of radial compressor impellers. The radial impeller flowfield is highly three dimensional, with tip clearance vortices and strong secondary flows. A full appreciation of this flowfield has only recently been attained through the use of CFD methods, see Cumpsty (1989).

Even with the advent of successful 3D methods for the calculation of impellers, most radial compressor designs are still drafted out with a relatively simple throughflow method coupled with a linear approximation to the blade-to-blade computation, see, for example, Casey and Roth (1984). These allow the basic design to be rapidly optimised, making use of engineering design criteria for impellers which are based on the work of Dallenbach (1961), Morris and Kenny (1971), Stiefel (1972) and Came (1978). These criteria relate to:

- selection of the blade incidence,
- the maximum allowable diffusion on any blade surface (minimum De Haller number typically $W_{exit}/W_{max} \approx 0.625$),
- the rate of deceleration of the mean flow (an initial rapid rate is desirable following Stratford (1959)),
- choice of smooth parameter variation through the impeller and across the span and
- the limitation of the blade-to-blade loading to avoid secondary flows (maximum blade-to-blade loading parameter $[\Delta p/(1/2)\rho W^2] = 0.7$).

The weakness of such a simple design system becomes clear when the flow measurements in radial impellers are compared to the Q3D predictions, see figure 10 from Casey (1985). Figure 10 compares the predictions of the simple Q3D design system with measurements made by Eckardt (1980) on a backswept impeller at two operating points. The Diagrams from left to right represent the six laser optical measurement planes through the impeller, denoted I, II, III, IIIa, IV and V. The upper row shows the hub to shroud relative velocity gradient, and the lower three rows show the blade-to-blade velocity gradients at three spanwise positions (near shroud, mid-span and near hub). The flow predictions are perfectly adequate for the inlet region of the impeller and up to the point where the strong secondary flows in the impeller passages lead to a wake-like distortion in the impeller outlet flow. Downstream of the formation of the wake the predictions have little relationship to the real flow. Nevertheless the use of a throughflow design procedure ensures that the leading edge incidence is correct, and allows some, albeit inadequate, preliminary optimisation of blade loading and diffusion.

Modern 3D methods provide the designer with a tool that can examine the important deviations between the simple Q3D model and the real flow, that is, the effects of secondary flows and tip clearance flows. Comparisons of the flowfield predictions of CFD codes with measurements using laser velocimetry in radial compressors are very impressive. The main features of the flow are well captured by the calculations, see, for example, figure 11 from Casey, Dalbert and Roth (1992). It should be noted, however, that the predictions of the impeller performance obtained with these codes are not sufficiently accurate for engineering assessment based on this alone, figure 12. The design rules given in section 4 above are necessary in order to assess and improve impeller performance. An example has recently been given by Dalbert (1993) using a 3D prediction with the Dawes code (Dawes (1988)) to examine an impeller designed using the simple Q3D throughflow method. The 3D code identified a flow separation that was not predicted in the throughflow design, and a redesign to remove this separation resulted in a performance improvement, figure 13.

The key design problem for radial compressor stages has now moved to the prediction of the diffuser flow and its performance. The most difficult task for a radial compressor designer remains the matching of the diffuser to the impeller (Cumpsty (1989)): this usually has to be optimised by means of extensive development testing. This is an active area of CFD research and one which is particularly difficult by virtue of the unsteady nature of the interaction between the impeller and the diffuser. The use of CFD has already started to help here, see Dalbert et al. (1993) and Drtina et al. (1993), but it may require fully unsteady 3D multi-blade-row methods to finally sort this out.

An example of the use of CFD in diffuser optimisation is given in figure 14, from Drtina et al. (1993). The position of the splitter vane leading edge and the location of the splitter between the two full vanes was examined using CFD computations in the diffuser with the commercially available Navier-Stokes program STAR-CD. The optimisation of the splitter position was carried out by eliminating unnecessarily high velocities caused by the flow blockage of the splitter vane leading edge, by obtaining a uniform distribution of the downstream flow, and by removing a flow separation in one of the flow channels.

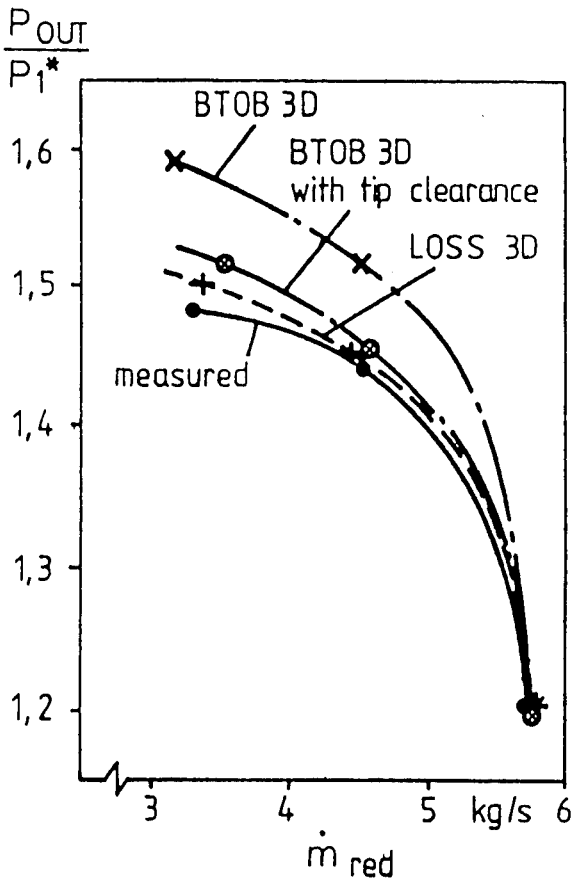

Figure 12: Performance prediction of a radial impeller using Denton LOSS3D code and Dawes BTOB3D codes, Casey et al. (1992)

5.2 Axial compressor design

The key aerodynamic problem facing axial compressor designers is the axial matching of the stages in a multistage compressor, especially for transonic blade rows in compressors operating at variable speed. The part-speed operation of an axial compressor designed for a high pressure ratio with the minimum number of stages inevitably introduces the likelihood of stalling in the early stages and choking in the end stages. Because of the difficulty they have in accurately capturing the blockage of the endwall boundary layers, multistage 3D Navier Stokes solvers have not yet advanced to the point where they can provide any useful design-worthy solutions to the axial matching problem of axial compressors. Designers remain fairly tied to throughflow design systems for the examination of this, with occasional flurries of activity looking at particular local blading phenomena with the 3D CFD methods.

The first serious attempts of axial compressor designers to make use of two-dimensional CFD in the optimisation of blade profiles was the development of blade profiles with tailored Mach number distributions and boundary layer behaviour, so-called "supercritical" profiles, "controlled diffusion" profiles, "prescribed velocity distribution" profiles and "custom-tailored" profiles. All of these design styles were attempting to control the deceleration of the flow such that the maximum diffusion occurred in the early part of the suction surface, where the boundary layers were still thin, see for example Starken (1989). The initial euphoria of this approach has somewhat abated as difficult problems were encountered with the profiles in practice, mainly in the endwall regions where the flow is not 2D, see Behlke (1985) and Tubbs and Rae (1991).

The engineering criteria for the design of such profiles have been summarised by Starken (1989) as:

- The front part of blade has accelerating flow, with peak velocity at around 30% of chord for space/chord ratios above about 0.7 and further upstream for lower space/chord ratios.
- Laminar to turbulent transition should occur in the forward part of the velocity distribution.
- The rear part of blade with decelerating flow with a continuously falling boundary layer shape parameter H_{32} (which is the ratio of the energy thickness to momentum thickness).

Similar criteria for advanced axial compressor profile design were recently given by Ginder (1991) and Katoh (1993). In Ginder's example the peak velocity occurs further forward than Starken's suggestion, corresponding to a lower pitch-chord, and the boundary layer shape parameter H_{12} (the ratio of displacement thickness to momentum thickness) is specified as rising to the trailing edge.

An idealised example of a modern profile design is given by Ginder. He shows the comparison between the blade-to-blade aerodynamics of a profile with a conventional circular arc camber line and a profile with a parabolic arc camber line having a similar space/chord and thickness/chord, see figure 15. It can be seen that the high forward curvature of the parabolic arc profile causes a more rapid acceleration on the forward part of the suction surface compared with the circular arc case and the peak Mach number is amost 0.1 higher. The parabolic arc design thus violates the rule given above concerning minimisation of the velocities. This high suction peak is followed by a diffusion rate which is initially much steeper than that for the circular arc case, becoming progressively less severe towards the trailing edge. The fundamental difference between the two profiles is that the loading on the parabolic blade has been moved forward to where the boundary layers are thinnest and are better able to withstand the diffusion. The boundary layer separation near 75% of axial chord on the circular arc profile (with the shape factor rising above 2.8) is thus almost entirely avoided and losses are predicted to be 30% lower, despite the higher peak Mach number.

Earlier forms of controlled diffusion profile tended to have a more severe diffusion on the early part of the suction surface such that the shape factor H_{12} peaked at around mid-chord. Whilst this may not be of concern near design incidence, it could become critical at high off-design incidence leading to early separation and loss of operating range. Tubbs and Rae (1991) mention that there was a tendency for stall to start at mid-chord in the early generation of controlled diffusion profiles. Ginder gives clear examples of the need to examine off-design operating points and choke margin.

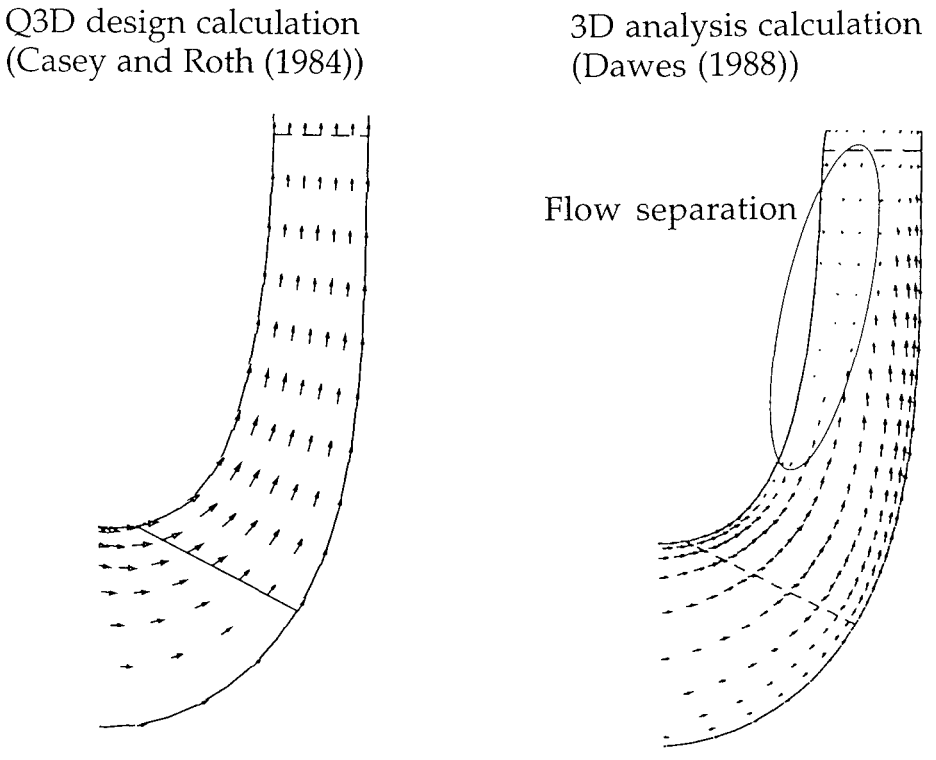

Figure 13: The 3D method of Dawes (1988) identifies a flow separation not observed in the Q3D design, Dalbert (1993)

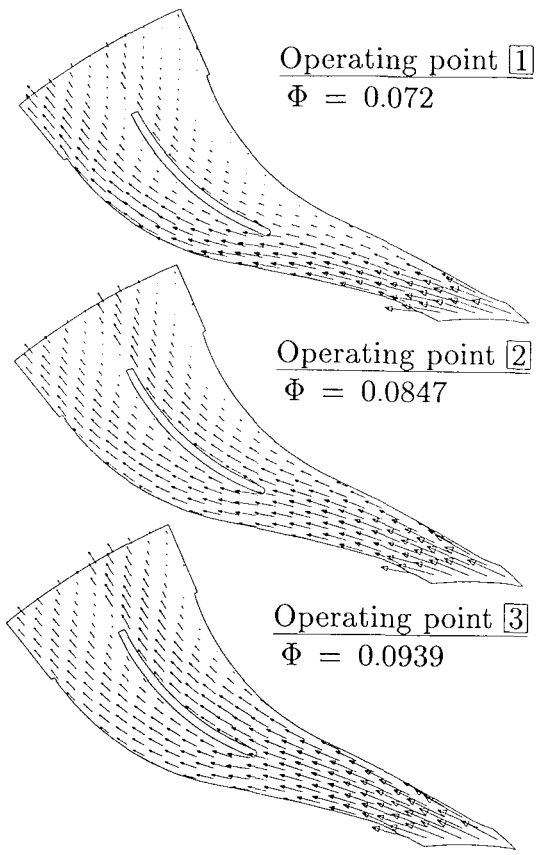

Figure 14: Radial compressor diffuser flowfield calculation with splitter vane at three operating points, Drtina et al. (1993).

Another excellent example of the use of CFD in the design of axial compressors is the paper by Wisler (1984). Here a four-stage low-speed rig compressor is used to test unconventional aerofoil shapes which have been designed using CFD methods. The best profiles can be selected on the basis of performance measurements in the four stage rig and then reproduced in high speed compressors by using similar velocity distributions for their design.

An area of compressor design which has benefited from the application of CFD methods is in the use of so-called end-bends to adapt the shape of the blade leading and trailing edges to the flow found in the endwall regions of the compressor. The initial designs of end-bends were mainly empirical and more careful analysis and design is required before such techniques can be applied without risk. Wadia and Beacher (1989) give examples of calculations using an Euler code on blades with end-bends and Robinson et al. (1989) describe calculations on conventional and end-bent stators using the Moore Elliptic Flow Progam, Moore (1985). More detail is given in Robinson (1991), where it is shown that the end-bend on a stator at the hub reduces the flow incidence onto the leading edge relative to that of a conventional stator, see figure 16.

The work of Howard and Gallimore (1992) is of interest here in that they show how a conventional streamline curvature throughflow method can be adapted to include the viscous wall layers so that the true incidence and flow field in the endwalls are already available in the throughflow design to provide the boundary conditions for the 3D computation.

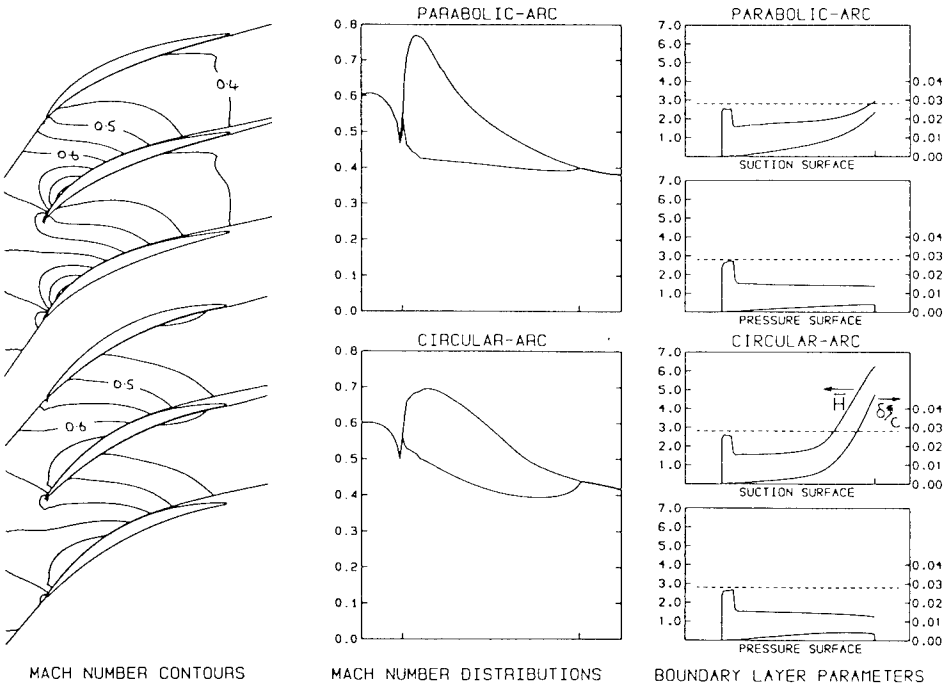

Figure 15: Comparison of compressor sections with circular arc and parabolic arc camber lines, showing Mach number distribution and boundary layer parameters, Ginder (1991)

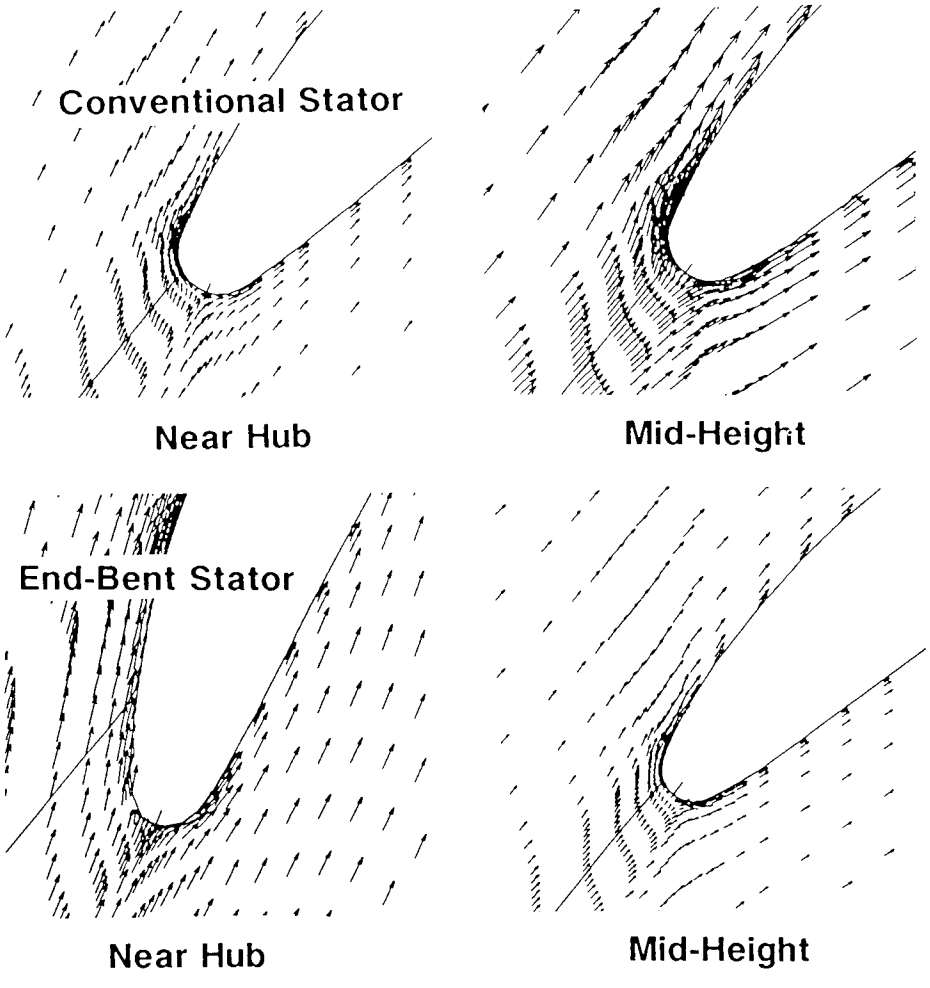

Figure 16: Predicted 3D flowfield in a conventional compressor stator and a stator with end bends, Robinson (1991). (Note location of stagnation point marked by a line on the profile leading edge).

5.3 Transonic and supersonic fan design

The design of transonic fans also relies heavily on CFD methods and many 3D codes have been validated on the various NASA fan stages. Several authors have described the use of CFD in the design of fans for commercial aero-engines. Ginder and Calvert (1987) describe the use of an S1-S2 system, Karamidas (1988) outlines the use of an Euler 3D code, and other authors make use of 3D Navier-Stokes solvers, for example, Jennions and Turner (1993), Goyal and Dawes (1993) and Rhie et al. (1993).

Ginder and Calvert (1987) are, however, the only authors who have clearly described some of the design rules and criteria that can be used for an engineering assessment of the individual sections of a conventional high bypass ratio civil aero-engine fan on the basis of the predicted flowfield. Here the key criteria are precompression and unique incidence in supersonic inlet flow, minimising the pre-shock Mach number in transonic flow and the distribution of camber to optimise the boundary layer development.

For convenience Ginder and Calvert consider three separate fan sections across the span, close to the hub, near mid span and towards the tip, each having their own particular design difficulties and profile design rules, figure 17. In the inner region close to the hub they suggest an optimum design in which most of the suction surface camber is concentrated in the first 80% of the chord, leading to a distinctly flat-backed profile. The low camber rate at the rear is carefully controlled to ensure that any boundary layer separation is concentrated towards the rear of the suction surface. The high camber at the front ensures that the throat area is large enough to avoid choking without too high an incidence setting and the rate of camber can be adjusted in the front of the blade to limit the peak suction surface Mach number.

In the middle region of the blade the duty required poses more difficult problems. The inlet Mach number is just sonic and the required camber is large. Any attempt to avoid flow separation through low camber on the rear of the suction surface leads to high camber rates at the front which in turn cause high peak Mach numbers. Ginder and Calvert discuss several possible solutions and adopt a compromise solution for the camber distribution in which the camber is mainly concentrated in the mid-chord region. Neither the peak Mach number nor the extent of the flow separation are reduced to their absolute minimum. The solution adopted is examined for its sensitivity to the position of the shock and the amount of the camber in the mid-chord region is chosen to ensure that the position of the foot of the shock is not unduly sensitive either to operating conditions or to inaccuracies in the flow prediction.

Near the tip of the fan the deflection required is quite small, the inlet Mach number is quite high ($\approx$1.5) and most of the pressure rise is caused by the shock. An important feature of the supersonic flow near the fan tip which may be used for blade optimisation is the fact that supersonic flow expands along a convex surface and compresses along a concave one. This gives the designer the opportunity to control the pre-shock Mach numbers, and hence shock losses, by suitable shaping of the suction surface to achieve a certain amount of pre-compression. The amount of pre-compression that can be used is limited by two factors. First, the more the suction surface is negatively cambered, the smaller the passage throat; this may cause problems of choking, especially when operating at part speed. Second, the negative camber in the forward part of the aerofoil must be made up by additional camber in the rear of the aerofoil with a consequent increase in loading and a risk of separation. Nor has the designer any choice for the incidence of the flow entering a supersonic cascade, since when the flow entering the covered passage of a supersonic cascade is wholly supersonic, there is only one possible value of incidence for a particular inlet Mach number, see Freeman and Cumpsty (1992). The solution adopted by Ginder and Calvert uses negative camber on the uncovered part of the suction surface to reduce the pre-shock Mach numbers. The boundary layer is predicted to separate momentarily near the shock foot and then remain just attached over the remainder of the suction surface. No further camber could be applied without causing separation of the flow.

The difficult nature of the aerodynamic design of such fans can be seen from the fact that these authors consider only a single design point optimisation. In a real fan design, the off-design operating points also need to be considered with care to avoid part-speed choking.

Three-dimensional codes can also be used for this type of optimisation, but in the publications listed above, it would appear that they have less resolution in predicting the detail of the boundary layer than the S1-S2 method described by Ginder and Calvert. It should, however, be noted that the Q3D method ignores the strong secondary flow that can occur in the rotor boundary layer in the hub sections, the spanwise flow that can occur in the separated boundary layer downstream of the shock, the swept nature of the actual shock front and the tip leakage flows.

Examples of the use of 3D methods are given by Adamczyk et al (1993), Jennions and Turner (1993) and Rhie et al. (1993). All of these authors present predictions of the characteristic curves of the NASA Lewis rotor 67 fan, using grids which are probably as fine or finer than those currently used for most design applications, (Adamczyk had 100,905 points, Rhie 108,000 points and Jennions 328,937 points). The codes predict the pressure rise characteristics of such fans with reasonable accuracy, even if the absolute predictive accuracy of the efficiency level is not sufficient, figures 18. This suggests that such codes can, with appropriate correction of the efficiency level, be used to predict the shape of characteristic curves.

Two of these authors demonstrate the extreme sensitivity of the results to the tip clearance used, showing clearly the importance of examining the sensitivity of fan calculations to the tip clearance values. The improved understanding of the 3D flowfield that is possible with CFD calculations is demonstrated clearly in the paper of Adamczyk et al (1993).

(a) Adamczyk et al. (1993)

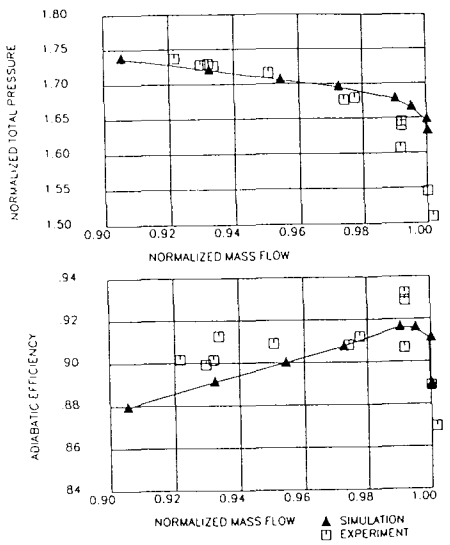

Comparison of predicted and measured pressure rise characteristic and adiabatic efficiency map of Rotor 67, tip clearance/tip chord = 0.25 percent

(b) Rhie et al. (1993)

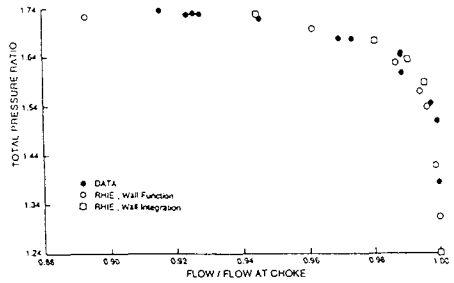

Total pressure ratio as function of flow at design speed

(c) Jennions and Turner (1993)

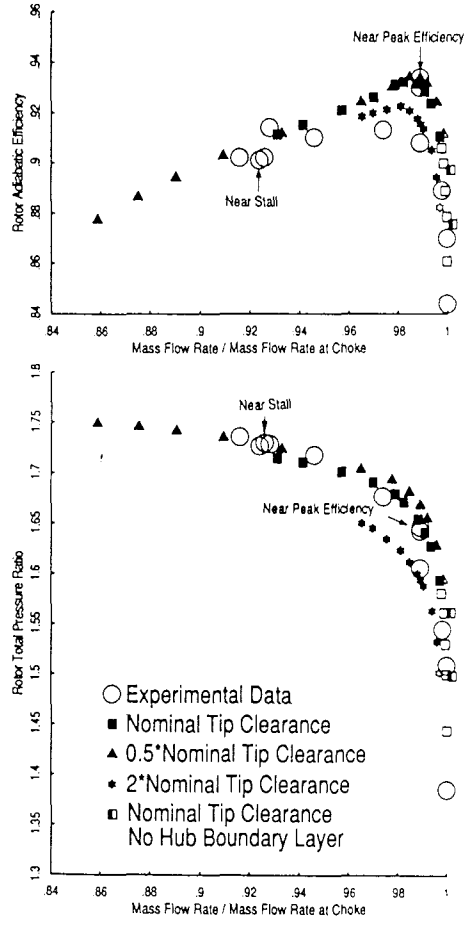

Rotor 67 Design Speed Operating Characteristics

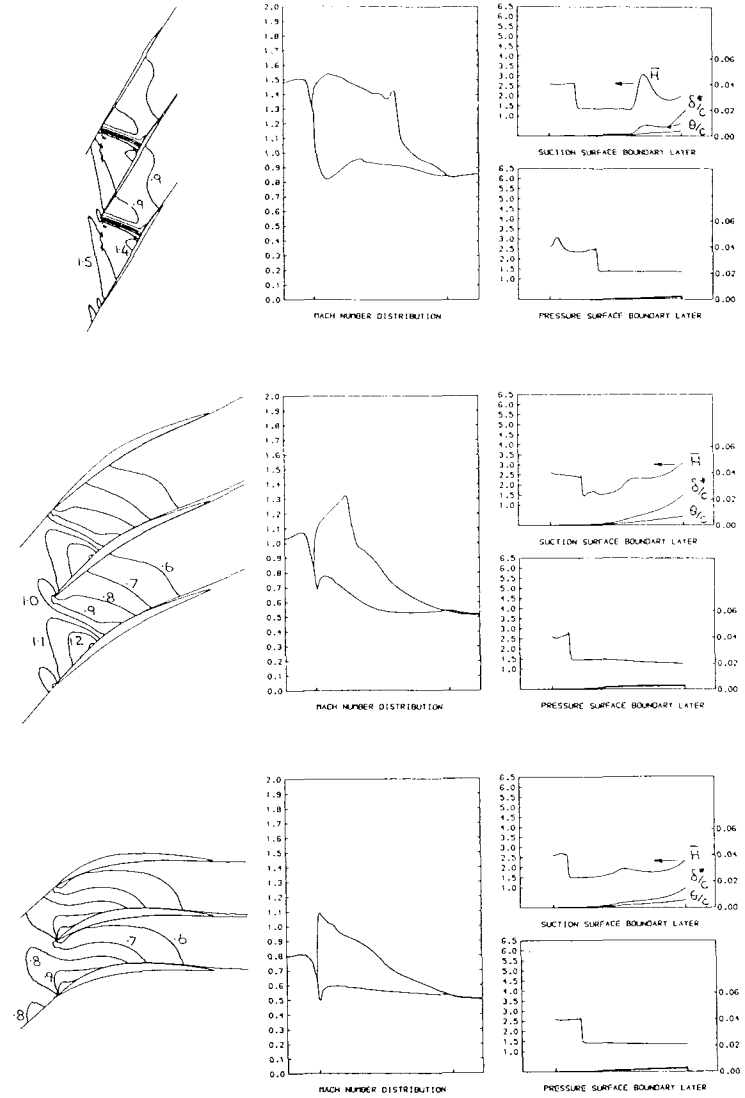

Figure 18: Predicted performance of NASA LEWIS Fan rotor 67
(a) Adamczyk et al. (1993)
(b) Rhie et al. (1993)
(c) Jennions and Turner (1993)

Figure 17: Q3D flowfield prediction of a the tip, mid-span and hub sections of a low aspect ratio civil aeroengine fan, showing Mach number distribution and boundary layer development, Ginder and Calvert (1987)

5.4 Axial turbine design

Axial turbines have regularly been one of the first areas in which new CFD methods have made a large impact and contribution to design. Turbine designers were the first to use blade-to-blade computations for profile optimisation, throughflow calculations for spanwise flow optimisation and 3D CFD methods for stacking optimisation.

While it was still commonplace in compressor design to use standard aerodynamic profiles (NACA 65, double circular arc etc.) supported by extensive data from cascade testing, turbine designers rapidly moved into blade profile optimisation. They were helped by the fact that the turbine flow is mainly accelerating, which gives favourable pressure gradients and thin surface boundary layers (boundary layer displacement thickness of typically less than 2% of the flow area). This meant that even the very first 2D Euler calculations of the Mach number distribution were sufficient to provide a good estimate of the flowfield.

The essential features of the Mach number distribution for a subsonic turbine blade are shown in figure 19. The leading edge of turbines is relatively thick but causes insignificant loss. The trailing edge can cause noticeable base pressure drag if it is too large, see Denton (1993). The flow on the pressure surface should accelerate to the trailing edge and lead to low loss production, although a small region of diffusion near the leading edge may be difficult to avoid. The flow on the suction surface accelerates fairly rapidly over the first third of the surface to the throat, followed by a more gradual acceleration to maximum velocity at the throat. The losses in this region are low because the presence of the favourable pressure gradient ensures that the boundary layers are laminar. In a subsonic profile, downstream of the throat the subsonic flow is decelerated over the convex surface and conventional diffusion criteria limit the amount of turning that can be achieved.

In a transonic turbine the flow continues to accelerate beyond the throat to produce additional turning. Shock waves occur around the throat and the downstream shock strength is affected by back surface deflection, trailing edge thickness, trailing edge wedge angle and suction side contour downstream of the throat.

Detailed rules for turbine profile design with controlled boundary layers are given by Hourmouziadis (1989) as follows:

- Minimise boundary layer thickness at trailing edge.
- Minimise trailing edge thickness.
- Avoid separation upstream of the trailing edge.
- Select the highest pitch possible.
- High acceleration of the pressure side upstream of the trailing edge.
- Delay transition on the suction surface as long as possible.
- Use suction side acceleration to control transition.
- Force suction side transition early enough to ensure reattachment of a bubble.
- Limit suction surface diffusion towards the trailing edge to keep the flow attached.

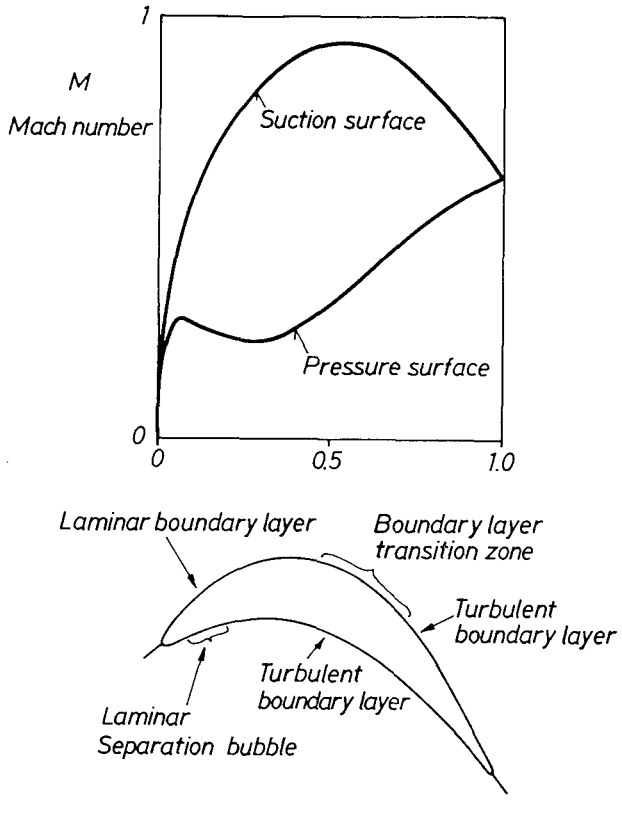

Figure 19: Mach number distribution for a turbine blade

The overlap with the general rules given in section 4 is apparent.

Another area of interest where turbine designers made an early use of CFD to improve designs was in the development of so-called forced vortex turbine designs, see Dorman et al. (1968). The use of streamline curvature throughflow techniques allowed turbine designers to move away from earlier free-vortex designs to forced vortex designs. These designs used the swirl and work distributions to control the radial distribution of the flow to avoid low reaction in the turbine roots. By increasing the reaction in the root, the pressure drop across the rotor root was increased and this avoided adverse pressure gradients and associated flow separations and losses.

Yet another first for turbine designers was the move to fully 3D designs of blading, in which blade stacking effects have been used to redistribute the flow across the annulus, giving a change in the radial distribution of flow parameters, and possibly a reduction of secondary flows, see Hourmouziadis (1989). An example of the optimisation of the stacking of a turbine blade is given in figure 20. This example is taken from a recent design calculation for a Francis hydraulic turbine (a radial machine), using the Euler method of Göde and Rhyming (1987), see section 5.5 below. The Euler method is very sensitive to the spanwise flows due to variations in the spanwise distribution of loading and shed vorticity. Figure 20 shows the effect of two different stacks of similar blade shapes on the streamline patterns close to the blade surface, Göde and Sebestyen (1994). In reality the strong spanwise flows near to the surface would be less than those calculated by a Euler method because of

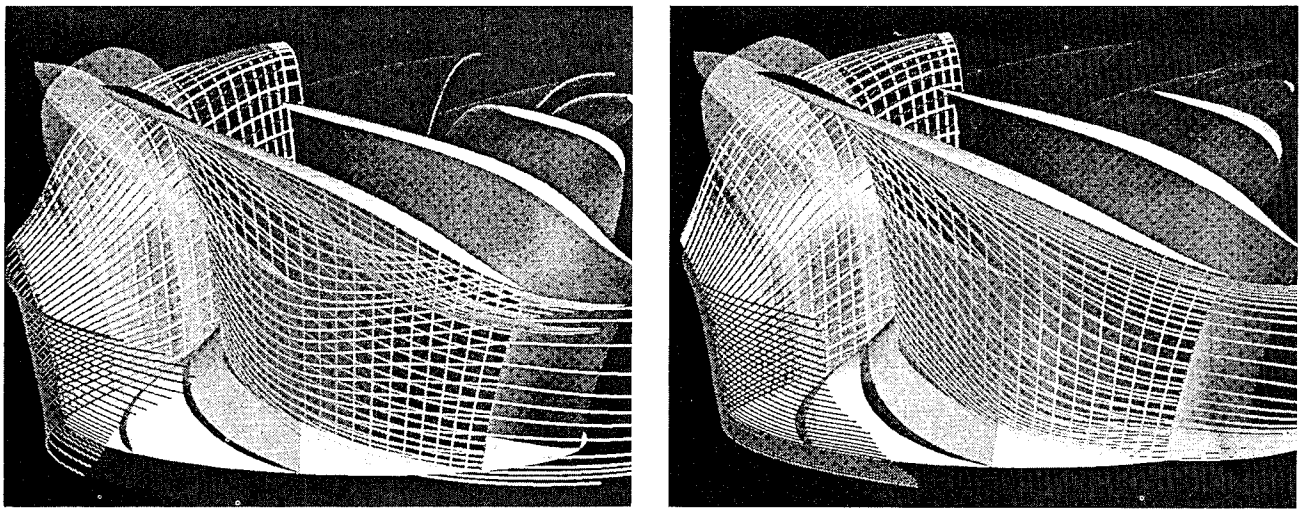

Figure 20: Effect of change of blade stacking on the spanwise flow in a Francis turbine, Göde and Sebestyen (1994)

the boundary layers, so the Euler method provides a sensitive tool for minimising these flows to optimise the stacking.

Unlike compressors, turbines have low endwall boundary layer blockage, and multistage CFD methods already offer a sensible approach to the axial matching of multistage turbines. An example of a recent multistage turbine calculation using the code of Dawes (1992), is given in figure 21, taken from Dalbert and Kmecl (1994). This calculation used 176,841 grid points and required 8 days and 6000 times steps to achieve convergence. This type of calculation can only be used as a final check of the design and is not yet quick enough to be part of the iterative design procedure.

An aspect of turbine blading design that is beginning to receive attention with CFD is the flow in shrouded turbine blades, and the associated interaction of the the discharge flow from the seal clearance and the secondary flows. The Dawes unstructured code (Dawes (1991)) appears to be suitable for tackling problems of this type.

5.5 Radial turbine design

The success of highly-loaded axial turbine designs in recent years has displaced radial turbines from many applications, but in hydraulic machinery radial turbines of the Francis type are still the preferred solution for medium specific speed applications. Some examples are presented here of the use of the above design rules in hydraulic turbomachinery design.

Until recently a very empirical approach to the design of Francis turbines was used, with little if any detailed flow calculation involved. Despite the limitations of the empirical techniques, hydraulic efficiencies in the region of 93% to 94% were commonplace. These classical techniques have now been replaced by more modern CFD Euler based methods, see Eriksson et al. (1984), Göde and Rhyming (1987) and Keck et al. (1990). The first applications of these techniques have proved highly successful, increasing turbine efficiencies by over 1% and more or less eliminating unwanted cavitation phenomena.

The use of an Euler method for these calculations means that detailed boundary layer considerations cannot be taken into account. Nevertheless, various criteria have been used for the interpretation of the CFD flowfield results. Figure 22 illustrates the calculated static pressure field of a Francis turbine runner; this has been highlighted in regions below the vapour pressure of water to identify the possible occurrence of cavitation inception. The Euler method used in conjunction with a blade geometry generator allow fine control in the design process over the surface static pressures and this now means that cavitation occurs more or less simultaneously over the whole blade trailing edge. Earlier designs were not optimum in this respect and were often prone to local areas of low pressure with early cavitation onset.

The main improvement in performance has come about through better control of the flow angles downstream of the Francis turbine runner. The Euler code is able to predict the flow exit angles with some precision, whereas earlier empirical methods were prone to error, Göde and Cuenod (1989). It is now possible to design the turbine with a specified swirl in the outlet flow (not necessarily zero swirl for reasons of stability at off-design operating points), see figure 23. Earlier designs tended to have either more swirl than intended, or an uneven distribution of swirl, leading to a strong vortex in the draught tube. Since one of the largest components of loss in such turbines was the leaving loss, the use of an Euler CFD method has been able to reduce losses and improve the performance. The Euler code also allows the leading edge of the blades, which are typically curved in two planes, to be accurately aligned with the inlet flow direction.

CFD has also contributed to the design of other flow elements of Francis turbines. Calculations with the commercially available Navier-Stokes code TASCflow have been used to examine the flow in the turbine draught tube with and without a splitter vane (Drtina et al. (1992)). The same code has been used to aid the understanding of erosion due to the passage of sand through a water turbine, making use of particle tracking techniques (Drtina and Krause (1994)).

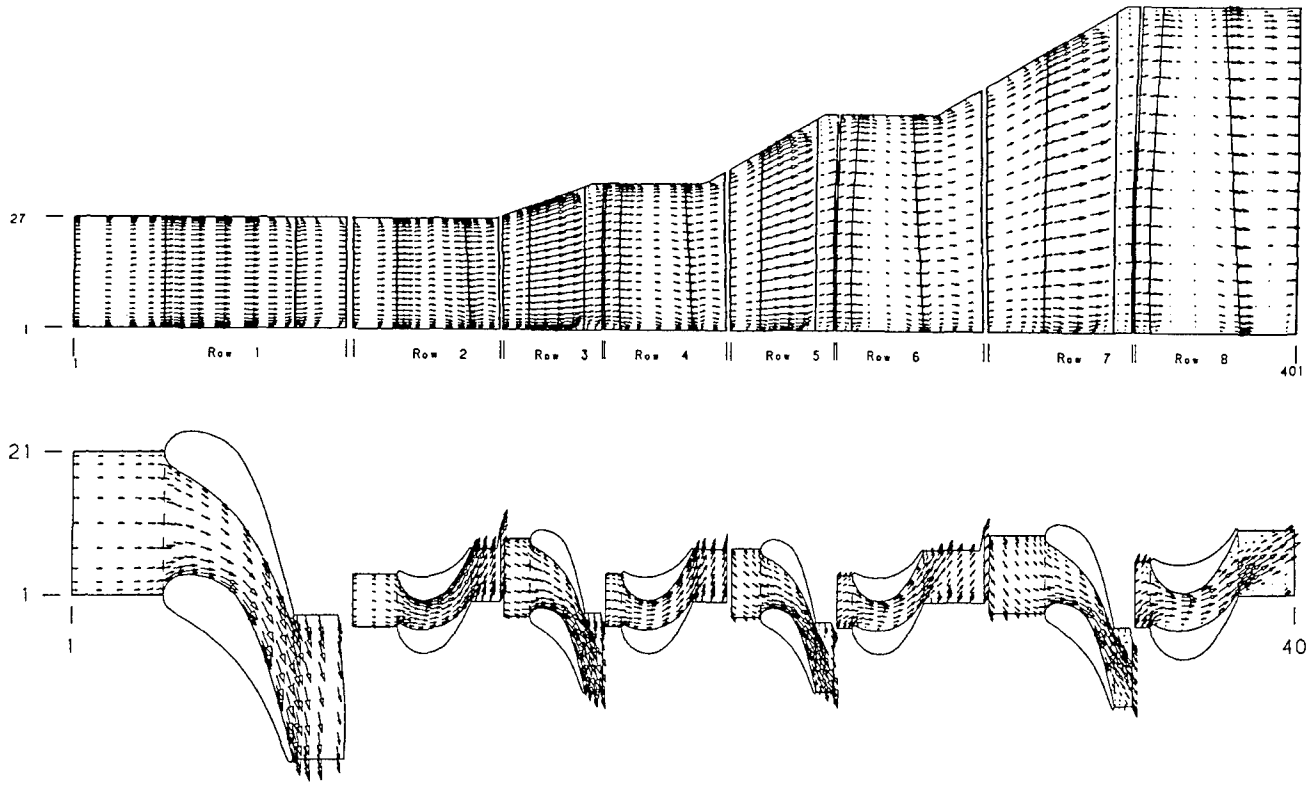

Figure 21: Multistage CFD calculation of a turbine, Dalbert and Kmecl (1994)

Figure 22: Predicted cavitation inception in a Francis turbine

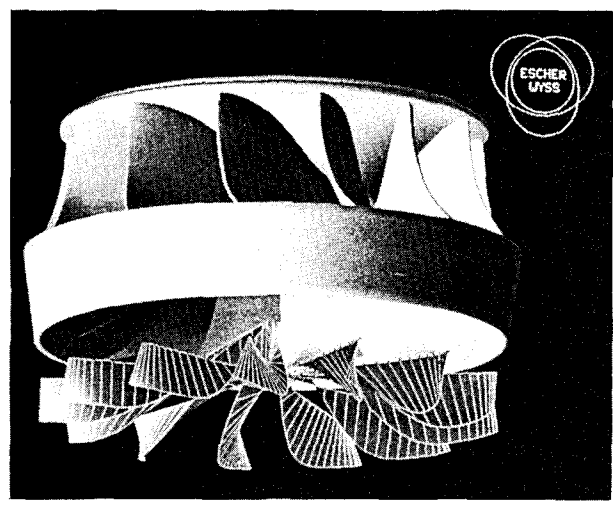

Figure 23: Downstream swirl in the outlet flow of a Francis turbine

6. USE OF CFD IN AN INTEGRATED DESIGN PROCESS

It is important to realise that a CFD code cannot stand alone in the engineering design process for turbomachinery. For their most effective use in turbomachinery blading design, CFD codes need to be part of an integrated design system, such as shown in figure 1, comprising a number of key elements such as:

- Fast and accurate preliminary design techniques.
- Blade and annulus geometry generator.
- Automatic links to mechanical and stress calculations.
- Automatic grid generation for the CFD codes.
- Validated, robust and user-friendly CFD methods.
- Calibration of CFD methods on test cases that are well understood.
- Effective graphical processing of the CFD results.
- Designers with experience of the limitations of the methods.

Simple, fast and reasonably accurate preliminary design techniques, coupled with flexible geometry definition methods and automatic grid generators, are crucially important in the design process. These permit the computationally intensive Navier-Stokes methods to be used as 'numerical wind tunnels' to verify the design rather than to be wasted in the process of generating suitable designs.

There are two ways in which the computational effort of Navier-Stokes methods may be reduced. Firstly, the knowledge gained from earlier 3D calculations should be incorporated into the simpler tools and rules used in the design process to avoid the need for hours of expensive computational effort for every design change.

Secondly, it is often worthwhile examining the computed CFD results before complete convergence has been attained. Errors and unwanted features in the flow often show up even if the flowfield is converged to engineering accuracy and time can be saved if the geometry is changed as soon as the calculations show it already looks bad - convergence to an optimum geometry can then take place together with the convergence of the program. The use of unconverged solutions may, however, be dangerous in some situations and should be done with care.

The value of high quality graphical output, both as an engineering tool and as a marketing aid (CFD = colourful fluid dynamics), should not be underestimated.

7. CLOSING REMARKS.

Despite the enormous progress in CFD methods over the last two decades, there are still some important aspects of turbomachinery design that CFD is not able to cope with (yet):

- Calculating the performance of a turbomachine with sufficient accuracy to eliminate the need for any further testing.
- Providing solutions to two crucial problems of the compressor designer - the axial matching of stages in a multistage axial compressor and the matching of the impeller with the diffuser in a radial compressor.
- Predicting boundary layer transition and flow separation with the necessary engineering accuracy for an accurate estimation of losses.
- Analysing and interpreting the predicted flowfield in terms of the probable sources of loss and the risk of the design.
- Eliminating the need for well-trained experienced turbomachinery designers to interpret the flowfield results, weigh up the conflicting engineering objectives and work out what to do when a new design doesn't quite work as it should.

Although there is still a lot to be done, CFD has already made a large contribution to our understanding of complicated turbomachinery flowfields. When used in combination with the design rules described in section 4, it has also increased the confidence with which new turbomachines can be designed to meet their performance objectives. The future of CFD in tubomachinery aerodynamic design is assured.

Several current CFD research developments are likely to strongly influence the use of CFD in the design of turbomachinery during the next decade. These are the use of multi-blade-row non-steady computations, the application of inverse methods, the computation of the interaction between the main flow and leakage flows over shrouds and clearance gaps, and the examination of unconventional geometric features such as non-axisymmetric wall contours and sculpted and leaning blade surfaces.

8. ACKNOWLEDGMENTS

This review is based on the author's personal experience of the use of CFD in the turbomachinery design environment. The author is greatly indebted to many friends (from the Fluid Dynamics Laboratory of Sulzer Innotec, the Turbocompressor and Hydraulic Divisions of Sulzer Escher Wyss, the Steam and Gas Turbine Divisions of ABB, the Compressor Engineering department of Rolls-Royce plc., the Whittle Laboratory, Cambridge and the DRA, Farnborough) for their comments on an early draft of this paper and for their continuing guidance and stimulation in the application of CFD to turbomachinery blading design. The author also wishes to thank Sulzer Innotec for the opportunity to publish this review.

9. REFERENCES.

Adamczyk, J. J., Celetina, M. L., Beach, T. A., and Barnett, M., "Simulation of three-dimensional viscous flow within a multistage turbine", ASME paper 89-GT-152.

Adamczyk, J. J., Celestina, M. L., Greitzer, E. M., 1993, "The role of tip clearance in high-speed fan stall", ASME Journal of Turbomachinery, Vol,115, No. 1, pp. 28-39.

AGARD-AR-256, 1988, "Technical status review on drag prediction and analysis from computational fluid dynamics: state of the art", AGARD Advisory Report No.256.

Barnett, M., Hobbs, D. E., and Edwards, D. E., 1991, "Inviscid-viscous interaction analysis of compressor cascade performance", Trans. ASME, Jounal of Turbomachinery, Vol. 113, Oct 1993, pp 538-552.

Behlke, R. F., 1985, "The development of a second-generation of controlled diffusion profiles for multistage compressors", ASME paper 85-IGT-9, 1985 Beijing International Gas Turbine Symposium, September 1985.

Calvert, W. J., 1982, "An inviscid-viscous interaction treatment to predict the blade-to-blade performance of axial compressors with leading edge normal shock waves", ASME Paper 82-GT-135.

Calvert, W. J., 1991, "Application of S1BYL2 to the AGARD WG18 Compressor test cases", RAE Tech Memo P1204, February 1991.

Casey, M. V., Dalbert, P., and Roth, P., 1992, "The use of 3D viscous flow calculations in the design and analysis of industrial centrifugal compressors". ASME Journal of Turbomachinery, Vol. 114, No. 1, pp 27 - 37

Casey, M. V., 1985, "The aerodynamic development of high performance radial compressor stages for industrial turbocompressors", VDI Bericht No. 572.1, *Thermische Strömungsmaschinen '85*, pp 167-181

Casey, M. V., and Roth, P., 1984, "A streamline curvature throughflow method for radial turbocompressors", I. Mech E. Conference Publication 1984-3, *Computational methods in turbomachnery*, paper C57/84.

Came, P.M., 1978, "The development, application and experimental evaluation of a design procedure for centrifugal compressors", Proc. I. Mech E., Vol. 192, No.5.

Cumpsty, N. A., 1989, *Compressor aerodynamics*, Longman.

Dalbert, P., 1993, "Turbocompressors optimised numerically", Sulzer Technical Review.2/93

Dalbert, P., Gyarmathy, G., and Sebestyen, A., 1993, "Flow phenomena in a vaned diffuser of a centrifugal compressor stage", ASME paper 93-GT-53

Dalbert, P., and Kmecl, T., (1994), Sulzer Escher Wyss, private communication.

Dallenbach, F., 1961, "The aerodynamic design and performance of centrifugal and mixedflow impellers", SAE Tech Prog. Series, Vol 3.

Dawes, W. N., 1988, "Development of a 3D Navier-Stokes solver for application to all types of turbomachinery, ASME paper 88-GT-70

Dawes, W. N., 1990, "Time marching solutions of the two and three dimensional Navier Stokes equations for turbomachinery flows", IGTI Course notes *Fluid Dynamics of Turbomachinery.*

Dawes, W. N., 1991, "The simulation of three-dimensional viscous flow in turbomachinery geometries using a solution-adaptive unstructured mesh methodology", ASME paper 91-GT-124

Dawes, W. N., 1992, "Towards improved throughflow capability - the use of three-dimensional viscous flow solvers in a multistage environment", ASME Journal of Turbomachinery, Vol. 114, No. 1, pp 8-17

Denton, J. D., 1982, "An improved time-marching calculation for turbomachinery flow calculation", ASME paper 82-GT-239.

Denton, J. D., 1992, "The calculation of three-dimensional viscous flow through multistage machines", ASME Journal of Turbomachinery, Vol. 114, No 1, pp 18-26.

Denton, J. D., 1993, "Loss Mechanisms in Turbomachines", ASME Journal of Turbomachinery, Vol. 115, October 1993, pp 621-656.

Dodge, P. R., 1973, "The use of a finite difference technique to predict cascade, stator and rotor deviation angles and optimum angles of attack", ASME Journal of Engineering for Power, July 1973, pp 185 - 190

Dong, Y., and Cumpsty, N. A., 1990, "Compressor blade boundary layers: part 2 - measurements with incident wakes", Trans. ASME Journal of Turbomachinery, Vol. 112, No. 2, pp 231 - 240.

Drtina, P., Göde, E., and Schachenmann, A., 1992, "Three-dimensional turbulent flow simulation for two different hydraulic turbine draft tubes", First European computational fluid dynamics conference, Brussels, 7-11 September.

Drtina, P., Dalbert, P., Rütti, K., and Schachenmann, A., 1993, "Optimization of a diffuser with splitter by numerical simulation", ASME paper 93-GT-110

Drtina, P., and Krause, M., 1994, In preparation for submission, "The prediction of sand abrasion in a francis turbine guide vane" IAHR Symposium, Peking,.

Dunham, J, 1993, "A new approach to predicting annulus wall boundary layers in axial compressors", I. Mech E. Seminar on Turbomachinery, October 1993.

Eckardt, D., 1980, "Flow field analysis of radial and backswept centrifugal impellers", ASME Conference publication, *Performance of Centrifugal pumps and compressors*, Gas Turbine conference, New Orleans, pp 77-86

Eriksson, L. E., Rizzi, A., and Therre, J. P., 1984, "Numerical solutions of the steady incompressible Euler equations applied to water turbines", AIAA Appl. Aerodynamics conference, Seattle

Ferziger, J. H., 1993, "Estimation and reduction of numerical error", ASME FED Publication Vol 158,

Quantification of uncertainty in Computational Fluid Dynamics.

Freeman, C., and Cumpsty, N. A., 1992, "A method for the prediction of supersonic compressor blade performance", AIAA Journal of Propulsion, Vol. 8, No. 1 ,pp 199 - 208.

Ginder, R. B., 1991, "Design and performance of advanced blading for a high speed HP compressor", ASME Paper 91-GT-374, ASME Gas Turbine Conference, Orlando, June 1991.

Ginder, R. B. and Calvert, W. J., 1987, "The design of an advanced civil fan rotor", ASME Jnl. of Turbomachinery, Vol.109, pp 340-345.

Göde, E.,and Cuenod, R., 1989, "Numerical simulation of the flow in a hydraulic turbine", Sulzer Technical Review, 4/1989.

Göde, E., and Rhyming, I.L, 1987, "3-D computation of the flow in a Francis Runner", Sulzer Technical Review, 4/1987.

Göde, E, and Sebestyen, A., 1994, Sulzer Escher Wyss, private communication.

Goyal, R. K., and Dawes, W. N., 1993, "A comparison of the measured and predicted flow field in a modern fan-bypass Configuration", ASME Jnl. of Turbomachinery, Vol. 115, No. 2, pp 273-282.

Hodson, H. P., 1984, "Boundary layer and loss measurements on the rotor of an axial-flow turbine", Trans. ASME, Journal of Engineering for Gas Turbines and Power, Vol.106, pp 391-399.

Hourmouziadis, J., 1989, "Aerodynamic design of low pressure turbines", AGARD-LS-167.

Howard, M., and Gallimore, S. J., 1992, "Viscous throughflow modelling for multi-stage compressor design", ASME paper 92-GT-302.

Jennions, I. K., and Turner, M. G., 1993, " Three-dimensional Navier-Stokes computations of transonic fan flow", ASME Jnl of Turbomachinery, Vol.115, No.2, pp 261-272.

Karamidas, G., 1988, "Design of high performance fans using advanced aerodynamic codes", ASME paper 88-GT-141.

Katoh, Y. et al., 1993, "Development of a transonic front stage of an axial compressor for industrial gas turbines", ASME paper 93-GT-304.

Katsanis, T., 1965, "Use of quasi-orthogonals for calculating flow distribution on a blade-to-blade surface in a turbomachine", NASA TN D2809.

Keck, H., Göde, E., and Pestalozzi, J., 1990, "Experience with 3-D Euler flow analysis as a prectical design tool", IAHR Symposium, Belgrade

Mayle, R. E., 1991, "The role of laminar-turbulent transition in gas turbine engines", Trans. ASME, Journal of Turbomachinery, pp 509 - 537.

Moore, J. G., 1985, "An elliptic calculation procedure for 3-D viscous flow", AGARD LS-140.

Morriss, R. E. and Kenny, D. P., 1971, "High pressure ratio centrifugal compressors for small engines", ASME publication *Advanced centrifugal compressors.*

Rhie, C. M., Zacharias, R. M., Hobbs, D. E. et al., 1993, "Advanced transonic fan design procedure based on a Navier Stokes method", ASME paper 93-GT-323

Robinson, C. R., 1991, "End-wall flows and blading design for axial flow compressors", Ph. D Thesis, Cranfield Institute of Technology, UK

Robinson, C. R., Northall, J. D., and McFarlane, C. W. R., 1989, "Measurement and calculation of the three-dimensional flow in axial compressor stators with and without end-bends", ASME paper 89-GT-6

Starken, H., 1989, "Design criteria for optimal blading design", AGARD-LS-167, Blading design for axial turbomachines.

Stiefel, W., 1972, "Experiences in the development of radial compressors", VKI Lecture series 50, *Advanced radial compressors.*

Stow, P., 1985, "Incorporation of viscous-inviscid interactions in turbomachinery design", in *Thermodynamics and Fluid Dynamics of Turbomachinery*, Ed. Ucer , Stow and Hirsch, Martinus Nijhoff Publishers, pp 887-921.

Stratford, B. S., 1959, "The prediction of separation of the turbulent boundary layer", Journal of Fluid Mechanics, Vol. 5, pages 1-16.

Tubbs, H., and Rae, A. J., 1991, "Aerodynamic development of the high pressure compressor for the IAE V2500 aero-engine", Paper C423/023, Institution of Mechanical Engineers.

Wadia, A. R., and Beacher, B. F., 1989, "Three-dimensional relief in turbomachinery blading", ASME paper 89-GT-151.

Wilcox, D. C., 1993, "Comparison of two-equation turbulence models for boundary layers with pressure gradient", AiAA Journal, Vol.31, No. 8, pp 1414 - 1421.

Wisler, D. C., 1984, "Loss reduction in axial-flow compressors through low-speed model testing", ASME paper 84-GT-184.

Youngren, H. and Drela, M., 1991, Viscous/Inviscid method for preliminary design of transonic cascades", AIAA paper 91.

NEW METHODS, NEW METHODOLOGY ADVANCED CFD IN THE SNECMA TURBOMACHINERY DESIGN PROCESS

Christophe VUILLEZ (*) - Bertrand PETOT (**)

Snecma - Division Recherches et Etudes Avancées
Centre de Villaroche - 77550 MOISSY CRAMAYEL -FRANCE

Abstract :

CFD tools represent a significant source of improvements in the design process of turbomachinery components, leading to higher performances, cost and cycle savings as well as lower associated risks.

Such methods are the backbone of compressor and turbine design methodologies at Snecma. In the 80s, the use of 3D Euler solvers was a key factor in designing fan blades with very high performance level. Counter rotating high speed propellers designed with this methodology reached measured performances very close to their ambitious objective from the first test series.

In the late 80s and the beginning of the 90s, new, more powerful methods were rapidly developed and are now commonly used in the design process : a quasi-3D, compressible, transsonic inverse method, quasi-3D and 3D Navier-Stokes solvers, 3D unsteady Euler solvers. As an example, several hundred 3D Navier-Stokes computations are run yearly for the design of low and high pressure compressor and turbine blades.

In addition to their modelling capabilities, the efficient use of such methods in the design process comes from their close integration in the global methodology and from an adequate exploitation environment. Their validation, their calibration, the correlations between different levels of modelling are of critical importance to an actual improvement in design know-how.

The integration of different methods in the design process is described. Several examples of application illustrate their practical utilisation. Comparisons between computational results and test results show their capabilities as well as their present limitations. The prospects linked to new developments currently under way are discussed.

(*) : Head of Compressor Research & Methods
(**) : Turbine Aero & Cooling Research Manager

1°) *INTRODUCTION*

The design of advanced turbomachinery components has to meet ever more demanding requirements. Higher performance must be reached within shorter design cycles and at lower cost. Ambitious objectives of weight, complexity and manufacturing costs reduction lead to lower the number of stages and thus to increase stage loadings.

For compressor and turbine designers, this implies the capability to control the very complex flow phenomena occurring in highly loaded stages, in all the operating range of the component, early in the programme. Besides aerodynamic performances, the aggressive design of advanced, fully 3D blades also requires an early focus on all the aspects related to engine integrity : blade flutter, forced response, turbine blade and disk cooling efficiency as examples.

Up to the end of the 70's, most of the design and optimisation process relied on an empirical approach, which meant a very large number of tests. The all-experimental optimisation strategy was very time and cost consuming for two reasons at least. Each iteration implied all the phases from design to manufacturing, instrumentation and testing. Secondly, determining what must be improved in the design required heavy instrumentation on each component, in order to identify the "hard spots".

For these reasons, Snecma started very early to take advantage of the fast-growing of computer power and of the concurrent advances in Computational Fluid Dynamics. The use of CFD tools in the design methodology has brought major improvements in the iterative optimisation process of each component.

An attempt to summarise this contribution could use the following keywords : faster response, broader range of alternative solutions, better description of flow complexity. Indeed, every computation node in a numerical simulation is also a "measurement" node, which allows an easy and comprehensive analysis of the flow prediction.

But unfortunately, CFD is far from faithfully reproducing reality yet. Even with the power of the most recent super computers, simulation capabilities still depend on models or are limited to component parts. The computation of a complete multistage high pressure compressor with 3D, unsteady and viscous, small scale phenomena is out of reach for a long time yet. So the major challenge for both the engine component designer and the CFD method developer consists in integrating new computational methods, with their capabilities and limitations, in the design process in a fast, safe and efficient way. Every new method brings new answers, but also raises new questions. The most obvious risks in using a new, more powerful tool are either misunderstanding or overoptimistic confidence in the results.

Presented at an AGARD Lecture Series on 'Turbomachinery Design Using CFD', May to June 1994.

A constant effort must be dedicated to methods comparison, validation and calibration. This means in particular that heavily instrumented rigs, representative of real engine component be used to produce a validation data-base.

At Snecma, a strong interaction between compressor and turbine designers and CFD tools developers allowed an early use of advanced methods in the design process : 3D Euler in 1984, Quasi-3D Navier-Stokes in 1988, 3D Navier-Stokes in 1992. Most of the CFD developments have been undertaken in close co-operation with research laboratories, and especially with the Theoretical Aerodynamics Division and Energetics Division at Onera.

This paper will present the numerical basis of currently used CFD codes at Snecma, as well as the combined efforts to develop homogeneous and user-friendly pre and post-processors. Then the applications of CFD tools will be presented for both compressor and turbine blade design. Comparison with experimental results will show the prediction capabilities of different methods. Finally, conclusions will be drawn on the current use of CFD tools in the design methodology. New directions for improvement will be discussed.

2°) OVERVIEW OF CFD TOOLS DEVELOPMENT AT SNECMA

2.1 CODE DEVELOPMENT AND INDUSTRIALISATION STRATEGY

For more than 25 years, Snecma has been heavily investing in building design systems which benefit from the latest advances in CFD techniques and existing computer technology [Karadimas, 89]. Although much is being done in such fields as combustion, engine/airplane integration, air intakes, exhaust systems or acoustics, this paper will only focus on applications to compressor and turbine design.

The aim of all efforts dedicated to CFD developments is to increase the capability to accurately simulate the very complex flows encountered in a turbomachine, i.e. three-dimensional, compressible, partially supersonic, viscous, turbulent flows. Other major aspects concerned are fluid/structure interaction involved in blade flutter or forced response phenomena, or fluid/solid surface heat transfer in turbines and internal cavities. Obviously, such an objective sounds like a Sisyphean task, and a correct and complete simulation of the flow through a whole multistage HP compressor would demand computing power far beyond what exists today or what is foreseeable in the mid-term future with parallel super computers. Basically, the computing requirements for a given simulation depend on two main choices :

- The level of modelling, i.e. how deep into details do we want to go, or in other words how realistic do we want the computation ?
- The size and complexity of the physical domain to be computed -from 2D blade-to-blade to whole compressor or turbine-.

So the questions that arise when dealing with the use of CFD tools in the design process are as follow :

1) At a given time, what kind of physical modelling can be successfully computed on the late generation of super computers, on which geometrical domain, at what cost, in terms of time and money ?

2) Which kind of design applications can be foreseen using this method, with which level of confidence ?

3) In which way must the design methodology be modified to successfully and efficiently integrate the new tool ?

For the industry, the answer to the first question comes from close cooperations with different research partners, and requires a permanent foresight of computer technology breakthroughs and availability, as well as new developments in numerical techniques. In many cases, Snecma played a leading role in inciting new research work. Cost evaluation is a key point. The fast cost decrease of a given computing power leads us to carefully choose the right time for acquiring new computing capabilities : too early is expensive, too late means using tools that are poorly competitive. This balance is a challenging problem for engine manufacturers who heavily depend on their computing, CAD and Data Base Management Systems in the design process.

The second question can be translated in terms of method accuracy, reliability and limitations. These aspects will be discussed in more details in the sections dedicated to compressor and turbine design. Let us only mention here that component design can take no advantage of advances in CFD techniques without adequate experimental data to validate and calibrate new generation codes. This means that combined efforts are definitely needed in designing, manufacturing, instrumenting and testing experimental rigs capable of bringing ever more detailed and reliable information on flows in engine-like components. In fact, it must be emphasised that the use of CFD in aero-engine design strongly depends upon the improvements in measurement techniques, in order to have access to the same detailed level of investigation as that of CFD (e.g. secondary and unsteady flows). Data acquisition on real engine components is important as well, but it cannot be considered sufficient, since the constraints specific to engine design make it difficult to implement enough instrumentation to directly validate advanced CFD tools.

The third point is a delicate matter. Up to this decisive step, only code developers familiar with computational techniques have been involved. The final objective here is to move from a solver to a tool that can be handled by designers who are not CFD specialists. To reach this objective, additional work is required to integrate the new code in a framework that is user-friendly. Simple user rules must help the designer to feel comfortable with advanced tools, which bring new answers but also question more traditional design procedure.

Within Snecma, this problem is tackled through the association of researchers and component designers within the same entity. CFD developers are thus spread in different departments such as Compressor Aerodynamics or Turbine Aero&Cooling. This allows component designers to be involved early in the validation and industrialisation of new codes. Once the code is in service, CFD developers can assist users in real time. A strong coordination guarantees the necessary synergy between the developments undertaken within each department.

The importance of pre and post processors must be underlined here. Beyond the computing time required for the calculation itself, these can be the limiting steps in the procedure. Pre- processing consists in mesh generation and initialisation. Mesh generation has been fully automated, with a few parameters that can be redefined interactively to adapt to a given blade passage geometry. Initialisation is directly provided by throughflow data for steady computations. Some adaptations may be necessary near endwalls and are discussed in section 3. Additional inputs are taken into account for unsteady calculations, like blade vibration modes for flutter simulation for instance.

To be efficient, post-processing tools must offer several levels of investigation. A straightforward, batch tool is necessary to have fast answers even from heavy 3D Navier-Stokes computations. This is particularly convenient in parametric studies around a configuration close to the final one. It provides spanwise distribution of standard flow quantities, or pressure distribution on blade profiles. But a deeper and interactive investigation may be necessary, with strong 3D visualisation capabilities. At

Snecma, the solution consists in the combination of in-house, modular tools specific to turbomachinery applications and of 3D visualisation software from vendors.

From a general point of view, a new application is considered operational once the complete cycle of pre-processing, computation, post-processing and conclusions can be executed within 24 hours. That means in particular that the calculation itself can be run overnight. 3D steady Navier-Stokes applications for instance have been implemented in this way in the design procedure in 1992. Since this entry into service, more than a thousand calculations have been performed for design purposes.

2.2 MAIN FEATURES OF COMPRESSIBLE EULER AND NAVIER-STOKES SOLVERS

2.2.1 TOWARDS CODE COMMONALITY

In the 70's and the early 80's, different codes have been developed separately for different applications. The poor memory capabilities of the computers put severe restrictions on code structure. CPU time considerations led to a deep optimisation of the software coding in a single direction. So each code would live its own life, would be dedicated to a given application and would include its own simple pre and post processors.

The outstanding development of computer technology in the 80's and the advances in numerical techniques made possible a large number of new applications for CFD. For the industrial user, this led to the obvious necessity to structure the new developments from a global point of view. There are two main objectives. Firstly, all applications, either steady or unsteady, 2D or 3D, inviscid or viscous, must benefit from work on any of them, in order to save time and money. Secondly, the amount of work necessary to maintain the codes and support users must be kept at a reasonable level.

Nowadays, most of Snecma solvers for compressible flows share the same modular coding and the same numerical basis, which will be described hereafter. This situation makes the implementation of advanced numerics fast and easy for a broad range of applications, i.e. compressors, turbines, air intakes or nozzles. It is noteworthy that most of the numerics presented here apply to inviscid or viscous, steady or unsteady simulations.

2.2.2 NUMERICS AND MODELS

The most recent developments at Snecma are the results of a long time co-operation with ONERA which started in the 70's [Veuillot, 75].

The general trend since then has been to move from 2D, steady, inviscid blade-to-blade computations to 3D, unsteady, viscous simulation. Let us just mention in this section parallel work on other topics of great interest such as throughflow methods or inverse methods, which will be shortly presented in section 3 and 4. Most of the applications that will be presented for compressor and turbine analysis are now based on the following numerical basis.

The technique used to solve compressible flows is a finite volume, time marching technique applied on multiblock structured grids. Structured grids are well adapted to blade-to-blade geometries which present a simple topology. The multi-domain approach offers a good compromise in order to benefit from structured grid simplicity and yet guarantee satisfactory qualities in terms of mesh regularity and orthogonality. The numerical scheme includes two steps : an explicit integration scheme and an implicit step. Several explicit schemes can be used : a 1 or 2 step Lax-Wendroff-Ni scheme, presented for instance in [Cambier, 89], or a Jameson-type space discretization combined with a 4 step Runge-Kutta time integration scheme. In both cases, those centered schemes have a second order accuracy when solving Euler equations. For simplicity purposes, Thommen's idea [Thommen, 66] is used for Navier-Stokes equations, leading to a first order accuracy in viscous regions. An additional numerical dissipation has been derived from Jameson [Jameson, 81] to ensure the stability of the explicit scheme in presence of flow discontinuities. For steady computations, a local time-stepping technique is used.

For some time, a multigrid technique has been implemented to significantly improve the convergence speed of the algorithm [Couaillier, 89]. Since 1991, an Implicit Residual Smoothing technique proposed by Lerat [Lerat et al., 82 ; Lerat, 85] and applied to turbomachinery cases by Chima and Yokota [Chima, 88] has been preferred [Vuillot, 93].

All boundary conditions are imposed through compatibility equations obtained from characteristic relations, as well as sub-domain matching [Viviand, 78], [Cambier, 83]. This approach is particularly efficient for unsteady calculations.

Because of its efficiency, this numerical basis has been widely implemented in most of steady and unsteady solvers used for compressor and turbine applications. For 3D steady computations on compressor blades, Euler solutions on a typical 20 000 points mesh require only 2 minutes on a Cray-YMP single processor. Using the standard mixing-length turbulence model described hereafter, Navier-Stokes computations need about 1 500 iterations to reach a satisfactory level of convergence, which represents approximately 5 hours on the same Cray-YMP single processor with a 800 000 node, H-O-H grid.

Figure C.1 shows the convergence history of a 3D Navier-Stokes computation on a transonic rotor blade of an HP compressor, using two criteria : flow rate convergence and residuals evolution.

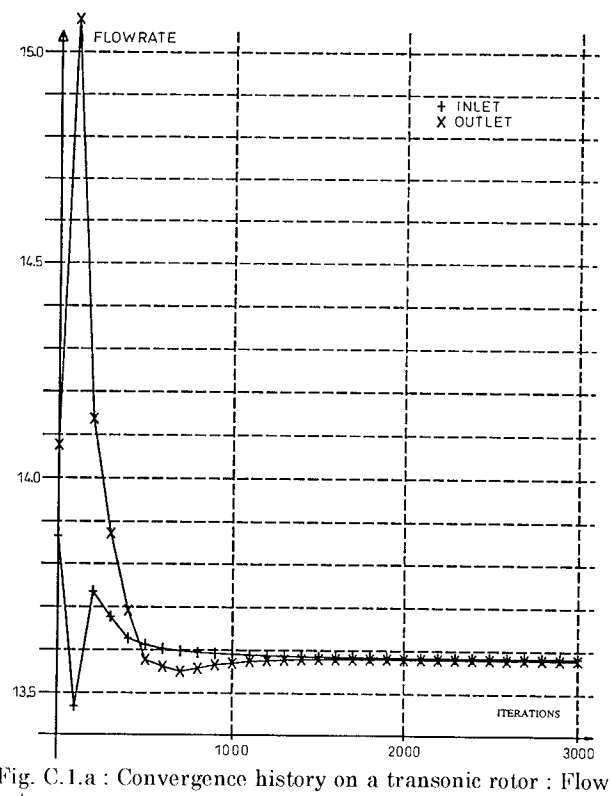

Fig. C.1.a : Convergence history on a transonic rotor : Flow rate

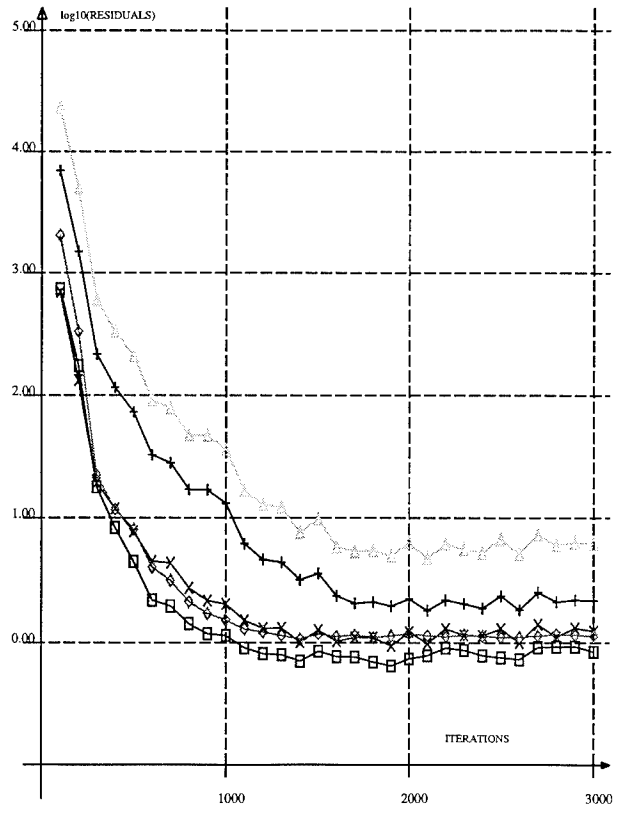

Fig. C.1.b : Convergence history on a transonic rotor : $||residuals||_{L2}$

These codes are highly vectorized. 3D Navier-Stokes solvers are parallelized on Cray computers with a reasonable speedup of 1.85 on two processors and 2.6 on 3 processors.

Before moving to compressor and turbine applications, a final word must be said on turbulence modelling for Navier-Stokes solvers. The codes which are currently used today for design application use the algebraic turbulence model proposed by Michel et al. [Michel, 69].

The use of an algebraic turbulence model guarantees good code robustness, with a reasonable accuracy, even if the extension of such a model to 3D applications requires special care to account for the influence of several walls (blade, hub and casing).

The general discussion on turbulence models accuracy is beyond the scope of this paper. Nevertheless, there are several practical limitations to the use of algebraic models in compressor and turbine environments. The first one comes from the necessity to describe each boundary layer with respect to the distance from a wall, which makes its use rapidly difficult when the geometry of the computational domain is complex, like in clearances or cooling channels. The second one is their inability to take into account free-stream turbulence, which is important in multistage components.

Two-equation transport models like the k-ε model developed by Jones and Launder [Jones, 72] can provide a solution to the two limitations. Solid surfaces are only taken into account using boundary conditions on k and ε, and the model is suitable for imposing free-stream turbulence conditions at inlet. But this model is far less robust than an algebraic model and more difficult to initialise. A lot of code developers overcome this difficulty in using endwall functions instead of a direct computation of the inner part of boundary layers. This makes the computation easier and faster because it requires less grid nodes, and allows larger cell size at solid walls.

However the general experience concerning this approach shows that the model accuracy is poor either with strong adverse pressure gradients leading to separation, or when computing heat transfer at endwalls. In consequence, Onera and Snecma prefer the low-Reynolds number correction of the k-ε model near solid surfaces [Jones, 73] for compressor and turbine applications. This model has given very accurate results prediction of a complex 3D shock-wave/boundary layer interaction [Cahen, 93]. A large effort is now under progress to turn it into an industrial tool.

3°) *CFD APPLICATIONS ON COMPRESSOR DESIGN*

3.1 EVOLUTION OF DESIGN PROCEDURE

The efficient integration of new computational tools, with increased simulation capabilities, is a real challenge for the industrial designer. To benefit from the fast advance in CFD developments, it is necessary to constantly adapt the design methodology and procedure according to new simulation capabilities. In January 1990, Falchetti and Thouraud presented a Methodology for advanced core compressor design [Falchetti, 90] which already emphasised the importance of advanced CFD methods and the improvements they brought in designing core compressors. Karadimas [Karadimas, 88] and more recently Brochet [Brochet, 93] demonstrated the usefulness of 3D Euler solvers in designing high bypass ratio fans for commercial engines with high efficiency at cruise and required thrust at take-off.

In all these cases, the methodology used could be summarised by the following diagram (fig. C.2). The procedure was rather linear, with regular feedback from the different steps.

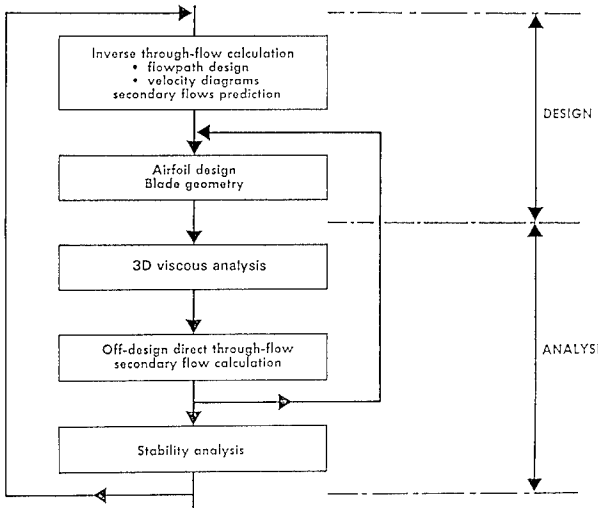

Fig. C.2 : Classical design procedure

This diagram points out the key role of 3D Euler and Quasi-3D Navier-Stokes solvers in the analysis process, allowing a real optimisation of the blade shape before any testing. As an example, the fan of the CFM56-5C which powers the Airbus A340 was designed using this set of tools. With a tip Mach number of 1.55 and a mid-span shroud, this fan exhibited a high maximum efficiency of 0.905 very early in the programme. This powerful approach was successfully extended to the design of counter rotating high speed propellers [Nicoud, 89]. A set of blades designed at Snecma was manufactured and tested in the Onera-Modane test facility. The measured performances were very close to the aero adiabatic efficiency objective of 0.925 at a flight Mach number of 0.78 with the very first version of

the blades. Tests could be run at a high flight Mach number of 0.9 without significant loss in performance.

A major new step has been made in 1992 with the integration of a 3D Navier-Stokes solver in the design procedure. This generation of codes brought the capability to directly take into account both 3D and viscous effects which were treated separately in the previous procedure.

The practical use of this solver is described below. The incidence on the design procedure is different depending on the application. For fan design, the relatively small number of degrees of freedom in flowpath definition allows a rather sequential process which remains similar to the diagram in fig. C.2. The major change consists in replacing 3D Euler and quasi-3D viscous analysis with 3D Navier-Stokes in the blade geometry analysis step.

As far as multistage compressors are concerned, the change in the procedure itself has been much more significant. To fully benefit from the capability of 3D viscous simulation, preliminary blade design is performed during the initial flowpath definition to substantiate the principal choices based on past experience and correlations, e.g. stage loading distribution, degree of reaction, spanwise work distribution. Fig. C.3 summarises the procedure currently used to design innovative, highly loaded HP compressors.

In the following sections, key methods in this process are reviewed.

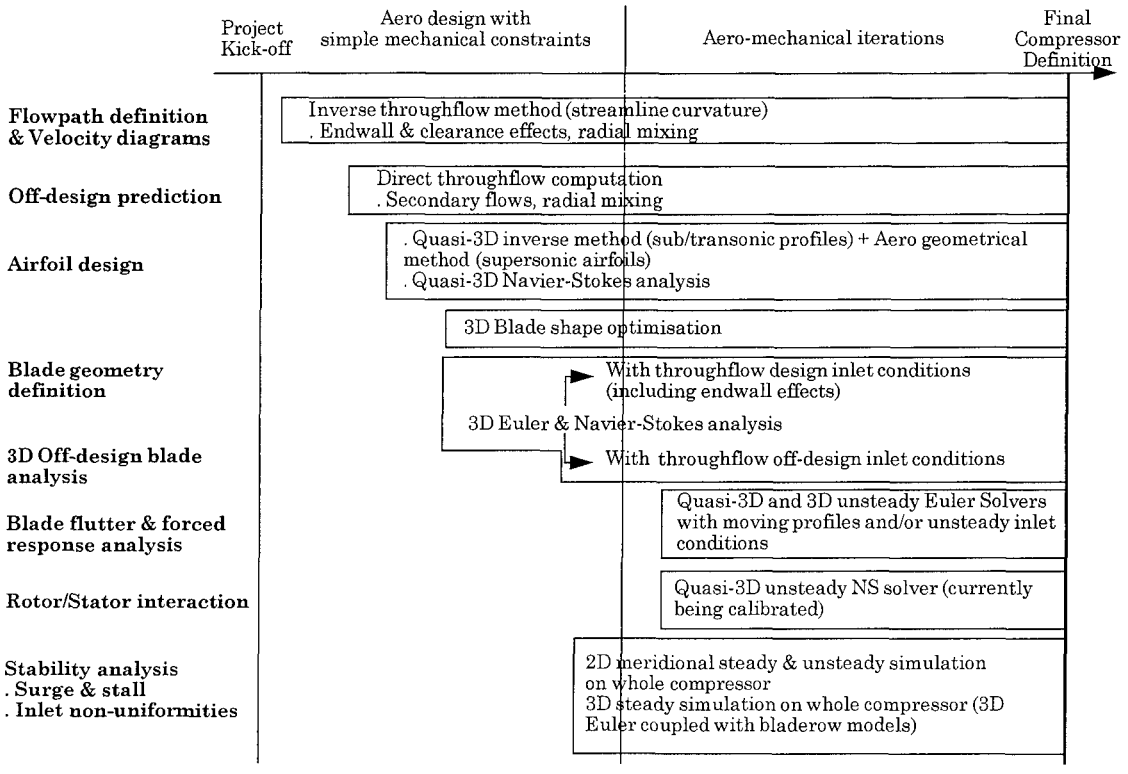

Fig. C.3 : New design procedure for innovative, highly loaded HP compressor

3.2 THROUGHFLOW COMPUTATION

As for all engine manufacturers, the throughflow method is the basis of compressor design. It allows a complete definition of the flowpath walls geometry as well as velocity diagrams for each blade row. For all further steps, the meridional flowpath represents a reference, for it is a simplified but comprehensive overview of a whole compressor.

The code uses a classic streamline curvature method. The input parameters are spanwise distributions of rotor pressure ratios and stator exit angles. Viscous losses on profiles are computed using semi-empirical correlations based on Snecma's experience. Shock losses are computed with simple models based on some aerodynamic and geometrical parameters.

The initial optimisation process leads to the definition of all the main parameters influencing the compressor aerodynamics : flowpath geometry, stage loading distribution, degree of reaction, spanwise work distribution, blade and vane numbers and aspect ratios.

A lot of industrial know-how is integrated in this method, using correlations and simple models that are calibrated according to past experience. As an example, a model of radial diffusion effects has been implemented. The importance of radial mixing in multistage compressors has been emphasised for instance by Gallimore and Cumsty [Gallimore, 86]. Snecma's model has been calibrated by application to several tested multistage HP compressors that cover a wide range of applications (civil & military, 6 to 10 stages).

To illustrate these effects, throughflow computations with and without spanwise mixing have been performed on the 4-stage H4 compressor. This research vehicle is representative of the rear stages of an engine HP compressor. The design pressure ratio is 2.2 at a rotational speed of 13 700 rpm. Increased axial gaps between rotors and stators allow traverse probe investigations behind each bladerow. Fig. C.4 summarises the H4 instrumentation capabilities.

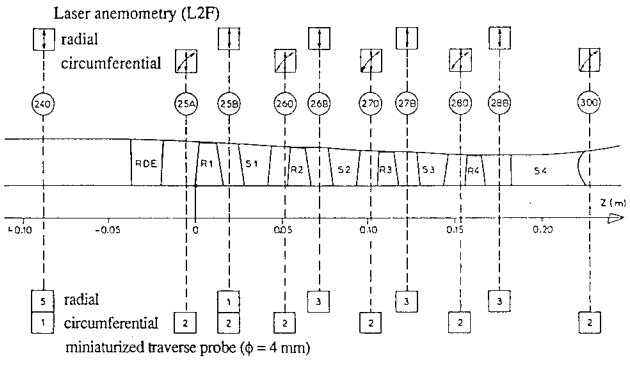

Fig. C.4 : Summary of H4 instrumentation

Using the same experimental input data, the two computations show large differences in total pressure and total temperature spanwise distributions downstream of stator 4 (fig. C.5). The discrepancies observed in the computation without mixing increase in compressors with higher pressure ratio. Conversely, the good results obtain with mixing terms confirm the validity of the model.

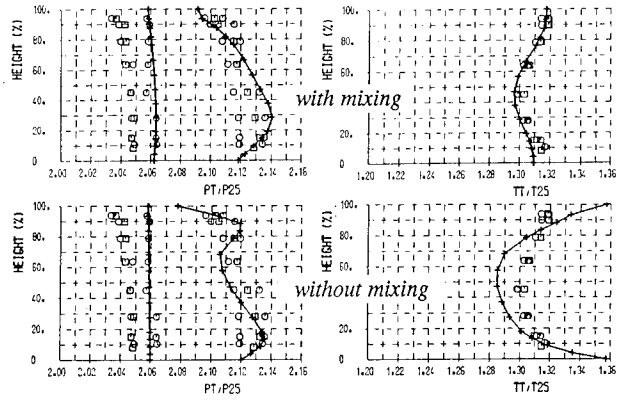

Fig. C.5 : Effects of radial mixing in the throughflow analysis of H4 compressor (downstream of stator 4)

The prediction of endwall effects is another major difficulty in multistage compressor design. A secondary flow prediction method has been successfully used on several compressors [Brochet, 87]. Today, the systematic use of 3D Navier-Stokes analysis on each blade enhances the capability to deal with secondary flow effects, as shown later in this paper.

3.3 BLADE DESIGN

Each blade design starts with the design of several profiles along the span. Different methods are used to design subsonic or supersonic profiles. Both integrate some structural specifications such as maximum thickness to chord ratio, leading edge and trailing edge thickness.

Supersonic profiles are designed using an aero-geometrical method developed at Snecma. Some input parameters are specified, such as suction side incidence, pitch-to-chord ratio, turning angle, deviation, throat margin. Iterations with a quasi-3D Navier-Stokes solver are necessary to reach aerodynamic objectives and minimise shock intensities and boundary layer diffusion.

For subsonic and transonic airfoils design, a quasi-3D inverse method is used. It has been jointly developed by Onera and Snecma and is described in [Nicoud, 91]. This finite element method solves the Quasi-3D compressible transsonic potential equations, using a variational formulation. The classic Quasi-3D approach takes into account radius and stream tube variations coming from throughflow calculation using additional source terms, and rotation effects in rotors. The inverse formulation, using a transpiration model, iteratively modifies a preliminary profile to match an imposed velocity distribution on the target profile. This allows a good control of boundary layer diffusion.

After optimisation, the aerodynamic performances of the profile are also analysed using the Quasi-3D Navier-Stokes solver, described in [Vuillez, 90]. This can lead to further modifications according to viscous effects and shock prediction.

Fig. C.6 illustrates the use of this method. Fig. C.6.a shows the velocity distribution of the initial profile and the objective velocity distribution. Fig. C.6.b compares the initial and modified geometries. Fig. C.7.a presents the isentropic Mach number distribution computed using Quasi-3D Navier-Stokes solver on the final profile. Fig. C.7.b shows the Mach number distribution in the final blade passage.

The optimised profiles are then stacked to generate the complete blade or vane geometry.

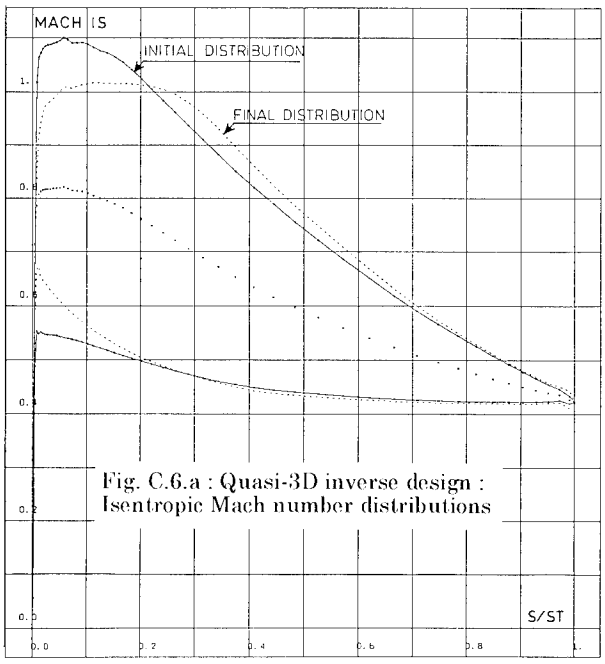

Fig. C.6.a : Quasi-3D inverse design : Isentropic Mach number distributions

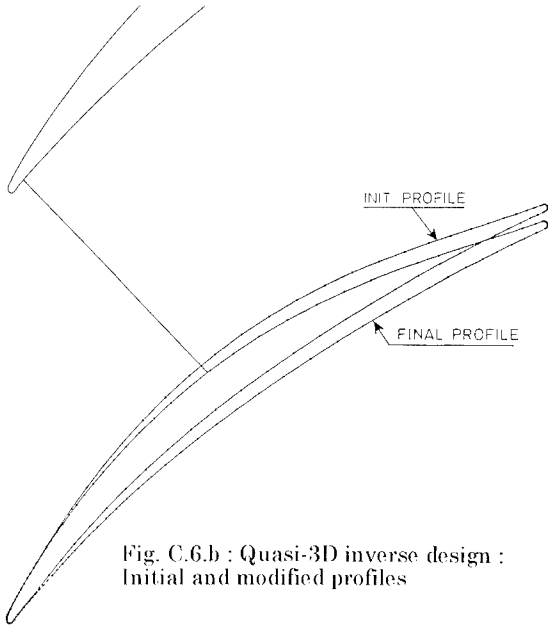

Fig. C.6.b : Quasi-3D inverse design : Initial and modified profiles

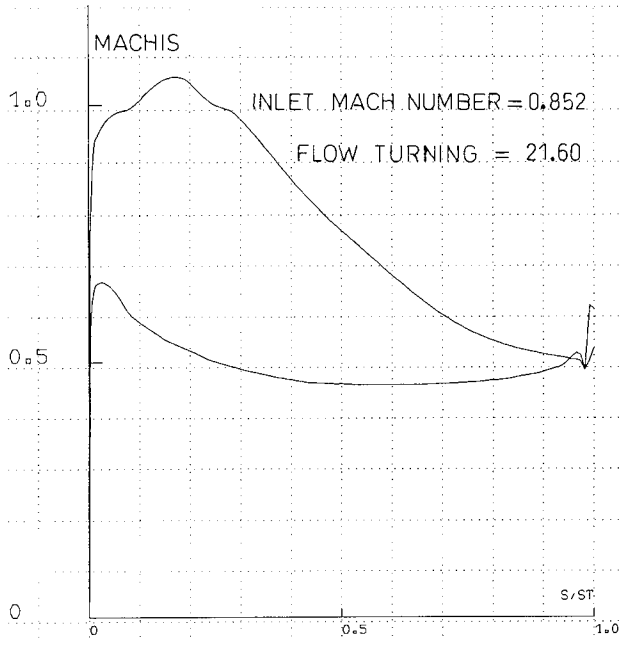

Fig. C.7.a : Quasi-3D Navier-Stokes computation : Isentropic Mach number distribution

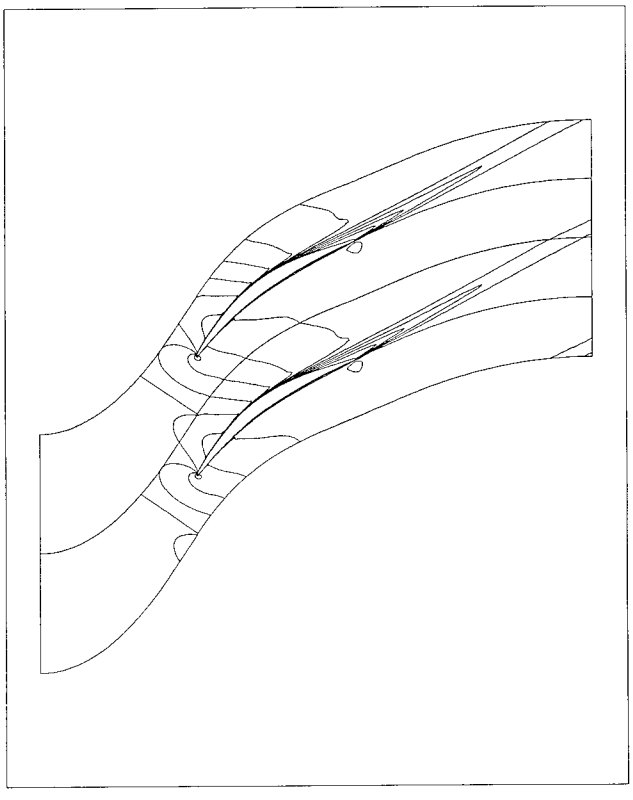

Fig. C.7.b : Quasi-3D Navier-Stokes computation : Iso-Mach lines

3.4 3D EULER AND NAVIER-STOKES STEADY ANALYSIS

As mentioned above, the integration of a 3D Navier-Stokes solver has deeply modified the design procedure. 3D Euler computations have been successfully used for years in designing high speed rotor blades with supersonic relative inlet flow. Civil engine fans have naturally been the most relevant application for this method in so far as they present high aspect ratio, low hub-to-tip ratio and as they work at high Reynolds numbers. Properly calibrated, 3D Euler analysis proved its effectiveness in predicting major features such as overall massflow in started conditions and start margin. Shock losses could also be optimised according to several operating conditions. Figure C.8 shows the shock structure in the mid-span shroud region of the CFM56-5C fan blade computed with the 3D Euler solver.

Unfortunately, viscous losses had to be estimated with the additional use of boundary-layer integral methods or Quasi-3D Navier-Stokes computations. Besides, the use of 3D Euler for HP compressor blade and vane analysis was hazardous, given the importance of viscous effects on endwalls in these cases.

3D Navier-Stokes capabilities have brought major advances in two fields. For fans and more generally for supersonic rotor blades, they ensure a much better consistency of the predicted flowrate, pressure ratio and efficiency with respect to experimental data. Before being heavily used for CFM56-7 wide chord fan optimisation, the 3D Navier-Stokes code has been carefully calibrated on 3 different wide chord fan blades with various pressure ratios (1.5 to 1.7), corrected tip speed (370 to 413 m/s) and diameters (22 to 61 inches). To illustrate the code's accuracy in terms of overall performance prediction, let us mention here the results obtained at peak efficiency on the TS27 wide chord fan blade. The TS27 wide chord fan has been designed at Snecma in 1984 and tested in 1985 and is shown on figure C.9. At nominal operating point, for a corrected tip speed of 400 m/s, the pressure ratio is 1.65 and the specific mass flow 208 kg/s/m². The measured bypass efficiency was 0.91. The computation was run on a 613 000 node computation grid. No tip clearance was taken into account, and a slip condition was imposed at the casing. Experimental values of absolute total pressure, total temperature and velocity direction were imposed at the inlet. The level of back pressure imposed downstream is also directly derived from test results.

Figure C.10 shows the good agreement concerning the shock location and the relative Mach number contours between the computation and L2F anemometer measurements. It must be emphasised that no correction was necessary on the back pressure level to reach this agreement.

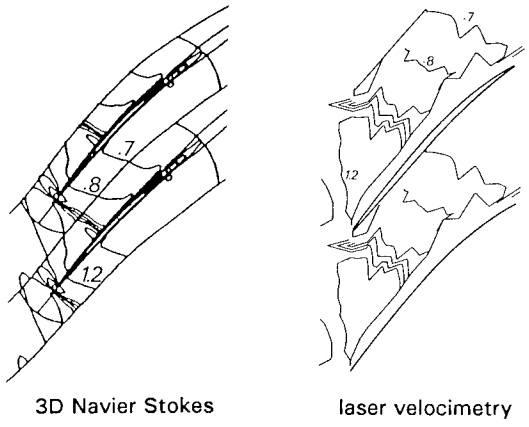

Fig. C.10 : Contours of relative Mach number at 95 % of blade height - TS27 wide chord fan

On figure C.11, pitchwise averaged values of computed total pressure and total temperature downstream are compared with traverse probe measurements. A very good agreement can be observed except for total temperature in the tip region where clearance and casing boundary layer have not been taken into account in the calculation. Another indication of the accuracy is a computed rotor efficiency of 0.936 for a measured value of 0.931. 3D Euler code calibration led to 5 to 10 % corrections on flowrate and pressure ratio predictions. With calibrated 3D Navier-Stokes, the required

corrections are less than 1 %. Figure C.12 presents the result of a 3D Navier-Stokes computation on an intermediate version of the CFM56-7 fan blade.

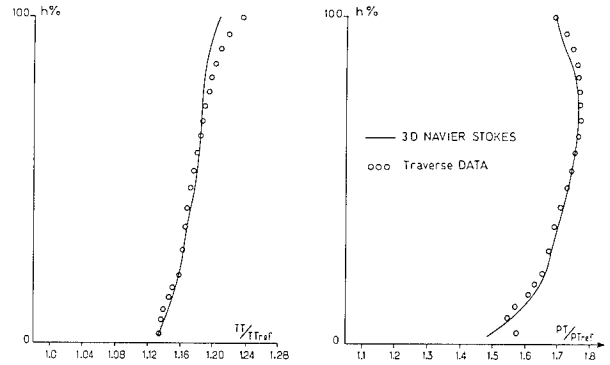

Fig. C.11 : 3D Navier-Stokes pitch-averaged values vs traverse data - Total temperature and total pressure distribution at TS27 rotor exit

The second field where 3D Navier-Stokes brought a major breakthrough is HP compressor blade and vane analysis. The close 3D interaction between viscous and inviscid flows makes 3D Navier-Stokes the right approach to deal with these bladings. For many applications, additional validation is obviously required. Some examples are given hereafter. The first one concerns the rotor blade of the ECL4, a single stage, highly loaded compressor. The rotor has a nominal corrected tip speed of 380 m/s. This compressor reached a peak efficiency of 0.845 with a pressure ratio of 2.22. Figure C.13 shows the flowpath of this compressor. On figures C.14 and C.15, several computation results are compared with experimental data for spanwise pressure ratio distribution and spanwise outlet angle distribution. 4 calculations have been performed : 3D Euler, 3D Navier-Stokes with slip conditions on both endwalls, 3D Navier-Stokes with no slip condition on hub and slip condition on casing and finally 3D Navier-Stokes with no slip conditions on both hub and casing and a 0.5 % tip clearance.

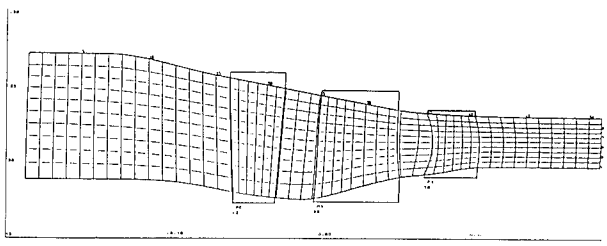

Fig. C.13 : ECL4 compressor flowpath

Experimental values have been measured with traverse probes. These comparisons show the importance of secondary flows and their spanwise influence. Taking hub boundary layer into account is obviously necessary for an accurate prediction of spanwise work distribution.

The experimental tip clearance is unfortunately too small to offer a validation of the prediction of its effects. But the two Navier-Stokes calculations which include the boundary layer at hub present an excellent agreement with the experimental data. The calculation with tip clearance shows a slight difference in the upper part for in both cases the back pressure used was directly derived from a throughflow calculation in which clearance effect had not been taken into account. Fig. C.16 shows the computed relative Mach number contours in the clearance region of another HP compressor rotor blade. Clearance vortex evolution is clearly captured.

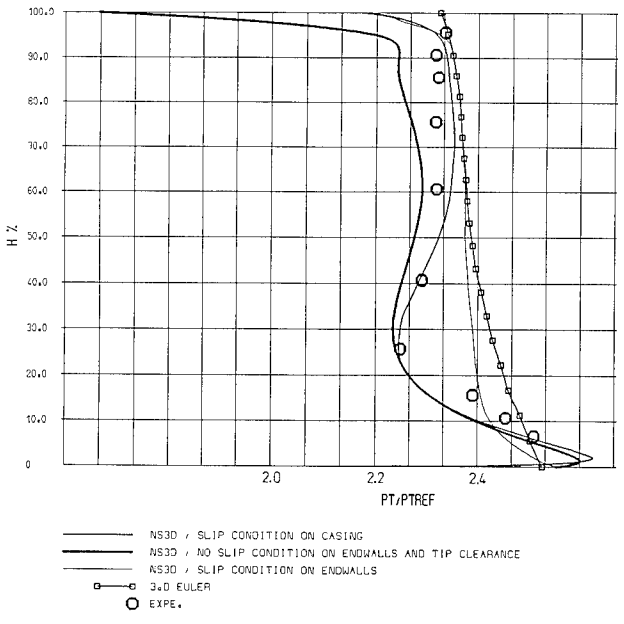

Fig. C.14 : ECL4 rotor outlet : Total pressure

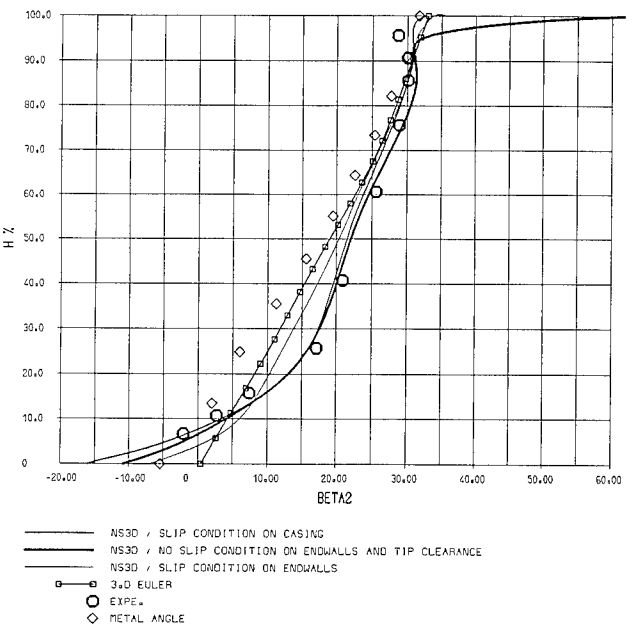

Fig. C.15 : ECL4 rotor outlet : relative flow angle

Another comparison of exit angles is presented on figure C.17. Several computations performed on stator 3 of the above mentioned H4 compressor are presented and compared with test throughflow analysis as well as traverse probe measurements. A 3D Euler and a 3D Navier-Stokes computation using slip conditions at endwalls have been performed with inlet conditions that take into account a total pressure defect near endwalls to represent the inlet boundary layers. Another 3D Navier-Stokes calculation has been run with no-slip conditions on endwalls.

Several conclusions can be drawn from this. On this type of blade, with a hub to tip ratio over 0.9 and a blade height lower than 20 millimetres, 3D viscous effects have a major influence. The deviation predicted by Quasi-3D Navier-Stokes calculations is almost constant along the span. On the opposite, all three 3D methods see large variations spanwise. Outlet streamwise vortices mainly depend on the vorticity coming in the inlet boundary layers.

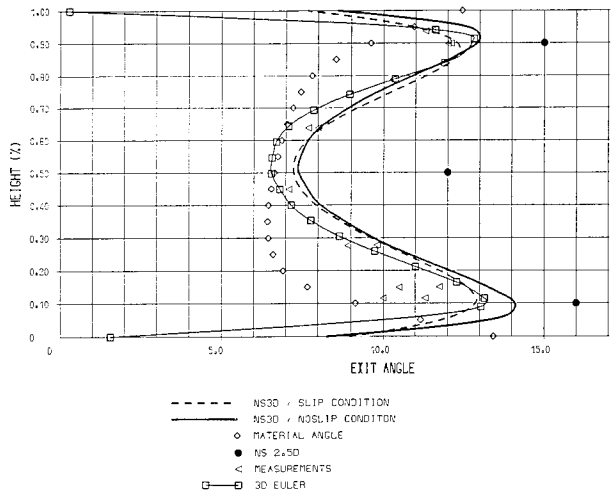

Fig. C.17 : H4 stator 3 vane outlet : Exit angle

Besides, it must be noticed that the order of magnitude of deviation variations along the span is 5°, while the average deviation coming from blade boundary layers is about 1° which is seen when comparing Euler and Navier-Stokes distributions.

This conclusion opens a new field of application for 3D Euler computation. In many cases, a number of optimisation iterations can be performed with simple, low cost 3D Euler analysis even on HP compressor bladings. A reduced set of 3D Navier-Stokes calculations is needed for calibration and final validation.

On figures C.18a and C.18b, 3D Navier-Stokes computation results on H4 rotor 3 blade and H4 stator 3 vane are shown. They illustrate the capability of the code to deal with small HP compressor blades and give an indication on the importance of the computed secondary flows.

A few conclusions can be drawn on the use of 3D Navier-Stokes codes in the design procedure. The combination of its intrinsic accuracy, of careful calibration and adapted inlet conditions in order to deal with the multistage environment leads to a very powerful prediction tool. The number of computations required in the blade design step can be optimised by combining it with low cost 3D Euler calculations.

Further improvements in the prediction of 3D flows in compressors will come from the industrial use of a two-equation transport turbulence modelling, allowing to deal with free stream turbulence influence, and from Quasi-3D and 3D unsteady viscous codes for a better description of rotor/stator and stator/rotor interaction. The Quasi-3D approach is already being tested (see section 4). The full 3D approach will be possible on the next parallel computer generation which will offer over 50 Gigaflops of sustained performances for CFD applications and available memory over 2 Gigawords.

3.5 UNSTEADY ANALYSIS

The flow in aero-engine compressors is fundamentally unsteady, given that energy transfer in a turbomachine is basically an unsteady phenomenon. The influence of flow unsteadiness on aerodynamic performances will not be discussed in this section. It has been said before that this aspect would be tackled using Quasi-3D and 3D rotor/stator analysis. Rather, this section focuses on stability considerations linked to flow unsteadiness. These can be divided in three aspects. Two concern fluid/structure interaction : blade flutter and forced response. The third one deals with the stability of compression system as a whole, namely stall and surge.

3.5.1 BLADE FLUTTER PREDICTION

Blade flutter is a major concern for the safety of compressor operation. It comes from an unstable coupling between the blade vibration modes and the resulting flow unsteadiness. This potential problem is also well known on aircraft wings. In aero-engine compressors, this phenomenon can have several origins according to the operating conditions. With supersonic inlet conditions, flutter can be initiated by strong shock wave unsteadiness in the blade passage. At lower rotation speed and high inlet angle of attack, an unstable flow separation occurring at the leading edge on the suction side can also be coupled with blade vibration. At high flow rate and low pressure ratio operating conditions, the instability may come from the choking of the blade passage.

Many of these phenomena directly involve viscous effects and require Navier-Stokes unsteady simulation capabilities. A lot of efforts is currently being put in that direction. Preliminary results have been obtained, which are encouraging. Nevertheless, these difficult problems are still treated in the design procedure by the use of empirical criteria based on past experience and dedicated research test series.

There is one major exception that can be efficiently tackled using CFD tools today, which is supersonic flutter. In this case, inviscid effects are considered preeminent, in so far as the unsteady component of blade pressure (which is what puts flow work in the blade vibration) mainly depends on the displacement of the strong shock wave in the blade passage. Thus, Euler computations are thought to be adequate to predict this form of flutter.

The analysis procedure is detailed in [Gerolymos1, 92]. First, a structural vibration mode analysis is performed in running conditions, i.e. taking centrifugal forces into account. This analysis is performed on the whole bladed disk using cyclic symmetry. The resulting blade surface displacement distribution for a given mode is used as an input to 3D Euler unsteady analysis. The unsteady calculation is performed around the vibrating 3D blade, and a chorochronic periodicity technique allows the computation to be run on a single interblade channel, regardless of the azimutal wave number of the vibration mode [Gerolymos2, 92]. As the computation progresses, the initial vibration mode can be iteratively modified to account for the flow influence, but the modification is not significant for full titanium blades, due to the high density ratio between blade material and air. In the case of composite or hollow titanium blades however, the aero-mechanical (coupled) mode can differ somewhat from the original mechanical mode, just like for aircraft wings. The results of the 3D computation is then summarised in terms of the distribution of the mean power due to unsteady pressure forces on the blade surface.

An example of such a distribution is shown on the TS27 wide chord fan suction side, for the 1st flex/4 diameters mode in unstarted operating conditions (fig. C.19). This picture shows that, as anticipated, the unsteady forces are concentrated around the strong shock wave location.

The mean power distribution can be integrated over the blade surface to yield the aerodynamic damping parameter, a measure of the stability of fluid/structure coupling. This can be evaluated for several operating conditions and thus used to determine probable supersonic flutter zones on the compressor map. This procedure has been validated on several civil engine and military engine fans. It is systematically used today in the fan design process, in order to anticipate a potential risk of supersonic flutter very early in the project.

3.5.2 FORCED RESPONSE ANALYSIS

Another source of fluid/structure interaction is the rotor/stator aerodynamic interaction. Each blade row is periodically impinged by the wakes coming from the upstream blade row(s) and submitted to potential interaction from the upstream and downstream blade row(s). The usual procedure in blade and vane design consists in avoiding too close proximity between the frequencies of blade or vane vibrating modes and the forced excitation frequencies linked to upstream and downstream bladerows, for rotation speeds corresponding to steady engine operation. This is achieved using the classic Campbell diagram.

In the case of most multistage compressor, however it is next to impossible to avoid all crossings with the required frequency margin. The designer therefore has to make a choice between several non-ideal configurations, mainly on the basis of prior empirical experience. But this is sometimes in conclusive or simply scarce, and it is possible to provide help in assessing how critical the possible configurations are, by using unsteady computations.

The first important piece of information is the aerodynamic damping of the vibration mode concerned by the interaction, at the rotation speed at which the frequency crossing occurs (and, say, on the compressor operating line). Considering that the flow on the operating line is not too far off-design, the aerodynamic damping is determined using the same 3D Euler code as for supersonic flutter studies.

The aerodynamic damping would probably be enough to choose between configurations but does not ascertain that any of the configuration of the blade forced response is in fact acceptable. This requires the computation of the blade forced response, which implies knowing the aerodynamic forcing function. As mentioned before, the origin of aerodynamic forcing is either potential (an effect which propagates upstream and downstream) or vortical (an effect which only propagates downstream by convection of the upstream airfoil wakes). Potential interaction can be dealt with using a full stage, rotor/stator computation, solving for example the Euler equations. Such a code is currently under development, for three dimensional configurations. Concerning vortical (i.e. blade/wake) interaction, the same 3D unsteady Euler code as for supersonic flutter is used, with vorticity (in the form of total pressure distributions) prescribed at the inlet of the computational domain.

Such a computation is illustrated on fig. C.10, showing contours of total pressure defect (with respect to the non-perturbed flow field) in the case of an HP blisk rotor submitted to upstream wakes [Berthillier et Al, 94]. In the general case, the wakes prescribed at the inlet are obtained using correlations. Unfortunately, this is probably a very poor approximation of reality in the case of a closed coupled rotor-stator configuration, where potential and wake effects strongly interact and cannot be considered separately. This would require full Navier-Stokes rotor stator simulation : such a code is currently under development, in quasi-3D, and has recently been run on a turbine configuration (see 4.3.2).

3.5.3 COMPRESSION SYSTEM STABILITY

In recent years, a large amount of work has been devoted to understanding the onset of stall and surge in axial compressors. This has mostly consisted in using simple (e.g. 2D, incompressible) models and experiments to provide a qualitative description of the phenomenon (although more and more high speed experiments are being run). More pragmatically, the compressor designer is faced with the important but difficult task of quantitatively predicting the surge line. Usually, this is done by using empirical criteria on parameters such as diffusion factors, flow incidence on blades or static pressure rise on endwalls, all obtained from an off-design throughflow calculation. By comparison, a numerical method capable of predicting surge on the basis of a theoretical model requires many features ; first, it must take into account the whole compression system, i.e. all parts involved in the compressor stability : the compressor itself, the downstream volume and the throttling device which controls the operating condition of the compressor. Secondly, boundary layer growth on the compressor blades and endwalls must be modelled in a way which permits to accurately predict the compressor speedline at off-design conditions (in this point lies the main limitation of the method's accuracy : it is commonly said that surge line prediction can be made accurate ... once the experimental compressor map is known !). Thirdly, it has to be an unsteady method in order to adequately reproduce the onset of the unstable phenomenon.

The simplest level of modelling which fits this description is a time-linearised method, with 1D fluid equations integrated on cells each comprising a blade row or a full stage. Fluid perturbations in the compressor are then solution of a linear system, the eigenvalues of which represent the frequency and growth of these perturbations. Such a method is currently in use at Snecma, integrated with a 1D throughflow method to provide fast and reliable surge line prediction for HP compressors.

However, the method mentioned above is not adequate to deal with low hub-to-tip ratio machines or ones with strong flowpath curvature and radial variations. Snecma recently developed a new method to compute the flow in the compressor using the meridional approach, in co-operation with BERTIN. Unlike the streamline curvature method, this code solves the pitch-averaged Euler equations with the same time-marching, finite volume technique used in 3D Euler solvers above mentioned. Additional source terms are used in the blade and vane areas to model the blade forces exerted on the flow as well as viscous losses generation. In particular, this technique allows the direct prediction of started configurations, as presented on fig. C.23.

This method has been extended to deal with surge prediction. The multi-domain approach allows an easy addition of the downstream volume using a Quasi-2D grid, as shown on fig. C.21 behind a single stage compressor. This enables to take large volume into account and to correctly propagate acoustic waves in the axial direction with minimum computing requirements. Finally, different models of downstream throttle can be used. Fig. C.22 shows the surge inception cycle in the pressure ratio vs flowrate diagram of the single stage compressor shown in fig. C.21. Several stable operating points are shown, as well as the time evolution once the instability is reached. This method needs further developments before it can be used as a prediction tool in the design procedure, but these are very promising results.

In addition to surge line prediction, such a time accurate method is very useful as an investigation tool to determine where the instability starts from in the compressor, thus allowing design improvements. It is with this capability in mind that this method is currently being extended in three dimensions in an attempt to reproduce tangential instability mode (i.e. stall) in addition to axial ones (surge). It should be noted that active control of compression system instabilities is probably not achievable industrially without this sort of capability.

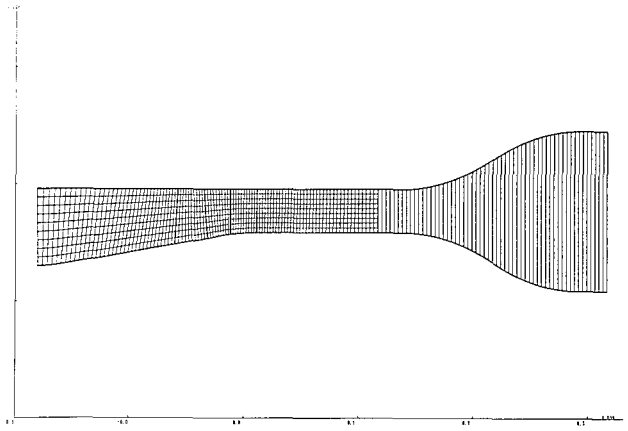

Fig. C.21 : Computational domain for unsteady throughflow calculation on CM7 compressor

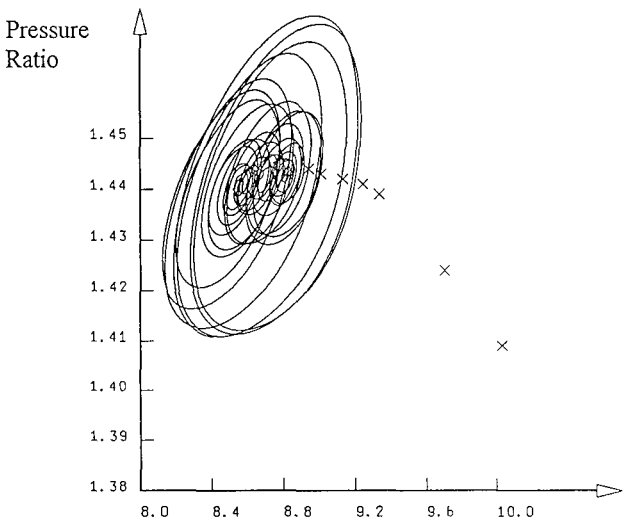

Fig. C.22 : Surge inception in CM7 compressor map computed with unsteady throughflow code

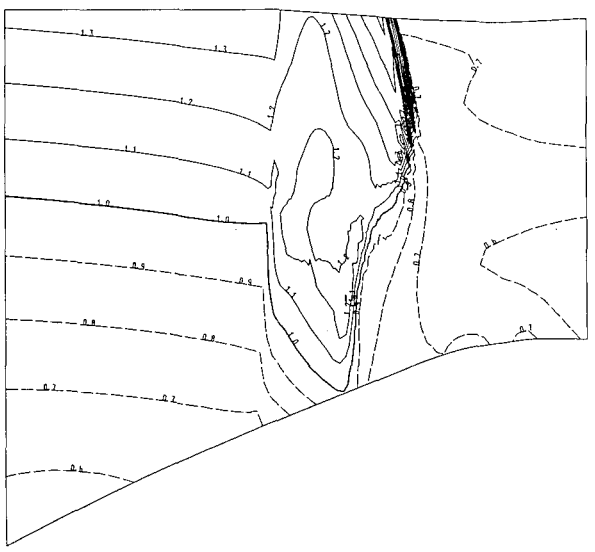

Fig. C.23 : TS27 time-marching throughflow computation of a steady started operating point : Relative Mach number

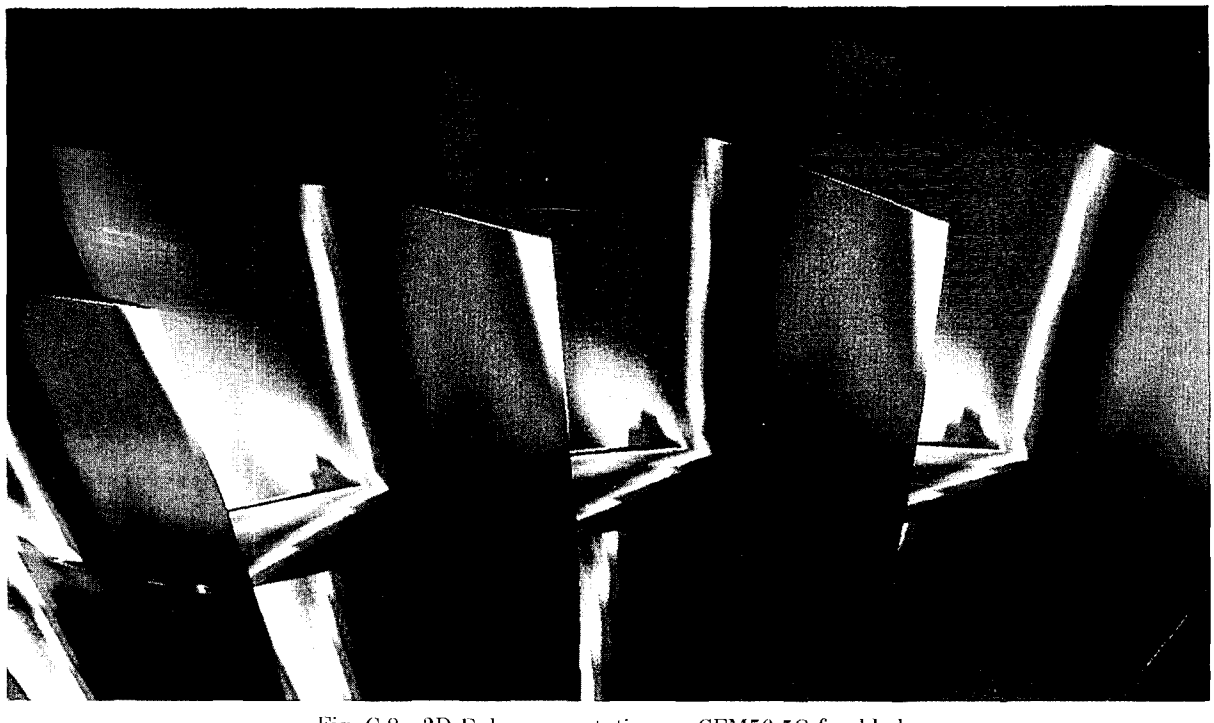

Fig. C.8 : 3D Euler computation on CFM56-5C fan blade : Mach number distribution around the shroud

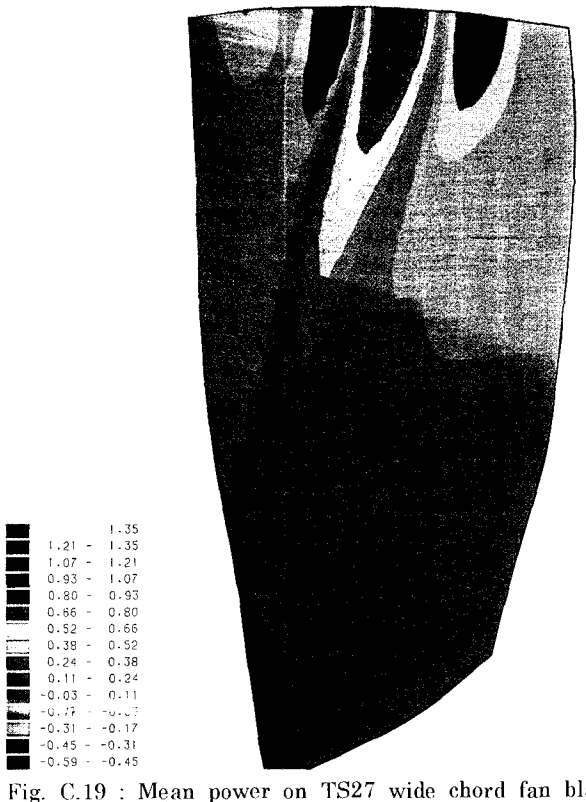

Fig. C.19 : Mean power on TS27 wide chord fan blade suction side. 1st flex/4 diameters mode

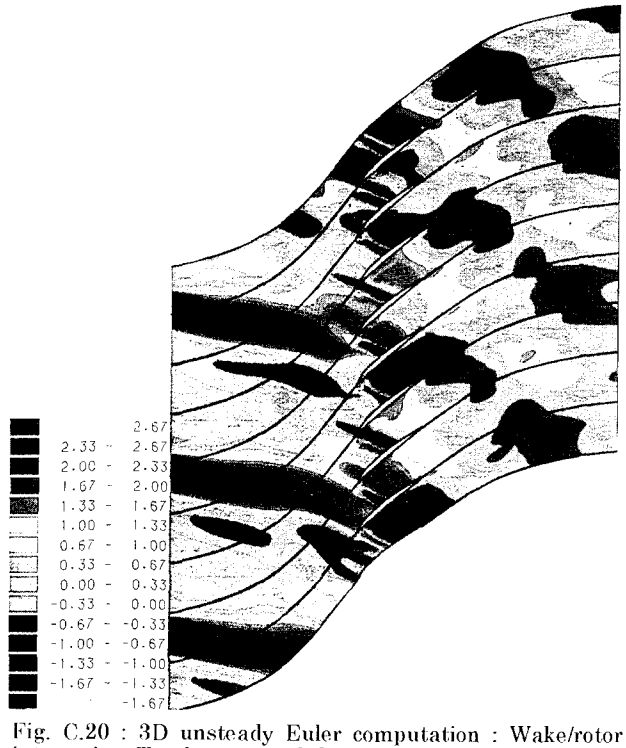

Fig. C.20 : 3D unsteady Euler computation : Wake/rotor interaction. Total pressure defect at mid-span

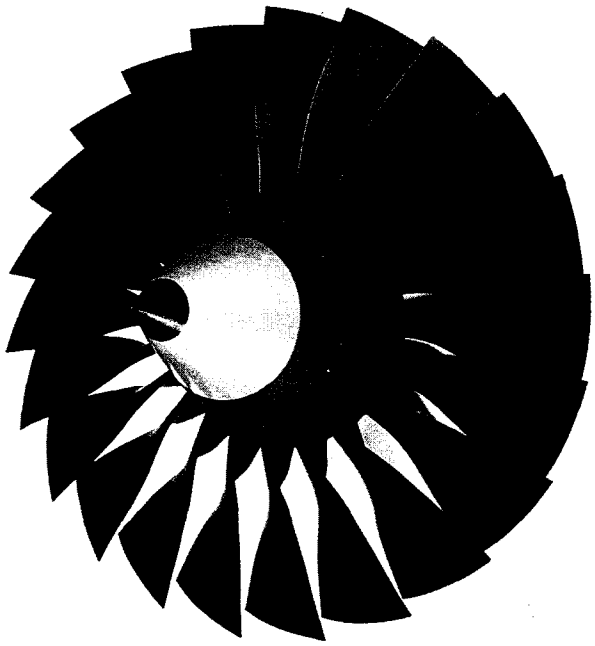

Fig. C.9 : TS27 experimental wide-chord fan

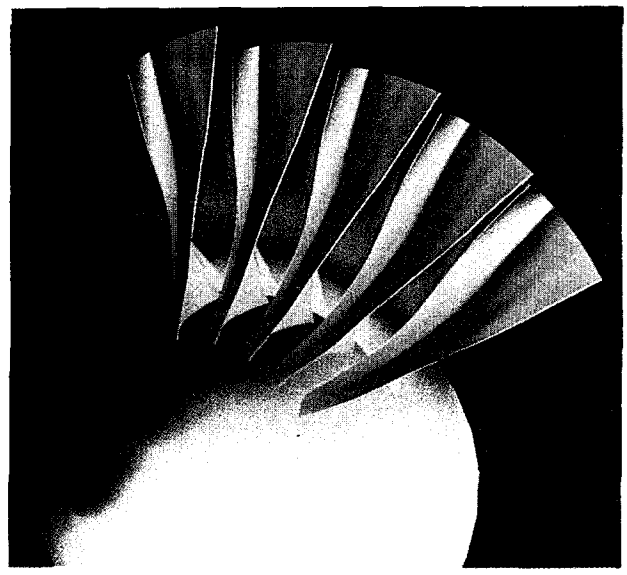

Fig. C.12 : 3D Navier-Stokes computation on a CFM56-7 fan intermediate version - Total relative pressure contours

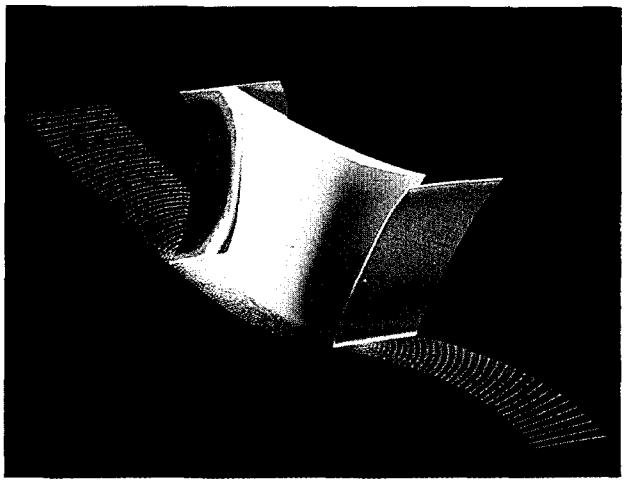

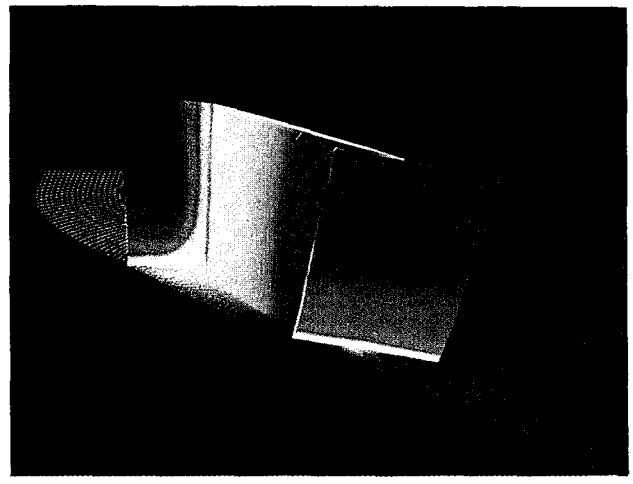

Fig. C.18 : 3D Navier-Stokes results on rotor 3 and stator 3 of H4 compressor : Relative total pressure

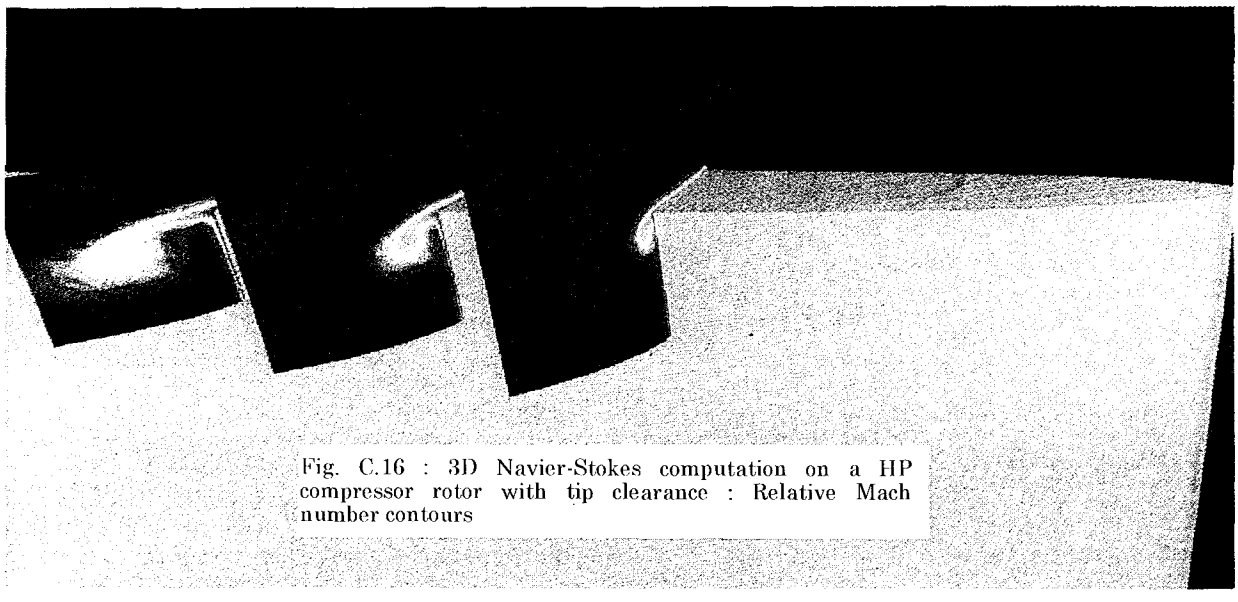

Fig. C.16 : 3D Navier-Stokes computation on a HP compressor rotor with tip clearance : Relative Mach number contours

4°) CFD APPLICATIONS ON TURBINE DESIGN

4.1 INTRODUCTION

We have seen that the same methods are used for the prediction of flows in compressors and turbines. However, these flows are much different : turbine blades are thick, have round leading and trailing edges and some of them are drilled by hundreds of cooling holes. The flows are strongly accelerated and boundary layers are usually thin. But of course, one major difference is due to the high temperatures encountered in high pressure turbines.

The turbine aero and cooling designer's task can be divided into the few several items :

1. To predict accurate through-flow and blade to blade flows and the associated losses including cooling flows,
2. To predict heat transfer at the wall with and without cooling,
3. To predict heat transfer inside the blades in the cooling channels,
4. To predict and to model the flows in rotating cavities (rotor/rotor and rotor/stator) of cooling devices.

In all these domains, the past five years have seen a very rapid evolution of the prediction methods (for a detailed review about the numerical methods and design methodology, written in the end of the 80s, see [Bry, 89]). For blade to blade flow analysis, the integration of steady viscous (quasi-3D and 3D) flow solvers in the design process is certainly the most important point. For the other points, the integration of new computation methods is not yet completed although many interesting calculations have been performed in 3D cooling channels or in rotating cavities.

In low pressure turbines, the profile and secondary flow losses are the primary cause of losses, but in high pressure turbines, many other sources of losses are also present : base losses, shock losses, tip leakage flow losses for unshrouded rotors, cooling and mixing losses and at last unsteady flow losses. Once added altogether, these individual losses lead to high levels of losses even for a single stage turbine, and they also have to be predicted accurately. Till now, the prediction method was based on the decoupling of all these individual sources and the global losses predicted were the result of a sequential process involving up to about ten different methods. The new methods as for instance the Navier-Stokes methods give the opportunity to treat all these phenomena in a fully integrated manner.

High pressure turbines are thus much more difficult to design than low pressure turbines because all the phenomena listed above have to be optimised simultaneously. That is why current research has been for a long time focused on the analysis and performance prediction of the flows in high pressure turbines. Heat transfer for instance must be predicted accurately as life duration or mass strongly depend on it. This is one of the most difficult task because wall heat transfer is characterised by local values that directly depend on the whole three-dimensional field of velocity, while wall pressure distributions can be more readily computed.

At last, the unsteady flows have to be computed. The principal purpose is to obtain the aerodynamic losses as they modify the operating conditions of the different turbine stages, but these phenomena have also an important effect on heat transfer; this is the case for the combustor emitted hot streaks that modify heat transfer on turbine rotor pressure surfaces.

Moreover, analysis must not only be considered as useful in the direct mode which enables the designer to make a final judgement about the performance of one given turbine, but also as able to give important information in the preliminary phases of a design. Thus, 3D design takes benefit from many direct analyses to deduce for example the 3D shape of an airfoil. This means that the analysis methods are part of the design process as early as possible.

The following sections will give a few examples illustrating the previously mentioned topics and show all the gains obtained from CFD for turbine design.

4.2 COMPUTATION OF STEADY FLOWS IN TURBINES

4.2.1 3D DESIGN

Three-dimensional design is based on the three-dimensional optimisation of the characteristics of the flow. This means that the designer tries to modify the three-dimensional shape of the turbine blades and flow-path in order to minimise the losses created by 3D components of the flow or to improve the working conditions for a stage as a whole. This cannot be obtained without full 3D calculation tools capable of predicting accurately the detailed flow characteristics, because most of the 3D phenomena and vortices are originally linked to very small aerodynamic structures such as corner vortices or leakage flows. The knowledge of the boundary conditions is also of major importance as it can be shown that part of the secondary flows in blade channels could take their origin in the sheared upstream boundary layers [Vialonga, 1992]. This is the reason why a section will be devoted to the comparison of pitch-averaged Navier-Stokes results and through-flow calculation results.

3D Euler studies

Before speaking about 3D Navier-Stokes numerical predictions, it may be useful to recall a few things about 3D Euler computations as they bring important information about the three-dimensional pressure field and can be useful tools for a first simple 3D optimisation [Vialonga, 1992]. This is due to the high Reynolds number encountered in turbine blade channels. It has thus been demonstrated that important pressure distribution changes could be obtained by the modification of the stacking line of the blades. The work was performed on a low pressure nozzle guide vane with adapted inlet total pressure profiles. The exit flow angles were modified as well.

3D Navier-Stokes method for turbine blade channels

As the actual flows are fully three-dimensional and viscous, the 3D Navier-Stokes codes are well adapted to 3D steady design. However, the so-called '3D design' cannot be efficient without completely validated and automated methods because the modifications of the profiles will be inferred from the informations obtained from the calculation results.

The computational grid used for turbine blade channels 3D Navier-Stokes calculations is a simple three zone grid (H+O+H) already described by Heider [Heider, 1993]. The current grid counts up to 700,000 points per channel. The same type of grid is used for any type of blades including turbine rear frame struts. Of course a few parameters can be chosen if necessary, because of the various possible deviations or 3d shapes of the blades.

The validation of the code has been performed on several types of blades including low pressure turbine blades as well as high pressure transonic turbine blades. The important parameters for the validation are the exit flow angles and the total pressure profiles. The informations obtained on the total temperature profiles are also of prime interest as they closely depend on the secondary flows and used to be calculated by empirical methods based on correlations.

Rotor with tip clearance

A calculation of a transonic rotor blade with tip clearance has been performed [Heider, 1993] at Snecma with the same tool. This calculation has shown that in the case of turbine rotors, the tip leakage region could be divided into three parts. The first part is 'casing-driven' near the leading edge of the blade. The two other parts can be described as two layers sheared by the relative motion of the blade and casing. One is close to the casing and the flow is driven by it from the suction surface towards the pressure surface; the other one close to the tip of the blade is the region where the leakage vortex is created by the pressure driven flow from the pressure side of the blade to the suction side of the blade. Figure T.1 displays the grid used and the details of the leakage flow region and the exit flow. The tip leakage vortex losses are clearly distinguished and can be compared to the two counter-rotating passage vortices.

Through-flow - 3D Navier-Stokes calculation methods

The averaging techniques used are very important in the numerical design methodology. Following the advices written in the AGARD report on that topic [AGARD], Snecma uses several 'problem adapted' averaging techniques. For 3D design, the flow characteristics have to be averaged in such a way that the conserved flow equations are exactly those treated by the through-flow calculation method. This technique improves a lot the adequacy between 3D Navier-Stokes and 2D through-flow predictions.

The comparison between through-flow predictions and pitchwise averaged three-dimensional Navier-Stokes calculations is shown in figure T.2. A low pressure turbine stator vane in a strongly diverging channel is calculated at subsonic conditions. This vane has been tested in a cascade facility [Vialonga, 1992] and the actual working conditions are imposed at the inlet and at the exit planes in the through-flow calculation in such a way that the experimental results are accurately matched in the upstream and downstream planes closer to the vane . The conditions calculated by the through-flow calculation are then imposed in the 3D Navier-Stokes calculation in the experimental planes. The results displayed show the two different calculated structures. The discrepancies between the two can be seen close downstream of the blade, but it must be pointed out that some three-dimensional characteristics of the flow are caught by the through-flow modelling, especially in the front upper part of the blade.

The adequacy between 3D Navier-Stokes and 2D through-flow calculations had to be checked as the three-dimensional design of turbine blades relies for an important part on the accuracy of the prescribed boundary conditions in the 3D Navier-Stokes code. To be consistent, the same averaging techniques are used for the classical quasi-3D design methodology.

4.2.2 HEAT TRANSFER IN COOLED BLADE TURBINE CHANNELS

Introduction

The ever increasing gas temperatures in turbines lead to the need to predict accurately the heat transfer at the wall of the blades and casing. These walls are currently protected by film cooling or by cooling flows emitted in slots at the trailing edges. In the past years, the design methodology relied on heat transfer computed by boundary layer calculation methods and by empirical methods for film cooled blades. These methods are still currently used but tend to be replaced by Navier-Stokes methods with longer calculation durations but with an increased range of applications.

The results presented in the previous sections were treating purely aerodynamic flow fields. The same numerical methods have been extended to the prediction of flows with heat transfer at the wall. Computational results have been obtained with quasi-3D as well as with full 3D Navier-Stokes codes. The multi-domain approach has been systematically used in order to obtain a precise description of the geometric details. Figure T.3 shows that it is possible to obtain reasonable results for the prediction of heat transfer in a transonic nozzle guide vane. The experimental results were obtained at the Von Karman Institute for Fluid Dynamics in Belgium [Chanez, 1993].

HP Nozzle guide vane with cooled trailing edge : quasi-3d Navier-Stokes calculation

An important part of the losses generated in a high pressure turbine nozzle guide vane channel is located in the region of the trailing edge of the blade. For choked HP turbines, this region is transonic and the flow pattern in this region is rather complicated with several shocks emitted on suction surface and on pressure surface and interacting with the wake of the blade or impinging on the neighbouring airfoils. That is why it is important to be able to compute accurately the flow in this region. The calculations are complicated by the presence of cooling slots in the trailing edge. Several quasi-3d calculations of a HP nozzle guide vane with cooled trailing edge have been performed. The temperature ratio of the mainstream vs coolant flow are close to the actual ones. These calculations demonstrated the ability of this kind of tools for the prediction of the detailed flow pattern : the modifications of the shock structure by the cooling flow is predicted (see figure T.4) and the cooling efficiency in the slot can also be computed (see figure T.5) as well as the associated aerodynamic losses. This allows the designer to choose among several blowing rates or cooling configurations [Chanez, 1993].

HP Nozzle guide vane without cooling : full 3D Navier-Stokes calculation

Heat transfer at the wall is very much influenced by 3D phenomena such as secondary flows. A full 3D Navier-Stokes calculation with heat transfer has been run recently for a validation purpose. The results show the influence of the secondary flows on heat transfer, especially in the transonic zone of suction surface (Figure T.6). These results have been compared to the experimental results from VKI [ARTS, 1994] and can be also be considered as close enough to use this code for design. However, although an increased number of points was used, the grid was not refined enough in the vicinity of the hub or casing to obtain good heat transfer results on those particularly interesting regions. Further calculations are needed for the improvement of the ability of the code to predict heat transfer on hub and casings.

HP Nozzle guide vane with film cooling : full 3D Navier-Stokes of a slice of a blade

We have seen that a high number of discretization points is necessary for accurate heat transfer calculations. A complete calculation of a HP nozzle guide vane channel with film cooling is thus impossible with current available storage computer memories. In order to overcome this difficulty, a calculation of a two millimetre thick slice of a HP nozzle guide vane with film cooling on suction side and on pressure side has been run [Fougères, 1994]. The prediction of the efficiency in the film cooled region is displayed on figure T.7 and compared to experimental results and demonstrates a reasonable accuracy. Although quite difficult to run, such a calculation shows the tendency of using 3D Navier-Stokes codes in very complex turbomachinery configurations.

A few words about turbulence modelling

Internal flows are certainly a domain of much interest and difficulty for turbulence modelling. The results shown above have been obtained with a simple mixing length model. It seems that on typical geometries of turbine channels, and for nominal conditions, the high value of Reynolds number makes the mixing length models accurate enough for the turbine designer even for heat transfer coefficient prediction. This may not be the case when trying to compute heat transfer with injections because of the various turbulence scales involved and this is certainly not the case for the flows encountered in cooling channels or in rotating cavities with complex geometries. For these application, two transport equation models are necessary and are sometimes not good enough especially in the case of strong anisotropy of turbulence.

4.3 COMPUTATION OF UNSTEADY FLOWS IN TURBINES

4.3.1 INTRODUCTION

In the preceding sections were presented the 'classical steady flow' design tools for turbine blade channels. This level of analysis is well adapted to current design methodology. But the designer has also to take into account -or at least to be able to assess- the influence of the unsteady phenomena. These phenomena are of several types; concerning stator-rotor interaction, the potential fields attached to either a rotor or a stator interact between them as the blades rotate. However this phenomenon is of little concern except in the case of very short interfaces between stator and rotor rows. Much more important is the influence of the shocks attached to transonic blades. These shocks either emitted at the trailing edge or reflected on the suction surfaces of the blades finally impact on the downstream row of airfoils, periodically modifying the nature of the boundary layer on these airfoils. The influence of the shocks is enhanced by the strong azimuthal static pressure variations associated with shock structures. This is the cause of strong modifications of the flow in the front part of the downstream airfoils, leading to increased profile losses associated to separations and recirculating zones. This can also modify the heat transfer on the profile as far as the blade is concerned. The potential flow field and shock waves can be assessed by inviscid numerical calculations such as 3D unsteady Euler calculations.

The wakes of the blades are also one major source of unsteadiness in turbines. As any entropy generation, the total pressure drop of the wakes is convected downstream by the fluid and impinge on the following rows, modifying the average flow at the inlet of the channel. The calculation of the influence of the wakes has to be computed by Navier-Stokes solvers and this makes the task much more difficult than the computation of inviscid flows.

For unsteady flows, the same family of numerical methods is used as they already solve the unsteady sets of fluid equations. The unchanged numerical schemes are used and the treatment of boundary conditions are adapted to unsteady flows.

For Navier-Stokes computations, the meshing techniques described above for steady flows lead to very short time steps in the region of the walls or regions of high shearing of the flow. For unsteady computations it is necessary to keep a uniform time step in the overall grid and this leads to very little absolute values of time steps due to stability criteria in the small cells and thus to slow down convergence of the calculations. This also implies the numerical scheme employed to be very stable at very low time steps for the large cells of the grid.

4.3.2 STATOR / ROTOR INTERACTION

3d inviscid multi-row interactions

The most commonly used tool capable of computing unsteady phenomena is the 3D unsteady Euler method. Thanks to the multi-zonal approach, the multi-row version of this code takes benefit from the previous works done for the computation of steady flows.

Several calculations have been performed at Snecma on the interface between a one stage HP turbine and a LP turbine. The calculation takes into account 5 HP rotor pitches versus six LP stator vanes. The grid counts around 700,000 points. Figure T.8 shows one eighth of the total annulus of this interface and clearly demonstrates that the major source of unsteadiness is associated to the shocks emitted on the suction surface of the trailing edge of the rotor. The lower part of the figure shows the Mach number distribution at several moments and points out that the front part of the stator is very much affected by the varying upstream flow field. The pressure gradient along the profile becomes periodically strongly positive.

Quasi-3d unsteady viscous analysis

Some more recent works have been performed at ONERA for the simulation of unsteady quasi-three-dimensional viscous analysis. The details of the work will be published in a future paper by A. Fourmaux [Fourmaux, 1994]. This type of analysis is made possible thanks to the high CFL numbers used in the code.

Some results have been obtained at Snecma for the study of stator rotor interactions. Several types of meshes are used for the unsteady computations.

On figure T.9 the calculation grid is made of five rotor pitches / six stator pitches for the same type of turbine interface as the one presented for the previous Euler computations. The actual ratio of blade numbers is respected and this allows to assess the influence of the rotor operating conditions on the stator blades. One computational result is shown on figure T.10.

The next figures (T.11 & T.12) show the calculation mesh and the pressure field at one particular moment of a transonic high pressure turbine stage. The 'one stator / two rotor' configuration is close to the actual one and allows to obtain a qualitative information on the interface. This calculation demonstrates that the coupling of the two rows of airfoils is very strong and that the transonic rear part of the stator downstream of the throat is affected by unsteady phenomena. The shocks are reflected on the front part of the rotor blades and the wakes affect periodically a large part of the downstream channel.

This type of tool cannot be considered yet as being part of the design methodology cycle because of the difficulty of some aspects of the work, but it is noteworthy that it already affords a new direction of thinking and investigation. One could for instance optimise the reaction of a stage thanks to these numerical methods and predict more accurately the flow function of a given turbine stage.

The results obtained with this type of computations are also very much dependent on the turbulence models used and certainly have to be taken with great care when trying to obtain quantitative results on the values of heat transfer on leading edges for instance.

The next step is the computation of full 3D unsteady rotor - stator interaction. As the convergence time can be simply extrapolated from the quasi-3D results, it will soon be available to turbine designers. This will allow a more complete understanding of the behaviour of the multi-stage turbines and will offer new ways of improvement.

4.3.3 HOT STREAKS MIGRATION

The stator/rotor interaction is one topic among unsteady phenomena; the 3D Euler code has also been used in order to assess the amplitude of the 'hot streaks' in turbines. The hot streaks emitted by the combustor can be simulated by azimuthal temperature heterogeneities. The amplitude of the increase of total temperature is considered as being sufficiently high to modify the velocity triangle at the exit of the nozzle guide vanes and to lead to a segregation of the hot/cold gases in the relative frame of reference. The hot streaks impinge on the pressure surface of the rotor blades and tend to increase wall heat transfer periodically. As the heat transfer coefficients on pressure surfaces of rotor blades are very often higher than the calculated ones, recent works have been devoted to this topic. In our calculation, a moving stripe of hot gases is imposed at the inlet boundary of the rotor channel. The segregation of the hot and cold gases appears and the periodic increased heat transfer on the rotor surface is computed. However, this overheating seems much lower than the emitted hot streak amplitude (figure T.13). This will have to be confirmed by complementary calculations like quasi-3D Navier-Stokes calculations.

4.4 INTERNAL COOLING DEVICES

4.4.1 INTRODUCTION

The above sections were devoted to blade-to-blade flow analysis. These flows are characterised by high mainstream Reynolds numbers that lead to the decoupling between mainstream inviscid flow regions and viscous flow regions near walls. This has permitted to perform accurate calculations very early thanks to inviscid flow solvers and thus to develop adapted techniques for turbine design. Of course, this could not be the case for internal flows such as those encountered in internal rotating cavities or internal blade cooling channels because these flows are much more complicated. They are highly three-dimensional and turbulent, and many effects appear that could be firstly neglected in the blade to blade analysis (i.e. influence of Coriolis forces or rotation on turbulence). To be computed accurately, these flows have to be treated with more elaborated turbulence models such as two transport equations models.

For internal flows in rotating cavities or in cooling channels, Snecma uses a numerical method that is being developed at ONERA. This 3D Navier-Stokes solver has been presented by Dutoya [Dutoya, 91],[Dutoya, 92], it is adapted to complex geometries and several turbulence models are available with or without wall functions and with or without low Reynolds number treatments near walls. The most currently used turbulence model is the two-transport equations k-l model, where k is the turbulent kinetic energy and l the mixing length [Vialonga, 1993].

4.4.2 COOLING CHANNELS

A full three dimensional calculation has been performed in a stator cooling channel. This channel is equipped with horizontal ribs on both suction and pressure surfaces. More than 150,000 points were necessary for the description of the geometry. Because of the large range of geometrical scales in this channel, the grid was difficult to build and may not be refined enough in the vicinity of the ribs.

The grid, the Mach number distribution and the total temperature distribution are presented on figure T.14 & T.15. The flow enters the channel in the front upper side and goes downwards to the exit for the supply of another cooling cavity. One can detect a zero-velocity zone in the upper part of the channel that has to be avoided for an efficient cooling. When studying in detail the three-dimensional structure of the flow, one can also notice that several ribs are passed over tangentially due to a secondary flow motion from the 'trailing edge' to the 'leading edge' of the cavity. This completely changes the rate of cooling efficiency in these zones and shows that the flow is far from being as simple as assumed in the classical correlation design methods. Although not completely quantitative, the results obtained in this calculation demonstrate that a first level of improvement of the cooling efficiency of blade channels can be inferred from the qualitative analysis of the computed cooling flow field.

4.4.3 INTERNAL ROTATING CAVITIES

The flows in the internal rotating cavities are very different from those encountered in the blade to blade channels or even in the internal cooling channels as they are very often driven by the rotation or even by buoyancy. The purpose of the designer is to be able to obtain a model of the flow in the complete cavity in order to choose among different types of correlations for the prediction of heat and momentum transfer at the disk walls. Thus, he wants to know precisely the way followed by the cooling flows emitted from any type of sealing. This cooling flow makes his way through an ensemble of large rotating structures at different rotational speeds and exchanges heat with walls. Figure T.16 shows the rotating structure in a typical rotor/rotor compressor cavity with axial flow at the axis. The lower part of the cavity is influenced by the axial flow and this leads to the existence of the three counter-rotating nuclei. The upper zone of the cavity shows a buoyancy region isolated from the axial flow. Two different radial temperature gradients lead to two different sizes of this region.

The validation of the numerical methods for these flow can be performed thanks to experimental results obtained on simple test configurations. The difficulty is here to obtain in the same time heat transfer and aerodynamical measurements.

The rotation momentum coefficients, heat transfer coefficients, etc... depend very much on boundary conditions and turbulence modelling, and it is admitted that classical turbulence models fail to predict accurate results in these configurations. Very often, the flow is assumed to be axisymmetric although the actual flows are certainly not. However, this assumption gives interesting results and avoids too heavy computational costs for full 3D calculation. Here again, the designer takes benefit from any information given by the analysis of the qualitative numerical results to build his model of the flow rotating in the cavity. As an illustration, Figure T.17 gives one example of the flow computed in a compressor stator well cavity, including the labyrinth seal.

4.5 TURBINE AND CFD : CONCLUSIONS

Current design of turbine blades integrates full 3D steady Navier-Stokes tools and has thus been partly modified by this new level of analysis. The designer has learned to pilot new parameters in his design such as averaged radial pressure distributions and to analyse more deeply the 3D components of the flow. This makes possible the optimisation of full stage operating conditions, by sometimes modifying the geometry of upstream blades without losses increase only to obtain a better behaviour of the downstream blade.

Moreover, quasi-3D unsteady Navier-Stokes codes can already be considered as available for turbine design. They allow the designer to study several parameters that are driving the unsteady losses as for instance the axial gap between two following rows of airfoils or the influence of reaction of a transonic stage on the losses.

For high aspect ratio turbine blades (especially shroudless), it is necessary to be able to predict the coupling between the mechanical stresses and the flow. As only subsonic turbines are concerned, it can be regarded as sufficient in a first time to run 3D Euler codes with unsteady upstream boundary conditions able to simulate wake passing. However, these problems are still very limited in current aircraft engines.

5°) CONCLUSION

The role of CFD in the design procedure of aeroengine compressor and turbine is fast-growing. Numerical simulation significantly contributes to reaching industrial objectives such as the reduction of cycle time and cost in a project development. It has already demonstrated its effectiveness on several applications, allowing an earlier and more reliable component optimisation.

The advances in computer technologies and the combined developments of CFD techniques constantly enlarge the field of possible applications. In this paper, a broad spectrum of examples in compressor and turbine design and analysis shows the capabilities of today's CFD methods.

However, the increasing importance of CFD requires special care to turn numerical methods into integrated tools easy to handle by component designers. Validation and calibration are essential to an effective use of advanced but still limited simulation techniques. Well instrumented experimental vehicles are definitely needed for this purpose.

The integration of 3D Navier-Stokes solvers in the design methodology of compressors and turbines represented a milestone and led to significant changes in the procedure. The development of unsteady applications makes the near future very promising. The next generation of computers using parallel architecture will make possible 3D viscous unsteady simulation on multiple row configurations, enabling a new step in component optimisation. However, much has to be done in numerical techniques and modelling of flow physics to turn this opportunity into an industrial achievement.

ACKNOWLEDGEMENTS :

A large part of the CFD developments presented in this paper has been supported by the French DRET and STPA. ONERA has been a major contributor to the development of the Euler and Navier-Stokes solvers. It must be emphasised that the results presented in this paper have been obtained by many co-workers at Snecma during the past three years. Their help in reviewing and shaping up the manuscript is also gratefully acknowledged.

The authors also wish to thank Snecma for permission to publish this paper.

REFERENCES :

AGARD ADVISORY REPORT N° 182 : Propulsion and Energetics Panel working group 14 on suitable averaging techniques in non uniform internal flows.

ARTS, T, HEIDER, R. : Aerodynamic and Thermal performances of a three-dimensional annular transonic guide vane. - Part 1 : Experimental investigation - Part 2 : 3D Navier-Stokes assessment, AIAA PAPER 94-2929 - 30th AIAA/ASME/SAE/ASEE Joint Propulsion Conference and Exhibit, Indianapolis, IN, June 27-29, 1994.

BERTHILLIER, M., DHAINAUT, M., BURGAUD, F., GARNIER, V. : A Numerical Method for the Prediction of Bladed Disk Forced Response, to be presented at ASME IGTI Turbo Expo 94.

BROCHET, J. : Aerodynamic Design of the CFM56-5C fan, The Leading Edge, GE Aircraft Engine Publication, April 1993.

BRY, P.F. : Blading design for cooled high pressure turbines, AGARD Lecture series 167 Blading Design for axial turbomachines, 1989.

CAHEN, J., COUAILLIER, V., DELERY, J., POT, T. : Validation of a Navier-Stokes Code using a k-ε turbulence model applied to a three-dimensional transsonic channel. AIAA Paper n° 93-0293, 1993.

CAMBIER, L., ESCANDE, B. : Three Dimensional Turbulent Flow Computation in a Linear Turbine Cascade. Paper n° 13, 74th AGARD PEP Conference, 1989.

CAMBIER, L., GHAZZI, W., VEUILLOT, J.P., VIVIAND, H. : A Multi-Domain Approach for the Computation of Viscous Transsonic Flows by Unsteady Type Methods. Recent Advances in Numerical Methods in Fluids, vol. III, Viscous Flow Computational Methods (W.G. HABASHI, ed.), Pineridge Pass, 1983.

CHANEZ, Ph., PETOT, B., JOURDREN, Ch. : Viscous analysis of high pressure inlet guide vane flow including cooling injections, AIAA Paper 93-1798, AIAA/SAE/ASME/ASEE 29th Joint propulsion conference and exhibit, MONTEREY, CA, June 28-30, 1993.

CHIMA, R.V., YOKOTA, J.W. : Numerical Analysis of Three-Dimensional Viscous Internal Flows, AIAA/ASME/ASCE/SIAM/APS First National Fluid Dynamics Congress, Cincinnati, 1988.

COUAILLIER, V. : Multigrid Method for Solving Euler and Navier-Stokes Equations in Two and Three Dimensions Proceedings of the 8th GAMM Conference on Numerical Methods in Fluid Mechanics, Delft, 1989.

COUAILLIER, V., VEYSSEYRE, Ph., VUILLOT, A.M. : 3D Navier-Stokes computations in transsonic compressor bladings. Xth ISOABE, Nottingham (U.K.), September 1-6, 1991.

DUTOYA, D., ERRERA, M. : Le code MATHILDA : modèles physiques, réseau de calcul et méthode numérique, ONERA RT N°42/3473, 1991.

DUTOYA, D., PONCELIN DE RAUCOURT, Ph. : Calculs aérothermiques dans les cavités interdisques de turbines, AGARD Conference proceedings 527 - Heat transfer and cooling in gas turbines (Le transfert thermique et le refroidissement dans les turbines à gaz).

FALCHETTI, F. and THOURAUD, P. : Methodology for Advanced Core Compressor Design. European Propulsion Forum, Köln, Conference Proceedings 90-014, DGLR-Bericht 90-01, pp 113-121, 1990.

FOUGERES, J.M., HEIDER, R. : Three dimensional Navier-Stokes prediction of heat transfer with film cooling, ASME Turbo Expo The Netherlands June 13-16, 1994.

FOURMAUX, A. : Assessment of a low storage technique for multi-stage turbomachine Navier-Stokes computations, Submitted to ASME Winter annual meeting, Chicago nov. 94, 1994.

GALLIMORE, S.J., CUMPSTY, N.A. : Spanwise Mixing in Multistage Axial Flow Compressors, ASME Journal of Turbomachinery, vol. 108, pp 2-16, 1986.

GEROLYMOS, G.A. : Advances in the Numerical Integration of the 3D Euler Equations in Vibrating Cascades, ASME Paper n° 92-GT-170, 1992.

GEROLYMOS, G.A. : Coupled 3D Aeroelastic Stability Analysis of Bladed Disks, ASME Paper n° 92-GT-171, 1992.

HEIDER, R., DUBOUE, J.M., PETOT, B., BILLONNET, G., COUAILLIER, V., LIAMIS, N. : Three-Dimensional analysis of turbine rotor flow including tip clearance, ASME paper 93-GT-111, 1993.

JAMESON A., SCHMIDT, W. and TURKEL E. : Numerical solution of the Euler Equations by Finite Volume Methods Using Runge-Kutta Time Stepping Schemes, AIAA paper n° 81-1259, 1981.

JONES, W.P., LAUNDER, B.E. : The Calculation of Low-Reynolds-Number Phenomena with a Two-Equation Model of Turbulence. J. of Heat and Mass Transfer, vol. 16, pp 1119-1130, 1973.

JONES, W.P., LAUNDER, B.E. : The Prediction of Laminarization with a Two-Equation Model of Turbulence. J. of Heat and Mass Transfer, vol. 15, pp 301-314, 1972.

KARADIMAS, G. : Application of Computational Systems to aircraft components development. 9th ISOABE, Athens, 1989.

KARADIMAS, G. : Design of High-Performance Fans Using Advanced Aerodynamic Codes, ASME Paper 88-GT-141, Amsterdam, 1988.

LERAT, A. : Implicit Methods of Second Order Accuracy for the Euler Equations, AIAA Journal, January 1985.

LERAT, A., SIDES, J. and DARU, V. : An Implicit Finite-Volume Method for Solving the Euler Equations, Lecture Notes in Physics, Vol. 170, pp 343-349, 1982.

MICHEL, R., QUEMARD, C. and DURAND, R. : Application d'un schéma de longueur de mélange à l'étude des couches limites turbulentes. ONERA NT n° 154, 1969.

NICOUD, D., BROCHET, J., GOUTINES, M. : A Methodology Proposal to Design and Analyse Counter Rotating High Speed Propellers, ASME Paper n° 89-GT-38, 1989.

NICOUD, D., LEBLOA, C., JACQUOTTE, O.P. : A Finite Element Inverse Method for the Design of Turbomachinery Blades, ASME Paper 91-GT-80, 1991.

THOMMEN, H.U. : Numerical Integration of the Navier-Stokes Equations, ZAMP, vol. 17, pp 369-384, 1966.

VEUILLOT, J.P. : Calcul Numérique de l'écoulement transsonique d'un fluide parfait dans une grille d'aubes. La Recherche Aérospatiale n° 1975-6, 1975.

VIALONGA, J., CHANEZ, Ph., PETOT, B. : Prédiction numérique de refroidissement et des échanges de chaleur dans les turbines de moteur d'avion, 30ème colloque AAAF, Nantes octobre 93, 1993.

VIALONGA, J., PETOT, B., CHIAPPA,T. : Assessment of a 3D Euler code for subsonic vane flows and study of the non radial stacking, ASME PAPER 92-GT-63, 1992.

VIVIAND, H., VEUILLOT, J.P. : Méthodes pseudo-instationnaires pour le calcul d'écoulements transsoniques. La Recherche Aérospatiale n° 1978-4, 1978.

VUILLEZ, C., VEUILLOT, J.P. : Quasi-3D Viscous Flow Computations in Subsonic and Transonic Turbomachinery Bladings, AIAA Paper n° 90-2126, 1990.

VUILLOT, A.M., COUAILLIER, V., LIAMIS, N. : 3-D Turbomachinery Euler and Navier-Stokes Calculations with a Multidomain Cell-Centered Approach. AIAA/SAE/ASME/ASEE 29th Joint Propulsion Conference and Exhibit, Monterey, CA (USA), 1993.

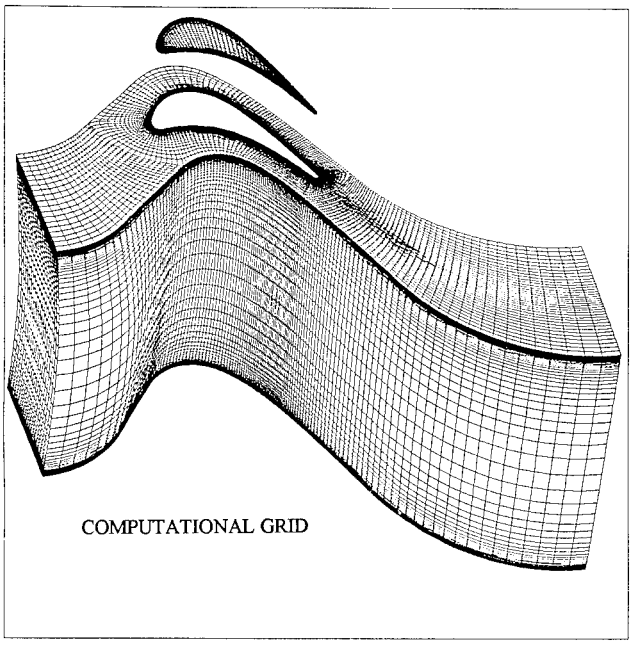

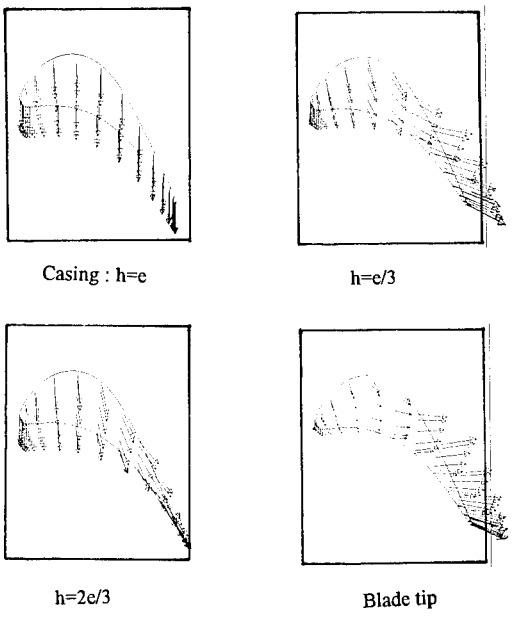

3D NAVIER-STOKES COMPUTATION OF A HIGH PRESSURE TURBINE ROTOR
WITH TIP CLEARANCE

FIGURE T1 :

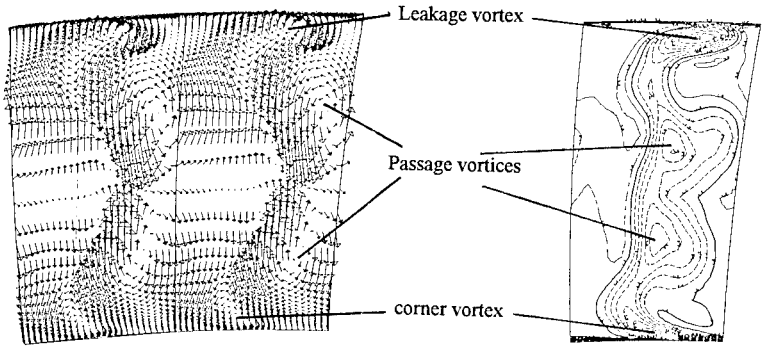

VELOCITY FIELD AFT LOOKING FWD TOTAL PRESSURE

AVERAGED 3D NAVIER-STOKES CALCULATION

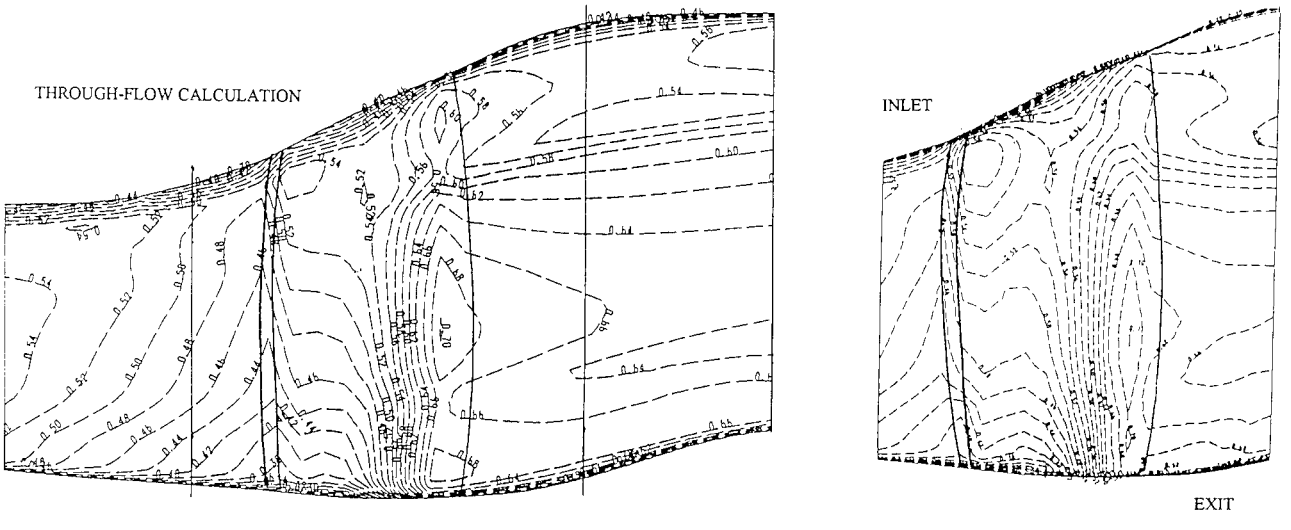

FIGURE T2 : COMPARISON OF PITCHWISE AVERAGED 3D NAVIER-STOKES AND 2D THROUGH-FLOW CALCULATION OF A LOW PRESSURE STATOR VANE

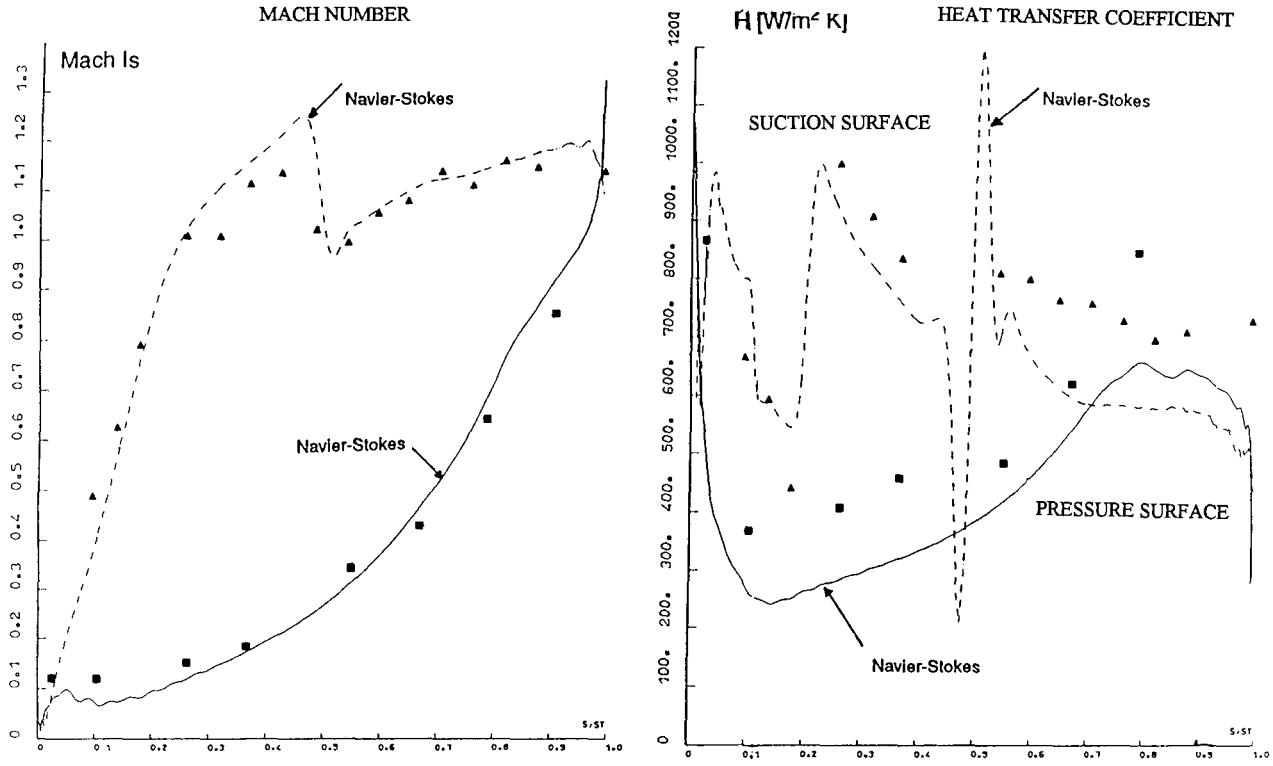

FIGURE T3 : VALIDATION OF QUASI-3D NAVIER-STOKES METHOD : MACH NUMBER DISTRIBUTION AND HEAT TRANSFER COEFFICIENT ON A HP TURBINE NOZZLE GUIDE VANE

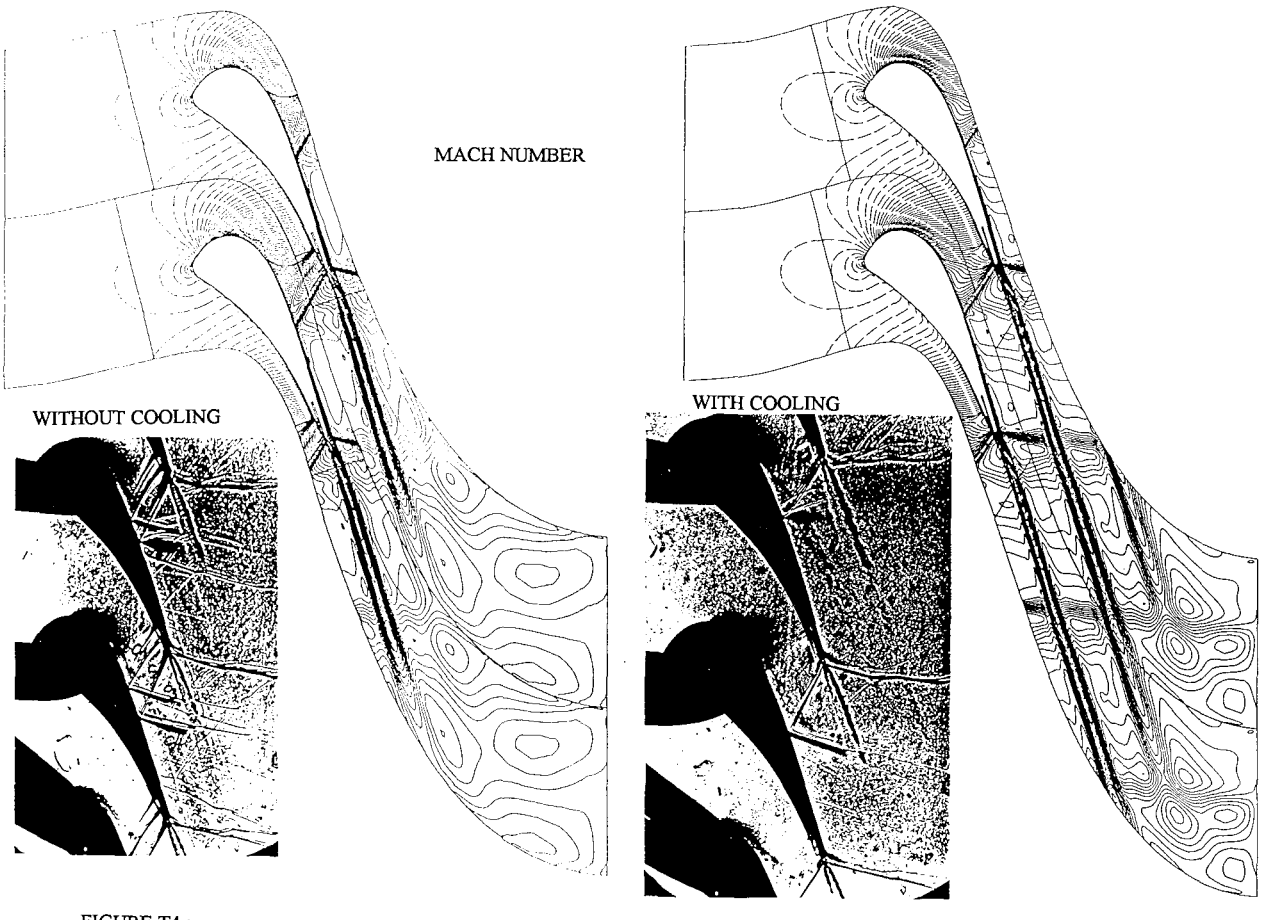

FIGURE T4 : VALIDATION OF QUASI-3D NAVIER-STOKES METHOD : MACH NUMBER DISTRIBUTION COEFFICIENT ON A HP TURBINE NOZZLE GUIDE VANE WITH AND WITHOUT COOLING FLOW AT TRAILING EDGE.

HP TURBINE INLET GUIDE VANE

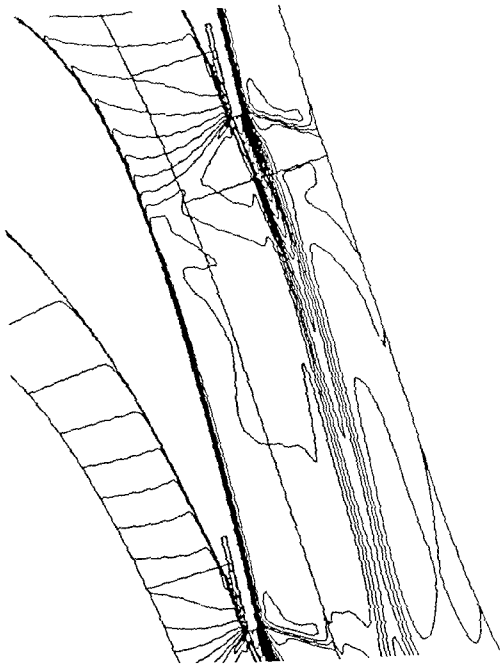

MACH NUMBER

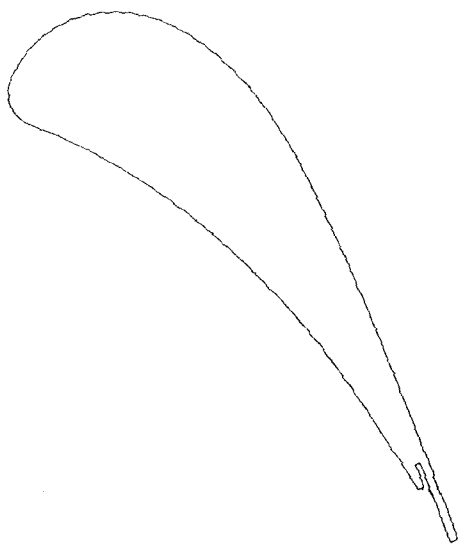

NOZZLE GUIDE VANE PROFILE

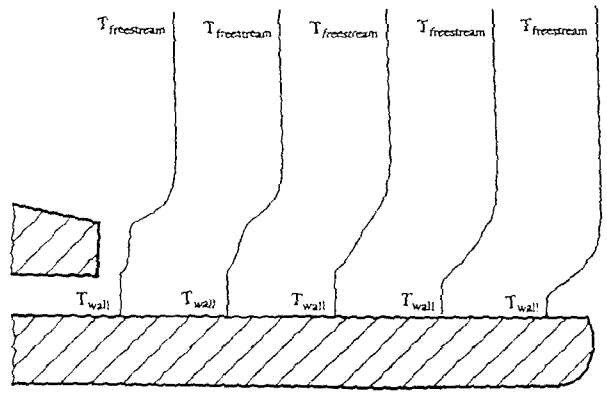

TRAILING EDGE COOLING

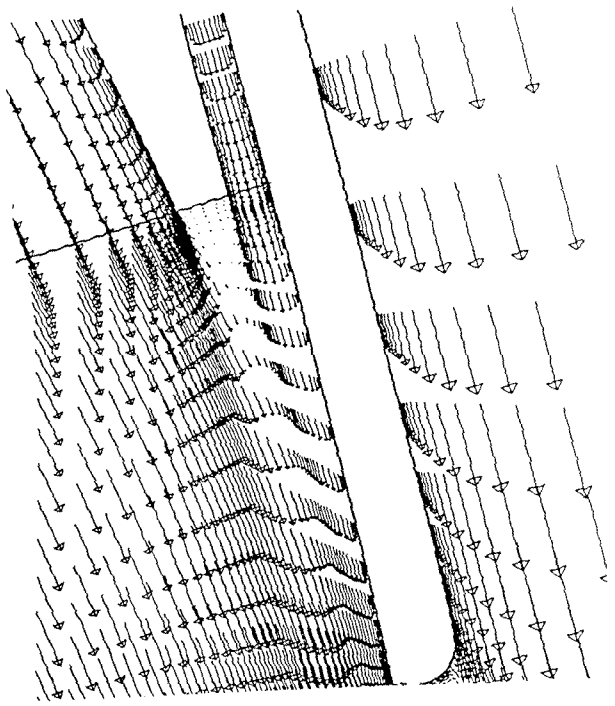

TRAILING EDGE VELOCITY FIELD

FIGURE T5 : VALIDATION OF QUASI-3D NAVIER-STOKES METHOD : HP TURBINE NOZZLE GUIDE VANE WITH COOLING FLOW AT TRAILING EDGE - DETAIL OF THE COOLING SLOT FLOW PATTERN.

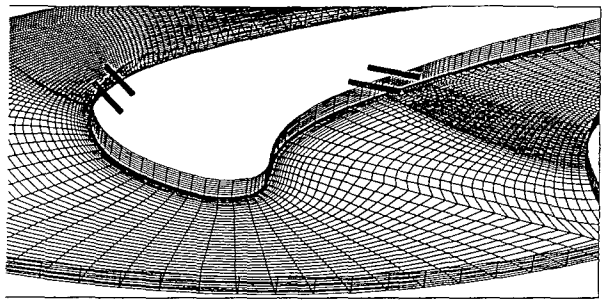

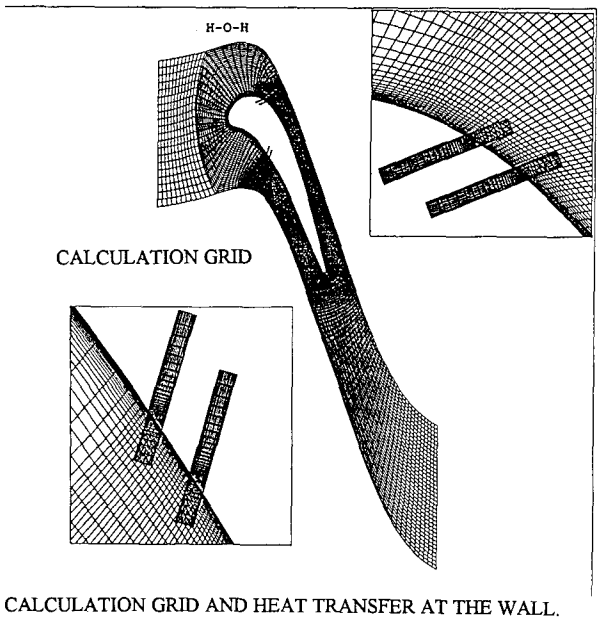

CALCULATION GRID AND HEAT TRANSFER AT THE WALL.

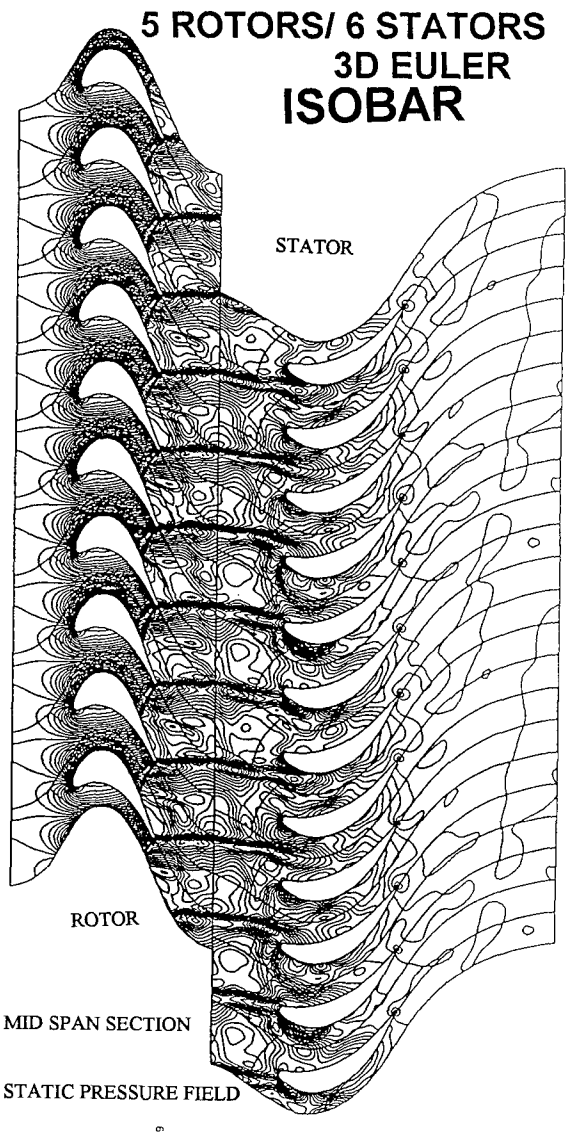

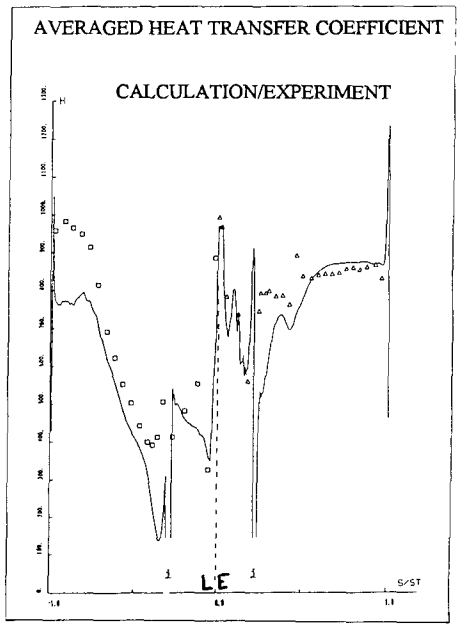

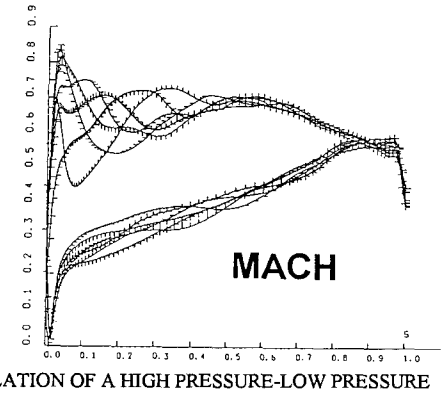

FIGURE T8 :
3D EULER UNSTEADY CALCULATION OF A HIGH PRESSURE-LOW PRESSURE TURBINE INTERFACE - STATIC PRESSURE FIELD - MACH NUMBER DISTRIBUTION ALONG THE LOW PRESSURE TURBINE STATOR VANE.

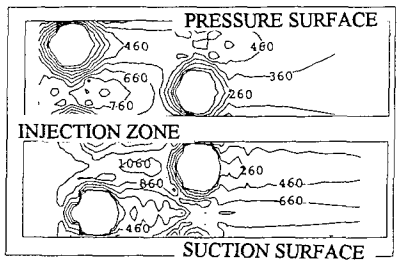

VALIDATION OF 3D NAVIER-STOKES METHOD
FIGURE T7 : HP TURBINE NOZZLE WITH FILM

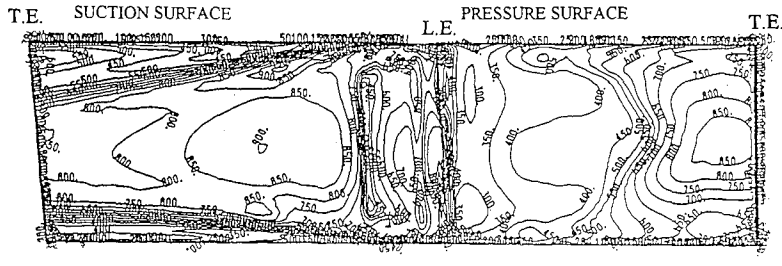

FIGURE T6 : VALIDATION OF 3D NAVIER-STOKES METHOD : HP TURBINE NOZZLE GUIDE VANE - HEAT TRANSFER COEFFICIENT ON BLADE SURFACE.

FIGURE T9 : COMPUTATIONAL GRID

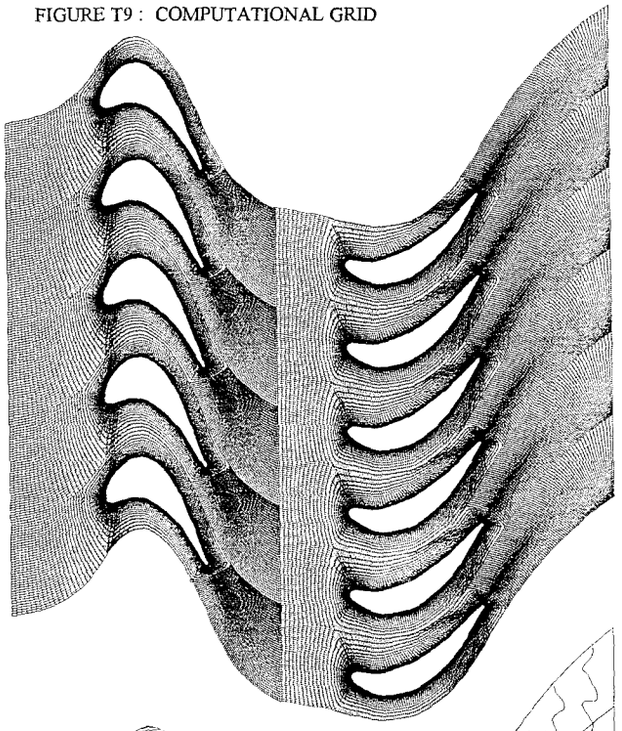

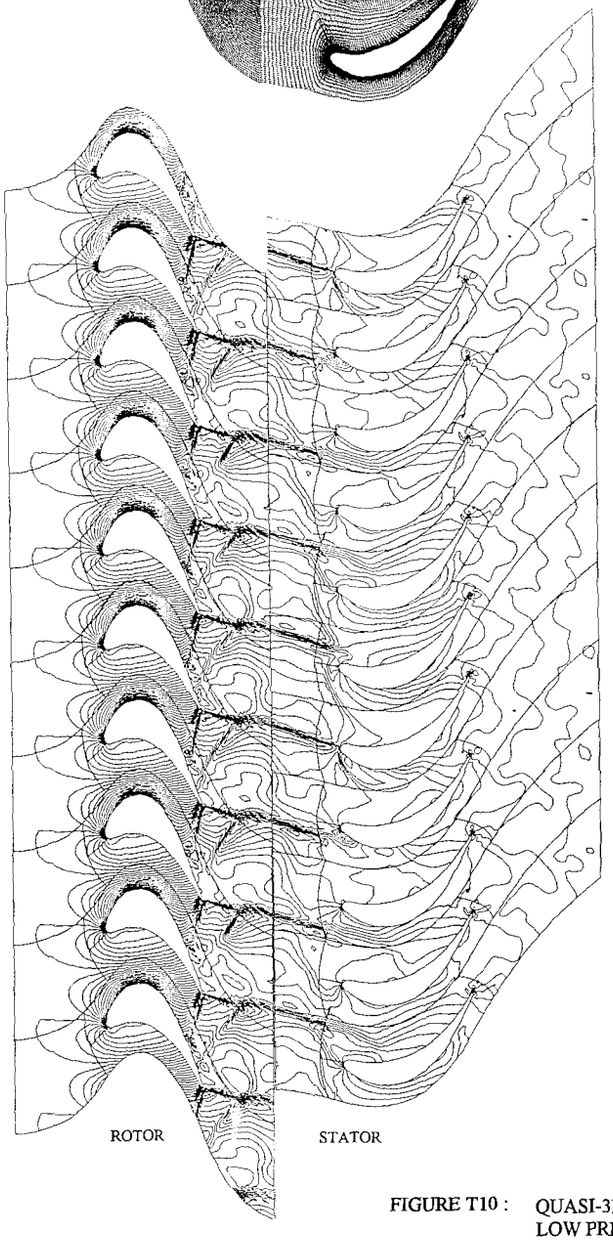

FIGURE T10 : QUASI-3D UNSTEADY NAVIER-STOKES COMPUTATION OF A HIGH PRESSURE-LOW PRESSURE TURBINE INTERFACE - STATIC PRESSURE FIELD

FIGURE T11 :
TRANSONIC TURBINE STAGE - COMPUTATIONAL GRID

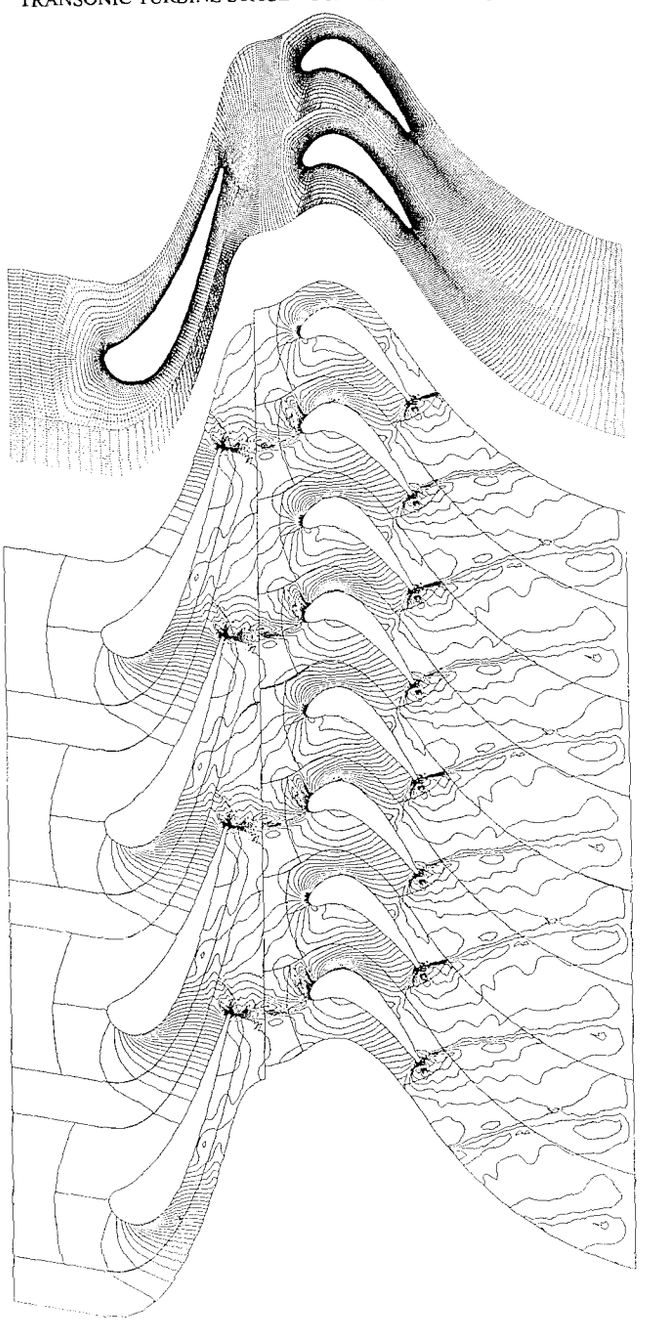

FIGURE T12 :
QUASI-3D UNSTEADY NAVIER-STOKES COMPUTATION
TRANSONIC TURBINE STAGE - STATIC PRESSURE FIELD

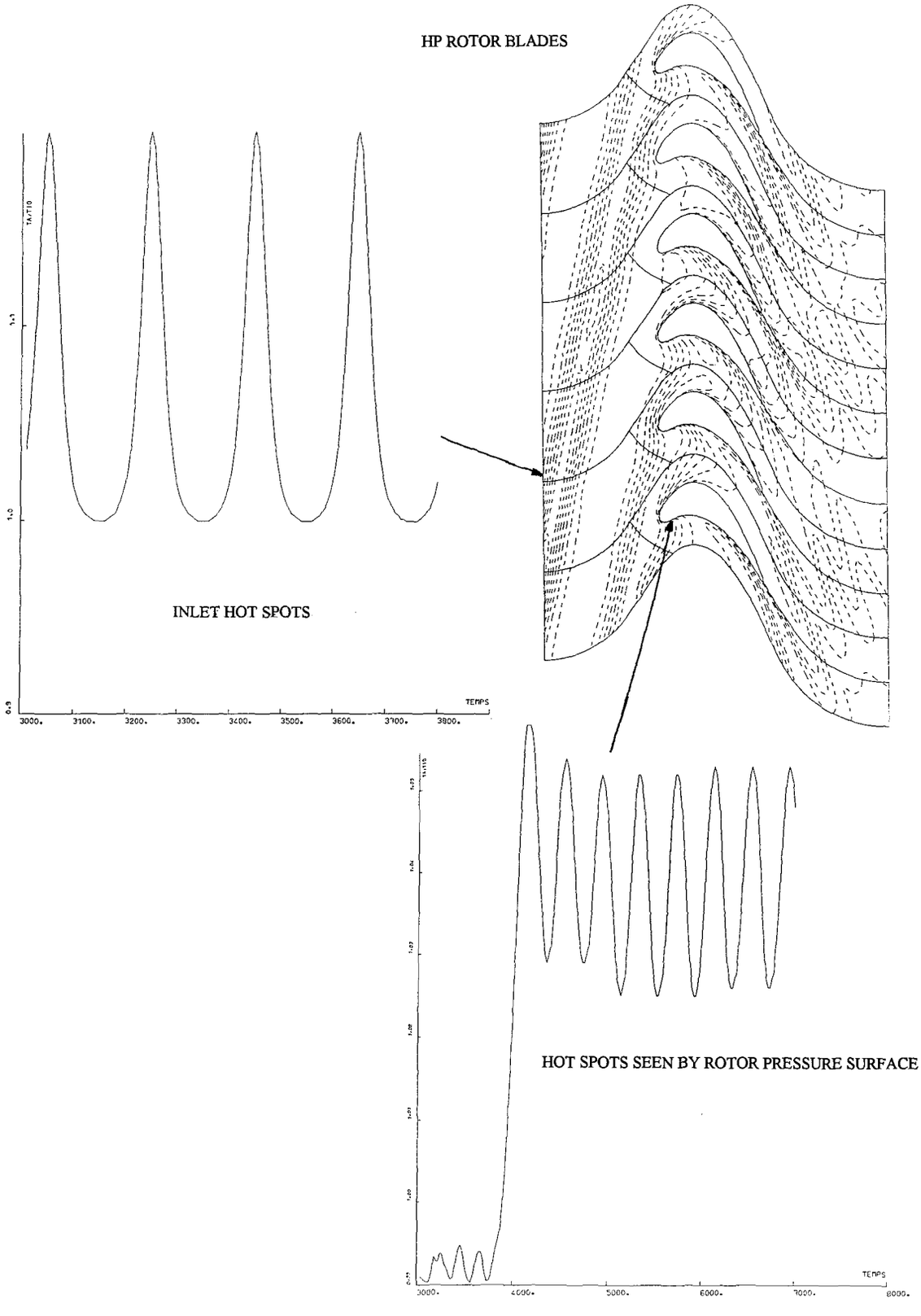

FIGURE T13 : HOT STREAKS INFLUENCE ON ROTOR BLADE PRESSURE SIDE - PERIODIC VARIATION OF TOTAL TEMPERATURE AT THE WALL

FIGURE T14 : 3D NAVIER-STOKES CALCULATION
COOLING CAVITY OF A LOW PRESSURE TURBINE STATOR

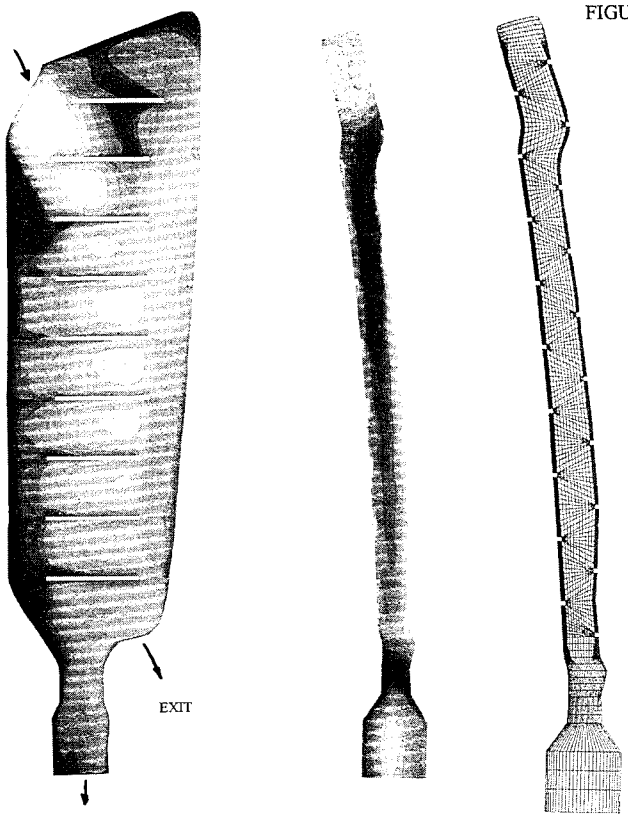

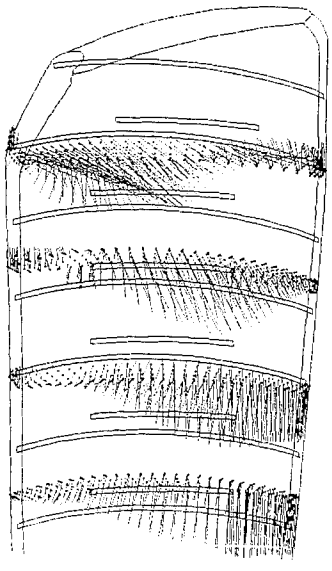

VELOCITY FIELD

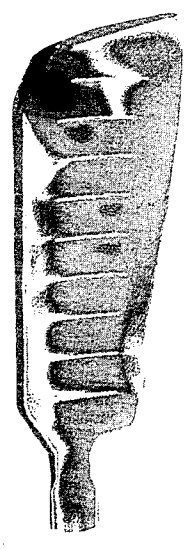

PRESSURE SURFACE

TOTAL TEMPERATURE FIELD

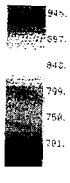

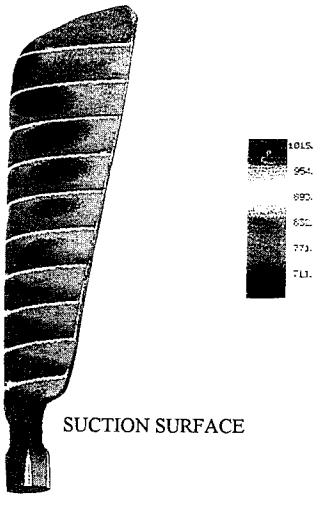

SUCTION SURFACE

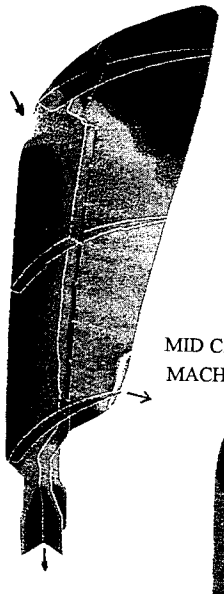

ZERO VELOCITY ZONE

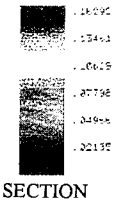

MID CAVITY SECTION
MACH NUMBER

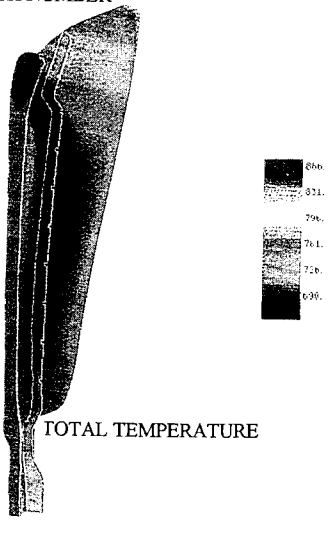

TOTAL TEMPERATURE

FIGURE T15 : 3D NAVIER-STOKES CALCULATION
COOLING CAVITY OF A LOW PRESSURE TURBINE STATOR

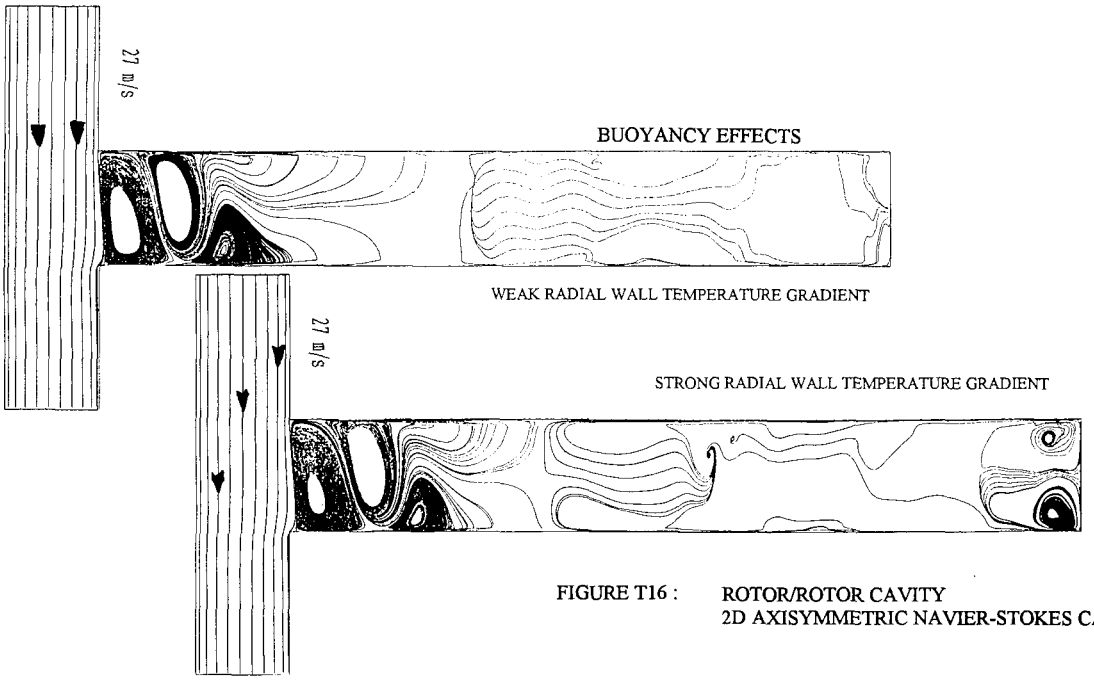

FIGURE T16 : ROTOR/ROTOR CAVITY
2D AXISYMMETRIC NAVIER-STOKES CALCULATION

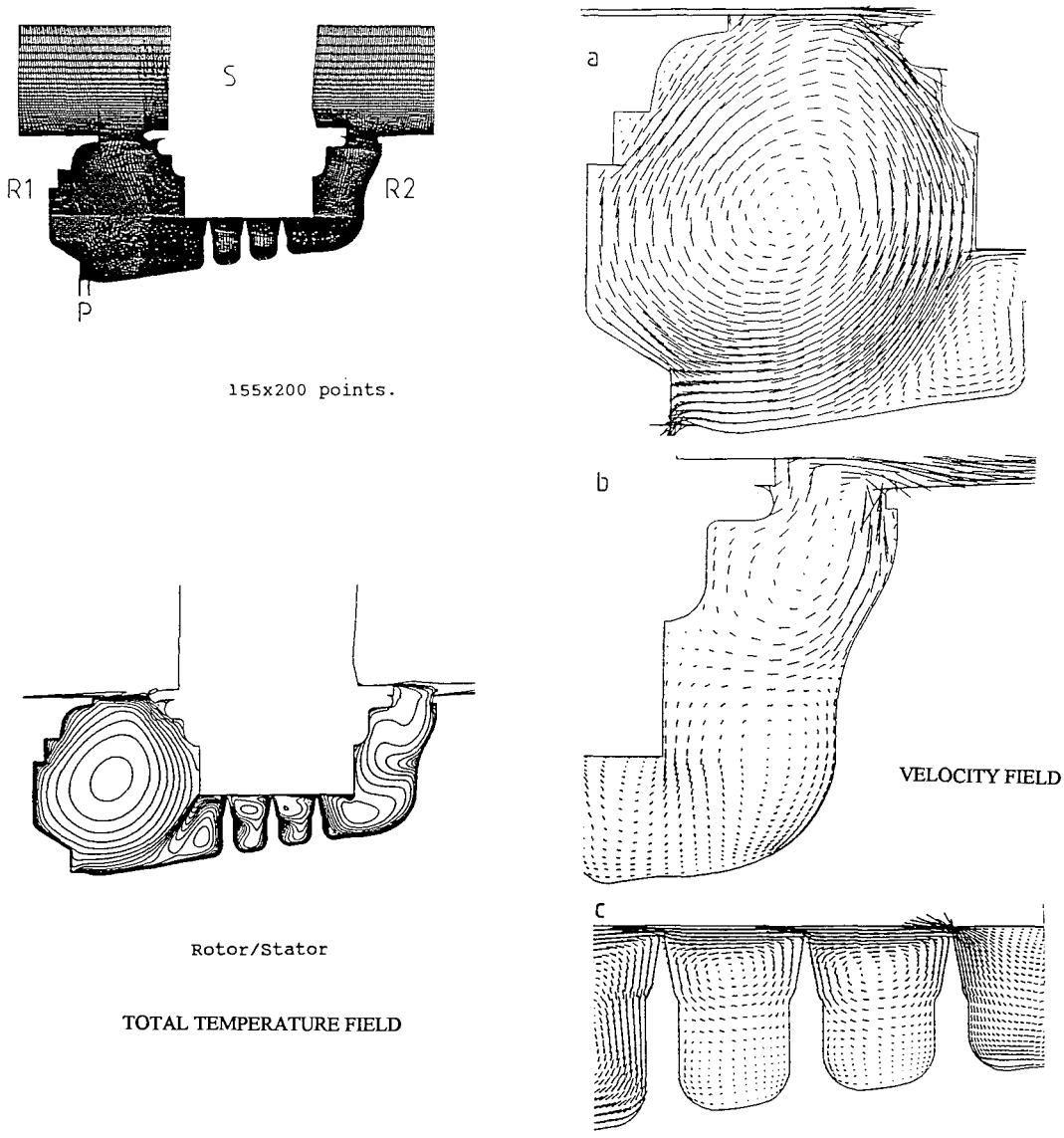

FIGURE T17 : 2D AXISYMMETRICAL NAVIER-STOKES CALCULATION
OF A COMPRESSOR STATOR WELL WITH LABYRINTH

THE ROLE OF CFD IN THE DESIGN PROCESS

by

Ian K. Jennions
GE Aircraft Engines
One Neumann Way, MD X409
Cincinnati, OH 45215-6301
United States

Abstract

Over the last decade the role played by CFD codes in turbomachinery design has changed remarkably. While convergence / stability or even the existance of unique solutions was discussed feverently ten years ago, CFD codes now form a valuable part of an overall integrated design system and have caused us to re-think much of what we do. The geometric and physical complexities addressed have also evolved, as have the number of software houses competing with in-house developers to provide solutions to daily design problems. This paper reviews how GE Aircraft Engines (GEAE) uses CFD in the turbomachinery design process and examines many of the issues faced in successful code implementation.

1 Introduction

This paper focusses on our own in-house efforts at GE Aircraft Engines (GEAE) and specifically on the development and design use of two codes : NOVAK2D and Viscous EULER. NOVAK2D is a quasi-3D unstructured adaptive solver while Viscous EULER is a 3D Navier-Stokes code specifically for the analysis of flow through blade rows. Issues such as grid generation and turbulence modelling will be discussed as they relate to each code. Some numerical background on each code is given in order that the capabilities and limitations of these codes are properly understood.

These codes will be discussed inside the framework of the GEAE design system with consideration given to pre-processing (geometry and grid generation) and post-processing (graphical and data output). As it is difficult to show actual commercial designs, this paper illustrates our current capabilities on geometries that are freely available. Design considerations and possibilities for improvement are pointed out.

The use of third party codes will also be discussed. Examples are taken from the heat transfer and installations areas where complex geometries are one of the main concerns.

Lastly, the lecture will address the current state of the art as viewed from industry. Topics surveyed will include multi-stage analysis, boundary layer transition and parallel processing. Examples from current development projects will be given.

2 NOVAK2D

2.1 Unstructured Background

During the mid 1980's it was realized that a structured grid code employing a single block grid would not allow designers to compute the flows around some of the more complex geometries they encounter. Multi-block approaches were becoming popular but limitations, particulary in terms of the number of grid points required to resolve the flow features, made them seem less attractive. Instead, a new approach based on an unstructured grid to which points could be adaptively added was pursued. The advantages claimed for this approach are: a) the capability of handling arbitrary geometries (e.g. multiple, dissimilar blades), b) the ability to resolve small scale features (e.g. flow around trailing edges, shocks), and c) freedom from the necessity of generating 'good' grids (the algorithm generates its own grid, given an initial

Presented at an AGARD Lecture Series on 'Turbomachinery Design Using CFD', May to June 1994.

coarse grid).

A two-dimensional inviscid code (TRIAD2D) was produced and is reported by Holmes et al. (1988). The code was subsequently extended to viscous flows (Connell et al., 1993) and renamed NOVAK2D in honor of Dick Novak, a longtime contributor to CFD at GEAE. Many changes in terms of grid generation and internal code structure were made along the way but the basic underlying philosophy given in these two papers remains essentially unchanged and is described below.

In order to aid the understanding of grid generation and the solution cycle, the inviscid capability is described before the viscous extension. The code solves the Euler or Navier-Stokes equations using a Runge-Kutta scheme, both Baldwin-Lomax and $k-\epsilon$ turbulence models are available. Emphasis is placed on the overall solution cycle rather than on the numerical details, which are very similar to those of Viscous EULER (discussed below), in order to give an appreciation of the power of this approach.

The extension of these codes to 3D has been made for inviscid flows (Connell and Holmes, 1993) and viscous flows are being worked. As these codes are not in production use for design, they are not included in this review.

2.2 Unstructured Solution Cycle

Figure 1 shows the overall structure of the solution process. The solution process is built around two key ideas. The first idea is that grids are made by creating solution points, without any knowledge of how they are to be connected into a grid, and then, in an entirely separate operation, connecting up the points into a triangular grid in some 'optimal' way. The second idea is that the solver is embedded in a cyclic process in which the solver alternates with grid adaption by refinement, i.e., by addition of solution points.

The solution process shown in Figure 1 begins with the creation of the initial grid points. The grid points need not be numerous enough to resolve all of the solution domain geometry, or all of the expected flow features; all that is needed is a crude set of points that can resolve the gross features of the flow. After the initial grid points are created, they are passed to the solution cycle. The solution cycle has four phases, and begins with the triangulator.

1. The grid points are connected by the triangulator into a grid. If the grid is the initial grid, all of the points are connected. If the grid is a refined grid, the new points are connected into the previous grid by local retriangulations, without the necessity of a complete new triangulation from scratch. The resulting grid is optimal in the sense that, given the point locations, the triangles created have the best possible aspect ratios.
2. The solver produces a solution on the grid from 1, converged only to the point at which the flow features have emerged. Full convergence is not required, or desirable.
3. The solution is tested to see if the flow is sufficiently well resolved. If it is, then the solver can be run to full convergence and the solution process is complete.
4. If more resolution is needed, new points are simply added where they are needed, without regard to how they will be connected into the grid. The refined grid is then thrown back into the triangulator (1) and the cycle continues.

2.3 Unstructured Mesh Generation

Fundamental to the mesh generation process is that the use of adaptive refinement greatly simplifies the task of creating the initial grid. The initial grid need not take into account the expected nature of the solution. A uniform and rather coarse distribution of points is sufficient.

Because the initial grid is uniform, the initial grid generation breaks down readily into a series of simple tasks.

1. The domain boundary is represented by a set of points that form the knots of parametric splines (Figure 2). Grid points are placed along the domain boundary. The boundary grid points are represented by square symbols in Figure 3. Parametric spline coefficients are computed from the input boundary data for later use in interpolating new boundary points.
2. A rectangular region, big enough to encompass the entire solution domain, is 'carpet bombed' with a uniform equilateral array of points, represented by the open and filled circular symbols in Figure 3.
3. The points outside the solution domain (the open circles in Figure 3) are deleted, as are points inside the domain, but too close to the boundary.
4. The remaining interior points and the exterior points are triangulated.

5. The grid is smoothed to eliminate possible grid irregularities near the boundaries, and retriangulated (Figure 4).

6. At this point the grid can be passed to the solver. It is usually worthwhile, however, to do some initial refinement based on the curvature of the grid boundaries. Each grid point on the boundary is examined, and if the angle between the boundary edges at that point exceeds some threshold - typically twenty degrees - all of the triangles sharing the boundary grid point are tagged for refinement. The refined grid is then retriangulated.

While the above process describes one method of generating meshes, an alternative, used more recently, is described by Holmes and Snyder (1988).

2.4 Unstructured Adaption

The criteria used for adaptive refinement of the grid are very simple. More complex criteria, such as truncation error estimates, might be used, but rather crude criteria have proved to be sufficient.

The solver is iterated until the solution approaches some specified level of convergence. This should not be complete convergence, but rather a level of convergence that assures some degree of stability in the solution. The refiner then checks the relative ranges of pressure, velocity, and total pressure in each triangle. If one of these relative ranges in a triangle exceeds some threshold, the refiner adds new points to increase the resolution of the solution in that triangle. The refinement may be done by adding three points at the midpoints of the triangle edges, or by adding one point at the triangle centroid (with a point added as well at the midpoint of any edge of the triangle that lies on the grid boundary). Either scheme produces acceptable refined grids. When the triangle size reaches some lower limit, the refinement is suppressed to prevent captured shocks from refining indefinitely. The Delauney triangulation then connects the refinement points, one by one, into the existing grid, using exactly the same algorithm as for the initial triangulation, and using the current triangulation as a starting point. Some grid smoothing may be used here to relax the grid point locations towards the average locations of the neighbouring points. This improves the grid point distribution. Finally, the solver takes the new grid and continues the solution cycle.

Special techniques must be used when adding refined points on curved grid boundaries. On a curved boundary, the edge midpoint will not fall on the true boundary (Figure 5). In this way, as the grid is refined, the true boundary shape emerges from the coarse initial grid.

Ni Bump. Over the years, three inviscid 'Ni bump' problems have become standard test cases for internal flow solvers (Ni, 1982). Solutions for the second Ni bump problem - a 10% height circular arc bump with a nominal Mach number of 0.675, are shown here to further explain the above procedure and show the quality of results that can be obtained with such an approach.

Before displaying the NOVAK2D solutions, we show a solution obtained for the second problem using EULER, i.e. Viscous EULER run inviscidly! This is a 3D structured mesh code, described in a subsequent Section. For this case only multigrid acceleration has been used. EULER is a 3D code that can also produce 2D solutions. There is some overhead involved in using EULER to solve a 2D problem: a true 2D solver would probably run about 50% faster than EULER.

The Ni bump grid for EULER contains 33x97 grid points, distributed uniformly. Figure 6 shows Mach number contours computed on this mesh, a bubble of supersonic flow appearing on the bump followed by a shock. The solution time on a CRAY XMP for 235 time steps, with four levels of multigrid, was 78 seconds, equivalent to roughly 50 seconds using a true 2D code.

The initial NOVAK2D grid has 53 grid points. Figure 7.g shows the Mach number contours obtained after NOVAK2D has solved and refined, producing a mesh containing 1263 grid points - less than half the number of mesh points of the EULER solution. Solution time on the CRAY XMP (which has the hardware gather/scatter needed to vectorize the key loops in NOVAK2D) for 2100 time steps was 33 seconds. Allowing for the difference in grid size, the EULER and NOVAK2D run times are comparable. One might have expected NOVAK2D to be ten or twenty times slower than EULER because it lacks multigrid and suffers a significant speed penalty on the CRAY because it can only vectorize via indirect addressing and hardware gather/scatter. NOVAK2D does as well as it does because much of the time-stepping is done on the initial coarser meshes.

The NOVAK2D solution is clearly much better - the shock is much more sharpely resolved than in the EULER solution. Figure 7 shows the whole sequence of grids and corresponding Mach number contours as the solution cycle (Figure 1) proceeds. Both the emergence of the body shape from the underlying cubic splines and the frugal use of grid points can clearly be seen.

2.5 Viscous Implementation

The usual practise in unstructured mesh codes is to employ a mesh comprised of purely triangular cells. When adaption by reinforcement is performed, the triangular cell divides into four smaller triangular cells (Figure 8). This can be very wasteful of points in regions such as boundary layers where only gradients in one direction need to be resolved. A better method is to use a control volume which may be preferentially refined in one direction, e.g. a quadrilateral (Figure 9).

The computationl mesh for viscous analyses is therefore generated by first placing a layer of quadrilateral elements around the body, extending down both sides of the expected wake centerline. Outside of this region, a triangular mesh generated as described above, is used.

Transonic Turbine Cascade. This geometry is the subject of experimental work at VPI&SU (Shelton et al., 1992) and represents a transonic rotor typical of modern gas turbine applications. This case was run over a range of pressure ratios. These pressure ratios are usually expressed in terms of an isentropic exit Mach number which ranged from 0.8 to 1.35.

The $k-\epsilon$ turbulence model was used for this case as trailing edge unsteadiness was observed with the Baldwin-Lomax model. Turbulence models are designed to enhance the laminar viscosity in order to model the small (sub grid) scale unsteadiness. However at the trailing edge of a turbine blade it is feasible to have a fine enough grid (especially with refinement) to resolve the vortex shedding process which is observed experimentally. The question arises as to what the turbulence model will do in these regions. Experimenting with both the Baldwin-Lomax and $k-\epsilon$ models indicated that the $k-\epsilon$ model produces a large enough turbulent viscosity to damp out the vortex shedding and hence make the trailing edge steady. The turbulent viscosity from the Baldwin-Lomax model tended to be too small to suppress this unsteadiness. On reflection this is not surprising as this model is designed for attached or mildly separated boundary layers which differ greatly from the trailing edge flow field.

The initial and final grids for an exit Mach number of 1.25 are shown in Figure 10. The quadrilateral region and the refinement performed to resolve the shocks and wakes can be clearly seen. Contours of Mach number are shown in Figure 11 for a range of exit Mach numbers. Comparisons with experimental data for pressure distribution and loss are given in Figures 12 and 13 respectively. The total pressure loss coefficient P_l is defined to be :

$$P_l = \frac{P_{t1} - P_{t2}}{P_{t1}}$$

where P_{t1} is the inlet total pressure and P_{t2} is the mass averaged exit total pressure.

The increase in loss with exit Mach number is well predicted and indicates that the loss arising from viscous and inviscid effects is being correctly predicted. The small shock on the suction surface which appears at an exit Mach number of 1.03 is not present in the experimental results

The final grids ranged in size from 2250 nodes for an exit Mach number of 0.83 to 7329 nodes for an exit Mach number of 1.25. CPU time on an HP720 workstation was between 25 minutes for the low exit Mach number case to 125 minutes for the high Mach number case. The increase in mesh size and consequent CPU time with exit Mach number is due to the presence of shocks. With an increase in Mach number to 1.35 the final mesh size jumps to 12,759 nodes as the wake moves outside the quadrilateral region and forces inefficient two dimensional refinement in the triangular region. This case serves to illustrate the efficiency of quadrilateral refinement for resolving viscous regions. Obviously to fix this problem the quadrilateral region would be expanded slightly.

Combustor dump diffuser. The previous case can be meshed and good quality solutions obtained with a structured mesh code. This case, however, demonstrates the capability of the algorithm on a complex geometry which is extremely difficult to mesh and solve using a structured mesh code. The geometry is an axisymmetric combustor dump diffuser. The function of the diffuser is not only to reduce the velocity of the combustor inlet air, but also to recover as much of the dynamic pressure as possible, and to present the liner with a smooth and stable flow (Lefebvre, 1983). The initial and final meshes are shown in Figure 14. The final mesh has 3584 nodes.

This case was run with the $k-\epsilon$ turbulence model. A velocity vector plot is given in Figure 15 where large recirculation regions can be clearly seen. The same flow features have been observed in a similar dump diffuser by other investigators (Shyy and Correa, 1985). The calculated flow split among the three exit passages is found to be in good agreement with experimental data from cold flow experiments conducted in a wooden diffuser model.

3 Viscous EULER

3.1 Background

In 1985 an Euler code (Holmes and Tong, 1985) was written for GE Aircraft Engines and subsequently used in the design of the Unducted Fan (Smith, 1987). The code was then further enhanced (Cedar and Holmes, 1989) to account for boundary layers, solid bodies such as part-span shrouds and engine splitters, and the presence of adjacent blade rows. It was used extensively in transonic fan design. Next, the viscous stress terms, viscous boundary conditions and Baldwin-Lomax turbulence model were added, followed by a novel implementation of the $k-\epsilon$ turbulence model as discussed by Turner and Jennions (1992). These progressive steps allowed for code development inside a common framework, both from a CFD code developer's and a designer's point of view, and consequently have increased designer productivity.

3.2 The Viscous EULER Code

The papers cited above describe the individual parts of the present code and Turner and Jennions (1992) describes the viscous numerics in some detail. This discussion of the code is therefore restricted to a brief description, emphasizing the main attributes of the solver, in order to provide background for the numerical simulations. As was mentioned previously, much of this discussion also applies to the NOVAK2D code.

The Reynolds averaged form of the full 3D Navier-Stokes equations including the energy equation written in Cartesian coordinates are solved. The flow is assumed to be compressible with adiabatic walls; supersonic and transonic solutions are allowed. The equations are cast in terms of absolute velocity but are solved in a relative non-Newtonian reference frame rotating with the blade. All that is needed to close this system of equations are models for the laminar and turbulent viscosity.

The laminar viscosity is modelled by Sutherland's law and a choice of turbulence model is provided. The Baldwin-Lomax model (Baldwin and Lomax, 1978) implemented as a nearest wall model for three-dimensional flows, was coded first. This model unfortunately contains very little turbomachinery physics as it was devised for external flows. In particular the model does not account for pressure gradient effects (Dawes, 1990), which we believe to be important in fans. As a consequence, the $k-\epsilon$ turbulence model (Launder and Spalding (1974) was also coded and used as the default model. In order to achieve engineering solutions in acceptable times both models use optional wall functions which yield the shear stress and shear work terms at wall boundaries. It is interesting to observe that as the Baldwin-Lomax model is not highly vectorized, as is the case with all Baldwin-Lomax models the authors have seen, both turbulence models take approximately the same computer time to execute.

The equations of motion are integrated to produce a cell centered finite volume flux balance which, with the addition of the usual second and fourth order smoothing terms, are solved using the explicit Runge-Kutta scheme of Jameson, Schmidt and Turkel (1981). Various stage schemes are available in the code with the default being the 5 stage scheme described by Cedar and Holmes (1989) which has good dissipative properties for use with multigrid. Velocity and temperature gradients are computed using auxiliary control volumes, an approach similar to that adopted by Kallinderis (1987). Local time stepping and multigrid are used to accelerate convergence. At present up to five levels of multigrid may be used, with V or W cycles and optional subiteration and smoothing. Residual averaging with constant coefficients (usually 1.0) is used to stabilize solutions rather than accelerate convergence. This was found to be necessary to converge fine grid cases with features such as overtip leakage and, as it adds very little computer time, is currently used as default. For a Runge-Kutta scheme with an odd number of partial steps the averaging is applied on the finest grid level and the odd steps only.

The $k-\epsilon$ turbulence model is discretized about the same flux balance control volumes used by the explicit flow solver, with k and ϵ stored at cell centers. The resulting equations are solved implicitly using an ADI scheme on a cross flow plane. Alternatively, the algebraic equations used in Baldwin-Lomax are solved on a cross flow plane with reference to the nearest wall. Although the number of explicit time steps per turbulent viscosity update (solving of the turbulence model) can be varied, in practice the viscosity is updated every time step. All viscous runs presented here use the $k-\epsilon$ model with wall functions.

Developing a code with this 'building block' approach results in a very flexible tool with many attractive features. Those that have not been mentioned so far are listed below.

- An option to use tip leakage has always been

available in the code and is being exercised with the viscous version.

- Solid bodies, e.g. part-span shrouds and engine splitters, are modeled as viscous and can be rotating or stationary. As we are using an implicit ADI solver for the k and ϵ equations this had to be modified to account for the triple grid lines which are used to define solid bodies in the code.

- Source terms are used to account for the average effects of adjacent blade rows. These source terms usually come from a through-flow analysis but could come from a separate 3D calculation in a manner similar to that used by Celestina, Mulac and Adamczyk (1986).

- The radial equilibrium exit boundary condition has been supplemented by the addition of an exit condition which allows no change in the cross stream pressure gradient between the next to last and the last streamwise cell center values. This boundary condition, although not totally non-reflective, allows vortices and shock waves to escape from the solution domain without causing spurious reflections.

Quality solutions depend on the control of numerical viscosity, i.e. an accurate differencing scheme, and a good grid. Because the Navier-Stokes solver is an extension of an Euler solver, the amount of numerical viscosity produced by the code for inviscid applications has been monitored extensively and gridding requirements have been established. The extension to quality viscous solutions can therefore be made knowing the underlying errors associated with a purely inviscid solution.

3.3 3D System

The 3D system of codes - preprocessing, solvers and postprocessing - is built around the use of binary files that separately contain the grid and flow information. These binary files permit storage of large amounts of data in a relatively small space. Conversion routines for transfer of files between computers (principally to and from the GE CRAY YMP), all of which are unseen by a designer, permit easy use of this format.

3.4 Overall Grid Generation

The grid generation part of the system consists of the following main steps, the exact number used depending on the complexity of the geometry to be modelled.

- Convert the quasi-3D design system files obtained from through-flow and blade-to-blade codes into a 3D blade passage description of the geometry. The meridional grid distribution on both suction and pressure surfaces is set in this code, which allows for the setting of lines along which solid bodies may appear.

- The passage wall distibution is then taken and a blade-to-blade grid is produced by solving a sequence of 2D grid sections from hub to casing. The blade-to-blade grid is generated by an elliptic grid generator which is described in more detail below. At this point we have a full 3D grid, which for a fixed stator would be complete.

- Tip and/or hub clearance is accomodated by placing grid lines in the tip/hub gap region and restretching the grid locally in order to obtain acceptable stretchings in the spanwise direction.

- Internal solid bodies are grown from an existing grid line that has been placed to run through the center of the body. Extra lines are placed to describe the upper and lower surfaces of the body, these lines being coincident with the central line upstream and downstream of the body. Leading and trailing edges are then matched to the real geometry and the grid relaxed in the neighbourhood of these bodies to produce lines that blend in smoothly with the surrounding grid.

- The flow conditions from the through-flow are mapped onto the grid to give a starting flow file for the 3D Navier-Stokes solver.

The grids produced by the above sequence are checked for near wall proximity in order that calculations are not performed outside the range of validity of the wall functions being used. Likewise, in all of the above gridding steps, multigrid requirements are adhered to. This amounts to areas with like boundary conditions, not crossing a triple line, being grouped together.

In the overall cycle time of producing a solution, a majority of the time is spent in creating good grids. The initial grid can take some time to produce, especially if new features (e.g. island splitters) have to be accomodated. However, once a gridding procedure is established future design iterations are regularly accomplished within a working day.

3.5 Grid Generation Details

The grid generation algorithm used is a modified form of the 2D NASA GRAPE program, developed by Sorenson (1980). The alterations maintain the basic core solver integrity while changing the general input and boundary setup routines to new turbomachinery specific routines which build a volume grid using an 'onion peel' approach. In addition, the program has an optional output format which allows a Quasi-3D grid to be developed. In this case a volume grid consisting of a single cell in the spanwise direction, whose height is adjusted to the lamina thickness predicted by a throughflow analysis, is generated. Although it lacks generality, the program requires few user inputs, making it more appropriate in an industrial design setting.

Two basic types of blade-to-blade grid are available : an H grid and an I grid (Figure 16). H grids are characterized by their cross-passage grid lines (outside of the blade row) beginning and ending at the same axial locations. This makes the imposition of periodic boundary conditions straightforward as there is good matching across the periodic boundary. An I grid has its cross-passage grid lines much more orthogonal to the streamwise running grid lines, resulting in a grid mismatch on the periodic boundaries. This makes the periodic boundary conditions much harder to implement (Turner et al., 1993) but gives much better shock resolution in cases were H grids would be highly sheared.

A simple illustration of this is given in Figure 17, where three types of grid are considered for the simple problem of a supersonic flow in a duct containing a small (3°) wedge in its bottom wall. The H grid with $\alpha = 0°$ represents the 'base case' and resolves the shock and resulting reflections reasonably well. However, if we now take exactly the same problem but shear the grid (Figure 17b), the shock system is degraded significantly at 70°(Figure 17e) and is completely lost at 80° (Figure 17f). As modern high pressure turbine vanes have exit metal angles around 80°, clearly any shock system would not be seen with this type of grid. The I grid, which for this case represents a simple rotation of the $\alpha = 0°$ H grid, produces the solution shown in Figure 17d and is therefore used for these high exit angle cases. A demonstration for a real case is given below. I grids could also be used for transonic fans were the tip staggers are very high and good H grids are hard to obtain.

3.6 Postprocessing

Postprocessing is mainly performed using an in-house code which runs in both interactive and batch modes on a number of different platforms, including the CRAY. The code principally deals with line or contour plots and for designer use runs in a batch mode with input dictating the plots to be produced. In this fashion the solver and postprocessor can be run together, plots of convergence history and engineering variables of interest being returned to the designer in order that the next design decision can be made.

Third party postprocessors are available on high-end workstations (e.g. IRIS). The FAST code (Walatka et al., 1992) is used for structured single and multi-block applications, while an implementation of Visual3 (Haimes and Giles, 1991) is used for unstructured and structured applications. Being a library of callable routines, Visual3 is extremely useful in that it enables the user to custom tailor the postprocessor to individual needs For example, the (m', θ) coordinate system is often used in turbomachinery to 'unwrap' surfaces. Using Visual3, calculations can be performed and displayed in this coordinate system, one that would not be found in a 'canned' postprocessor. The use of these tools (and others) in rendering complex 3D information in a meaningful way is growing rapidly.

3.7 Viscous EULER Simulations

VKI-LS82, 2D Turbine Nozzle. A Von Karman Institute (VKI) gas turbine nozzle guide vane (VKI-LS82) presented at a VKI Workshop (1982) demonstrates the relative capabilities of H versus I grid on a real 2D geometry. This vane has a leaving angle around 80° and test data, including surface static pressure measurements, are available for comparison.

The entire 2D I grid, with 48 cells in the blade-to-blade direction and 224 cells in the flow-wise direction, is shown in Figure 18a (where only every fourth line is shown for clarity) with an enlargement of the throat region (for the full grid) in Figure 18b. The grid is reasonably orthogonal, given that a good number of points are required around the trailing edge and the grid must be pulled into this region by the elliptic solver in order to maintain good definition. The blade is positioned in the center of the grid with the periodic lines, across which there is a grid mis-match, running between two adjacent blades. The grid shape (Figure 18a) mimics the axial inlet of the flow and the turning of the flow through the vane, while being gradually turned back to axial from the trailing edge.

The resulting isentropic Mach numbers from both test and computation are shown in Figure

18d for a variety of exit isentropic Mach numbers, ranging from subsonic to supersonic. The two subsonic conditions are well predicted, including a slight overspeed on the suction surface that develops at x/c = 0.27 for the $M_{2,isen}$ = 0.70 case and x/c = 0.29 for the $M_{2,isen}$ = 0.85 case. As the exit flow becomes supersonic the effect of the pressure surface trailing edge flow is felt on the vane suction surface. Figure 18c shows computed interferometry pictures (from Visual3) for these three cases and Figure 18e shows an enlargement of the trailing edge region for the $M_{2,isen}$ = 1.43 case. Interferograms are contours of constant density using an alternating grey scale which clearly show shock and wake action. They are used in experimental visualization and make the assimilation of complex phenomena easier. On the pressure surface, the flow rapidly accelerates as the effect of the round trailing edge is felt. It then encounters the flow from the suction surface and is deflected, producing the pressure surface leg of the classic fish-tailed shock system characteristic of this type of flow. The suction surface feels the effects of this pressure surface trailing edge flow by first accelerating in response to the expansion and then rapidly decelerating in response to the pressure surface shock. These features can readily be seen in both the experimental and computed profiles shown in Figure 18d. It appears that the $M_{2,isen}$ = 1.12 data point at x/c = 0.4 may well be in error as it does not track the trend being set by the rest of the data.

To complement the simple example of grid shear presented in the previous section, a study of the effects of H versus I grid on this geometry have been performed. An H grid, conforming to rules on aspect ratio found from the duct case above, and using the same number of cells as the I grid was generated by using the elliptic solver previously described. Figure 19a shows the same portion of this grid as Figure 18b did for the I grid. The H grid shown has one quarter the number of points in each direction for clarity, the difference in shear being self evident. Figure 19b shows the result of running this grid was to obtain a solution that rivals that from the I grid. The suction surface peak Mach number is not quite as high as that from the I grid, but the pressure surface trailing edge expansion and shock are being correctly generated and transmitted by the H grid. For this case, to obtain a solution with the H grid the CFL number had to be dropped by 30% in order to obtain a stable solution. Even with this, the convergence history was not as smooth as the I grid, demonstrating that I grids are easier to run and converge than the highly sheared H grids.

In order to demonstrate grid dependence the number of blade-to-blade points in each calculation was halved, the results in terms of isentropic surface Mach number being cross-plotted on Figure 19b and contours of absolute Mach number for both calculations being shown in Figure 19c and 19d. The H grid is now failing to pick up and transmit the pressure surface shock system while the I grid results are remarkably unaffected by the halving of the grid. It seems for this case that the initially chosen I grid was far denser than it needed to have been to capture the relevant physics. These results indicate that the cost of running an I grid calculation would be significantly cheaper than its H grid counterpart.

NASA Rotor 67. Rotor 67 was designed and tested at NASA Lewis. It has 22 blades with a design pressure ratio of 1.63 and mass flow of 33.25 kg/sec at 100% speed, corresponding to 16,043 rpm with a tip relative Mach number of 1.38. Extensive test data, available both from laser measurements and static probes, is given by Strasizar, Wood, Hathaway and Suder (1989) and this has been carefully compared to the results of Viscous EULER simulations in Jennions and Turner (1992). Here, the results are shown for the operating map only, for three values of tip clearance : nominal (0.024 ins, the observed running clearance), half nominal and twice nominal.

The simulations employed 328,937 grid points; 49 points in the blade-to-blade direction, 49 in the spanwise direction (4 being in the tip gap) and 137 in the axial direction. The code took 1 to 1.5 hours on the GE CRAY YMP to produce results for one point on the performance map. Other points can take less time being restarted from previous solutions.

Computed and experimental performance maps are shown in Figure 20. Three individually computed tip clearance cases are shown with higher pressure rise, greater peak adiabatic efficiency and greater flow range being obtained as the clearance is reduced. The computed mass flows are non-dimensionalised with respect to the choked mass flow for the nominal tip clearance case. This mass flow was found to be 1.2% lower than the experimentally observed value. The leftmost point on each of the computed characteristics represents the highest downstream static pressure at which the code would converge. Raising the static pressure further produced reverse flow near the tip through the inlet and hence no solution was possible. This is not what would happen in practice as the rotor would probably experience rotating stall before being pushed to its ultimate stall point, but as only a single passage is being modelled it is the

closest the simulation can come to the stall point.

As the exit pressure was lowered from stall past the peak efficiency point, a separated region observed near the hub / suction surface trailing edge at all operating conditions began to grow and become unsteady. This behavior manifests itself in the solution neither converging nor diverging, with slowly fluctuating errors in the solution domain being encountered only in the separated region. These solutions are marked with open symbols. There are a number of ways to produce a steady state result, such as increasing the smoothing to damp out the unsteadiness. For this simulation we chose to remove the small inlet hub boundary layer and hence produce the converged points shown at a (consistently) slightly higher mass flow. While no other inlet boundary layer profiles have been investigated it is clear that reasonably fine grids are needed for an accurate definition of this profile.

Efficiencies seem to be reasonably well predicted with the nominal clearance except that the dramatic fall off from 93.4% to 91.3% as the mass flow changes from 0.989 to 0.974 is not seen in the calculations. Instead a smooth curve extending out towards stall is predicted. It is not understood what phenomena causes the sudden efficiency loss in the experiment (hysteresis effects have been proposed) and so it is difficult to explain the behaviour of the computations which, on an isolated basis, look reasonable.

Three tip clearance cases were run to test the sensitivity of the results to the modelled clearance and hence aid with future tip clearance modelling. The tip of the blade is formed by simply closing the cross flow plane grid at this location resulting in a roof type structure on the top of the blade. The clearance is then the distance from the roof apex to the casing, modelled as the true tip clearance for the nominal case. What this distance should actually be set to is the subject of some debate. If the flow perpendicular to the chord over the tip is likened to the flow through a sharp two-dimensional slot then it can be argued that in shaping the tip of the blade in this manner we have in some way modelled the limiting streamline emanating from the upstream blade corner and the tip gap should be reduced according to a coefficient of discharge for such a geometry. Alternately, the current results show a 14.4% peak pressure loss for a 1% increase in tip gap. Existing experimental data could be correlated and the modelled tip gap sized to produce the correct pressure loss effect. At present this data is viewed as a first attempt to understand tip clearance effects and no definite conclusions regarding the tip gap sizing have been drawn.

Much care needs to be taken to ensure consistency between experimental and computed data in a comparison such as the one above (Jennions and Shin, 1993). In the experimental calculation of efficiency, the total pressure is 'energy averaged' by converting it to its enthalpy equivalent, while the total temperature is mass averaged. The efficiency is then formed as a simple average of the 9 radial locations at which data is taken. While the same procedure is followed for the computational results presented here, it is interesting to observe the effects of what may seem reasonable assumptions. Two such assumptions are explored in Table 1.

	Computed Efficiencies		
	$P_{T,9}$	$P_{T,49}$	$P^*_{T,9}$
Near Stall	91.125	88.981	89.898
Near Peak Efficiency	93.162	90.810	91.416
Near Choke	86.095	83.992	84.824

Table 1. Effect of Averaging on Efficiencies.

The efficiencies calculated using all the spanwise points ($P_{T,49}$) are 2-3% lower than those using just the experimental data points ($P_{T,9}$). This is because the endwall boundary layer effects, which lower the efficiency, are present in the full span average but are missed when only 9 points are used. If total pressure and total temperature are area averaged in the circumferential direction before enthalpy averaging in the spanwise direction (using 9 points) then the efficiencies shown under $P^*_{T,9}$ are found. These are lower than the $P_{T,9}$ values by $1\frac{1}{2}$-2%. Obviously, reducing the computational data in the same way as the experimental data is crucial to meaningful comparisons.

GE/NASA E^3 Fan. The last, and most complex, simulation is that of the GE/NASA E^3 fan (Sullivan and Hager, 1983). This fan was chosen because it is one of the few high efficiency, high bypass ratio fans typical of modern aeroengines for which test data is available and because it had previously been simulated by Cedar and Holmes (1989) using an Euler plus boundary layer approach. Figure 21 shows the fan configuration, part-span shroud, island splitter and quarter stage booster. The meridional grid for the current fully viscous calculation is shown in Figure 22. It has 81 points in the spanwise direction including 4 points in the tip gap. Such a high number is needed in order to model viscous effects on the endwalls and solid bodies. There are 157 points in the axial direction to enable an accurate description of all the geometry present, an enlargement of the part-span shroud and blade leading

edge region being shown in Figure 22. Finally, 49 points are used in the blade-to-blade direction giving a total grid of 623,133 points.

An initial estimate of the flow field is made by mapping the throughflow datamatch onto the 3D grid. Even so, starting a calculation as complex as this can be difficult with a 5 stage Runge-Kutta scheme and usually a 2 stage scheme, which has been found to be more robust, is run for the first 100 time steps after which the 5 stage scheme is run as normal. For the present case, including the effect of the booster blade rows as source terms, a converged solution was obtained in a total of 500 time steps, taking some 3.6 hours on the GE CRAY YMP. Of course, in the normal design process, changes of back pressure will have to be made to obtain the correct bypass ratio etc., such runs typically taking a further 300-400 iterations to converge depending on the severity of the change that is made.

The current simulation models a 97.2% speed case. The datamatch through-flow analysis that was performed subsequent to the fan being tested gave a bypass ratio of 3.52. The calculation, which was essentially run to the datamatch bypass exit and booster vane leading edge static pressures, predicted a bypass ratio of 3.51 with the individual mass flows being predicted to better than 1%.

Figure 23 shows contours of static pressure on the casing from kulite measurements and from the calculation. Agreement is reasonable with both showing a two shock system, the calculation predicting a more noticeable tip clearance vortex from the leading edge. This vortex is also evident in the relative Mach number contours, plotted midway between the tip and casing in Figure 24. It is accompanied by a second stronger vortex, driven by the pressure difference created across the tip by the in passage shock. This second vortex interacts more strongly with the in passage shock than does the leading edge vortex.

The measured pressures show an almost constant pressure on the 'pressure' surface behind the first shock (static pressures ratios around 1.3) whereas the computation shows a rapid acceleration into the second shock. This is further seen in the average endwall statics shown in Figure 25 where the higher pressure from experiment is again evident. This discrepancy is not fully understood at the present time but a combination of probe error and tip clearance gap sizing might be the cause. Possible probe error was investigated by Weyer and Schodl (1971) where they concluded that a pneumatic measuring system such as that used here could record up to 5% high at the frequencies and pressure ratios encountered in this rotor. For the other two rotors simulated in this paper, probe error would be much lower, as their rotational speeds and hence their excitation frequencies are much higher. Studies of the effect of tip clearance gap are underway.

Total pressure and temperature measurements were available at the booster vane leading edge and on the bypass OGV. These are compared with the prediction in Figures 26 and 27 and show remarkably good agreement. Island static pressure taps were also taken and are shown in Figure 28. As the main interest of this simulation was with the fan, matching the booster leading edge pressure was judged to be important, the other pressures on the island inner side depending critically on the source term modelling.

Recent design interest in cases like this has focussed on the part-span shroud as being an area for possible performance improvement. Ideally, this body would be non-lifting to cause minimal disturbance to the surrounding flow, a situation that cannot be fully achieved due to the presence of the fan's shock system. The loading on the part-span shroud is shown in Figure 29, the near suction surface velocity vectors in Figure 30 and the local velocity vectors around the part-span shroud at three locations across the passage in Figure 31. Near the suction surface, the pressure inbalance between the upper and lower part-span shroud surfaces causes flow around the trailing edge and a small separation to form on the upper surface. This radial flow then joins the radial flow produced by the action of the passage shock on the suction surface boundary layer as it is centrifuged out towards the tip, action that is confined to a region very close to the blade surface. At mid-passage the flow appears healthy, the loading being mostly from the interaction of the part-span shroud with the passage shock. Over near the pressure surface an overspeed is observed near the leading edge on the upper surface and the flow in the trailing edge region behaves in a more orderly manner than that near the suction surface. Design improvements aimed at better aligning the part-span shroud with the flow, to remove the leading edge overspeed and trailing edge flow migration, would improve the efficiency of the part-span shroud.

4 Third Party Codes

The use of third party codes has become more popular over the last ten years due to three main reasons. The first is that with so many different physical problems needing attention, it is not possible to develop all the capability needed in-

house. When outside sources have codes that contain the right physical models e.g. turbulence models or unsteady flow, then it makes sense to pick up a code that already exists rather than put a lot of money into developing the same capability in-house. The second reason is one of geometric complexity. Designers constantly want to know what the flow around the next widget looks like. These are mostly one-off calculations and speed in setting up the grid and getting a solution are of paramount importance. Unfortunately the overall process may still take a long time, as grid generation for complex geometries is by no means easy, but third party codes can be used to expedite the process. The third and perhaps most important reason is that third party codes have now developed to the point were results are more consistently correct then previously. This aspect has led some codes to have bad reputations in the past, but overall it is felt that this phase of development is over. We are not to the same point as stress analysis codes where there are industry 'standards' and virtually no in-house codes are written, but this position is gradually being approached.

In contrast to the above, the reasons for developing in-house codes must also be considered and these are primarily two fold. When there exists a large user base for an in-house code, then it is difficult to justify the considerable effort required to retrain and recalibrate designers to the new tool. Adding new features to such a code then becomes a judgement choice. For relatively simple changes, such as different boundary conditions, the in-house code should be extended; whereas for a change to a different turbulence model it is a much more difficult choice. The second reason is where a competitive advantage is sought by solving a problem to which there does not exist an 'off the shelf' solution. An example of this type of development is the current interest in linearized unsteady flows to study forced response problems or the use of unstructured grids to simplify the grid generation / solution / postprocessing cycle. The question becomes whether a company considers the money put into such a development worth the pay-back in the short term, before such an analysis is available on the open market.

With the above comments made, third party codes originate from two principal sources - NASA and software companies. Over the years GEAE has made use of a number of NASA codes, some of which are : GRAPE, GRIDGEN, PLOT3D / FAST, ROTOR1 / STAGE2, ROTOR3, F3D and CFL3D, the last two being in the installation area. The unsteady codes (ROTOR1 / STAGE2 and ROTOR3) were brought in because no in-house code was positioned to solve these unsteady problems without significant work and, through government contracts, much of the basic ground work of calibration had already been done.

CFL3D was brought in for basically the same reason, no in-house capability existed and it was deemed more prudent to team up with NASA than try to develop our own method. A measure of the power of this approach can be gained from the paper by Cedar et al. (1993). The approach uses CFL3D with Chimera grid oversetting to solve for a cleanwing and for the wing with the nacelle and pylon present. The cleanwing results are shown in Figure 32 where inviscid, viscous and fine grid viscous runs against experimental data are shown. It is clear that a fine grid viscous computation is needed to match the experimental data, a conclusion consistent with the findings of many other researchers. Further, Figure 33 shows the results when the pylon and nacelle are included in the calculation. The CFD solutions capture the trends in the experimental data, the Mach numbers inboard of the installation on the upper wing surface are elevated due to the presence of the nacelle.

A number of different codes from software houses have been used at GEAE. An example to illustrate the use of just one is given here. Discrete jet film cooling, often used in conjunction with internal convective cooling, is a popular method of extending the life of turbine hot section components. Although there are many configurations of film cooling, one common feature is the highly complex nature of the flowfield created by a coolant jet interacting with a hot cross-stream. Leylek and Zerkle (1993) reported on a joint experimental / computational study of a jet in a crossflow (Figure 34). A single hole, including the plenum, was gridded as shown in Figure 35. Much consideration was given to produce a highly orthogonal, non-uniform, fine grid consisting of 200,090 points. The standard $k-\epsilon$ turbulence model was used in order to ascertain how well it could perform and hence remedy its shortcomings in future studies. Results showing the computed temperature contours for two cases, a blowing ratio (M) of 0.5 and a density ratio (DR) of 2.0 and then an increase in the blowing ratio to 2.0, are given in Figure 36. The deduced streamwise variation of adiabatic effectiveness is shown in Figure 37 along with the experimental data. It is evident that the computations are not spreading the jet as quickly as the experimental data suggests. Much of the flow physics has been captured, e.g. turbulence generated as the cooling flow moves from the plenum out through the hole, and it was thought that the lack of lateral spreading was caused by the inability of

the $k-\epsilon$ model to cope with non-uniform rates of diffusion in different directions.

5 Current Development Issues

In this Section, a number of topics that are currently being worked and are of significant importance are discussed.

Multi-Stage Calculations. Single blade row 3D Navier-Stokes solvers have now been used in industry for some time but their application to a stage calculation is still a matter of some concern. For a single stage a mixing plane (Dring, 1990) can be postulated to exist between the two blades and conditions mixed out circumferentially in order that the downstream blade row sees a steady flow. Unfortunately, this does not seem to produce the same results as time averaging a complete unsteady solution for the stage. Figure 38, taken from Fritsch and Giles, illustrates this point. Here, a stator followed by a rotor has been modelled both by a fully unsteady calculation and by a steady stage calculation using an interface approach such as previously discussed. The jump in entropy at the interface plane, produce by the mixing procedure, causes a discrepancy between the two calculations. From a designer's point of view the downstream rotor, if examined in isolation, looks better from the steady calculation than from the unsteady and may lead to design decisions that would not work in practice. Physically, the unsteady solution is allowing such effects as the upstream wakes to be reenergized by the downstream blade (Smith, 1993) and not completely lost to mixing, which is irrecoverable. Work has been done on solving the time average unsteady flow equations through a multi-stage machine in which account of the upstream blade rows is taken when solving for the current row. These interactions appear as stress terms which can be modelled (Adamczyk, 1992) and currently this looks the most promising form in which to attack this problem.

Boundary Layer Transition. Evidence from a number of sources suggests that boundary layers, particularly on low pressure (LP) turbines are more laminar and transitional than had previously been assumed (e.g. Mayle, 1991). Hodson et al. (1993) published data on the Rolls-Royce Trent LP turbine (Figure 39) where, with surface mounted constant temperature hot-film anemometers, the suction surface boundary layer could be investigated in detail. Much laminar and transitional flow was found on the third stage stator, but not much evidence of fully turbulent flow. This is in agreement with work done at GEAE (Figure 40) which shows the variation of total pressure downstream of an LP turbine vane compared with calculations performed using a high Reynolds number form of a $k-\epsilon$ turbulence model and wall functions. The agreement is fairly good, but the small difference, particaulrly at mid-span, is thought to be due to the real boundary layer being transitional. Work described by Dailey et al. (1994) aimed at addressing this problem by incorporating a low Reynolds number $k-\epsilon$ model into the computer code (Viscous EULER). Flat plate transition could be predicted as the inlet turbulence intensity (TU0) was changed (Figure 41), but grid considerations (Figure 42) and the CPU times to run the calculation (1 to 2 hours on a CRAY YMP) make the approach impractical for design use. There is a need for practical transition predictions within the framework of a Navier-Stokes code.

Parallel Processing. As the speed of single processors begins to asymptote, the use of a number of processors in parallel to achieve greater speed with price/performance benefits looks very attractive. There are still problems with vendors choosing different architectures but sufficient experience has been gained to enable an optimistic view of the future to be taken in this area.

Braaten (1992) describes the application of a parallel pressure-correction algorithm to 3D turbomachinery flows. The algorithm solves the compressible form of the Euler or Navier-Stokes equations via a compressible pressure-correction formulation. Table 2 shows measured performance for the calculation of an inviscid transonic turbine cascade on a grid with 130x18x66 points (154,440 point in total). Here, comparisons are made between one processor of a CRAY Y-MP and a number of procesors on iPSC/860s at GE CR&D and NASA Ames and the Touchstone Delta machine at the California Institute of Technology. Overall, performance in excess of the CRAY was achieved with only 32 nodes and speeds 2.4 times the CRAY could be achieved with 128 nodes. As the increase in speed of the chips used in these cases continues to outpace their supercomputer equivalents, these figures will only become more impressive in the future.

Since this case is too large to run on a single processor, the parallel efficiency must be estimated. This was done using the method described by Braaten (1991). Parallel efficiency drops below 50% around the level of 64 processors, suggesting that the given problem is too small for a much greater number of processors. The loss in parallel efficiency is due primarily to load imbal-

ances caused by the use of a staggered grid and from the application of different boundary conditions on different processors, as well as the cost of communication between processors during the solution step.

6 Concluding Remarks

This paper has explored the main uses of CFD in the turbomachinery design process at GE Aircraft Engines. The two main in-house codes, NOVAK2D and Viscous EULER, have been discussed in some detail, with examples given as to their accuracy and hence potential use within a design system. The use of third party codes, either from NASA or from software houses, has also been discussed, as has current development issues.

The impact of these CFD solvers on the traditional design system cannot be understated. Navier-Stokes calculations are being performed on a regular basis, giving valuable insight into flow problems that did not seem tractable even a few years ago. It therefore seems that CFD has a sure future in aiding the design process.

Acknowledgement

The author would like to thank GE Aircraft Engiones for permission to publish this paper.

References

Adamczyk, J. J., 1992, "Unsteady Aerodynamic Interaction Effects on Turbomachinery Blade Life and Performance", AIAA 92-0149.

Baldwin, B. and Lomax, H., 1978, "Thin Layer Approximation and Algebraic Model for Seperated Turbulent Flows", AIAA 78-257.

Braaten, M. E., 1991, "Development of a Parallel Computational Fluid Dynamics Algorithm on a Hypercube Computer", *Int. Journal for Numerical Methods in Fluids*, 12, pp. 947-963.

Braaten, M. E., 1992, "Applications of a Parallel Pressure-Correction Algorithm to 3D Turbomachinery Flows", in: Parallel Computational Fluid Dynamics, edited by: Pelz, Ecer and Hauser. North-Holland.

Cedar, R. D., Dietrich, D. A. and Ostrander, M. J., 1993, "Engine/Airframe Installation CFD for Commercial Transports An Engine Manufacturers Perspective", SAE Aerotech '93, Paper No. 932623.

Cedar, R. D. and Holmes, D. G., 1989, "The Calculation of the Three-Dimensional Flow Through a Transonic Fan Including the Effects of Blade Surface Boundary Layers, Part-Span Shroud, Engine Splitter and Adjacent Blade Rows", ASME 89-GT-325.

Connell, S. D., Holmes, D. G. and Braaten, M. E., 1993, "Adaptive Unstructured 2D Navier-Stokes Solutions on Mixed Quadrilaterals/Triangular Meshes", ASME 93-GT-99.

Connell, S. D. and Holmes, D. G., 1993, "A 3D Unstructured Adaptive Multigrid Scheme for the Euler Equations", AIAA 93-3339.

Dailey, L. D., Jennions, I. K. and Orkwis, P. D., "Simulating Laminar-Turbulent Transition with a Low Reynolds Number $k - \epsilon$ Turbulence Model in a Navier-Stokes Solver", AIAA 94-0189.

Dawes, W. N., 1990, "A Comparison of Zero and One Equation Turbulence Modelling for Turbomachinery Calculations", ASME 90-GT-303.

Dring, R. P. and Spear, D. A., 1990, "The Effects of Wake Mixing on Compressor Aerodynamics", ASME 90-GT-132.

Haimes, R. and Giles, M., 1991, "VISUAL3: Interactive Unsteady Unstructured 3D Visualization", AIAA-91-0794.

Holmes, D. G. and Tong S. S., 1985, "A 3-D Euler Solver for Turbomachinery Blade Rows", ASME *Journal of Engineering for Gas Turbines and Power*, 107.

Holmes, D. G., Lamson, S. H. and Connell, S. D., 1988, "Quasi-3D Solutions for Transonic, Inviscid Flows by Adaptive Triangulation", ASME 88-GT-83.

Holmes, D. G. and Snyder, D., 1988, "The Generation of Unstructured Triangular Meshes Using Delaunay Triangulation", in: Numerical Grid Generation in Computational Fluid Mechanics, edited by: Sengupta, Hauser, Eiseman and Thompson. Pineridge Press.

Jameson, A., Schmidt, W., and Turkel, E., 1981, "Numerical Solutions of the Euler Equations by Finite Volume Methods using Runge-Kutta time-stepping scheme AIAA 81-1259.

Jennions, I.K. and Shin, C. T., 1993, "An Exhaustive Study of the Flow in a Transonic Rotor", Second ISAIF Conference, Prague.

Jennions, I.K. and Turner, M. G., 1993, "Three-Dimensional Navier-Stokes Computations

of Transonic Fan Flow Using an Explicit Flow Solver and an Implicit $k-\epsilon$ Solver", ASME *Journal of Turbomachinery*, Vol. 115, pp. 261-272.

Kallinderis, J. G., and Baron, J. R., 1987, "Adaptation methods for a new Navier-Stokes algorithm", AIAA 87-1167.

Launder, B. E., and Spalding, D. B., 1974, "The Numerical Computation of Turbulent Flows". In *Computer Methods in Applied Mechanics and Engineering 3*, p. 269, North-Holland Publishing Company.

Lefebvre, A. H., 1983, *Gas Turbine Combustion*, McGraw Hill, pp. 4-9.

Leylek, J. H. and Zerkle, R. D., 1993, "Discrete-Jet Film Cooling: A Comparison of Computational Results with Experiments", ASME 93-GT-207.

Ni, R. H., 1982, "A Multiple Grid Scheme for Solving the Euler Equations", AIAA Journal, Vol. 20, p.1565.

Shelton, M. L., Gregory, B. A., Doughty, R. L., Kiss, T. and Moses, H.L., 1992, "A Statistical Approach to the Experimental Evaluation of Transonic Airfoils in a Linear Cascade", ASME 92-GT-5.

Shyy, W. and Correa, S. M., 1985, "A Systematic Comparison of Several Numerical Schemes for Complex Flow Calculations", AIAA 85-0440.

Smith, L. H., 1987, "Unducted Fan Aerodynamic Design", ASME *Journal of Turbomachinery*, Vol. 109, pp. 313-324.

Smith, L. H., 1993, "Wake Ingestion Propulsion Benefit", ASME *Journal of Propulsion for Power*, Vol. 9, pp. 74-82.

Sorenson, R. L., 1980, "A Computer Program to generate Two-Dimensional Grids About Airfoils and Other Shapes by the Use of Poisson's Equation", NASA Technical Memorandum 81198.

Strazisar, A. J., Wood, J. R., Hathaway, M. D. and Suder, K.L., 1989, "Laser Anemometer Measurements in a Transonic Axial-Flow Fan Rotor", NASA Technical Paper 2879.

Sullivan, T. J. and Hager, R. D., 1983, "The Aerodynamic Design and Performance of the General Electric / NASA E^3 Fan", AIAA-83-1160.

Turner, M. G. and Jennions, I.K., 1992, "An Investigation of Turbulence Modelling in Transonic Fans Including a Novel Implementation of an Implicit $k-\epsilon$ Turbulence Model", ASME *Journal of Turbomachinery*, Vol. 115, pp. 249-260.

Turner, M. G., Liang, T., Beauchamp, P. P. and Jennions, I.K., 1993, "The Use of Orthogonal Grids in Turbine CFD Computations", ASME 93-GT-38.

Walatka, P. P., Clucas, J., McCabe, R. K., Plessel, T. and Potter R., 1992, "FAST User Guide", NASA Ames, Report No. RND-92-015.

Workshop on Two- and Three-Dimensional Flow Calculations in Turbine Bladings, 1982, Von Karman Institute.

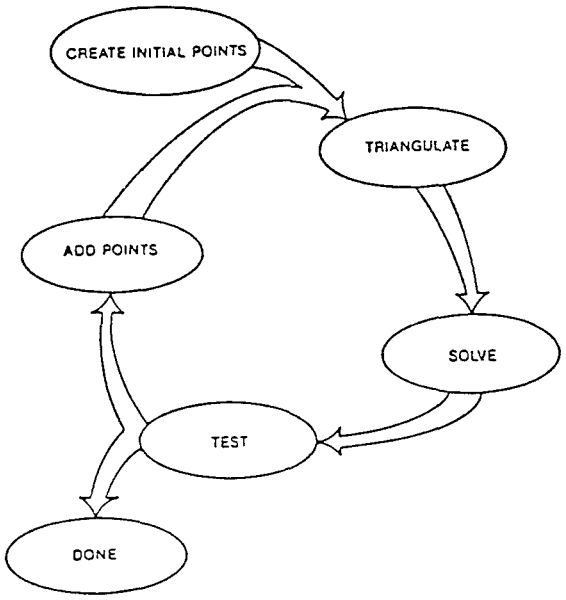

Figure 1. Unstructured Solution Cycle.

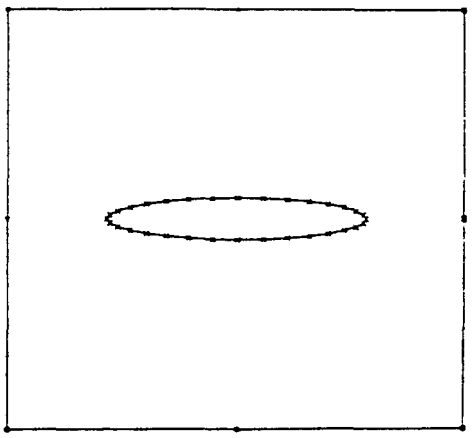

Figure 2. Input Points Form the Knots of the Parametric Spline Representation of the Boundary.

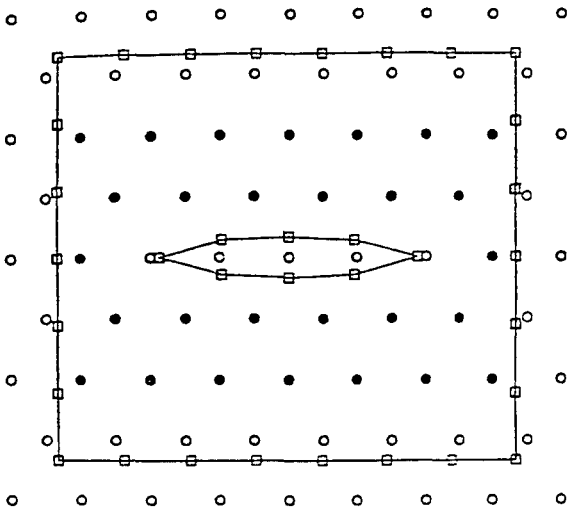

Figure 3. Boundary and Interior Points.

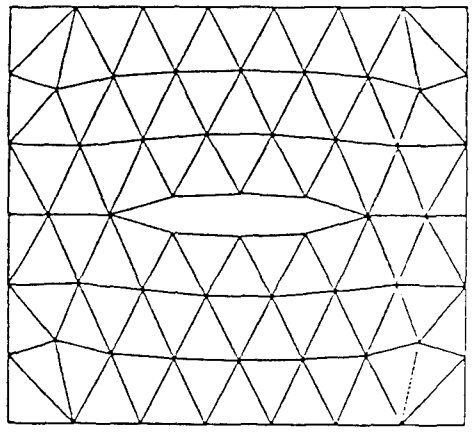

Figure 4. Triangulated and Smoothed Grid.

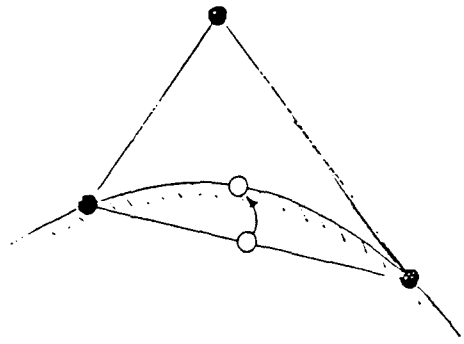

Figure 5. Adding a New Point on the Boundary.

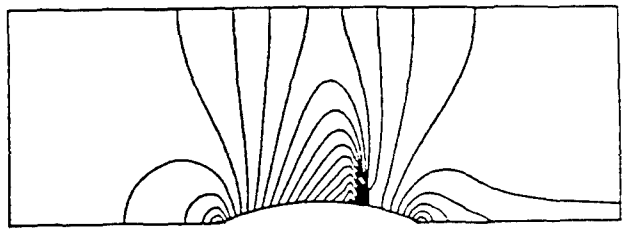

Figure 6. EULER Ni Bump Solution, 33x97 Grid.

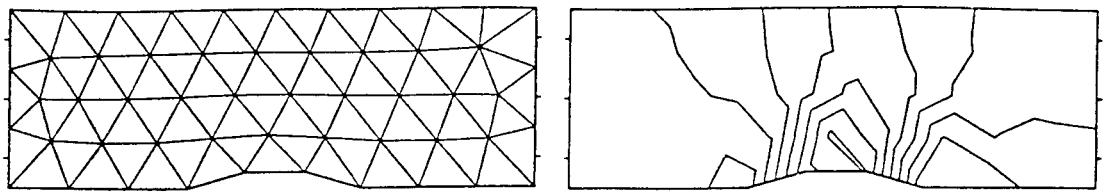

a. 53 grid points

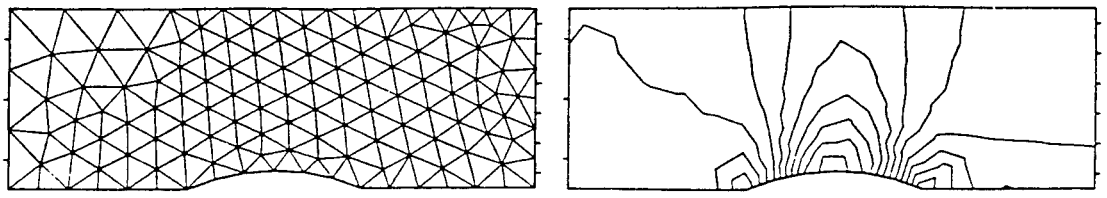

b. 136 grid points

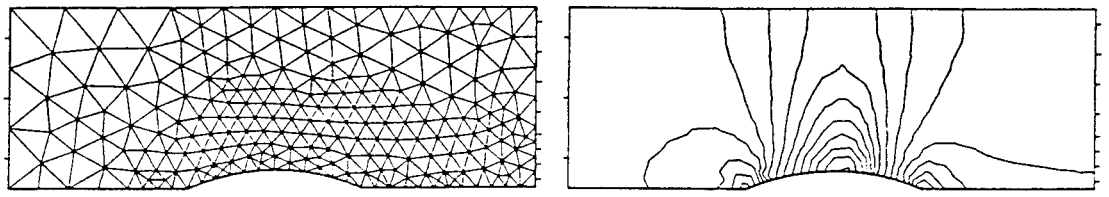

c. 241 grid points

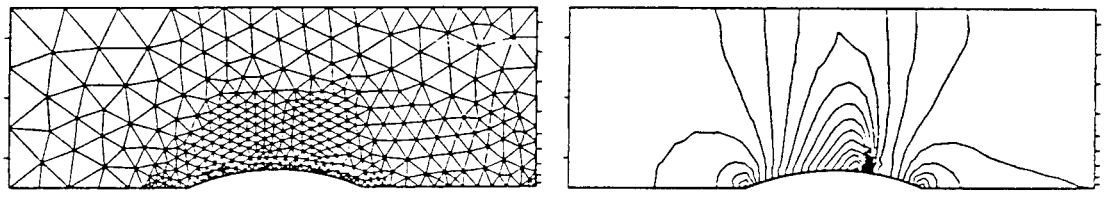

d. 393 grid points

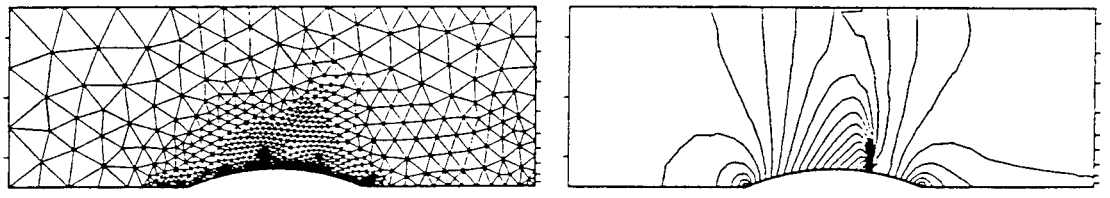

e. 658 grid points

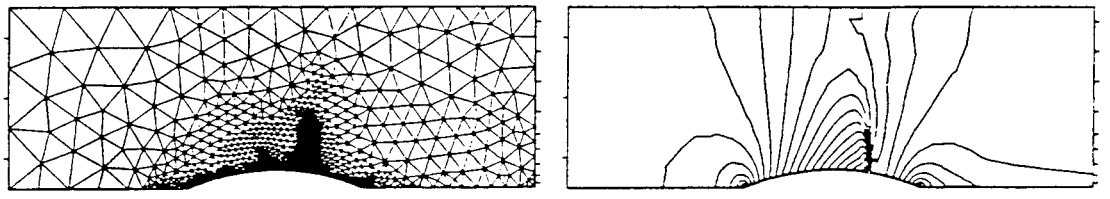

f. 850 grid points

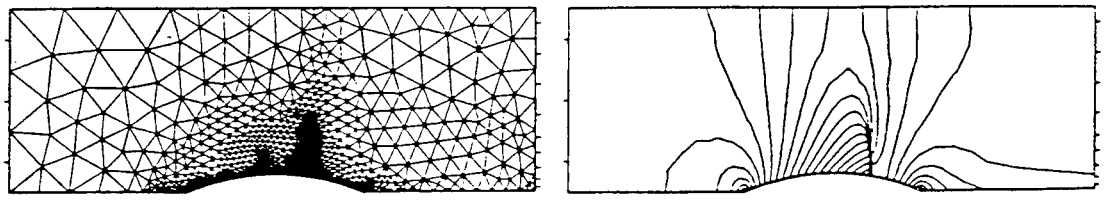

g. 1263 grid points

Figure 7. The Succession of Grids and Mach Number Contours Produced by the Solution Cycle for the Ni Bump Case.

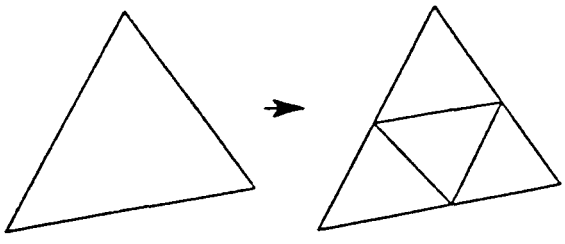

Figure 8. Subdivision of Triangular Cells.

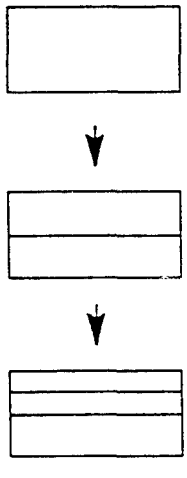

Figure 9. One Dimensional Refinement of Quadrilateral Cells.

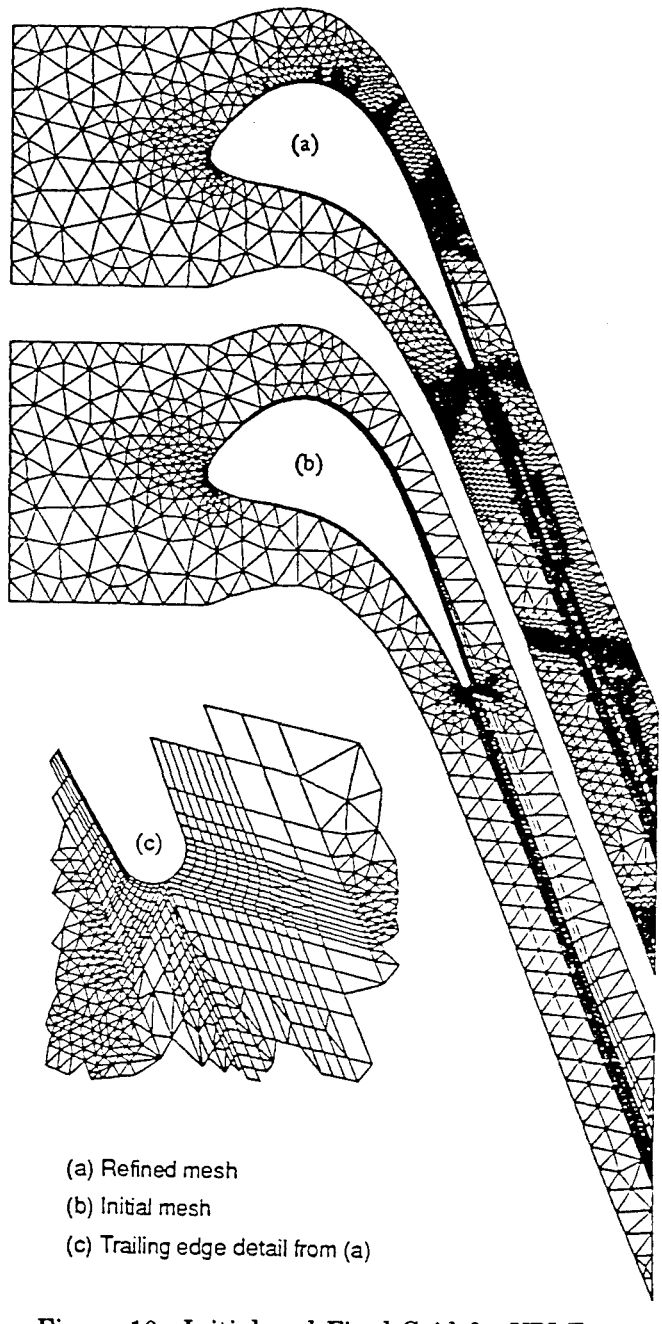

Figure 10. Initial and Final Grid for VPI Turbine Cascade (M_{ex} = 1.25).

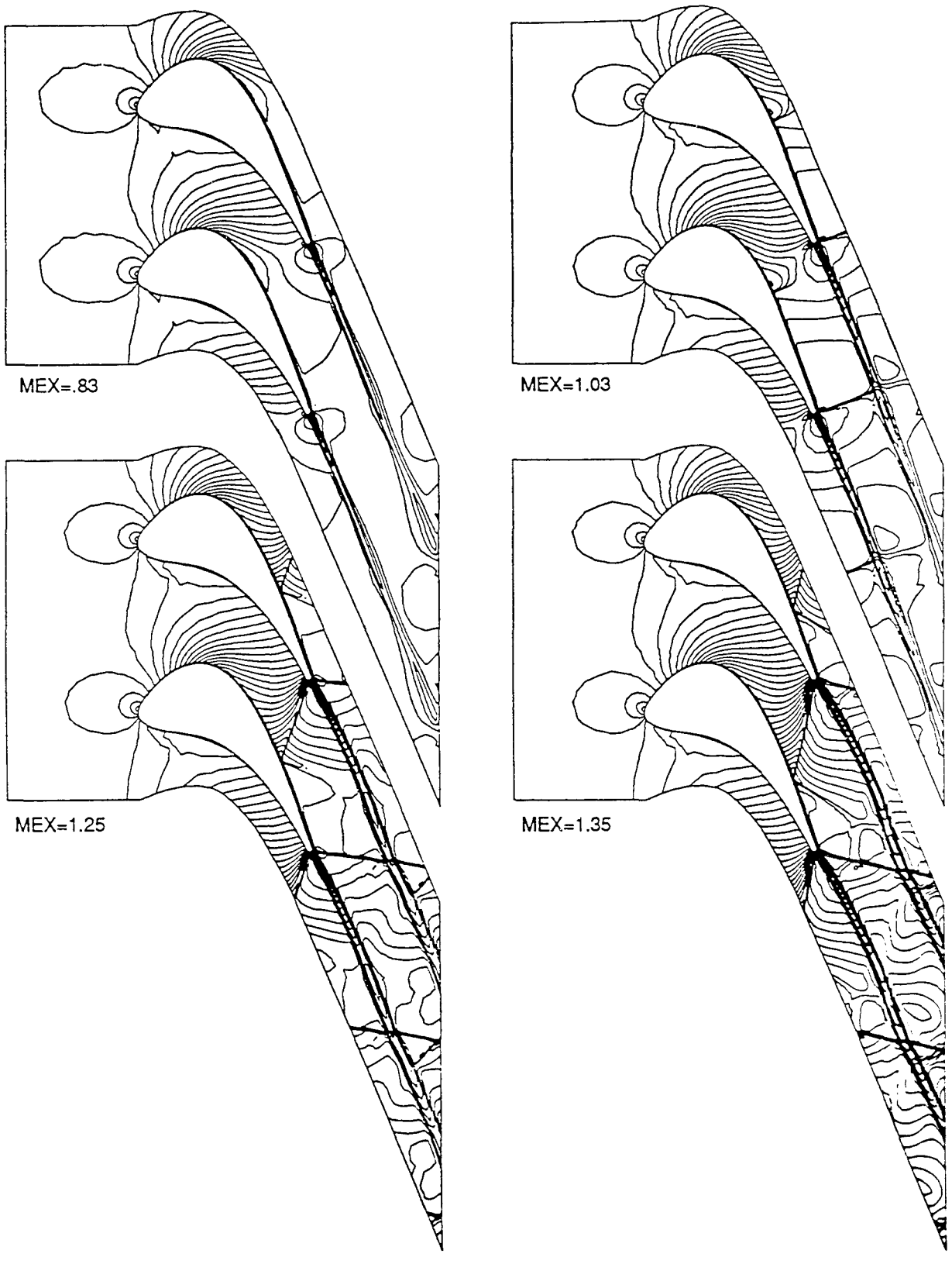

Figure 11. Mach Contours for a Variety of Exit Pressures.

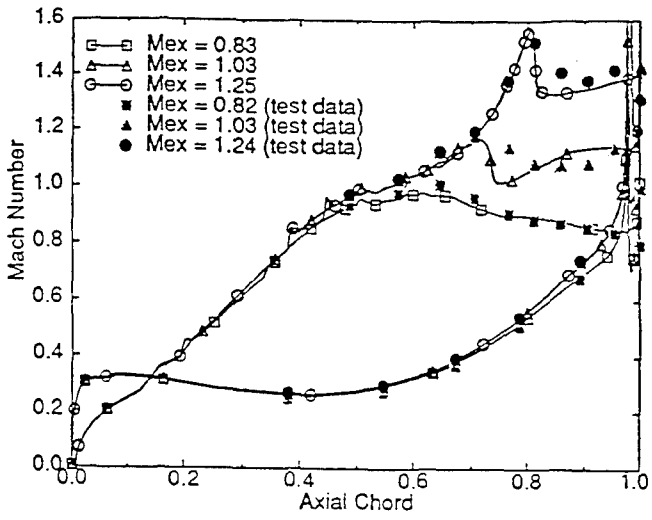

Figure 12. Surface Mach Number Distributions for VPI Turbine.

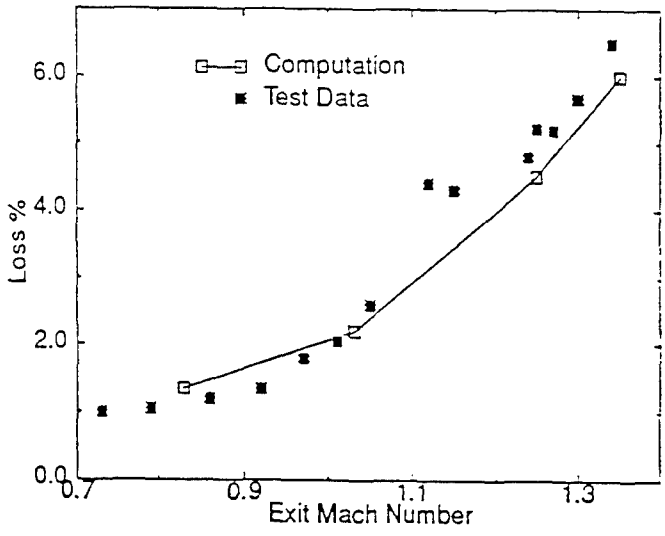

Figure 13. Loss Prediction for VPI Turbine.

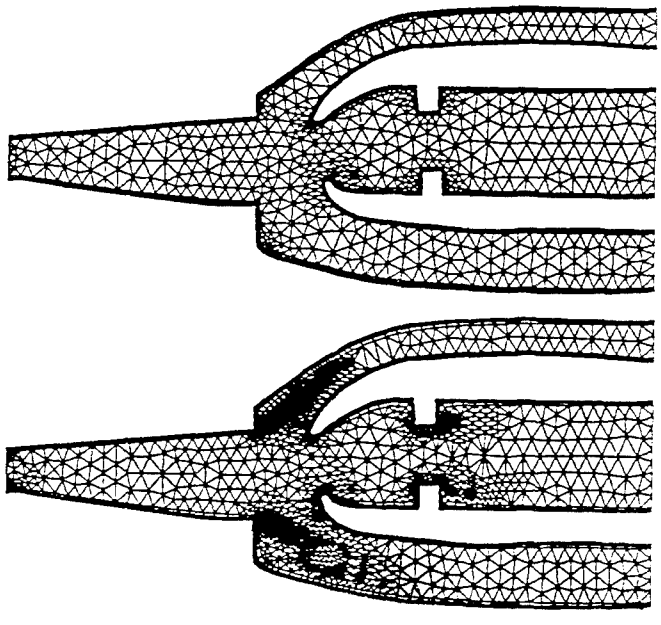

Figure 14. Initial and Final Grids for Combustor Diffuser.

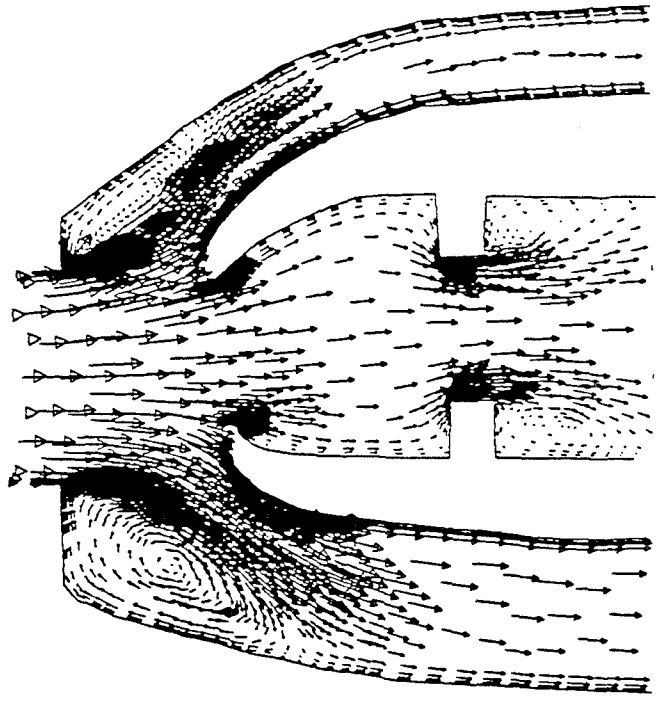

Figure 15. Velocity Vector Plot for Combustor Diffuser.

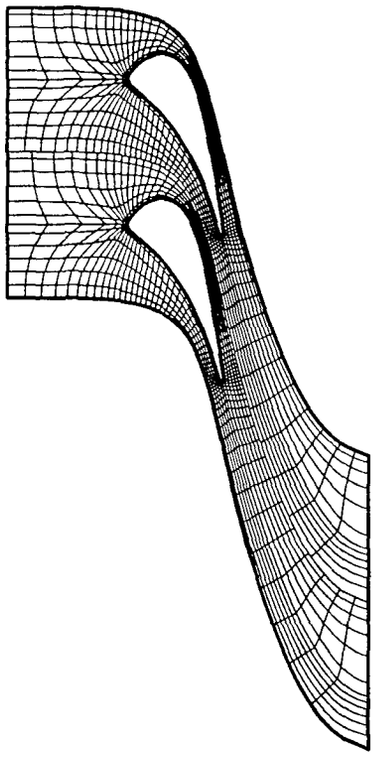

a) I Grid (every fourth line shown)

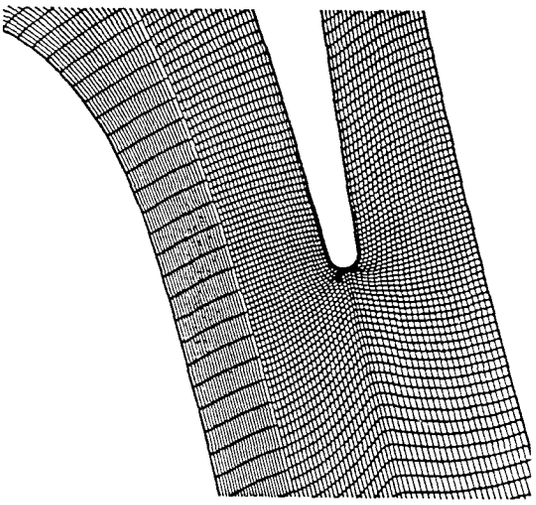

b) Enlargement of I Grid Throat Region (full grid)

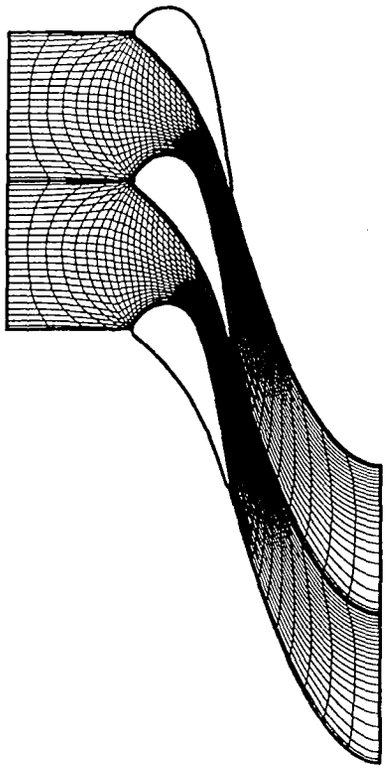

c) H Grid (every fourth line shown)

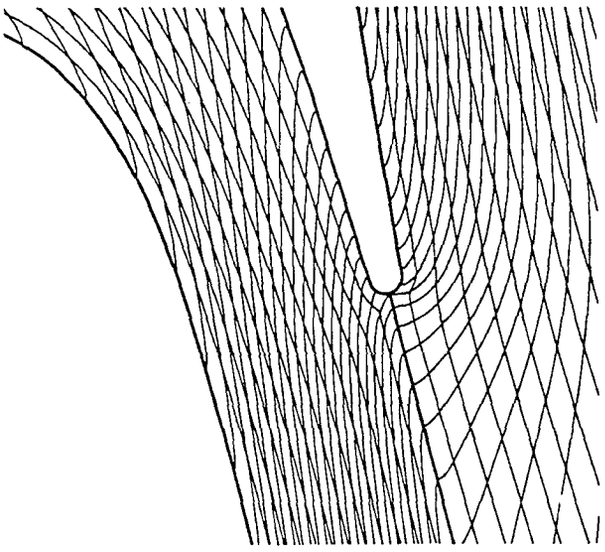

d) Enlargement of H Grid Throat Region (every fourth line shown)

Figure 16. H and I Grids

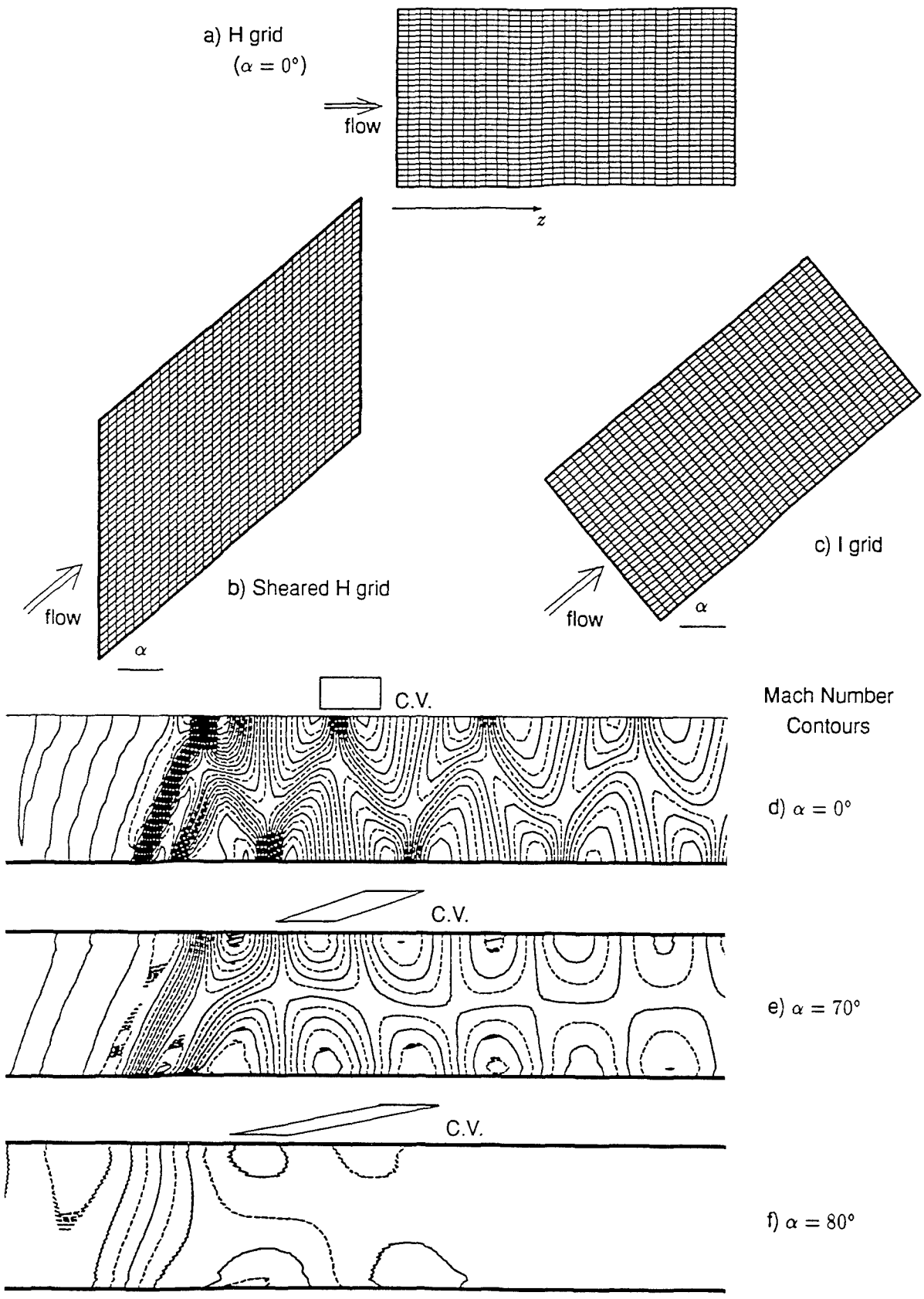

Figure 17. Simple Duct Example.

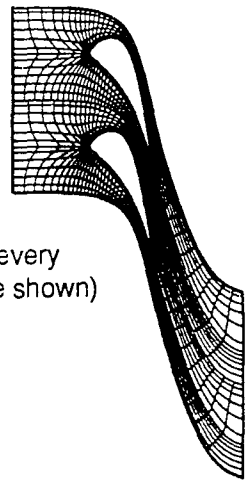

a) I grid (every fourth line shown)

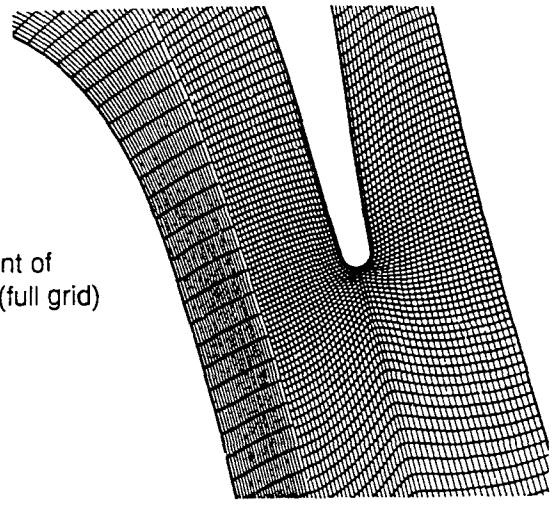

b) Enlargement of throat region (full grid)

$M_{2,isen}$=1.00 $M_{2,isen}$=1.12 $M_{2,isen}$=1.43

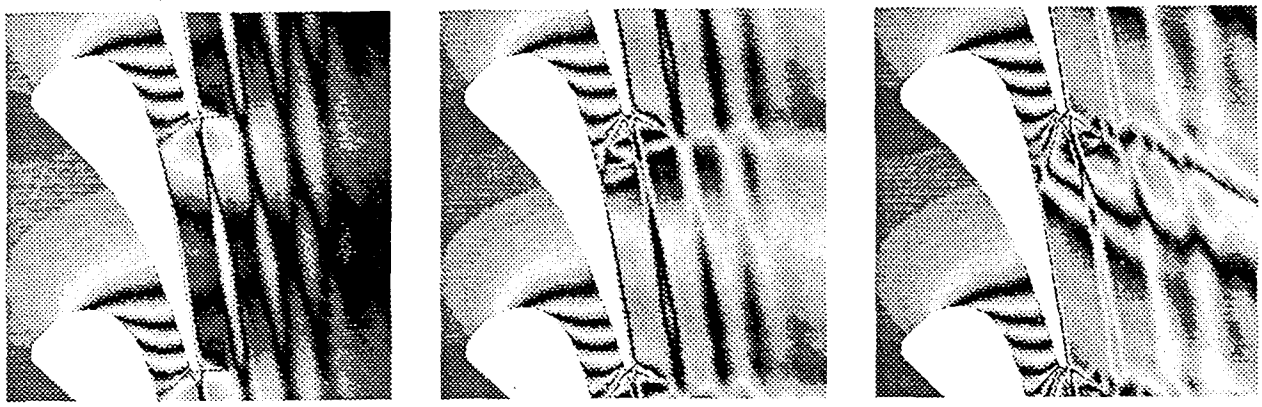

c) Computed interferograms (density contours using an alternating grey scale)

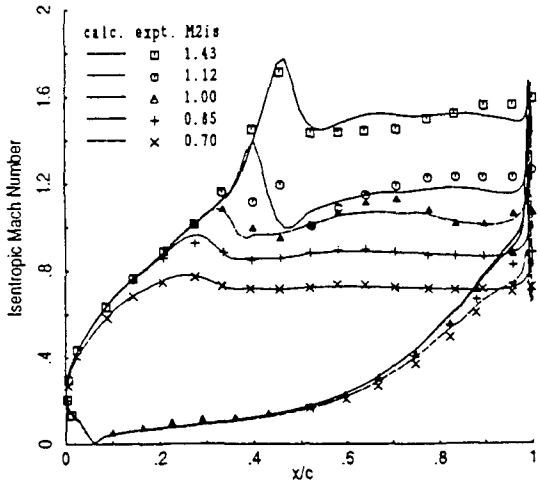

d) Loading comparison

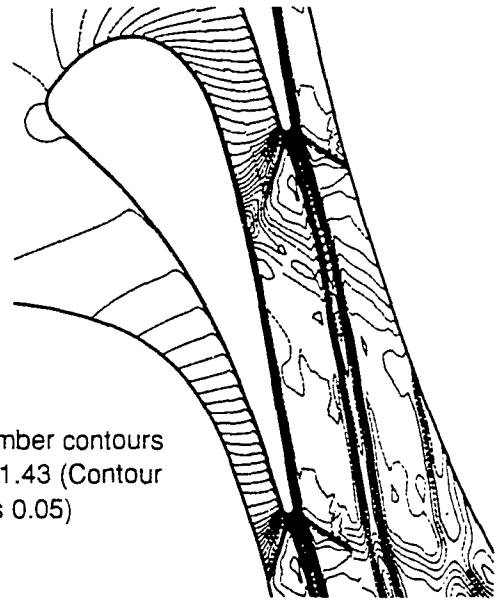

e) Mach number contours for $M_{2,isen}$=1.43 (Contour increment is 0.05)

Figure 18. VKI-LS82 I Grid Results.

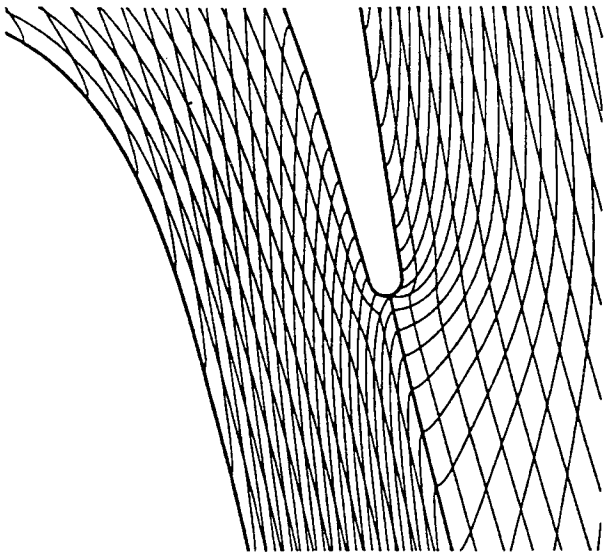

a) H grid near throat (every fourth line shown)
cf. Figure 3b for I grid

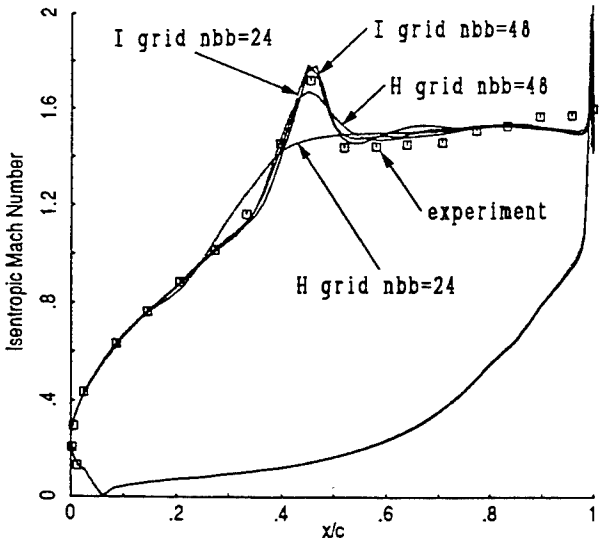

b) Loading with different grids

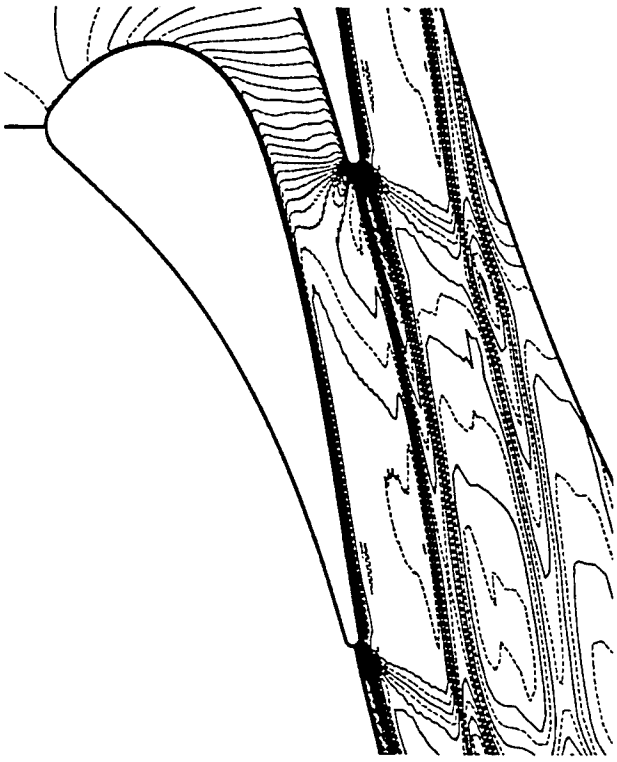

c) H grid

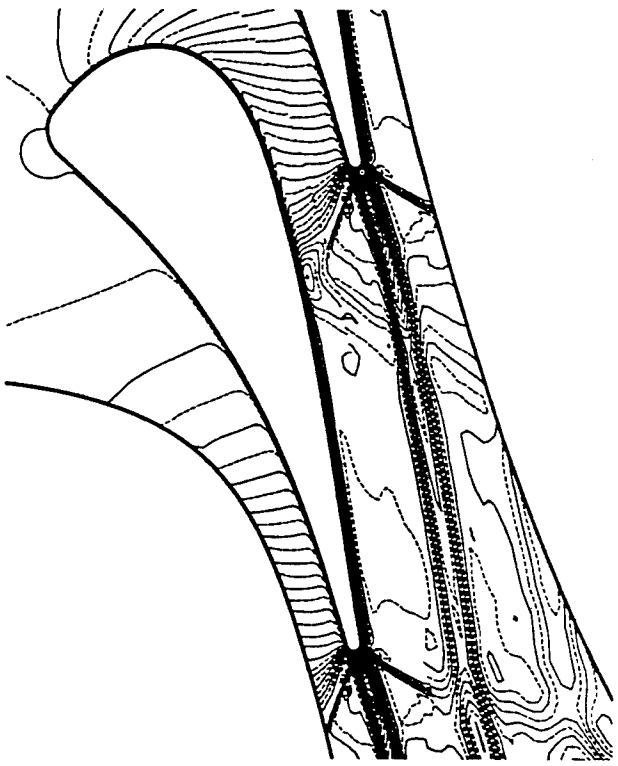

d) I grid

Mach number contours for the coarse grids (24 blade-to-blade cells)
Contour interval is 0.05

Figure 19. Derefinement Study on the VKI-LS82 at $M_{2,isen} = 1.43$.

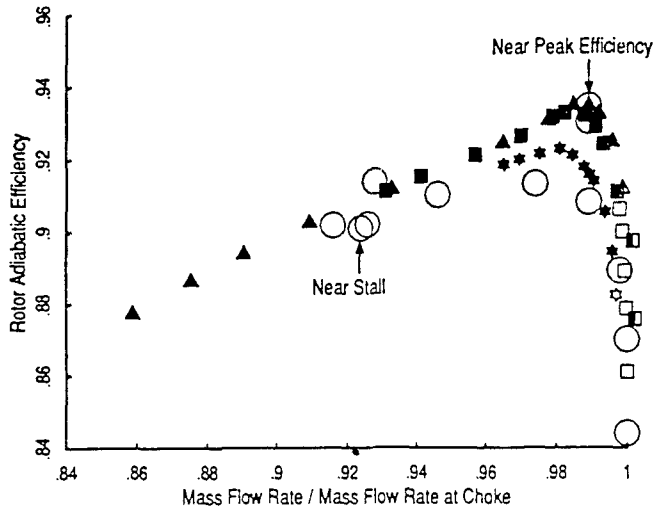

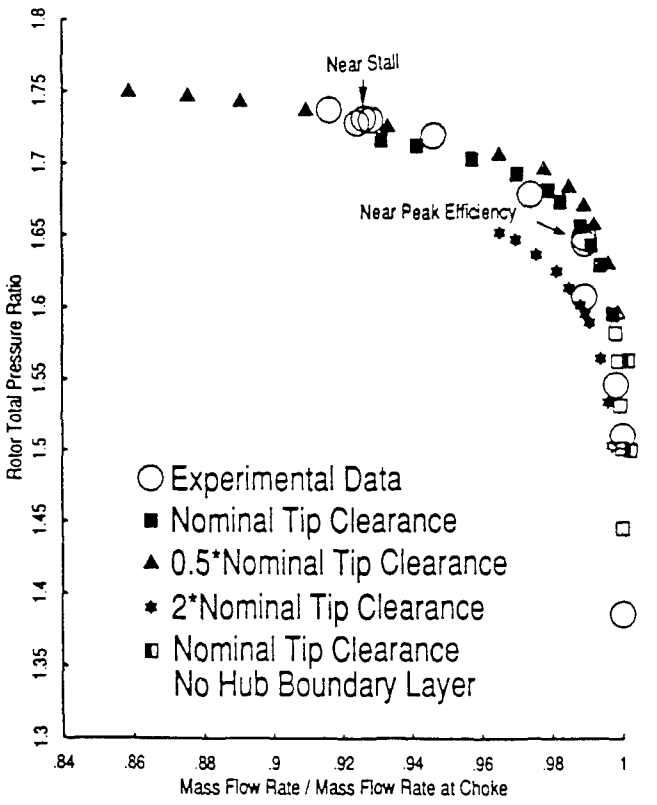

Figure 20. Rotor 67 Design Speed Operating Characteristics.

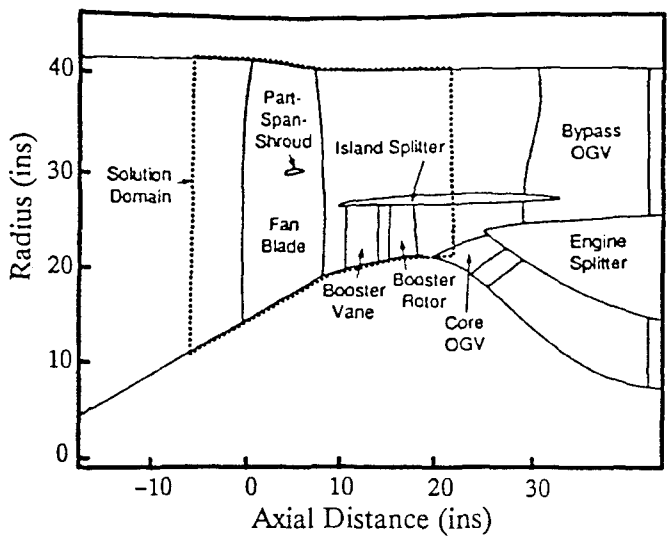

Figure 21. E^3 Fan Configuration.

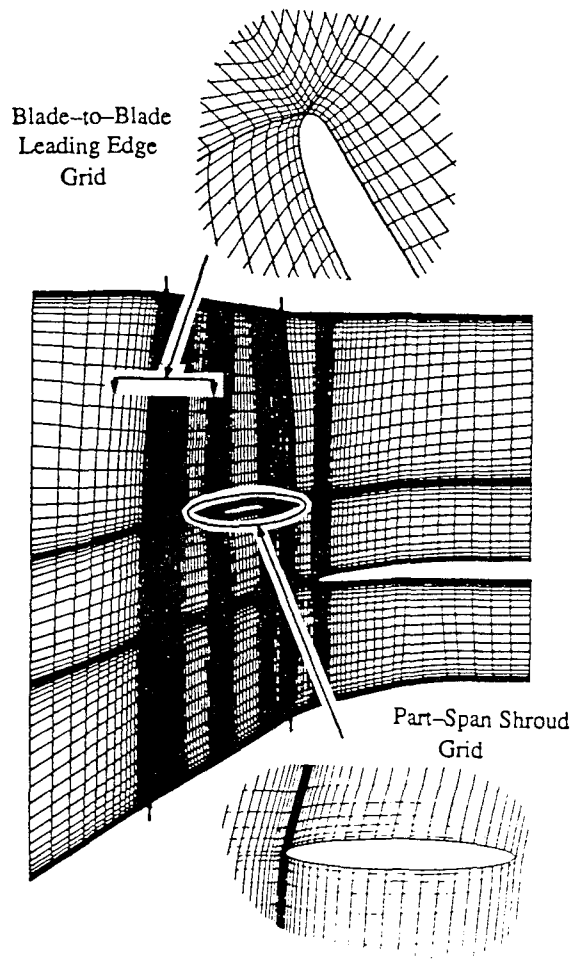

Figure 22. E^3 Fan Grid Details.

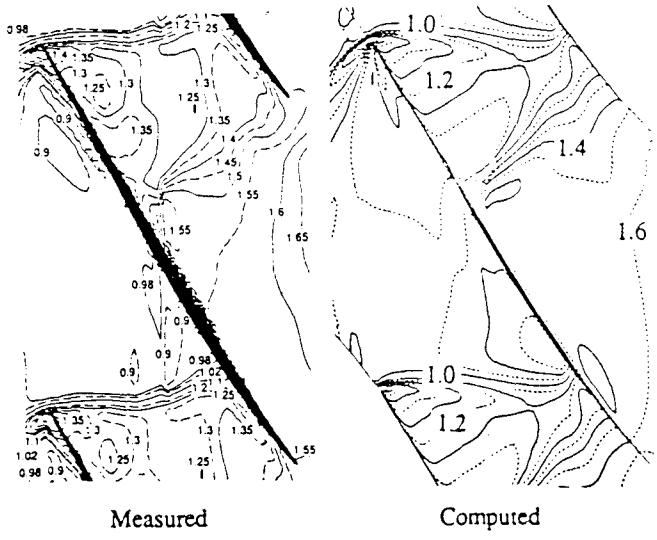

Figure 23. E^3 Casing Normalized Static Pressure Contours.

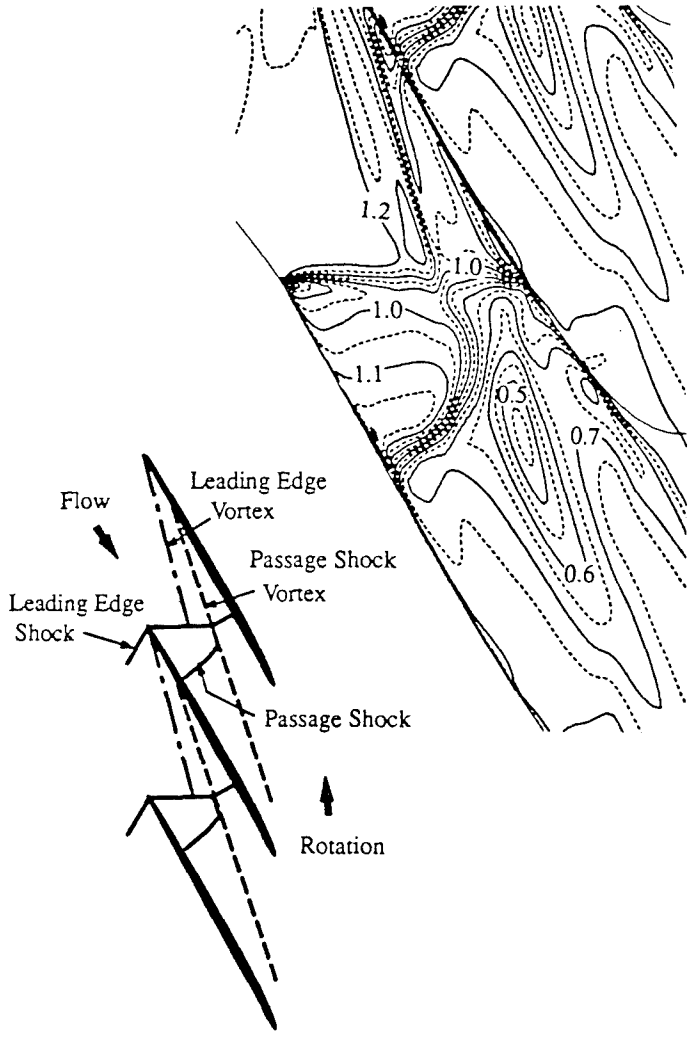

Figure 24. Computed E^3 Relative Mach Number Contours between Tip and Casing and Schematic Showing Tip Vortex / Shock Interaction. Contour interval of 0.05.

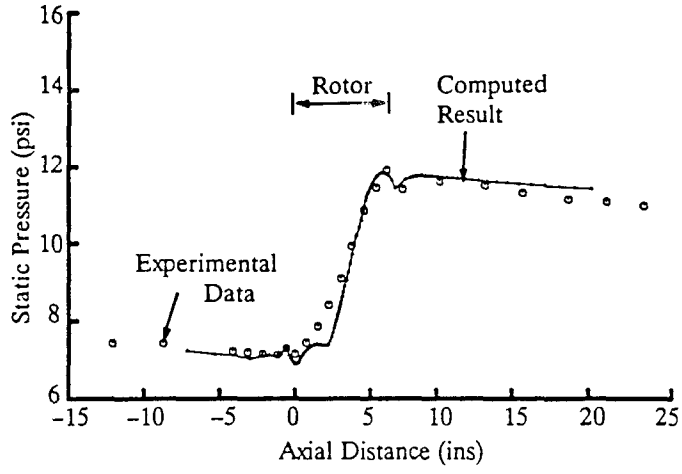

Figure 25. E^3 Casing Static Pressure Comparison.

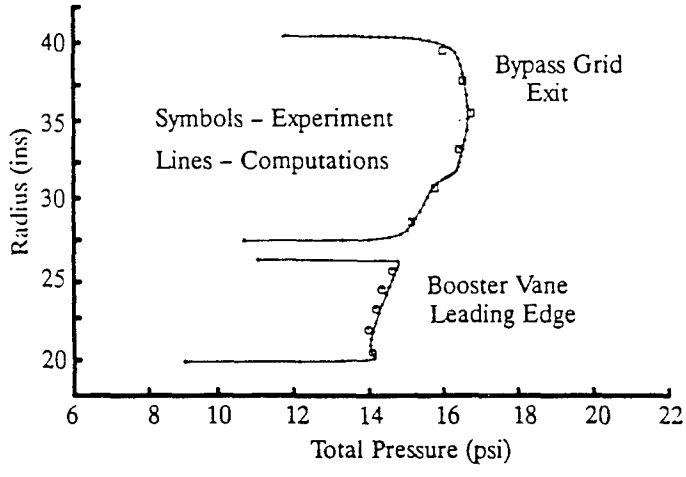

Figure 26. E^3 Downstream Total Pressure Profiles.

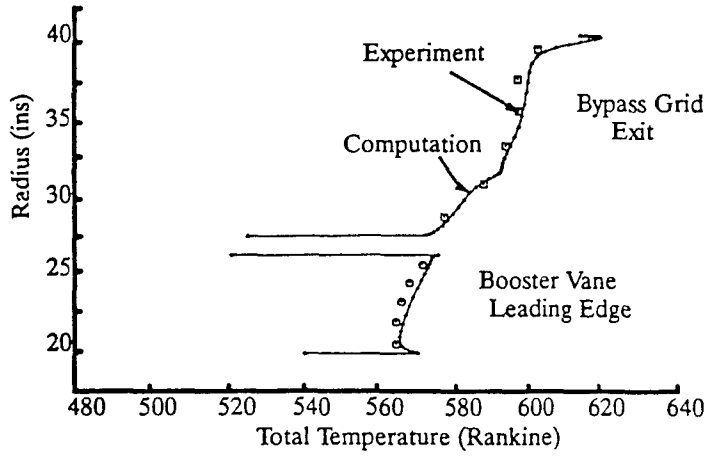

Figure 27. E^3 Downstream Total Temperature Profiles.

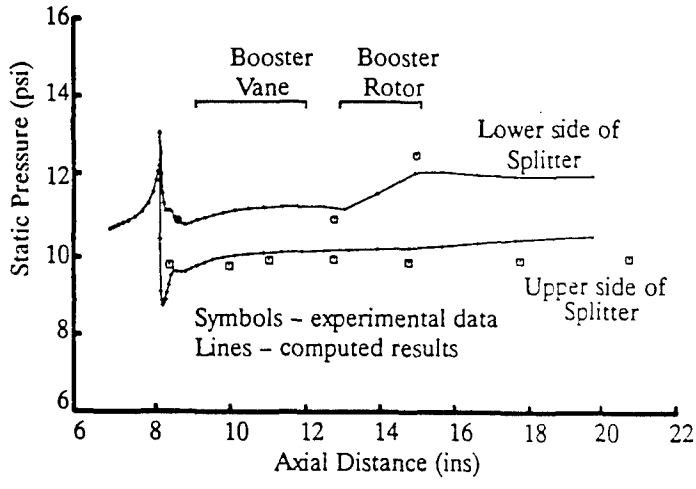

Figure 28. E^3 **Island Static Pressure Distribution.**

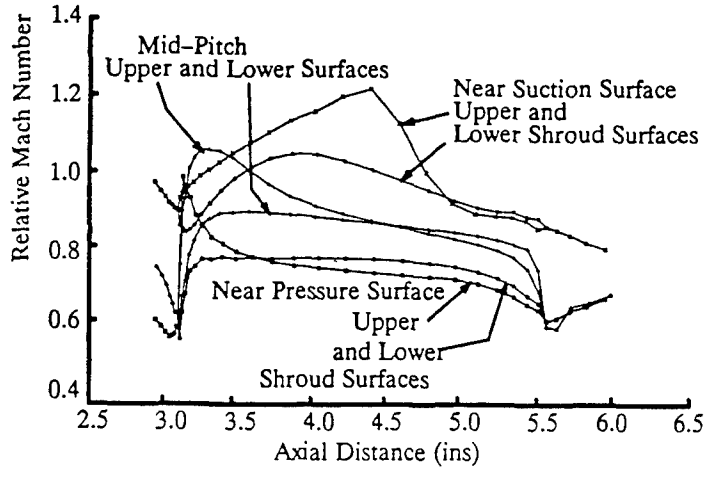

Figure 29. E^3 **Part-Span Shroud Loading Distributions.**

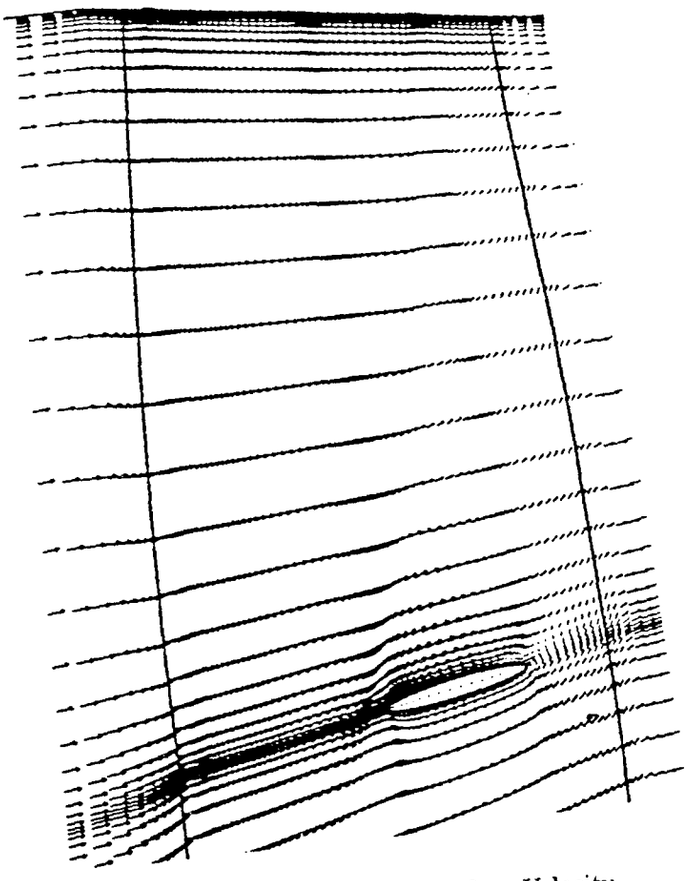

Figure 30. E^3 Near Suction Surface Velocity Vectors.

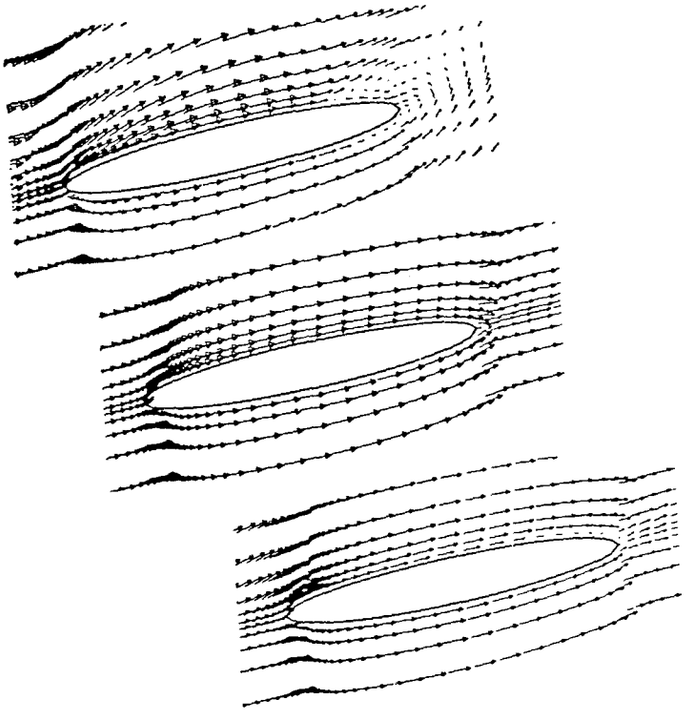

Figure 31. Velocity Vectors around the Part-Span Shroud near the Suction Surface (left), at mid-passage, and near the Pressure Surface (right) for E^3.

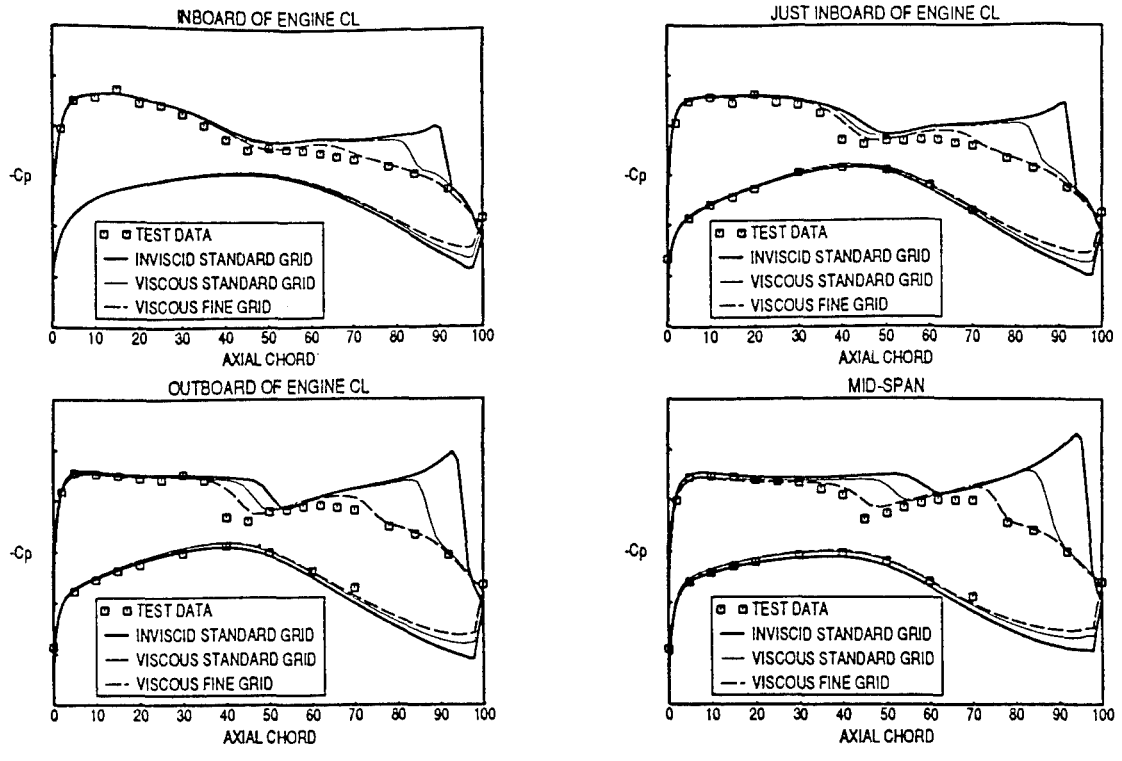

Figure 32. Cleanwing Surface Pressure Distributions.

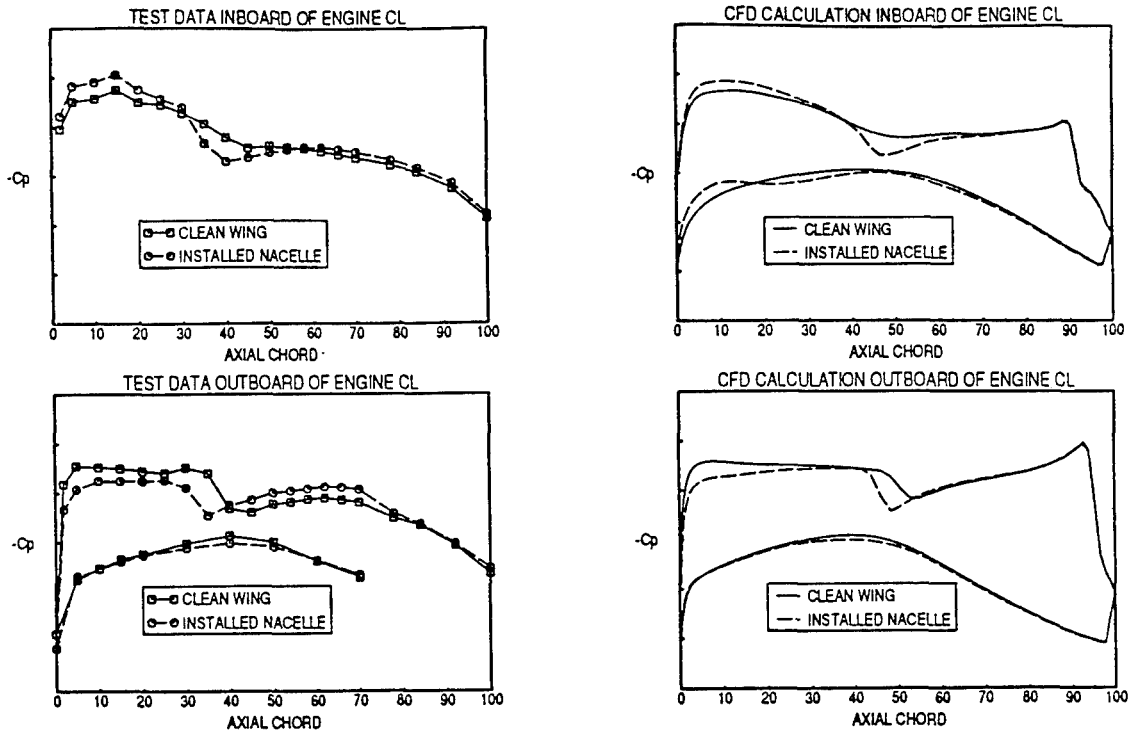

Figure 33. Wing Surface Pressure Distributions for Cleanwing and Installed Nacelle.

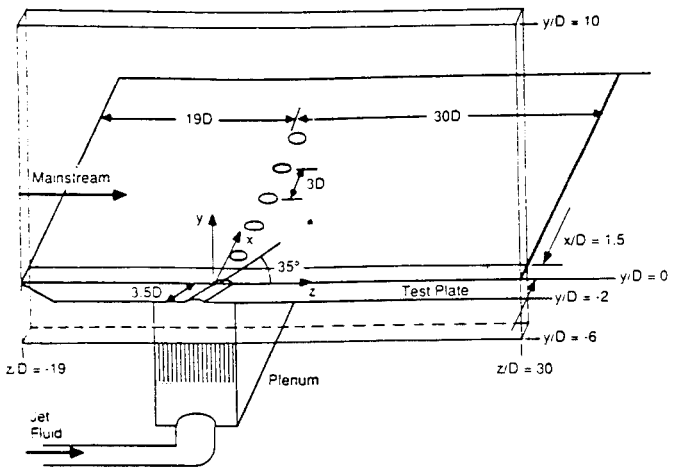

Figure 34. Essential Features of Experimental Film Cooling Configuration Showing Overall Extent of Computational Domain.

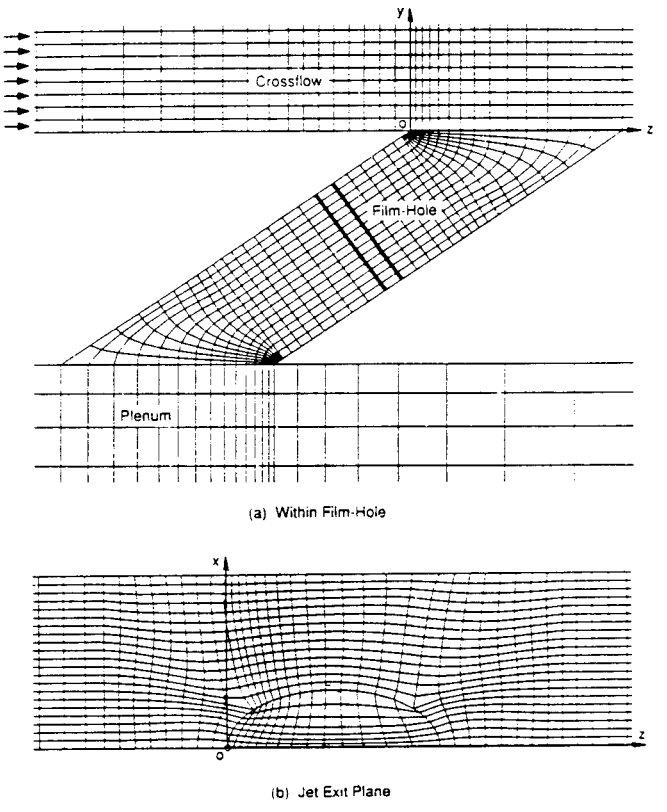

Figure 35. Computational Grid for 3D Discrete Jet Film Cooling: 200,090 Grid Points with 22 Lateral, 85 Vertical, and 107 Streamwise.

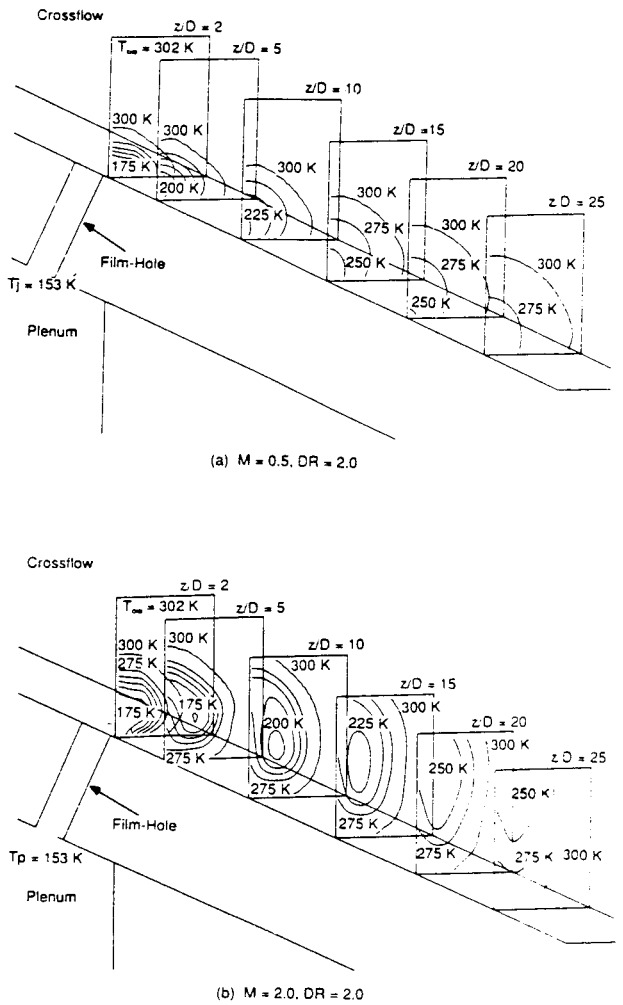

Figure 36. Isometric View of Computed Temperature Contours on Many Crossflow Planes showing Coolant Jet Trajectories and Lateral Diffusion.

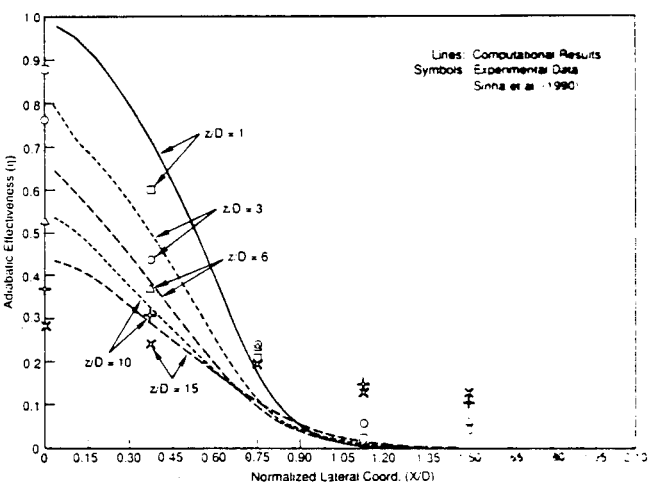

Figure 37. Lateral Variation of Adiabatic Effectiveness from Computations and Experiments for a Blowing Ratio of 0.5 at Five Streamwise Stations.

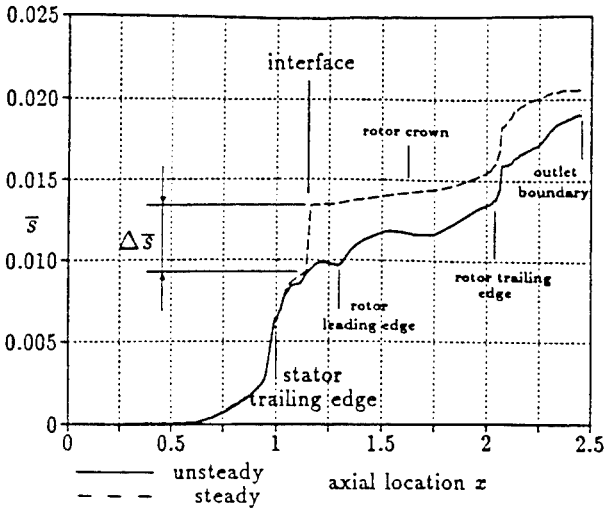

Figure 38. Entropy Rise in Numerical Simulations of the ACE Stage (turbulent boundary layers/no free stream turbulence).

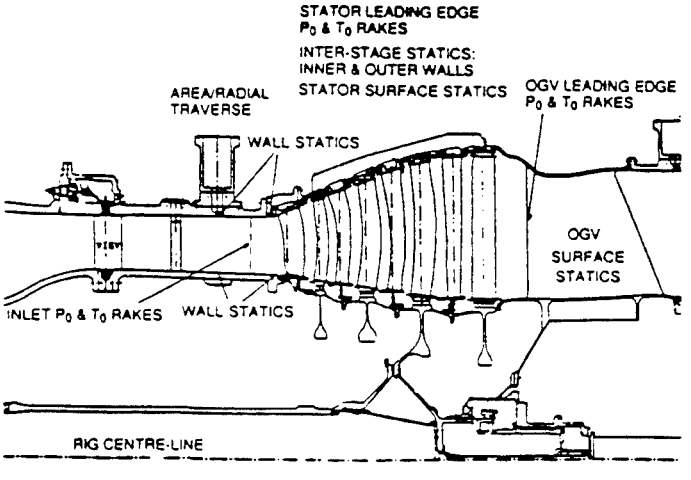

Figure 39. Schematic of Trent 700 LP Turbine Parts Rig.

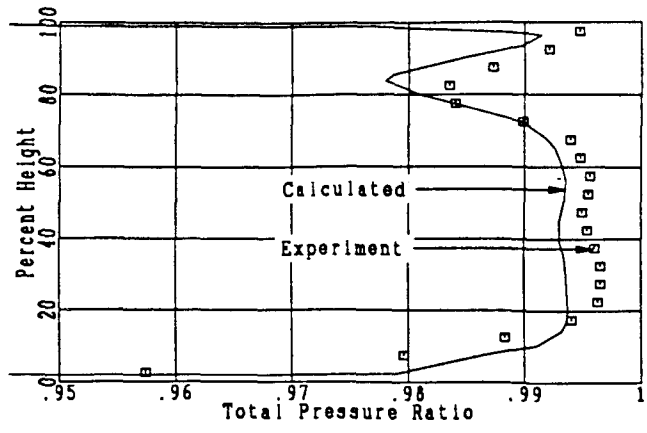

Figure 40. Downstream Total Pressure Profile for the E^3 LP Turbine Vane.

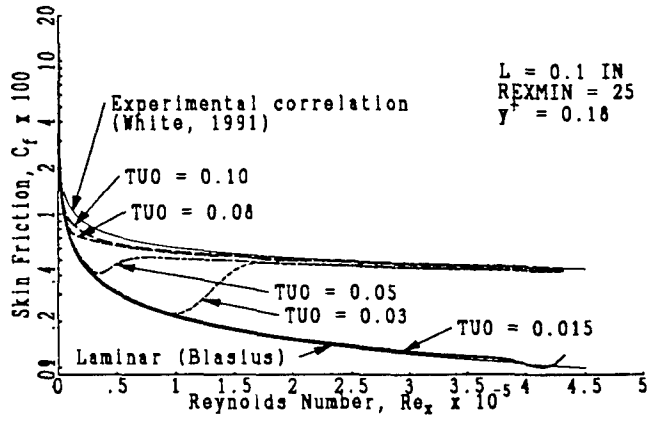

Figure 41. Effect of Freestream Turbulence Intensity for Transitional Flat Plate Flow with Viscous EULER.

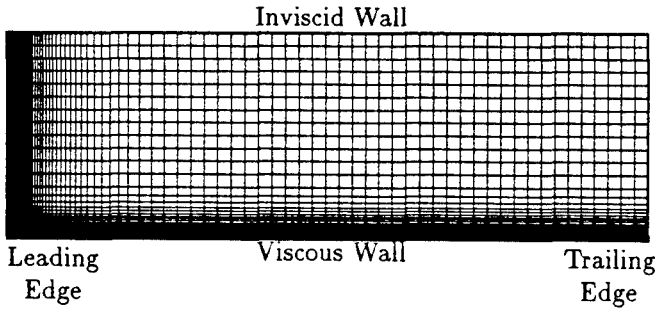

Figure 42. Typical Flat Plate Grid - 81x81 grid (7561 grid points).

Table 2. Performance of parallel algorithm on inviscid transonic turbine cascade (154,000 grid points)

# Processors	sec/iter/point/equation	Performance/Cray	Parallel Efficiency
Cray Y-MP (1)	1.10×10^{-5}	1.00	——
iPSC/860			
4 x 2 x 2 (16)	1.51×10^{-5}	0.73	80.9 %
4 x 2 x 4 (32)	8.85×10^{-6}	1.24	67.1 %
4 x 4 x 4 (64)	6.29×10^{-6}	1.75	50.1 %
8 x 4 x 4 (128)	4.59×10^{-6}	2.40	33.3 %
Touchstone Delta			
4 x 2 x 2 (16)	1.36 x 10–5	0.81	74.8 %
4 x 2 x 4 (32)	8.09 x 10–5	1.36	58.9 %
4 x 4 x 4 (64)	5.84 x 10–6	1.89	41.4 %
8 x 4 x 4 (128)	4.47 x 10–6	2.46	25.9 %
8 x 4 x 8 (256)	4.30 x 10–6	2.56	14.9 %

AERO DESIGN OF TURBOMACHINERY COMPONENTS – CFD IN COMPLEX SYSTEMS

by

K. Broichhausen
MTU München
Postfach 50 06 40
Dachauer Strasse 665
D-8000 München 50
Germany

I. Introduction

The importance of CFD in the design of turbocomponents is no longer a matter of discussion. Since the fundamental publications of Wu and the first successfull attempts to determine the potential 2D flow in blade rows the position of computational fluid dynamics in the design of jet-engine turbocomponents has increased continuously. This mainly has been driven by the two factors "time" and "cost".

As a result the design engineer of today can rely on a mature set of numerical approaches for the aerodynamic optimization of turbomachines. This design system is structured differently in the specific companies. Generally, however, an inverse correlation between the complexity of the problem and the complexity of the numerical approach can be observed: The most complex problems rely on relatively simple codes with a big portion of empiricism and vice versa. An overview of the design problems and the application of computational methods is given in Fig. 1. Related to the progress in computational fluid dynamics and computer hardware quality (cost and speed) a trend towards the use of more complex numerical tools for more complex design problems is obvious. The remarkable improvement of the design tools (i. e. numerical methods and experience basis) can be shown impressively by the reduction of the time being necessary to get the design performance for the last two European military engines, the RB199 and the EJ200. There is, however, still a remarkable gap between the capability of the design tools to define the components of a new generation engine and the desired status. This relation between the standard reached in analysis and modelling can be composed with the technically desirable standard and the scientifically correct standard according to an assessment of different specialists summarized by Grieb /1/. This analysis shows that aerodynamic and aeroelasticity are stil about 40 - 50% away from the desirable standard. Compared to the scientifically correct standard the status is of course even worse.

II. Symbols

a	velocity of sound
$D\sigma/Dm$	change of blockage
h	enthalpy
m	meridional direction
m'	perturbation amplitude
M_{S2}	mass flow on hub-to-tip surface
O	surface
p	static pressure
r	radius
S2	hub-to-tip surface
V	volume
w	relative velocity
ϕ	circumferential direction
ϕ'	perturbation amplitude
z	axial direction
β	flow angle
δ	angle of quasi-orthogonal plane
ρ	density
σ	blockage
ν	coordinate of quasi-orthogonal plane
ψ	streamfunction
ω	annular velocity
ω	vibration frequency

Presented at an AGARD Lecture Series on 'Turbomachinery Design Using CFD', May to June 1994.

III. Hub to Tip solutions

The design of turbo-components from scratch is generally started by an approximate computation of the flow pattern between hub and tip in the gaps between the blade rows. For this simple modelling of the complex turbomachinery flow streamline curvature methods are appropriate tools.

For these methods a parametric description of the coordinates as shown in Fig. 2 can be chosen. By this procedure the meridional flow can be calculated for both, radial and axial flow turbomachines. By combining the
- geometry of the meridional streamlines,
- the continuity equation along the streamlines,
- the momentum equations,
- the energy equation and
- the equation of state in differential form

a linear equation system can be established.

As the pressure gradient on the quasi-orthogonal computational plane and the streamline is described by

$$\left[\frac{dp}{dv}\right]_{S2} = \left[\frac{\partial p}{\partial r}\right]_{S2,z} \sin\delta + \left[\frac{\partial p}{\partial z}\right]_{S2,r} \cos\delta$$

the essential portions of the pressure gradient in the radial and axial direction must be derived by the differential equation system as shown in Tab. 1.

It is obvious that for Mach number unity the change of the pressure has a singularity. For practical design purposes the stability in the unstable domain around sonic Mach number can be improved by simple interpolation between the two branches of the hyperbola $(1 - Ma^2)^{-1}$.

The numerical solution procedure of the whole algorithm is as follows

- For the upstream boundary total pressure and temperature are given.
- For the different computational planes mass-flow and rotor speed are defined together with hub and tip coordinates. Also blockage, losses and turning is computed by appropriate models.
- The computation is started with an area averaged quasi-streamline system formulated by cubic splines. On that basis all geometry data and derivatives can be established.
- The differential equations describing the pressure distributions are solved iteratively starting with the Laval number at the mean streamline. This iteration is finished by achieving the prescribed integral mass-flow within a given tolerance band.
- As different radial distributions can result in the same integral mass flow, a difference between the computed mass flow for neighbouring streamlines and the prescribed one might be detected. In this case a new position for the relevant streamlines is computed by interpolation.

As a final result the computation can give all the data relevant for turbomachinery design. In the case of a real duct flow method all the parts related to threedimensional blade effects (in literature frequently denoted as "blade forces") are zero. Including those terms, however, the method is valid also for the internal flow in the blade rows and thus can be used as a through flow method. For that purpose also computational planes in the blade passage have to be introduced.

In combination with a blade to blade computation method (S1-flow calculation) and taking the flow angles on the rotational surface between the blade rows from the computed blade to blade flow, the streamline curvature methods cover the most substantial threedimensional effects like bow and lean in an appropriate way.

If such a method is combined with adequate loss models and/or mixing models it can also be developed as a useful tool for performance calculation of turbomachinery components.

The limit of the streamline curvature methods is sonic meridional flow. So, for example, the determination of the choke margin is hard to perform.

Another limit is the accuracy referring to details of the flow pattern:
- Greater number of computation planes within the blade rows result in stability problems.
- The resolution of hub and casing boundary layers is poor. The overall effects are generally introduced by a blockage factor. A combination of a streamline curvature method with a more exact hub/casing boundary method seems to be not adequate.

The extraordinary flexibility of the streamline curvature method is demonstrated by Fig. 3 which refers to a combination of a transonic fan, the bypass duct including the stator and the inner duct with the stator, the interduct and an ax-rad high pressure compressor. The LPC and the HPC are rotating with different speeds. The figure shows the resulting streamlines. The computation planes are indicated by the squares, inlet and outlet planes of vanes/blades by the dashed lines.

Because of their short computation times the streamline curvature methods are also predestinate tools for parametric studies. As an example Fig. 4 shows the influence of different bypass back pressures on the bypass ratio and the resulting flow pattern in the compressors of a military jet engine (low pressure compressor, interduct and high pressure compressor).

Finally the capability of the described simple methods is demonstrated by the performance map of a multistage low pressure turbine. The convergence rate for the choking limit, of course, is very poor in this case (Fig. 5).

The discussed short comings of the streamline curvature methods can be overcome by field methods applied on a representative stream surface extending from hub to casing. In the streamline curvature methods the up- and downstream influence is only produced by the geometry (position and curvature) of the streamlines, whereas for the field methods the meridional coupling is guaranteed by the basic differential equations.

Starting with the continuity equation, and the momentum equation in all coordinate directions (formulated for a hub to tip streamsurface) the circumferential gradient in axial and radial momentum equation and can be substituted. Taking the energy equation, the basic thermodynamic equations and defining the streamfunction as

$$\left[\frac{\partial \psi}{\partial r}\right]_{S2,z} = \sigma r \rho w_z ,$$

$$\left[\frac{\partial \psi}{\partial z}\right]_{S2,r} = - \sigma r \rho w_r$$

a system of partial differential equations for radial and axial direction can be derived. Taking into account that the total derivatives of entropy and rothalpy between different streamlines are independent of the way (which corresponds to the conservation of rothalpy and entropy) a single partial differential equation for the twodimensional meridional flow along a representative streamsurface can be derived. By means of the Stoke's theorem an integral formulation can be given (Tab. 2).

For the streamfunction equation the basic equations for steady flow have been the basis. Taking the unsteady conversation equations, a time dependent Euler method can be designed for application on the meridional plane. For this purpose the procedure is comparable to the derivation of the streamfunction equation. The resulting equations are given in Tab. 3.

The capability of the differential methods for computing meridional flows described above is discussed in the following.

As these methods basically are non-viscous the loss-terms here are generally not included. The streamfunction method is applied to stator and rotor of a turbine for ultra-high-bypass propfan. The data are compared to an 3D Euler solver. The basic geometry and the numerical grid is shown in Fig. 6. The resulting static pressure distribution along streamlines representing hub, mean and tip radius show basic agreement between the two methods (Fig. 7). Some inconsistencies are observed for the Euler solver with respect to the system changes between rotor and stator. This basic similarity is also confirmed by the axial velocities shown in Fig. 8. The big advantage of the Euler solver on the meridional plane can be demonstrated by its application to a highly loaded transonic compressor rotor (Fig. 9). The shock waves in the outer part of the meridional surface are reproduced with good accuracy. The shock itself generates a sudden turning angle of the meridional streamlines.

IV. Consideration of viscous effects (Hub to Tip)

The methods for hub to tip flow calculation discussed so far have been derived by a formulation of the momentum equation neglecting the viscosity of the fluid. To get quantitive data on the basis of this simplified assumption, the losses are considered in most cases incosistently within the

description of the thermodynamic properties of the fluid.

To improve this situation casing boundary layers are often calculated separately on the basis of boundary layer equations. In extension to these methods coupling the non-viscous core flow calculation with a casing boundary layer calculation, the viscous 2D meridional flow can be computed on the basis of the circumferentially averaged 3D Navier-Stokes equations /2/. Doing that it would also be possible to incorporate the gradients in circumferential direction by means of additional terms. The resulting equations for rotational symmetric flow are given in Tab. 3.

The equations are solved numerically on an H-Grid which is adopted to the blade/vane-inlet and -outlet planes (Fig. 10). For the casing boundary layer a grid refinement should be applied. The solution of the equations can be done iteratively by means of a pressure correction method /3/. Progressing in downstream direction the parabolized equations of motion and the energy equation are solved for a given pressure field. By means of a correction step the continuity is covered and an improved pressure field is generated.

The viscous computation is performed turbulent with a simple mixing length model. Radial mixing may be incorporated by models described by Adkins, Smith /4/ or Gallimore, Cumpsty /5/. Additional losses because of tip clearance flow, blade wake and secondary flow can be considered inconsistently like in the described streamline curvature and streamfunction methods. The resulting meridional flow pattern is shown in Fig. 11. In contrary to the methods described before with an inconsistent description of the losses near the wall the hub and casing boundary layers are represented extremely good with the parabolized Navier-Stokes methods on a meridional plane.

V. Blade to Blade Flow

The methods for computing the blade to blade flow including streamline contraction from hub to tip (axial velocity density ratio) and radial shift of the stream surface extend from simple potential methods to Navier-Stokes methods. Details of those methods are described in /6, 7, 8/. In this context some single topics referring to transonic viscous "blade to blade" flow shall be discussed.

To avoid problems arising from type change of the differential equations the hyperbolic character can be simulated in the elliptic numerics without a change of the basic algorithm (as proposed by Jameson /9/) by introducing artificial density. Efficient procedures are described by Giese und Eberle /10, 11/ and give the possibility to extend the Mach number range of subsonic methods up to $Ma \leq 1.2$. As the streamfunction methods have a reduced accuracy near the sonic point because of the maximum of the flow function (ρw) the application of artificial density to potential methods is preferred.

The problems arising with the character change of the basic equations around Mach number unity can be avoided by using time marching methods based on the unsteady conservation laws which are hyperbolic for both sub- and supersonic flows. The steady solution is achieved by marching in time directions from an initial data surface satisfying the boundary conditions until a steady solution is found. An overview on the methods used is given by Hänel /12/.

Special aspects regarding the application to turbomachinery flow are discussed for example by /13, 14/.

Despite of using time marching or steady numerical codes for the computation of blade to blade flow the results are still neglecting viscous effect. This, however, does no longer meet the todays and future requirements on blade design methods. The viscous effects which result in losses and underturning can be dealt with by the boundary layer approximation or by applying full Navier-Stokes codes to the blade to blade flow.

For transonic flows the coupling of Euler solver and a boundary layer integral method have proved to be an efficient tool for blade designs covering viscous effects. The coupling is performed by a transpiration model. After a certain number of Euler-time steps the corresponding boundary layer is calculated by a fast integral methods. Special semi-empirical models for the determination of the boundary layer status near compression shocks /15/ laminar separation bubbles /16/ and turbulent separation criteria can be insorted. The numerical damping by additional 2nd and 4th order terms is done according to Jameson/Schmidt /17/. For turbulent boundary layers and wakes the Baldwin/Lomax

turbulence model is applied. The examples regarding the interaction of cooling air and shocks in a turbine passage and shock pattern strongly influenced by shock boundary layer interaction prove the general capability of methods like this (Fig. 12).

The methods for the calculation of blade to blade flows as discussed above are the most frequently used ones during the design phase. Thus computation time and cost are important factors from the users point of view. A comparison for different approaches for viscous effects shows Fig. 13. It becomes obvious that with the use of advanced computers the difference of calculation time is no longer a matter of discussion for 2D methods. Overall costs and the time for pre- and post-processing are the focal point for the future.

VI. 3D-Methods

Basically the same classes of numerical procedures as discussed for blade to blade and hub to tip flow are used for 3D flows through blade rows. The real iterative coupling of hub to tip flow and blade to blade flow already gives the threedimensional non-viscous flow pattern. For that purpose the hub to tip flow surface is generated by the streamlines ψ = 0,5 on the blade to blade surface /18/. This method can give a first quick impression on basic 3D effects. Generally, however, the distribution of losses is of primary interest regarding 3D computations. For subsonic flows this can be done very efficient by 3D partial parabolized Navier-Stokes methods. The equations are formulated for primary and secondary flow velocities.

The diffusion in the main flow direction is neglected. Then a downward stepping integration is possible if the static pressures are taken as known (in the first iteration from a couple S1/S2 surface calculation). As it is described already with respect to the circumferentially averaged Naver-Stokes equation the continuity equation is taken to correct the pressure field /19/. This pressure correction is applied to the overall mass flow and to the discrete finite volume element.

The application of these methods is restricted to subsonic flows with attached boundary layers. So, for example, regarding turbines the horseshoe vortex is not reproducable.

To overcome the Mach number related limitation 3D Euler methods are applied in transonic/supersonic flows. A lot of numerical solvers for Euler methods have been established so far /20, 21/. For design purposes the use of an H-grid has proved to be quite successful. As shown in Fig. 14 the grid is more closely spaced near the profile suction and pressure sides. The grid structure is refined in a simple multigrid procedure. The resulting local Mach numbers are shown in Fig. 15. It seems to be of interest to compare the above discussed quasi 3D procedure with the 3D Euler method. This is done for the data presented in /22/ and summarized in Fig. 16. The laser data are related to both the results of a quasi-3D procedure (streamline curvature method for hub to tip flow and 2D Euler/2D Navier-Stokes blade to blade flow) and the results of the 3D Euler code. The quasi 3D procedure represents the data qualitatively. Near the hub the quasi 3D computation shows a distinct bow shock which is smoothed out to great extend in case of the Navier-Stokes blade to blade flow. The better agreement of the Navier-Stokes data with respect to the laser data can also be seen by comparing the exit Mach number and the shock pattern for 70% and 90% span. The use of the 3D code also improves the situation at the hub, however, the strong interaction of the shock waves and the blade boundary layers is of course not covered. As a result, the exit Mach numbers for 70% and 90% span are again lower than the measured ones.

The situation regarding the non-viscous Euler code is improved, if viscosity near the wall is simulated by means of body forces as also described in /23/. The rough procedure is outlined in Tab. 4. The exponent function is calibrated with respect to experiments. The influence of the pseudo-viscosity in the blade pressure distribution of a turbine and the radial distribution of relative Mach number, flow angle, static and total pressure at the blade exit is shown in Fig. 18. The more realistic shape of these distributions gives an explanation for the fact that the 3D Euler solvers including pseudo-viscosity are (after careful calibration) important tools for the design of turbomachines. The potential of this relatively simple 3D quasi-viscous methods like this is demonstrated in Fig. 19 by comparing the exit flow field of a highly loaded turbine vane with experimental data. The comparison refers to two vanes with different 3D structure (lean and bow). The difference in secondary flow pattern is reproduced

well by the quasi-viscous Euler method. This becomes especially obvious by comparing the streamwise vorticity. Even details of the separated flow as for example the separation of the secondary vortices near the trailing edge are covered by this simplified simulation of viscosity in combination with the Euler method.

A further improvement can only be achieved if the fully 3D Navier-Stokes equations are used. For solving these equation a strongly conservative formulation according to Tab. 5 is used. As for 2D solvers this formulation guarantees a stable behaviour in shock-waves. The solver established by Jameson et al /24/ has proved its practicability. The basic equations are solved cell centered. A two/- four step Runge-Kutta solver is used. For stabilization second and fourth order terms are used for artificial dissipation. This is governed by a sensor function based on the 2nd derivative of the density. For convergence improvement the maximum local time step is used according to the CFL-criterium. As not only the blade/vane flow but also complex geometries are the focus point of interest the application of a block structured grid has big advantages /25/. The grid generation is relatively independent of neighbouring blocks. Data referring to a special block can be stored if they are not used for the computation. An example referring to the tip clearance flow in a compressor cascade is shown in Fig. 20 and 21.

The cascade has been experimentally investigated by Flot /26/ with 1.1% tip clearance. As shown in Fig. 20 the cascade is discretized by a C-grid the clearance by an H-grid. The resulting flow pattern in comparison to an experimental flow visualization is shown in Fig. 21.

Regarding the complex environment of turbomachines the computation of a single blade row is only a valid tool to understand details of the flow. For real design purposes the interaction of the blade rows and stages is of predominant importance. To cover these effects during a standard design without leaving out of consideration the high quality of 3D effects resolution offered by 3D methods it is standard practise to average the 3D flow pattern behind rotor and stator. The averaged status is then taken as the inlet boundary condition for the next blade row. A simple, but proven method for this coupling, is explained in Tab. 6. At the inner boundaries the upstream influence is managed by energy averaging the downstream status taking into account

W_R, $W_u + \omega R$, w_z, ρ, p

From this averaged status the pressure is taken as downstream boundary condition for the upstream flow field. With the same procedure the upstream part of the internal boundary is averaged. According to the characteristic theory the averaged three velocity components and the density are imposed as differences on the downstream flow field.

Examples for the application for coupled 3D Euler solvers including the pseudo-viscosity are shown in Fig. 22 for multistage turbines and Fig. 23 for multistage compressors. The turbine pressure distribution show an excellently matched design. The compressor case is shown for two back pressures. Clearly to be seen are the shocks moving upstream even in the first rotor if the back pressure is raised.

A comparable coupling technique is also possible for 3D Navier-Stokes codes. As an example the meridional flow for three turbine stages is shown in Fig. 24. This computation is done for analysis reasons. In the design practise the 3D Euler with pseudo-viscosity is of superior quality and applicability.

VII. Unsteady flow

The strong requirements with respect to a minimum engine weight are the reason for increasing importance of aeroelasticity. In this context blade row interaction, flutter, rotating stall and distortion has to be addressed.

Generally for the computation of the unsteady flow effects hyperbolic method are the most suitable tools. Into the lowest level of complexity the linearized methods can be classified. For those methods the unsteady flow is formulated as a small harmonic oscillating disturbance of the steady flow. Similarly, the computational grid is assumed to oscillate harmonically with the same frequency at a small perturbation amplitude (ϕ', m'). By doing this the unsteady flow can be described by the frequency of the oscillation ω and the vector of the complex disturbation amplitudes. Introducing these correlations into the Euler equations in finite volume form for blade to blade

flow with variable radius and variable streamtube-thickness a system of equations shown in Tab. 7 can be derived. Second order terms are neglected. The left hand side corresponds to the Jacobians of the vectors of the conservative variables U, the fluxes F and G and the source terms H resulting from the streamsurface-geometry of the Euler equations. The right hand side which is rather complex is resulting from the moving grid. It is not depending on the variation of the flow properties and thus can be computed in front of the aero computation and stored. It has to be noticed that in the described method, which has proved to be an excellent working tool, the time derivative of the disturbance velocity is included. This is physically not necessary. It, however, makes it possible to use existing time marching solvers, for example /15/, to calculate the finally steady complex perturbation quantities. So for the steady and for the unsteady flow field similar solvers can be used.

The following boundary conditions are applied

- non reflecting boundaries up and downstream /27, 28/
- equal disturbance amplitudes on corresponding points of the periodic boundaries,
- normal flow velocity equal to normal mechanical velocity of the blade on the blade surface.

For the increase of convergence rate a multigrid algorithm has proved to be successful (Fig. 25).

As realistic test the standard-configuration 4 of /29/ is used. This is a transonic turbine cascade with a reduced 1st bending frequency between 0.6 and 0.75. Looking at the unsteady suction side pressure distribution shown in Fig. 26 for an exit Mach number of 1.19 a quality improvement in comparison to standard methods is obvious. The resolution of the shock induced pulsation has improved remarkably. Also the summary chart showing the unsteady work for all Mach number clearly indicates the unstable region in conformity with the experiment.

In extension of the linearized methods the full Euler equation can be used to simulate unsteady flow effects. Comparing the results and the effort (CPU-time) the linearized methods seem to be more advantageous for practical design work. For calibration of the linearized methods, however, the full Euler solvers are extremely important.

More relevant with respect to practical work seems to be the incorporation of viscous effects. Very efficiently this can be done by coupling Euler and boudary layer methods.

An excellent practical tool proved to be an integral method according to /30, 31, 32/. The unsteady compressible boundary equations in form of the momentum equation and the mechanical energy equation are integrated layer for the two variables momentum thickness and shape factor. For turbulent boundary layers also a transport equation for turbulent dissipation is solved. The position of transition is detected by the e^n-method. For the coupling with an unsteady Euler code a direct/inverse (semi-inverse) formulation is used and unsteady separation bubbles can be computed. The upstream wake is addressed by an empirical law. The resulting wakes, the wake transport, the wake deformation and the resulting vorticity passing through blade row are demonstrated in Fig. 27. Comparing the time mean skin friction of the unsteady calculation with a steady calculation a difference with regard to the losses can be found (Fig. 28).

Another important complex aeroelastic problem of increasing importance is the transfer of distortion in the compressor and the resulting blade forces. This can be reproduced with good accuracy by a 2D calculation (circumferential and axial) of the inlet duct, the compressor and the exit duct for a given inlet and/or exit flow non-uniformity (see Fig. 29).

The compressor is represented by its geometry and blade row characteristics (radially averaged). The calculation is again performed on the basis of linearized Euler equations. Careful modelling of the unsteady blade row response and wave propagation effects allows the calculation of short scale and long scale disturbances. This feature gives an important advantage in comparison to parallel compressor models as it can be used for both the aerodynamic behaviour due to (small scale) disturbances and (long scale) distortion as well as for the determination of the resulting blade loads. A representative result is given in Fig. 30 regarding the calculation of distortion transfer through a 5-stage HP-compressor. The response of the compressor to the incoming total pressure distortion leads to the development of a total temperature distortion. The profile of the temperature distortion is shifted relative to the pressure pattern

due to different propagation speeds. Local entropy gradients at the fringes of the pressure drop cause localized (small scale) increase/decrease of the temperature which is also found in test results.

With this set of methods for the standard design procedure tools are available to attach problems resulting from the complex interaction between aerodynamics and structures and vibration.

In the phase of numerical development and testing the coupled methods (Euler and boundary layers) are extended to unsteady Navier-Stokes. From the designers point of view these codes, however, have not yet proven a decisive advantage in comparison to the discussed simplified solutions.

VIII. System

With the improvement of the numerical CFD codes, as outlined above, the management of the design process and of the available data becomes more and more important. This, on the one hand, holds true for visualization systems, pre- and postprocessors and program interfaces. On the other hand automatic optimization techniques and expert systems will be - and are already today - the corner stones for design systems.

Examples for optimization techniques are the evolution strategy, hill climbing strategies and penalty -/barrier methods /33/. As an example the evolution-strategy which has proved to be extremely robust but time consuming shall be discussed shortly. The evolution in nature with its recombination, mutation and selection process is adapted.

For a simple optimization problem one optimum shall be existing. A certain combination of parameters (genes) results in a certain status of the subject with respect to the optimum. Different descendants have more or less optimum qualities than the parents with respect to the goal. This basic procedure is now performed for generations (see Fig. 31). The parents A to D of the k-generation, have the genes X1, ..., Xn. In case of an optimization of work split and annulus of a compressor these genes represent the stage work, the flow angles, the solidity and so on. Two stochastically chosen parents generate 6 descendants which genes are taken randomly again from one of the parents. By mutation the genes of the six descendants are changed slightly. The quality of the resulting descendants are decisive for survival and reproduction. The strategy and the controll of the mutation is extremely important with respect to the result and the convergence /34/.

As a lot of generations have to pass (100 - 300) till the optimum is found, CPU time again has a different importance. An example for the optimization of a high-speed low pressure compressor of an advanced ducted propfan (ADP) engine is shown in Fig. 31. Efficiency and surge margin have been the quality indicators. For blading optimization the design turning, the Mach numbers and the overall loss and boundary layer development are the quality indicators. For the purpose of optimization a fast streamfunction method including a transonic approximation for local supersonic flow coupled with an integral boundary layer code (as described above) is chosen.

It should not be neglected that the blind application of the described algorithm might also lead to quite unusual results (Fig. 32). Because of the high computation times the optimization techniques up to now are not widely used in the standard design process. Only for special and often very complex problems they are used, more or less as a sparrings partner for the design engineer.

On the other hand they can produce data for an expert system. For those systems rules are extracted from experts knowledge and existing, optimized solutions. The rules for profiles are generated basically by approximiation of the interdependency between geometry parameters like stagger, angles and so on and aerodynamic inlet conditions. If the rules are adjusted continuously those systems have proved to generate 95% solutions which are a good basis for further improvement.

References

/1/ H. Grieb
The Changing Role of Experimentation in Aero-Engine Research and Development - The Perception of an Engine, Manufacturer
Third European Propulsion Forum, Paris Nov. 1991

/2/ J.J. Adamczyk
Model Equation for Simulating Flows in Multistage Turbomachinery
ASME paper 85-GT-226, Houston, March 1985

/3/ J. Moore; J.G. Moore
Lecture Notes on Viscous Flow Calculations in Turbomachinery,
VKI-LS 1982-05, 1982

/4/ G.G. Adkins; L.H. Smith
Spanwise Mixing in Axial-Flow Turbomachines
Trans. of the ASME, Journal of Engineering for Power, Vol. 104, 1982

/5/ S.J. Gallimore; N.A. Cumpsty
Spanwise Mixing in Multistage Axial Flow Compressors
Part I - Experimental Investigation
Trans. ASME, Vol. 108, July 1986

/6/ W.H. Isay
Beitrag zur Potentialströmung durch axiale Schaufelgitter
ZAMM 33, S. 397-409, 1953

/7/ Th. Katsanis; W.D. McNally
Revised Fortran Program for Calculating Velocities and Streamlines on a Blade-to-Blade Streamsurface of Turbomachine
NASA TM X-1764, 1969

/8/ R.V. Chima
Develpment of an explicit multigrid algorithm for quasi three-dimensional viscous flows in turbomachinery
NASA TM 87128, 1986

/9/ A. Jameson
Iterative Solution of Transonic Flows over Airfoils and Wings, Including Flows at Mach 1
Comm. Pure Appl. Math. Vol. 27, pp 283/309, 1974

/10/ U. Giese
Berechnung schallnaher Einlaufströmungen
Diss. RWTH Aachen, 1983

/11/ A. Eberle
Eine Methode finiter Elemente zur Berechnung der transsonischen Potential-Strömung um Profile
MBB-Bericht Nr. UFE 1352, 1977

/12/ D. Hänel
Computational Techniques for solving the Navier-Stokes Equations
AGARD-CP-510, St. Antonio, 1992

/13/ J.D. Denton
A Time Marching Method for Two- and Three-dimensional Blade to Blade Flows
R & M No. 3775, Oct. 1974

/14/ H.-W. Happel; H.-J. Dietrichs, K. Lehmann
Computation of Transonic 2D Cascade Flow
AGARD-CP-401, 1986

/15/ M. Hoeger; K. Broichhausen
Prediction of 2D Viscous Transonic Flow in Compressor Cascades Using a Semi-Empirical Shock/Boundary-Layer Interaction Method
ASME Paper 92-GT-277; Cologne 1992

/16/ J. Rannacher,
Vorgang des Grenzschichtumschlages in laminaren Ablösewirbeln und seine Berücksichtigung bei Grenzschichtrechnungen
Maschinenbautechnik 31, 322-326, 1982

/17/ W.B. Roberts
The Effect of Reynolds Number and Laminar Separation on Axial Cascade Performance
ASME paper 74-GT-68, 1974

/18/ P. Lücking, H.E. Gallus
Berechnung der dreidimensionalen kompressiblen reibungsfreien Unterschallströmung durch Gitter und Stufen von axialen Turbomaschinen mit Hilfe eines Differenzenverfahrens.
Inst. f. Strahlantriebe, Mi-Nr. 79-12, RWTH Aachen 1979

/19/ P. Lücking
Three-Dimensional viscous calculation techniques for radial and axial turbomachinery (partially-parabolic calculations)
Advanced Topics in Turbomachinery Technology, PLS-2, Concepts ETI, Inc., 1986

/20/ J.D. Denton
Extension of the Finite Area Time Marching Method to Three-Dimensions
VKI-LS 84

/21/ H.-W. Happel; B. Stubert
Computation of Transonic 3D Cascade Flow and Comparison with Experiments
AGARD-CP-437,

/22/ J.R. Wood; T. Strazisar; M. Hathaway
Test Cases for Computation of Internal Flows in Aero Engine Components; Test Case E/CO-2 Single Transonic Fan Rotor
AGARD-Advisory Report-275, July 1990

/23/ J.D. Denton
The Use of Distributed Body Force to Simulate Viscous Effects in 3D Flow Calculations
ASME Paper 86-GT-144, June 1986

/24/ A. Jameson, W. Schmidt
Some Recent Developments in Numerical Methods for Transonic Flow
Stuttgart: Fenomech-84 Conference
Seite 467, ..., 493, 1984

/25/ R. Radespiel
Progress in the Development of an Efficienct Finite Volume Code for the Three-Dimensional Euler Equations.
DFVLR-FB 85-31, 1985

/26/ F. Lebeuff; R. Flot
Low Subsonic Compressor Cascade NACA-86.
AGARD-AR-275, 1975

/27/ K.C. Hall; E.F. Crawley
A Linearized Euler Analysis of Unsteady Inviscid Flow in Turbomachinery
NASA-CR 180987, Mass. Inst. of Technology 1987

/28/ E. Acton; A.M. Cargill
Non-Reflecting Boundary Conditions for Computations of Unsteady flows in Turbomachines
UAATP Proc. of 4th Symposium, pp. 211-228 Aachen 1987

/29/ A. Bölcs; T.H. Fransson
Aeroelasticity in Turbomachines: comparison of Theoretical and Experimental Cascade Results
Communication du Laboratoire de Thermique Apliquée et de Turbomachines Nr. 13, L'Ecole Polytechnique Fédérale de Lausanne, 1986

/30/ Drela; Giles
A Two-Dimensional Viscous Aerodynamic Design and Analysis Code
AIAA 86-0424, 1986

/31/ Drela
Two-Dimensional Transonic Aerodynamic Design and Analysis Using Euler Equations
MIT GTL Report No. 187, Feb. 1986

/32/ Fenno; Newman; Hassan
Unsteady Viscous-Inviscid Interaction Procedures for Transonic Airfoils Using Cartesian Grids,
88-2591-CP, 1988

/33/ P.E. Gill; W. Murray; M.H. Wright
Practical Optimization
Academic Press; 1981

/34/ I. Rechenberg
Evolution Strategy Natures Way of Optimization
in: Methods and Applications, Possibilities and Limitations
Lecture Notes in Engineering, Vol. 47, Ed. H.W. Bergmann, Springer Berlin 1989

/35/ G. Kahl; A. Klose
Computation of time linearized Transonic Flow in oscillating cascades
ASME-Paper 93-TG-269, Cincinnati, May 1993

Acknowledgement

The author likes to thank MTU Motoren- und Turbinen-Union München GmbH for the permission for publication. Special acknowledgement should be given to the MTU-specialists on CFD which have not been mentioned in the references.

These are Gerhard Kahl, Dr. Andreas Fiala, Stephan Servaty for unsteady aerodynamics, Ralf-Dietmar Baier for turbine cooling, Dr. Martin Lawerenz, Erwin Wischmeier and Manfred Dupslaff for S2-flow and optimization techniques and Ernst Fischer for Navier-Stokes.

They have extremely contributed with their material and knowledge to the content of the paper.

Tables

$$\frac{1-\left(\frac{w_m}{a}\right)^2}{\rho}\frac{\partial p}{\partial r} = -b_3\frac{Dr}{Dm} + b_1\left\{1+(\kappa-1)\left(\frac{w_m}{a}\right)^2-\kappa\left(\frac{w_m}{a}\right)^2\left(\frac{Dz}{Dm}\right)^2\right\} + b_2\left\{\kappa\left(\frac{w_m}{a}\right)^2\frac{Dr}{Dm}\frac{Dz}{Dm}\right\}$$

$$\frac{1-\left(\frac{w_m}{a}\right)^2}{\rho}\frac{\partial p}{\partial z} = -b_3\frac{Dz}{Dm} + b_1\left\{\kappa\left(\frac{w_m}{a}\right)^2\frac{Dr}{Dm}\frac{Dz}{Dm}\right\} + b_2\left\{1+(\kappa-1)\left(\frac{w_m}{a}\right)^2-\kappa\left(\frac{w_m}{a}\right)^2\left(\frac{Dr}{Dm}\right)^2\right\}$$

$$b_1 = -w_m^2\frac{D^2r}{Dm^2}+\frac{(w_\varphi+wr)^2}{r},\qquad b_2 = -w_m^2\frac{D^2z}{Dm^2},$$

$$b_3 = -w_m^2\left\{\frac{1}{\sigma r}\frac{D(\sigma r)}{Dm}+\frac{\partial}{\partial r}\left(\frac{Dr}{Dm}\right)+\frac{\partial}{\partial z}\left(\frac{Dz}{Dm}\right) - (\kappa-1)\left(\frac{w_\varphi+\omega r}{a}\right)^2\frac{1}{r}\frac{Dr}{Dm}\right\}$$

Tab. 1 Equation system of streamline curvature system on hub-to-tip surface

$$\oint\left(\left[-\frac{1}{\sigma r\rho}\frac{\partial\psi^*}{\partial z}\left(1+\cot^2\beta_{r\varphi}\right)+\frac{1}{\sigma r\rho}\frac{\partial\psi^*}{\partial r}\cot\beta_{r\varphi}\cot\beta_{z\varphi}+\frac{\omega r\cot\beta_{r\varphi}}{\dot M_{S2}}\right]dr + \left[\frac{1}{\sigma r\rho}\frac{\partial\psi^*}{\partial r}\left(1+\cot^2\beta_{z\varphi}\right)-\frac{1}{\sigma r\rho}\frac{\partial\psi^*}{\partial z}\cot\beta_{r\varphi}\cot\beta_{z\varphi}+\frac{\omega r\cot\beta_{z\varphi}}{\dot M_{S2}}\right]dz\right)$$

$$= \iint\left(\left[\frac{1}{\sigma\rho}\left(-\frac{\partial\psi^*}{\partial z}\cot\beta_{r\varphi}+\frac{\partial\psi^*}{\partial r}\cot\beta_{z\varphi}\right)+\frac{\omega r^2}{\dot M_{S2}}\right]\cdot\left(\left[\frac{\partial}{\partial z}\left(\frac{\cot\beta_{r\varphi}}{r}\right)\right]_{S2,r}-\left[\frac{\partial}{\partial r}\left(\frac{\cot\beta_{z\varphi}}{r}\right)\right]_{S2,z}\right)dr\,dz\right)$$

$$+\iint\left(\frac{\sigma r\rho}{\dot M_{S2}^2}\left(T\left[\frac{ds}{d\psi^*}\right]_{S2}-\left[\frac{dh_{Rot}}{d\psi^*}\right]_{S2}\right)dr\,dz\right).$$

Tab. 2 Integral formulation of streamfunction equation on hub-to-tip surface

$$\int_V\frac{\partial\vec U}{\partial t}\,dV+\int_O\left\{\vec F\,dO_r+\vec G\,dO_z\right\}=\int_V\vec H\,dV$$

$$dV := \sigma\,r\,dr\,dz \qquad dO_r := -\sigma\,r\,dz \qquad dO_z := \sigma\,r\,dr$$

$$\vec U := \begin{vmatrix}\rho\\ \rho(w_r+c_\varphi\cot\beta_{r\varphi})\\ \rho(w_z+c_\varphi\cot\beta_{z\varphi})\\ \rho(u+\frac{w^2}{2}-\frac{\omega^2r^2}{2})\end{vmatrix}$$

$$\vec F := \begin{vmatrix}\rho w_r\\ \rho(w_r+c_\varphi\cot\beta_{r\varphi})w_r+p\\ \rho(w_z+c_\varphi\cot\beta_{z\varphi})w_r\\ \rho(h+\frac{w^2}{2}-\frac{\omega^2r^2}{2})w_r\end{vmatrix}$$

$$\vec G := \begin{vmatrix}\rho w_z\\ \rho(w_r+c_\varphi\cot\beta_{r\varphi})w_z\\ \rho(w_z+c_\varphi\cot\beta_{z\varphi})w_z+p\\ \rho(h+\frac{w^2}{2}-\frac{\omega^2r^2}{2})w_z\end{vmatrix}$$

$$\vec H := \begin{vmatrix}0\\ \frac{p}{\sigma r}\left[\frac{\partial(\sigma r)}{\partial r}\right]_{S2,z}+\rho r c_\varphi\left\{w_r\left[\frac{\partial}{\partial r}\left(\frac{\cot\beta_{r\varphi}}{r}\right)\right]_{S2,z}+w_z\left[\frac{\partial}{\partial z}\left(\frac{\cot\beta_{r\varphi}}{r}\right)\right]_{S2,r}\right\}+\rho\frac{c_\varphi^2}{r}\\ \frac{p}{\sigma r}\left[\frac{\partial(\sigma r)}{\partial z}\right]_{S2,r}+\rho r c_\varphi\left\{w_r\left[\frac{\partial}{\partial r}\left(\frac{\cot\beta_{z\varphi}}{r}\right)\right]_{S2,z}+w_z\left[\frac{\partial}{\partial z}\left(\frac{\cot\beta_{z\varphi}}{r}\right)\right]_{S2,r}\right\}\\ 0\end{vmatrix}$$

Tab. 3 Euler equations on representative hub-to-tip surface

$$CF(R) = CF(N)*\left[\frac{R(G)-R}{R(G)-R(N)}\right]^{EXP(N)} - CF(G)*\left[\frac{R-R(N)}{R(G)-R(N)}\right]^{EXP(G)}$$

$$\tau(R) = CF(R)*\frac{\rho}{2}w^2$$

$$\vec{FV} = \frac{\partial\tau(R)}{\partial R}\cdot\frac{\vec w}{|\vec w|}$$

Tab. 4 Incorporation of body-forces into a non viscous Euler-code

$$\iiint_V (\vec{W}_t - \vec{W}_{t_0})\, dV + \int_{t_0}^{t} \left[\oint\oint_{\partial V} \vec{A}\, dydz + \vec{B}\, dxdz + \vec{C}\, dxdy \right] dt = \vec{0}$$

$$\vec{W} = \begin{pmatrix} \rho \\ \rho u \\ \rho v \\ \rho w \\ e_t \end{pmatrix}, \qquad \vec{A} = \begin{pmatrix} \rho u \\ \rho u^2 - \sigma_{xx} \\ \rho uv - \sigma_{xy} \\ \rho uw - \sigma_{xz} \\ e_t u - \sigma_{xx} u - \sigma_{xy} v - \sigma_{xz} w - k\dfrac{\partial T}{\partial x} \end{pmatrix},$$

$$\vec{B} = \begin{pmatrix} \rho v \\ \rho uv - \sigma_{xy} \\ \rho v^2 - \sigma_{yy} \\ \rho vw - \sigma_{yz} \\ e_t v - \sigma_{xy} u - \sigma_{yy} v - \sigma_{yz} w - k\dfrac{\partial T}{\partial y} \end{pmatrix},$$

$$\vec{C} = \begin{pmatrix} \rho w \\ \rho uw - \sigma_{xz} \\ \rho vw - \sigma_{yz} \\ \rho w^2 - \sigma_{zz} \\ e_t w - \sigma_{xz} u - \sigma_{yz} v - \sigma_{zz} w - k\dfrac{\partial T}{\partial z} \end{pmatrix}$$

Tab. 5 3D Navier-Stokes equation in strongly conservative formulation

$$\int_V \left[\frac{\partial \mathbf{u}}{\partial t} - \frac{\partial m}{\partial t}\frac{\partial \mathbf{u}}{\partial m} - \frac{\partial \phi}{\partial t}\frac{\partial \mathbf{u}}{\partial \phi} \right] dV + \int_S \left[hr\, \mathbf{G}\, d\phi - h\, \mathbf{F}\, dm \right] = \int_V \mathbf{H}\, dV$$

with

$$\mathbf{u} = \begin{bmatrix} \rho \\ \rho w_m \\ \rho r v_\phi \\ \rho e_{rot} \end{bmatrix} \qquad \mathbf{F} = \begin{bmatrix} \rho w_\phi \\ \rho w_m w_\phi \\ \rho r v_\phi w_\phi + r p \\ \rho h_{rot} w_\phi \end{bmatrix}$$

$$\mathbf{G} = \begin{bmatrix} \rho w_m \\ \rho w_m^2 + p \\ \rho r v_\phi w_m \\ \rho h_{rot} w_m \end{bmatrix} \qquad \mathbf{H} = \begin{bmatrix} 0 \\ \dfrac{\rho v_\phi^2}{r}\dfrac{dr}{dm} + \dfrac{p}{hr}\dfrac{d\,hr}{dm} \\ 0 \\ 0 \end{bmatrix}$$

$$v_\phi = w_\phi + \Omega r$$

$$e_{rnt} = \frac{1}{\gamma - 1}\frac{p}{\rho} + \frac{1}{2}[w_m^2 + w_\phi^2 - (\Omega r)^2]$$

$$h_{rot} = \frac{\gamma}{\gamma - 1}\frac{p}{\rho} + \frac{1}{2}[w_m^2 + w_\phi^2 - (\Omega r)^2]$$

$$\int_V \frac{\partial \mathbf{u}'}{\partial t} + (i\omega \mathbf{E} - \mathbf{C})\, \mathbf{u}' d\bar{V} + \int_S (hr\, \mathbf{B}\, \mathbf{u}'\, d\bar{\phi} - h\, \mathbf{A}\, \mathbf{u}'\, d\bar{m}) =$$
$$- \int_V i\omega\, \bar{\mathbf{u}} \left[\frac{\partial \phi'}{\partial \phi} + \frac{\partial m'}{\partial \bar{m}} \right] d\bar{V} + \int_S i\omega\, hr\, \bar{\mathbf{u}} \left[m'\, d\bar{\phi} - \phi'\, d\bar{m} \right]$$
$$- \int_S \left[hr\, \bar{\mathbf{G}} \left[\frac{\partial \phi'}{\partial \bar{\phi}} d\bar{\phi} + \frac{\partial \phi'}{\partial \bar{m}} d\bar{m} \right] - h\, \bar{\mathbf{F}} \left[\frac{\partial m'}{\partial \bar{\phi}} d\bar{\phi} + \frac{\partial m'}{\partial \bar{m}} d\bar{m} \right] \right]$$
$$- \int_S \left[\bar{\mathbf{G}} \frac{d\,hr}{d\bar{m}}\, m'\, d\bar{\phi} - \bar{\mathbf{F}} \frac{dh}{d\bar{m}}\, m'\, d\bar{m} \right]$$
$$- \int_S \left[hr \frac{\partial \bar{\mathbf{G}}}{\partial r}\frac{dr}{d\bar{m}} m' d\bar{\phi} - h \frac{\partial \bar{\mathbf{F}}}{\partial r}\frac{dr}{d\bar{m}} m'\, d\bar{m} \right]$$
$$+ \int_S hr\, \bar{\mathbf{H}} \left[m' d\bar{\phi} - \phi' d\bar{m} \right] + \int_V \frac{\partial \bar{\mathbf{H}}}{\partial \bar{m}} m'\, d\bar{V}$$

$$\mathbf{A} = \left.\frac{\partial \mathbf{F}}{\partial \mathbf{u}}\right|_{\mathbf{u}=\bar{\mathbf{u}}} \qquad \mathbf{B} = \left.\frac{\partial \mathbf{G}}{\partial \mathbf{u}}\right|_{\mathbf{u}=\bar{\mathbf{u}}} \qquad \mathbf{C} = \left.\frac{\partial \mathbf{H}}{\partial \mathbf{u}}\right|_{\mathbf{u}=\bar{\mathbf{u}}}$$

Tab. 7 Linearized Euler equations for unsteady blade to blade flow

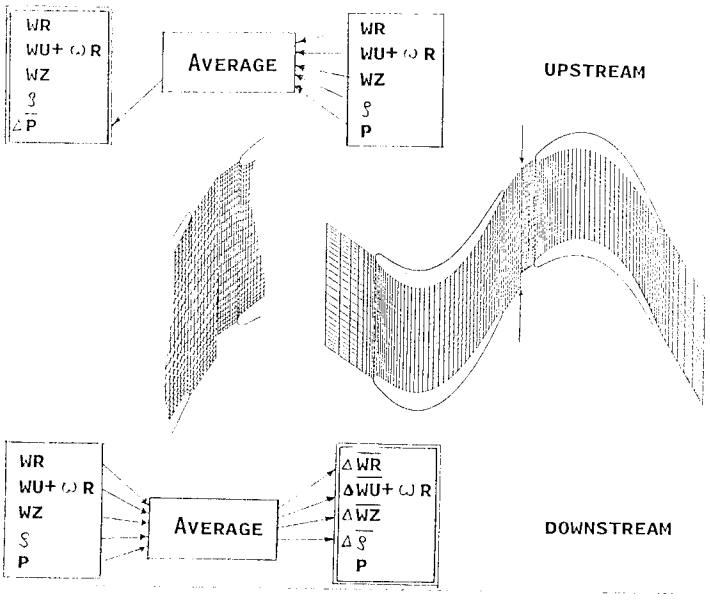

Tab. 6 Coupling at internal boundaries for multi-stage 3D procedures

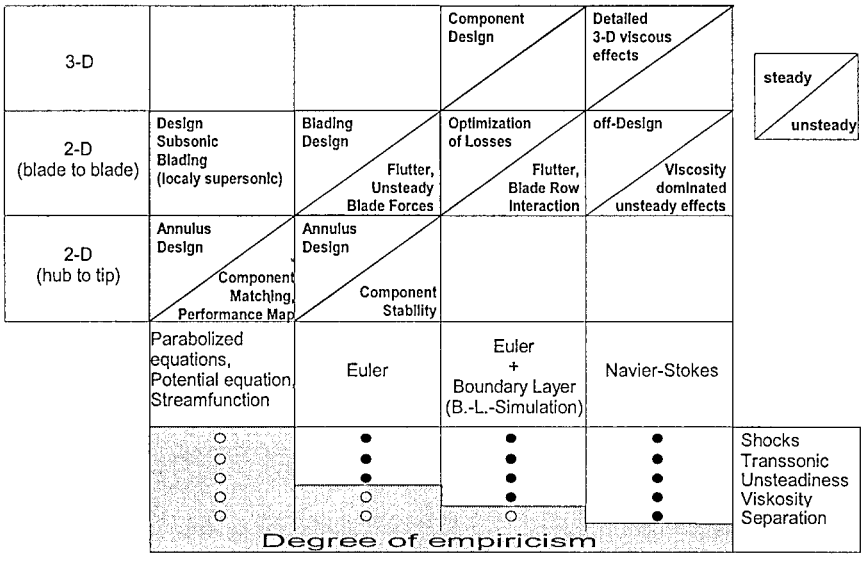

Fig. 1: Design problems and application of CFD methods

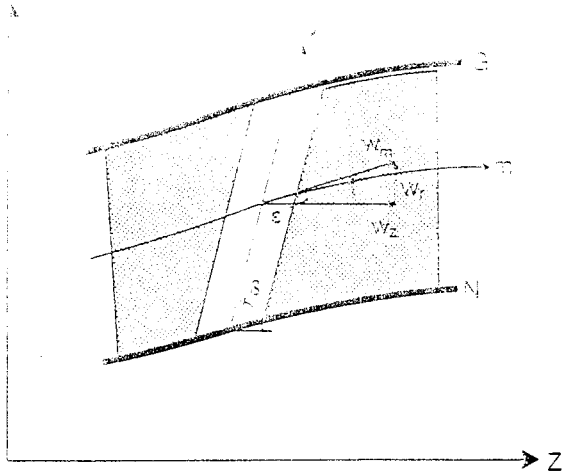

$$w_r = w_m \frac{Dr}{Dm}, \quad \varepsilon = \text{arc sin}\left(\frac{Dr}{Dm}\right), \quad w_z = w_m \frac{Dz}{Dm}$$

Fig. 2: Parametric description of the coordinates for streamline curvature methods

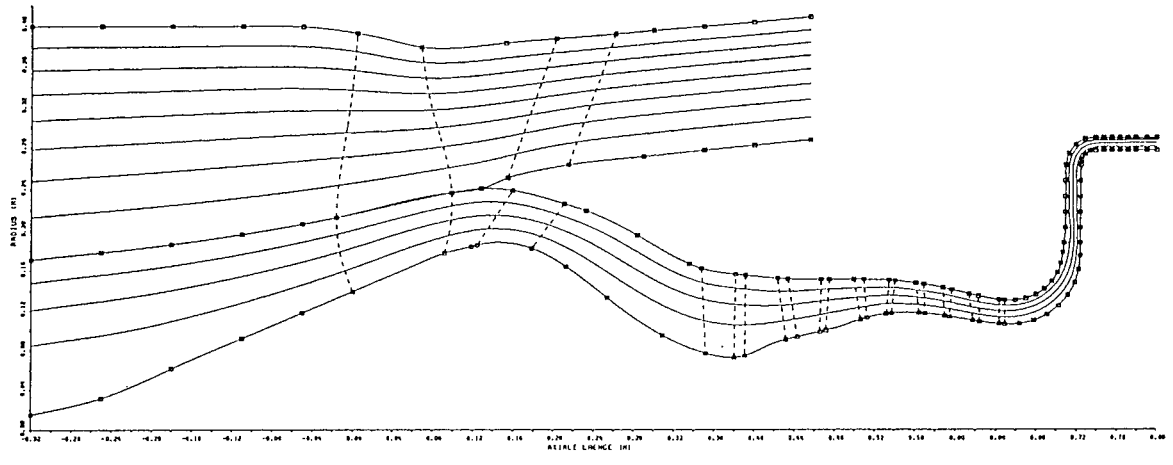

Fig. 3: Application of streamline curvature method for a complex compressor system

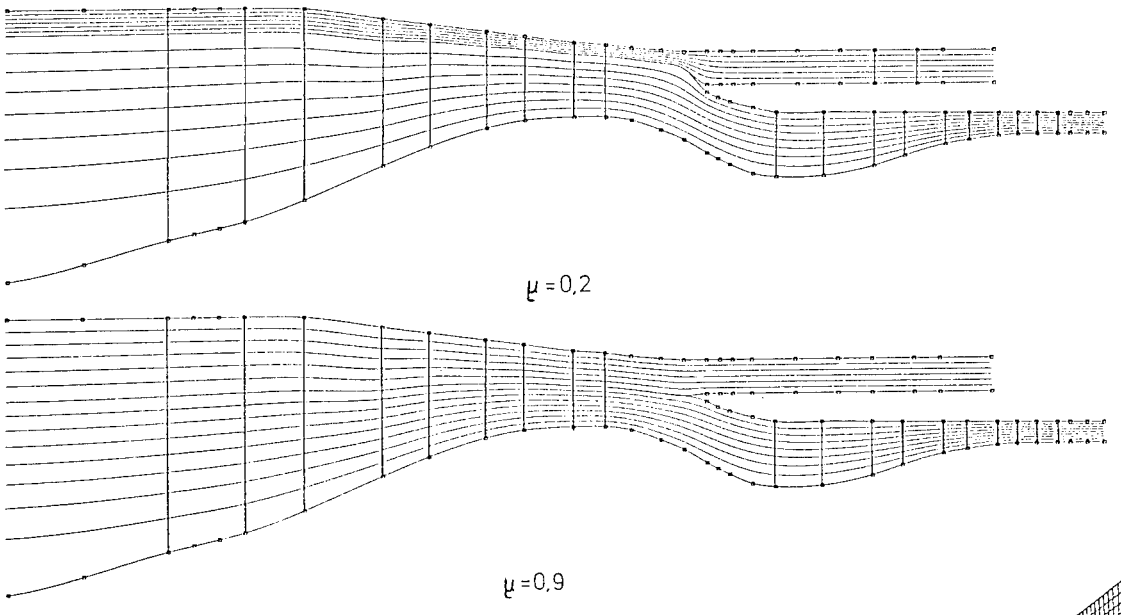

Fig. 4: Influence of different bypass-ratios on LPC, bypass duct and HPC, calculated by a streamline-curvature method

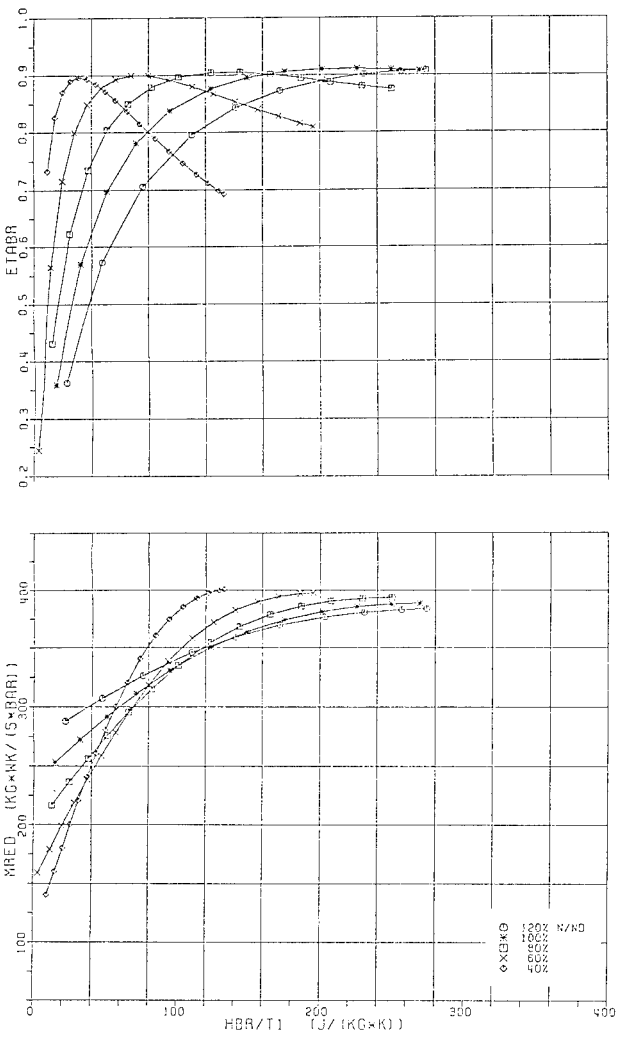

Fig. 5: Streamline-curvature-method simulation of a turbine performance map

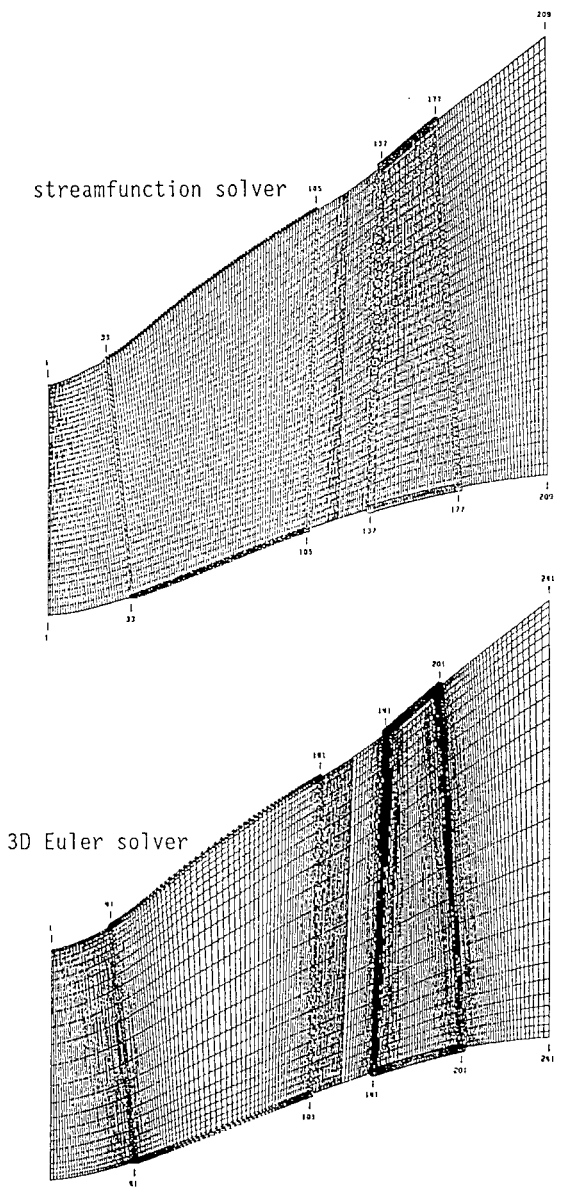

Fig. 6: Numerical grid for hub-to-tip flow streamfunction solver in comparison to the grid of a 3D Euler solver (transonic turbine)

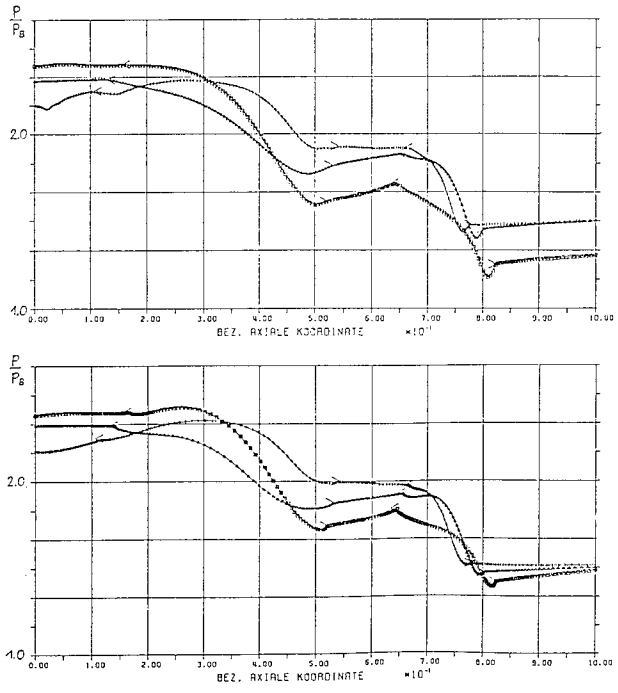

Fig. 7: Axial distribution of static pressure on hub, tip and mean streamlines (streamfunction and Euler solver)

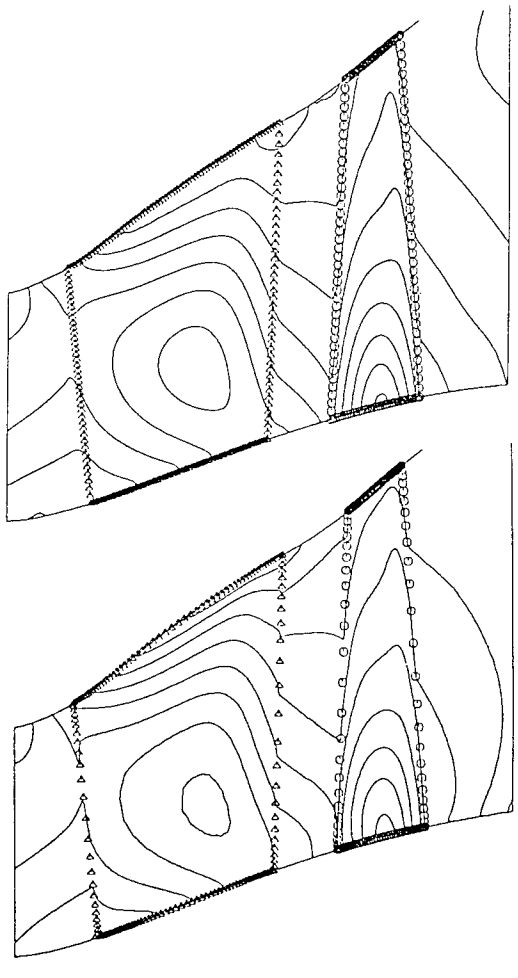

Fig. 8: Axial velocities (streamfunction and Euler solver)

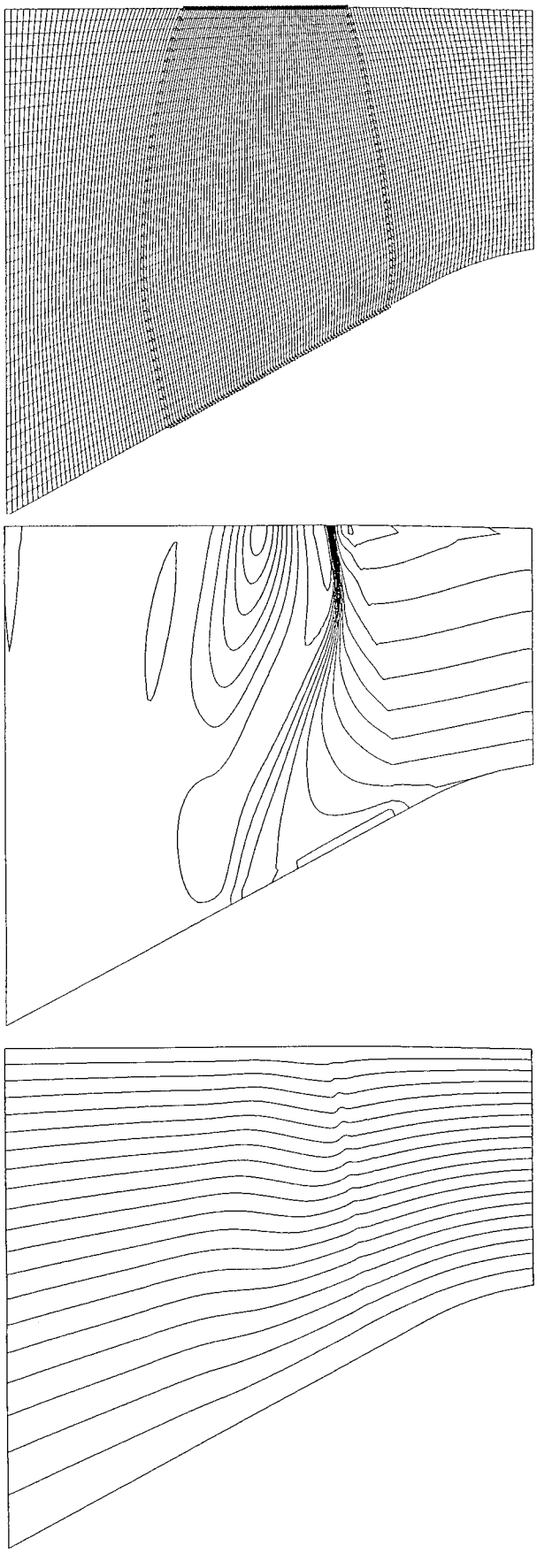

Fig. 9: Application of a 2D hub-to-tip Euler solver to a highly loaded transonic compressor rotor

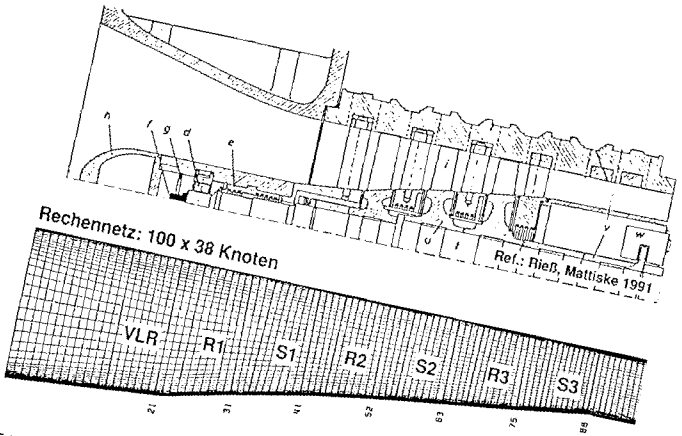

Fig. 10: Numerical grid for circumferentially averaged Navier-Stokes equation

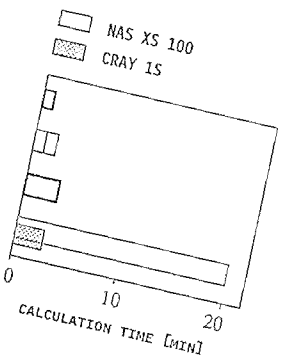

METHOD	CPU-MIN
EULER + INTEGRAL B.L.	1 + 0.025
EULER + FIN. DIFF. B.L.	1 + 1
EULER/ INTEGRAL B.L. INTERACT.	2 - 3
NAVIER-STOKES	20 (2.5)

Fig. 13: CPU-Comparison of different methods for the computation of viscous effects

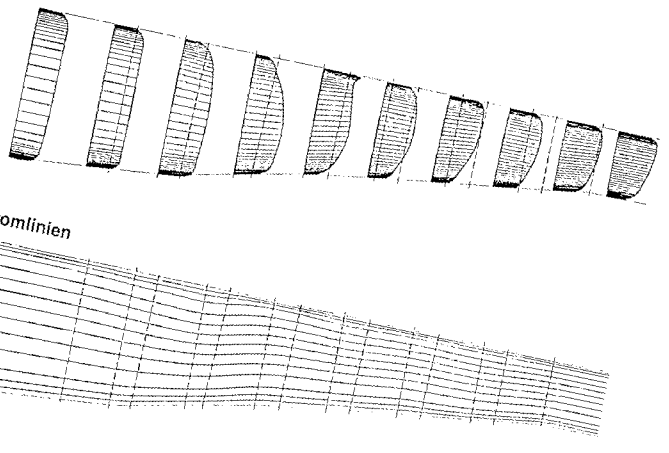

Fig. 11: Meridional flow pattern on the basis of circumferentially averaged Navier-Stokes equations

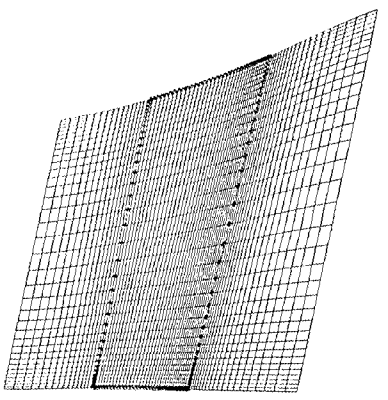

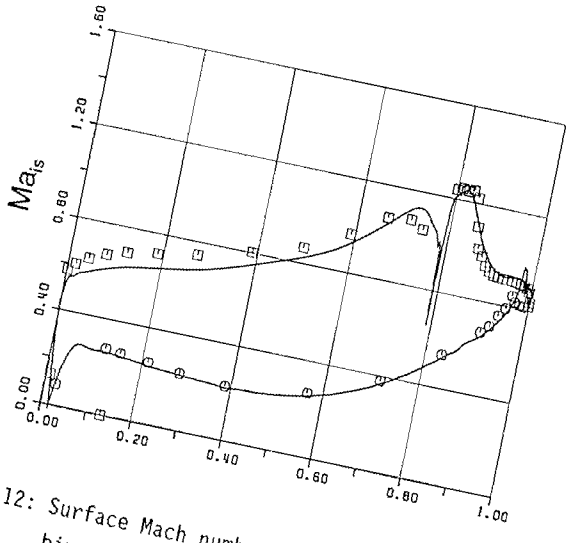

Fig. 12: Surface Mach number of a transonic turbine with film cooling

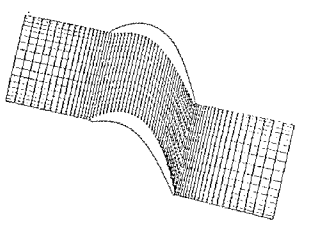

Fig. 14: Grid for 3D Euler solver

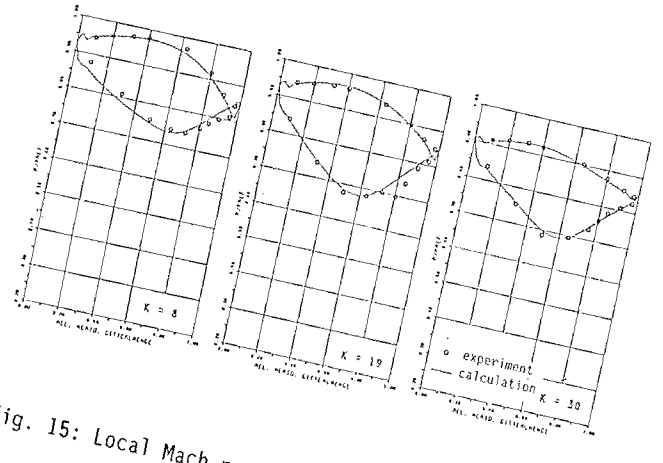

Fig. 15: Local Mach numbers resulting for 3D Euler computation

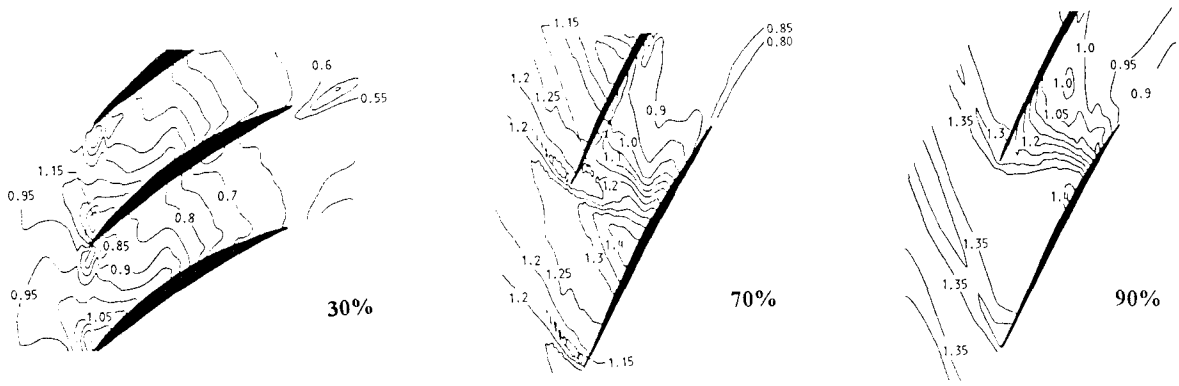

Fig. 16: Iso-Mach number-lines for a transonic rotor /22/

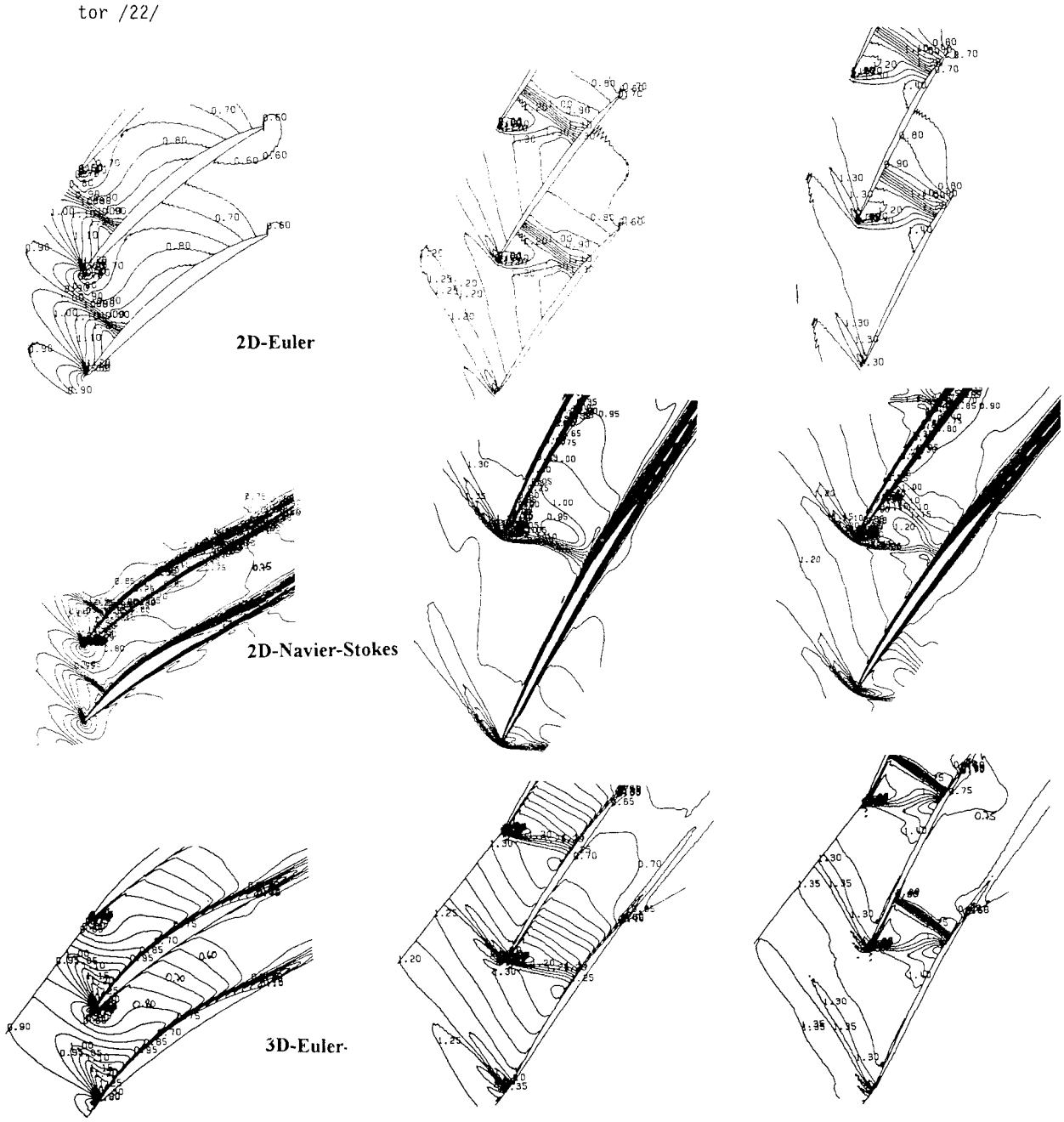

Fig. 17: Comparison of quasi-3D procedure (Euler and Navier-Stokes blade to blade flow) with 3D-Euler solver

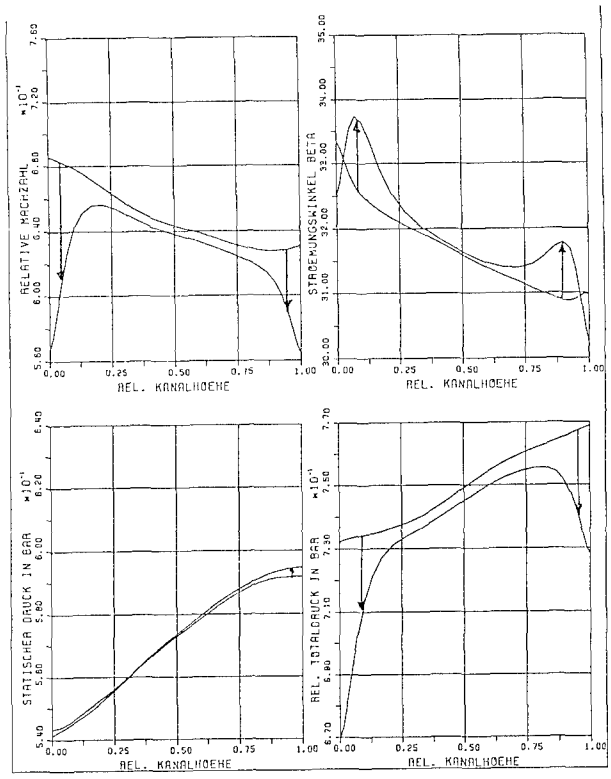

Fig. 18: Influence of pseudo-viscosity by body-forces on radial distribution of flow properties

BOW-Schaufel, nominal

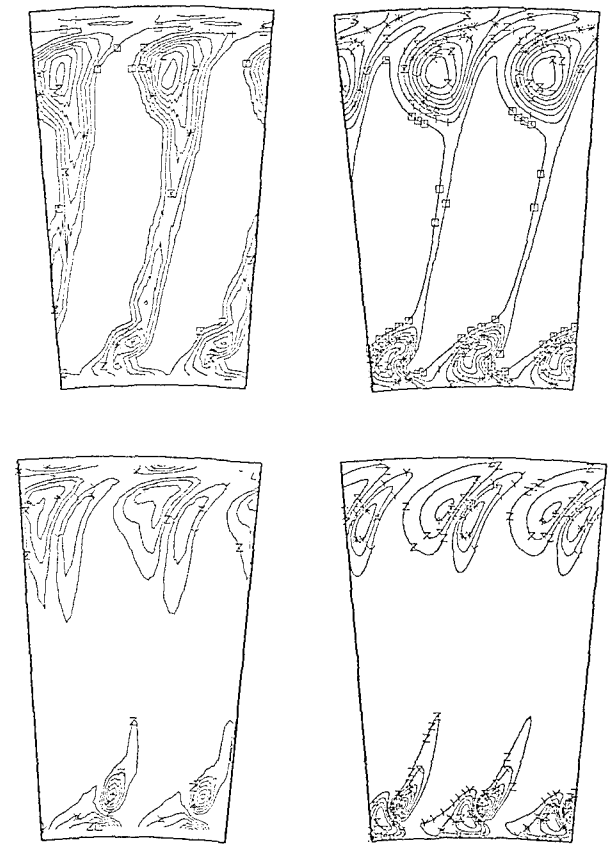

LEAN-Schaufel, nominal

Fig. 19: Secondary flow at the exit of a turbine vane

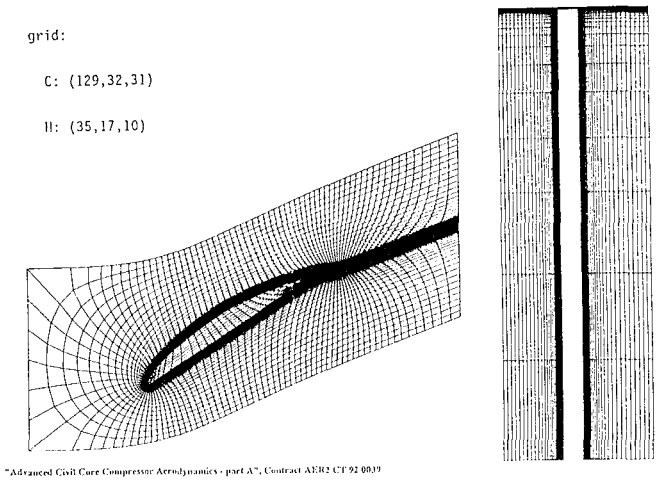

"Advanced Civil Core Compressor Aerodynamics - part A", Contract AER2 CT 92 0039

Fig. 20: Tip clearance flow in a compressor cascade /26/ simulated by 3D Navier-Stokes solver (grid)

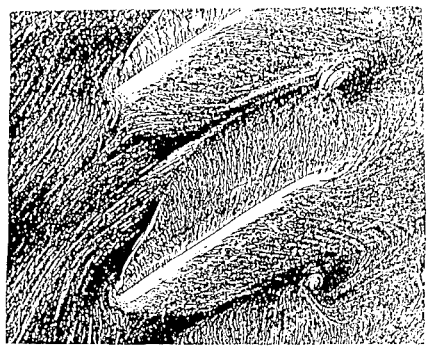

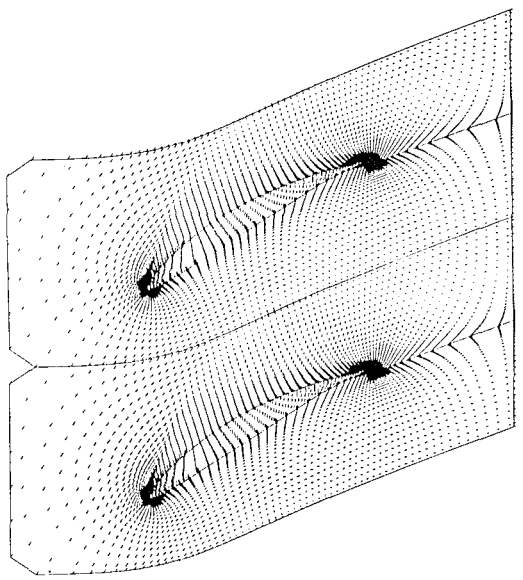

"Advanced Civil Core Compressor Aerodynamics - part A", Contract AER2 CT 92 0039

Fig. 21: Tip clearance flow in a compressor cascade /26/ simulated by 3D Navier-Stokes solver (flow pattern)

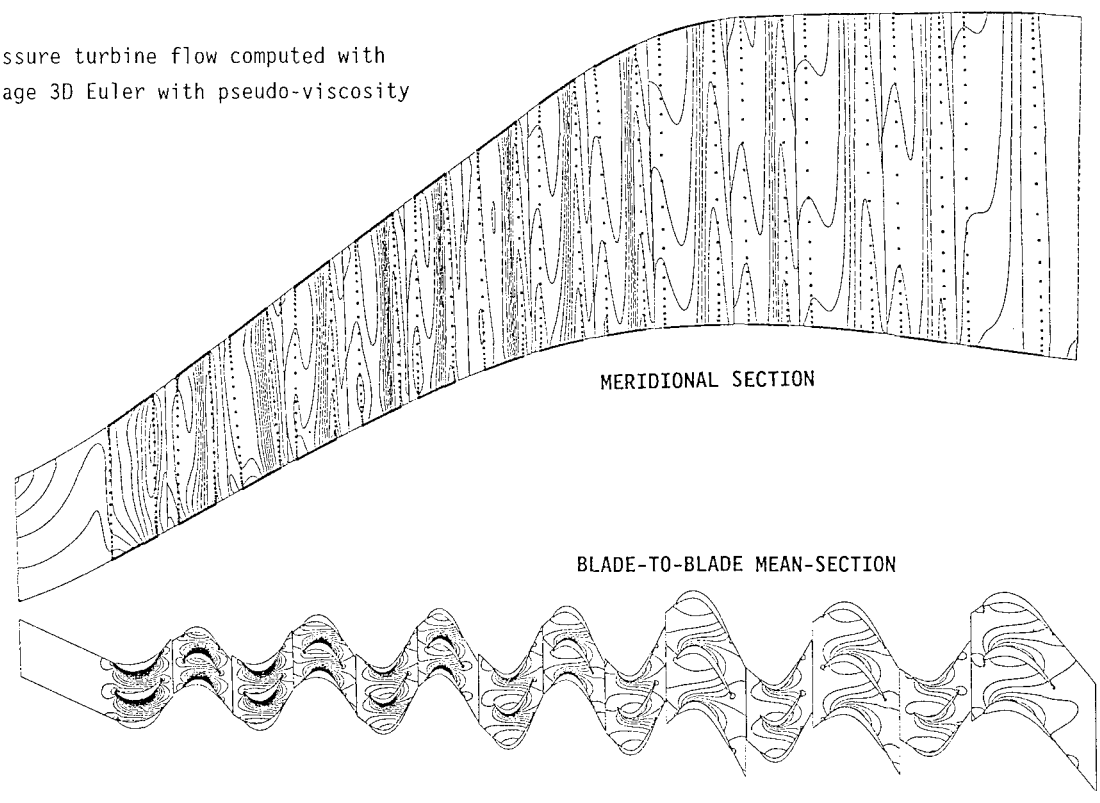

Fig. 22: Low pressure turbine flow computed with multistage 3D Euler with pseudo-viscosity

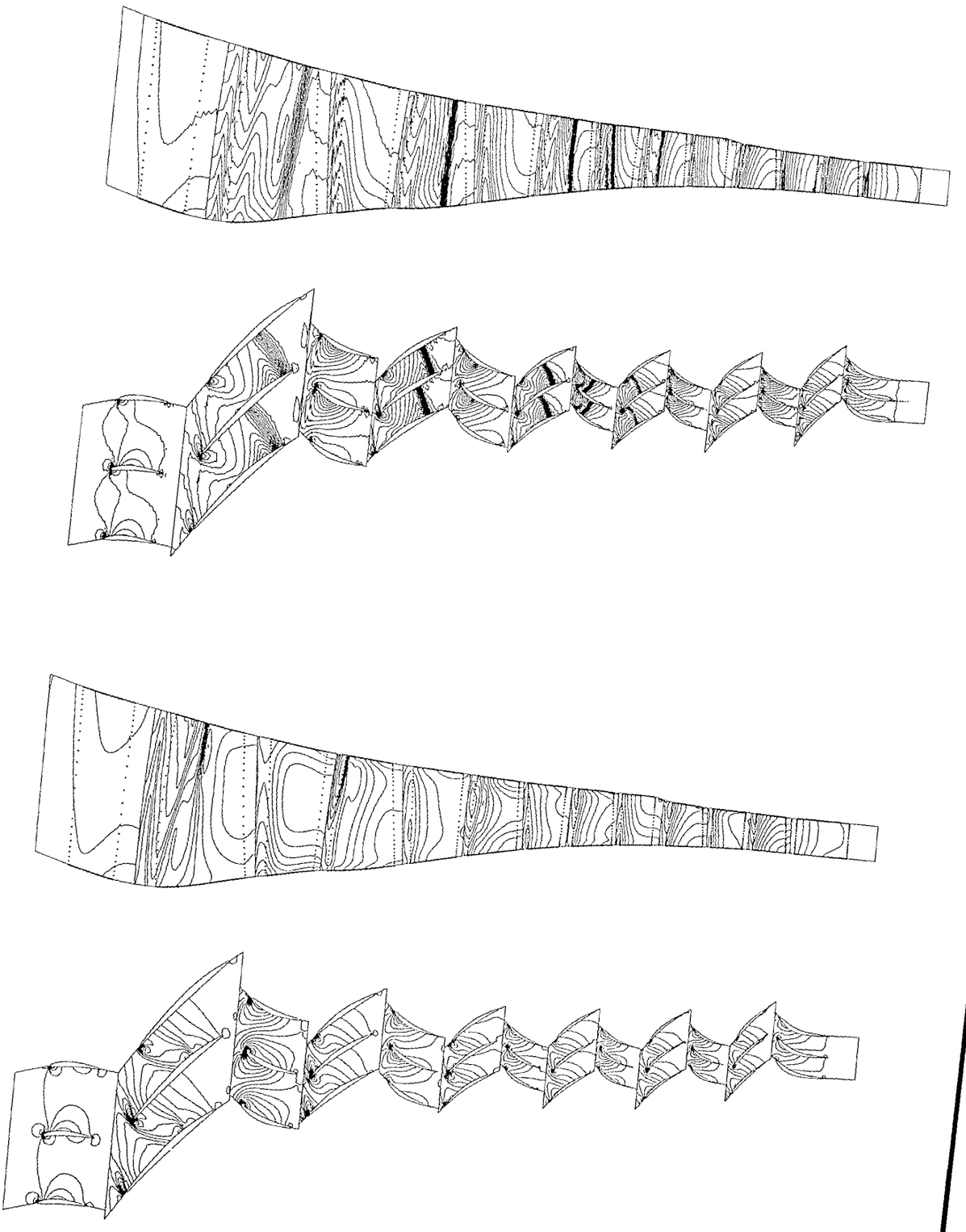

Fig. 23: High pressure compressor flow computed with multistage 3D Euler with pseudo-viscosity

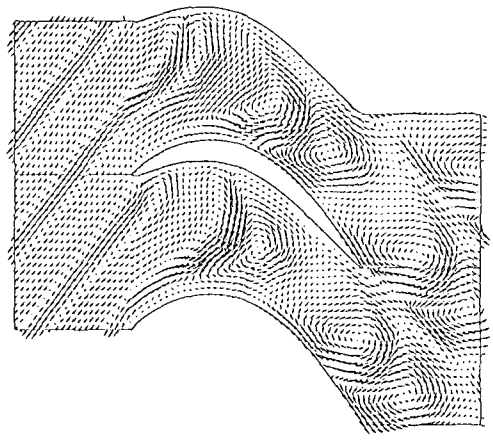

Fig. 27: Wake induced unsteady flow in a turbine blade

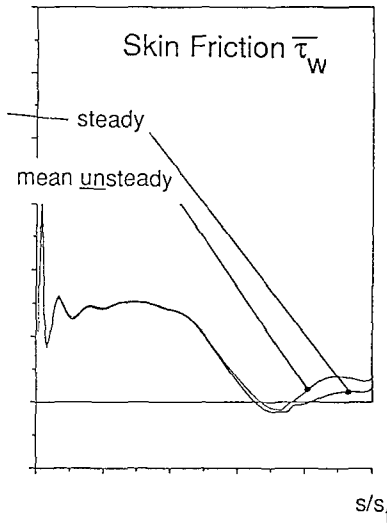

Fig. 28: Influence of Unsteadiness on skin friction

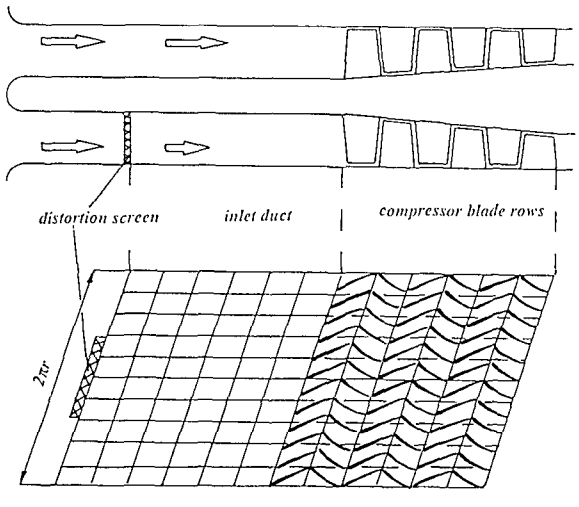

Fig. 29: System for distortion calculation

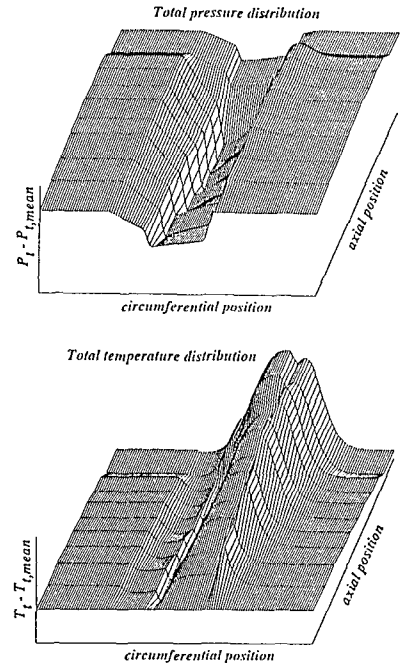

Fig. 30: Distortion transfer in multistage compressor

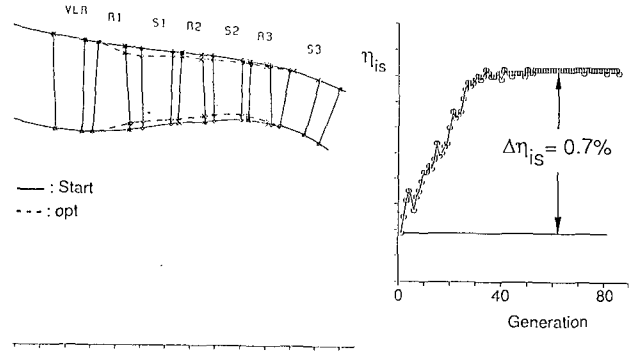

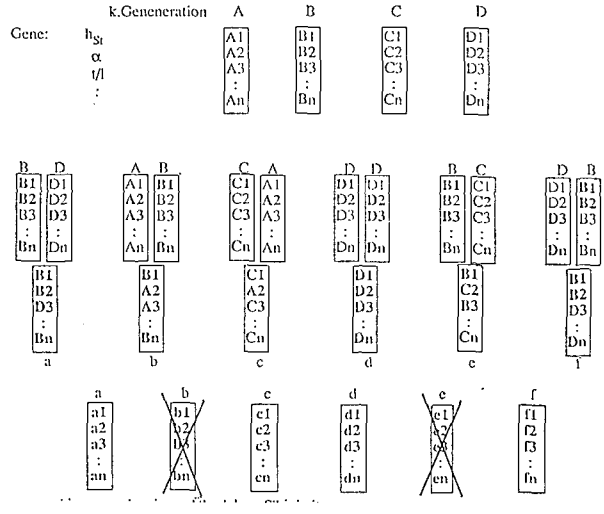

Fig. 31: Application of an evolution-strategy on a compressor

Fig. 24: Flow field in a low pressure turbine computed by a Multistage 3D Navier-Stokes solver

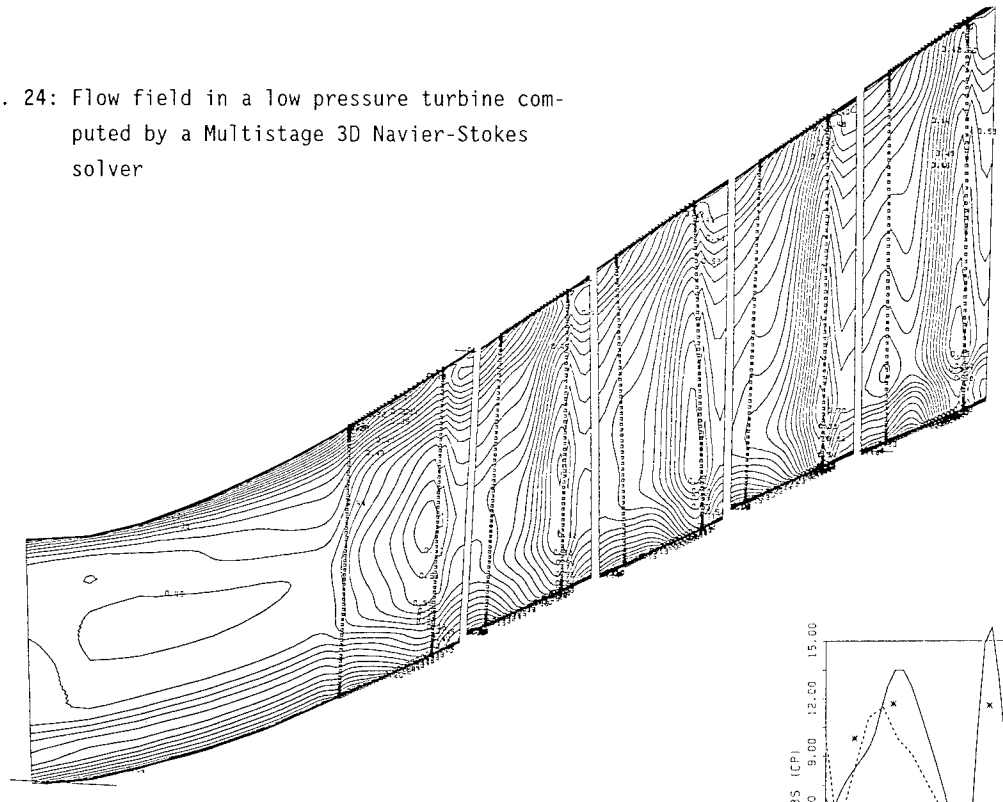

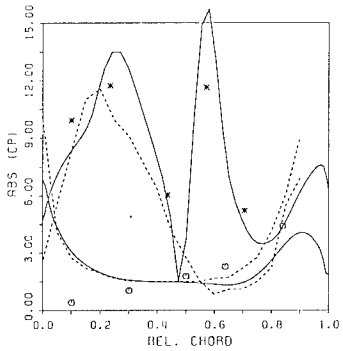

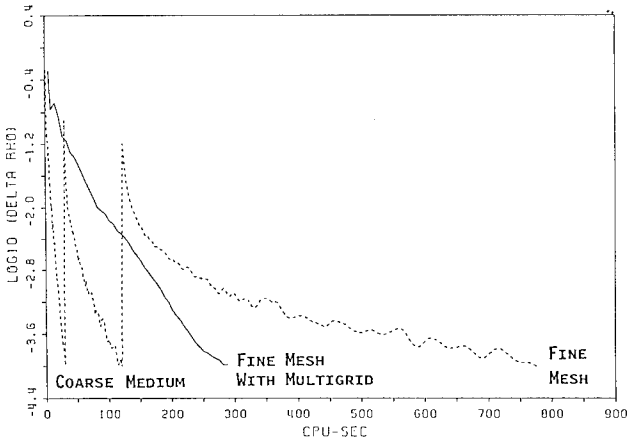

Fig. 25: Improvement of convergence rate by multigrid technique

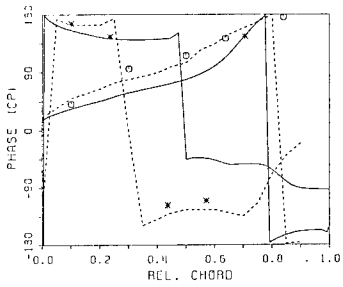

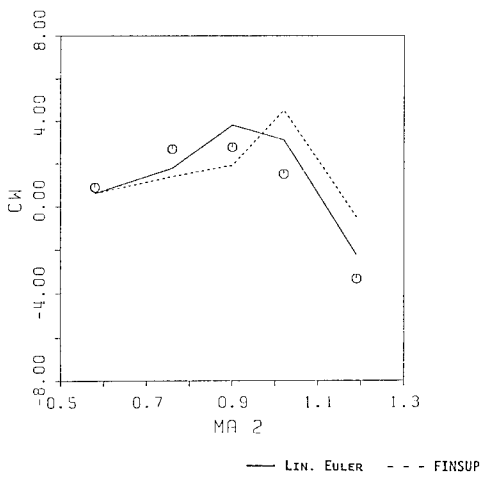

Fig. 26: Unsteady pressure distribution and work transonic turbine blade /29, 35/

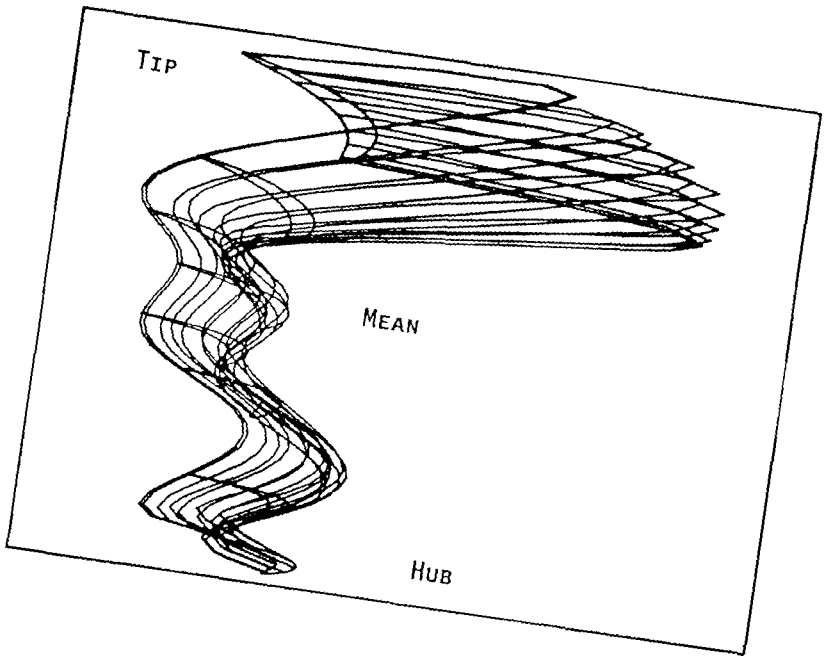

Fig. 32: Optimized "Mega-Bow" - today's limitation of optimization-strategies

REPORT DOCUMENTATION PAGE			
1. Recipient's Reference	**2. Originator's Reference**	**3. Further Reference**	**4. Security Classification of Document**
	AGARD-LS-195	ISBN 92-835-0749-5	UNCLASSIFIED/ UNLIMITED

5. Originator	Advisory Group for Aerospace Research and Development North Atlantic Treaty Organization 7 rue Ancelle, 92200 Neuilly sur Seine, France
6. Title	TURBOMACHINERY DESIGN USING CFD
7. Presented on	24th–25th May 1994 in Ohio, United States, 6th–7th June 1994 in Ankara, Turkey, and 9th–10th June 1994 in Munich, Germany.

8. Author(s)/Editor(s)	**9. Date**
Various	May 1994
10. Author(s)/Editor's Address	**11. Pages**
Various	252

12. Distribution Statement	There are no restrictions on the distribution of this document. Information about the availability of this and other AGARD unclassified publications is given on the back cover.

13. Keywords/Descriptors

Computational fluid dynamics	Turbulent flow
Design	Unsteady flow
Gas turbines	Aircraft engines
Jet flow	

14. Abstract

Computational Fluid Dynamics (CFD) has become a major design tool for designers of turbomachinery. The progress in this area is fast, and the use of 3-D methods is becoming increasingly applicable to the design process. This Lecture Series will improve the knowledge in the NATO nations on how to utilize the modern tools of CFD to increase the efficiency, reduce the fuel consumption, and increase the affordability of aircraft engines. Its aim is a unique forum in which the designers from leading gas turbine manufacturers and CFD code developers will present their points of view on the role of CFD in design.

The Lecture Series will cover the recent advances in the use of CFD for turbomachinery design. The role of CFD in the final design phase and the use of computational techniques in the preliminary design phases will be emphasized. Topics to be covered will include:

- Computational methods for preliminary design and geometry definitions;
- Methods for computing through-flows, blade-to-blade flows and geometry generation;
- Optimization strategies;
- Designing in three dimensions;
- Code validation, mesh influence on solution accuracy;
- Turbulence and transition modelling;
- Comparison of time averaged flow solvers and 3-D unsteady CFD codes;
- Industrial use of CFD and the points of view of the designers.

This Lecture Series, sponsored by the Propulsion and Energetics Panel of AGARD, has been implemented by the Consultant and Exchange Programme.

AGARD Lecture Series 195
Advisory Group for Aerospace Research and Development, NATO
TURBOMACHINERY DESIGN USING CFD
Published May 1994
252 pages

Computational Fluid Dynamics (CFD) has become a major design tool for designers of turbomachinery. The progress in this area is fast, and the use of 3-D methods is becoming increasingly applicable to the design process. This Lecture Series will improve the knowledge in the NATO nations on how to utilize the modern tools of CFD to increase the efficiency, reduce the fuel consumption, and increase the affordability of aircraft engines. Its aim is a unique forum in which the designers from leading gas turbine manufacturers and CFD code developers will present their points of view on the role of CFD in design.

P.T.O.

AGARD-LS-195

Computational fluid dynamics
Design
Gas turbines
Jet flow
Turbulent flow
Unsteady flow
Aircraft engines

AGARD Lecture Series 195
Advisory Group for Aerospace Research and Development, NATO
TURBOMACHINERY DESIGN USING CFD
Published May 1994
252 pages

Computational Fluid Dynamics (CFD) has become a major design tool for designers of turbomachinery. The progress in this area is fast, and the use of 3-D methods is becoming increasingly applicable to the design process. This Lecture Series will improve the knowledge in the NATO nations on how to utilize the modern tools of CFD to increase the efficiency, reduce the fuel consumption, and increase the affordability of aircraft engines. Its aim is a unique forum in which the designers from leading gas turbine manufacturers and CFD code developers will present their points of view on the role of CFD in design.

P.T.O.

AGARD-LS-195

Computational fluid dynamics
Design
Gas turbines
Jet flow
Turbulent flow
Unsteady flow
Aircraft engines

AGARD Lecture Series 195
Advisory Group for Aerospace Research and Development, NATO
TURBOMACHINERY DESIGN USING CFD
Published May 1994
252 pages

Computational Fluid Dynamics (CFD) has become a major design tool for designers of turbomachinery. The progress in this area is fast, and the use of 3-D methods is becoming increasingly applicable to the design process. This Lecture Series will improve the knowledge in the NATO nations on how to utilize the modern tools of CFD to increase the efficiency, reduce the fuel consumption, and increase the affordability of aircraft engines. Its aim is a unique forum in which the designers from leading gas turbine manufacturers and CFD code developers will present their points of view on the role of CFD in design.

P.T.O.

AGARD-LS-195

Computational fluid dynamics
Design
Gas turbines
Jet flow
Turbulent flow
Unsteady flow
Aircraft engines

AGARD Lecture Series 195
Advisory Group for Aerospace Research and Development, NATO
TURBOMACHINERY DESIGN USING CFD
Published May 1994
252 pages

Computational Fluid Dynamics (CFD) has become a major design tool for designers of turbomachinery. The progress in this area is fast, and the use of 3-D methods is becoming increasingly applicable to the design process. This Lecture Series will improve the knowledge in the NATO nations on how to utilize the modern tools of CFD to increase the efficiency, reduce the fuel consumption, and increase the affordability of aircraft engines. Its aim is a unique forum in which the designers from leading gas turbine manufacturers and CFD code developers will present their points of view on the role of CFD in design.

P.T.O.

AGARD-LS-195

Computational fluid dynamics
Design
Gas turbines
Jet flow
Turbulent flow
Unsteady flow
Aircraft engines

The Lecture Series will cover the recent advances in the use of CFD for turbomachinery design. The role of CFD in the final design phase and the use of computational techniques in the preliminary design phases will be emphasized. Topics to be covered will include:

- Computational methods for preliminary design and geometry definitions;
- Methods for computing through-flows, blade-to-blade flows and geometry generation;
- Optimization strategies;
- Designing in three dimensions;
- Code validation, mesh influence on solution accuracy;
- Turbulence and transition modelling;
- Comparison of time averaged flow solvers and 3-D unsteady CFD codes;
- Industrial use of CFD and the points of view of the designers.

This Lecture Series, sponsored by the Propulsion and Energetics Panel of AGARD, has been implemented by the Consultant and Exchange Programme, presented on 24th–25th May 1994 in Ohio, United States 6th–7th June 1994 in Ankara, Turkey, and 9th–10th June 1994 in Munich, Germany.

ISBN 92-835-0749-5

The Lecture Series will cover the recent advances in the use of CFD for turbomachinery design. The role of CFD in the final design phase and the use of computational techniques in the preliminary design phases will be emphasized. Topics to be covered will include:

- Computational methods for preliminary design and geometry definitions;
- Methods for computing through-flows, blade-to-blade flows and geometry generation;
- Optimization strategies;
- Designing in three dimensions;
- Code validation, mesh influence on solution accuracy;
- Turbulence and transition modelling;
- Comparison of time averaged flow solvers and 3-D unsteady CFD codes;
- Industrial use of CFD and the points of view of the designers.

This Lecture Series, sponsored by the Propulsion and Energetics Panel of AGARD, has been implemented by the Consultant and Exchange Programme, presented on 24th–25th May 1994 in Ohio, United States 6th–7th June 1994 in Ankara, Turkey, and 9th–10th June 1994 in Munich, Germany.

ISBN 92-835-0749-5

The Lecture Series will cover the recent advances in the use of CFD for turbomachinery design. The role of CFD in the final design phase and the use of computational techniques in the preliminary design phases will be emphasized. Topics to be covered will include:

- Computational methods for preliminary design and geometry definitions;
- Methods for computing through-flows, blade-to-blade flows and geometry generation;
- Optimization strategies;
- Designing in three dimensions;
- Code validation, mesh influence on solution accuracy;
- Turbulence and transition modelling;
- Comparison of time averaged flow solvers and 3-D unsteady CFD codes;
- Industrial use of CFD and the points of view of the designers.

This Lecture Series, sponsored by the Propulsion and Energetics Panel of AGARD, has been implemented by the Consultant and Exchange Programme, presented on 24th–25th May 1994 in Ohio, United States 6th–7th June 1994 in Ankara, Turkey, and 9th–10th June 1994 in Munich, Germany.

ISBN 92-835-0749-5

The Lecture Series will cover the recent advances in the use of CFD for turbomachinery design. The role of CFD in the final design phase and the use of computational techniques in the preliminary design phases will be emphasized. Topics to be covered will include:

- Computational methods for preliminary design and geometry definitions;
- Methods for computing through-flows, blade-to-blade flows and geometry generation;
- Optimization strategies;
- Designing in three dimensions;
- Code validation, mesh influence on solution accuracy;
- Turbulence and transition modelling;
- Comparison of time averaged flow solvers and 3-D unsteady CFD codes;
- Industrial use of CFD and the points of view of the designers.

This Lecture Series, sponsored by the Propulsion and Energetics Panel of AGARD, has been implemented by the Consultant and Exchange Programme, presented on 24th–25th May 1994 in Ohio, United States 6th–7th June 1994 in Ankara, Turkey, and 9th–10th June 1994 in Munich, Germany.

ISBN 92-835-0749-5

AGARD

NATO OTAN

7 RUE ANCELLE · 92200 NEUILLY-SUR-SEINE

FRANCE

Télécopie (1)47.38.57.99 · Télex 610 176

DIFFUSION DES PUBLICATIONS

AGARD NON CLASSIFIEES

Aucun stock de publications n'a existé à AGARD. A partir de 1993, AGARD détiendra un stock limité des publications associées aux cycles de conférences et cours spéciaux ainsi que les AGARDographies et les rapports des groupes de travail, organisés et publiés à partir de 1993 inclus. Les demandes de renseignements doivent être adressées à AGARD par lettre ou par fax à l'adresse indiquée ci-dessus. *Veuillez ne pas téléphoner.* La diffusion initiale de toutes les publications de l'AGARD est effectuée auprès des pays membres de l'OTAN par l'intermédiaire des centres de distribution nationaux indiqués ci-dessous. Des exemplaires supplémentaires peuvent parfois être obtenus auprès de ces centres (à l'exception des Etats-Unis). Si vous souhaitez reçevoir toutes les publications de l'AGARD, ou simplement celles qui concernent certains Panels, vous pouvez demander à être inclu sur la liste d'envoi de l'un de ces centres. Les publications de l'AGARD sont en vente auprès des agences indiquées ci-dessous, sous forme de photocopie ou de microfiche.

CENTRES DE DIFFUSION NATIONAUX

ALLEMAGNE
Fachinformationszentrum,
Karlsruhe
D-7514 Eggenstein-Leopoldshafen 2

BELGIQUE
Coordonnateur AGARD-VSL
Etat-Major de la Force Aérienne
Quartier Reine Elisabeth
Rue d'Evere, 1140 Bruxelles

CANADA
Directeur du Service des Renseignements Scientifiques
Ministère de la Défense Nationale
Ottawa, Ontario K1A 0K2

DANEMARK
Danish Defence Research Establishment
Ryvangs Allé 1
P.O. Box 2715
DK-2100 Copenhagen Ø

ESPAGNE
INTA (AGARD Publications)
Pintor Rosales 34
28008 Madrid

ETATS-UNIS
NASA Headquarters
Attention: CF 37, Distribution Center
300 E Street, S.W.
Washington, D.C. 20546

FRANCE
O.N.E.R.A. (Direction)
29, Avenue de la Division Leclerc
92322 Châtillon Cedex

GRECE
Hellenic Air Force
Air War College
Scientific and Technical Library
Dekelia Air Force Base
Dekelia, Athens TGA 1010

ISLANDE
Director of Aviation
c/o Flugrad
Reykjavik

ITALIE
Aeronautica Militare
Ufficio del Delegato Nazionale all'AGARD
Aeroporto Pratica di Mare
00040 Pomezia (Roma)

LUXEMBOURG
Voir Belgique

NORVEGE
Norwegian Defence Research Establishment
Attn: Biblioteket
P.O. Box 25
N-2007 Kjeller

PAYS-BAS
Netherlands Delegation to AGARD
National Aerospace Laboratory NLR
P.O. Box 90502
1006 BM Amsterdam

PORTUGAL
Força Aérea Portuguesa
Centro de Documentação e Informação
Alfragide
2700 Amadora

ROYAUME UNI
Defence Research Information Centre
Kentigern House
65 Brown Street
Glasgow G2 8EX

TURQUIE
Millî Savunma Başkanlığı (MSB)
ARGE Daire Başkanlığı (ARGE)
Ankara

Le centre de distribution national des Etats-Unis ne détient PAS de stocks des publications de l'AGARD.
D'éventuelles demandes de photocopies doivent être formulées directement auprès du NASA Center for Aerospace Information (CASI) à l'adresse suivante:

AGENCES DE VENTE

NASA Center for
Aerospace Information (CASI)
800 Elkridge Landing Road
Linthicum Heights, MD 21090-2934
United States

ESA/Information Retrieval Service
European Space Agency
10, rue Mario Nikis
75015 Paris
France

The British Library
Document Supply Division
Boston Spa, Wetherby
West Yorkshire LS23 7BQ
Royaume Uni

Les demandes de microfiches ou de photocopies de documents AGARD (y compris les demandes faites auprès du CASI) doivent comporter la dénomination AGARD, ainsi que le numéro de série d'AGARD (par exemple AGARD-AG-315). Des informations analogues, telles que le titre et la date de publication sont souhaitables. Veuiller noter qu'il y a lieu de spécifier AGARD-R-nnn et AGARD-AR-nnn lors de la commande des rapports AGARD et des rapports consultatifs AGARD respectivement. Des références bibliographiques complètes ainsi que des résumés des publications AGARD figurent dans les journaux suivants:

Scientifique and Technical Aerospace Reports (STAR)
publié par la NASA Scientific and Technical
Information Program
NASA Headquarters (JTT)
Washington D.C. 20546
Etats-Unis

Government Reports Announcements and Index (GRA&I)
publié par le National Technical Information Service
Springfield
Virginia 22161
Etats-Unis

(accessible également en mode interactif dans la base de données bibliographiques en ligne du NTIS, et sur CD-ROM)

Imprimé par Specialised Printing Services Limited
40 Chigwell Lane, Loughton, Essex IG10 3TZ

AGARD

NATO OTAN

7 RUE ANCELLE · 92200 NEUILLY-SUR-SEINE

FRANCE

Telefax (1)47.38.57.99 · Telex 610 176

DISTRIBUTION OF UNCLASSIFIED AGARD PUBLICATIONS

AGARD holds limited quantities of the publications that accompanied Lecture Series and Special Courses held in 1993 or later, and of AGARDographs and Working Group reports published from 1993 onward. For details, write or send a telefax to the address given above. *Please do not telephone.*

AGARD does not hold stocks of publications that accompanied earlier Lecture Series or Courses or of any other publications. Initial distribution of all AGARD publications is made to NATO nations through the National Distribution Centres listed below. Further copies are sometimes available from these centres (except in the United States). If you have a need to receive all AGARD publications, or just those relating to one or more specific AGARD Panels, they may be willing to include you (or your organisation) on their distribution list. AGARD publications may be purchased from the Sales Agencies listed below, in photocopy or microfiche form.

NATIONAL DISTRIBUTION CENTRES

BELGIUM
Coordonnateur AGARD — VSL
Etat-Major de la Force Aérienne
Quartier Reine Elisabeth
Rue d'Evere, 1140 Bruxelles

CANADA
Director Scientific Information Services
Dept of National Defence
Ottawa, Ontario K1A 0K2

DENMARK
Danish Defence Research Establishment
Ryvangs Allé 1
P.O. Box 2715
DK-2100 Copenhagen Ø

FRANCE
O.N.E.R.A. (Direction)
29 Avenue de la Division Leclerc
92322 Châtillon Cedex

GERMANY
Fachinformationszentrum
Karlsruhe
D-7514 Eggenstein-Leopoldshafen 2

GREECE
Hellenic Air Force
Air War College
Scientific and Technical Library
Dekelia Air Force Base
Dekelia, Athens TGA 1010

ICELAND
Director of Aviation
c/o Flugrad
Reykjavik

ITALY
Aeronautica Militare
Ufficio del Delegato Nazionale all'AGARD
Aeroporto Pratica di Mare
00040 Pomezia (Roma)

LUXEMBOURG
See Belgium

NETHERLANDS
Netherlands Delegation to AGARD
National Aerospace Laboratory, NLR
P.O. Box 90502
1006 BM Amsterdam

NORWAY
Norwegian Defence Research Establishment
Attn: Biblioteket
P.O. Box 25
N-2007 Kjeller

PORTUGAL
Força Aérea Portuguesa
Centro de Documentação e Informação
Alfragide
2700 Amadora

SPAIN
INTA (AGARD Publications)
Pintor Rosales 34
28008 Madrid

TURKEY
Milli Savunma Başkanlığı (MSB)
ARGE Daire Başkanlığı (ARGE)
Ankara

UNITED KINGDOM
Defence Research Information Centre
Kentigern House
65 Brown Street
Glasgow G2 8EX

UNITED STATES
NASA Headquarters
Attention: CF 37, Distribution Center
300 E Street, S.W.
Washington, D.C. 20546

The United States National Distribution Centre does NOT hold stocks of AGARD publications.
Applications for copies should be made direct to the NASA Center for Aerospace Information (CASI) at the address below.

SALES AGENCIES

NASA Center for
Aerospace Information (CASI)
800 Elkridge Landing Road
Linthicum Heights, MD 21090-2934
United States

ESA/Information Retrieval Service
European Space Agency
10, rue Mario Nikis
75015 Paris
France

The British Library
Document Supply Centre
Boston Spa, Wetherby
West Yorkshire LS23 7BQ
United Kingdom

Requests for microfiches or photocopies of AGARD documents (including requests to CASI) should include the word 'AGARD' and the AGARD serial number (for example AGARD-AG-315). Collateral information such as title and publication date is desirable. Note that AGARD Reports and Advisory Reports should be specified as AGARD-R-nnn and AGARD-AR-nnn, respectively. Full bibliographical references and abstracts of AGARD publications are given in the following journals:

Scientific and Technical Aerospace Reports (STAR)
published by NASA Scientific and Technical
Information Program
NASA Headquarters (JTT)
Washington D.C. 20546
United States

Government Reports Announcements and Index (GRA&I)
published by the National Technical Information Service
Springfield
Virginia 22161
United States
(also available online in the NTIS Bibliographic
Database or on CD-ROM)

Printed by Specialised Printing Services Limited
40 Chigwell Lane, Loughton, Essex IG10 3TZ

ISBN 92-835-0749-5